Advances in Natural and Technological Hazards Research

Vikas Thakur
Jean-Sébastien L'Heureux
Ariane Locat *Editors*

Landslides in Sensitive Clays

From Research to Implementation

Springer

Advances in Natural and Technological Hazards Research

Volume 46

The book series entitled *Advances in Natural and Technological Hazards* is dedicated to serving the growing community of scholars, practitioners and policy makers concerned with the different scientific, socio-economic and political aspects of natural and technological hazards. The series aims to provide rapid, refereed publications of topical contributions about recent advances in natural and technological hazards research. Each volume is a thorough treatment of a specific topic of importance for proper management and mitigation practices and will shed light on the fundamental and applied aspects of natural and technological hazards.

Comments or suggestions for future volumes are welcomed.

More information about this series at http://www.springer.com/series/6362

Vikas Thakur • Jean-Sébastien L'Heureux
Ariane Locat
Editors

Landslides in Sensitive Clays

From Research to Implementation

Springer

Editors
Vikas Thakur
Department of Civil
and Environmental Engineering
Norwegian University of Science
and Technology (NTNU)
Trondheim, Norway

Jean-Sébastien L'Heureux
Trondheim Division
Norwegian Geotechnical Institute (NGI)
Trondheim, Norway

Ariane Locat
Département de génie civil et de génie
des eaux
Université Laval
Québec City, QC, Canada

ISSN 1878-9897 ISSN 2213-6959 (electronic)
Advances in Natural and Technological Hazards Research
ISBN 978-3-319-56486-9 ISBN 978-3-319-56487-6 (eBook)
DOI 10.1007/978-3-319-56487-6

Library of Congress Control Number: 2017941619

Printed on acid-free paper

This Springer imprint is published by Springer Nature
The registered company is Springer International Publishing AG
The registered company address is: Gewerbestrasse 11, 6330 Cham, Switzerland

Preface

Sensitive clays are known for their potential for large landslides, which poses a serious risk to human lives, infrastructure and surrounding ecosystems within their reach. This has been reminded by the recent catastrophic landslides at, e.g., Sørum in 2016, Skjeggestad in 2015, Statland in 2014, Byneset in 2012, Saint-Jude in 2010, Lyngen in 2010 and Kattmarka in 2009. Alone, the collapse of Skjeggestad Bridge in Norway in 2015 due to a landslide in sensitive clay costs millions of dollars in repairs. Efforts are being made recently to increase society's ability to cope with such landslide hazards. Geoscientists are now expected to provide input to agencies responsible for preparedness work for the landslide risk at an acceptable level. In other words, geoscientists' role is not only to act as technologists to establish new theories but also to go the extra mile to implement them in the practice in order to find solutions to geotechnical problems.

In recent years, there have been significant research activities in the Scandinavian countries and Canada with respect to the characterisation, identification, mapping and testing of sensitive clays. Closer collaborations between geophysicists and geoengineers have enhanced the use of geophysical methods for site characterisation and bridging gaps between geophysics and geoengineering. New techniques for the identification and assessment of sensitive clays have been tested, while chemical stabilisation of sensitive clays is under investigation in the field and in the laboratory. Furthermore, some related knowledge on landslides in sensitive sediments, climate change, innovative stabilisation methods, effective preparedness and early warning systems is being developed.

This book gathers the most recent scientific research by international experts dealing with geological, geotechnical and geophysical aspects of slope failure in sensitive clays and focuses on understanding the complete and practical spectrum of challenges presented by landslides in such complex materials. Recommendations for the implementation of research results in the practice cover topics including the characterisation and behaviour of sensitive clays; pre-failure, failure and post-failure stages of sensitive clays; mapping and identification methods; climate change; hazard assessment; and risk management.

Keywords
Sensitive clay, Quick clay, Landslide, Site investigation, Modelling, Hazard assessment, Hazard mitigation, Risk assessment, Climate change

Trondheim, Norway — Vikas Thakur
Trondheim, Norway — Jean-Sébastien L'Heureux
Québec City, QC, Canada — Ariane Locat

Contents

Contributors

Per Aagaard University in Oslo, Oslo, Norway

Matthew Adamson Norwegian University of Science and Technology (NTNU), Trondheim, Norway

H. Ali GHD Ltd, Waterloo, ON, Canada

Helene Alexandra Amundsen Norwegian University of Science and Technology (NTNU), Trondheim, Norway

Norwegian Public Roads Administration (NPRA), Trondheim, Norway

Lars Andresen Norwegian Geotechnical Institute (NGI), Oslo, Norway

Helgard Anschütz Norwegian Geotechnical Institute (NGI), Oslo, Norway

Kristian Aunaas Norwegian Public Roads Administration (NPRA), Oslo, Norway

Synnøve W. Austefjord Norwegian University of Science and Technology (NTNU), Trondheim, Norway

Vikas Chand Baranwal Geological Survey of Norway (NGU), Trondheim, Norway

Mehrdad Bastani Geological Survey of Sweden (SGU), Uppsala, Sweden

Sara Bazin Norwegian Geotechnical Institute (NGI), Oslo, Norway

Anders Beijer ELU Konsult AB, Stockholm, Sweden

Karine Bélanger Ministrère des Transports, de la Mobilité durable et de l'Électrification des transports (MTMDET), Quebec City, QC, Canada

K. Bergdahl Swedish Geotechnical Institute (SGI), Linköping, Sweden

Chantal Bilodeau Ministère de la Sécurité publique du Québec, Québec, QC, Canada

Régis Bouchard SNC-Lavalin, Montréal, QC, Canada

Sarah Bouchard Department de génie civil et de génie des eaux, Université Laval, Québec, Canada

Djamalddine Boumezerane Department of Civil and Transport Engineering, Norwegian University of Science and Technology (NTNU), Trondheim, Norway

Brian D. Carlton Norwegian Geotechnical Institute (NGI), Oslo, Norway

G. Cascante Civil Engineering Department, Waterloo University, Waterloo, ON, Canada

Jung Chan Choi Norwegian Geotechnical Institute (NGI), Oslo, Norway

Stein Christensen SINTEF Building and Infrastructure, Oslo, Norway

Catherine Cloutier Département de géologie et de génie géologique, Université Laval, Quebec, QC, Canada

Einar Dalsegg Geological Survey of Norway (NGU), Trondheim, Norway

H. Dang Norwegian University of Science and Technology (NTNU), Trondheim, Norway

Multiconsult, Fredrikstad, Norway

Samson Abate Degago Norwegian Public Roads Administration (NPRA), Trondheim, Norway

Denis Demers Ministrère des Transports, de la Mobilité durable et de l'Électrification des transports (MTMDET), Quebec, QC, Canada

M. Demers Bonin Golder Associés Ltée, Montréal, QC, Canada

Ivan Depina SINTEF Building and Infrastructure, Rock and Geotechnical Engineering, Trondheim, Norway

L. Desbiens Ville de Saguenay, Quebec City, QC, Canada

Bruno Di Buò Tampere University of Technology (TUT), Tampere, Finland

Marco D'Ignazio Norwegian Geotechnical Institute (NGI), Oslo, Norway

Bjorn Kristoffer Dolva Norwegian Public Roads Administration (NPRA), Oslo, Norway

Shane Donohue Queen's University Belfast, Belfast, Northern Ireland, UK

J. Ekström Swedish Transport Administration, Borlänge, Sweden

Arnfinn Emdal Norwegian University of Science and Technology (NTNU), Trondheim, Norway

Odd Arne Fauskerud Multiconsult AS, Oslo, Norway

Trine Flobak Rambøll Norge AS, Oslo, Norway

Petter Fornes Norwegian Geotechnical Institute (NGI), Oslo, Norway
Norwegian University of Science and Technology (NTNU), Trondheim, Norway

Carl Fredrik Forsberg Norwegian Geotechnical Institute (NGI), Oslo, Norway

Richard Fortier Département de géologie et de génie géologique, Université Laval (UL), Québec City, QC, Canada

Alexis Fortin Ministère des Transports, de la Mobilité durable et de l'électrification des transports du Québec, Quebec City, QC, Canada

M.H. Frekhaug Norwegian Public Roads Administration (NPRA), Oslo, Norway

Tone Furuberg Municipality of Trondheim, Trondheim, Norway

Vidar Gjelsvik Norwegian Geotechnical Institute (NGI), Oslo, Norway

G. Göransson Swedish Geotechnical Institute (SGI), Linköping, Sweden

Shane Gribben Queen's University Belfast, Belfast, Northern Ireland, UK

Bjørn Ove Grøtan Geological Survey of Norway, Trondheim, Norway

Ragnhild Håøy Grue Multiconsult ASA, Oslo, Norway

S. Gulbrandsen Geological Survey of Norway, Trondheim, Norway

Anders Samstad Gylland Multiconsult ASA, Trondheim, Norway

Louise Hansen Geological Survey of Norway (NGU), Trondheim, Norway

Ellen D. Haugen Norwegian Water Resources and Energy Directorate (NVE), Tønsberg, Norway

Ingrid Havnen Norwegian Water Resources and Energy Directorate (NVE), Trondheim, Norway

J. Hedfors Swedish Geotechnical Institute (SGI), Linköping, Sweden

Tonje Eide Helle Norwegian University of Science and Technology (NTNU), Trondheim, Norway
Norwegian Public Roads Administration (NPRA), Trondheim, Norway

Håkon Heyerdahl Norwegian Geotechnical Institute (NGI), Oslo, Norway

Dieter Issler Natural Hazards Division, Norwegian Geotechnical Institute, Oslo, Norway

A. Jarna Geological Survey of Norway (NGU), Trondheim, Norway

Jörgen Johansson Norwegian Geotechnical Institute (NGI), Oslo, Norway

Å. Jönsson Swedish Geotechnical Institute (SGI), Linköping, Sweden

Hans Petter Jostad Norwegian Geotechnical Institute (NGI), Oslo, Norway

Konstantinos Kalomoiris Multiconsult ASA, Trondheim, Norway

Kjell Karlsrud Norwegian Geotechnical Institute (NGI), Oslo, Norway

Mats Karlsson Department of Civil and Environmental Enginering, Chalmers University of Technology, Gothenburg, Sweden

Minna Karstunen Department of Civil and Environmental Enginering, Chalmers University of Technology, Gothenburg, Sweden

Kristoffer Kåsin Norwegian Geotechnical Institute (NGI), Oslo, Norway

Huynh D. V. Khoa Norwegian Geotechnical Institute (NGI), Oslo, Norway

R. Kiilsgaard Swedish Geotechnical Institute (SGI), Linköping, Sweden

Jihwan Kim University of Oslo (UiO), Oslo, Norway
Norwegian Geotechnical Institute (NGI), Oslo, Norway

Suzanne Lacasse Norwegian Geotechnical Institute (NGI), Oslo, Norway

Tim Länsivaara Tampere University of Technology (TUT), Tampere, Finland

Alexandre Lavoie Ministère des Transports, de la Mobilité durable et de l'électrification des transports du Québec, Quebec City, QC, Canada

Denise Leahy SNC-Lavalin, Montréal, QC, Canada

D. LeBoeuf Département de génie civil et de génie des eaux, Université Laval, Quebec City, QC, Canada

Guy Lefebvre University of Sherbrook, Sherbrooke, QC, Canada

Ville Lehtonen Tampere University of Technology (TUT), Tampere, Finland
Ramboll Finland Oy, Tampere, Finland

Jean-Michel Lemieux Département de géologie et de génie géologique, Université Laval, Québec, QC, Canada

M. Lemieux Golder Associés Ltée, Montréal, QC, Canada

Serge Leroueil Département de génie civil et de génie des eaux, Université Laval, Québec City, QC, Canada

M. Létourneau Ministère des Transports, de la Mobilité durable et de l'électrification des transports, Quebec City, QC, Canada

Jean-Sébastien L'Heureux Trondheim Division, Norwegian Geotechnical Institute (NGI), Trondheim, Norway

M. Limoges Golder Associés Ltée, Montréal, QC, Canada

Zhongqiang Liu Norwegian Geotechnical Institute (NGI), Oslo, Norway

Ariane Locat Département de génie civil et de génie des eaux, Université Laval, Québec City, QC, Canada

Jacques Locat Department of Civil Engineering and Water Engineering, Laval University, Québec City, QC, Canada

Pascal Locat Ministère des Transports, de la Mobilité durable et de l'électrification des transports, Quebec City, QC, Canada

Hjördis Löfroth Swedish Geotechnical Institute (SGI), Linköping, Sweden

Mike Long School of Civil Engineering, University College Dublin (UCD), Dublin, Ireland

Anders Beijer Lundberg ELU Konsult AB, Stockholm, Sweden

Karin Lundström Swedish Geotechnical Institute (SGI), Linköping, Sweden

Asgeir Lysdahl Norwegian Geotechnical Institute (NGI), Oslo, Norway

Juho Mansikkamäki Tampere University of Technology (TUT), Tampere, Finland

Christopher Meehan University of Delaware (UD), Newark, NJ, USA

R. Mompin Ministère des Transports, de la Mobilité durable et de l'Électrification des transports du Québec, Quebec City, QC, Canada

Alberto Montafia Multiconsult ASA, Trondheim, Norway

Farrokh Nadim Norwegian Geotechnical Institute (NGI), Oslo, Norway

Bo Nordahl Geological Survey of Norway (NGU), Trondheim, Norway

Steinar Nordal Norwegian University of Science and Technology (NTNU), Trondheim, Norway

Trude Nyheim Norwegian Water Resources and Energy Directorate (NVE), Trondheim, Norway

M. Öberg Swedish Geotechnical Institute (SGI), Linköping, Sweden

Karin Odén Swedish Geotechnical Institute (SGI), Linköping, Sweden

Frode Oset Norwegian Public Roads Administration (NPRA), Oslo, Norway

H. Ottesen Norwegian Public Roads Administration (NPRA), Oslo, Norway

Daniel Ouellet Ministère des Transports, de la Mobilité durable et de l'électrification des transports du Québec, Quebec City, QC, Canada

Stéphane Paradis Ministère des Transports, de la Mobilité durable et de l'électrification des transports du Québec, Quebec City, QC, Canada

N. Pépin Golder Associés Ltée, Montréal, QC, Canada

Lena Persson Geological Survey of Sweden (SGU), Uppsala, Sweden

Gordana Petkovic Norwegian Public Roads Administration (NPRA), Oslo, Norway

Andreas Aspmo Pfaffhuber Norwegian Geotechnical Institute (NGI), Oslo, Norway

Janelle Potvin Ministère des Transports, de la Mobilité durable et de l'Électrification des transports du Québec, Quebec City, QC, Canada

Katherine Price University of Washington (UW), Seattle, USA

Ernst Pytten Rambøll Norge AS, Kristiansand, Norway

Denis Robitaille Ministère des Transports, de la Mobilité durable et de l'électrification des transports du Québec, Quebec City, QC, Canada

Jan Steinar Rønning Geological Survey of Norway (NGU), Trondheim, Norway
Norwegian University of Science and Technology (NTNU), Trondheim, Norway

Anders Rosenquist af Åkershult Trimble, Sunnyvale, CA, USA

David Schälin Swedish Geotechnical Institute (SGI), Linköping, Sweden

Juha Selänpää Tampere University of Technology (TUT), Tampere, Finland

V. Sivakumar Queen's University Belfast, Belfast, Northern Ireland, UK

Colby A. Smith Geological Survey of Sweden (SGU), Uppsala, Sweden

Inger-Lise Solberg Geological Survey of Norway (NGU), Trondheim, Norway

Wojciech Solowski Department of Civil Engineering, Aalto University, Espoo, Finland

Stein-Are Strand Norwegian Water Resources and Energy Directorate, Oslo, Norway

Vikas Thakur Norwegian University of Science and Technology (NTNU), Trondheim, Norway

Julie Therrien Ministère des Transports, de la Mobilité durable et de l'Électrification des transports (MTMDET), Québec, QC, Canada

Catherine Thibault Ministère des Transports, de la Mobilité durable et de l'électrification des transports du Québec, Quebec City, QC, Canada

Jan Fredrik Tønnesen Geological Survey of Norway (NGU), Trondheim, Norway

J. Kenneth Torrance Geography and Environmental Studies, Carleton University, Ottawa, ON, Canada

Quoc Anh Tran Department of Civil Engineering, Aalto University, Espoo, Finland

Dominique Turmel Laboratoire d'études sur les risques naturels (LERN), Université Laval, Québec, QC, Canada

Morten Tveit Rambøll Norge AS, Kristiansand, Norway

Cecilia Ulmke Department of Civil and Transport Engineering, Norwegian University of Science and Technology (NTNU), Trondheim, Norway

Maarten Vanneste Norwegian Geotechnical Institute (NGI), Oslo, Norway

Margareta Viklund Norwegian National Rail Administration (NNRA), Oslo, Norway

Tara Wood Chalmers University, Gothenburg, Sweden

Ashenafi Lulseged Yifru Norwegian University of Science and Technology (NTNU), Trondheim, Norway

Chapter 1
Landslide in Sensitive Clays – From Research to Implementation

Vikas Thakur, Jean-Sébastien L'Heureux, and Ariane Locat

1.1 Introduction

Sensitive clays, when provoked by manmade or natural causes, have led to several landslide disasters throughout history. This has been reminded by the recent catastrophic landslides at e.g. St. Jude (2010), Lyngen (2010), Kattmarka (2009), Byneset (2012), Skjeggestad landslide (2015) and Sørum (2016). In the last 40 years there has been approximately 1 or 2 slides per decade with a volume $\geq$ 500,000 m^3 (Thakur et al. 2014). Alone, the collapse of Skjeggestad bridge in Norway in 2015 resulted in damages for over several millions of dollars and was associated to a landslide in sensitive clay. Since landslides in sensitive clays possess huge destructive capabilities, there is a need for accurate assessment and prediction of landslide potential in such materials. However, this is not a straightforward task due to the complexity associated with characterization, identification, mapping and testing of such materials.

In recent years, there have been significant research activities in the Scandinavian countries and Canada with respect to landslides in sensitive clays in a close collaborations between geophysicists and geo-engineers. For example, a large Inter-governmental R&D programme "Natural Hazards – Flood and landslides" in

V. Thakur (✉)
Department of Civil and Environmental Engineering, Norwegian University of Science and Technology (NTNU), Trondheim, Norway
e-mail: vikas.thakur@ntnu.no

J.-S. L'Heureux
Trondheim Division, Norwegian Geotechnical Institute (NGI), Trondheim, Norway
e-mail: jsl@ngi.no

A. Locat
Département de génie civil et de génie des eaux, Université Laval, Québec City, QC, Canada
e-mail: ariane.locat@gci.ulaval.ca

V. Thakur et al. (eds.), *Landslides in Sensitive Clays*, Advances in Natural and Technological Hazards Research 46, DOI 10.1007/978-3-319-56487-6_1

Norway have proposed several assessment, mitigation and management strategies (Dolva and Pektovik, Chap. 46, this volume). This book is an effort to gather the most recent scientific research by international experts dealing with geological, geotechnical and geophysical aspects of slope failure in sensitive clays and focuses on understanding the complete and practical spectrum of challenges presented by landslides in such complex materials. This book, which is the second in the series of "International Workshop of Landslides in Sensitive Clays" arranged in Trondheim in Norway, builds further on the first book "*Landslides in sensitive clays: from geoscience to risk management*" that was edited by L'Heureux et al. (2014).

This book contains 49 chapters. The main objective of the book has been on the implementation of research results into the practice. To be able to use academic results in real practice confidently one must implement them in code of practice or guidelines. The real scenarios are usually much more complex than the idealization made during research. Therefore results must be validated against real cases or observations. Accordingly, this book presents selected numbers of recommendations which are based on sound and validated research results and they have the potential to be implemented in the guidelines or code-of-practice. The recommendations cover the various themes including characterization and behaviour of sensitive clays, the pre-failure, failure and post-failure stages of sensitive clays, mapping and identification methods, climate change, hazard assessment, and risk management. The book is thematically divided in six major parts and they are discussed one by one hereafter.

1.2 Part I: Characterization and Behaviour of Sensitive Clays

Sensitive clays are leached marine clays that may change from a relatively stiff and brittle material into a viscous liquid when remoulded (Rosenqvist 1953). They are typically classified in terms of their ratio of intact shear strength to the corresponding remoulded shear strength measured using the fall cone test at the same water content. Several classification systems have been proposed in the literature (Skempton and Northey 1952; Rosenqvist 1953; Norwegian Geotechnical Society (NGF) 1974; Broms and Stål 1980; Le Bihan and Leroueil 1981).

Reliable characterisation is essential to understand the behaviour of sensitive clays. This requires a proper understanding of their origin, pore water chemistry, geological history, and geotechnical and geophysical properties, among other factors. Chemistry's dominating role in sensitive clay development and behaviour provides the starting point for developing approaches to ameliorate the sensitive-clay landslide problem (Torrance 1983). The interactions of chemical factors – depositional environment, particle mineralogy, changes in pore-water chemistry, oxidizing or reducing conditions, cementation (or lack thereof) and more – determines the physical properties of the sensitive clays (Torrance, Chap. 3, this volume).

Moreover, this complex interaction can also improve the properties of sensitive clay deposits when potential chloride is infiltrated in it (Moum et al. 1971; Helle et al. 2016). The recent work on this remediation method by Helle et al. (Chap. 4, this volume) indicates a significant improvement of the post-failure properties of a sensitive clay deposit in Trondheim, Norway.

When looking at the results of geotechnical investigations, it is important to establish rational links between each soundings in order to develop a general understanding of the nature, extend and position of the soil strata one expects to find at the site (Lefebvre, Chap. 2, this volume). In this regards, the integrated approach of geotechnical and geophysical methods for characterization of sensitive clay formations has advanced considerably (Long et al., Chap. 6, this volume). Cone penetration testing (CPTU) with an option to measure electrical resistivity (R-CPTU) or shear wave velocity (SCPTU) are becoming valuable tools in geotechnical engineering because the results can be used for supplementary classification and determination of soil parameters (Long et al., Chap. 6, this volume; Gylland et al., Chap. 5, this volume; Bélanger et al., Chap. 7, this volume; Gribben et al., Chap. 8, this volume; Bouchard et al., Chap. 15, this volume). Field vane test traditionally gives information about the *in situ* undrained shear strength (undisturbed and remoulded), and the sensitivity. Previous studies have shown that the results obtained by using field vane tests involve many uncertainties. However, the field electric vane shear apparatus with a possibility to measure torque down at the vanes in general has good repeatability. Also, this new apparatus can assist in generating a continuous shear stress versus vane-rotation diagram which can be used for the determination of remoulding energy of sensitive clay e.g., Thakur et al. (2015), Sandven et al. (Chap. 36, this volume), Thakur et al. (Chap. 1, this volume), and Selänpää et al. (Chap. 10, this volume).

Sensitive clays are prone to sample disturbance, especially when retrieving samples from piston and tube samplers (e.g. Bjerrum (1967), Lunne et al. (1997)) On the contrary, block sampling is among the best methods of collecting high quality samples of soft clays. However, even block samples may fail to capture the true and unique response of sensitive clay if they are not sampled and handled properly. For instance, stress relief, transportation effects, storage procedure time and testing procedures may lead to an inaccurate response, e.g., Skempton and Sowa (1963), Lundberg (Chap. 12, this volume). In this connection, Amundsen et al. (Chap. 11, this volume) suggests a new laboratory approach to study the effect of stress relief in sample quality.

1.3 Part II: Pre-failure and Failure Stages

The processes and mechanisms governing the landslides in slopes of sensitive clay are very complex. Leroueil et al. (1996) and Vaunat and Leroueil (2002) suggested dividing slope movements into four stages. Accordingly, the stages are i) pre-failure,

ii) onset of failure, iii) post failure and iv) reactivation stage. This part of the book deals with the first two stages and refers to all the deformation processes leading to failure. Triggering of landslide in sensitive clay is usually attributed to natural factors (e.g. river erosion, rainfall, etc.), human activity (e.g. placement of fill), or a combination of both. Recent experience also shows that vibrations from blasting, earthquake or compaction work (e.g. Perret et al. 2011; Johansson et al. 2013; Bouchard et al., Chap. 15, this volume) may lead to landslides in sensitive clay deposits. The triggering load and the extent of the initial part of the landslide depends upon the formation and propagation of the failure zones namely shear bands and in particular upon their thickness (Jostad et al. 2006; Thakur 2007; Locat et al. 2011; Gylland et al. 2014; Thakur et al. 2017). Leahy et al. (Chap. 19, this volume) and Andresen and Jostad (Chap. 16, this volume) methodically explains the ingredients for a proper modelling of the failure process involving the emergence and progressive development of shear band localisation in sensitive clay slopes. It must be realised that progressive failure modelling to account for the strain softening is demanding because it requires a special ad-hoc computational scheme namely an appropriate regularization method. However, the role of local pore water drainage and rate dependency in the formation and propagation of the localised shear bands is yet to be fully understood (Thakur et al. 2006; Thakur 2011; Locat et al. 2011; Andresen and Jostad, Chap. 16, this volume). In practice, slope stability assessments are generally performed by limit equilibrium methods (LEM). In such assessment neglecting strain softening behaviour, an overestimation of the safety margin can be expected especially when the input parameters, namely undrained shear strength profile, is based on high quality block samples. To compensate this, an indirect approach is common in Scandinavia (i.e. the strength values are reduced by a factor in the calculation or the minimum allowable safety margin is increased (Oset et al. 2014)). Fornes and Jostad (Chap. 20, this volume) suggest that when a sensitive clay slope is subjected to an undrained load (e.g. fill), the effect of strain softening is between 5–15% depending on the location of sensitive clay layer, the inclination of strength profile.

Sensitive clays are usually anisotropic in nature. Therefore, their undrained shear strength is not identical when they are subjected to a compression/active, direct shear and extension/passive loading. Thakur et al. (Chap. 9, this volume) suggests a recommended practice for selection and use of anisotropy factors in stability calculations. They also did a benchmark stability calculation to illustrating the overall impact of various anisotropy factors on the factor of safety. The recommended anisotropy factor is valid for Norwegian soft clays regardless of their sensitivity. The reliability of stability calculations are also dependent on the uncertainty involved in the assessment of input parameters including the modelling of excess pore pressure that has traditionally been a source of most uncertainty in undrained effective stress analyses (e.g., Lacasse 2017; Depina et al., Chap. 18, this volume; Lehtonen, Chap. 21, this volume).

1.4 Part III: Post-failure Stage

The post failure stage of a landslide in sensitive clay include its retrogressive behaviour and potential extensive runout distance. It has been empirically, as well as experimentally, validated that large retrogressive flow slides in sensitive clays only occur when the remoulded shear strength of the soil is less than 1.0 kPa and when the liquidity index is larger than 1.2 (Lebuis and Rissmann 1979; Tavenas et al. 1983; L'Heureux 2012; Thakur and Degago 2012; Thakur et al. 2014; Demers et al. 2014). Several researchers have also shown that the post failure movements of landslide in sensitive clays involve aspects of geometry, material properties and other external controls such as infrastructures, and vegetation (e.g. Mitchell and Markell 1974; Tavenas et al. 1983; Geertsema and L'Heureux 2014; Thakur et al. 2014). In addition, Strand et al. (Chap. 26, this volume) suggests that flowslides in sensitive clays are likely only if 40% of the soil material over the failure surface is composed of clays with remoulded shear strength less than 1 kPa. Such criteria is yet to be established for spreads type landslides. Locat et al. (2008), Locat and Lee (2005, 2009), Thakur and Degago (2013), and Thakur et al. (2015, Chap. 9, this volume) stipulates that the energy involved in remoulding of sensitive clays can assist in identifying various landslide types including spreads in sensitive clay. More work is needed in this direction.

Post failure assessment can be done in many ways e.g. empirical approaches, analytical approaches or by surveys. The use of LiDAR for the purposes of landslides inventory and mapping has been increasingly popular in the recent years (McKean and Roering 2004; Van Den Eeckhaut et al. 2005; Ardizonne et al. 2007; Mora et al. 2014). Based on an extensive study from over 50 large landslides in the Quebec region, Demers et al. (Chap. 25, this volume) suggests that LiDAR surveys may provide much more reliable inventories and a far more detailed knowledge of hazards in an area. Strand et al. (Chap. 26, this volume) proposes an empirical approach to calculate runout of sensitive clay debris. Their recommendation is based on the data from 51 large Norwegian landslides in sensitive clays. However, an accurate assessment of runout distance demands an advanced continuum based simulation model. Some approaches and methods have been developed in the past for a quantitative risk analysis using dynamic runout models for debris flows and avalanches such as BING, NIS, and quasi-three-dimensional models such as DAN3D, MassMov2D, LS-RAIPD and RAMMS. None of these tools are specifically meant for sensitive clay landslides (Yifru et al., Chap. 30, this volume), however an effort is being made in Norway by the GeoFuture II project to develop a slope runout module (Strand et al., Chap. 26, this volume).

Experimental results suggest that Canadian and Norwegian sensitive clays are shear thinning in nature (e.g. Locat and Demers (1988); Grue et al. [Chap. 14, this volume]). The flow behaviour of such clays can be approximated using Herchel-Belkley rhehology. Tran et al. (Chap. 29, this volume) and Turmel et al. (Chap. 27, this volume) modelled the flow behaviour of sensitive clays, numerically.

Fornes et al. (Chap. 31, this volume) studied the Vestfossen landslide (1984) in Norway using a Coupled Eulerian-Lagrangian, which allowed for capturing the full progressive failure mechanism (initiation, propagation and breakoff) involved in the Vestfossen landslide. In summary, there is a significant development made in the past few years in terms of experimental numerical studies related to the post failure movements of sensitive clays.

1.5 Part IV: Historical Landslides and Case Study of Area Prone to Landslides in Sensitive Clays

Much knowledge can be obtained by carefully studying historical landslides and by analysing their cause(s) and failure mechanisms. In this book two well-described historical cases are presented; i.e. the 1908 Notre-Dame-de-la-Salette landslide (Locat et al., Chap. 32, this volume) and the 1959 landslide at Sokkelvik. These events have respectively been the deadliest in Eastern Canada and Scandinavia in the last century. They also show that landslides in sensitive clay have the potential to trigger devastating tsunamis when occurring in near shore environments.

An accurate assessment and mitigation strategy for landslides hazards in sensitive clays necessitates a good understanding of the phenomenon at hand. Three case studies are well presented in this volume and includes assessment of sensitive clay slopes in Eastern Canada and in Norway (Flobak et al., Chap. 33, this volume; Bonin et al., Chap. 34, this volume; Sandven et al., Chap. 36, this volume; Potvin et al., Chap. 37, this volume). These very vital case studies range from understanding and characterization of soil behaviours, stability calculations, hazard mapping and risk management.

1.6 Part V: Sensitive Clays Mapping and Identification

Recently, airborne transient electromagnetic measurements (ATEM or TEM) or helicopter born electromagnetic measurements (AEM) have been tested for the mapping of sensitive layer in various locations in Scandinavia (Anschütz et al. 2014; Sandven et al., Chap. 36, this volume; Lysdahl et al., Chap. 39, this volume; Löfroth et al., Chap. 38, this volume; Bastani et al., Chap. 41, this volume). Though the higher initial costs involved, the airborne methods give promising results. Quaternary geological maps display fjord-marine deposit distributions and various features of importance, among others, for sensitive clay mapping (Hansen et al., Chap. 40, this volume). Since there is a close connection between clay strength and pre-consolidation pressure, it is important to understand the Quaternary geology of the area of interest. This includes knowledge about the soil depositional history and subsequent natural processes that have shaped the landscape due to, for example,

erosion and landslide activity (Thakur et al. 2016). It must be realised that the quaternary map provides information only on the top layer of sediment deposition. The maps provide geological overviews and are often used for their predictive power and for setting local investigations such as for the conventional geotechnical testing. Therefore, it is important to combine with site investigation to identify sensitive clay deposits. Conventional sounding methods such as rotary sounding or total sounding are now being complemented by cone penetration test, optionally with resistivity measurements because these tools have great potential for detection of sensitive clay through combined recordings of cone resistance, sleeve friction, pore pressure and resistivity or shear wave velocity.

1.7 Part VI: Hazard Assessment and Risk Management

One of the distinct features of geotechnical engineering is the need to deal with uncertainties in analysis and design (Degago et al., Chap. 9, this volume). Currently there is an increased activity towards probabilistic based reliability approaches to achieve a systematic risk assessment of landslides (e.g. Lacasse 2017). Risk and probabilistic methods have reached a level of maturity that makes them effective to use in practice. Lacasse et al. (Chap. 45, this volume) propose a probabilistic model in an event tree format that can be included to ensure that all failure modes and the uncertainties have been covered and that slope failure mitigation measures are in place. Despite this, one must realise that reliability approaches do not remove uncertainty nor do they alleviate the need for judgment. They provide a way to quantify the uncertainties and to handle them consistently. The occurrences of the recent man-made landslides in sensitive clay deposits have more to do with unforeseen events or unplanned activities at the sites than calculation methods. Unplanned activities that are not foreseen during design may alter the *in situ* conditions of a slope and result in a different factor of safety or probability of failure. Thus, as much as establishing the factor of safety or the probability of failure is important in design phase, one should also equally focus on trying to reassure the analysis/assessment done during the design phase remains valid during and after construction (Degago and Thakur, Chap. 48, this volume).

Hazard maps for landslides in sensitive clays has been available to the public domain in Norway many years through web-based solutions. Of great value is also the recently launched National site Investigation database i.e. NADAG (Solberg et al., Chap. 43, this volume) in several of the Nordic countries. Such tools are necessary for proper land-use planning and to ensure fewer landslides in the future (Havnen et al., Chap. 50, this volume).

In recent years, researchers have looked at the impact of climate change on the occurrence of landslides in sensitive clays, but the trends are still unclear. The predicted effect of climate changes, such as increased precipitation and erosion, is expected to result in an increase frequency of landslides. The short and long-term

monitoring of clay slopes are therefore becoming important. The monitoring should allow a better evaluation of the occurrence of landslides and develop warning criteria adapted for climate change potential impacts. These aspects are studied in detail by Cloutier et al. (Chap. 47, this volume) and Dolva and Pektovik (Chap. 46, this volume).

1.8 Closing Remarks

Significant development has been made to assess and to mitigate landslides in sensitive clays in recent years. The majority of the work is being performed in a close collaboration between the academia, the industry and public authorities. Application of geophysical methods for site characterization, airborne mapping of sensitive clay deposits, high quality sampling, established database, and state-of-the-art laboratory tests give us new possibilities to better understand the development of sensitive clays, to perform more realistic slope stability analyses, and to better map the hazards posed by such landslides. Advanced computational tools and new mathematical models will help in an accurate assessment of the extent of landslide and the mobility of landslide debris. Reliability approaches are becoming increasing popular. However, one must realise that these approaches do not remove uncertainty nor do they alleviate the need for judgment. Recent developments are very promising and in our opinion most of these developments are ready to be implemented in guidelines. In fact, some of the findings are already in practice. On the other hand, there remain some issues to solve. Unforeseen events or unplanned activities threaten the safety of sensitive clay slopes and they remain as a matter of concern. This challenge could be alleviated to some extent by public awareness, training, and by making information available on web-based solutions. Climate change induced landslides in sensitive clays are mainly related to erosion at the toe, change in ground water hydrology or change in pore water pressure profile in the ground. In time, short term and long term monitoring of critically stable slopes will become an important aspect of landslide hazard mitigation.

This book, which is a result of *the Second International Workshop on Landslides in Sensitive Clays* arranged in Trondheim in Norway, put forward the recommendations made by the international experts dealing with geological, geotechnical and geophysical aspects of landslides in sensitive clay slopes. The book also highlights the areas and topics where more research and development is necessary. Therefore, such international workshops are important to arrange on regular basis so that scientists, engineers, students, authorities and others can be discuss and exchange the challenges and the possibilities within the wide spectrum of landslide in sensitive clays.

References

Anschütz H, Bazin S, Pfaffhuber AA (2014) AEM method description & project examples. Norwegian Geotechnical Institute, Report 20130058–02-R_ENG, Oslo

Ardizzone F, Cardinali M, Galli M, Guzzetti F, Reichenbach P (2007) Identification and mapping of recent rainfall-induced landslides using elevation data collected by airborne Lidar. Nat Hazards Earth Syst Sci 7:637–650

Bjerrum L (1967) Engineering geology of Norwegian normally-consolidated marine clays as related to settlements of buildings. Géotechnique 17(2):83–118

Broms BB, Stål T (1980) Landslides in sensitive clays. In: Proceedings of the international symposium on landslides, vol 2. New Delhi, pp 39–66

Demers D, Robitaille D, Locat P, Potvin J (2014) Inventory of large landslides in sensitive clays in the province of Quebec, Canada: preliminary analysis. Natural hazards book: advances in natural and technological hazards research, ISSN: 1878–9897 (Print) pp 2213–6959 (Online), pp 77–89

Geertsema M., L'Heureux JS (2014) Controls on the dimensions of landslides in sensitive clays. Advances in natural and technological hazards research, ISSN: 1878–9897 (Print) 2213–6959 (Online), pp 105–117

Gylland AS, Jostad HP, Nordal S (2014) Experimental study of strain localization in sensitive clays. Acta Geotech 9:227–240

Helle TE, Nordal S, Aagaard P et al (2016) Long-term effect of potassium chloride treatment on improving the soil behavior of highly sensitive clay — Ulvensplitten, Norway. Can Geotech J 53(3):410–422. doi:10.1139/cgj-2015-0077

Johansson J, Løvolt F, Andersen KH, Madshus C, Aabøe R (2013) Impact of blast vibrations on the release of quick clay slides. In Proceedings of the 18th ICSMGE, Paris

Jostad HP, Andresen L, Thakur V (2006) Calculation of shear band thickness in sensitive clays. In: Conference of the 6th numerical methods in geotechnical engineering, At Graz, vol 1

L'Heureux JS (2012) A study of the retrogressive behaviour and mobility of Norwegian quick clay landslides. In: Proceedings of the 11th INASL, Banff, Canada, vol. 1, pp 981–988

L'Heureux JS, Locat A, Leroueil S, Demers D, Locat J (2014) Landslides in sensitive clays: from geosciences to risk management, Advances in natural and technological hazards research 36. Springer, Dordrecht. doi:10.1007/978-94-007-7079-9_1

Lacasse S (2017) 55th Rankine lecture. Hazard, risk and reliability in geotechnical practice. Paper submitted to *Geotechnique*

Le Bihan JP, Leroueil S (1981) The fall cone and the behaviour of remoulded clay. Terratech Ltd. Research Report, Montreal

Lebuis J, Rissmann P (1979) Les coulées argileuses dans le région de Québec et de Shawinigan. In: Argiles sensibles, pentes instables, mesures correctives et coulées des régions de Québec et Shawinigan. Geo. Assoc. of Canada Guidebook, pp 19–40

Leroueil, S, Locat, J, and Vaunat J (1996) Geotechnical characterisation of slope movements. In: Proceedings of the 7th international symposium on landslides, pp 53–74

Locat J, Demers D (1988) Viscosity, yield stress, remolded strength, and liquidity index relationships for sensitive clays. Can Geotech J 25(4):799–806. doi:10.1139/t88-088

Locat J, Lee HJ (2005) Subaqueous debris flow. Debris-flow hazards and related phenomena. Springer, Berlin/New York, pp 203–246. ISBN:3-540-20726-0

Locat J, Lee H (2009) Submarine mass movements and their consequences: an overview landslides – disaster risk reduction. Springer, 115–142 http://link.springer.com/chapter/10.1007/978-3-540-69970-5_6

Locat P, Leroueil S, Locat J (2008) Remaniement et mobilité des débris de glissements de terrain dans les argiles sensible de l'est du Canada. In: Proceedings of the 4th Canadian conference on geohazards: from causes to management. Presse de l'Université Laval, Québec, pp 97–106

Locat A, Leroueil S, Bernander S, Demers D, Jostad HP, Ouehb L (2011) Progressive failures in eastern Canadian and Scandinavian sensitive clays. Can Geotech J 48(11):1696–1712

Lunne T, Berre T, Strandvik S (1997) Sample disturbance effects in soft low plastic Norwegian clay. In: Proceedings of the symposium on recent development in soil and pavement mechanical, Rio de Janeiro, Brazil, pp 81–102

McKean J, Roering J (2004) Objective landslide detection and surface morphology mapping using high-resolution airbone laser altimetry. Geomorphology 57:331–351

Mitchell RJ, Markell AR (1974) Flow slides in sensitive soils. Can Geotech J 11(1):11–31

Mora OE, Liu JK, Lenzano MG, Toth CK, Grejner-Brzezinska DA (2014) Small landslide susceptibility and hazard assessment based on airbone lidar data. Photogramm Eng Remote Sens 81:239–247

Moum J, Løken T, Torrance JK (1971) A geochemical investigation of the sensitivity of a normally consolidated clay from Drammen, Norway. Géotechnique 21(4):329–340

Norsk Geoteknisk Forening (NGF) (1974) Retningslinjer for presentasjon av geotekniske undersøkelser. Oslo, 16 p (In Norwegian)

Oset F, Thakur V, Dolva BK, Aunaas K, Sæter MB, Robsrud A, Viklund M, Nyheim T, Lyche E, Jensen OA (2014) Regulatory framework for road and railway construction on the sensitive clays of Norway. 1st IWSLC, Québec. In: L'Heureux JS et al (eds) Landslides in sensitive clays: from geosciences to risk management, Advances in natural and technological hazards research 36. Springer, Dordrecht, pp 343–352. doi:10.1007/978-94-007-7079-9_27

Perret D, Mompin R, Bossé F, Demers D (2011) Stop 2-5B: the Binette road earth fl ow induced by the June 23rd, 2010 Val-des-Bois earthquake. In: Russell HAJ, Brooks GR, Cummins DI (eds) Deglacial history of the Champlain Sea basin and implications for urbanization. Joint annual meeting GAC-MAC-SEG-SGA, Ottawa, Ontario, May 25–27, 2011, Field Guide Book, pp 72–74. Geological Survey of Canada, Open File 6947

Rosenqvist IT (1953) Consideration on the sensitivity of Norwegian quick-clays. Geotechnique 3:195–200

Skempton AW, Northey RD (1952) Sensitivity of clays. Geotechnique 3(1):40–51

Skempton AW, Sowa VA (1963) The behaviour of saturated clays during sampling and testing. Géotechnique 13(4):269–290

Tavenas F, Flon P, Lerouil S et al (1983) Remolding energy and risk of slide retrogression in sensitive clays. In: Proceedings of the symposium slopes on soft clays, Linköping, Sweden, pp 423–454

Thakur V (2007) Strain localization in soft sensitive clays. PhD thesis. Norwegian University of Science and Technology, NTNU, Trondheim, Norway

Thakur V (2011) Numerically observed shear bands in soft sensitive clays. J Geomech Geoeng 6:131–146

Thakur V, Degago SA (2012) Quickness of sensitive clays. Géotechnique Lett 2(3):87–95

Thakur V, Degago SA (2013) Disintegration energy of sensitive clays. Géotechnique Lett 3:21–25

Thakur V, Grimstad G, Nordal S (2006) Instability in soft sensitive clays. In: Proceedings of the ECI conference on geohazards, Lillehammer, Norway Eds. Nadim, Pöttler, Einstein, Klapperich and Kramer

Thakur V, Degago SA, Oset F, Dolva BK, Aabøe R, Aunaas K, Nyheim T, Lyche E, Jensen OA, Viklund M, Sæter MB, Robsrud A, Nigguise D, L'Heureux JS (2014) Characterization of post-failure movements of landslides in soft sensitive clays. Natural hazards book: advances in natural and technological hazards research, ISSN: 1878–9897 (Print) pp 2213–6959 (Online), pp 91–104

Thakur, V, Degago SA, Oset F, Gylland SA, Sandven R (2015) In-situ measurement of remoulding energy of sensitive clay. In: 68th Canadian geotechnical conference, *GeoQuebec*, Quebec

Thakur V, Fauskerud OA, Gjelsvik V, Christensen S, Oset F, Viklund M, Strand SA, Nordal S (2016) A procedure for the assessment of undrained shear strength profile in soft clays. In: Proceedings of the 17th nordic geotechnical meeting, Iceland, pp 533–546

Thakur, V, Nordal S, Viggiani, G, Charrier P (2017) Plane strain testing on Norwegian quick clays. Submitted to Canadian Geotechnical Journal

Torrance JK (1983) Towards a general model of quick clay development. Sedimentology 30:547–555

Van Den Eeckhaut M, Poesen J, Verstraeten G, Vanacker V, Moeyerson J, Nyssen J, van Beek LPH (2005) The effectiveness of hillshade maps and expert knowledge in mapping old deep-seated landslides. Geomorphology 67:351–363

Vaunat J, Leroueil S (2002) Analysis of post-failure slope movements within the framework of hazard and risk analysis. Nat Hazards 26:83–102

Part I
Characterization and Behavior of Sensitive Clays

Chapter 2
Sensitive Clays of Eastern Canada: From Geology to Slope Stability

Guy Lefebvre

Abstract Landslides in Eastern Canadian sensitive clay deposits are generally located along river or stream valleys. The stratigraphy of these deposits can be simplified as an impervious clay deposit between two pervious boundaries, a weathered fissured crust at the top and a coarse till layer at the bottom. The paper examines the evolution of the ground water regime as the valleys are formed by erosion and discusses the impact of the valleys formation on the requirements for slope stability analysis and determination of shear strength. A large data bank of laboratory test results are then presented and treated to arrive at a determination of the shear strength parameters based only on the preconsolidation pressure.

2.1 Introduction

Looking back in the literature, in fact as far back as the literature existed in Scandinavia and Eastern Canada, one can find descriptions of catastrophic landslides where the ground was reported as flowing toward river or stream, houses being destroyed and lives being lost. Such events still happen in modern time even if the phenomena is today relatively well understood. Methods and ways to evaluated the stability of a slope against sliding were developed early in the last century. And since the fifties, the nature of these soils susceptible to "flow", the sensitive clays, is relatively well known, starting with works carried on in Scandinavia, namely at the Norwegian Geotechnical Institute under Bjerrum leadership. In Scandinavia and in Eastern Canada, the risk associated to landslide in sensitive clays is today generally accounted for in measures to protect the populations. This is the results of intensive studies during the last 50 years including the documentation and analysis of numerous case records, which have greatly expended our knowledge and contributed at the same time to the formation of competent engineers. Compared to all the knowledge existing today on sensitive clay, this paper is rather limited in

G. Lefebvre (✉)
University of Sherbrooke, Sherbrooke, QC, Canada
e-mail: Guy.Lefebvre@Usherbrooke.ca

V. Thakur et al. (eds.), *Landslides in Sensitive Clays*, Advances in Natural and Technological Hazards Research 46, DOI 10.1007/978-3-319-56487-6_2

scope considering only some slope stability aspects for the sensitive clays of Easter Canada. The purpose is first to examine the evolution of the ground water regime associated with the formation of the river or stream valleys through the clay deposits, in order to appreciate its impact on the stability of the valleys slopes. In the second part, the use of the post-peak shear strength for the analysis of slope stability in sensitive clays of Eastern Canada is revisited using both laboratory results and back analysis data together with the development of correlations allowing determining the shear strength parameters from the oedometric preconsolidation pressure.

2.2 Clay Deposits of Eastern Canada

The different clay deposition basins of Easter Canada are shown on Fig. 2.1. They were formed in depressions left by the Laurentian ice sheet that covered Easter Canada some 14,000 years ago. The postglacial marine clays in the Champlain sea were deposited some 12,000 years ago (Hilaire–Marcel 1979) while the clay deposits of the Tyrrel sea basin are considered to be younger than 6000 years. The isostatic rebound associated with the retreat of the ice sheet has resulted in the emergence of the clay deposits with an impact on the groundwater regime. Due to hydraulic gradients and concentration gradients, the pore water salt content, initially as high as 32 g/L in some area, was greatly reduced. In very sensitive clay deposits, pore water salt content could be today lower than 1 g/L. The reduction of the liquid limit and of the plasticity as well as the reduction of the remolded shear strength associated with the reduction of the pore water salinity is today well documented. Because of their geologic origin, the sensitive clays of Easter Canada have characteristic composition and mineralogy. The silt fraction is most often high, typically in the range of 30 to 70 percent. The clay fraction (<2 micron) generally contains more rock flour than clay mineral the latter being predominantly illite (Quigley 1980, Locat et al. 1984).

2.3 Stratigraphy

Due to the cleaning of the bedrock surface by the ice sheet, the layering in the clay deposition basin is relatively simple. In large depositional basin, marine clay deposits are generally massive and notably uniform. Most often if not always a layer of till, made of silt, sand and gravel with relatively little clay is identified between the bedrock and the clay deposit.

The lower boundary of the clay deposit is thus characterized most generally, by a contrast of hydraulic conductivity higher than 100. The upper boundary is made generally of a weathered fissured crust or sometime by a surficial layer of silty or sandy soil from the final depositional stages resulting also in a high contrast of hydraulic conductivity. In small depositional basins or close to the limit of

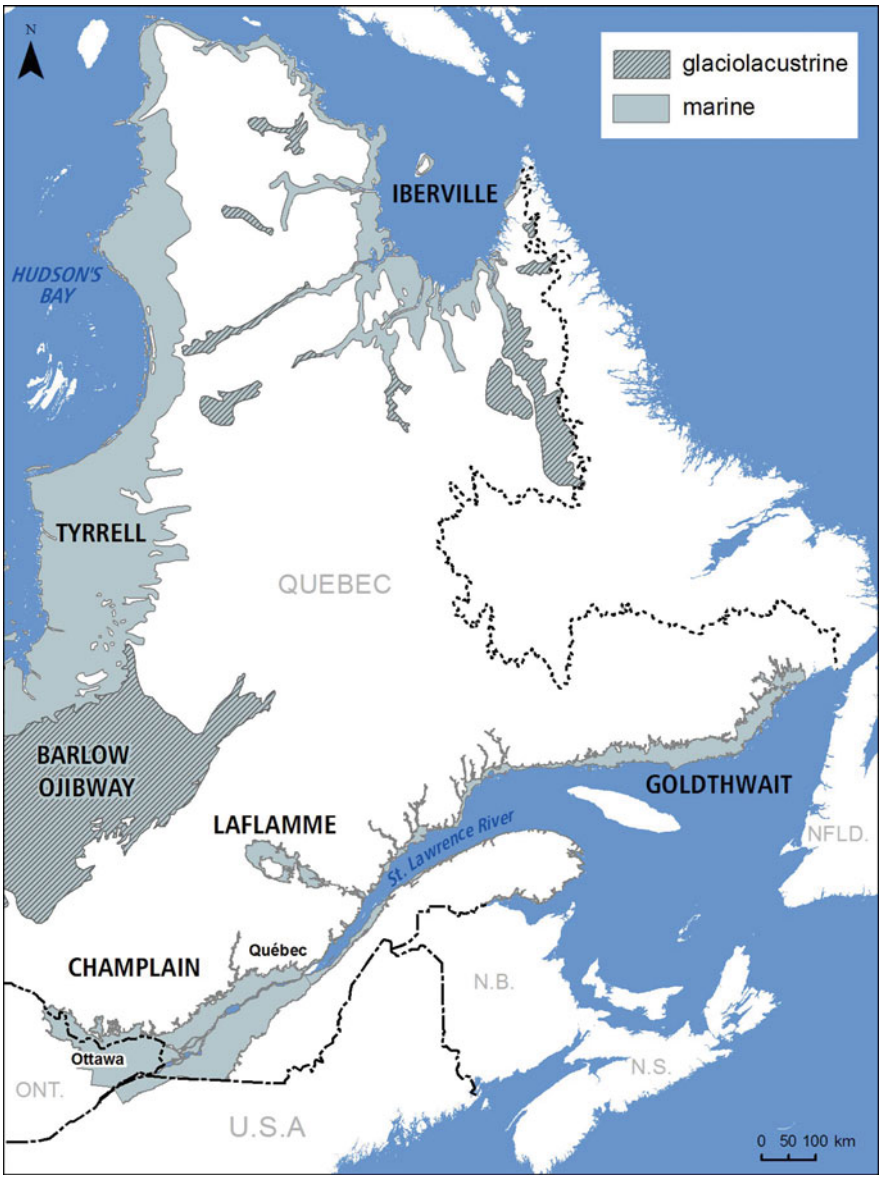

Fig. 2.1 Clay deposits of Eastern Canada

large basins, the marine clay deposits can be interlayered with granular soil (Gadd 1975) resulting in a slightly more complex stratigraphy. In most cases and at least to develop an understanding of the ground water conditions, one can consider a simple model of a relatively impervious clay deposit confined between two pervious boundary as illustrated on Fig. 2.2.

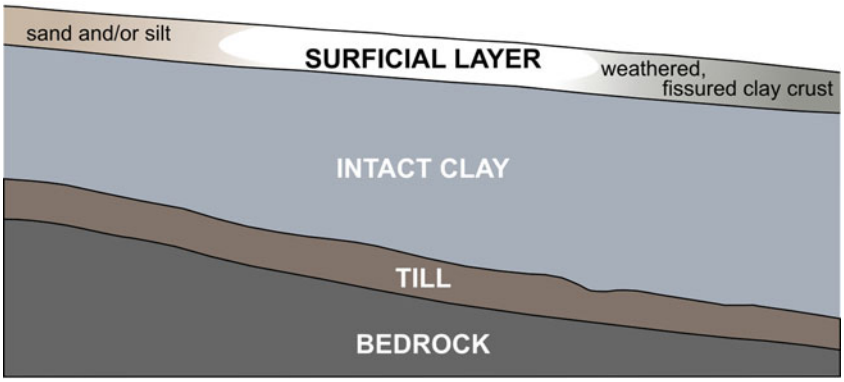

Fig. 2.2 Simplified statigraphy of a typical marine clay deposit of Eastern Canada

2.4 Valley Formation and Groundwater Regime

Landslides in sensitive clays of Eastern Canada are most generally located along river or stream valleys. Slopes have been created by the gradual erosion of these valleys in initially horizontal clay deposits. Stability analyses in sensitive clays concern most generally slopes along river or stream valleys created by the erosion of valleys through the deposit. In the Champlain sea basin, the preconsolidation pressure is, in general in agreement with the maximum filling level of the valley (Bouchard et al. 1983, Crawford and Eden 1965) even if secondary consolidation (Bjerrum 1967) and structuration (Locat and Lefebvre 1986) can also play a role. River and stream valleys can be identified today in different stages of formation as illustrated on Fig. 2.3. The ground water regime can change drastically depending of the stages of the valley formation through the clay deposit due to the contrast of hydraulic conductivity at the clay boundaries. One can see that at the intermediate stage, (Fig. 2.3b) where the river valley has not yet completely cut through the clay deposit, the river still flowing on a clay bottom, the ground water regime is characterized by upward hydraulic gradients (i) at the toe of the slope, creating conditions detrimental to slope stability and prone to deep failure surface. On the contrary, once the valley has cut completely through the clay deposit (Fig. 2.3c), the river flowing on till or bedrock, the till layer is discharging in the valley with a water head at equilibrium with the water level in the river. This creates a strong underdrainage of the whole slope, a condition highly favourable to slope stability. Once the boundary conditions are established, it is a simple matter to produce a flow net for a given geometry since the hydraulic conductivity of the marine clays of Eastern Canada can for practical purpose, be considered as isotropic (Tavenas et al. 1983). Ground water flow patterns are presented on Fig. 2.4 for the geometric conditions corresponding to the three stages of valley formation shown on Fig. 2.3 (from Lafleur and Lefebvre 1980).

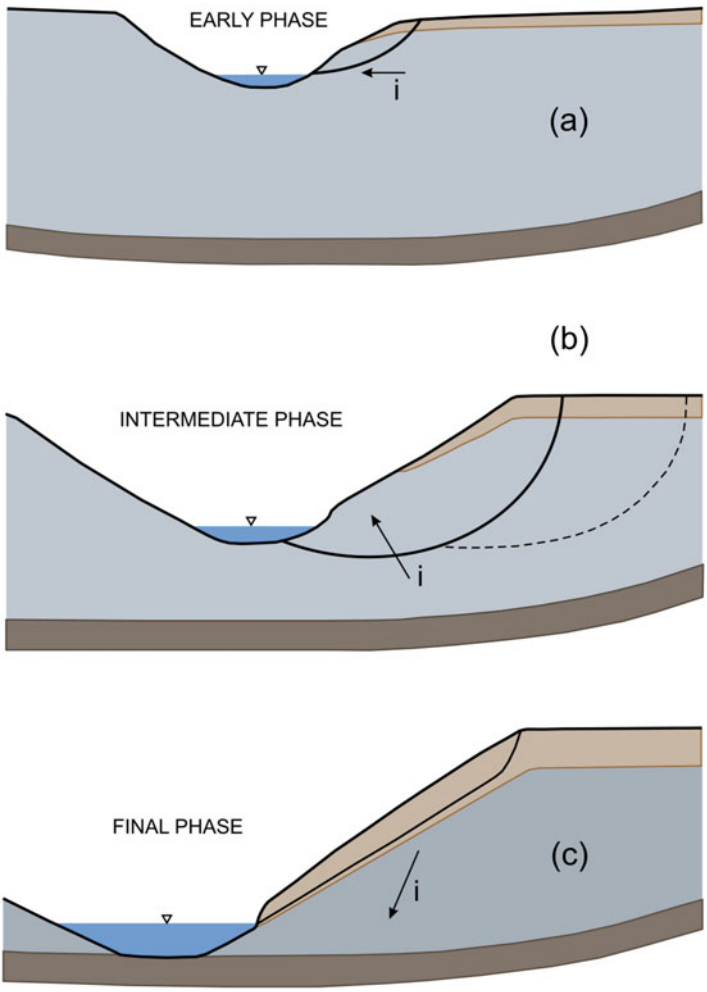

Fig. 2.3 Simplified model of a valley formation in the clay deposits of Eastern Canada

These flow nets have been determined numerically assuming an hydraulic conductivity contrast of only 10 between the clay deposit and the till layer at the bottom. This hydraulic conductivity (k) contrast of only 10 is however sufficient to result in artesian conditions and upward gradients in the lower portion of the slope for the intermediate stage of valley formation (Fig. 2.4b) and in a generalized underdrainage of the whole slope when the till layer discharges into the river. These considerations and analyses allow to distinguish in the process of valley formation between a critical intermediate phase before the till freely discharges into the river and a stable or final phase once the till layer freely discharges into the river.

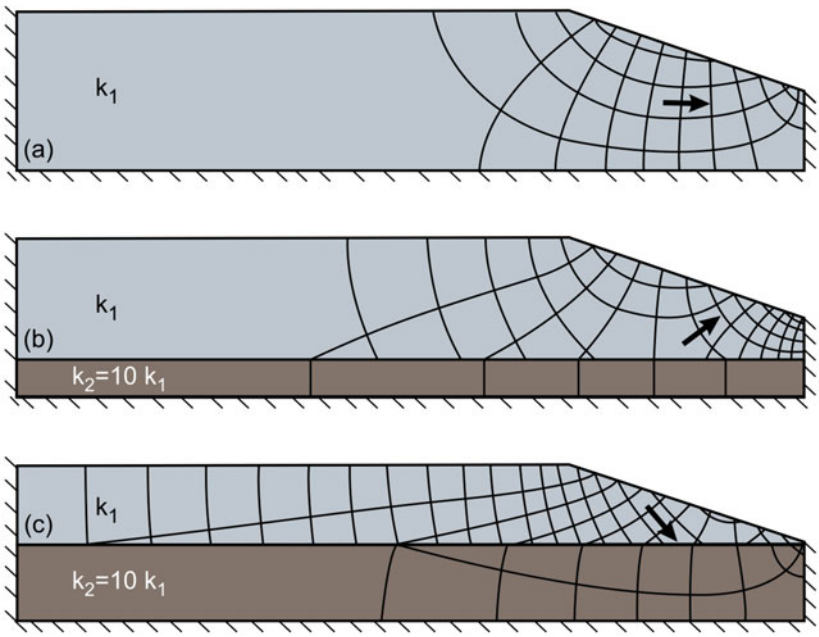

Fig. 2.4 Ground water regime in the vicinity of a clay slope

2.5 Examples of Ground Water Regimes from Case Records

Two examples of ground water regimes in the vicinity of a clay slope are presented, one where the valley is at its final stage having cut completely through the clay deposit as in Figs. 2.3c and 2.4c and the other for the critical intermediate stage as in Figs. 2.3b and 2.4b. The first case record is on the Broadback river in the Tyrrel sea basin in Northern Québec (Fig. 2.1). The site was well documented with numerous borings and piezometers (Lefebvre 1986). The slope is about 25 m high with a typical stratigraphy where a deposit of sensitive marine clay with a weathered surficial crust rests on a layer of till. Two ground water regimes are presented for this site on Fig. 2.5 with the stratigraphic information. In the first ground water regime, the experimental regime, (Fig. 2.5a), the equipotential lines are based only on the piezometer readings (November 1980). The ground water regime is characterized by a strong underdrainage, the till layer, the pervious boundary at the lower limit of the clay deposit, freely discharges into the river which is flowing directly on the till strata. Under the crest of the slope, the piezometric head in the till is just slightly higher than the water level in the river. In the surficial fissured weathered crust, the water level however rises to ground surface during wet seasons with nearly hydrostatic conditions inside the pervious weathered surficial crust. In the intact clay, the pore pressure under the crest of the slope increases with depth in the upper

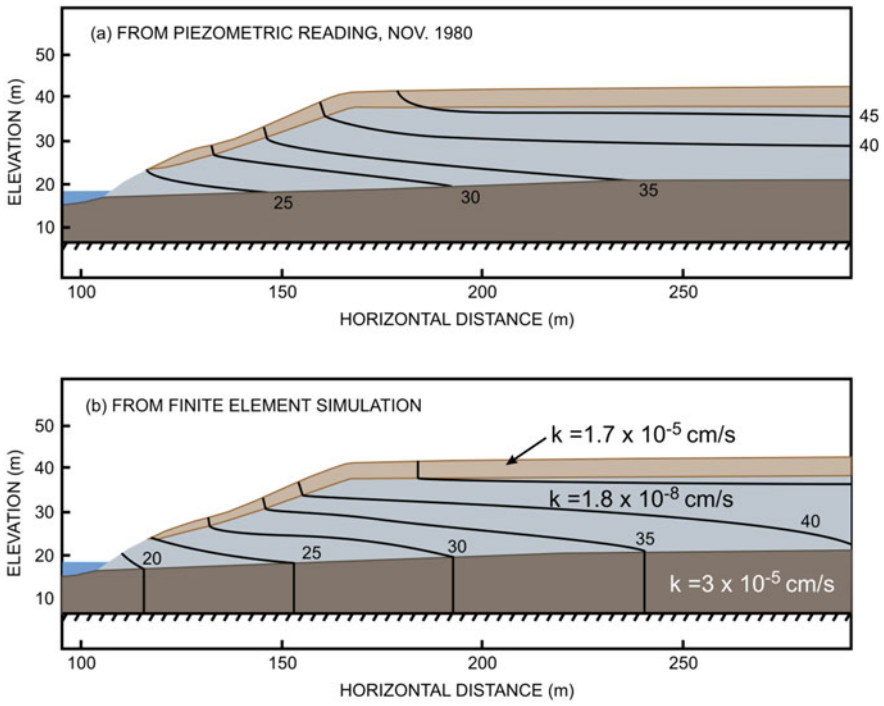

Fig. 2.5 Example of ground water regime for a slope in a valley at final stage

part of the deposit then decreases with depth until equilibrium with the potential in the till strata discharging into the river. The second ground water regime for the same site has been determined by numerical analysis using the site stratigraphy and hydraulic conductivities measured in several field permeability tests performed in driven piezometers or at end of casing (Fig. 2.5b).

The two ground water regimes, the experimental and the numerical, are remarkably similar and confirm the very beneficial underdrainage of the slope when the river or stream valley reaches its final or maturity stage. The field measurements of hydraulic conductivity as presented on Fig. 2.5b also confirm that the contrast of hydraulic conductivity between the intact clay deposit and its boundary layers, the till strata at the base and the weathered crust at the top is higher than 100. These boundary layers can thus be considered as pervious when compared to the intact clay deposit. This means that the pore pressure in the intact clay deposit does not necessary follows or comes to equilibrium with the relatively rapid seasonal variations in the boundary layers (Lefebvre 1986).

The second example concerns the critical intermediate stage in the process of valley formation when the lower pervious boundary does not yet discharge into the valley, the river still flowing on a clay bottom as illustrated on Figs. 2.3b and 2.4b.

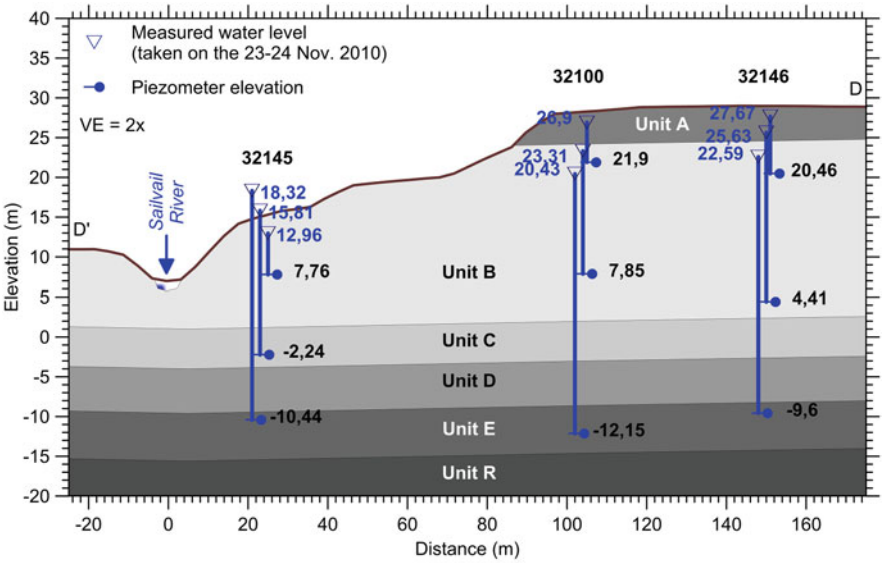

Fig. 2.6 Example of ground water regime for a slope in a valley at intermediate stage (Locat et al. 2012b)

The site of the Saint-Jude May 2010 landslide is one of the best documented in Eastern Canada (Locat et al. 2012a, b). The geometry and the stratigraphy before the landslide as well as the piezometric readings of November 2010 are reproduced on Fig. 2.6. The piezometric readings have been obtained in piezometers installed in intact ground at 100 to 200 m from the landslide crater. The piezometric readings presented on Fig. 2.6 were confirmed by numerical analyses based on stratigraphy and hydraulic conductivity. Unit R on Fig. 2.6 is the bedrock while unit E is the till. The till is more than a thousand time more pervious than the clay, unit B. While units C and D are slightly different than unit B in term of general properties, the hydraulic conductivity appears fairly similar based on a limited number of laboratory permeability tests. The slope is 22 m high above the river bottom. The layer of clay between the till and the river bottom is about 16 m thick restricting the discharge of the pervious till strata into the river. This is evidenced by the water head in the till strata who decreases very slowly from the piezometer behind the crest to the one near the river, resulting in a high artesian condition in the lower part of the slope. The extrapolation of the piezometric level in the till would indicate in the center of the valley a water head rising about 10 m above the river bottom, creating a situation prone to bottom heave and to the development of a deep failure surface.

The piezometric measurements as well as the numerical analysis of the ground water regime at this Saint-Jude site fully support the considerations and analyses presented on Figs. 2.3b and 2.4b.

The two case records presented here illustrated the large impact of the phases of valley formation on the groundwater regime and on the stability conditions, in the intermediate critical phase, strong artesian conditions as compared to a generalized under drainage in the final or maturity phase.

2.6 Conditions for Slope Stability Analysis

The first question to examine in relation to slope stability analysis concerns the drainage conditions. A clay failure is always undrained in the sense that the pore pressure generated during the failure cannot dissipate as rapidly as the movement. What we want to model however in our analysis is not only the failure phenomena but the loading leading to the failure. The system of shear stress existing today in a stable slope has developed over centuries as the valley was formed. In other words, the stress path leading to the present condition is a drained stress path as illustrated on Fig. 2.7. Let's look at the state of stress in a soil element existing today on a potential failure surface, represented by point B in the Mohr Coulomb space of Fig. 2.7. As the valley is being eroded, the confinement stress is reduced and the shear stress increases under the slopes. The phenomena takes place over many centuries and can be considered fully drained with the pore pressure at equilibrium with the state of stress. If the state of stress get near the shear resistance envelope, failure may develop due to a rapid increase of the shear stress associated for example to a rapid toe erosion. The failure phenomena which develops rapidly is then undrained. A drained or effective stress analysis thus respects the field stress path until the incipience of failure and the error associated with the undrained failure (stress path BO or BN, Fig. 2.7) remains small. An important consideration when looking at Fig. 2.7 is that the stress path associated with valley formation represent a decrease of the confining stress on the soil element. Even for a normally consolidated deposit, a soil element under the bottom or under the slope of the valley is overconsolidated and will behave as such under shear loading. The pore pressure generation during the shearing of a clay element decreases as the overconsolidation degree increases. The error associated with an undrained failure at the end of the

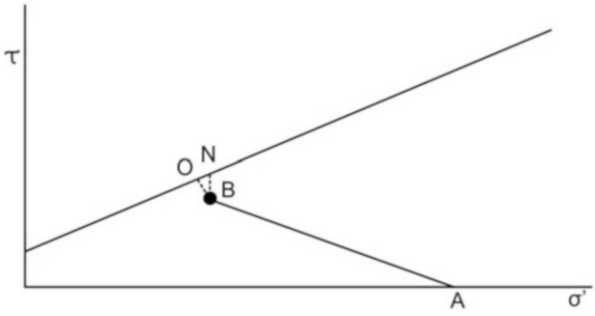

Fig. 2.7 Approximate stress path during valley formation for a clay element on a potential failure surface

drained stress path of Fig. 2.7 may thus become rather negligible. The process of valley formation in the Easter Canadian sensitive clay deposits has thus an important impact on the choice of the methodology to evaluate the slope stability, dictating the use of an effective stress analysis and of a shear strength reflecting the behaviour of an overconsolidated clay.

2.7 Determination of the Shear Strength Parameters

Overconsolidated soils, in particular overconsolidated clays, exhibit a brittle behaviour when loaded up to failure. This is illustrated Fig. 2.8 using the stress strain curves obtained in isotropically consolidated drained triaxial compression tests (CID) for two undisturbed specimens cut in block samples from the Champlaim sea basin. The specimens where reconsolidated under low isotropic pressures, 10 and 15 kPa, so that they remains in the overconsolidated range throughout the loading. In both tests, the stress strain curve is characterized by a brittle failure at an axial deformation of about 1% followed by a rapid strength decrease until a post peak plateau at an axial deformation of about 6 or 7%. Even if qualified as

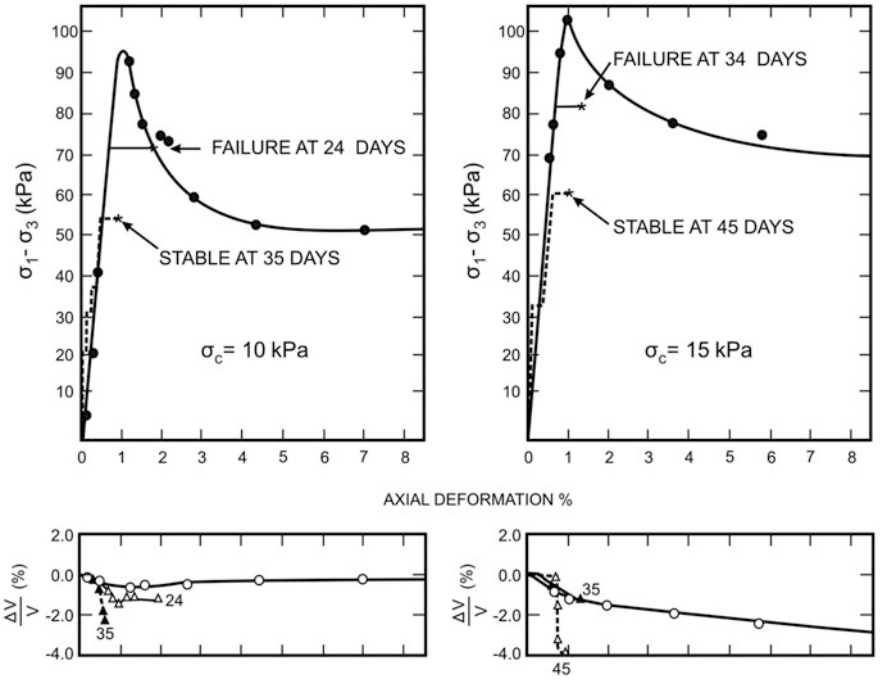

Fig. 2.8 Results of isotropically consolidated triaxial compression tests, conventional and creep tests (From Lefebvre 1981)

overconsolidated, it is important to note that the clay deposits of Eastern Canada have not in general been compressed under relatively high past consolidation pressure as it is the case for example for the well documented overconsolidated London clay (Skempton 1964) where the natural water content has been reduced practically to its plastic limit. In the Easter Canadian clay deposits qualified as overconsolidaded or lightly overconsolidated, the natural water content has remained generally close to or above the liquid limit, the liquidity index being generally close to or above 1.0 and as high as 2.0 in the very sensitive deposits. It is as if the water content and the void ratio had not adjusted to the reduction of the liquid limit associated with the reduction of the pore water salinity. The brittle behaviour observed on Fig. 2.8 is interpreted as a fairly rigid clay microstructure until failure followed by an adjustment of the shear resistance to the present void ratio of the soil.

The large deformation or post peak shear strength determined on Fig. 2.8 should not thus be confused with the residual shear strength determined at large deformation on heavily overconsolidated clays. While the development of the residual state in highly overconsolidated clays is associated with dilatancy and a certain realignment of the particles (Skempton 1964), the shearing of Canadian soft clay is typically associated to a compressive behaviour as illustrated on Fig. 2.8 and the post peak can be seen as a state of equilibrium between the shear strength and the void ratio. The results of four creep tests are also presented on Fig. 2.8 together with the stress strain curves of the two conventional CID tests.

The specimens for the creep tests were cut from the same block sample, prepared and consolidated under the same pressures than for the conventional tests and loaded in compression as in the conventional tests except that the loading was stopped well before failure at different percentage of the peak strength. The axial and volumetric deformations were then monitored for a long period of time. Depending of the stress level, axial deformation either started to increase after a certain number of days and ended up in failure of the sample or tended to stabilize in a manner very similar to the behaviour observed by Singh and Mitchell (1968). The creep tests thus indicated that the peak strength is reduced significantly with time but that there exist a stability threshold. The 8 creep tests performed after reconsolidation pressures between 5 and 25 kPa show indeed that the specimens under a stress level higher than the post-peak strength have ended up in failure but that the samples under a stress level lower than the post-peak strength have stabilized and remained stable as shown on Fig. 2.9.

This Fig. 2.9 presents the envelopes for both the peak and post-peak strength. The results of the 8 creep tests presented on this figure identify the post-peak envelop as a stability threshold separating the specimens which have remained stable and those which have failed with time. It is interesting to note that the specimens which have remained stable had stabilized at axial deformation significantly lower than observed at failure in conventional CID tests.

The recognition of the effect of time and of the existence of a stability threshold has a major bearing on the understanding of the stability analysis based on limit equilibrium for brittle soft clays as existing in Eastern Canada. Contrary to the assumption of the classical progressive failure model, the peak strength which is

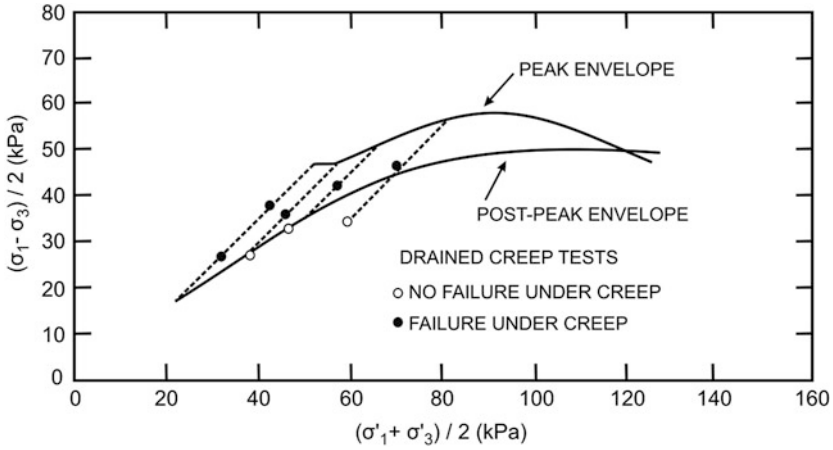

Fig. 2.9 Comparison of creep test results with the peak and post-peak strength envelopes, Nicolet clay

observed in conventional laboratory tests is not necessarily mobilized in the field at a certain time. The stresses do not have to exceed the peak strength in one location to initiate the failure. In other words, the concept of progressive failure, developed to account for the failure of highly overconsolidated materials like the London clay, is not necessary to explain slope failure in Canadian soft clay. The post-peak strength, as measured in a conventional CID test appears to provide a good evaluation of the stability threshold above which failure will develop with time. The range of reconsolidation pressure must however be low enough for the specimens to remain in the overconsolidated range not only at the end of the reconsolidation, but also during the loading stress path leading to failure, and for the state of stress during the tests to be representative of the stress on potential failure surfaces in the field. One must realize that isotropic reconsolidation pressures of 15 or 20 kPa would lead in a CID test to a vertical stress at failure of about 100 kPa with a normal stress of the order of 40 kPa.

2.8 Generalization of the Post-peak Envelop

The analysis of several case records in the seventies confirmed that the post peak strength determined in conventional CID tests was providing a good evaluation of the shear strength mobilized at slope failures in Eastern Canadian clay deposits (Lefebvre and LaRochelle 1974, Lefebvre 1981). The clay specimens in these studies were generally cut from block samples and reconsolidated under relatively low stresses. Conventional CID tests are not routinely performed in general practice. The test requires well trained technicians, relatively sophisticated equipment and

automated monitoring, the test lasting about a week. There was consequently an incentive to examine if the post-peak shear strength parameters could be obtained using correlations with routinely determined parameters. Due to the development of the Sherbrooke sampler (Lefebvre and Poulin 1979), block samples were obtained at several locations in the different clay basin of Eastern Canada. The post-peak strength envelop was then determined for 20 different sites with block sampling, from CID tests with reconsolidation pressures of 5, 10, 20 and 30 kPa, allowing to examine different correlations with routinely determined parameters, namely the natural water content, the plasticity index, the field vane strength and the oedometric preconsolidation pressure. The correlations with the post-peak strength were examined individually for each reconsolidation pressure. The correlations with the post-peak shear strength determined for all 20 sites in CID tests where the specimens were reconsolidate under on isotropic pressure of 10 kPa are presented on Fig. 2.10 reproduced from Lefebvre 1981. The correlations were determined by linear regression with each time the determination of the correlation coefficient r^2. Fig. 2.10 allows in addition to appreciate the range of natural water content,plasticity index, field vane strength and preconsolidation pressure covered by the 20 sites of the study.

The post-peak shear strength decreases significantly as the water content or as the plasticity index increases. The tendency is clear and logical but the correlation coefficients are rather low at 0.27 and 0.18 (Fig. 2.10). The post-peak strength increases with the field vane strength with again a fairly low correlation coefficient of 0.23. The correlation of the post-peak shear strength with the preconsolidation pressure as determined in the oedometer shows however a relatively high correlation coefficient, 0.81, much higher than with the three other properties. The same exercise was repeated with the post-peak strength determined in CID tests with reconsolidation pressures of 5, 20 and 30 kPa showing when correlated with the oedometric preconsolidation pressure correlation coefficients of 0.25, 0.85 and 0.73 respectively. Post-peak shear strength envelopes were then reconstituted for preconsolidation pressures of 100, 200, 300 and 400 kPa as presented on Fig. 2.11.

The 4 points on each of the envelops on this figure were simply obtained from the correlations of the preconsolidated pressure with the post-peak strength determined with reconsolidation pressure of 5, 10, 20 and 30 kPa as shown on Fig. 2.10 for a reconsolidation pressure of 10 kPa. The 4 points used to reconstitute the post-peak strength envelop show a certain curvature of the envelope with a tendency of the envelope to be steeper toward the origin. This has been confirmed in back analysis of shallow failures in relatively low slopes, leading to strength envelopes defined by lower cohesion and higher friction angle (Lefebvre 1981). In slope stability analysis the shear strength envelope is generally assumed to be linear and simply defined by a cohesion intercept and a friction angle. The use of a linear approximation in the present case would not introduced significant errors but still raises the question of what is the most appropriate range of stresses to consider for the linear approximation. As mentioned before, the range of reconsolidation pressures in the CID tests should cover the range of stresses on potential failure surfaces and be

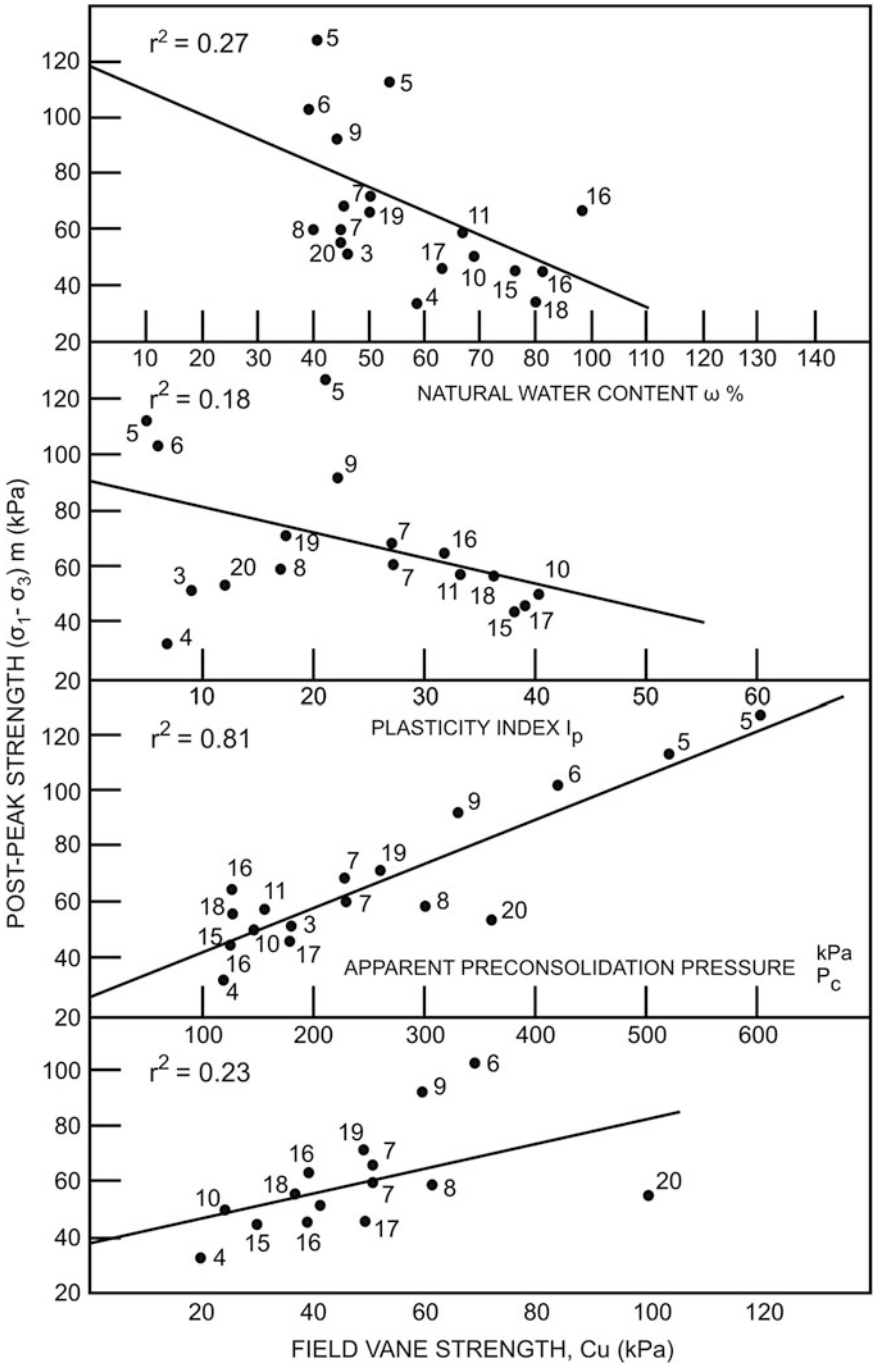

Fig. 2.10 Correlation of the post-peak strength with different properties for specimens reconsolidated at 10 kPa (See Lefebvre 1981 for site numbering)

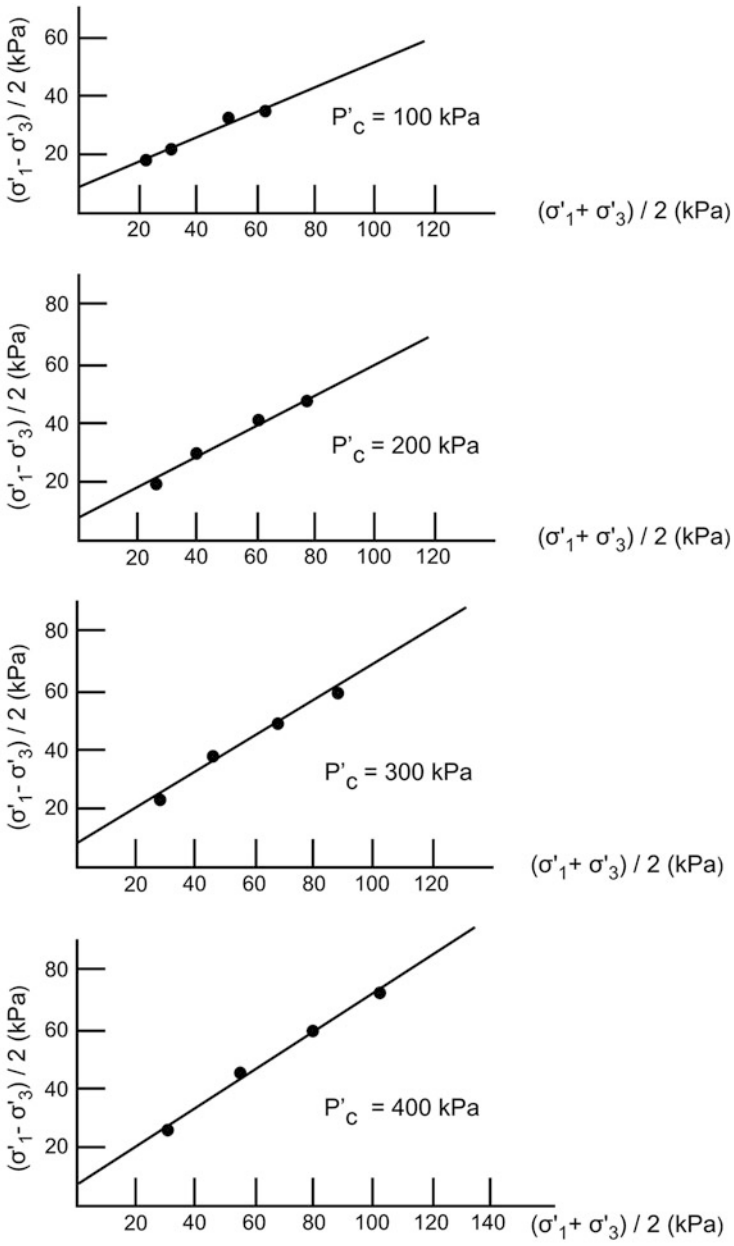

Fig. 2.11 Post-peak strength envelopes deducted from the correlations with the preconsolidation pressure

Table 2.1 Parameters of the post-peak strength envelopes obtained from the correlations with the preconsolidation pressures

Range of reconsolidation pressure (kPa)	σ'_p (kPa)	C_m' (kPa)	φ_m' (°)
5–20	100	7.4	28.7
	200	7.7	34.7
	300	7.7	39.8
	400	7.5	43.6
5–30	100	9.5	24.2
	200	9.6	30.7
	300	9.8	36.2
	400	9.8	39.8

low enough for the entire stress path to remain in the overconsolidated range. A reconsolidation pressure of 30 kPa is susceptible to end up at failure with an effective vertical stress near 150 kPa, thus over the preconsolidation pressure for some deposits and with a normal stress over 50 kPa which may exceed what is expected generally on a failure surface. The range of stresses associated with reconsolidation pressures of 5 to 20 kPa appears more representative of the operative stresses in most slopes in Eeastern Canadian deposits. Reconsolidation pressures of 5 to 30 kPa will be more representative of the operative stresses in higher slopes. The shear strength parameters describing the post-peak envelope were computed by linear regression for oedometric preconsolidation pressures of 100, 200, 300 and 400 kPa and are presented on Table 2.1 for reconsolidation stresses of 5 to 20 kPa and also for 5 to 30 kPa. The increase of the post-peak strength with the preconsolation pressure is evident on Table 2.1. For the reconsolidation stresses of 5 to 20 kPa and assuming a normal stress of 30 kPa, one calculates a post-peak strength increasing from 24 to 36 kPa, an increase of 50%, when the preconsolidation pressure increases from 100 to 400 kPa. It is however interesting to note that for both reconsolidation ranges, the cohesion intercept remains constant, only the friction angle increases with the preconsolidation pressure. Considering a higher reconsolidation range has the effect of rotating the linear strength envelope leading to a higher cohesion intercept and lower friction angles (Table 2.1). For the reconsolidation stresses of 5 to 30 kPa, and assuming again a normal stress of 30 kPa, the post-peak strength increases from 23 to 34.5 kPa when the preconsolidation pressure increases from 100 to 400 kPa, values slightly lower than with the 5 to 20 range but still showing an increase of 50%. For low values of normal stress, the 5 to 30 range would however yield higher values of shear strength due to a higher cohesion intercept than the 5 to 20 range. Overall the difference between the two sets of strength envelopes presented in Table 2.1 should be small in term of strength but may have an impact on the position of the critical failure surface. The influence of the oedometric preconsolidation pressure on the post-peak strength is well illustrated by Table 2.1 and Fig. 2.11. This influence becomes still more obvious when the state of stresses corresponding to the post-peak strength determined in all the CID

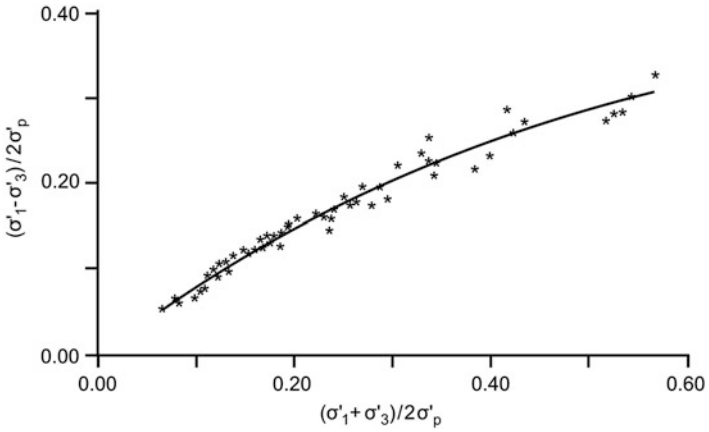

Fig. 2.12 Post-peak strength envelope normalized by the preconsolidation pressure

tests are normalized by the preconsolidation pressure as presented on Fig. 2.12. While the natural water content, the plasticity index, the field vane strength and the preconsolidation pressure shows large variation among the sites considered in the study (Fig. 2.10), the state of stresses corresponding to the post-peak strength values define a unique envelope with a surprising low scatter when normalized by the preconsolidation pressure (Fig. 2.12). The curvature of the normalized envelope is readily apparent. This curvature explains why the friction angle increases with the preconsolidation pressure while the cohesion intercept remains constant for a given range of reconsolidation pressure (Table 2.1). For a preconsolidation pressure of 100 kPa, the portion of the normalized envelope defining the strength for a range of reconsolidation pressure, say of 5 to 30 kPa, is at the flatter extremity of the envelope, thus a low friction angle. For a preconsolidation pressure of 400 kPa, and for the same range of reconsolidation pressure, the strength is defined by the steeper portion of the envelope near the origin with thus a high friction angle.

2.9 A Recent Case Record

The May 10 2010 Saint-Jude landslide is remarkably well documented (Locat et al. 2012a, b) and is thus an interesting case to verify the resistance mobilized at failure. Slope stability effective stress analyses were performed using the Bishop method and a shear strength envelope defined by a friction angle of 35 degree and a cohesion intercept of 7.7 kPa as proposed in Table 2.1 for a preconsolidation pressure of 200 kPa. All sliding surfaces for the minimum factors of safety, in fact for factors of safety between 0.99 and 1.05, are presented on Fig. 2.13. The back analysis of the Saint Jude landslide confirms not only that the post-peak shear strength is a good

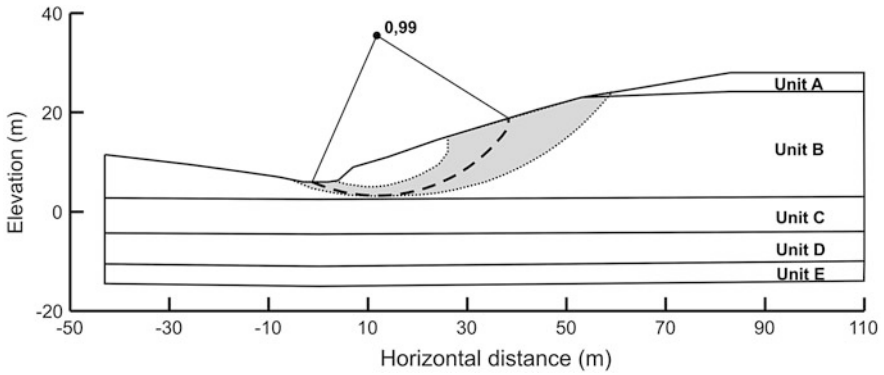

Fig. 2.13 Back analysis of the Saint-Jude slope failure using post-peak strength deducted from the preconsolidation pressure; array of the failure circles with the minimum factors of safety, between 0.99 and 1.05

evaluation of the shear strength mobilized at slope failure in the Eastern Canadian clay deposits but also that its determination based on the preconsolidation pressure as presented in Table 2.1 is a reliable approach. The critical sliding surfaces on Fig. 2.13 reached the bottom of the clay layer, some 2.5 m below the river bottom and thus models relatively well the position of the sliding surface observed after failure. Note that the sliding surface has progressed inland almost horizontally over some 100 m.

2.10 Slide Retrogression in Sensitive Clay Deposits

Landslides are basically part of a process by which slopes adjust to changes of geometry and of ground water conditions associated with valley formation or sometimes human activities. Landslides in sensitive clay are peculiar because the debris move away instead of stabilizing the newly formed slope. The clay sensitivity or the severe reduction of the undrained shear strength associated with the first failure is thus the primary cause of the retrogression in sensitive clay deposits. Its amplitude is difficult to evaluate. One rule which is generally accepted is however that retrogression would develop only following a significant initial or triggering landslide. While the retrogression is often a series of rotational slides, it is described at Saint-Jude as a "spread" with a post-slide morphology characterized by horst and graben shapes. The sliding surface is at 2.5 m below the river bottom and propagated inland nearly horizontally over about 100 m. The purpose here is not to discuss the mechanism of retrogression but simply to point out to a particular state of stress associated with valley formation which may play a role in the initiation of the retrogression. As noted before the erosion of the valley has resulted in an overconsolidation of the deposit under the valley. This has a significant

impact on the state of stress, the value of K_0, the stress ratio, increasing with OCR (overconsolidated ratio), particularly in the Eastern Canadian clay deposits. Hydraulic fracture tests at 5 different sites in the Champlaim clay with OCR varying between 1.7 and 4.7 have indeed indicated that the horizontal stresses have remained practically unchanged (Lefebvre et al. 1991) when the deposits became overconsolidated due to a reduction of the vertical stress by erosion, seemingly due to the rigidity of the microstructure. Even if the Saint-Jude deposit was only lightly overconsolidated, the erosion of the valley should have increased the OCR above 2.0 in the lower half of the slope and even more after the initial failure. Immediately after the triggering slide, there were thus significant horizontal forces tending to push out the block of intact clay behind the initial failure. Such a stress system could contribute to initiate slide retrogression either as a spread or as rotational failures.

2.11 Conclusion

When looking at the results of geotechnical investigations, it is important to establish rational links between each borings or soundings in order to develop a general understanding of the nature, extend and position of the soil strata one expects to find at the site. This allows normally to arrive at a better interpolation or extrapolation of the stratigraphy and of the soil properties, and in the vicinity of a slope to have an idea of the ground water regime. Such an analysis is always useful in particular for geology and stratigraphy as simple as generally observed in the clay deposits of Eastern Canada. The examples of ground water regime presented in this paper illustrate the relation between the stratigraphy and the ground water regime in the vicinity of slopes and show the drastic difference of the ground water regime associated to the stages of valley formation.

The shear strength, the other important parameter in a slope stability analysis, should be determined in a drained loading in the overconsolidated range to model the stresses under a slope associated with the erosion of the valleys over the age. The post peak strength determined in conventional CID tests on intact specimens under low reconsolidation stresses appears as a good evaluation of the shear strength mobilized at the failure of a slope in Eastern Canadian clays as confirmed in several back analyses. Long term creep tests have shown that the CID peak strength decrease with time but that the post peak shear strength envelope acts as a stability threshold below which creep deformations stabilized, the specimens remaining stable. The post peak strength is related to the presonsolidation pressure and to avoid the need of CID tests, correlations have been developed to obtain with a sufficient accuracy the post peak strength from the consolidation pressure, routinely determined in geotechnical investigations.

Acknowledgments The material presented in this paper resulted from the work of many graduated students in the soil mechanics laboratory at the University of Sherbrooke in the province of Québec, Canada. Working with these graduated students has been the highlight of the author career at the

university. The author is grateful in the preparation of this paper for the support of the «Ministère des Transports, de la Mobilité durable et de l'Électrification des transports» of the province of Québec, namely Denis Robitaille, Denis Demers and Mélissa Raymond, and also of Ariane Locat at the University Laval.

References

Bjerrum L (1967) Engineering geology of Norwegian normally consolidated clays as related to settlements of buildings. Geotechnique 17:81–118

Bouchard R, Dion D, Tavenas F (1983) Origine de la préconsolidation des argiles du Saguenay. Can Geotech J 20(2):315–328

Crawford CG, Eden WJ (1965) A comparison of laboratory results with in situ properties of Leda clay. In: Sixth international conference on soil mechanics and foundation engineering. Montreal, Canada 1, 31–35

Gadd N R (1975) Geology of Leda clay. In: Fourth Guelph symposium on geomorphology, pp 137–151

Hilaire-Marcel C (1979) Les mers post-glaciaires du Québec: quelques aspects. Thèse de doctorat, Université Pierre et Marie Curie, France

Lafleur J, Lefebvre G (1980) Groundwater regime associated with slope stability in Champlain clay deposits. Can Geotech J 17(1):44–53

Lefebvre G (1981) Strength and slope stability in Canadian soft clay deposits. Can Geotech J 18(3):420–442

Lefebvre G (1986) Slope instability and valley formation in Canadian soft clay deposits. Can Geotech J 23(3):261–270

Lefebvre G, LaRochelle P (1974) The analysis of two slope failures in cemented Champlaim clays. Can Geotech J 11(1):89–108

Lefebvre G, Poulin C (1979) A new method of sampling in sensitive clay. Can Geotech J 16(1):226–233

Lefebvre G, Bozozuk M, Philibert A, Hornych P (1991) Evaluating K_0 in Champlaim clays with hydraulic fracture tests. Can Geotech J 28(3):365–377

Locat J, Lefebvre G, Ballivy G (1984) Mineralogy,chemistry and physical properties interrelationships of some sensitive clays from Eastern Canada. Can Geotech J 21(3):530–540

Locat J, Lefebvre G (1986) The origin of structuration of the Grande-Baleine marine sediments. Quart J Eng Geol 19:365–374

Locat P, Demers D, Robitaille D, Fournier T, Noël F, Leroueil F, Locat A, Lefebvre (2012a) The Saint-Jude landslide of May 10, 2012. In: Second North American symposium on landslides, Banff, Canada, pp 635–640

Locat A, Leroueil S, Locat P, Demers D, Robitaille D, Lefebvre G (2012b) In situ characterization of the Saint-Jude landslide, Québec, Canada. In: Fourth international conference on geotechnical and geophysical site characterisation, Porto de Galinhas, Brazil, 1, 501–514

Quigley RM (1980) Geology, mineralogy and geochemistry of Canadian soft soils: a geotechnical perspective. Can Geotech J 17(2):261–285

Singh A, Mitchell JK (1968) General stress-strain-time function for soils. ASCE J Soil Mech Found Div 94(SM1):21–46

Skempton AW (1964) Long term stability of clay slopes. Géotechnique 20(14):75–102

Tavenas F, Jean P, Leblond P, Leroueuil S (1983) The permeability of natural soft clays, part II: permeability characteristics. Can Geotech J 20:645–660

Chapter 3
Chemistry: An Essential Key to Understanding High-Sensitivity and Quick Clays and to Addressing Landslide Risk

J. Kenneth Torrance

Abstract The property of silty-clay to clayey-silt quick clays, whereby apparently solid soil transforms to the liquid state when subjected to sufficient stress, derives from chemical factors: mineralogy (low activity); depositional environment (marine-to-brackish conditions causing flocculation and high water content); and post-depositional chemical changes (development of cementation and displacement of marine-to-brackish water by infiltrating rainwater). The stability of slopes developed by river incision is affected (negatively) by physical factors (drainage and fluctuating water tables) and chemical weathering reactions that have led to weak, fissured, blocky, nodular structures. Immediate causes of quick clay landslides are commonly the physical factors of: river erosion; high water contents in the fissured slopes; and human actions. Regardless, the characteristics of the resulting landslides are primarily determined by the chemical factors.

3.1 Introduction

Chemical influences on physical factors dominate the development of quick clays. Knowledge of these influences is essential to understanding and managing the challenges that the physical properties of quick clays present. Indeed, chemistry's dominating role in quick clay development (Fig. 3.1) and behavior provides the starting point for developing approaches to ameliorate the quick-clay landslide problem and other challenges presented by these unusual natural materials.

'Quick clay', used alone, refers to the undisturbed material, *in situ*, and to samples that retain their microstructure. After structural breakdown, by any means, it has been transformed to 'disturbed', 'remolded' or 'post-failure' quick clay.

The vast majority of quick clays accumulated in marine to brackish water during the late stages of the last continental glaciations. Their main mineral components are

J.K. Torrance (✉)
Geography and Environmental Studies, Carleton University, Ottawa, ON, Canada K1S 5B6
e-mail: ken.torrance@carleton.ca

V. Thakur et al. (eds.), *Landslides in Sensitive Clays*, Advances in Natural and Technological Hazards Research 46, DOI 10.1007/978-3-319-56487-6_3

Factors producing high undisturbed strength	
Depositional	**Post-depositional**
Flocculation[1,2] • Salinity[1] • Polyvalent cations dominate[2] • High suspension concentration	Cementation • Rapidly developed • Slowly developed Slow load increase Time-dependent diagenetic changes
Factors producing low remolded strength	
Material properties • Domination by low activity minerals[1,2]	Decrease in liquid limit > decrease in water content • Leaching of salt[1] • Dispersants[2] Reducing Conditions Inhibition of high-swelling smectite formation Minimal consolidation

1 Essential in marine clays 2 Essential in fresh water clays (Modified from Torrance 1983, 2012)

Fig. 3.1 The general model for quick clay development

glacially ground silt- and clay-sized particles of common rock-forming minerals – mostly quartz, feldspars, amphiboles, micas and chlorites. They also contain iron oxide nanoparticles, produced by grinding. The marine sediments in Scandinavia, Canada (east of Hudson Bay) and immediately adjacent states of the USA, and in coastal British – are similar, but not identical in terms of their mineralogy and development. Sensitive marine sediments in Ariake Bay, Japan, represent a major variation (Torrance and Ohtsubo 1995). They are 'post-glacial', having accumulated during the sea-level-rise period that accompanied glacial melting. They differ in being dominated by high-iron, low-swelling, smectitic clay minerals and volcanic ash. They have similar high sensitivities and bearing capacity problems and their sensitivity development has followed the same basic rules as the Scandinavian and North American sediments.

3.2 Development of High Sensitivity

Salinity-induced flocculation gives the sediment strength, and its open structure holds a high water content. High sensitivity develops when fresh water entering the sediment displaces the salt water. Salinity reduction to <2 g/l creates a situation

where, if the flocculated structure breaks down, the soil behaves as a liquid; quick clay has been produced. In Eastern Quebec and Labrador, cementation by iron oxides greatly increases the undisturbed soil strength and increases the sensitivity and has implications for the post-failure strength as well.

3.3 Cementation in Eastern Canadian, Sensitive Clays

Cementation, which increases undisturbed strength, is important for sensitivity in parts of Quebec and Labrador. The Scandinavian, Japanese, British Columbian and Ottawa Valley sensitive clays are considered 'soft' – meaning 'not cemented'.

It is not unusual to find the occasional small carbonate-cemented concretion at landslide sites. At Green Creek Valley in Ottawa, many concretions weighing 100 gm to several kilograms have been exposed by river erosion. The carbonate has locally impregnated the pore space. Their presence shows that, in water-saturated conditions, the carbonates, when in small amounts, prefer to congregate to form concretions, rather than to act as a widely dispersed cementing agent.

Within the St. Lawrence River Basin, the only compounds of sufficient abundance and low solubility to act as cementing agents are hematite and magnetite. Magnetite is more effective, probably because it has the highest stability toward weathering of the iron oxides (Murad 1988) and it is magnetic. From west to east in Quebec, the dominant iron oxide changes from: hematite (~1% by wt) in the Ottawa Valley (Torrance and Percival 2003); to magnetite at St. Leon le Grande, near Trois Rivières (Torrance et al. 1986). The magnetite almost certainly originated by grinding (to nanometer sizes) of magnetite-rich, iron ore (from western Labrador) during glacial transport outward and southward to where it ultimately co-sedimented with the other glacially ground minerals, in the Champlain, Laflamme and Goldthwaite Seas, The location and abruptness of the transition to magnetite dominance are undetermined; based on ice-flow patterns and terrain features, it probably occurs over a short distance near Jolliette, about 60 km SSW of Trois Rivières. The degree of cementation trends higher towards the eastern portions of the marine sediment accumulation areas of Quebec and Labrador.

Studies on the effect of EDTA, as an extractant for iron oxides, have been conducted on clays from Outardes, Québec, in the Goldthwaite Sea (Loiselle et al. 1971) and from Labrador (Kenney et al. 1967); both locations lie 'down-ice-flow' from the Québec/Labrador magnetite deposits. In both cases, EDTA was percolated through undisturbed samples of cemented marine clay and the percolate was collected. The most Fe^{+3} that Loiselle et al. extracted was 0.94% of the soil dry weight. The most Fe^{+3} that Kenney et al. extracted was 0.37% of the soil dry weight. Bulk extraction by EDTA at the end of the latter experiment revealed that the percolation experiment, which extracted about 20% of the magnetite originally present, led to substantial decrease in the *'apparent'* preconsolidation' pressures. Another overall conclusions, from Mössbauer spectroscopy and the extraction

experiments, are that nano-crystalline magnetite co-sedimented with the other glacially ground minerals, and that it is a remarkable cementing agent.

In 'Landslides in Sensitive Clays' (L'Heureux et al. 2014), clays with cementation were commonly referred to as being 'over-consolidated'. This is misleading. It is preferable to think of them as exhibiting '*apparent preconsolidation pressures'* (Kenney et al. 1967), because their high resistance to consolidation arose from cementation, not by volume decrease from prior greater loading. In the consolidation context, they are, in a way, 'under-consolidated' in that relatively little post-depositional consolidation occurred, when compared to the non-cemented Champlain Sea sediments. This reconceptualization may be of little consequence if one is only concerned with bearing capacity; but arguably, it is very important in the context of sensitive-clay landslides. These *'apparently preconsolidated'* sediments have somewhat greater water contents than do non-cemented sediments bearing the same load. Consequently, their greater cementation and lesser consolidation results in greater hydraulic conductivities, which facilitates more rapid leaching of salt from the sediment, and to a lower post-failure strength. Where valleys are: deeply incised into sediments with cementation; the riverbanks high and steep; and the weathered, surface zone thin compared to the depth of quick clay that underlies it, the size and severity of landslides would be enhanced. The presence of cementation by magnetite at St. Jean Vianney, and the 'under consolidation' that resulted, were factors in the high fluidity of the quick clay debris. This affected both the on-site and the downstream impact of the landslide. This consequence of cementation is important in the landslide amelioration context.

3.4 Geomorphic Influences on Landslide Types

The sensitive marine clay landscapes of Eastern Canada and those of Norway and Sweden differ greatly. The Champlain Sea sediments accumulated as broad, level expanses into which rivers incised their valleys; hills are scarce in the Basin. In the Laflamme Sea Basin, level expanses are less extensive, although most marine sediment surfaces are remote from hills. In the Goldthwaite Sea Basin and through to Labrador much of the exposed marine sediment is within sight of rocky uplands. In Scandinavia, many of sensitive-marine-sediment areas abut rock uplands, particularly in coastal Norway. Even in muted topography north of Oslo, rock outcrops and glacial till knolls interrupt the marine sediment surface continuity. In Sweden, western coast marine sediments and those now inland along rivers are adjacent to rock uplands, as are the brackish-water, Baltic Sea sediments in the muted topography of eastern and southern Sweden. These different geomorphological settings influence salt leaching in important manners.

3.5 Leaching and Weathering Dynamics: Flat Expanses

On large flat areas, salt removal occurs by water infiltration through the soil surface. Near riverbanks, the flow path is short; further away, water follows longer and deeper paths through the sub-surface drainage system. Water infiltration is accompanied by the physical and chemical changes of soil profile development (soil scientist view) and weathering crust development (geotechnical engineer view). In addition wetting and drying, freezing and thawing, oxidative weathering and transport of soluble products develop a several meters thick weathered crust zone.

The near-surface processes change the originally massive structure of the surface zone and valley slopes. Roots and the soil fauna introduce organic matter into the soil to produce a few-centimeter-thick zone of friable aggregates, the A horizon, below which angular, blocky aggregates become increasingly large until a massive zone is reached. In eastern Canada, Eden and Mitchell (1970), described the upper angular, blocky zones as having a 'nodular' structure'. In these angular, blocky zones, the vertical surfaces of the aggregates, throughout their depth range, have 'cutans' (thin layers of clay, iron oxides and black organic material) on their surfaces. This presence of cutans indicates that the spaces between blocky units are open and occupied by air or water, depending on the hydrologic conditions. These open spaces in the weathering crust, particularly on slopes, are locations of weakness. Hence, the angular, blocky aggregation that dominate the river valley slopes, throughout the zone within which the water table fluctuates during floods and heavy rainfalls, contribute to slope instability; local riverbank failures commonly constitute the triggering events for sensitive clay landslides.

3.6 Leaching and Weathering Dynamics: Near Uplands

Adjacent to uplands, salt leaching proceeds differently. The marine sediment interfaces directly with areas where the water table is higher than the sediment surface. The resultant artesian pressures at the lateral and basal contacts cause flow of water through the marine sediment, displacing the salty pore water upward. The rain that falls on the surface penetrates only a short distance before it is deflected towards the drainage system. The weathered surface zone's interface with quick clay may be as shallow as one meter. Also, after salt water has been displaced to produce the leached quick clay, continuing upward flow of water may bring with it potassium and magnesium ions, weathered from potassium feldspars, illite, and chlorite) in an oxidizing environment, that will slowly decrease the sensitivity from the sediment base upward (Moum et al. 1971). Such situations are expected in Norway, Sweden (along the Gota River and elsewhere), and in Canada where nearby uplands create artesian pressures at the sediment base.

3.7 Landslide Types: Flows and Spreads

Quick clay landslides commence with a failure that involves mostly the fractured, nodular, weathered material of the riverbank. This failure is commonly triggered by the combination of erosion at the river bank base (which steepens the slope) and water saturation in the weathered zone (which decreases the frictional component of its strength). The landslide may be a 'flow' or a 'spread'. A few slides exhibit elements of both types. Flows tend to occur in a step-wise fashion; whereas spreads tend to occur as a continuous, uninterrupted event. The different patterns arise from the transporting ability of the liquefied zone, which relates to the ratio of the thickness of the zone that liquefies relative to that of the low-sensitivity, weathered crust and any sensitive material above the failure zone that does not liquefy (Torrance 2012, 2014).

When related to the geomorphological influences, 'flows' tend to occur where salt leaching occurred from below (thin weathered crust), and 'spreads' where salt leaching was from above (thick weathered crusts). Hence, 'flow' slides should dominate in Scandinavia, while in eastern Canada, 'flow' slides are concentrated: (1) in the northern portions of the Champlain Sea Basin where the sediments are relatively shallow and adjacent to Canadian Shield uplands; (2) along river channels where the river is deeply incised and the liquefiable quick clay zone is very thick relative to the weathering crusts, as at St Jean Vianney in the Laflamme Basin (Tavenas et al. 1971), and the Rivière du Loup and Rivière Yamachiche basins west of Trois Rivières in the central Champlain Sea Basin (Karrow 1972); and 3) where sediments are in fjord-like settings such as the lower Rivière Gouffre valley near Baie St Paul in the Goldthwaite Sea Basin (Filion et al. 1991). In other situations, 'spreads' would be expected to be the norm. Demers et al. (2014) provide an inventory and some imagery of large landslides in Quebec. Some landslides exhibit elements of both flow- and spread-landslides.

3.8 Flow Slide Examples

In the 1951 'flow' landslide at Ullensaker, Norway, the farm owner observed 'fissures at the lower parts of the slope towards the brook' (Bjerrum 1955). His awareness that the cracks could lead to a bank failure and subsequent landslide led him to evacuate his family to a neighbor's farm. The slide occurred shortly after midnight, taking all the farm buildings and about 10 hectares of farmland. It left a 'classic' bottle-neck scar with a narrow opening to the creek valley.

On May 4, 1971, 31 people died in a disastrous flow slide at St. Jean Vianney, along the Petit Bras River, near Chicoutimi, Quebec (Tavenas et al. 1971). Ten days before, a 100 m long, river-bank failure extended 60 m into the steep and high river bank. It was discovered by the farm owner and photographed, but not

reported. On the evening of May 4, a St. Jean Vianney resident felt a slight "earth shaking" and could see Chicoutimi's lights from her window (never before visible), phoned a neighbor to ask if she had felt anything. Neither interpreted these signs to indicate a landslide was under way. In contrast to the folk knowledge about quick-clay landslides in the Norwegian sensitive clays, local knowledge of quick clay landslides was almost non-existent in the Laflamme Basin. This is probably because few quick-clay landslides have occurred during historical times. The first scientific report on quick-clay landslides in the basin was published in 1968 (La Salle and Chagnon 1968), only 3 years before the landslide. The publicity that followed this landslide has narrowed the knowledge gap.

3.9 Spread Slide Example

For spread slides, the failure begins when a relatively thin, quasi-horizontal layer of quick clay near the riverbank slope, fails and liquefies, upon which, the riverbank soil commences its movement into the valley and the failure plane retrogressively advances into the landscape. Sequential breaking of the overburden into slightly-rotated slices and/or a horst and graben-like sequence of intact-triangular-ridges and debris-occupied-valleys follows. These features are pushed forward by an ongoing supply of new ridges and liquefied debris. The landslide ceases when the capacity of the valley or plain to accommodate more debris is exhausted. The stalled sequences of ridges and troughs, inside the scar and in the debris field beyond, leads these spreads to often be referred to as 'ribbed' landslides.

The 1989 landslide at St. Liquori, Quebec, which disrupted a golf course, was triggered by a night-time, riverbank failure that was followed, essentially instantaneously, by a rapidly-advancing retrogressive stage. The retrogression distance extended to include several hectares on which a single-storey house had been constructed. While the occupants were rudely awakened and their house was irreparably damaged, they 'rode out the landslide' without injury. Locat et al. (2014) discussed some of the apparent differences among spread-type landslides.

3.10 Chemical Amelioration of Sensitive Marine Clays

3.10.1 Salt Addition – NaCl

The first application of chemistry to a quick-clay landslide problem was in 1953 after a 100,000m^3 spread at Bekkelaget destroyed 100 m of the highway connecting Oslo to the rest of Europe (Eide and Bjerrum 1955). The debris liquidity inhibited rebuilding of the highway. Professor Ivan Rosenqvist, University of Oslo,

demonstrated how mixing NaCl into the liquid debris would transform it into a plastic material of sufficient strength to allow reconstruction of the highway.

3.10.2 Lime Piles and Hydroxy-Aluminium Piles

Broms and Boman (1979) introduced 'lime piles' as a means of increasing the bearing capacity of sensitive clays. Unslaked lime is mixed into the sensitive soil, and pozzolanic (cementing) reactions of the calcium oxide with the aluminum-bearing minerals strengthen the soil. Lime piles have become a standard practice. Bryhn et al. (1983) investigated hydroxy-aluminium, ($Al(OH)_{2.5}Cl_{0.5}$), as an additive to strengthen sensitive clays. It works if calcium carbonate is present, or if additives that generate the pozzolanic reactions are introduced. Over time, the strengthening effects of both methods extend into the untreated adjacent soil; the hydroxy-aluminium effects extend further and more rapidly. Neither method is readily adaptable to application over large areas, or great depths. Soil disturbance during mixing of additives into the clay, the number of piles required and the pile length limit the application of the pile methods to landslide amelioration.

3.11 KCl Introduction by Diffusion from Salt Wells

In the early 1970s, when a new highway intersection in Northeastern Oslo was designed, it was decided to use salt addition to increase the undisturbed strengths of the sensitive clay sediments. The salt would also reflocculate and strengthen high sensitivity sediments disturbed by construction activities. Moum et al. (1968) had demonstrated that K^+ diffused most quickly through samples of intact quick-clay, and was the most effective in increasing the undisturbed and remolded strengths While Na^+ (0.99 Å) is smaller than K^+ (1.37 Å), hydrated Na^+ is larger than hydrated K^+ and its diffusion coefficient is only 2/3 that of K^+. Also, hydrated K^+ has a greater affinity to cation exchange sites and a 50% greater effect on the soil behavior. 2629 salt wells of 15 cm diameter and 15–16 m depth, at a grid spacing of 1.5 m, were drilled over an area of 6000 m^2 and filled with solid KCl (Helle et al. 2017). Investigations a few years after installation showed remarkably improved geotechnical behavior, and the highway interchange was completed. Subsequently, 3 boreholes were investigated in 2002 and 2 more in 2013. The results are analyzed by Helle et al. (2016). Their assessment was that KCl salt wells are very promising. A long-term advantage of KCl is that, as leaching continues over centuries and the salt concentration gradually decreases, K^+ should remain as the dominant pore-water and exchangeable cation for centuries; consequently, the sediment's sensitivity will remain low. This approach is truly long term.

3.12 Chemical Amelioration of Landsliding in Sensitive Clays

The quick-clay landslide problem can be addressed by: 1) prevent the triggering landslide in the weathered riverbank; or 2) prevent the slide from advancing into the quick clay beyond the weathered zone. Strategy one requires: earthworks at the slope base and/or slope height and slope angle reductions. These actions have safety and soil disposal challenges that make them impractical for most sites. Strategy two can be addressed by chemical modification of the high-sensitivity clay adjacent to the weathering crust using salt wells; the design of the salt-well array would be site dependent.

KCl introduction by diffusion from salt wells is feasible: installation need not disturb the riverbank; the wells are of small diameter; and the hydraulic pressure remains hydrostatic. KCl diffusion progressively improves undisturbed and post-failure soil strengths (Helle et al. 2016, 2017); and is long term. KCl leaching should not pose a river water quality problem and the site can be avoided as a drinking water source. This approach should be very effective in Scandinavia, and in non- to lightly-cemented sediments in North America. It should also be beneficial in cemented, high-sensitivity sediments.

3.13 Concluding Remarks

The interactions of chemical factors – depositional environment, particle mineralogy, changes in pore-water chemistry, oxidizing or reducing conditions, cementation (or lack thereof) and more – in determining the physical properties of the post-glacial, sensitive, marine clays and in changing their behavior, pose a challenge to the geotechnical community. Limits to bearing capacity, susceptibility to disastrous landslides and the ease with which limits can be exceeded, demand that practitioners be familiar with their properties and how those properties can change, for better or worse, as a consequence of what seem to be innocuous actions. Chemistry played many roles in the development of the high sensitivity sediments; it shows great promise in providing solutions to problems, including for the most dramatic one of quick clay landslides.

Acknowledgements I wish to recognize: Murray Milford who introduced me to clay mineralogy; the late Cand. Real Johan Moum who introduced me to the chemistry of quick-clays, and the late L. H. Bowen who identified the iron oxides in the quick clays as being nanometer-sized, detrital, crystalline hematite and magnetite. I thank Dr. Mike Long for his insightful comments.

References

Bjerrum L (1955) Stability of natural slopes in quick clay. Géotechnique 5:101–119
Broms BB, Boman P (1979) Lime columns – a new foundation method. In: American Society of Civil Engineers, Proceedings 105, GT4, pp 539–556
Bryhn OR, Löken T, Aas G (1983) Stabilization of sensitive clays with hydroxy-aluminium compared with unslaked lime. In: Proceedings of the eighth European conference on soil mechanics and foundation engineering, Helsinki, vol 2, pp 885–896
Demers D, Robitaille, Locat P, Potvin J (2014) Landslides in sensitive clays. Springer, Dordrecht
Eden WJ, Mitchell RJ (1970) The mechanics of landslides in Leda clay. Can Geotech J 7:285–296
Eide O, Bjerrum L (1955) The landslide at Bekkelaget. Géotechnique 5:88–100
Filion L, Quinty F, Bégin C (1991) A chronology of landslide activity in the valley of Rivière du Gouffre, Charlevoix, Quebec. Can J Earth Sci 28:150–256
Helle TE, Nordal N, Aagaard P, Lied OK (2016) Long-term-effect of potassium chloride treatment on improving the soil behavior of highly sensitive clay – Ulvensplitten, Norway. Can Geotech J 53:400–422
Helle TE, Aagaard P, Nordal S (2017) Improving the post-failure properties in quick clays by treatment with potassium chloride. In: Thakur V, L'Heureux J-S, Locat A (eds) Landslides in sensitive clays. From research to implementation. Springer, Dordrecht, pp 45–55
Karrrow PF (1972) Earth flows in the Grondines and Trois Rivières areas, Quebec. Can J Earth Sci 9:561–573
Kenney TC, Moum J, Berre T (1967) An experimental study of bonds in natural clay. In: Proceedings of the geotechnical conference, Oslo, vol 1
La Salle P, Chagnon J-Y (1968) An ancient landslide along the Saguenay River, Quebec. Can J Earth Sci 5:548–549
L'Heureux J-S, Locat A, Leroueil S, Demers D, Locat J (2014) Landslides in sensitive clay. ISSN 1878–9897, pp 15–24
Locat A, Leroueil S, Jostad HP (2014) Failure mechanisms of spreads in sensitive clays. Landslides in sensitive clay, ISSN 1878–9897, pp 279–290
Loiselle A, Massiera M, Sianani UR (1971) A study of the cementation bonds of the sensitive clays of the Outardes River region. Can Geotech J 8:479–498
Moum J, Sopp OI, Løken T (1968) Stabilization of undisturbed quick clay by salt wells. Norwegian Geotechnical Institute, Publication 81
Moum J, Löken T, Torrance JK (1971) A geochemical investigation of the sensitivity of a normally consolidated clay from Drammen, Norway. Géotechnique 21(4):329–340
Murad E (1988) Properties and behavior of iron oxides as determined by Mössbauer spectroscopy. Iron in soils and clay minerals. D. Reidel Publishing Company, Dordrecht
Tavenas F, Chagnon J-Y, LaRochelle P (1971) The Saint-Jean-Vianney landslide: observations and eyewitnesses accounts. Can Geotech J 8:463–478
Torrance JK (1983) Towards a general model of quick clay development. Sedimentology 30:547–555
Torrance JK (2012) Landslides in quick clay. In: Landslides: types, mechanisms and modeling. Cambridge University Press, Cambridge, pp 83–94
Torrance JK (2014) Chemistry, sensitivity and quick-clay landslide amelioration. Landslides in sensitive clay. ISSN 1878–9897
Torrance JK, Ohtsubo M (1995) Ariake Bay quick clays: a comparison with the general model. Soils Found 35:11–19
Torrance JK, Percival JB (2003) Experiences with selective extraction procedures for iron oxides. In: 2001. A clay odyssey, Proceedings of the 12th international clay conference, Bahia Blanca, Argentina, Elsevier, Amsterdam
Torrance JK, Hedges SW, Bowen LH (1986) Mössbauer spectroscopic study of the iron mineralogy of post-glacial marine clays. Clay Clay Miner 34(3):314–322

Chapter 4
Improving the Post-failure Properties in Quick Clays by Treatment with Potassium Chloride

Tonje Eide Helle, Per Aagaard, and Steinar Nordal

Abstract Installation of salt wells filled with potassium chloride may be used as a ground improvement method in quick-clay hazard areas. The migration of potassium chloride is self-driven by molecular diffusion. The effectiveness of improving the geotechnical properties and the time to do so, depend on hydrogeological conditions at the site, original pore water composition and concentration, adsorbed ions, mineral type, and cation exchange capacity. Increased salt content in the pore water decreases the repulsive forces acting between the mineral surfaces. By decreasing the repulsive forces, the liquid limit and remolded shear strength increase, indicating the improvement of the post-failure properties. The clay particles no longer repel one another, ultimately preventing development of retrogressive landslides.

4.1 Introduction

In Norway, quick clays are defined by a remolded shear strength of less than 0.5 kPa (NGF 1982). The salt content in quick clays is almost always less than 2 g/l (Torrance 1979), and at salt contents below 1 g/l they may behave as a liquid when remolded due to large repulsive forces between the clay mineral surfaces caused by overlapping diffuse-double layers (van Olphen 1963; Bjerrum et al. 1969; Moum et al. 1971). Clays with a remolded shear strength of less than 1 kPa (Thakur et al. 2014), or a liquidity index exceeding 1.2 (Leroueil et al. 1983), pose a risk for large, retrogressive flow-slides.

T.E. Helle (✉)
Norwegian University of Science and Technology (NTNU), Trondheim, Norway

Norwegian Public Roads Administration (NPRA), Trondheim, Norway
e-mail: tonje.eide.helle@ntnu.no

P. Aagaard
University in Oslo, Oslo, Norway
e-mail: per.aagaard@geo.uio.no

S. Nordal
Norwegian University of Science and Technology (NTNU), Trondheim, Norway
e-mail: steinar.nordal@ntnu.no

V. Thakur et al. (eds.), *Landslides in Sensitive Clays*, Advances in Natural and Technological Hazards Research 46, DOI 10.1007/978-3-319-56487-6_4

Great emphasis is placed on preventing triggering of initial slides in Norwegian quick clay hazard zones. Counter fills, soil added at the foot of quick-clay slopes, are often used as landslide mitigation. However, many quick clay hazard zones are situated in areas where counter fills are not a preferable solution, either due to the terrain constraints, environmental issues, existing buildings or areas of historical value, amongst others. Preventing retrogressive development by treating the quick clay with salt wells may be a better solution. Retrogressive development can be inhibited by increasing the liquid limit beyond the natural water content, preventing the soil material from being liquid when remolded.

The liquid limit and the remolded shear strength increase with increasing salt content in the pore water (Moum et al. 1968; Løken 1968 amongst others). Potassium, especially has a greater beneficial effect on the post-failure properties in quick clay compared to other additives (Moum et al. 1968; Løken 1968; Torrance 1975). Potassium chloride (KCl) was successfully used in salt wells for ground improvement on a construction site in a quick clay area at Ulvensplitten, Oslo, Norway in the 1970s (Eggestad and Sem 1976), improving the fall cone undrained and remolded shear strength and the Atterberg limits. Ground investigations carried out 40 years after installation show that the effect of the treatment remains, and is considered to be a permanent effect in an engineering time scale (Helle et al. 2016).

Salt wells filled with KCl were installed in January 2013 at the Dragvoll research site in Trondheim, Norway in order to get a better understanding of how the geochemical treatment improves the geochemical properties and how the salt migration is affected by local hydrogeology.

4.2 Changed Ion Composition Due to Leaching of Post-glacial Clays

The salt content in the depositional environment for the Scandinavian clays may have been 30–35 g/l, dominated by NaCl (Moum et al. 1971; Mitchell and Soga 2005). Clay minerals flocculate at such high salt contents in their depositional environment, and orient themselves in complex edge-to-edge and edge-to-face orientations. Creating a structure of agglomerates of flocculated particles with large water-filled voids, forming a very complicated ‘house-of-cards’-like structure with both clay and silt sized particles in the matrix (Rosenqvist 1946; Torrance 2012). The high salt content suppresses the diffuse double-layer surrounding the clay minerals, and the repulsive forces between the mineral surfaces becomes low. As long as the salt content is high, and the repulsive forces are small, the structure is stable (van Olphen 1963). Sodium (Na^+) is initially the abundant ion both in the pore water and in the adsorbed positions on the mineral surface in clays sedimented in a marine environment (Fig. 4.1a).

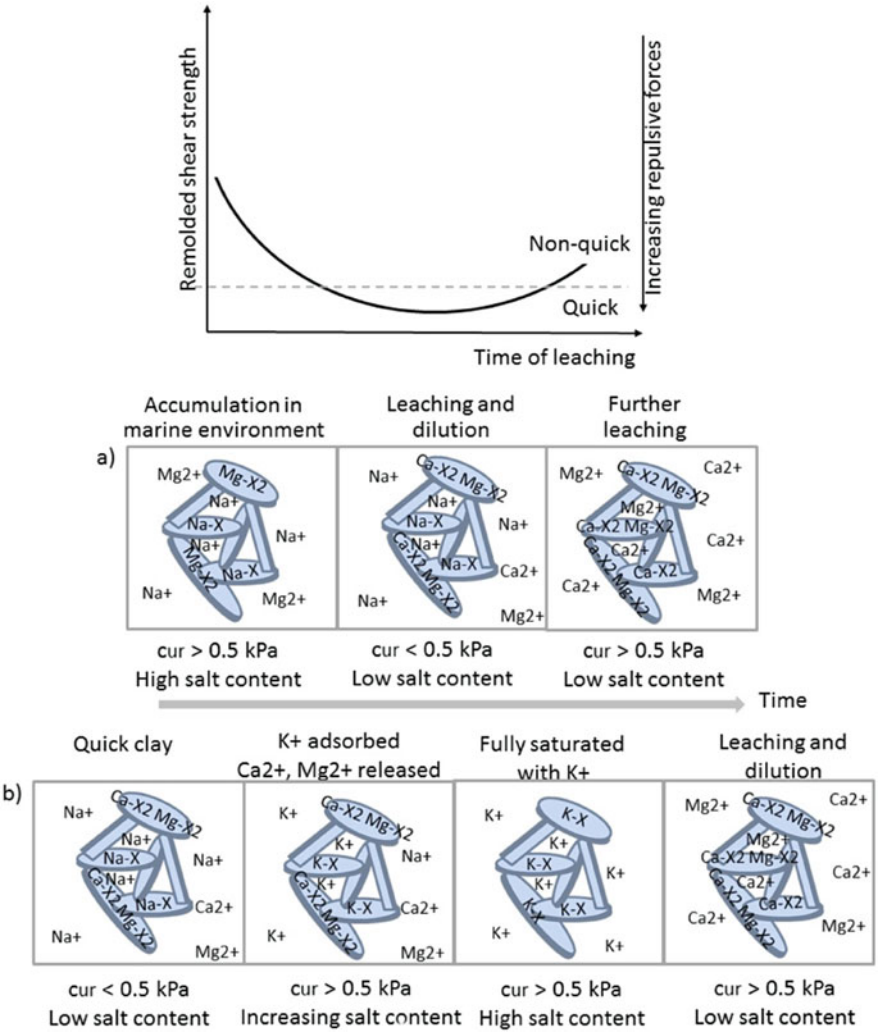

Fig. 4.1 Ions in solution (I^{i+}) and adsorbed on the mineral surfaces ($I\text{-}X_i$), where i is the valence and X_i is the number of occupied charge sites on the mineral surface. (**a**) The natural process of leaching and diluting the pore water in marine clays, and (**b**) the introduction of KCl to the clay-water system

Torrance (1983, 2014) states that chemical factors play a major role in quick-clay development. Isostatic uplift has allowed meteoric groundwater flow to migrate through the clay deposits, diluting and changing the ion composition in the pore water. Flowing groundwater is often dominated by divalent ions such as calcium (Ca^{2+}) and magnesium (Mg^{2+}), both of which are preferred over Na^{+} by the

mineral surface (Løken 1968; Appelo and Postma 2005; Mitchell and Soga 2005). Ca^{2+} and Mg^{2+} are adsorbed on the mineral surface (Ca-X_2 and Mg-X_2 in Fig. 4.1), and Na^{+} is released into the pore water (Fig. 4.1a). At this stage, the salt content is decreased to such an extent that the diffuse double-layer thicknesses increase, the repulsive forces between the mineral surfaces increase and the soil turns liquid when remolded.

Over a long period of leaching, more and more Ca^{2+} and Mg^{2+} is introduced, and Na^{+} is depleted in the clay-water system. The divalent ions then dominate both the composition in the pore water and the adsorbed positions. According to van Olphen (1963), the thickness of the double layer decreases by a factor of two in a divalent solute compared to a monovalent solute at the same normality. Even though the salt content is still low, the divalent ions suppress the diffuse double-layer to a greater extent than does Na^{+}. Consequently, the repulsive forces decrease, and the clay particles no longer disperse when remolded, and the clay ceases to behave as a quick clay.

4.3 Potassium Chloride as Ground Improvement

Potassium (K^{+}) is preferred over Na^{+} by the clay mineral surface due to a smaller hydrated radius and larger ionic potential. Thus, the charge of K^{+} is more 'effective' than for Na^{+}, even though they are cations of same valence. Therefore, K^{+} has a greater effect on suppressing the diffuse double-layer and reducing the repulsive forces. Introducing potassium chloride (KCl) to the clay-water system in quick clays increases the salt content in the pore water, and reduces the repulsive forces between the clay mineral surfaces (Fig. 4.1b). K^{+} has lower exchange power than Mg^{2+} and Ca^{2+}. Nevertheless, introducing large concentrations of K^{+}, the clay mineral surface releases the divalent ions into the pore water, adsorbing K^{+}. With time, leaching will take place, reducing the salt content. However, as Na^{+} is washed out of the system, remaining K^{+} and the divalent ions introduced by the leaching water will keep suppressing the diffuse double layer to such an extent that the remolded shear strength exceeds 1.0 kPa (Helle et al. Submitted).

The described process is tested in the field. Salt wells were installed to 15–16 m depth in a quick clay deposit at Ulvensplitten, Oslo, Norway in 1972, covering an area of 6000 m^2 (Eggestad and Sem 1976). Two years after installation, the remolded shear strength was increased from less than 0.5 kPa to 10–45 kPa, reducing the sensitivity from 12–80 to 1–3. Ground investigations 40 years after installation, show that the non-quick behavior remains. Even though the clay deposit has been leached to its original salt content of only 0.5 g/l at 14.5 m depth, the clay is not quick. This is caused by the ion composition in the pore water having changed from being dominated by Na^{+}, to being dominated by K^{+} and divalent ions with a higher ability to suppress the diffuse double layer, reducing the repulsive forces (Helle et al. 2016). Helle et al. (Submitted) suggest that a presence as little as 20%

of the major cations consisting of K^+, Mg^{2+} and Ca^{2+} (all in meq/l) inhibits the clay to develop highly sensitive, quick behavior, even at low salt contents.

4.4 Dragvoll Research Site

The Dragvoll research site in Trondheim, Norway is located at around 156 m above present sea level. The marine limit in the Trondheim area is around 175–180 m above present sea level (Kjemperud 1981; Hafsten 1983). The total thickness of the sediments is around 50 m, lying in between distantly outcropping bedrock. Due to the isostatic uplift, the accumulation of sediments with time took place at shallower water. Beach sediments are found at 160 m above sea level in the area (Hafsten 1989).

The ground water table at the site varies between 0.5 m and 1.0 m. Gravel, shells and shell fragments are commonly found in the upper 4 m of the soil and are occasionally found at greater depths. The soil changes from dry crust at the top with quick clay being encountered at 3 m and 4 m (Bryntesen 2013). Millimeter thick silt and sand layers are found with few cm spacing throughout the clay deposit. At around 7.5–8.0 m depth the thickness of these closely spaced silt/sand layers are around 1–2 cm.

The quick clay at Dragvoll is very sensitive, with a remolded shear strength of 0.5 kPa at 4 m depth, decreasing to less than 0.1 kPa at 5 m depth. The plastic limit decreases from 18% at 4 m depth to 15% at 8 m depth. The liquid limit is lower than the natural water content; 21–24%, also decreasing with depth. Leaching has reduced the salt content to as little as 0.6–0.7 g/l, with Na^+ as the abundant cation in the pore water (Helle et al. Submitted).

Six salt wells constructed of PE pipes with an outer diameter of 63 mm, were installed January 2013. The pipes were slotted from 4 m to 8 m depth, covered with a geotextile, allowing salt to migrate into the quick clay. The wells were filled with granular KCl, and refilled regularly to maintain high concentration. RCPTU soundings and 54 mm piston samples were extracted around salt-well no. 2 in April 2016; 3.2 years after installation.

4.5 Salt Migration and Improved Post-failure Properties

The conductivity measurements carried out with the resistivity piezocone (RCPTU), reflect the extent and direction of the salt plumes around the well. The salt migration is greatly affected by permeable layers. Permeable layers were detected at around 7–8 m depth allowing a greater salt plume extent at these depths (Fig. 4.2).

Increased conductivity with depth, and decreasing conductivity with distance from the well correspond well with the salt content in extracted pore water samples

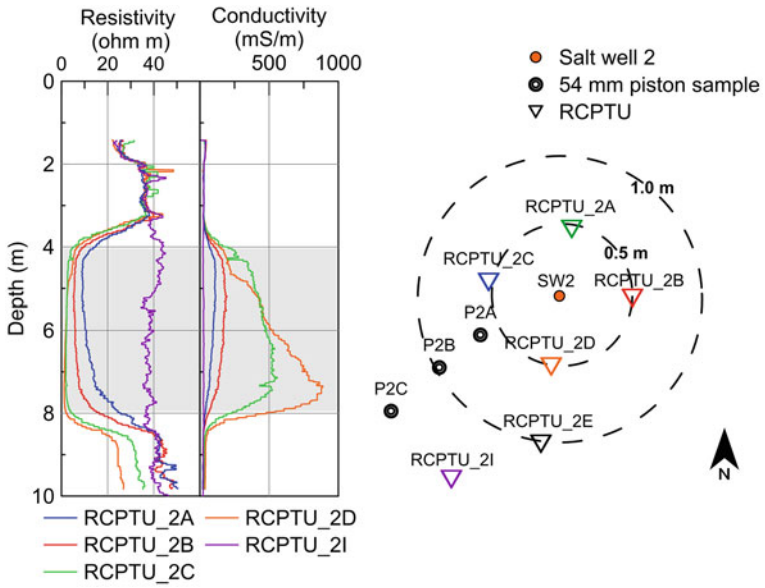

Fig. 4.2 Resistivity and conductivity profiles in a distance of 50 cm from salt-well no. 2. RCPTU2I 1.5 m from the salt well, is included to illustrate the initial condition of the quick clay

from clay samples in nearby boreholes (Fig. 4.3). Increasing salt content increased the remolded shear strength as well as the fall cone undrained shear strength.

The water content is practically unchanged in the salt-treated clay (Fig. 4.3), whereas the plastic limit increased to a maximum of around 22%. The liquid limit increased up to, and a little beyond, the natural water content. The remolded shear strength increased beyond 0.5 kPa, to a maximum of 6 kPa at 6.5 m depth 64 cm from the salt well. The undrained fall-cone shear strength increased up to around 40 kPa at the level of the bottom of the salt well. The remolded shear strength is unchanged and around 0.5 kPa at 0.5 m below the bottom of the salt well at distances of 64 cm and 100 cm from the salt well. At the same depth, the conductivity is at its initial value (solid red and blue line in Fig. 4.3).

Increased concentrations of K^+ are found in the samples in a distance of 64 cm and 100 cm form the well (Fig. 4.4). There is a simultaneous increase of Na^+, Mg^{2+} and Ca^{2+}. This is due to the ion exchange reactions on the clay mineral surfaces when K^+ enters the adsorbed positions. At the same time the clay mineral surfaces release Na^+, Mg^{2+} and Ca^{2+} to the pore water, and the cations migrate to distances from the well, accompanied by the increased concentration of chloride migrating from the salt wells. No changes from the initial concentrations are observed in the samples extracted 1.5 m from the salt well. The cation concentrations are at their initial values at 8.5 m depth, 64 cm from the salt well, as detected in the conductivity measurements (Fig. 4.3).

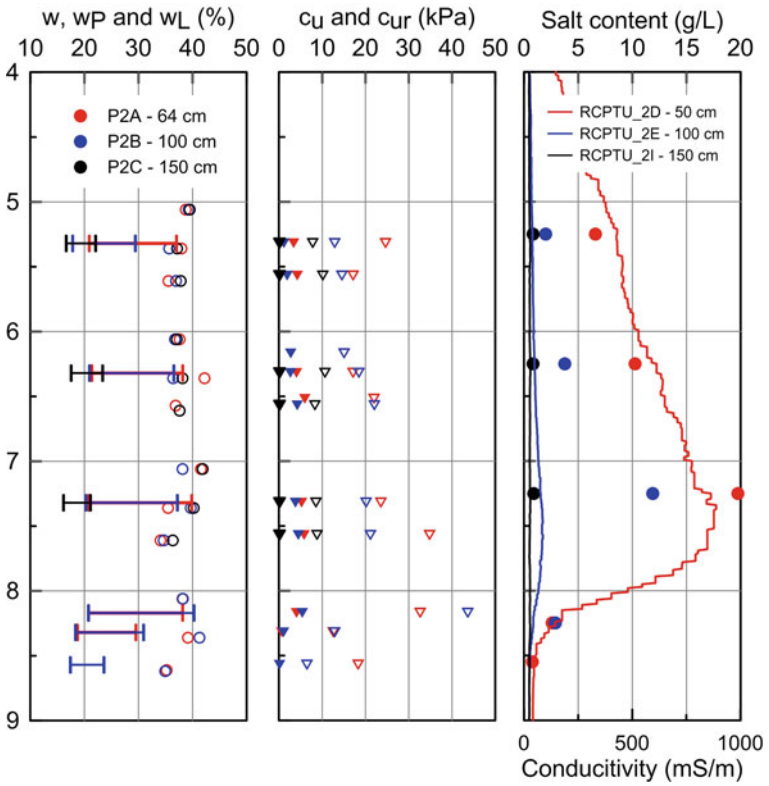

Fig. 4.3 Water content (w), plasticity (w_P) and liquid limit (w_L), undrained fall cone (c_u) and remolded (c_{ur}) shear strength, salt content and conductivity (*solid lines*) along, or in close vicinity to the fastest flow-line around salt-well no. 2

4.6 Discussion and Conclusions

Before installing the salt wells, the ratio of Na^+ over the sum of major cations (Na^+, K^+, Mg^{2+} and Ca^{2+}), all in meq/l, in the pore water in the original quick clay at Dragvoll was more than 85%. K^+, Mg^{2+} and Ca^{2+} all have a greater impact on suppressing the diffuse double-layer, and reducing the repulsive forces between the mineral surfaces, than Na^+ (Løken 1968; Appelo and Postma 2005; Mitchell and Soga 2005). Decreasing the repulsive forces between the minerals, the silt and clay particles are more prone to interacting with one another, and the soil is less prone to turn into a liquid when remolded (Fig. 4.5). Treating the quick clays at Dragvoll and Ulvensplitten with KCl, increased the remolded shear strength significantly from below 0.5 kPa to more than 1 kPa, and reduced the liquidity index to less than 1.2. The previously low-plasticity clay was changed to be of medium plasticity. This improvement is still found in Ulvensplitten clay with low salt content (< 1 g/L) whereas the ratio of K^+, Mg^{2+} and Ca^{2+} over major cations in the pore water exceeds only 20% (Helle et al. 2016, Submitted).

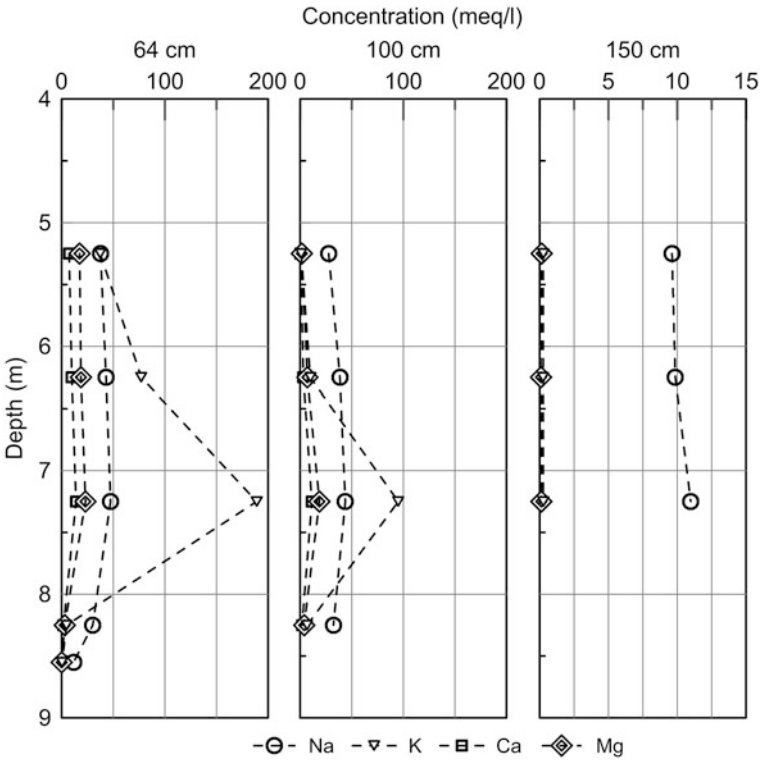

Fig. 4.4 Cations in the extracted pore water from clay samples 64–150 cm from salt-well no. 2 (Note that the scale of the horizontal axis 150 cm from the well is different than the others. Results also presented in Helle et al. (Submitted))

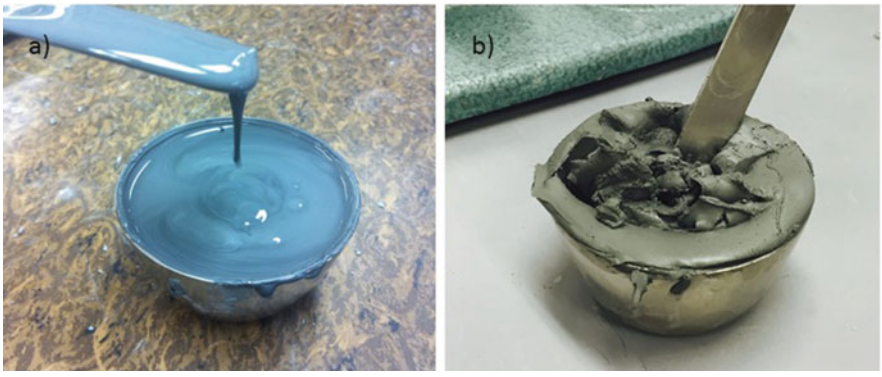

Fig. 4.5 (**a**) Remolded quick clay from Dragvoll. (**b**) Remolded salt-treated clay from Dragvoll

The salt migration at Dragvoll is partly driven by diffusion due to the steep concentration gradient away from the salt wells. Furthermore, the density difference of the fluid in the well and in the pore water in the surrounding clay, may cause increased velocity along permeable layers. The salt in the permeable layers will in addition to the horizontal transport, also diffuse vertically into the clay volume surrounding the permeable layers, reducing the time it takes to stabilize the quick-clay volume. The salt transport on the opposite side of the well is slightly slower as the salt migrates in one predominant direction from each well. Nevertheless, installing the salt-well grid with a center-to-center distance of 1.5–2.0 m may be sufficient to stabilize the quick clay volume within 3 years due to overlapping oppositely directed salt plumes (Helle et al. Submitted). This is, however, greatly dependent on the site conditions.

The time it takes for the salt to migrate into the clay volume depends on the hydrogeological conditions in the field together with mineral type, cation exchange capacity, adsorbed ions and original pore water composition and concentration. Helle et al. (Submitted) suggest that a ratio of the sum of K^{+}, Mg^{2+}, Ca^{2+} over the sum of major cations in the order of 20%, is sufficient to change the clay behavior from quick to non-quick, even at low salt contents.

KCl improves the post-failure properties in the quick clay without the necessity of mixing, causing major soil disturbance. The migration of salt is a self-driven process, and the stabilized clay volume increases with time due to concentration and density gradients (Fig. 4.6). The remolded shear strength in the KCl-treated quick clay exceeds 1 kPa, and the liquidity index is reduced below 1.2. Consequently, the sensitive clay particles will no longer liquefy when remolded, and the KCl-stabilized clay volume will work as a barrier against flow slides and spreads. The effect is considered to be permanent due to the irreversibly changed pore water composition (Helle et al. 2016, Submitted).

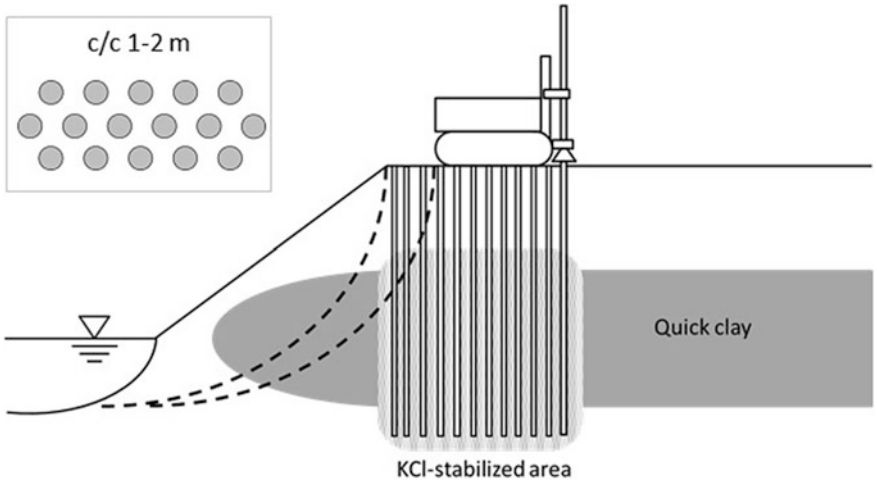

Fig. 4.6 The KCl-stabilized clay volume increases with time due to diffusion and advective flow. The KCl-stabilized clay works as a barrier against successive backscarp failures

Acknowledgments The authors express their sincere gratitude to Prof. Emeritus J.K. Torrance for his discussions and comments, improving the manuscript, as well as all the people that have contributed in discussions during this project; especially Arnfinn Emdal, Mike Long, Tor Løken, Øyvind A. Høydal, Elisabeth Gundersen and Anders Samstad Gylland. A number of people have contributed in ground investigations and laboratory work, all of which made it possible to carry out this extensive work.

References

Appelo C, Postma D (2005) Geochemistry, groundwater and pollution, 2nd edn. Balkema, Leiden

Bjerrum L, Løken T, Heiberg S et al (1969) A field study of factors responsible for quick clay slides. In: Proceedings of the 7th International Conference on Soil Mechanics and Foundation Engineering (ICSMFE), vol 2, Mexico 1969, pp 531–540

Bryntesen RN (2013) Block Sample Testing at Dragvoll. Project thesis, Norwegian University of Science and Technology

Eggestad A, Sem H (1976) Stability of excavations improved by salt diffusion from deep wells. In: Proceedings of the 6th European conference on soil mechanics and foundation engineering, Vienna, March 1976, pp 211–216

Hafsten U (1983) Shore-level changes in South Norway during the last 13,000 years, traced by biostratigraphical methods and radiometric datings. Nor Geogr Tidsskr 37:63–79

Hafsten U (1989) Dragvoll-Stokkan området ca. 11 500 år før nå. UnitNytt, no. 2/1989. pp 16–20 (In Norwegian)

Helle TE, Nordal S, Aagaard P et al (2016) Long-term effect of potassium chloride treatment on improving the soil behavior of highly sensitive clay — Ulvensplitten, Norway. Can Geotech J 53(3):410–422. doi:10.1139/cgj-2015-0077

Helle TE, Aagaard P, Nordal S (Submitted) In-situ improvement of highly sensitive clays by potassium chloride migration. Submitted to J Geotech Geoenviron

Kjemperud A (1981) A shoreline displacement investigation from Frosta in Trondheimsfjorden, Nord-Trøndelag, Norway. Nor Geol Tidsskr 61:1–15

Leroueil S, Tavenas F, Le Bihan JP (1983) Propriétés caracteristiqués des argiles de l'est du Canada. Can Geotech J 20(4):681–705. doi:10.1139/t83-076

Løken T (1968) Kvikkleiredannelse og kjemisk forvitring i norske leirer. Norwegian Geotechnical Institute, Oslo, Norway. NGI Publication No. 75 (In Norwegian)

Mitchell JK, Soga K (2005) Fundamentals of soil behavior, 3rd edn. Wiley, New Jersey

Moum J, Sopp OI, Løken T (1968) Stabilization of undisturbed quick clay by salt wells. Norwegian Geotechnical Institute, Oslo, Norway. NGI Publication No. 81

Moum J, Løken T, Torrance JK (1971) A geochemical investigation of the sensitivity of a normally consolidated clay from Drammen, Norway. Géotechnique 21(4):329–340

Norwegian Geotechnical Society (NGF) (1982) Veiledning for symboler og definisjoner i geoteknikk: Identifisering og klassifisering av jord. Norwegian Geotechnical Society, Oslo, Norway. NGF notification No. 2 (In Norwegian)

Rosenqvist IT (1946) Om leirers kvikkaktighet. Norwegian Public Road Administrations, Oslo, Norway. Meddelelsen fra Vegdirektøren No. 3. pp. 29–36 (In Norwegian)

Thakur V, Degago S, Oset F et al (2014) Characterisation of post-failure movements of landslides in soft sensitive clays. In: L'Heureux, Locat, Leroueil et al (eds) Landslides in sensitive clays: From geoscience to risk management. 1st international workshop on landslides in sensitive clays, Quebec, October 2013. Springer, Dordrecht, pp 91–104

Torrance JK (1975) On the role of chemistry in the development and behaviour of the sensitive marine clays of Canada and Scandinavia. Can Geotech J 12:326–335

Torrance JK (1979) Post-depositional changes in the pore water chemistry of the sensitive marine clays of the Ottawa area, eastern Canada. Eng Geol 114:135–147

Torrance JK (1983) Towards a general model of quick clay development. Sedimentology 30: 547–555

Torrance JK (2012) Landslides in quick clay. In: Clague, Stead (eds) Landslides: types, mechanisms and modeling. Cambridge University Press, Cambridge, pp 83–94

Torrance JK (2014) Chemistry, sensitivity and quick-clay landslide amelioration. In: L'Heureux, Locat, Leroueil et al (eds) Landslides in sensitive clays: From geoscience to risk management. 1st international workshop on landslides in sensitive clays, Quebec, October 2013. Springer, Dordrecht, pp 15–24

van Olphen H (1963) An introduction to clay colloid chemistry. Wiley, New York

Chapter 5
CPTU Classification Diagrams for Identification of Sensitive Clays

Anders Samstad Gylland, Rolf Sandven, Alberto Montafia, Andreas Aspmo Pfaffhuber, Kristoffer Kåsin, and Mike Long

Abstract When dealing with slope stability considerations in deposits where sensitive and quick clays might be encountered it is vital to map the extent of these clays. For the geotechnical engineer, the cone penetration test with pore pressure measurement (CPTU) is a powerful tool in this respect. With its combined measurement of tip resistance, pore pressure and sleeve friction, the CPTU holds a great potential for identification of quick and sensitive clays. Such interpretations can be done based on measured data directly or by combining parameters in dimensionless numbers. Amongst the more popular dimensionless numbers are the pore pressure ratio (B_q), the cone resistance number (N_m) and the friction ratio (R_f). Diagrams exist which allow classification of soils based on the combination of such numbers. Robertson (Can Geotech J 27:151–158, 1990) is one widely used example. However, In Norway, it is found that existing diagrams to a large extent fail to identify sensitive and quick clays. Based on a database of 10 Norwegian sites a new set of classification diagrams are presented with focus on identifying quick and sensitive clays. The diagrams are based on a pore pressure ratio where the tip pore pressure is used (u_1) rather than the u_2-position as this is found to better capture the actual collapsible response of sensitive clays. The cone resistance number is modified to also include an effect of overconsolidation (OCR) instead of only accounting for vertical effective overburden. Also, the friction ratio is normalized with pore pressure (u_1) rather than the cone resistance. Electrical resistivity values from R-CPTU-soundings are also included in the considerations. The outcome is a set of revised classification diagrams that provides more accurate identification of Norwegian sensitive and quick clays compared to existing classification diagrams.

A.S. Gylland (✉) • R. Sandven (deceased) • A. Montafia
Multiconsult ASA, Trondheim, Norway
e-mail: anders.gylland@multiconsult.no; Alberto.montafia@multiconsult.no

A.A. Pfaffhuber • K. Kåsin
Norwegian Geotechnical Institute (NGI), Oslo, Norway
e-mail: Andreas.a.pfaffhuber@ngi.no; Kristoffer.kaasin@ngi.no

M. Long
School of Civil Engineering, University College Dublin (UCD), Dublin, Ireland
e-mail: Mike.Long@ucd.ie

V. Thakur et al. (eds.), *Landslides in Sensitive Clays*, Advances in Natural and Technological Hazards Research 46, DOI 10.1007/978-3-319-56487-6_5

5.1 Motivation and Scope

Sensitive and quick clays are typically found in Norway, Sweden and Canada, and are characterized by a remoulded undrained shear strength (c_{ur}) that is considerably lower than the undisturbed shear strength (c_u). If the remoulded shear strength is less than 2.0 kPa, the material is classified as brittle in Norway and prone to progressive slope failure. If the remoulded shear strength is less than 0.5 kPa the material behaves like a liquid and is by the Norwegian definition termed quick clay. In geotechnical engineering, the presence of sensitive clays poses a major challenge. The landslides at Rissa in 1978, and more recently at the Skjeggestad bridge in Norway, are reminders of the potential devastating threats related to such soils. In a project, the geotechnical engineer must hence (1) determine if there is brittle clay present and (2) clarify its extent.

Of the several methods in the geotechnical toolbox, the CPTU is, with its combined measurement of tip resistance, pore pressure and sleeve friction, one of the most useful for soil classification and parameter determination. This field test has a great potential for identifying soft sensitive clays, but up to now, the available classification methods have not been accurate enough for this purpose.

This topic has been investigated in the NIFS project. NIFS is a joint venture between the Norwegian Water Resources and Energy Directorate (NVE), The Norwegian Railroad Administration (NNRA) and the Norwegian Public Roads Administration (NPRA). A main goal of the project is to coordinate guidelines and develop better tools for geotechnical design in quick clay areas. In this context, the possibility to create CPTU based classification diagrams that allow for a more accurate identification of sensitive and quick clays has been studied.

5.2 Basis for Study

The basis for the study has been a comprehensive collection and analysis of data from 10 different sites in Norway. The key sites and performed tests are listed in Table 5.1. The main focus has been on detection of brittle clays by means of multiple methods, and the main findings are available in NIFS report no. 2015-126 and Sandven et al. (2016a, b).

5.3 CPTU

In Norway, the Cone Penetration Test with pore pressure measurement (CPTU) is one of the most popular field-testing methods. The test is performed with an instrumented cylindrical probe with conical tip that is pushed into the ground at a constant rate of 20 mm/sec. The probe contains electronic transducers for recording

Table 5.1 Main sites and methods included in the study

Test site	Methods
Smørgrav	DT, CPTU, R-CPTU, ERT, PS
Kløfta	TOT, CPTU, R-CPTU, ERT, AEM, PS, BS
Klett	DT, TOT, CPTU, R-CPTU, ERT, EFVT, PS, BS
Fallan	TOT, CPTU, R-CPTU, ERT, EFVT, PS
Tiller	TOT, CPTU, R-CPTU, ERT, EFVT, PS, BS
Esp, Byneset	TOT, CPTU, R-CPTU, ERT, EFVT, PS, BS
Dragvoll	CPTU, R-CPTU, ERT, BS
Tiller	CPTU, R-CPTU, ERT, PS, BS, EFVT
Rissa	TOT, DRT, CPTU, R-CPTU, PS, BS

DT Rotational weight sounding, *DRT* Rotational pressure sounding, *TOT* Total sounding, *R-CPTU* CPTU with resistivity measurement, *ERT* Electrical Resistivity Tomography, *AEM* Airborne electro magnetics, *EFVT* Electrical field vane test, *PS* Piston sampling, *BS* Block sampling.

of the load against the cone, the force against the friction sleeve and the pore pressure at the location of the porous filter. A location immediately above the cone tip is selected as reference level for the pore pressure measurement (u_2). Pore pressure measured at the conical tip is referred to as u_1.

Measurements of corrected tip resistance (q_t), pore pressure (u_2) and sleeve friction (f_s) can be interpreted separately or combined to form various corrected and/or normalized parameters. There are both theoretical and empirical frameworks that allow interpretation of strength and stiffness parameters as well as aspects related to stress history and consolidation properties. There are also frameworks for classification of soil type (Begemann 1965, Jones and Rust 1982, Larsson and Mulabdic 1991, Olsen and Mitchell 1995, Robertson 1990, Robertson and Campanella 1983, Schmertmann 1978, Schneider et al. 2008, Senneset et al. 1989).

The classification diagram presented in Robertson (1990) is one of the more used in Norway. It incorporates the following parameters:

- The cone resistance number is defined as: $N_m = (q_t - \sigma_{v0})/\sigma_{v0}'$. $(q_t - \sigma_{v0})$ is often given as the net cone resistance q_n so that $N_m = q_n/\sigma_{v0}'$. σ_{v0} and σ_{v0}' are the total and effective vertical overburden stress respectively.
- The pore pressure ratio is given by: $B_q = (u_2 - u_0)/q_n$ where u_0 is the in situ pore pressure.
- The friction ratio is given by: $R_f = f_s * 100\,\%\,/q_t$

The classification diagrams from Robertson (1990) are shown in Fig. 5.1 together with readings from CPTU-soundings performed at the 10 test sites. It contains about 7000 data points. The CPTU-data is classified in three categories based on parallel sampling at the sites. Green: non-sensitive clay ($c_{ur} > 2.0$ kPa), Orange: sensitive/brittle clay ($0.5 < c_{ur} < 2.0$ kPa), Red: quick clay ($c_{ur} < 0.5$ kPa).

Although some of the basic properties of the classification chart are reflected through the dataset, such as increasing sensitivity with increasing B_q, one can see that the red "quick clay"-points are spread over ID 1, 3 and to some extent 4. In the

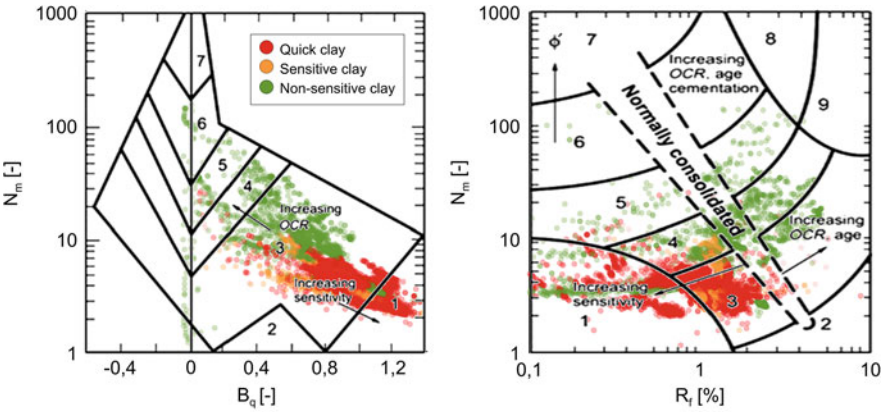

ID	Material	ID	Material
1	Sensitive, fine grained	6	Sands – clean sand to silty sand
2	Organic soils – peats	7	Gravelly sand to sand
3	Clays – clays to silty clays	8	Very stiff sand to OC clayey sand
4	Silt mixtures – clayey silt to silty clay	9	Very stiff, fine grained OC
5	Sand mixtures – silty sand to sandy silt		

Fig. 5.1 Robertson (1990) classification diagrams with data from the present study

original classification, only ID 1 suggests sensitive clay. Hence, there is a mismatch between the classification of Robertson (1990) and the behaviour of Norwegian sensitive clays. One reason is, of course, that the Robertson diagram is based mainly on Canadian soils, not Norwegian soils. Another factor is that the chosen parameters do not fully relate to the clay being sensitive or not. This is further elaborated in the following.

5.4 New Classification Diagrams

As demonstrated, there are mixed experiences with CPTU-based classification diagrams for detection of brittle materials and in many cases previously developed diagrams are misleading for indication of sensitive Norwegian clays. Recently Valsson (2016) improved the interpretation by developing 3D charts using B_q as well as q_t and f_s normalized with the vertical effective overburden stress. Here however, we here take the interpretation even one step further. Based on the Robertson (1990) charts new classification parameters are introduced to better capture the collapsible nature of sensitive clays and hence improve the accuracy of the classification.

5.4.1 Parameters

5.4.1.1 Cone Resistance Number, N_{mc}

The cone resistance number is the ratio between net resistance and vertical overburden stress. Its construction is hence of a similar nature as a bearing capacity factor relating shear stress and shear strength. The value of N_m should thus represent the failure mode around the cone. This is a useful aspect to cover in a classification diagram as one can expect different modes of mobilization and failure in a non-brittle material compared to a brittle material. However, in this respect one should take care in using parameters in the formulation that represents the desired effects as closely as possible. While q_n is a fair representation of the acting shear stress, σ_{v0}' is not optimal for representing shear strength. At a penetration rate of 20 mm/sec in clay, undrained conditions apply. Ladd and Foott (1974) have in their SHANSEP-adaption demonstrated that the preconsolidation stress is an important factor in determining the undrained shear strength of a clay. A revised cone resistance number, N_{mc}, is therefore constructed as shown in Eq. 5.1.

$$N_{mc} = q_n / \left(\sigma_A' + a\right) \tag{5.1}$$

In this equation a is the attraction and σ_A' the reference stress as defined in Eq. 5.2.

$$\sigma_A' = \sigma_c'^{m} \cdot \sigma_{v0}'^{(1-m)} \tag{5.2}$$

This expression is derived from the SHANSEP-framework where σ_c' is the preconsolidation stress and the stress exponent m accounts for the effect of unloading and swelling of the sediment. For Norwegian clays m is in the order of 0.7–0.8 (Karlsrud and Hernandez-Martinez 2013). This expression requires reliable values of the preconsolidation stress σ_c' so that a depth profile can be established. The preconsolidation stress should primarily be determined from oedometer test data, from known topographical information and previous terrain level. Secondarily from independent interpretation of CPTU data.

5.4.1.2 Pore Pressure Ratio, B_{q1}

As the collapse and remoulding of sensitive clays generates high pore pressures, the pore pressure ratio is an effective indicator of such materials. In normally consolidated clays $B_{q2} \geq 1.0$ (based on u_2) is common. In stiffer, overconsolidated clays, the B_{q2} – values in quick clays are usually significantly lower, often between 0.6 and 0.9 depending on the overconsolidation ratio. This difference in B_{q2} can to some extent be related to the location of the pore pressure sensor. Due to dilatancy

effects when the material flows around the cone edge, the measured pore pressures at the u_2 location are smaller than the pore pressure in the compression zone just beneath the tip (u_1). Due to this influence, the pore pressure ratio B_{q2} (based on u_2) is not a unique identification parameter in brittle materials and a pore pressure ratio based on u_1 (B_{q1}) might be better suited.

The revised expression for the pore pressure ratio B_{q1} hence becomes (Eq. 5.3):

$$\begin{aligned} B_{q1} &= (u_1 - u_0) / (q_n) \\ &= k^* (u_2 - u_0) / q_n \end{aligned} \tag{5.3}$$

In Eq. 5.3 the constant k is an empirical correction factor expressing the ratio between the pore pressure at various locations on the probe. Tentative values of k in various clays are according to Sandven (1990): Soft NC-clay: $k = 1.25$; Medium soft clay, low OCR: $k = 1.50$; Stiff OC-clay, high OCR: $k = 1.90$. Empirical relations between over-consolidation ratio OCR and pore pressure distribution around the probe can also be used (see e.g. Sully et al. 1988), see Eq. 5.4:

$$u_1 = u_2 + u_0{}^* (OCR - 0,66) / 1,43 \tag{5.4}$$

5.4.1.3 Friction Ratio, R_{fu}

The friction ratio, R_f, is usually created with the net cone resistance, q_n, as the normalizing reference. However, in soft sensitive clays, the most reliable parameter is often the pore pressure. This is due to the cone resistance showing values so low that effects of load cell resolution and accuracy comes into account. The pore pressure however is well within the accuracy range of the sensor. Further, interpretation of undrained shear strength from the pore pressure has shown to be the most reliable, compared to cone resistance, in Norwegian soft sensitive clays (Karlsrud et al. 2005). On this basis, the friction ratio is redefined using the excess pore pressure as shown in Eq. 5.5.

$$R_{fu} = f_s{}^* 100\% / \Delta u_1 \tag{5.5}$$

Here $\Delta u_1 = u_1 - u_0$ is based on the tip pore pressure using the same corrections as shown in Eqs. 5.3 or 5.4. This formulation has also the advantage of highlighting differences in pore pressure response, e.g. when passing from a sensitive clay into a silt layer.

5.4.1.4 Resistivity – R-CPTU

Resistivity readings from R-CPTU-soundings were available from several of the test sites and the interpreted resistivity values were included in the study for developing

classification diagrams. Unfortunately, the span in resistivity values in the zones of sensitive, quick and non-sensitive clay overlapped to such an extent that they were evaluated to not possess sufficient accuracy to be used as a general classification indicator in the type of diagrams as presented here. The measured resistivity depends on a magnitude of factors, including local mineralogy, and in order to be accurate, local correlations should be established for each site.

5.4.2 $N_{mc} - B_{q1}$ – Diagram

A classification diagram using N_{mc} and B_{q1} is shown in Fig. 5.2. The figure incorporates all 7000 data points from the 10 test sites included in this study as also shown in Fig. 5.1. Based on this, the following classification is suggested:

- $N_{mc} \leq 3.5$ and $B_{q1} \geq 0.75$: Sensitive/brittle clay
- $N_{mc} \leq 2.5$ and $B_{q1} \geq 1.00$: Quick clay

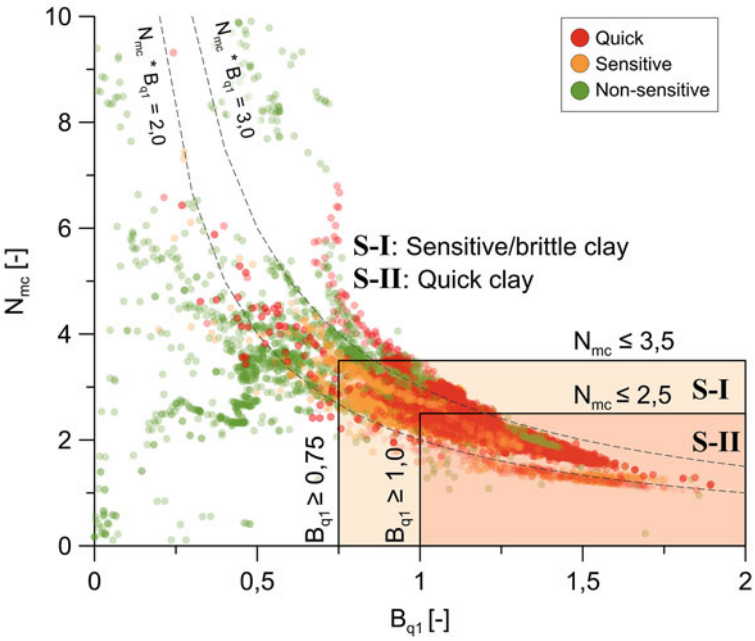

Fig. 5.2 N_{mc}—B_{q1} classification diagram

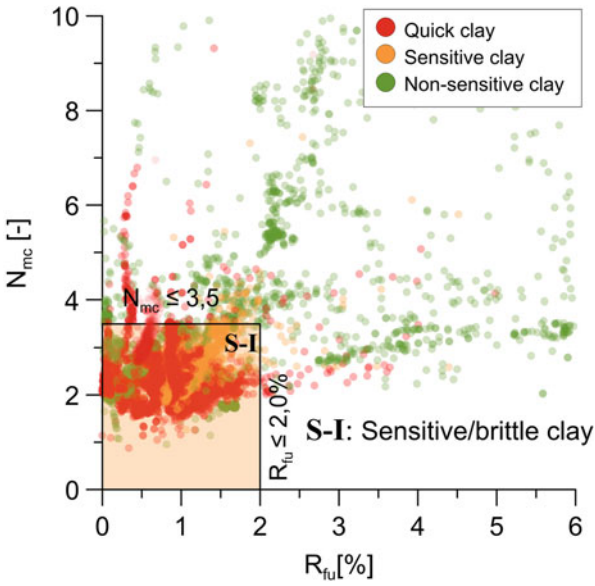

Fig. 5.3 N_{mc}–R_{fu} classification diagram

5.4.3 N_{mc} – R_{fu} – Diagram

Figure 5.3 includes the classification diagram using N_{mc} and R_{fu}. Based on this, the following classification is suggested:

- $N_{mc} \leq 3.5$ and $R_{fu} \leq 2.0\%$: Sensitive/brittle clay

5.5 Evaluation and Recommendations

The new diagrams in Figs. 5.2 and 5.3 gives a more accurate classification compared to the classification diagram by Robertson (1990) in Fig. 5.1. This is partly related to new limits for the boxes in the diagram and partly related to the modified parameters used. These new parameters stretch the data points to a larger extent along both axis, allowing more precise classification lines to be drawn. The classification diagrams are not ideal and there are some examples of sensitive clays falling outside the box and non-sensitive clays falling inside. However, for the main bulk of the data points, the classification is satisfactory.

Most CPTU-probes measure pore pressure at the u_2-position and hence the use of the presented diagrams rely on a correlation between u_1 and u_2. This introduces some uncertainty, but in general, using Eq. 5.4, the correlation between u_1 and u_2 is good for moderate levels of OCR, typical for most Norwegian sensitive clays. NIFS report no. 2015-126 includes a correlation diagram using only u_2 where the limits are S-1: $N_{mc} \leq 3.5$ and $B_{q2} \geq 0.65$, S-II: $N_{mc} \leq 2.5$ and $B_{q2} \geq 0.90$.

N_{mc} and B_{q1} are not independent parameters. Both parameters describe the same phenomenon, the failure mode around the cone tip. For sensitive clays, the failure mechanism gives low tip resistance and high pore pressures; reducing N_{mc} and increasing B_{q1} for increasing sensitivity. Following the data analysis of Karlsrud et al. (2005), both N_m and B_q (and hence N_{mc} and B_{q1}) relate to OCR. Mathematically it can be shown that $N_{mc} * B_{q1}$ should be in the order of 1.8–3.2 in sensitive clays. Lines showing $N_{mc} * B_{q1} = 2$ and 3 are included in Fig. 5.2 to illustrate this relationship. In turn this implies that N_{mc} alone can be a good classification parameter. This is utilized in Fig. 5.3 where N_{mc} is combined with R_{fu} in a classification diagram. However, this classification diagram is not as robust as the N_{mc}–B_{q1}-version. The main reason is uncertainties related to the sleeve friction. The first penetration of the CPTU-cone in a typical Norwegian sensitive clay is usually not sufficient to achieve complete remoulding of the material. As such, the sleeve friction measures then a state somewhere in-between intact and remoulded state. For two clays with the same remoulded fall cone reading, but with different toughness against remoulding, the sleeve friction can give distinctly different readings. Further, the measured sleeve friction in these clays is so low that it challenges the accuracy of the load cell.

To detect and classify sensitive and quick clays it is important to evaluate all available data and indicators, such as simple soundings and direct readings from the CPTU, in a unified interpretation. The proposed classification diagrams are a supplement to this, not a replacement. Further, the proposed diagrams are based on data from 10 sites and do not span all possible variations of soft sensitive clays. The authors therefore encourage a careful implementation of these diagrams into geotechnical practice in order to gain experience with their accuracy. This again would form the basis for a revised set of classification diagrams.

Acknowledgements Partners in the NIFS project are greatly acknowledged for the financial support and good discussions throughout the study. The board of the Norwegian Geotechnical Society (NGF) are also acknowledged for financial support. The authors want to extend thanks to Rambøll, Multiconsult, NGI, Norwegian Public Roads Administration and NGU for allowing the use of data in the study. The authors also wish to express their gratitude to the reviewer Dr. Maj Gøril Bæverfjord for her valuable comments.

References

Begemann HKS (1965) The friction jacket cone as an aid in determining the soil profile. In: Proceedings of the 6th ICSMFE, 2, (17–20). Montreal, 8–15 September

Jones GA, Rust E (1982) Piezometer penetration testing, CUPT. In: Proceedings of the 2nd European Symposium on Penetration Testing, ESOPT-2, 2, (607–614), Amsterdam, 24–27 May

Karlsrud K, Hernandez-Martinez FG (2013) Strength and deformation properties of Norwegian clays from laboratory tests on high-quality block samples. Can Geotech J 50(12):1273–1293

Karlsrud K, Lunne T, Kort DA, Strandvik S (2005) CPTU correlations for clays. International conference on soil mechanics and foundation engineering, 16, Osaka 2005, pp 693–702

Ladd CC, Foott R (1974) New design procedure for stability of soft clays. J Geotech Eng Div ASCE 100(7):763–786

Larsson R, Mulabdic M (1991) Piezocone tests in clay. Swedish Geotechnical Institute, SGI, Report No. 42, 240

NIFS report no 2015-126 2015 Detection of quick clay – final report, Sandven et al. In Norwegian

Olsen RS, Mitchell JK (1995) CPT stress normalization and prediction of soil classification. CPT95, Linköping, 2, (257–262). Sweden, SGI Report 3:95

Robertson PK (1990) Soil classification using cone penetration test. Can Geotech J 27:151–158

Robertson PK, Campanella RG (1983) Interpretation of cone penetrometer tests, Part I sand. Can Geotech J 20(4):718–733

Sandven R (1990) Strength and deformation parameters from piezocone tests. Ph.D. thesis, Norwegian University of Science and Technology

Sandven R, Gylland A, Montafia A, Kåsin K, Pfaffhuber AA, Long M (2016a) In situ detection of sensitive clays – Part I: selected test methods. NGM 2016 Reykjavik Proceedings, 123–132

Sandven R, Gylland A, Montafia A, Kåsin K, Pfaffhuber AA, Long M (2016b) In situ detection of sensitive clays – Part II: results. NGM 2016 Reykjavik Proceedings, 113–122

Schmertmann JH (1978) Guidelines for cone test, performance, and design. Federal Highway Administration, Report FHWA-TS-78209, Washington

Schneider J, Randolph M, Mayne P, Ramsey N (2008) Analysis of factors influencing soil classification using normalized piezocone tip resistance and pore pressure parameters. J Geotech Geoenviron Eng ASCE 134(11):1569–1586

Senneset K, Sandven R, Janbu N (1989) Evaluation of soil parameters from piezocone test. In-situ Test. Soil property for transportation. Transportation Research Record, No. 1235. C., 24–37

Sully JP, Campanella RG, Robertson PK (1988) Overconsolidation ratio of clays from penetration pore water pressures. ASCE J Geotech Eng 114(2):209–215

Valsson SM (2016) Detecting quick clay with CPTu. NGM 2016 Reykjavik Proceedings, 143–152

Chapter 6
Relationships Between Shear Wave Velocity and Geotechnical Parameters for Norwegian and Swedish Sensitive Clays

Mike Long, Tara Wood, and Jean-Sébastien L'Heureux

Abstract Shear wave velocity (V_s) is an important parameter in various geotechnical investigations especially in dynamic problems but is also useful in general characterisation studies and for problems such as landslide hazard assessment. This paper presents V_s data for sites in Norway and Sweden and shows that V_s can be measured reliably and repeatability using a variety of intrusive and non-intrusive techniques. Norwegian and Swedish V_s profiles show similar trends with depth. However the values for Norwegian soils are much higher. When correlated against the index properties water content and density the reason for the differences can be seen and the correlations apply across the soils from the two areas. Good correlations are found between V_s and s_u and V_s and p_c' and it is also shown that one can predict V_s from CPTU data. However it is not possible to use correlations developed for Norwegian soils for Swedish clays and the results of this work show that locally derived correlations are needed. This work also shows that it is not possible to predict whether a clay is quick or not from V_s measurements alone.

6.1 Introduction

Shear-wave velocity (V_s) is an important parameter needed for site characterisation in geotechnical engineering. It is particularly useful for assessing the stability of slopes in sensitive clays prone to dynamic loading such as earthquakes and blast

M. Long (✉)
School of Civil Engineering, University College Dublin (UCD), Dublin, Ireland
e-mail: Mike.Long@ucd.ie

T. Wood
Chalmers University, Göteborg, Sweden
e-mail: Tara.Wood@ncc.se

J.-S. L'Heureux
Trondheim Division, Norwegian Geotechnical Institute (NGI), Trondheim, Norway
e-mail: jsl@ngi.no

V. Thakur et al. (eds.), *Landslides in Sensitive Clays*, Advances in Natural and Technological Hazards Research 46, DOI 10.1007/978-3-319-56487-6_6

vibrations. In Europe and in Canada the building codes and seismic design criteria require site classification based on V_s of the top 30 m of the soil profile (V_{s30}). In addition to site classification, V_s may be required for site-specific seismic evaluation or dynamic analysis when required by the seismic design criteria.

In this paper some data is presented from several sensitive clay sites in Norway and Sweden where V_s values were determined using different methods, including seismic cone tests (SCPTU), seismic dilatometer tests (SDMT) and surface wave analysis (principally MASW). Some correlations between V_s and key geotechnical parameters for landslide hazard analysis, such as undrained shear strength and preconsolidation stress are presented. Finally attempts are made to assess if V_s profiles can be used to predict the sensitivity of the clays or if it is possible to distinguish quick clay from non-quick clay.

6.2 Methods

Geophysical methods can be divided into two categories: invasive and non-invasive. Invasive methods require drilling into the ground. Common invasive methods include: down-hole, cross-hole and suspension logging, seismic dilatometer (SDMT) and the seismic cone penetration test (SCPTU). In Norway and Sweden, most invasive testing is done with the SCPTU (Robertson et al. 1986) or the SDMT (Marchetti et al. 2008), which essentially use the same equipment.

Non-invasive geophysical methods include: spectral analysis of surface waves (SASW), multichannel analysis of surface waves (MASW), continuous surface waves (CSW), f-k spectrum method, seismic refraction, and seismic reflection. MASW data was acquired on 28 Norwegian clay sites and 15 Swedish locations. For more information about the procedures used to acquire and process the MASW data the reader is referred to NGI (2015), Sauvin et al. (2016) and to L'Heureux and Long (2017).

A database of Norwegian sites where V_s data, high quality laboratory data and CPTU tests are available has been established. The reader is referred to NGI (2015) and L'Heureux and Long (2017) for a detailed overview of all sites in the database. The data used for correlation purposes originates from a total of 29 sites. Out of these sites, 28 are located in Norway. The last site included in the database is the Bothkennar clay site in Scotland. The various invasive and non-invasive methods were compared, and it was found that for all practical engineering purposes the resulting V_s profiles were very similar.

6.3 Typical V_s Data from Norway and Sweden

Typical profiles for two of the research sites studied here, one in Norway and one in Sweden, are presented on Figs. 6.1 and 6.2. Data for the Klett South site near Trondheim, Norway is shown on Fig. 6.1. The Klett research site was developed by

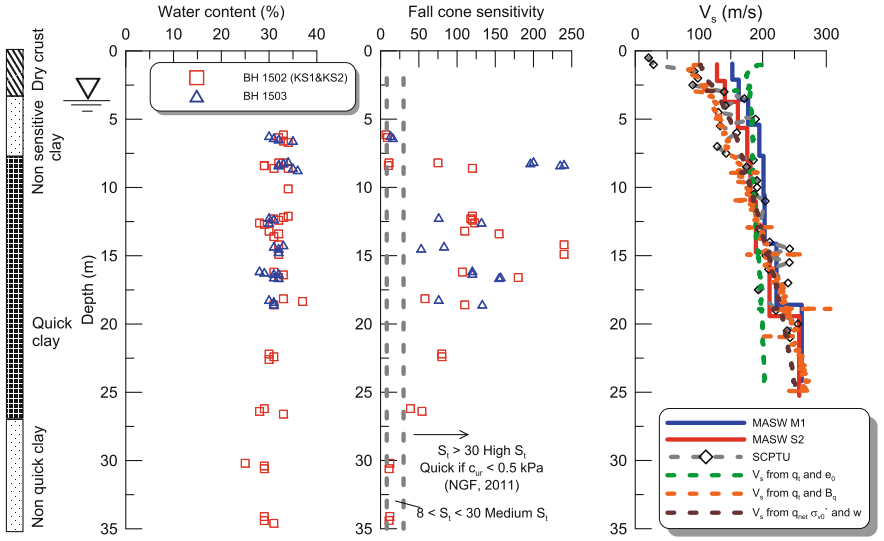

Fig. 6.1 Geotechnical profile from Klett-South, Trondheim with profiles of V_s

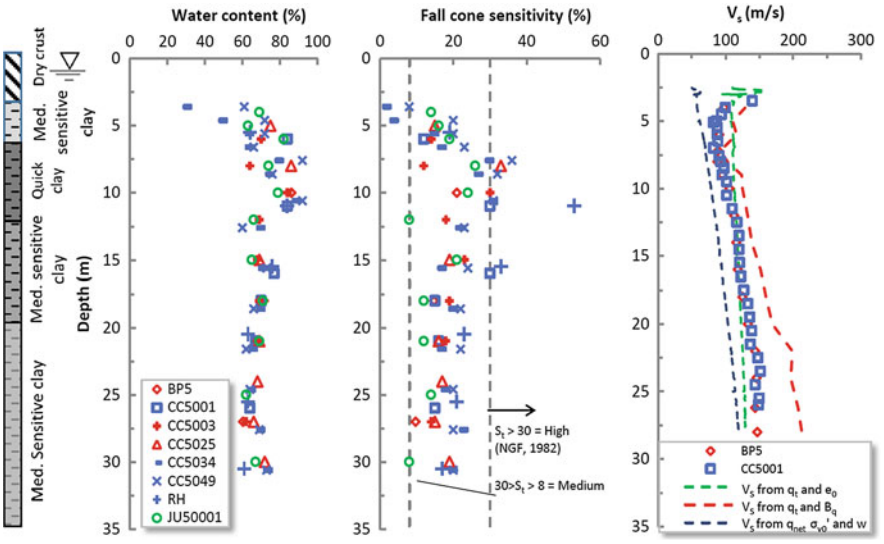

Fig. 6.2 Geotechnical profile from Göteborg Central Station site in Sweden with profiles of shear wave velocity (Modified from Wood (2015) and Trafikverket (2014))

Statens vegvesen, NGI and Multiconsult in conjunction with the upgrading of the E6 motorway in this area. Note this site is located to the south of the existing E6. Another research area was subsequently developed to the north of the E6. Several aspects of quick clay behaviour have been inspected including use of RCPTU, improved in situ vane testing and the use of lime-cement columns.

Ground conditions are typical for this area of Norway and the site is underlain by a thin layer of medium sensitive clay over quick clay and again medium sensitive clay at 27 m. Here the Norwegian definition of quick clay is used, i.e. clay with remoulded shear strength (c_{ur}) less than 0.5 kPa, according to NGF (2011). Water content decreases slightly with depth and has an average value of about 31.4%. Average values of bulk unit weight (γ), plasticity index (I_p) and clay content are 19.4 kN/m^3, 6.1%, and 31% respectively.

Two MASW profiles are available near to boreholes 1502 and 1503, where SCPTU testing was also carried out. Results show only a slight increase in situ V_s with depth. The SCPTU and MASW results agree well.

Similar data for the Göteborg Central Station Site is shown on Fig. 6.2. The site is underlain by a large thickness of soft clay with a quick clay layer (using the Norwegian definition of quick clay) being encountered between 7.5 m and 11 m. Water content values are much higher than for the Norwegian site and increases from about 60% near the surface to 90% at 10 m depth before reducing again and remaining reasonably constant with depth at about 65%. Average values of γ, I_p and clay content are 15.7 kN/m^3, 43%, and 60% respectively. V_s values measured by SDMT are lower than for Klett South and also show a slight increase with depth.

6.4 Comparison of Norwegian and Swedish Data

L'Heureux and Long (2017) separated the Norwegian shear wave velocity data into that from south-east Norway and from mid-Norway/Trondheim. They found V_s values for both areas were very similar and showed a consistent trend increasing with depth. Here selected Norwegian data is shown on Fig. 6.3a. These data are from sites which are referred to elsewhere in this paper. All sites show very similar results. An exception is the very soft, high water content and organic clay at Onsøy which shows a much lower values of V_s.

A summary of all the available data from Sweden is shown on Fig. 6.3b. These data were obtained from the work of Andréasson (1981), Larsson and Mulabdić (1991), Svensson and Möller (2001) and Wood (2015). A similar pattern to the Norwegian data can be seen with the values gradually increasing with depth. However the measured values are significantly lower than those from Norway. The range of values measured for sites in south-east Norway is also shown on Fig. 6.3b in order to illustrate this. Also the slope with depth of the Swedish profiles are not as steep as those of the Norwegian sites.

For both the Norwegian and Swedish data the V_s values deduced from the different geophysical methods (i.e. MASW, SASW, SCPTU and CHT) at a given

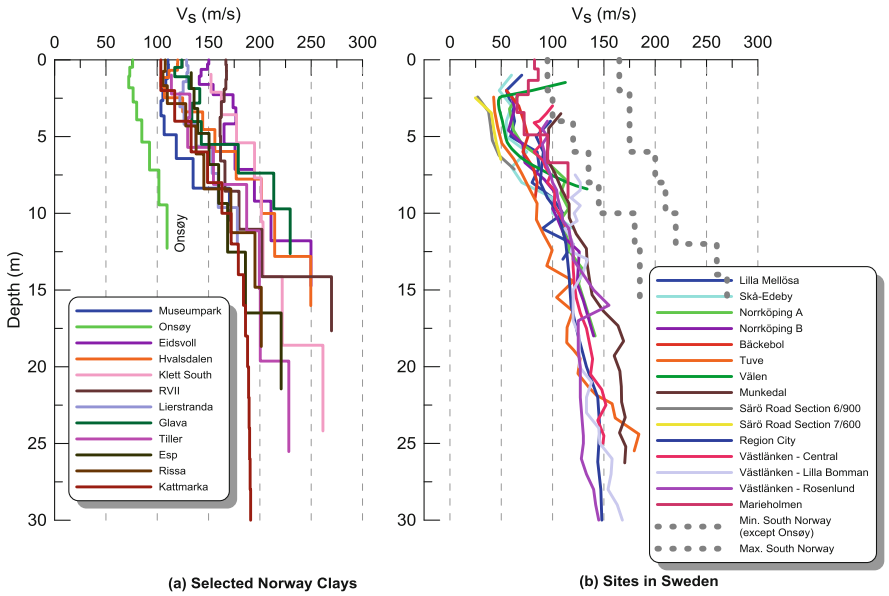

Fig. 6.3 Representative shear wave velocity profiles with depth from (**a**) Norway and (**b**) Sweden

site generally give very similar results. For the data presented here, the results do not seem to be affected by the technique used or the directions of propagation and polarization of the waves. This is likely to be due to the largely isotropic nature of these materials in the small strain range.

All sites show a very similar trend between V_s and depth and differ only in the value of V_s close to the surface and the slope of the profile. Teachavorasinskun and Lukkunaprasit (2004) found a similar pattern for soft Bangkok clays and they expressed the relationship in the form:

$$V_{sz} = V_{sg} + mz \tag{6.1}$$

where:

$V_{sz} = V_s$ at any depth z (m/s)
$V_{sg} = V_s$ close to the ground surface (m/s)
m = slope of the line of V_s versus depth (units m/s/m)

The coefficients V_{sg} and m in Eq. 6.1 are plotted against average water content (w) and unit weight (γ) for each site (over the interval where V_s data is available) on Fig. 6.4. It can be seen that both parameters decrease with increasing w and increase with increasing γ as would be expected. Data from Norway and Sweden are shown separately. It can be seen that the Swedish data shows lower V_{sg} and m values. These lower values are compatible with the higher w and lower γ values of the Swedish clays. Nonetheless the three sets of data follow the same trend and the values are consistent with one another. It would seem that the value of the parameter

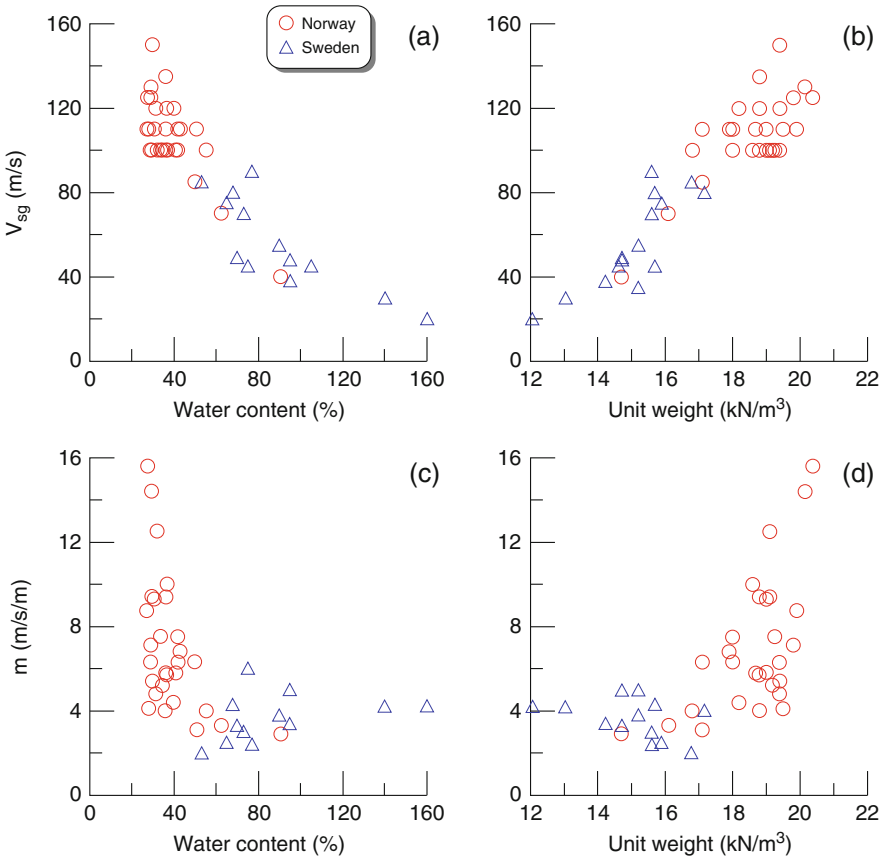

Fig. 6.4 Coefficients V_{sg} and m as a function of water content and unit weight

m reaches a minimum of 3.5 m/s/m to 4 m/s/m at high w/low γ. Attempts were also made to correlate V_{sg} and m against plasticity index. Broad trends exist but there was significant scatter in the data.

Overall it can be concluded that the trend between the parameters is reasonably good and these relationships could therefore be used for first order estimates of V_s or for validating site measurements.

6.5 Correlation Between V_s and Key Geotechnical Parameters

Many correlations between V_s and various geotechnical parameters have been presented in the literature. As an example correlations between V_s and two key geotechnical parameters namely undrained shear strength (s_u) and preconsolidation stress (p_c') are presented here.

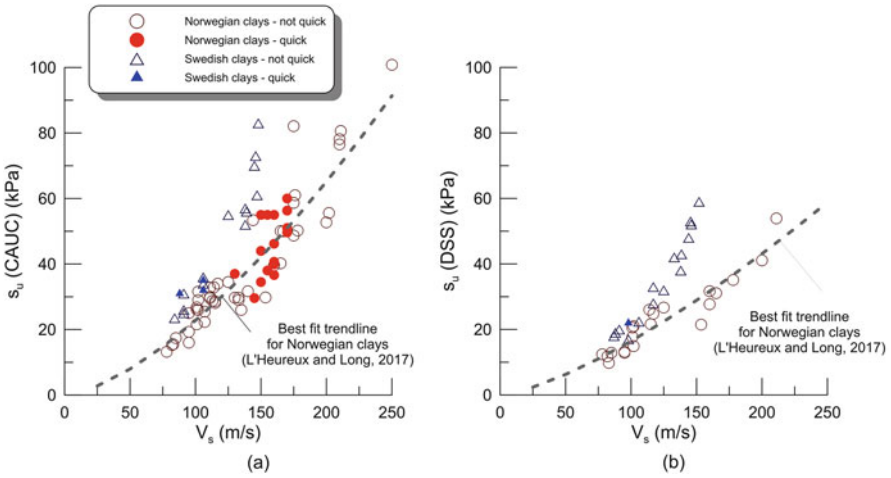

Fig. 6.5 V_s data versus (**a**) s_{u-CAUC} and (**b**) s_{u-DSS}

V_s has been frequently related to undrained shear strength (s_u) since both properties depend on common parameters. Care needs to be taken when correlating between V_s and s_u as the latter depends on the mode of failure in the testing method used and the rate of loading, amongst other factors.

The s_u values obtained from CAUC triaxial tests on high quality samples of Norwegian and Swedish clay together with the results of direct simple shear tests (DSS), which are relevant to landslide hazard assessment are plotted against in situ shear wave velocity on Fig. 6.5. Data are separated into those from Sweden and Norway and also for quick clays (Norwegian definition of quick clay used) and non-quick clays.

For both sets of data the results show an increase in s_u with increasing V_s. The best fit relationship for the Norwegian sites, as derived by L'Heureux and Long (2017), is also shown on the plots. These relationships had shown relatively high R^2 values of 0.85 and 0.87 for the CAUC and DSS tests respectively. Similar correlations have also been established for Norwegian clays using s_u values from CAUE tests. The Swedish results follow the same trend as those from Norway but the data points fall somewhat above the Norwegian data. There is no difference between the results from the quick and non-quick sites. This shows that V_s is independent of clay sensitivity and that V_s values alone are not able to distinguish quick from non-quick clays.

Results from oedometer tests have been analysed using the framework of Janbu (1963). Values of p_c' are plotted against V_s on Fig. 6.6. A reasonable correlation is expected here as the shear wave velocity is strongly dependent on the maximum past stress experienced by the clay. The best fit relationship for the Norwegian clays as found by L'Heureux and Long (2017) is also shown on the figure. Again this relationship had shown a good R^2 value of 0.80.

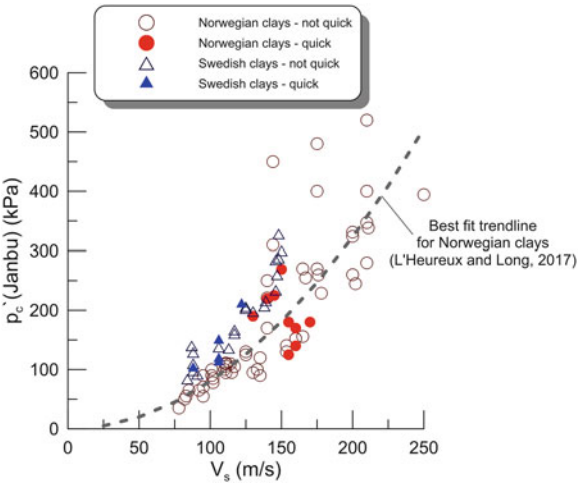

Fig. 6.6 V_s data versus p'_c for Norwegian and Swedish clays

Similar to the s_u data, the p_c' values for both Sweden and Norway increase with increasing V_s. Both sets of data show similar trends. Again similar to the s_u data the Swedish results lie above the Norwegian ones.

The differences between the Swedish and Norwegian results are mainly due to variations in the composition of the material (e.g. water content, unit weight, clay content and organic matter), see e.g. Fig. 6.4, and also in situ effective stresses. In addition, some of the differences are likely to be due to a combination of factors such as sampling disturbance, time between sampling and testing, small differences in the test procedures such as time allowed for consolidation, rate of loading effects and differences in the interpretation methods used. The findings for both s_u and p_c' show that correlations such as those shown can be very useful for first order estimates of soil properties and for checking laboratory test results. However it is clear that local correlations need to be made and reliance should not be placed on a correlation developed elsewhere even for Swedish and Norwegian soils which have similar geological background and basic parameters.

6.6 V_s and CPTU Correlations

Various researchers have studied relationships between CPTU parameters and V_s in clayey soils. These studies have explored relationships between in situ V_s and various parameters such as CPTU tip resistance (q_c), corrected tip resistance (q_t), cone net resistance (q_{net}), sleeve friction (f_s), pore pressure parameter (B_q), effective stress (σ'_v), water content (w) and initial void ratio (e_0). Long and Donohue (2010) developed two equations specifically for Norwegian clays as follows:

$$V_s = 65.00 q_t^{0.150} e_0^{-0.714}, \text{ with } R^2 = 0.76 \tag{6.2}$$

$$V_s = 1.961 q_t^{0.579} \left(1 + B_q\right)^{1.202}, \text{with } R^2 = 0.78 \tag{6.3}$$

L'Heureux and Long (2017) used the Norwegian clay database and found the following expression with the highest R^2:

$$\boldsymbol{V_s = 71.7 \cdot (q_{net})^{0.09} \cdot \left(\frac{\sigma'_{v0}}{w}\right)^{0.33}}, \text{with } R^2 = 0.89 \tag{6.4}$$

An example of these comparisons is shown on Fig. 6.1 for the Klett South site. V_s values obtained from CPTU correlations compared well to those from MASW and SCPTU results. Arguably the relationship between V_s and q_{net}, σ_{v0}' and w performs best as it gives V_s values closest to those measured. The relationship with q_t and e_0 does not capture the increase in V_s with depth and the relationship with q_t and B_q slightly overestimates V_s.

A similar set of data from SDMT for the Göteborg Central Station site is shown on Fig. 6.2. The approach involving q_t and e_0 best matches the measured data especially down to 17 m depth but thereafter underestimates V_s and fails to capture the increase in V_s with depth. The approach involving q_t and B_q and q_{net}, σ_{v0}' and w respectively overestimate and underestimate the measured data.

It is clear then that local correlations need to be made to link V_s and CPTU data and correlations developed elsewhere, even for similar soils, should not be used.

6.7 Conclusions

The objectives of this paper were to present V_s data from sensitive clays sites in Norway and Sweden. Some conclusions from the work are as follows:

- V_s can be measured reliably and repeatedly using a variety of different techniques such as SCPTU, SDMT and MASW.
- Norwegian and Swedish V_s profiles show similar trends with depth. However the values for Norwegian soils are much higher. This is due to differences in effective stresses, water content and higher unit weight of these materials amongst other factors.
- Good correlations were found between V_s and s_u and V_s and p_c'. However it is not possible to use correlations developed for Norwegian soils for Swedish clays and the results of this work show that local correlations are needed. A similar conclusion applies to CPTU correlations.
- This work shows that V_s is independent of sensitivity and that it is not possible to predict whether a clay is quick or not from V_s measurements alone.

Acknowledgments This work was funded in part by the Norwegian Geotechnical Society (NGF) through NGF stipend 2014–2015 and through the NFR strategic research project SP8- GEODIP at NGI. For the Swedish Gothenburg sites funding was provided by BIG (Better Interaction

in Geotechnics) funded by the Swedish Transport Administration (Trafikverket), the Swedish Railway Stations (Jernhusen) and the Swedish Building, Development and Research fund (SBUF). The authors would also like to thank Petter Fornes for his constructive comments.

References

Andréasson B (1981) Dynamic deformation characteristics of a soft clay. Paper presented at the International conference on recent advances in geotechnical earthquake engineering and soil dynamics, St. Louis, MO, April–May, 1981. vol 1

Janbu N (1963) Soil compressibility as determined by oedometer and triaxial tests. In: Proceedings of the 3rd European conference on soil mechanics and foundation engineering 1:19–25

L'Heureux J-S, Long M (2017) Relationship between shear wave velocity and geotechnical parameters for Norwegian clays. ASCE J Geotech Geoenviron Eng 21:04017013-1–04017013-20. First published online, February 13 2017. http://dx.doi.org/10.1061/(ASCE)GT.1943-5606.0001645

Larsson R, Mulabdić M (1991) Shear moduli in Scandinavian clays. Swedish Geotechnical Institute, Swedish Geotechnical Institute, Report No. 40, Linköping, Sweden

Long M, Donohue S (2010) Characterisation of Norwegian marine clays with combined shear wave velocity and CPTU data. Can Geotech J 47:709–718

Marchetti S, Monaco P, Totani G, Marchetti D (2008) In situ tests by seismic dilatometer. Paper presented at the from research to practice in geotechnical engineering, A Geotechnical Special Publication Honoring John H. Schmertmann

NGF (2011) Veilding for symboler og definisjoner i geoteknikk – identifisering og klassifisering av jord – Melding Nr. 2, Revidert 2011. Norwegian Geotechnical Society (Norsk Geoteknisk Forening) (In Norwegian), Oslo, Norway

NGI (2015) Correlations between shear wave velocity and geotechnical parameters in Norwegian clays, Report 20150030–04-R. Norwegian Geotechnical Institute (NGI), Oslo, Norway

Robertson PK, Campanella RG, Gillespie D, Rice A (1986) Seismic CPT to measure in situ shear wave velocity. J Geotech Eng ASCE 112(8):791–803

Sauvin G, Vanneste M, L'Heureux J-S, O'Connor P, O'Rourke S, O'Connell Y, Lombard T, Long M (2016) Impacts of data acquisition parameters and processing techniques on S-wave velocity profiles from MASW – examples from Trondheim, Norway. Proceedings 17th Nordic Geotechnical Meeting (NGM), Reykjavik, May, pp 1297–1306. ISBN 978-9935-24-002-6

Svensson M, Möller B (2001) Geophysics in soil mechanics – in situ shear moduli determined by SASW-technique and more traditional geotechnical methods vol Varia 508. Swedish Geotechnical Institute, Linköping, Sweden

Teachavorasinskun S, Lukkunaprasit P (2004) A simple correlation for shear wave velocity of soft Bangkok clays. Géotechnique 54(5):323–326

Trafikverket (2014) Tillhör systemhandling 2014-12-01, PM Geotekniska material parametrar, Km 456+900–457+800, Station Centralen", Västlänken document referens: PM F 05-010, 2014. (In Swedish)

Wood T (2015) Re-appraisal of the dilatometer for in-situ assessment of geotechnical properties of Swedish glacio-marine clays. Paper presented at the DMT 2015 3rd international conference on the flat dilatometer, Rome, Italy, June

Chapter 7
Geophysical and Geotechnical Characterization of a Sensitive Clay Deposit in Brownsburg, Quebec

Karine Bélanger, Ariane Locat, Richard Fortier, and Denis Demers

Abstract The results of a geophysical and geotechnical investigation in a sensitive clay deposit affected by numerous landslide scars in Vases Creek Valley near Brownsburg, Quebec, Canada are presented herein. The main objective of this investigation was to assess the suitability of electrical resistivity measurements in marine clay deposits for mapping out areas prone to flowslides. In addition to a 1.6 km-long electrical resistivity tomography (ERT) carried out perpendicular to the axis of the Vases Creek Valley, six piezocone penetration tests and five boreholes with sampling were also performed along the geophysical survey line. Moreover, standard geotechnical parameters and pore water salinity, as well as electrical resistivity of undisturbed clay samples were measured in the laboratory. According to the correlations found between the remoulded shear strength, the pore water salinity and the electrical resistivity, clay samples with salinity below 6.2 g/l are characterized by remoulded shear strength below 1 kPa and electrical resistivity above 2.8 and 10 Ωm measured respectively in the field and in the laboratory. In such conditions, sensitive clay deposits can be prone to flowslides if all other criteria are also met. Based on this resistivity limit value, only one small area of non-sensitive clay was identified in the interpretative stratigraphic cross-section assessed from the field investigation. Otherwise, the deposit is entirely composed of sensitive clay. The ERT is a promising geophysical tool for the delineation of areas prone to large landslides in eastern Canada.

K. Bélanger (✉) • D. Demers
Ministère des Transports, de la Mobilité durable et de l'Électrification des transports (MTMDET), Québec City, QC, Canada
e-mail: karine.belanger@transports.gouv.qc.ca; denis.demers@transports.gouv.qc.ca

A. Locat
Département de génie civil et de génie des eaux, Université Laval, Québec City, QC, Canada
e-mail: ariane.locat@gci.ulaval.ca

R. Fortier
Département de géologie et de génie géologique, Université Laval (UL), Québec City, QC, Canada
e-mail: richard.fortier@ggl.ulaval.ca

V. Thakur et al. (eds.), *Landslides in Sensitive Clays*, Advances in Natural and Technological Hazards Research 46, DOI 10.1007/978-3-319-56487-6_7

7.1 Introduction

In the province of Quebec, Canada, approximately 89% of the population is settled within the limits of marine transgression of the Champlain, Laflamme and Goldthwait seas (Demers et al. 2014). The effects of leaching on geotechnical properties of such marine clays are well documented (Rosenqvist 1966). Leached clay deposits can be prone to flowslides, which is a great hazard for the population and for man-made infrastructures, justifying the need to develop tools to identify vulnerable areas. According to many recent Scandinavian studies, (Solberg et al. 2008; Lundström et al. 2009; Long et al. 2012; Dahlin et al. 2014; Pfaffhuber et al. 2014), areas of leached clay can be efficiently delineated using geophysical surveys along with standard geotechnical investigations. As a part of its mandate to map landslide-prone areas and assess the associated risk (Potvin et al. 2014), the Quebec government has recently undertaken, in collaboration with researchers at Université Laval, the characterization of a sensitive clay deposit affected by numerous large landslides in the Vases Creek Valley near Brownsburg, Quebec. The results of this investigation are presented herein.

7.2 Site Description

The study area is located in the upstream part of Vases Creek Valley (Fig. 7.1). It is bordered to the north by the Canadian Shield's igneous and metamorphic rocks and to the south by a rise in the sedimentary bedrock of the St. Lawrence Lowlands. The center of the valley is buried under up to 60 m-thick clayey deposit of the Champlain Sea (Ross 2004). According to Carson (1981), up to 35 m of fluvioglacial sediments are present south of Vases Creek, between the marine clay deposit and the underlying till. Banks of 10 to 15 m high formed in the deposit along the creek. Following the study of landslides and geotechnical properties of the clay deposit in the valley, numerous large landslide scars were mapped by Fortin-Rhéaume (2013) (Fig. 7.1).

7.3 Methodology

A 1.6 km-long induced polarization profiling was performed across the Vases creek valley using a Tx II transmitter and a GRx8–32 receiver from *Instrumentation GDD inc* (see location in Fig. 7.1). A dipole-dipole array with 20 m electrode spacing and a 10-m array displacement were used to perform the profiling. This configuration allows to investigate the entire clay deposit which reaches up to almost 50-m thick along the profiling. The polarity of the current was switched each 2 s with 2 s

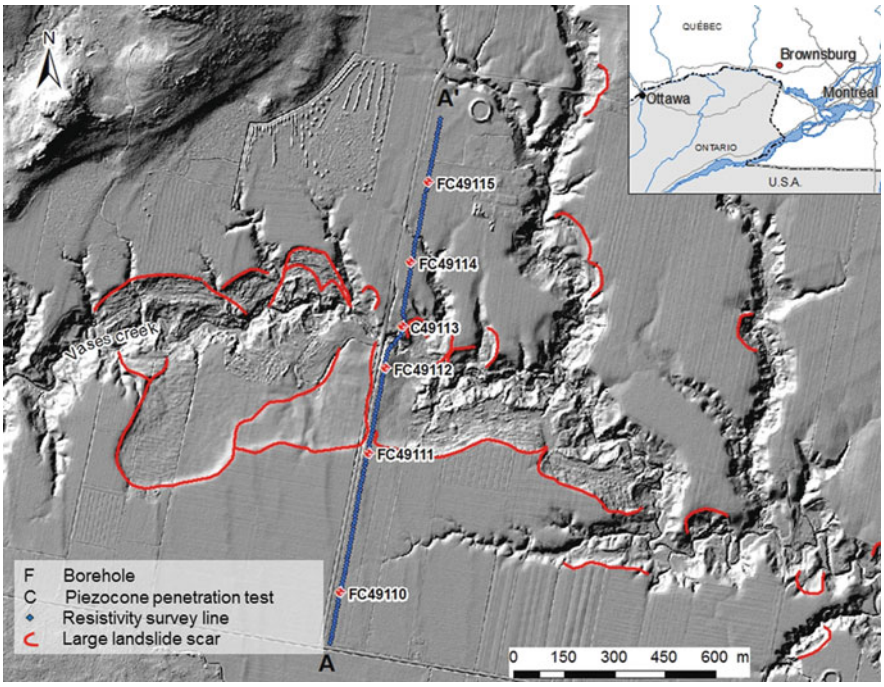

Fig. 7.1 Map of the Vases Creek Valley near Brownsburg, Quebec, showing the location of the geophysical and geotechnical investigation. Large landslide scars are delineated by *red lines* on a hillshade background

without electrical current flow in between to avoid the polarization of the electrodes. Inversion of the electrical resistivity data was performed with RES2DINV software using a smoothness-regularized least-square method.

Six piezocone penetration tests with pore pressure measurements (CPTU) were performed along the geophysical survey line (see location in Fig. 7.1). The cone has a 5 T capacity and was pushed at a constant rate of 1 cm/s in order to obtain a good resolution in clay. In addition to the CPTUs, clay samples were recovered with a stationary piston sampler and thin wall tube during drilling at five of the six CPTU sites. Some granular soil and bedrock samples were recovered by drilling.

Standard geotechnical tests, including grain size analysis, Atterberg limits and fall cone tests, were performed in the laboratory on each sample. Pore water salinity was determined with three methods: refractometry, electrical conductivity and X-ray fluorescence. Electrical resistivity was also measured on each samples with an apparatus made of two 85 mm copper electrodes called "SCIP" from *Instrumentation GDD inc*. The samples were 200 mm long, which is the same length that was used for standard geotechnical laboratory tests. Constant current of 500 μA was applied and a current cycle of 2 s was used as for induced polarization profiling.

7.4 Results

According to the geotechnical investigation, three different stratigraphic units called A, B and C were identified in the marine clay deposit. For instance, the geotechnical profiles of borehole F49114 is presented in Fig. 7.2 (see location in Fig. 7.1). Location of the CPTUs with the identification of these three units is shown on a cross-section along the AA' geophysical survey line on Fig. 7.3a. Unit A corresponds to the surficial weathered clayey crust and is located from the surface to a depth of 2.5 to 3.0 m. Unit B is located between elevation 85 and 65 m.a.s.l. and is characterized with a linear increase of CPTU undrained shear strength. This unit is composed of pale grey clay with pink and blackish banding. The clay and silt content of this unit are between 70 and 86% and between 13 and 42% respectively. Its water content is generally higher than 75% and can reach up to 104%. The plasticity and liquidity limits in this unit vary between 24 and 30% and between 49 and 77% respectively. The intact and remoulded shear strength vary between 14 and 43 kPa and between 0.1 and 1.7 kPa respectively. The liquidity index varies between 1.2 and 2.5. Unit C is located from elevation 72 and 48 m.a.s.l. and it is composed of dark grey silt and clay with a mottled black pattern. This unit is composed of 33 to 56% of clay with 43 to 58% of silt. The water content of this unit varies between 35 and 64% and the plasticity and liquidity limits varies respectively between 20 and 26% and between 30 and 46%. The intact and remoulded shear strength vary between 35 and 71 kPa, and between 0.07 and 2.7 kPa respectively.

Pore water salinity of clay samples is also given in Fig. 7.2. Results from electrical conductivity and X-ray fluorescence are similar, with less than 0.3 g/l difference between the methods. However, for the samples with the highest salt content, gaps of up to 2 g/l are observed when comparing the salinity values from these two methods and the results from the refractometer. Apart from the previous results from refractometry, the pore water salinity varies between 0.3 and 7.6 g/l. Salinity values are below 1 g/l for samples collected in borehole F49111 and F49112, and below 2 g/l in boreholes F49110 and F49115. Only the samples from borehole F49114 have salinity values above 2 g/l.

The model of electrical resistivity obtained from the inversion of the induced polarization profiling is presented in Fig. 7.3b. Two areas having a resistivity below 10 Ωm, appearing in blue in the model, correspond to slightly leached marine clay. The first area is located south of the Vases Creek, while the second one is north of the creek. According to the different boreholes and CPTUs, leached clay has resistivity values between 10 and 80 Ωm and sand or gravel has resistivity values between 20 and up to 160 Ωm.

Resistivity values higher than 160 Ωm in the southern area and higher than 500 Ωm in the center of the profile indicates the presence of bedrock, which was confirmed by the dolomite sample intercepted at depth in borehole F49110 and by the gneissic roc in borehole F49112.

Electrical resistivity log assessed from the model of electrical resistivity at the location of the borehole F49114 is also given in Fig. 7.2 along with the

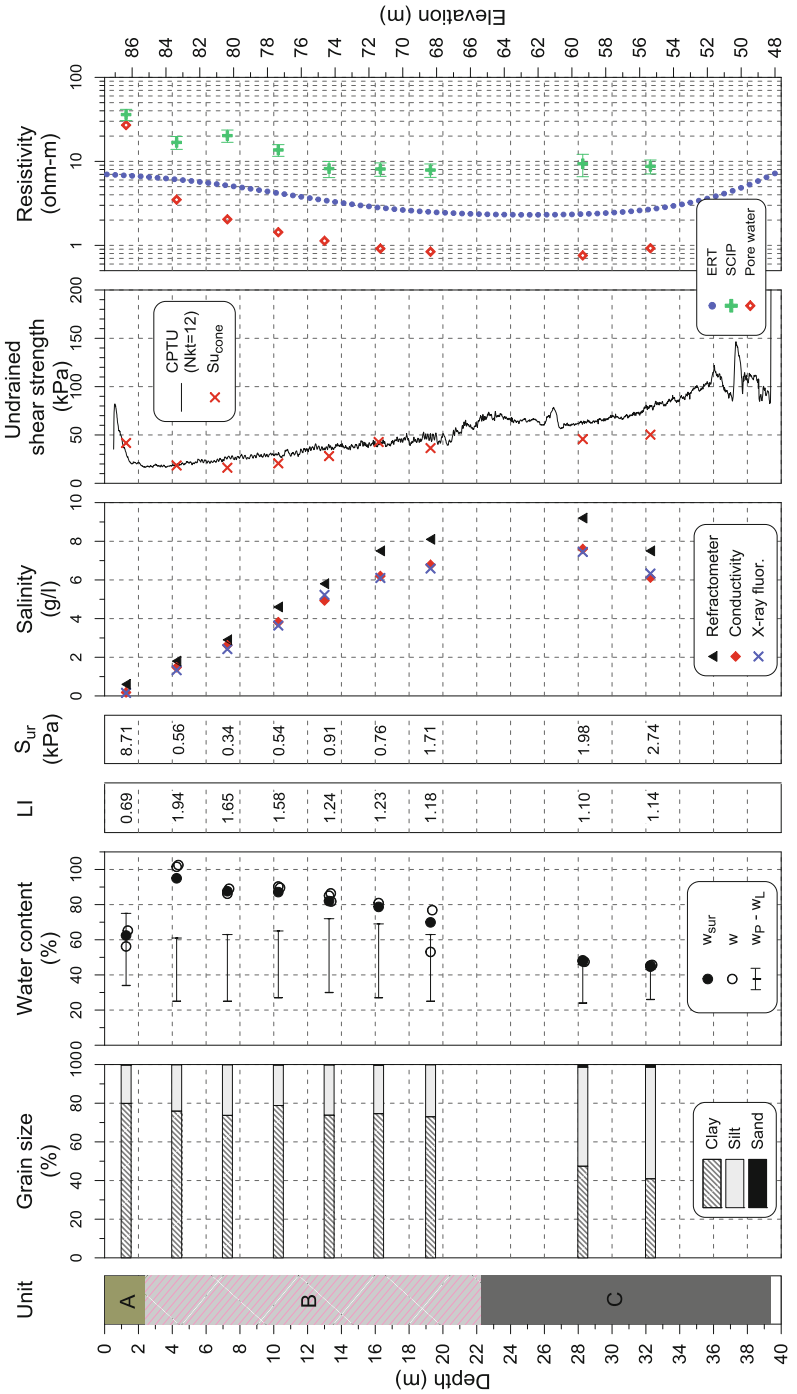

Fig. 7.2 Geotechnical and electrical resistivity profiles of borehole F49114 in the marine clay deposit of Brownsburg, Quebec

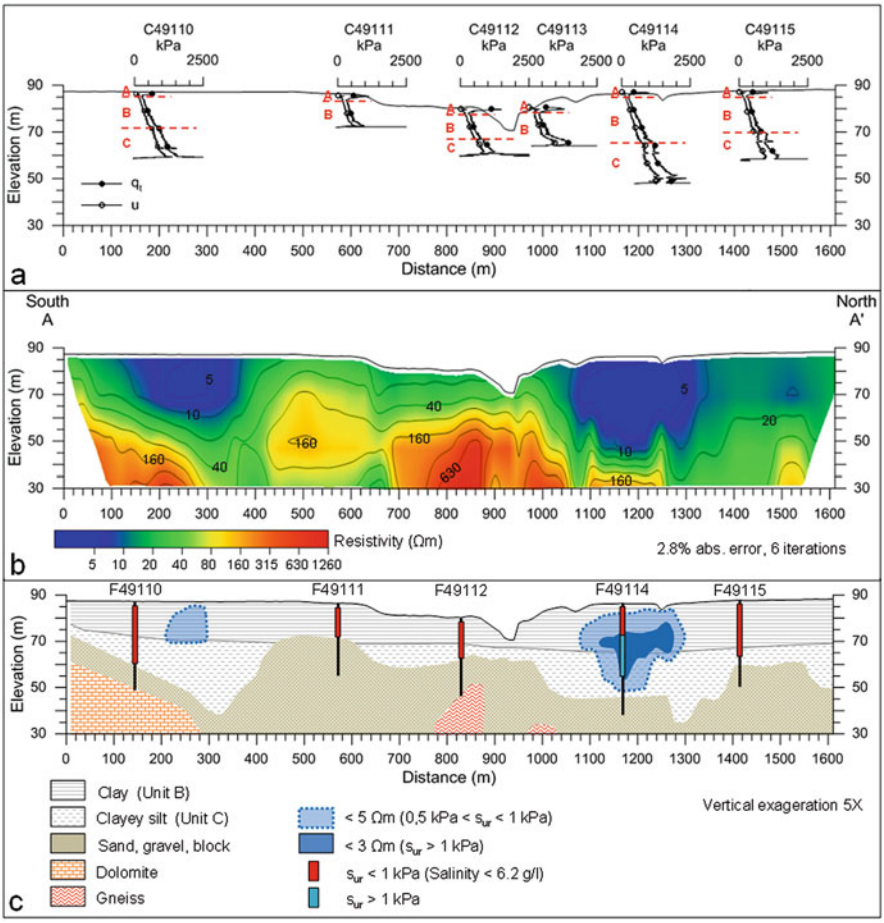

Fig. 7.3 (**a**) Stratigraphy of the marine clay deposit in the Vases Creek Valley near Brownsburg, Quebec assessed from the CPTU profiles. (**b**) Model of electrical resistivity obtained from the inversion of the induced polarization profiling. (**c**) Stratigraphic cross-section of the marine clay deposit assessed from the combined interpretation of geotechnical and geophysical characterization. Most of the investigated clay deposit is prone to flowslides (s_{ur} < 1 kPa), except for the dark blue area with electrical resistivity below 3 Ωm and s_{ur} > 1 kPa

measurements of electrical resistivity on clay samples and pore water. The electrical resistivity data show the same trend. Minimum values of electrical resistivity are 0.8 Ωm for pore water, 2.4 Ωm in the log assessed from the resistivity model and 7.9 Ωm with the SCIP measurements on clay samples. The difference between the resistivity values obtained from ERT and SCIP measurements is most likely due to the current flow in the soil. On one hand, during ERT, the current flows parallel to the bedding principally in the most conductive layers which reduces somewhat

the electrical resistivity. On the other hand, in the SCIP cell, the current flows perpendicular to the bedding in all the layers even the most resistive ones which increases the electrical resistivity.

7.5 Discussion

According to Tavenas (1984), one of the criteria for the assessment of sensitive clays prone to flowslides is a s_{ur} below 1 kPa, which also corresponds to a liquidity index above 1.2. For this reason, this criterion was used in this study in order to delimit areas prone to flowslides. Clay samples of units B and C have s_{ur} between 0.07 and 2.7 kPa while values of pore water salinity assessed from the X-ray fluorescence vary between 0.3 and 7.5 g/l. The correlation between remoulded shear strength and pore water salinity is shown in Fig. 7.4. Clay samples with s_{ur} below 1 kPa have salinity values below 6.2 g/l. A salinity value of 2.5 g/l was found in the Brownsburg clays for s_{ur} below 0.5 kPa, which is similar to the salinity value of 2 g/l proposed by Torrance (1975) for quick clays.

Values of electrical resistivity were taken from the model of induced polarisation at the location of each clay sample. In Fig. 7.5, values of electrical resistivity assessed from resistivity model and from SCIP measurements are related to the pore water salinity. For salinity values below 2.5 g/l, the resistivity assessed from ERT varies between 5 and 85 Ωm and forms a scatter plot with no evident trend, possibly caused by the large volume of soil involved. For salinity values above 2.5 g/l, the ERT resistivity values line up according to a semi-log law. Using the salinity limit

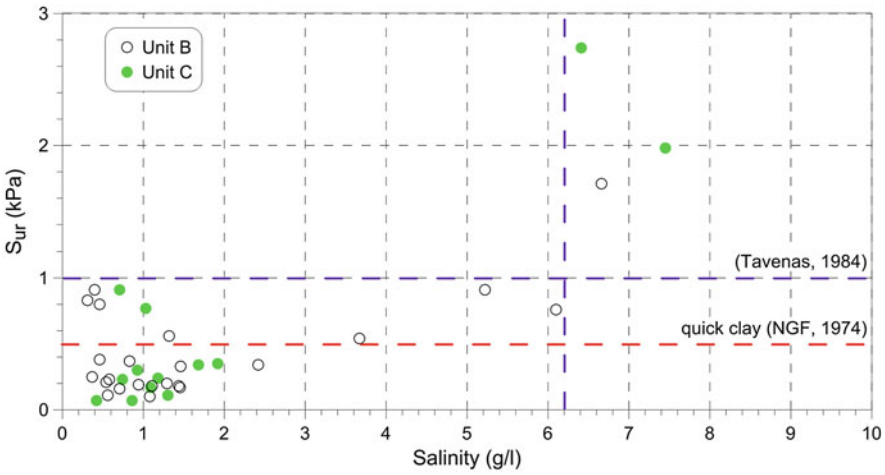

Fig. 7.4 Relationship between the remoulded shear strength and pore water salinity for units B and C of marine clays of Brownsburg, Quebec

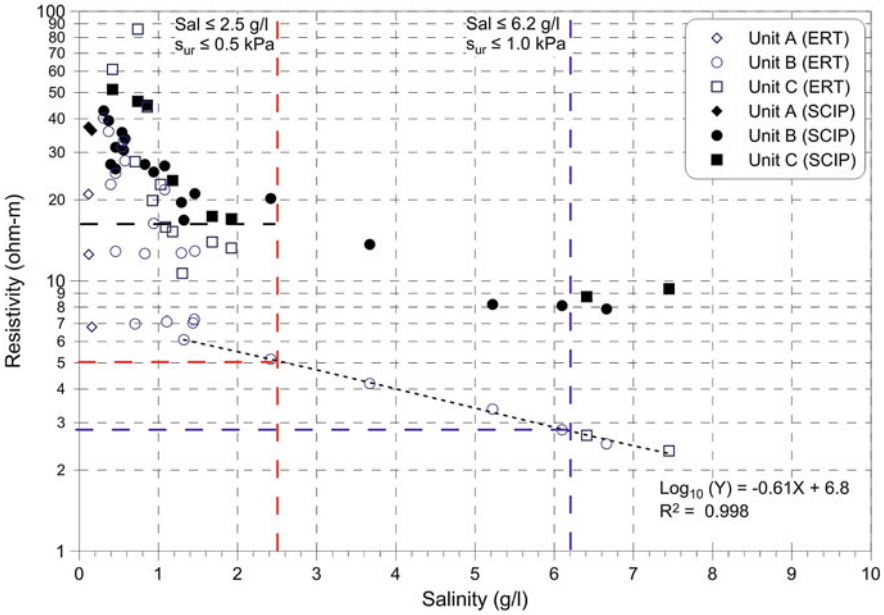

Fig. 7.5 Relationship between the electrical resistivity and pore water salinity of marine clays of Brownsburg, Quebec

value of 6.2 g/l which corresponds to a s_{ur} of 1 kPa (Fig. 7.4), a resistivity of 2.8 Ωm is found as a limit value to identify sensitive clays prone to flowslides in Brownsburg (see Fig. 7.5). This resistivity limit is found for a dipole-dipole array with electrode spacing of 20 m. Using the same semi-log relation, a value of 5 Ωm is bound to a salinity of 2.5 g/l which also corresponds to a s_{ur} of 0.5 kPa. Resistivity values from laboratory measurements are higher and less scattered than ERT resistivity values. For salinities below 2.5 g/l, resistivity is above 17 Ωm and for salinities between 5 and 7.5 g/l the SCIP resistivity values are between 7 and 10 Ωm. According to Solberg et al. (2008), Long et al. (2012), and Donohue et al. (2012), a limit value of 10 Ωm is generally admitted for quick clay in Norway ($s_{ur} < 0.5$ kPa). However, a limit value of about 6 Ωm is presented in Swedish studies for $s_{ur} < 0.4$ kPa (Dahlin et al. 2014; Lundström et al. 2009).

In Fig. 7.3c, the interpretation of the geotechnical and geophysical investigation is presented as a stratigraphic cross-section along the AA' geophysical survey line. Sections of boreholes with clay samples that have s_{ur} values below 1 kPa are identified with red boxes while the section with s_{ur} above 1 kPa is identified with a blue box. Two light blue areas with resistivity below 5 Ωm are identified in Fig. 7.3c. These areas correspond to inferred salinity between 2.5 and 6.2 g/l and s_{ur} values between 0.5 and 1 kPa. Therefore, the clay in these areas is assumed to be sensitive but not quick. A dark blue area within the light blue area north of the Vases Creek, corresponding to resistivity below 3 Ωm, was also delineated. According to the

relationship presented in Fig. 7.5, this area has pore water salinity above 6.2 g/l and s_{ur} above 1 kPa. Clay in dark blue area would therefore not be sufficiently leached to be prone to flowslides. Based on Tavenas (1984) flowslide criteria of s_{ur} below 1 kPa and the criterion of resistivity above 3 Ωm proposed in this study, most of the investigated section of marine clay deposit in the Vases Creek Valley would be prone to flowslides, except for the dark blue area in the interpretative stratigraphic cross-section north of the Vases Creek in Fig. 7.3c. The results obtained in this study are similar to those obtained by Carson (1981).

7.6 Conclusions

A geophysical and geotechnical investigation of a marine clay deposit was performed in the Vases Creek Valley, near Brownsburg, Quebec to characterize the standard geotechnical properties, pore water salinity and electrical resistivity, and to assess the areas prone to flowslides. According to the results of this investigation, clay samples with pore water salinity below 6.2 g/l in Brownsburg are characterized by remoulded shear strength below 1 kPa and electrical resistivity above 2.8 and 10 Ωm measured respectively in the field and in the laboratory. In such conditions, sensitive clay deposits can be prone to flowslides if all other criteria are also met. Based on the limit of 2.8 Ωm, one area of clay was identified as not prone to flowslides ($s_{ur} > 1$ kPa) in the interpretative stratigraphic cross-section, but otherwise, most of the investigated section is composed of sensitive clay prone to flowslides ($s_{ur} < 1$ kPa). The ERT is a promising geophysical tool for the delineation of areas prone to large landslides in sensitive clay deposits. The achievement of future studies in other sensitive clay deposits is needed to improve the relationships between the geotechnical and geophysical properties given herein and to refine the limit values of pore water salinity, remoulded shear strength and electrical resistivity. Areas having different geological contexts in Quebec should be also studied in order to check if these relationships and limit values are applicable to all the sensitive clay deposits found in eastern Canada.

Acknowledgments The research funding for this study was provided by the *Plan d'action 2013-2020 sur les changements climatiques* (PACC 2013-2020) and by the *Fonds vert* of Quebec government. The authors also wish to express their gratitude to the reviewer Jean-Sébastien L'Heureux for his valuable comments and to Thomas Fournier for the linguistic revision.

References

Carson MA (1981) Influence of porefluid salinity on instability of sensitive marine clays: a new approach to an old problem. Earth Surf Process Landf 6(6):499–515

Dahlin T, Schälin D, Tornborg J (2014) Mapping of quick clay by ERT and CPT-R in the Göta Älv river valley, First international workshop on landslide in sensitive clays, Quebec, Canada

Demers D, Robitaille D, Locat P, Potvin J (2014) Inventory of large landslides in sensitive clay in the province of Québec, Canada: preliminary analysis. First international workshop on landslide in sensitive clays, Quebec, Canada

Donohue S, Long M, O'Connor P, Helle TE, Pfaffhuber A, Rømoen M (2012) Geophysical mapping of quick clay: a case study from Smørgrav, Norway. Near Surface Geophysics 10:207–219

Fortin-Rhéaume A-A (2013) Étude de l'étalement latéral de 1988 et des autres glissements de terrain le long de la vallée à Brownsburg-Chatham, Québec. M.Sc. thesis in civil engineering, Université Laval

Long M, Donohue S, L'Heureux JS, Solberg IL, Rønning JS, Limacher R, O'Connor P, Sauvin G, Rømoen M, Lecompte I (2012) Relationship between electrical resistivity and basic geotechnical parameters for marine clays. Can Geotech J 49:1158–1168

Lundström K, Larsson R, Dahlin T (2009) Mapping of quick clay formations using geotechnical and geophysical methods. Landslides 6:1–15

Pfaffhuber AA, Bazin S, Helle TE (2014) An integrated approach to Quick-clay mapping based on resistivity measurements and geotechnical investigations. First international workshop on landslide in sensitive clays, Quebec, Canada

Potvin J, Thibault C, Demers D, Bilodeau C (2014) An overview of the mapping of landslide-prone areas and risk management strategies in the province of Quebec, Canada. First international workshop on landslide in sensitive clays, Quebec, Canada

Rosenqvist IT (1966) Norwegian research into the properties of quick clay – a review. Eng Geol 1:445–450

Ross M (2004) Stratigraphie et architecture des formations Quaternaires au nord-ouest de Montréal – Applications en hydrogéologie régionale. Ph.D. thesis in Earth sciences, Université du Québec

Solberg IL, Rønning JS, Dalsegg E, Hansen L, Rokoengen K, Sandven R (2008) Resistivity measurements as a tool for outlining quick-clay extent and valley-fill stratigraphy: a feasibility study from Buvika, central Norway. Can Geotech J 45:210–225

Tavenas F (1984) Landslides in Canadian sensitive clays – a state-of-the-art. In: 4th International Symposium on Landslides, Toronto

Torrance JK (1975) On the role of chemistry in the development and behavior of the sensitive marine clays of Canada and Scandinavia. Can Geotech J 12:326–335

Chapter 8
Investigating How the Changes in Geotechnical Properties of Sensitive Clays Influence Their Geophysical Properties

Shane Gribben, Sara Bazin, Shane Donohue, V. Sivakumar, and Jean-Sébastien L'Heureux

Abstract This laboratory study involves leaching clay from Onsøy, Norway. Deaired deionised water reduced the pore water salinity, potentially forming a quick clay, in a triaxial cell, modified to allow shear wave velocity and resistivity measurements to be made. This project aims to assess how changes in the geotechnical properties of the clay influence its geophysical properties. The testing procedure has been able to create a quick clay with a remoulded shear strength of 0.2 kPa, and a final salt content of 2.0 g/l. This corresponded to an increase in the resistivity of the clay from initially 0.9 Ωm to a final resistivity of 14.0 Ωm.

8.1 Introduction

Sensitive clays present a serious geological hazard, and are involved in some of the largest landslides that threaten infrastructure and people in countries such as Canada and Norway as demonstrated by the landslides at St-Jude in 2009 and Rissa in 1978. Deposits of quick clays are typically found in post glacial regions of Alaska, Canada and Scandinavia (Holmsen 1953; Engdahl 2006; Sauvin et al. 2014).

Quick clays are highly sensitive soils whose structure completely collapses upon remoulding, resulting in a significant reduction in its shear strength. Remoulded shear strengths less than 0.5 kPa are typical, due to the natural water content of the clay being greater than its liquid limit (Bjerrum 1954; Lundström et al. 2009). In

S. Gribben (✉) • S. Donohue • V. Sivakumar
Queen's University Belfast, Belfast, Northern Ireland, UK
e-mail: sgribben02@qub.ac.uk; s.donohue@qub.ac.uk; V.Sivakumar@qub.ac.uk

S. Bazin
Norwegian Geotechnical Institute (NGI), Oslo, Norway
e-mail: sara.bazin@ngi.no

J.-S. L'Heureux
Trondheim Division, Norwegian Geotechnical Institute (NGI), Trondheim, Norway
e-mail: jsl@ngi.no

V. Thakur et al. (eds.), *Landslides in Sensitive Clays*, Advances in Natural and Technological Hazards Research 46, DOI 10.1007/978-3-319-56487-6_8

Norway a clay is considered to be quick if its remoulded shear strength is less than 0.5 kPa (Torrance 1983; Lundström et al. 2009; NIFS 2015).

These clays are formed as a result of fine glacial outwash material being deposited in a high salt content marine environment. This has resulted in a clay with a highly flocculated structure, a high pore water salt content and a natural water content that is greater than its liquid limit. Post depositional processes such as isostatic uplift has resulted in these deposits being above sea level, as well as percolation and groundwater flow have reduced the pore water salt content of the clay (Bjerrum 1954).

The reduction in the pore water salt content has been linked to the increase in sensitivity of the clay deposit, in particular the reduction in the remoulded shear strength, and reductions in consistency limits. Threshold values for pore water salt content of 2 g/l and 5 g/l have been suggested to identify quick clay (Bjerrum 1954; Torrance 1974), however quick clays with pore water salt content as high as 5.6 g/l have been found in south west Sweden (Lundström et al. 2009).

Current methods for identifying deposits of highly sensitive clays are based on a combination of *in situ* characterisation and geotechnical assessment in the lab. The Norwegian method of identification is based upon a combination of *in situ* testing using total soundings, cone penetration tests, and lab testing to confirm field observations (Lundström et al. 2009; Rankka et al. 2004; NIFS 2015).

Recent developments in the identification of sensitive clays have involved the use of geophysical methods to locate and map the extent of these deposits (Solberg et al. 2008; Lundström et al. 2009; Long et al. 2012; Donohue et al. 2012; Donohue et al. 2014). In particular, there has been a considerable amount of work published on the use of geoelectrical measurements (e.g. Electrical Resistivity Tomography (ERT)) for mapping quick clay. The resistivity of clays typically fall in the range of 1–100 Ωm. Solberg et al. (2008, 2012) suggested for Norwegian clays, that unleached marine clays had resistivities between 1–10 Ωm, fully leached potentially quick clay deposits typically have resistivities in the range of 10–80 Ωm and resistivities of 80+ Ωm are typical of dry crusts, slide deposits and bedrock. The change in resistivity is linked to the reduction in salt content (Long et al. 2012; Solberg et al. 2008). However recent investigations have shown that local conditions can have a major impact upon the threshold resistivity values for quick clays, Lundström et al. (2009) reported Swedish quick clays have resistivity values as low as 5 Ωm.

The purpose of this project is to identify and understand the factors that influence the geophysical properties of sensitive clays.

8.2 Methodology

The experimental procedure involved testing a sample of clay from Onsøy, Norway. The test samples were cut from a block sample, obtained using a Sherbrooke sampler used by the Norwegian Geotechnical Institute (NGI). The site is located 100 km South East of Oslo near the city of Fredrikstad. This site has been used by NGI as a research site for decades. As a result, the site is well characterised.

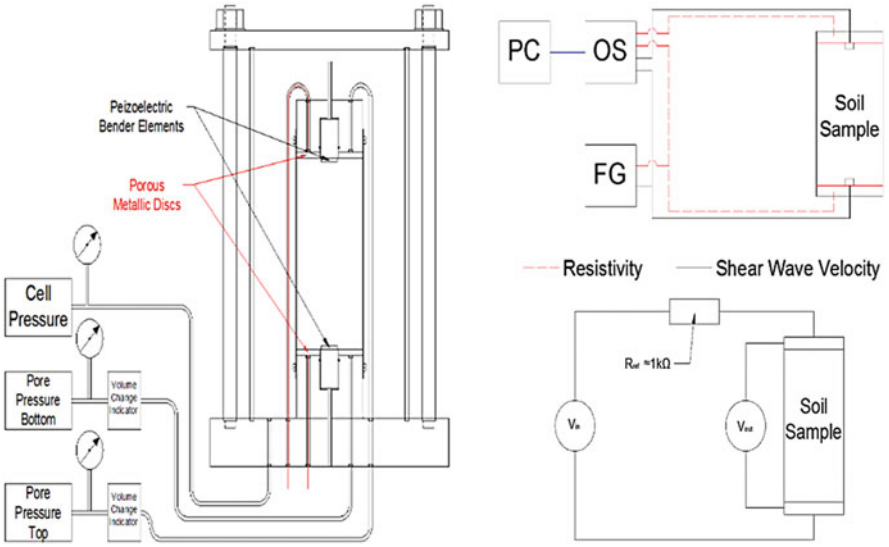

Fig. 8.1 (**a**) Triaxial cell with piezoelectric elements and axial resistance. (**b**) Schematic of sensors, Picoscope (*OS*), Function Generator (*FG*), and Computer (*PC*). (**c**) Electrode arrangement used to measure the complex impedance of the sample (After Wang et al. 2009)

The test procedure has been designed to reduce the pore water salt content of the sample by applying a hydraulic gradient to the sample, which was used to drive a flow of deaired, deionised water through the sample, reducing the pore water salt content of the marine clay, potentially forming a quick clay.

A triaxial cell, Fig. 8.1a, has been modified to measure the changes in resistivity and shear wave velocity of the sample as the pore water salt content is reduced. The shear wave velocity (V_s) is measured using piezoelectric bender element pairs and calculated from the travel time between the tips of the bender elements. Resistivity is measured by applying a current to the sample and measuring the potential difference, which allows the resistance to be determined, and the corresponding resistivity from the sample geometry and the resistance.

Figure 8.1a shows the layout of the triaxial cell including the configuration of the piezoelectric bender elements, used to measure V_s, and the metal porous discs used to measure the electrical resistance of the sample.

The hydraulic gradient across the sample was maintained using two pressure control systems. The pore water pressure at the bottom of the sample was 20 kPa higher than the top of the sample. Volume change due to consolidation/swelling of the sample was monitored using two volume change indicators connected to the pressure control systems that regulated the pore water pressure distribution.

Shear wave velocity and resistivity were measured at regular intervals during the test, using the set up shown in Fig. 8.1b, c. The resistance was measured using a setup modelled after Wang et al. (2009). An input voltage, V_{in}, generated by a

sinusoidal function at the function generator (FG), was passed through a reference resistor, R_{ref}, and the potential difference across the sample, V_{out}, was measured by a Picoscope (OS), Fig. 8.1b, c.

The fluid that was flushed out of the sample was collected in the volume change unit connected to the top of the sample, and the salt content of the pore water fluid was measured using a WTW Cond 3110 conductivity probe. The sample was subsequently sheared to obtain the final undisturbed shear strength and a fall cone test, with a 60 g 60° cone, was used to obtain the final remoulded shear strength.

8.3 Results

Table 8.1 summarises information about the tests that have been carried out. Figures 8.2 and 8.3 illustrate the change in resistivity of the various tests as a function of (a) time and (b) the pore water salt content of the sample, respectively.

Table 8.1 Summary of the tests carried out to date

	Test number			
	1	2	3	4
Depth of Sample (m)	12.5	8.0	8.0	8.0
Initial Salt Content (g/l)	9.0	32.6	32.6	32.6
Final Salt Content (g/l)	0.3	0.6	2.0	0.9
Duration of test (days)	130	140	70	125
Initial Undisturbed Shear Strength (kPa)		20	20	20
Initial Remoulded Shear Strength (kPa)		2	2	2
Final Undisturbed Shear Strength (kPa)	–	–	9.0	14.0
Final Remoulded Shear Strength (kPa)	–	–	0.2	0.4

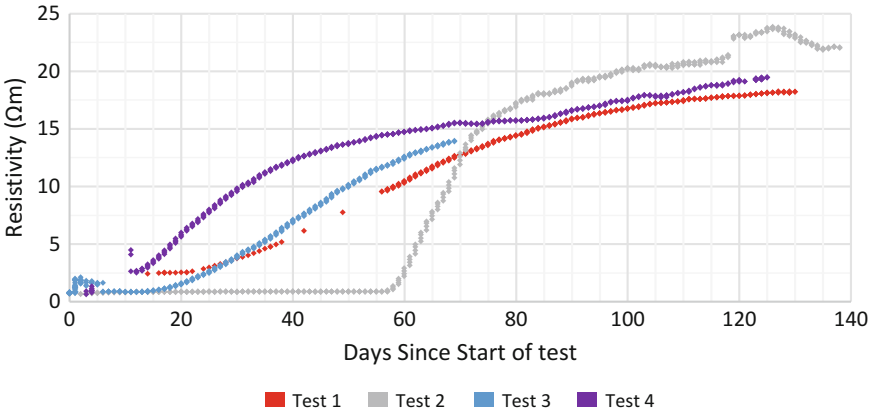

Fig. 8.2 Change in resistivity of the clay sample while undergoing leaching

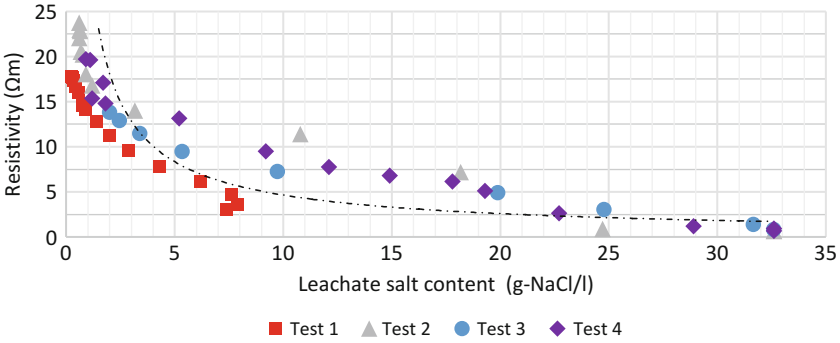

Fig. 8.3 Change in the resistivity of the clay sample as a function of pore water salinity. Dashed line is trend suggested by Long et al. (2012) of the form $y = Ax^n$

Test 1 was used to verify that the system was able to measure the change in resistivity and shear wave velocity as the pore water salt content was reduced by leaching. The sample used in Test 1 was a reconstituted sample of Onsøy clay, it was reconstituted using a pug mill in NGI's Schmertmann Research Laboratory.

The pore water salinity at the start of the test was 9 g-NaCl/l, the pore water salt content was reduced by the leaching method, described previously, to a salinity of 0.3 g-NaCl/l. This reduction in pore water salt content increased the resistivity of the sample from an initial resistivity of 2.4 Ωm to a final resistivity of 17.7 Ωm, see Fig. 8.2. The final shear strengths of this sample were not determined as the sample was reconstituted, this process destroyed the natural structure of the clay and, as a result, significant changes to the undisturbed shear strength, remoulded shear strength and resultant sensitivity were not expected.

Tests 2, 3 and 4 were conducted using a sample cut from a Sherbrooke block sample obtained from a depth of 8.0 m. Each sample had a starting pore water salt content of 32.6 g–NaCl/l. At this depth Onsøy clay typically has an undisturbed shear strength between 20 and 30 kPa, depending upon sampling and testing methods, and a remoulded shear strength of 2–3 kPa, and a resulting sensitivity between 8 and 16, according to Lunne et al. (2003).

During Test 2, one of the drainage lines was blocked, this is clearly visible in Fig. 8.2, as between days 20 and 60 there was no noticeable change in the resistivity of the sample. The method of clearing the drainage lines may have damaged the microstructure of the clay, and in this case neither the undisturbed or remoulded shear strength was calculated.

Figure 8.3 shows the change in resistivity of the marine clay as it was leached of its pore water salt content. Test 2 (shown in grey) had an initial pore water salt content of 32.6 g–NaCl/l and was leached to final pore water salt content of 0.6 g–NaCl/l. The reduction in pore water salinity resulted in an increase in the sample resistivity, from an initial value of 0.7 Ωm to a final resistivity value of 18.1 Ωm.

In Test 3, (shown in light blue), the pore water salt content was reduced to 1.8 g–NaCl/l. The resistivity of the sample increased from an initial value of 0.7 Ωm to a final value of 13.8 Ωm. The remoulded shear strength, measured using the fall cone method, decreased from an initial value of 2.0 kPa to a final value 0.2 kPa, which according to the Norwegian definition, making this leached marine clay, quick.

In Test 4, (purple), the pore water salt content was reduced to 0.9 g–NaCl/l. The resistivity of the sample increased from an initial value of 0.9 Ωm to a final value of 19.7 Ωm. The remoulded shear strength of this sample, measured via fall cone test, was found to have decreased from initially 2 kPa to 0.4 kPa, making the clay quick.

Figure 8.4 shows the change in the shear wave velocity of the sample in Tests 1, 2 and 4, as the sample was leached. No measurements were possible for Test 3 due to equipment malfunction. In Test 1 the initial V_s was 118 m/s which increased to a final velocity of 126 m/s this occurred over the same time period as a reduction in the pore water salt content, as previously stated, from 9.0 g–NaCl/l to 0.3 g–NaCl/l, Fig. 8.5.

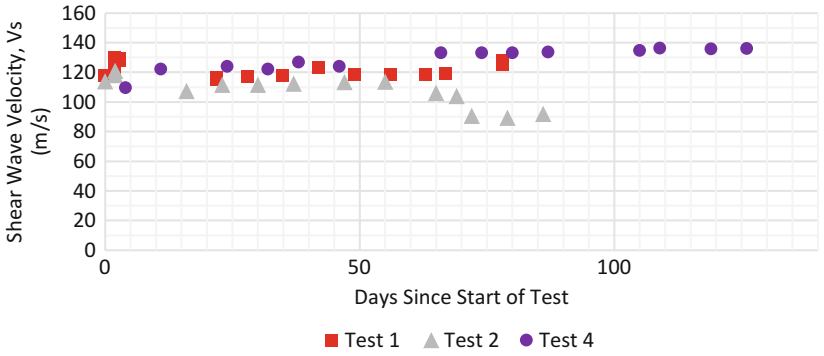

Fig. 8.4 Change in shear wave velocity of the clay samples while undergoing leaching

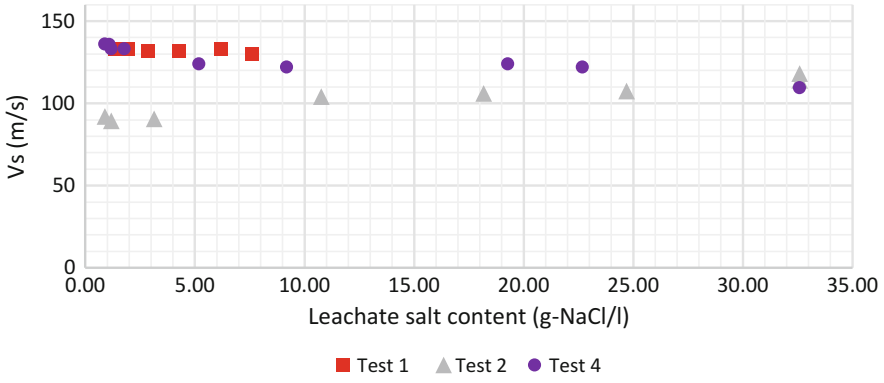

Fig. 8.5 Change in the shear wave velocity of the sample as a function of the pore water salinity

In Test 2 V_s decreased from 114 m/s to a final value of 92 m/s. This reduction in the shear wave velocity occurred over the same time period that the pore water salt content was reduced from an initial value of 32.6 g–NaCl/l to 0.6 g–NaCl/l, see Fig. 8.5. Due to the blockage in the drainage line in Test 2, nothing conclusive can be drawn from this reduction in V_s as any change in stiffness may be due to clearing the blockage.

In Test 4V_s increased from 109 m/s to a final value of 136 m/s. This increase in value occurred over the same time period that the pore water salt content reduced from an initial value of 32.6 g–NaCl/l to a final value of 0.9 g–NaCl/l, see Fig. 8.5.

8.4 Discussion

The reduction in the pore water salt content and consequent increase in the resistivity of the clay sample was expected as pore water salt is typically comprised of fully dissociated salts containing Na^+, K^+, Mg^{2+}, and Ca^{2+} ions which have lower electrolytic resistivity's than the clay dominated matrix. This was consistent in all four tests. The increase in the resistivity of the sample as a function of the salt content as shown in Fig. 8.3 appears to be of the form $y = Ax^n$ which is the same form as suggested by Long et al. (2012).

The results of Tests 3 & 4 suggest that the reduction in the remoulded shear strength, from 2 kPa in both cases to 0.2 kPa and 0.4 kPa in Tests 3 & 4 respectively, hence increase in the sensitivity, of the clay is linked to the reduction in the pore water salt content of the clay. This is consistent with Bjerrum (1954) conclusions regards the influence of salt content and the remoulded shear strength.

The initial laboratory resistivity and shear wave velocity measurements have been compared to values obtained from seismic and ERT surveys of the Onsøy research site, the values for resistivity measured in the lab for a sample at 8 m depth are in the range of 0.7–0.9 Ωm, while the value obtained from the ERT profile the resistivity at this depth is 0.8 Ωm (Bazin et al. 2016).

The small variation between the resistivity measured in the laboratory and those determined from ERT surveys indicates the laboratory setup is capable of accurately replicating the conditions encountered in the field. This also indicates that the storage method used for these samples had limited impact upon the salt content of the block sample, although more information on the ion composition and concentrations would be required to verify this.

It should, however, be noted that the pore water salinity according to Lunne et al. (2003), was expected to be 35 g/l whereas in both samples of Onsøy clay, the initial salinity was 32.6 g/l. A higher initial resistivity would therefore have been expected in the lab resistivity measurement, if the stress conditions in the lab accurately the *in situ* conditions at the site, than that obtained from the ERT survey (Bazin et al. 2016).

The lower than expected resistivity, given the salt content and stress conditions, is possibly as a result of changes in the consistency limits of the soil due to aging

of the soil during storage including a possible increase in moisture content due to the sampling technique, and changes in the salinity of the sample due to oxidation (NGI 2013) which has been shown to cause variations in resistivity, in particular the moisture content and salinity, (Samouëlian et al. 2005; Hazreek et al. 2015).

The V_s measurements from laboratory tests suggest that the initial shear wave velocity is between 109 m/s and 127 m/s, whereas the seismic data in the field gives a value of 105 m/s to109m/s (Bazin et al. 2016). The difference between the value in the field and the laboratory is likely due to a number of factors including, sample disturbance during preparation of the sample for testing, ageing of the samples while they were kept in storage and methodological uncertainty associated with selecting travel time between bender elements.

The increase in V_s observed during Test 1 is likely due to a combination of volume change and the effects of secondary consolidation. Research by Anderson and Stokoe (1978) propose that the increase in V_s with time is expected to be about 5–20% for every log cycle of time, for normally consolidated clays.

Test 2 showed a reduction in V_s from 114 m/s to 92 m/s, this was likely caused by clearing a blockage in the drainage lines, which would have disturbed the sample, however the reduction in V_s of the sample does occur when the pore water salt content of the sample falls below a threshold value of 5 g/l, and this corresponds to the expected changes in strength and stiffness of highly sensitive and quick clays (Bjerrum 1954). However the results of Test 4 show a 5% increase in V_s, per log cycle time, of the sample which is likely due to a combination of volume change and the effects of secondary consolidation which is in line with what was proposed by Anderson and Stokoe (1978), indicating that the reduction in V_s shown in Test 2 was due to sample disturbance during testing.

The pore water salt content is determined by measuring the conductivity of the fluid collected in the volume control unit. There are a few issues with this method, firstly, the salinity of the fluid that was flushed out of the sample may not be the same as the salinity of the pore water in the sample at the time of collecting the fluid (i.e. there will be a time lag). Secondly the exact geochemical composition of the pore water is unknown, and it is unknown whether the change in conductivity is a result of changes in Na^+, K^+, Ca^{2+}, and Mg^{2+} and not as a result of other oxidised stabilising ions.

8.5 Conclusion

The results of the preliminary tests show that using a modified triaxial cell to quantify the changes in geotechnical and geophysical properties of a marine clay as its pore water salt content is reduced is possible. The results of Tests 3 and 4 show that it is possible to create a highly sensitive (or quick) clay using the leaching method outlined.

In addition to determining the changes in the undisturbed and remoulded shear strengths due to reduction in the pore water salt content, it is proposed that future

work will assess the affect of moisture content, density, grain size distribution, consistency limits, pore water chemistry, grain size distribution and clay content on the geophysical properties during leaching of 'salt' clay samples.

Acknowledgements The authors wish to extend their sincere gratitude to Toralv Berre, Morten Andreas Sjursen, and Rune Dyvik at NGI geotechnical laboratory for all the help and expertise offered in laboratory work. We would also like to thank both NGI and Prof. JH Schmertmann for the use of both time and equipment in NGI's Schmertmann Research Laboratory. Funding for this research has been provided by both the Department for Employment and Learning (NI) and the NGI Schmertmann Research Laboratory.

References

Anderson DG, Stokoe KH (1978) Shear modulus: a time-dependent soil property. ASTM Special Technical Publication, Philadelphia, pp 66–90

Bazin S, Anschütz H, Sauvin G, Gribben S, Donohue S, Long M (2016) Geophysical characterisation of marine and quick clay sites: field and laboratory tests. In: 5th International conference on geotechnical and geophysical site characterisation. pp 0–5

Bjerrum L (1954) Geotechnical properties of Norwegian marine clays. Géotechnique 4(2):49–69

Donohue S, Long M, L'Heureux JS, Solberg IL, Sauvin G, Rømoen M, Kalscheuer T, Bastani M, Persson L, Lecomte I, O'Connor P (2014) Landslides in sensitive clays: from geosciences to risk management. In J.-S. L'Heureux et al., (eds) Dordrecht, Springer Netherlands, pp 159–178

Donohue S, Long M, O'Connor P, Eide Helle T, Pfaffhuber AA, Rømoen M (2012) Multi-method geophysical mapping of quick clay. Near Surf Geophy 10(1828):207–219

Engdahl M (2006) Natural hazards in Nordic countries. Episodes J Int Geosci 31(1):176–184

Hazreek ZAM, Aziman M, Azhar ATS, Chitral WD, Fauziah A, Rosli S (2015) The behaviour of laboratory soil electrical resistivity value under basic soil properties influences. Aero Earth 23:12002

Holmsen PER (1953) Landslips in Norwegian quick-clays. Géotechnique 3(5):187–194

Long M, Donohue S, L'Heureux JS, Solberg IL, Rønning JS, Limacher R, O'Connor P, Sauvin G, Rømoen M, Lecomte I (2012) Relationship between electrical resistivity and basic geotechnical parameters for marine clays. Can Geotech J 49(10):1158–1168

Lundström K, Larsson R, Dahlin T (2009) Mapping of quick clay formations using geotechnical and geophysical methods. Landslides 6(1):1–15

Lunne T, Long M, Forsberg CF (2003) Characterisation and engineering properties of Onsøy clay. In: Characterisation and engineering properties of natural soils. Swets & Zeitlinger, Lisse, pp 395–428

NGI (2013) Effect of storage time on sample quality, Report number 68-2014

NIFS (2015) Detektering av kvikkleire - Sluttrapport (Detection of Sensitive Material), Report number 126-2015. ISSN 1501–2832

Rankka K, Andersson-Sköld Y, Hultén C, Larsson R, Leroux V, Dahlin T, (2004) Quick clay in Sweden, Linkoping, Goteborg. Lund

Samouëlian A, Cousin I, Tabbagh A, Bruand A, Richard G (2005) Electrical resistivity survey in soil science: a review. Soil Tillage Res 83(2):173–193

Sauvin G, Lecomte I, Bazin S, Hansen L, Vanneste M, L'Heureux JS (2014) On the integrated use of geophysics for quick-clay mapping: the Hvittingfoss case study, Norway. J Appl Geophys 106:1–13

Solberg IL, Hansen L, Rønning JS, Haugen ED, Dalsegg E, Tønnesen JF (2012) Combined geophysical and geotechnical approach to ground investigations and hazard zonation of a quick clay area, mid Norway. Bull Eng Geol Environ 71(1):119–133

Solberg IL, Rønning JS, Dalsegg E, Hansen L, Rokoengen K, Sandven R (2008) Resistivity measurements as a tool for outlining quick-clay extent and valley-fill stratigraphy: a feasibility study from Buvika, central Norway. Can Geotech J 45(2):210–225

Torrance JK (1974) A laboratory investigation of the effect of leaching on the compressibility and shear strength of Norwegian marine clays. Géotechnique 24(2):155–173

Torrance JK (1983) Towards a general model of quick clay development. Sedimentology 30(4):547–555

Wang Z, Gelius LJ, Kong FN (2009) Simultaneous core sample measurements of elastic properties and resistivity at reservoir conditions employing a modified triaxial cell – a feasibility study. Geophys Prospect 57(6):1009–1026

Chapter 9
Determination of Remoulding Energy of Sensitive Clays

Vikas Thakur, Samson Abate Degago, Juha Selänpää, and Tim Länsivaara

Abstract Energy involved in disintegrating of sensitive clays from an intact to a fully remoulded state is one of the key aspects in assessing the post failure movements of sensitive clay landslides. This energy is referred to as remoulding energy. In this paper, the energy approach is conceptualised using an analytical approach. A comprehensive review of the empirical, laboratory and field techniques to estimate remoulding energy are presented and discussed in detail.

9.1 Introduction

Sensitive clays are strain-softening materials characterized by a decrease in shear strength with increasing deformation once the peak shear strength is attained. These clays transform from an intact state to highly viscous fluid when subjected to large deformation during retrogressive landslides, e.g. flow slides and spreads. This may result in a large run-out of slide debris, which may cause damage to the infrastructures and the nearby environment. This aspect is schematically illustrated in Fig. 9.1 using a Norwegian sensitive clay sample along with the run-out of the slide debris involved in the Hobol sensitive clay landslide in Norway in 2014. Additional factors, such as the topography and the stability of the area behind the initial slide zone, may influence the post failure movement of slide debris. However, if the involved sensitive clays are not sufficiently remoulded, vast landslides, such as those mentioned in the literature e.g. Karlsrud et al. (1985), Tavenas et al. (1983), Thakur and Degago (2014), are less likely to occur. Several indicators for occurrence

V. Thakur (✉)
Department of Civil and Environmental Engineering, Norwegian University of Science and Technology (NTNU), Trondheim, Norway
e-mail: vikas.thakur@ntnu.no

S.A. Degago
Norwegian Public Roads Administration (NPRA), Trondheim, Norway
e-mail: samson.degago@vegvesen.no

J. Selänpää • T. Länsivaara
Tampere University of Technology (TUT), Tampere, Finland
e-mail: juha.selanpaa@tut.fi; tim.lansivaara@tut.fi

V. Thakur et al. (eds.), *Landslides in Sensitive Clays*, Advances in Natural and Technological Hazards Research 46, DOI 10.1007/978-3-319-56487-6_9

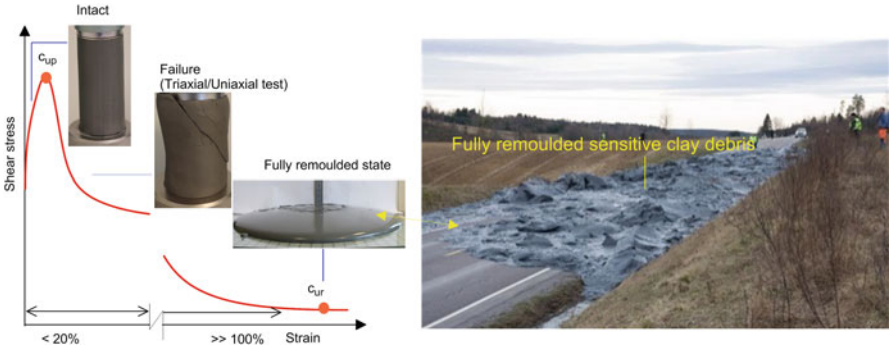

Fig. 9.1 Process of remoulding of sensitive clays illustrated using an ideal shear stress-shear strain plot (*Left*) along with the run-out of the slide debris involved in the Hobol sensitive clay landslide in Norway in 2014 (*Right*, photo taken by NGI)

of retrogressive landslides such as remoulded shear strength (c_{ur}), liquidity index (I_L), sensitivity (S_t), quickness (Q) or stability number (N_c), have been suggested in the literature. Thakur et al. (2014) carried out a detailed study using data from 33 Norwegian landslides, which suggests that these geotechnical parameters, although useful indicators of potential for flow slides, cannot be used individually to assess whether or not a flow slide will actually occur. In addition to the topographical aspects, a complete stress-strain behaviour of the involved soft sensitive clays must be accounted in the assessment process, which can be done using the remoulding energy concept.

During a landslide in sensitive clays, the change in the potential energy (ΔE^P) is equal to the energy consumed in the disintegrating of the soil to its remoulding state (ΔE^R) and in the slide movement (kinetic and frictional energy, ΔE^K), Eq. 9.1.

$$\Delta \mathrm{E}^{\mathrm{P}} = \Delta \mathrm{E}^{\mathrm{R}} + \Delta \mathrm{E}^{\mathrm{K}} \tag{9.1}$$

Equation 9.1 implies that the available potential energy to be transformed (E^P) and the required remoulding energy (E^R) have huge significance in deciding the extent of landslides in sensitive clays. Equation 9.1 also implies that for a given change in E^P, sensitive clays with higher E^R result in smaller slide movement (because of lesser E^K) than sensitive clays with lower E^R. The slide movement is characterised by the run-out distance and the retrogression distance, which is controlled by the amount of energy transferred to E^K during the slide process (Thakur and Degago 2014). Similarly, Locat et al. (2008) have made an effort to correlate the remoulding energy with run-out distances for 22 sensitive clay landslides in Canada and their study indicated a promising trend. In summary, an accurate assessment and prediction of retrogressive landslides in sensitive clays requires knowledge about the energy involved in the remoulding of sensitive clays. However, experimental determination of remoulding energy is not a straightforward

task, as it requires some special arrangements. In this paper, an attempt has been made to discuss the remoulding energy concept and various field and laboratory approaches that can be used to estimate it.

9.2 An Analytical Framework for the Remoulding Energy Concept

Remoulding energy (E^R) can simply be defined as the strain energy involved in the remoulding of a material. Considering clays that display elastic hardening followed by a strain-softening behaviour, the shear stress (τ)-shear strain (γ) response can schematically be idealised as in Fig. 9.2. The subscripts p and r represent the peak and the residual states, respectively. The area (B) under the τ-γ curve after the peak undrained shear strength (c_{up}) represents the second-order work or the strain energy dissipated during the remoulding process, i.e. the required E^R.

For an ideal behaviour of sensitive clays (Fig. 9.2), the total remoulding energy (area B) can be defined as;

$$E^R = c_{ur}\left(\gamma_r - \gamma_p\right) + \frac{1}{2}\left(c_{up} - c_{ur}\right)\left(\gamma_r - \gamma_p\right) \tag{9.2}$$

Equation 9.2 can be rewritten as;

$$E^R = \frac{(n-1)}{2}\left(c_{up} + c_{ur}\right)\gamma_p \tag{9.3}$$

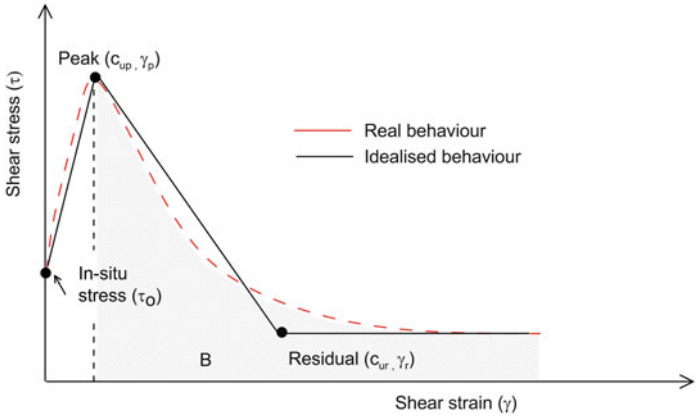

Fig. 9.2 Stress–strain behaviour of sensitive clays. The real soil response is shown as the *dotted line*; the continuous line is adopted in estimation of remoulding energy

where $n = \frac{\gamma_r}{\gamma_p}$ gives a measure of sensitivity or softening in terms of strain and is referred in this article as strain softening index. Higher n indicates that larger E^R is required to disintegrate a material. Normally $c_{ur} << c_{up}$ for sensitive clays, therefore Eq. 9.3 can be approximated as;

$$E^R \sim \frac{(n-1)}{2} c_{up}.\gamma_p \tag{9.4}$$

Such approximation will only underestimate E^R by 1% for sensitive clays having sensitivity greater than 100. Whereas the same will be underestimated by 2% and up to 5% when $50 > S_t > 100$ and $S_t < 50$, respectively. Majority of sensitive clays responsible for landslides have a sensitivity over 100. Therefore, Eq. 9.4 shall be considered a reasonable approximation.

Undrained shear strength (c_{up}) is a function of pre-consolidation pressure (σ_c') such that it can be related as $c_{up} = \alpha.\sigma'_c$. Accordingly, Eq. 9.4 can be further re-written as

$$\boldsymbol{E^R \sim \frac{(n-1)}{2} \alpha.\sigma'_c.\gamma_p} \tag{9.5}$$

It can be noted from Eq. 9.5 that E^R is directly related to the pre-consolidation pressure (or undrained shear strength), the strain softening index n and strain at fully disintegration state γ_p. Therefore, the often anticipated single parameters such as sensitivity S_t ($= c_{up}/c_{ur}$) are not sufficient to describe the ability of sensitive clays to remould. Previous studies e.g., Tavenas et al. (1983), Thakur et al. (2014) indicate that index test parameters such as liquid limits, remoulded shear strength, plasticity index influences the remoulding energy of sensitive clays.

9.3 Determination of Remoulding Energy Based on Laboratory Tests

Various researchers have attempted to investigate the role of E^R in large retrogressive landslides (e.g. Bishop 1967; Eigenbrod 1972; Flon 1982; Tavenas et al. 1983; D'Elia et al. 1998; Karlsrud et al. 1985; Leroueil et al. 1996; Leroueil 2001; Hutchinson 2002; Vaunat and Leroueil 2002; Locat et al. 2008; Quinn et al. 2011; Thakur and Degago 2013; Thakur et al. 2012, 2013, 2014, 2015). However, Tavenas et al. (1983) was the first to attempt the determination of E^R of sensitive clays using laboratory investigations. They estimated the remoulding energy of seven different Canadian sensitive clays using innovative approaches where different processes by which a sensitive clay may disintegrate during a landslide event were simulated using laboratory set-ups (see Fig. 9.3). Accordingly, these processes are the shearing along with continuous straining and displacement along a failure surface; squeezing

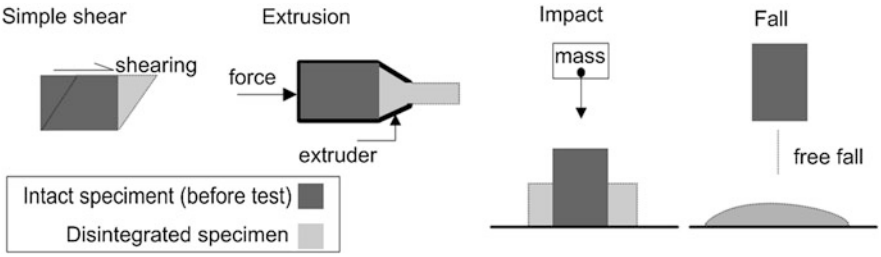

Fig. 9.3 Illustrations of the laboratory set-up to simulate the processes responsible for the remoulding of sensitive clays involved in a landslide (After Tavenas et al. 1983)

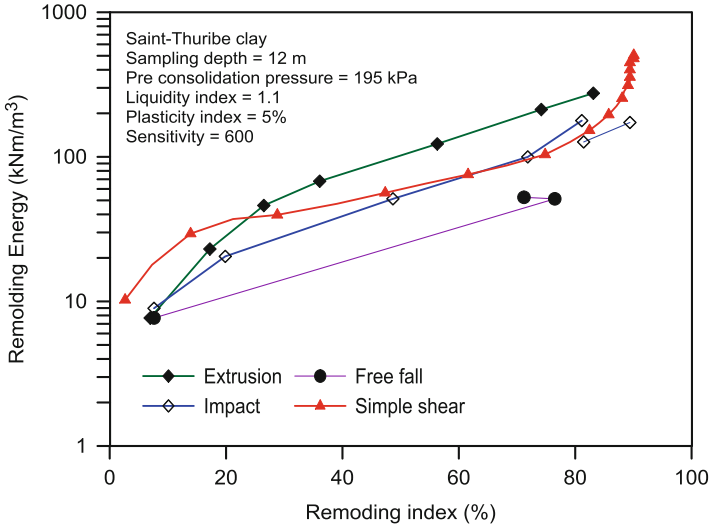

Fig. 9.4 Remoulding Energy at different remoulding index of the Saint-Thuribe specimen as tested by Tavenas et al. (1983)

and extrusion between relatively intact clay blocks; impact of clay block on the bottom of the slide bowl or impact on clay blocks from falling objects or soil. The energy involved in the remoulding process depends on the degree of remoulding. The term remoulding index (I_r) is thus used to indicate the degree of remoulding and can be defined as a ratio between (c_{up}−c_{ux}) and (c_{up}−c_{ur}), where c_{ux} is the undrained shear strength between c_{up} and c_{ur} for which I_r is being defined. $I_r = 0$ and 1 refers to a fully intact, fully remoulded state, respectively. For the tested clays, Tavenas et al. (1983) found that the remoulding process induced by the extrusion method required the highest amount of energy, whereas the free fall method disintegrated the tested sample on a much lower energy level. This is illustrated in Fig. 9.4 for Saint-Thuribe clay as tested by Tavenas et al. (1983).

Tavenas et al. (1983) observed (Fig. 9.4) that the extrusion method might overestimate the remoulding energy due to the friction between the tested specimen

and the apparatus, while the free fall method may underestimate the same due to a non-uniform remoulding of specimen. They recommend that the simple shear test is the best suited approach. The remoulded energy for the tested clays varied between 150–500 kNm/m^3 depending on the liquid limit, over-consolidation ratio and the plasticity index of the tested clays. Based on the laboratory experiments by Tavenas et al. (1983), Leroueil et al. (1996) proposed a pragmatic approach to calculate remoulding energy required as given in Eq. 9.6.

$$E^R = 16\, c_{up}\, I_p \tag{9.6}$$

Locat et al. (2008) have validated Eq. 9.6 using data from 22 landslides in Canadian sensitive clays. Thakur and Degago (2013) proposed an analytical solution to estimate the remoulding energy of Norwegian sensitive clays based on 18 Norwegian landslide sites.

9.4 Determination of Remoulding Energy Based on In-situ Tests

Recently, Thakur et al. (2015) made an effort to determine remoulding energy of Norwegian sensitive clays using a field vane shear apparatus. Following this approach, this work presents remoulding energy determined for three different low plastic sensitive soft clay deposits located in Central Norway as well as for a high plastic sensitive Perniö clay deposit in Finland. A representative stress-strain behaviour of soft sensitive clays can be established using the electric field vane shear method. Therefore, the registered total torque per unit volume (T_{tot}) in the field vane test was considered equivalent to the remoulding energy. In doing so, the shear stress, τ, was calculated using Eq. 9.7;

$$\tau = \frac{6}{7}\frac{T_{tot}}{\pi D^3} \tag{9.7}$$

In the field tests, 65 mm diameter (D) and 135 mm high vane were used, At the desired depth, a constant rotation rate of 2° per second was applied. A continuous measurement of the torque was made till the vane is rotated to 360°. The interpretation were based on following assumptions;

- The failure surface has cylindrical shape
- The soil is completely undrained during the test i.e. no local drainage of pore water from the shear zones occurs
- Isotropic strength condition in the soil volume
- There is no progressive failure in the soils subjected to shear.

Table 9.1 Soil properties of the tested sensitive clays in this study

Parameters (units)	Tiller clay	Klett clay	Fallan clay	Perniö clay
Natural water content (%)	40	33	33	95.1
Unit weight (kN/m^3)	19	20.2	18.8	14.5
Salt content (g/l)	1.0	1.0	0.8	–
Fall cone remoulded strength (kPa)	0.1	0.1	0.2	0.3
Fall cone sensitivity (−)	300	240	99	66
Liquidity index (−)	4.5	2.1	4.4	1.68
Plasticity index (%)	5	7	5	28
Fine silt fraction (%)	62	20	23	15
Coarse silt fraction (%)	0	11	8	0
Clay fraction (%)	38	32	34	83
Pre consolidation pressure (kPa)	112.5	120	260	64
In-situ vertical effective stress (kPa)	86.5	100	87	48

The soil properties and the interpreted shear stress-vane rotation plots of the tested clays are shown in Table 9.1 and Fig. 9.5, respectively. The tested Norwegian clays i.e. Tiller clay, Klett clay, Fallan clay are low plastic in nature whereas the Finnish Perniö clay, which is very well documented in the literature (e.g. Lehtonen et al. 2015), is highly plastic yet soft and sensitive in nature. All these tests were carried out at depths between 7.4 and 8.5 m below terrain level.

Figure 9.5 suggests that a representative stress-strain behaviour of soft sensitive clays can be established using the shear stress-vane rotation relationship established from electric field vane shear method. However, the field vane measurements beyond 90^o rotation indicate that the undrained shear strength remains more or less unchanged. Such behaviour is believed to be the result of the drainage of excess pore water pressure from the sheared zone or due to the cutting of partly intact clay at the bottom or at the side of the shear surface. These are considered to be major inherent limitation of the test. Therefore, the shear stress-vane rotation response beyond 90^o rotation is not considered in the determination of remoulding energy. Instead, to calculate the total remoulding energy at fully remoulded state, a linear extrapolation of the downward curve of the shear stress-radial displacement (vane rotation) part is made until the residual shear stress is achieved as shown in the Fig. 9.5 using the dotted lines.

Results of the estimated remoulding energy are presented in Fig. 9.6 along with Norwegian and Canadian data from earlier studies. The data are seen to follow a similar trend with an indication that the Canadian sensitive clays require higher energy to fully disintegrate as compared to the rest of the data. Remoulding energy as estimated by the empirical correlation given in Eq. 9.6 is also plotted in Fig. 9.6 using a solid line and this is seen to be in reasonably good agreement with the majority of the data. However, it may over predict remoulding energy for some sensitive clays.

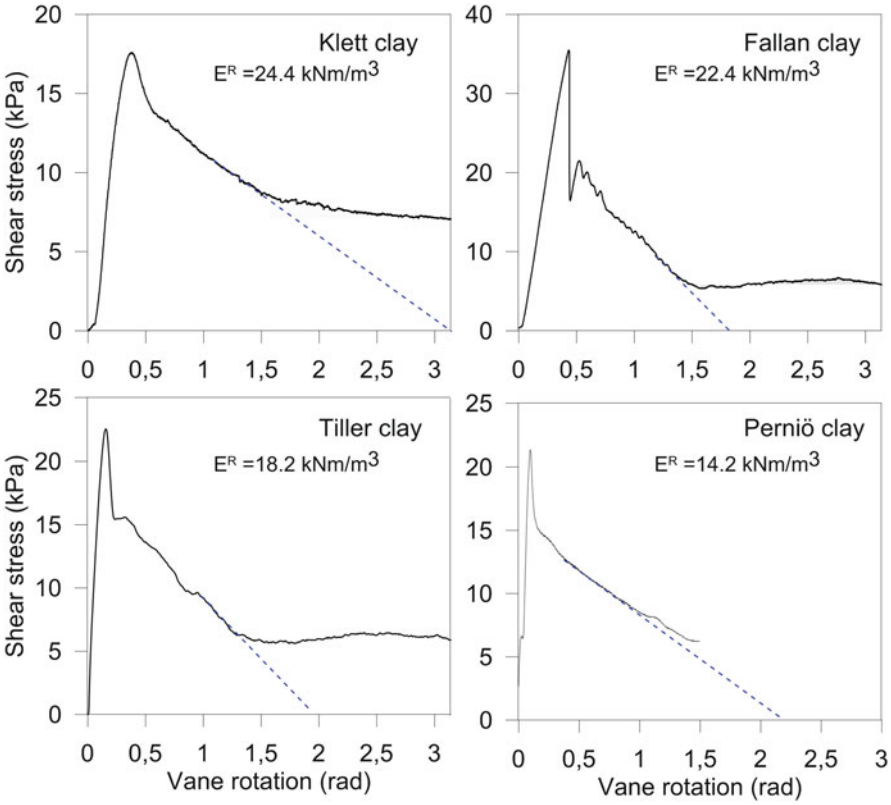

Fig. 9.5 Shear stress-vane rotation curve for four Scandinavian clays

It is worth mentioning that low plastic sensitive clays e.g., Norwegian sensitive clays are known to be easily affected by sample disturbance. Therefore, soil parameters derived from such laboratory tests are not always representative of the in-situ condition. Even with samples of high quality, determination of remoulding energy in the laboratory is not a straightforward task as it requires some special arrangement so that specimen can be deformed their residual strain level γ_p (see Fig. 9.1 right). Therefore, an in-situ methodology such as the vane shear apparatus for an in-situ measurement of the remoulding energy could be a sound alternative. In doing so, one need to account for the progressive failure and the shear band thickness in low plastic sensitive clays (e.g., Gylland et al. 2013; Jostad et al. 2014).

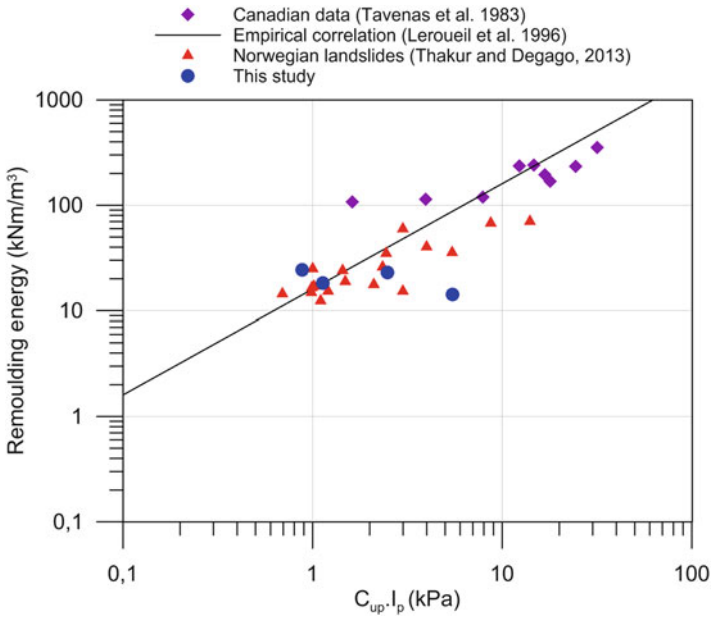

Fig. 9.6 A comparison between various approaches to determine remoulding energy

9.5 Conclusions

This paper presents some fundamental aspects of energy involved in remoulding of sensitive clays. An analytical solution to estimate remoulding energy is proposed. Determination of remoulding energy based on shear stress-vane rotation relationship of sensitive clays using field vane shear tests is also illustrated. This work shows that a representative stress-strain behaviour of soft sensitive clays can be established using the electric field vane shear apparatus. Despite the limitations associated with the testing procedure, the preliminary results are promising. This study also shows that the trend obtained using the empirical solution proposed by Leroueil et al. (1996) and the analytical solution proposed by Thakur and Degago (2014) are applicable for various sensitive clay data. However, further efforts should be made to validate the obtained results using extensive field-testing for different in-situ conditions.

Acknowledgements The cooperative research program «Natural hazards: Infrastructure for Floods and Slides (NIFS)» by the Norwegian Public Roads Administration, the Norwegian National Rail Administration and the Norwegian Water Resources and Energy Directorate is acknowledged for its support. The GeoFuture II project, partly financed by the Research Council of Norway, also is gratefully acknowledged for providing necessary resources. The authors also wish to express their gratitude to the reviewer Petter Fornes at NTNU and NGI.

References

Bishop AW (1967) Progressive failure – with special reference to the mechanism causing it. In: Proceedings of the geotechnical conference on shear strength properties of natural soils and rocks, vol 1, pp 142–150

D'Elia B, Picarelli L, Leroueil S (1998) Geotechnical characterization of slope movements in structurally complex clay soils and stiff jointed clays. Rivista Italiana di Geotecnica XXXIII:5–32

Eigenbrod KD (1972) Progressive failure in OC clays and mudstones. PhD Thesis, University of Alberta

Flon P (1982) Énergie de remaniement et régression des coulées d'argiles. MSc thesis, Department of Civil Engineering, Laval University, Québec

Gylland AS, Jostad HP, Nordal S, Emdal A (2013) Micro-level investigation of the in situ shear vane failure geometry in sensitive clay. Geotechnique 63(14):1264–1270

Hutchinson JN (2002) Chalk flows from the coastal cliffs of northwest Europe, Catastrophic landslides: effects, occurrence, and mechanisms. Geol Soc Am Rev Eng Geol 1:257–302

Jostad HP, Fornes P, Thakur V (2014) Effect of strain-softening in design of fills in gently inclined areas with soft sensitive clays. First international workshop on landslide in sensitive clays. Advances in Natural and Technological Hazards Research 36, Chapter: 24, Publisher: Springer, pp 305–316

Karlsrud K, Aas G, Gregersen O (1985) Can we predict landslide hazards in soft sensitive clays? Summary of Norwegian practice and experience. NGI Publication 158

Lehtonen VJ, Meehan CL, Länsivaara TT (2015) Full-scale embankment failure test under simulated train loading. Geotechnique 65(12):961–974

Leroueil S (2001) Natural slopes and cuts: movement and failure mechanisms. Géotechnique 51(2):197–243

Leroueil S, Vaunat J, Picarelli L, Locat J, Faure R, Lee H (1996) A geotechnical characterisation of slope movements. In: Proceedings of 7th international symposium on landslides, Trondheim, vol 1, pp 53–74, Balkema, Rotterdam

Locat P, Leroueil S, Locat J (2008) Remaniement et mobilité des débris de glissements de terrain dans les argiles sensible de l'est du Canada. In: Proceedings of the 4th Canadian conference on geohazards: from causes to management, Presse de l'Université Laval, Québec, pp 97–106

Quinn PE, Diederichs MS, Rowe K (2011) A new model for large landslides in sensitive clay using a fracture mechanics approach. Can Geotech J 48(8):1151–1162

Tavenas F, Flon P, Lerouil S, Lebuis J (1983) Remoulding energy and risk of slide retrogression in sensitive clays. In: Symposium on slopes on Soft Clays, Linköping, Sweden, pp 423–454

Thakur V, Degago SA (2013) Disintegration energy of sensitive clays. Géotechnique Lett 3(1):21–25

Thakur V, Degago SA (2014) Quickness test approach for assessment of flow slide potentials. Int Geotech Eng J SEAGS AGSSEA 45(1):85–94

Thakur V, Oset F, Degago S A, Berg P O, Aabøe R, Wiig T, Elisabeth E D, Lyche E, Sæter M B, Robsrud A (2012) A critical appraisal of the definition of Brittle clays (Sprøbruddmateriale). In: Proceedings of the 16th Nordic Geotechnical Meeting Copenhagen, vol 1, pp 451–462

Thakur V, Degago A, Oset F, Dolva BK, Aabøe R (2013) A new approach to assess the potential for flow slide in sensitive clays. In: 18th international conference on soil mechanics and geotechnical engineering, pp 2265–2268

Thakur V, Degago S A, Oset F, Aabøe R, Dolva BK, Aunaas K, Nyheim T, Lyche E, Jensen OA, Sæter MB, Robsrud A, Viklund M, Nigussie D (2014) Characterization of post-failure movements of landslides in soft sensitive clays. First international workshop on landslide in sensitive clays. Advances in Natural and Technological Hazards Research 36, Chapter: 24, Publisher: Springer, pp 91–103

Thakur V, Degago SA, Oset F, Gylland SA, Sandven R (2015) In-situ measurement of remolding energy of sensitive clay. In: 68th Canadian geotechnical conference, GeoQuebec, Quebec

Vaunat J, Leroueil S (2002) Analysis of post-failure slope movements within the framework of hazard and risk analysis. Nat Hazards 26:83–102

Chapter 10
Problems Related to Field Vane Testing in Soft Soil Conditions and Improved Reliability of Measurements Using an Innovative Field Vane Device

Juha Selänpää, Bruno Di Buò, Tim Länsivaara, and Marco D'Ignazio

Abstract In Finland, undrained shear strength is commonly measured using the field vane shear test (FV). Currently, the most commonly used field vane testers are the Nilcon vane and the electrical vane with shear rotation and measuring systems located above the ground level. Vane testing is normally carried out using vanes equipped with slip coupling, while the use of casing for protecting the vane is not very common. Recent studies from Finland have shown that the undrained shear strength of clays can be significantly underestimated when casing is not used. Experimental observations suggest that the slip coupling might not always be sufficient to remove all of the rod friction effects that occur during testing. Tampere University of Technology has recently purchased an innovative field vane apparatus with a vane tester unit, where torque and rotations are measured right above the vane. In this way, the effect of rod friction is minimized and the measured stress-rotation behavior is less biased. In this study, issues related to practical applications, testing devices and interpretation methods are discussed. Then, a critical comparison between test results in soft clays from both the traditional and new field vane testers is performed.

10.1 Principle of Field Vane Testing

The main advantage of the field vane test (FV) is that it gives an almost direct measurement of the in-situ undrained shear strength (s_u) (SGY 1995). In principle, the residual and remolded s_u can also be determined. The test is conducted by

J. Selänpää (✉) • B. Di Buò • T. Länsivaara
Tampere University of Technology (TUT), Tampere, Finland
e-mail: juha.selanpaa@tut.fi; bruno.dibuo@tut.fi; tim.lansivaara@tut.fi

M. D'Ignazio
Norwegian Geotechnical Institute (NGI), Oslo, Norway
e-mail: marco.dignazio@ngi.no

V. Thakur et al. (eds.), *Landslides in Sensitive Clays*, Advances in Natural and Technological Hazards Research 46, DOI 10.1007/978-3-319-56487-6_10

inserting and rotating a four-bladed vane at the desired depth, and measuring the applied torque and angular rotation (ASTM D2573-1 2007). For a successful test, the key issues are: (i) insertion of the blade to the desired depth with as little disturbance of the soil as possible, (ii) measurement of the actual torque produced by soil shearing. For traditional vanes the latter goal is addressed by applying and measuring the torque above ground level (herein referred to as uphole). In this situation, it is of utmost importance to avoid any additional friction caused by the presence of soil that is pressing against the vane shear test rods. Rod friction has traditionally been avoided by using casing around the rods, which prevents direct contact between the rods and the surrounding soil. This eliminates most of the friction, even though some may still occur between the rods and the casing, especially at greater depths (Ortigao and Collet 1988). The use of a slip coupling enables measurement of rod friction so that it can be subtracted from the final result. Slip couplings are often used without casing, trusting that the total rod friction can be accurately measured. Given the mechanism of rod friction, the most accurate way to measure the torque is to place the torque sensor and the measurement unit as close as possible to the vane (herein referred to as downhole).

The applied torque, reduced when necessary by the measured rod friction, is transformed into s_u by accounting for the shape and the size of the vane. For a rectangular vane and a rectangular vane with a taper at the bottom [Nilcon vane (Brand and Brenner 1981)] the relationship between torque (T) and s_u is given by Eq. 10.1 (Silvestri et al. 1993).

$$T = \frac{\pi D^2 H}{2}\left[1 + \frac{D}{6H}\left(1 + \frac{1}{\cos\alpha}\right)\right] s_u \tag{10.1}$$

Undrained conditions during testing are ensured by the high applied rate of rotation of the vane, i.e., 0.1°/s. The failure state is thus reached in approximately 1 min in soft soils. The measured values, corresponding to a relatively high shearing rate, must be corrected to account for anisotropy and rate effects, as suggested by Bjerrum (1973).

10.2 Factors Influencing Field Vane Test Accuracy

The measurement accuracy of a given FV test can be affected by uncertainties originating from the test procedure, apparatus used and operator. In Table 10.1, the main problems related to FV testing are summarized, based on a review of existing literature and on experience gained from FV testing conducted in Finland by personnel from Tampere University of Technology (TUT).

Slip coupling has a major role in measurement accuracy. Lack of maintenance of the slip coupling system can lead to inaccurate evaluation of the soil-rod friction.

Table 10.1 Problems commonly associated with FV testing

Soil disturbance induced by predrilling (Flaate 1966) and vane insertion (Cadling and Odenstad 1948; Flaate 1966; La Rochelle et al. 1973; TUT)
Strain rate effects (Bjerrum 1972)
Non-uniform shear stress distribution around the vane (Donald et al. 1977; Menzies and Merrifield 1980; Gylland et al. 2012)
Uncertainties in soil-rod friction evaluations (Ortigao and Collett 1988; TUT)
Influence of waiting time between vane insertion and rotation (Aas 1965; Flaate 1966; TUT)
Lack of apparatus maintenance and calibration (Flaate 1966; Kulhawy et al. 1983; TUT) [applies specially to malfunction of slip-coupling (TUT)]
Accuracy of measurement system and measurement errors (e.g. old calibration methods, non-linearity of calibration curve) (TUT)
Influence of vane size and thickness (Chandler 1988); variability in blade thickness (TUT)
Lateral disturbance induced by vane shaft (Flaate 1966; TUT)
Malfunctioning during the test such as rods twisting, joints tightening, change of vane position (Flaate 1966; TUT)
In Finland FV testing is typically performed without centralizers, which prevents the rods from bending inside the casing (TUT)

Moreover, the rod friction behavior after free-slip of the slip coupling is quite difficult to evaluate (Ortigao and Collet 1988). Some of the uncertainties relate to the assumptions made to convert torque into shear strength. A comparison between these general assumptions and the actual soil behavior is presented in Table 10.2.

10.3 Field Vane Measurements in Finnish Soft Soils

In order to improve the quality of ground investigation data, various studies have been conducted recently at TUT on FV testing, piezocone testing (CPTU) and undisturbed sampling. In order to study the accuracy and repeatability of the FV test, measurements have been performed using different apparatuses such as the Nilcon FV, two different uphole electrical FV and a new downhole FV (A.P. van den Berg (n.d.)). The main features of the new equipment can be summarized as: (i) torque sensor and drive are placed inside the tool itself and close to the vane, (ii) the apparatus is equipped with a robust case and the vane is pushed out and retracted prior to and after the test, (iii) the drive motor is electronically limited to a torque of 100 Nm.

Results from three different soft soil test sites (Perniö, Lempäälä, and Masku) are presented and discussed in this paper. Extensive field site investigation has been conducted at all sites, as partly reported by Di Buò et al. (2016).

Table 10.2 General assumptions made to convert torque moment into shear strength

Assumption	Reality	Source
1. Penetration of the vane causes negligible disturbance, both in terms of changes in effective stress and shear distortion	Disturbance of soil can cause a loss of s_u	Cadling and Odenstad (1948), Flaate (1966) and La Rochelle et al. (1973)
2. No drainage occurs before or during shearing	Dissipation of pore pressure can occur during rotation. Thin undetected drainage layers may be present	Roy and Leblanc (1988), Kimura and Saitoh (1983) and Kulhawy et al. (1983)
3. The soil is isotropic and homogeneous	Soft clays are almost always anisotropic and sometimes also layered due to sedimentation process	Mitchell and Soga (1976), Donald et al. (1977) and Silvestri and Aubertin (1988)
4. The soil fails on a cylindrical shear surface	In the beginning of the rotation, the shape of the progressing shear surface is more like a rounded square	Roy and Leblanc (1988), Chandler (1988) and Gylland et al. (2012)
5. The diameter of the shear surface is equal to the width of the vane blades	Shear surface could be a little bit larger than the diameter of the vane	Roy and Leblanc (1988) and Chandler (1988)
6. At the peak and remolded strength there is a uniform shear stress distribution across the shear surface	On horizontal planes, shear resistance is a function of the radius when the lowest mobilized shear resistance is close to the vane axle	Donald et al. (1977) and Wroth (1984)
7. There is no progressive failure, so that at maximum torque the shear stress at all points on the shear surface is equal to s_u	Numerical analyses have shown that the FV test interpretation depends upon the complete stress-strain curve of the material	Donald et al. (1977), De Alencar et al. (1988) and Griffiths and Lane (1990)

10.3.1 Lempäälä

This site is located in the southwest region of Finland next to the city of Tampere. The stratigraphy consists of a 3 m thick heterogeneous layer of peat and clay (possibly a fill layer), which overlies a 6–7 m thick soft sensitive clay deposit. At this site, both Nilcon and electrical vane tests were performed using the slip coupling system (Fig. 10.1). The raw data shown includes the effects of rotation of the slip coupling and some tightening/twisting of rods at the beginning of the test.

The stress-strain behavior measured by the downhole FV apparatus seems to give a higher peak strength with lower deformation, indicating better quality of the test. The uphole apparatus is generally affected by higher uncertainties, since the rotating and measuring system are placed at the ground level. Therefore, the measurement seems more vulnerable to rods twisting during the test.

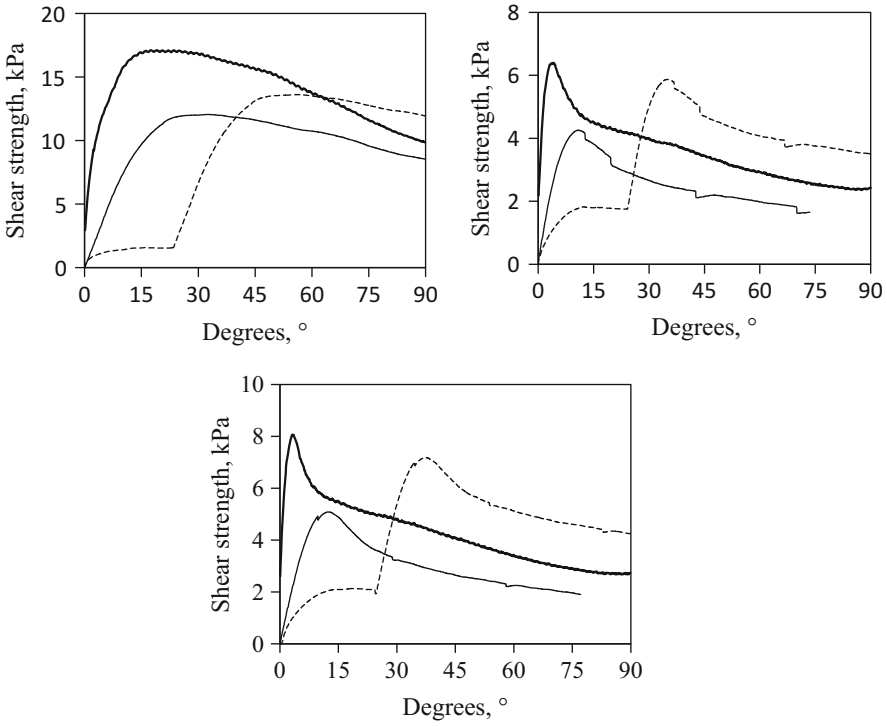

Fig. 10.1 Results from Lempäälä FV tests performed at depths of: (**a**) 2.2 m, (**b**) 4.7 m, (**c**) 6.1 m

The uncorrected peak shear strength evaluated with the four different apparatus is shown in Fig. 10.2. Good repeatability can be noticed for both the electrical vanes and downhole FV, even if the data is highly influenced by the apparatus. The strength measured by the Nilcon and the electrical vane is generally lower than the one provided by the downhole FV. One possible explanation is the amount of disturbance induced into the soil since none of the apparatus are equipped with casing. Another reason is a possible malfunctioning of the slip coupling system.

10.3.2 Perniö

The Perniö test site has been extensively investigated, as in 2009 a full-scale embankment failure test was conducted at this location (Lehtonen et al. 2015; D'Ignazio et al. 2017). The site is located in the southwest coast of Finland, next to the railway track connecting the cities of Helsinki and Turku. The stratigraphy consists of a 1–1.5 m of dry crust layer overlaying an 8–9 m thick soft clay layer.

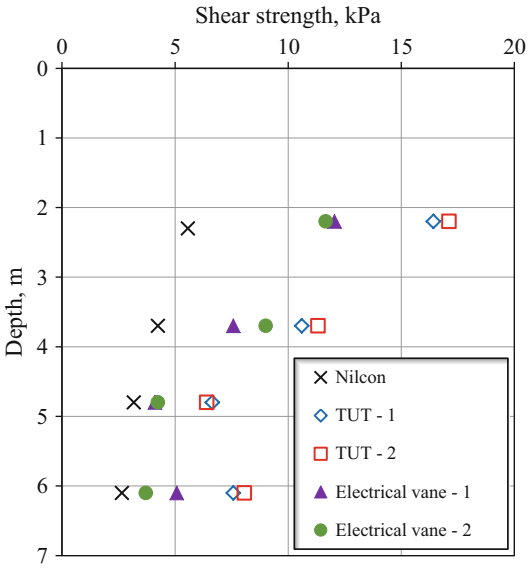

Fig. 10.2 Uncorrected s_u vs depth with different vane apparatuses, Lempäälä

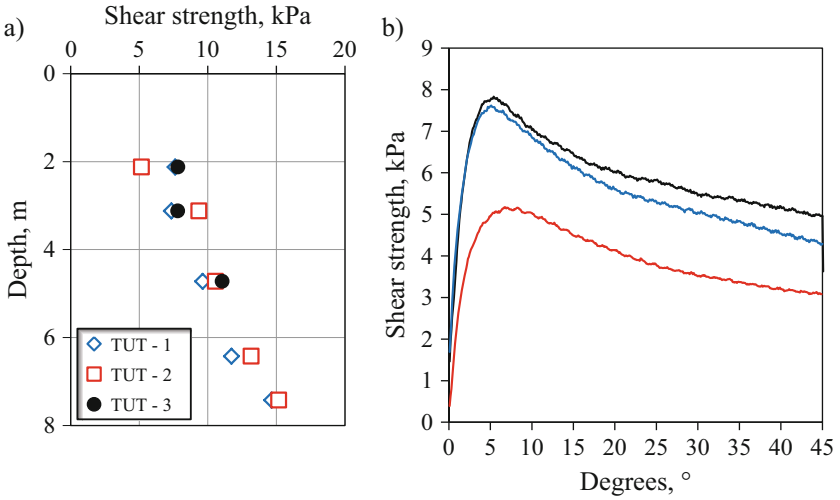

Fig. 10.3 (**a**) Uncorrected undrained shear strength vs depth with downhole FV, (**b**) FV test performed at 2.10 m depth, Perniö

The most recent field investigation has been conducted using the downhole FV apparatus. Data from other vane types are not available. Figure 10.3a shows the uncorrected shear strength plotted versus depth for the Perniö site. Data clearly shows that measurements in the homogeneous soft clay layer are repeatable. Scatter can be noticed at shallow depth probably due to the presence of the dry crust layer. Tests performed at a 2.1 m depth are shown in Fig. 10.3b. During the vane insertion,

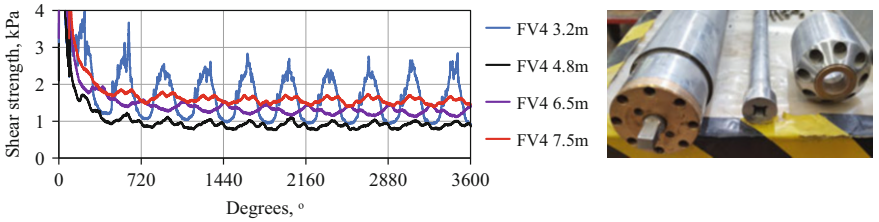

Fig. 10.4 (**a**) All shear stress vs. angular rotation FV stages at different depths from Perniö. (**b**) Connection between vane shaft and drive unit

some material from the upper layer might have entered into the casing and remained stuck to the blades, thus influencing the measurements. To avoid such a problem, pre-drilling into the dry crust layer should be performed prior to vane insertion.

The FV is considered to be a suitable device for measuring residual and remolded shear strength. The residual strength is usually determined after a vane rotation of 180° at slow speed (0.1°/s). To evaluate the remolded shear strength, the speed is increased up to 6 °/s. The measurement is performed after a 3600° rotation of the vane. Measured remolded strength of Perniö clay is shown in Fig. 10.4a. The data shown is clearly affected by errors, which are probably due to a loose connection between the vane axle and the rotating system. The authors believe that the vane was subjected to tilt movement, which caused the "wave" effect that can be observed in the figure. Figure 10.4b shows the connection between the vane and the drive unit.

Figure 10.5 shows remolded shear strengths measured from FV (in-situ) and fall cone test (laboratory). Higher values of remolded shear strengths measured by FV may depend on several reasons: (i) extra movement of the vane allows the vane to cut more undisturbed soil, (ii) the level of the vane might not stay constant, (iii) remolded shear strength includes about 395 mm friction between soil and shaft of the vane, (iv) pore pressure can be dissipated during the rotation (Kimura and Saitoh 1983). It should be further pointed out that the overall accuracy of the FV test device that was used is at least 0.5 Nm, which corresponds to 0.32 kPa for a vane size of 75 × 150 mm. The fall cone test should not be considered as an absolute reference test.

10.3.3 Masku

The Masku test site is located on the southwest coast of Finland. The stratigraphy consists of a 1.5 m thick weathered clay crust layer overlaying a 11 m thick soft clay deposit. The field investigation at this site was conducted using both a Nilcon vane equipped with casing, and the downhole FV apparatus. Measured FV results are shown in Fig. 10.6a. In this case, where casing was used, the difference in terms of measured shear strength between the Nilcon and the new FV downhole vane is

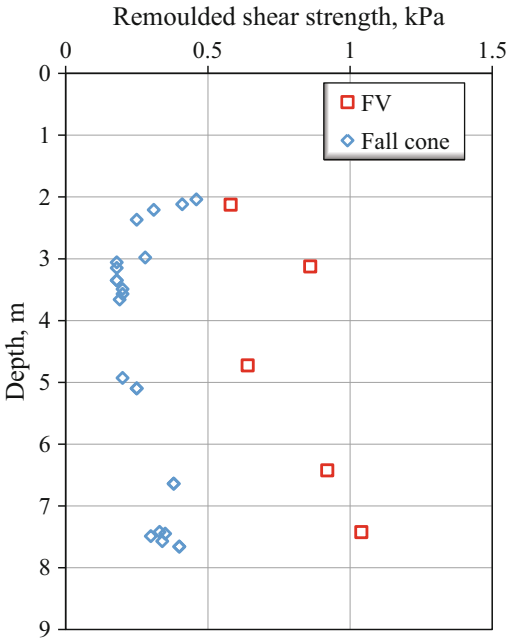

Fig. 10.5 Remolded s_u against depth (m) measured by FV and fall cone test, Perniö

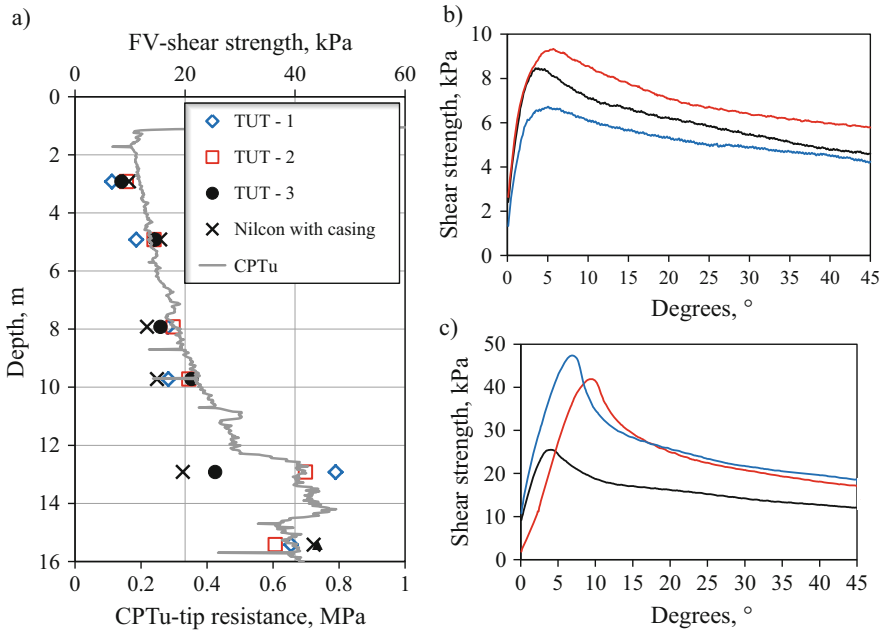

Fig. 10.6 (**a**) uncorrected undrained shear strength and tip resistance vs depth, (**b**) FV test (TUT apparatus) at 3.00 m depth, (**c**) FV test (TUT apparatus) at 13 m depth, Masku

lower than when casing was not used. The presence of the dry crust layer does not seem to affect the measurements at shallow depth, as was observed at the Perniö site. However, some scatter is noticeable at each measurement point. The scatter becomes very high at 13 m depth (Fig. 10.6c). This might be explained by some soil layering, as also suggested by the CPTU test (Fig. 10.6a).

10.4 Conclusions and Further Study

The field vane test is often seen as a rather simple and direct test to evaluate the undrained strength properties of clays. However, previous studies as well as this study have shown that many uncertainties are involved in the equipment and its maintenance, the procedure of testing and its interpretation. In recent years, there has been increasing interest to develop the FV test further. An obvious improvement is to place the measuring unit and possibly also the torque application unit right above the vane. In this study, the performance of this type of downhole equipment is compared to more traditional FV equipment. The study shows that the downhole FV gives often a very distinct stress-rotation behavior. The obtained peak strength was obtained at a smaller rotation compared to the uphole FV. Also, if no casing is used for the traditional FV, the downhole gives a clearly higher peak strength. These results emphasize the importance of using casing with traditional FV tests.

The repeatability of the new downhole FV is generally good, even though some scatter in results was observed. This can be partly avoided with improved testing procedures, e.g. by predrilling through the dry crust layer. Some of the scatter in results can also reasonably be attributed to natural soil variation, as only one measurement was performed at each given depth.

The results also show that the remolded strength obtained by the FV is generally higher than the one obtained by the fall cone test. Although some improvements can be made to the used downhole equipment, the authors think that because of the nature of the test the FV will probably always give too high values for the remolded strength, especially at larger depths.

The presented study is part of ongoing research at TUT to develop ground investigation methods. The FV results will be compared to CPTU tests and extensive laboratory tests including triaxial compression and extension tests and DSS tests on mini block samples.

Acknowledgements The research is funded by the Finnish Transport Agency, which is greatly appreciated. The authors would also like to thank Professor Christopher Meehan from the University of Delaware for his valuable comments when reviewing this article.

References

Aas G (1965) Study of the effect of vane shape and rate of strain on measured values of in-situ shear strength of clays. In: Proceedings of the conference on shear strength of soils, Oslo, 1, pp 141–145

ASTM D2573-01 (2007) Standard test m,ethod for field vane shear test in cohesive soil, ASTM International, West Conshohocken, PA, 2007, www.astm.org

Bjerrum L (1972) Embankments on soft ground, ASCE specialty conference on performance of earth and earth-supported structures. 2, pp 1–54

Bjerrum L (1973) Problems of soil mechanics and construction on soft clays. State-of-the-art report. In: Proceedings of the 8th ICSMFE, Moscow, 3, pp 111–159

Brand EW, Brenner RP (eds) (1981) Soft clay engineering, 20. Elsevier, Amsterdam/New York

Cadling L, Odenstad S (1948) The Vane Borer. In: Proceedings of the Royal Swedish Geotechnical Institute, 2, pp 1–87

Chandler RJ (1988) The in-situ measurement of the undrained shear strength of clays using the field vane. Vane shear strength testing in soils: field and laboratory studies, pp 13–44

De Alencar JA, Chan DH, Morgenstern NR (1988) Progressive failure in the vane test, vane shear strength testing in soils: field and laboratory studies, ASTM STP 1014, AF

Di Buò B, D'Ignazio M, Selänpää J, Länsivaara T (2016) Preliminary results from a study aiming to improve ground investigation data. In: Proceedings of the 17th Nordic Geotechnical Meeting, Reykjavik, 25–28 May 2016, 1, pp 187–197

D'Ignazio M, Länsivaara T, Jostad HP (2017) Failure in anisotropic sensitive clays: a Finite Element study of the Perniö failure test. Can Geotechl J. doi:10.1139/cgj-2015-0313.

Donald IB, Jordan DO, Parker RJ, Toh CT (1977) The vane test-a critical appraisal. In: Proceedings of the 9th international conference on soil mechanics and foundation engineering, 1, pp 81–88

Flaate K (1966) Factors influencing the results of vane tests. Can Geotech J 3:18–31

Griffiths DV, Lane PA (1990) Finite element analysis of the shear vane test. Comput Struct 37(6):1105–1116

Gylland AS, Jostad HP, Nordal SN (2012) Failure geometry around the shear vane in soft sensitive clay. In: Proceedings of the 16th Nordic Geotechnical Meeting (NGM), Copenhagen, pp 103–110

Kimura T, Saitoh K (1983) Effect of disturbance due to insertion on vane shear strength of normally consolidated cohesive soils. Soils Found 23:113–124

Kulhawy FH, O'Rourke TD, Stewart JP, Beech JF (1983) Transmission line structure foundations for uplift-compression loading, load test summaries: appendix to EPRI Final Report EL-2870. Electric Power Research Institute

La Rochelle P, Roy M, Tavenas F (1973) Field measurements of cohesion in Champlain clays. In: Proceedings of the 8th international conference on soil mechanics and foundation engineering, Moscow, 1, pp 229–236

Lehtonen V, Meehan C, Länsivaara T, Mansikkamäki J (2015) Full-scale embankment failure test under simulated train loading. Géotechnique 65(12):961–974

Menzies BK, Merrifield CM (1980) Measurements of shear distribution at the edges of a shear vane blade. Géotechnique 30(3):314–318

Mitchell JK, Soga K (1976) Fundamentals of soil behavior. Wiley, New York

Ortigao JAR, Collet HB (1988) Errors caused by friction in field vane tests. In: Vane shear strength testing in soils: field and laboratory studies. ASTM International, Philadelphia

Roy M, Leblanc A (1988) Factors affecting the measurements and interpretation of the vane strength in soft sensitive clays. In: Vane shear strength testing in soils: field and laboratory studies. ASTM International, Philadelphia

SGY (1995) Kairausopas II. 2. painos, 1999. Helsinki: Suomen Geoteknillinen yhdistys r.y. Finnish Geotechnical Society

Silvestri V, Aubertin M (1988) Anisotropy and in-situ vane tests. In: Vane shear strength testing in soils: field and laboratory studies. ASTM International, Philadelphia

Silvestri V, Aubertin M, Chapuis RP (1993) A study of undrained shear strength using various vanes. Geotech Test J 16(2):228–237

van den Berg AP (n.d.) User manual Icone vane tester Onshore http://www.apvandenberg.com/

Wroth CP (1984) The interpretation of in-situ soil tests. Rankine Lecture Geotéchnique 34(4):449–489

Chapter 11
A New Laboratory Procedure to Study Stress Relief in Soil Samples

Helene Alexandra Amundsen, H. Dang, Matthew Adamson, Arnfinn Emdal, and Vikas Thakur

Abstract During block sampling the in situ total stresses reduces to zero. This ultimately allows the soil sample to swell, leading to a weaker soil structure. In this paper, an attempt has been made to investigate this mechanism experimentally. In doing so, a new laboratory test procedure has been developed where the formation of a soil is simulated with a built in piezometer to study the stress changes in soil samples during and after sampling. The results show that the tested sample tends to lose a significant part of its residual effective stresses instantaneously, allowing the sample to swell.

11.1 Introduction

The mechanical behaviour, e.g. strength and stiffness, of soft sensitive clays depends on, among other things, soil structure, rheology, stress history and test conditions (e.g., Bjerrum 1967; Janbu 1985; Leroueil 2001). Moreover, the strength and stiffness of sensitive clays when determined in the laboratory are heavily influenced by the degree of disturbance induced during sampling and testing, referred to as sample disturbance. The term sample disturbance generally accounts for all the undesired physical processes which arise during sampling and testing. This includes processes such as drilling and coring, management during transport and storage,

H.A. Amundsen (✉)
Norwegian University of Science and Technology (NTNU), Trondheim, Norway

Norwegian Public Roads Administration (NPRA), Trondheim, Norway
e-mail: helene.amundsen@ntnu.no

H. Dang
Norwegian University of Science and Technology (NTNU), Trondheim, Norway

Multiconsult, Fredrikstad, Norway
e-mail: helena.dang@multiconsult.no

M. Adamson • A. Emdal • V. Thakur
Norwegian University of Science and Technology (NTNU), Trondheim, Norway
e-mail: matthewa@stud.ntnu.no; arnfinn.emdal@ntnu.no

V. Thakur et al. (eds.), *Landslides in Sensitive Clays*, Advances in Natural and Technological Hazards Research 46, DOI 10.1007/978-3-319-56487-6_11

handling while trimming and mounting of the sample, and recompression back to initial conditions. Sample disturbance due to sampling may be divided into two categories; sampler induced disturbance and disturbance induced due to stress relief. The sampler induced disturbance may be minimized with special sampling techniques, such as Sherbrooke block sampling, and expert personnel to handle the samples. However, the disturbance which is caused by stress relief is unavoidable even in cylinder samplers (e.g., Ladd and DeGroot 2003; Degago and Grimstad 2014) since after sampling the soil must be extracted prior to testing in a laboratory.

Stress relief results in the rearrangement or weakening of interparticle contacts and changes the stress-strain behaviour of the clay (e.g., Ladd and Lambe 1963; Skempton and Sowa 1963; Tanaka and Tanaka 2006). Disturbance induced due to stress relief may be increased if the pore water releases dissolved gases (Okumara 1971; Fredlund et al. 2012). This is crucial for samples with high in situ stresses such as offshore samples (Tanaka et al. 2002). Drainage or access to water during storage and testing may also increase the effect of disturbance induced due to stress relief (e.g., Adams and Radhakrishna 1971; Schjetne 1971).

In short, disturbance induced due to stress relief may result in a different stress-deformation response compared to the actual in situ response. For this reason, an understanding of stress changes as a result of sampling is essential to assess the sample quality of sensitive clays. Accordingly, this paper presents a novel test setup and a methodology to simulate the stress relief a sample may experience during sampling. Effect of stress relief on the tested samples are discussed in light of literature.

11.2 Stress Relief: Basic Concept and Earlier Work

In block sampling, the reduction of in situ total stresses to zero causes the soil sample to develop a negative pore pressure (u_r), which is equal to the residual mean effective stress (p'_r). A reduction of negative pore pressure in a sample is assumed to contribute to its quality deterioration and the degree of sample disturbance can be evaluated by a comparison between measured and theoretical pore pressure. The theoretical maximum negative pore pressure ($-u_{ps}$) in a perfectly undisturbed sample can be evaluated assuming a pure elastic unloading of a saturated sample (Ladd and Lambe 1963):

$$-u_{ps} = \sigma'_{v0}\left(1 + 2K'_0\right)/3 = p'_{ps} \tag{11.1}$$

where σ'_{v0} is the in situ effective vertical stress and K'_0 is the at-rest earth pressure coefficient. The maximum negative pore pressure in a perfectly undisturbed sample ($-u_{ps}$) is then equal to the mean effective stress (p'_{ps}).

The typical stress path performed on consolidated soil is shown in Fig. 11.1. Theoretically, complete stress relief may be achieved by starting at the in situ stress state (a) and, following path (a)–(b), reducing the deviatoric stress q to zero (b)

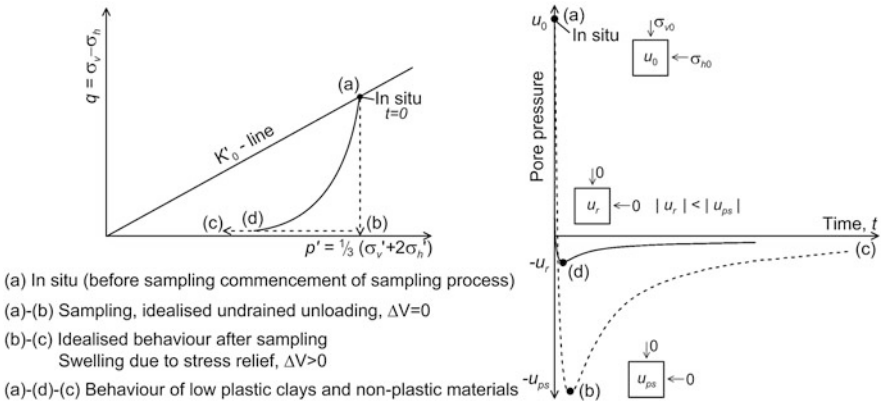

Fig. 11.1 Sampling induced stress changes, stress path and pore pressure response with time (Modified after Amundsen et al. 2017)

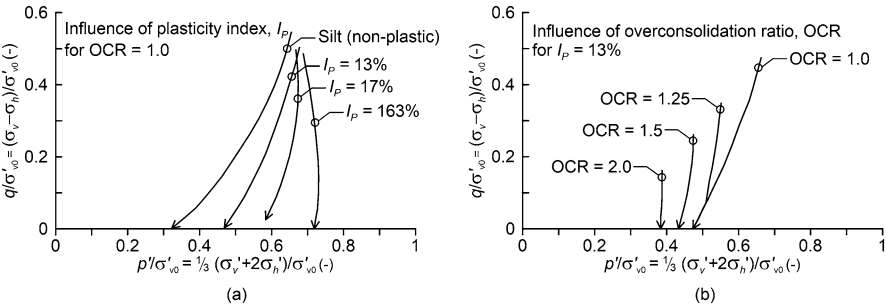

Fig. 11.2 The effect of (**a**) plasticity index (I_P) and (**b**) overconsolidation ratio (OCR) on perfect sampling stress paths for soils, after Hight and Burland (1990)

(corresponding to a pore pressure of $-u_{ps}$ in the sample, see Fig. 11.1). With time, the deviatoric stress remains unaltered while the mean effective stress p' is reduced, thus giving path (b)–(c). Realistically, stress relief is more likely to occur along the path (a)–(d)–(c), ending up at the point $-u_r$. This is especially the case for materials of low overconsolidation and low plasticity, which are exemplified in Fig. 11.2 Similar observations are also reported in the literature; see Table 11.1.

Stress relief and its effects has been studied by many researchers. Kirkpatrick and Khan (1984) investigated the effect of stress relief on the undrained stress-strain behaviour of normally consolidated clays, kaolin and illite, stored as large samples in laboratory. They concluded that storage time caused a significant reduction in undrained shear strength, increased the failure strain and produced a different effective stress path to failure. They observed that this behaviour became more pronounced with increasing time and dissipation of residual pore pressure.

Table 11.1 Some laboratory studies on stress relief using reconstituted samples

References	Site	w (−)	I_P (%)	OCR (%)	Range of p'_r (kPa)	Range of p'_r/p'_{ps} (−)	Range of p'_r/σ'_{v0} (−)
Skempton and Sowa (1963)	Weald[a]	33–49	24	NC	117–676	0.78–0.80	0.57–0.61
Adams and Radhakrishna (1971)	Lambton	31	18	OC	46	0.30	0.17
Kirkpatrick and Khan (1984)	Kaolin	40–46	30	NC	54–124	0.14–0.31	0.10–0.22
	Illite	34–41	40	NC	98–188	0.25–0.48	0.18–0.34
Graham et al. (1987), Graham and Lau (1988)	Illite	36–43	32	NC	57–90	0.52–0.84	0.36–0.58
	Illite	36–43	32	OC	44–52	0.80–0.95	0.55–0.65
Hight and Burland (1990) and Gens (1982)	Silt[a]			NC			0.32
	Till[a]		13	NC			0.45
	Magnus[a]		17	NC			0.67
Carrubba (2000)	Sandy silt		6	NC	15–88		0.11–0.31
	Clayey silt		11	NC	16–114		0.14–0.31
	Silty clay		25	NC	30–308		0.38–0.60

[a]Study on perfect sampling (see Ladd and Lambe (1963) for definition of perfect sampling)
w is natural water content, I_P is plasticity index, *OCR* is overconsolidation ratio, *NC* is normally consolidated and *OC* is overconsolidated, p'_r is residual mean effective stress, p'_{ps} is mean effective stress at perfect sampling and σ'_{v0} is in situ vertical effective stress

In another study conducted by Graham et al. (1987), the reconstituted illite samples were stored undrained in a triaxial apparatus. They have also concluded that a relaxation of the negative pore pressure occurred even with undrained storage of the samples. A similar study was carried out by Graham and Lau (1988), with some of the reconstituted clay samples having free access to water during storage. It was observed that drained storage decreased the undrained shear strength of the samples, especially for normally consolidated samples. All three studies confirm the established practice that the best result is obtained from samples that are stored at constant volume without access to water, and for as short a time as possible. However, it is doubtful that this procedure is possible to implement in practice. Expansion will occur either in the tube during and after sampling (Schjetne 1971) or during the extrusion in the laboratory.

The effects of the plasticity index (6–75%) on disturbance induced due to stress relief were examined by Carrubba (2000). He concluded that low plastic normally and anisotropically consolidated soils are sensitive to disturbance induced due to stress relief and may experience a loss of suction of up to 90% after unloading. This leads to a reduction of about 40% of the undrained shear strength.

A recent study was conducted in situ (Amundsen et al. 2017), where the pore pressure changes were measured during and after sampling in a block sample of a marine quick clay. The conclusion was that the sample swelled during the extraction from the ground due to access to water and the measured pore pressure was about 20% of the mean effective stress.

11.3 Instrumentation, Methodology and Material

Currently no commercial equipment is available to study the effects of stress relief. For this reason a new apparatus has been developed by NTNU. Figure 11.3 shows a cylinder with 150 mm diameter and 360 mm height (1), which is split in two and consists of two walls that are locked together during consolidation. Inside the cylinder, there is a pedestal (2) with three outlets, two for drainage (3) and one for the pressure sensor (4). The pressure sensor is connected to a tube, which has a high air-entry ceramic filter (5) on the end. The tube with the filter is placed above the pedestal, as shown in Fig. 11.3b. When the slurry is poured into the cylinder, it covers the filter allowing the soil to consolidate around it. On the top, the sample is covered with a cap (6) with two drainage outlets (7) and two contact pressure sensors (8). The load cell (9) controls the vertical stress and measures the deformation during the test. The contact pressure sensors (8) measure the actual pressure on the soil, avoiding frictional losses. All of the drainage tubes are attached to a burette (10), which measures volumetric changes and applies the backpressure (11).

The laboratory testing was performed on a remoulded natural cohesive soil sampled at Tiller, Trondheim, Norway (Gylland et al. 2013). The liquid limit was 32%, the plasticity index (I_P) was 13%, and the clay content (<2 μm) was 45%. The clay was remoulded with de-aired distilled water to achieve a water content twice its liquid limit. The shear strength of the slurry was less than 0.1 kPa.

After the slurry was poured into the cylinder, shown in Fig. 11.3a, the sample was confined by a rubber membrane, within a fixed cylinder, with vertical stress

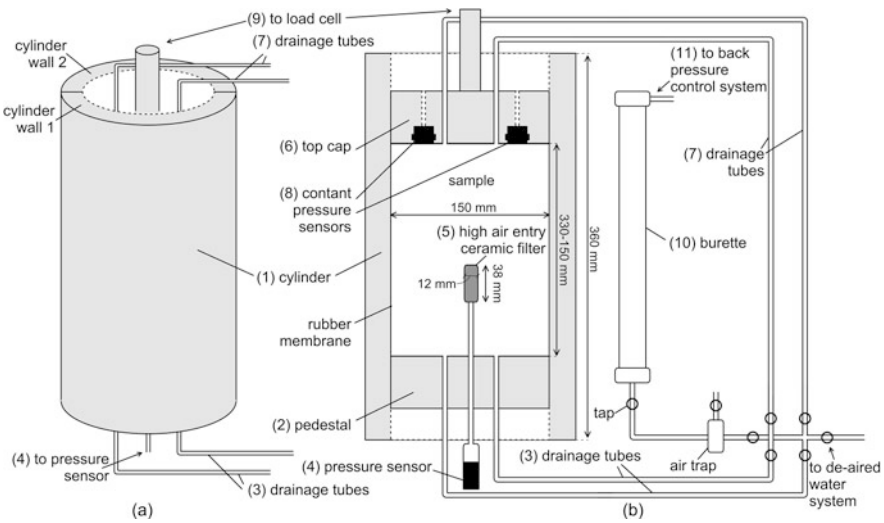

Fig. 11.3 Test setup, (**a**) an overview and (**b**) cross section (After Amundsen et al. 2017)

applied by means of a load cell. The saturation of the samples was controlled with the B-value ($B = \Delta u/\Delta\sigma$), which was higher than 0.95 throughout the consolidation. Thereafter the back pressure was applied through a burette while the volume of the sample was kept constant to simulate the in situ pore pressure (u_0).

This produced a specimen that was intended to represent normally consolidated clay located 5 m beneath the surface, with a simulated ground water level at 0.2 m beneath the surface. As soon as the sample achieved a stable stress state, the process of sampling was simulated. The total vertical stress was reduced, after which the total horizontal stresses were reduced to zero by removing the confining cylinder. With this procedure, the mechanical disturbance during installation of piezometer is eliminated and it is possible to monitor the pore pressure changes caused by stress relief and assess its effects. After the unloading the sample was divided and tested.

11.4 Laboratory Test Results

Two unloading tests were carried out, Test 1 and Test 2. During the testing the pore pressure was monitored inside the samples by means of a high air-entry ceramic filter which was connected to a pressure sensor, which is shown in Figs. 11.3b and 11.4a. The filter was placed in the middle of the samples, before consolidation and hence was not disturbing the soil around it. An at-rest pressure coefficient (K'_0) of 0.5 was assumed and the samples were consolidated to an anisotropic stress state, the initial stress condition are in Fig. 11.4a, d.

The unloading of the samples consisted of removal of the back pressure, followed by vertical unloading over a 15 min period and removal of the split cylinder. This is illustrated in Fig. 11.5a by the changes in mean total stress (p) and the pore pressure (u) with time for Test 1. The pore pressure response for both tests, Test 1 and Test 2, are shown in Fig. 11.5d, where the lowest values correspond to the p'_r-values

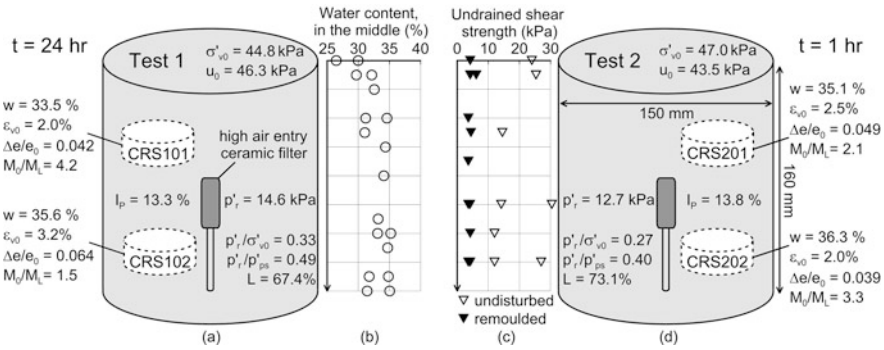

Fig. 11.4 Soil samples from (**a**) Test 1 and (**c**) Test 2, and a summary of (**b**) water content and (**c**) undrained shear strength (Swedish fall cone) in both samples (After Amundsen et al. 2017)

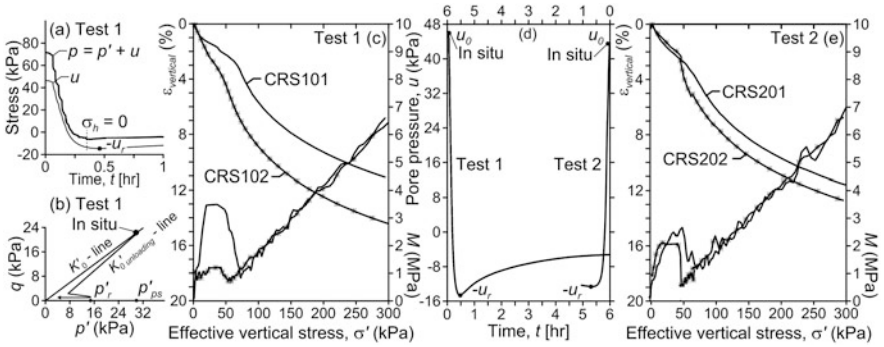

Fig. 11.5 Results from (**a**)–(**d**) Test 1 and (**e**)–(**f**) Test 2

in Fig. 11.4a and d. The p'_r-values are also normalised with the in situ effective vertical (σ'_{v0}) and maximum residual mean effective stress (p'_{ps}), in addition to L ($= (\sigma'_{v0} - p'_r)/\sigma'_{v0}$) which represents a loss of suction.

The sample from Test 1 was opened 24 h after unloading, and its lower part had access to 15 ml of water during that time. The sample from Test 2 was opened 1 h after unloading and had no access to water. Immediately after opening the samples, the water content and the fall cone shear strength were measured. The results are given in Fig. 11.4b and c, and are similar for both tests. In addition, it was conducted two Constant Rate of Strain (CRS) oedometer tests on each sample, as illustrated in Fig. 11.4a and d, with the results given in Fig. 11.5c and e.

11.5 Discussion

The test data in Fig. 11.4b and c suggest some variability in terms of water content and undrained shear strength distribution inside the reconstituted samples. The variation is pronounced in the upper part of the sample whereas the rest of the sample is fairly homogeneous. The samples are slightly overconsolidated due to creep during the consolidation, especially the upper part. The water content varies between 34.1% and 35.2% and the shear strength is about 12–15 kPa.

During 24 h of storage in the rubber membrane, the sample in Test 1 had access to 15 ml of free water. The presence of water is reminiscent of in situ sampling, as a natural sample will be surrounded by remoulded soil. After 24 h the added water was completely absorbed by the sample. The consequences of this are visible in Fig. 11.5d, where Test 1 was allowed to swell for 24 h, whereas Test 2 was allowed to swell for only 1 h during storage. In addition, there are variations in water content in oedometer test specimens in the same sample, see Fig. 11.4a. This variation can be attributed by the absorbed water. The oedometer test sample CRS102 had a 2.1

percentage point increase compared to CRS101. The variation in water content was smaller in Test 2, i.e. CRS202 has 1.2 percentage points increase in water content compared to CRS201.

It is interesting to check the sample quality using the M_0/M_L criterion (Karlsrud and Hernandez-Martinez 2013). Here M_0 is the maximum constrained modulus in the overconsolidated area and M_L is the minimum constrained modulus after the preconsolidation stress. The M_0/M_{L} ratio was 4.2 and 1.5 for CRS101 and 102, in Test 1. The reduction of M_0/M_{L} ratio indicates a poorer quality of the CRS102 sample due to access of water during a storage time of 24 h This is also reflected by a lower preconsolidation pressure measured for CRS102, there is a 29% decrease compared to 101. In case of Test 2, the decrease in preconsolidation pressure is 24% for CRS202 compared to 201. In general, the oedometer test results in Test 2, see in Fig. 11.5e, show smaller variations in stiffness, preconsolidation stress and sample quality due to a shorter storage time of only 1 h From these observations it is concluded that a longer storage time has a negative impact on sample quality.

The sample quality data of oedometer tests evaluated after normalised change in void ratio ($\Delta e/e_0$) are shown in Fig. 11.4a and d. The quality criteria depends on the volumetric strain (ε_{v0}) in a sample at in situ stresses (Lunne et al. 1997). The data show that CRS102 had a 1.2 percentage points increase in volumetric strain from CRS101. This difference could be related to the 15 ml of water, which corresponds to a 0.5% volumetric strain in the sample (or 1.1%, assuming that only half of the sample was influenced). In the sample that had no access to water, a difference of only 0.5 percentage points was found.

The process of unloading in Test 1 is illustrated in Fig. 11.5b (assuming $\nu = 0.26$ with a corresponding $K'_0 = 0.35$) by a reduction of the mean total stress to almost zero. In the Fig. 11.5a, the time at which the cylinder was removed is annotated in the diagram by "$\sigma_h = 0$", and about 4 min later the lowest residual pore pressure was registered. It was found to be −14.6 kPa and −12.7 kPa for Test 1 and Test 2, respectively. This means that the samples had a delayed maximum residual effective stress (p'_r) after unloading, before it started dissipating with time. This is also shown in a tentative effective stress path plot in Fig. 11.5a with a p'_r-value as a small peak along the p'-axis. It illustrates how the soil sample was subjected to a loss of negative pore pressure throughout the unloading process.

One cannot rule out that a possible reason for the low pore pressure values and the delayed reaction could be trapped air pockets, which could be present even with use of de-aired water and a saturated filter. There are always some limitations in the assembling of the equipment and the preparations of the sample prior to testing.

In the conducted tests, the p'_r/σ'_{v0} was 0.33 and p'_r/p'_{ps} was 0.49 for Test 1 and for the Test 2 they were 0.27 and 0.40, respectively. These values fit well with other similar studies on reconstituted soils, as shown in Table 11.1, where a greater loss of suction was found for slightly overconsolidated soils with low plasticity. Furthermore, the residual effective stress response in the tests, 14.6 kPa and 12.7 kPa, was similar to what one would anticipate during in situ sampling (Amundsen et al. 2017). Figure 11.5d shows how the pore pressure dissipated

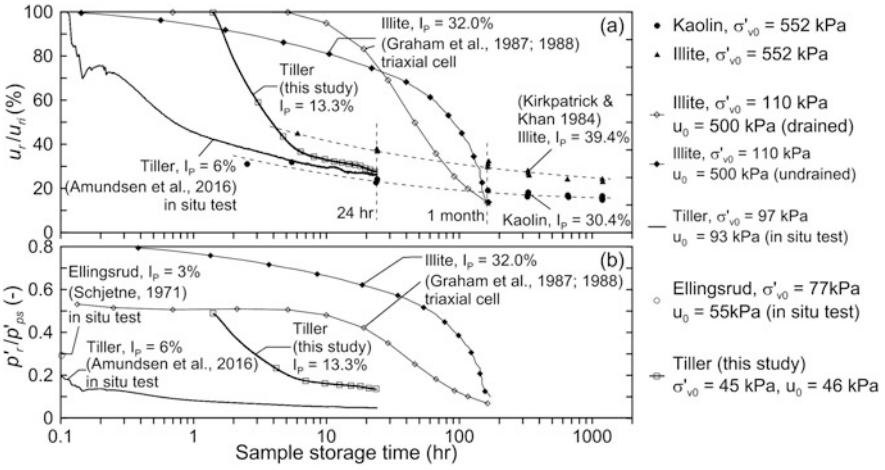

Fig. 11.6 Normalised (**a**) loss of suction (u_r/u_{ri}) and (**b**) residual effective stress (p'_r/p'_{ps}) versus sample storage time on reconstituted normally consolidated clay samples

gradually resulting in swelling, and after the 24 h storage period it had reached −4 kPa. The swelling, in turn, leads to sample disturbance, which is illustrated with two sets of oedometer tests in Fig. 11.5c and e.

Figure 11.6b shows two in situ tests that were carried out in marine sensitive clays, the maximum p'_r/p'_{ps}-values measured by Schjetne (1971) and Amundsen et al. (2017) were 0.27 and 0.20, respectively. The measured values are small, indicating that the sample was allowed to swell during sampling and extraction from the ground due to access of water from the remoulded material around the sample.

In addition to the in situ tests, several laboratory studies were conducted on reconstituted clay samples, shown in Fig. 11.6a and b, such as kaolin and illite. For normally consolidated clays, stored undrained, the p'_r/p'_{ps}-values were 0.52–0.84 for samples stored in a triaxial cell (Graham et al. 1987 and Graham and Lau 1988) and 0.14–0.48 for samples stored as large specimens which were later cut into smaller samples (Kirkpatrick and Khan 1984). Figure 11.6a indicate that clay stored as large samples lost its residual negative pore pressure faster compared to smaller samples which were stored in a triaxial cell. This observation is in line with the laboratory tests conducted in this study and the in situ tests (Schjetne 1971; Amundsen et al. 2017), which were all stored as large samples. Therefore these observations indicate that the new test setup presented in this paper is a realistic simulation of sampling and storage process of natural clays.

It is remarked that while the reconstituted samples are much more homogeneous than in situ samples, variation in material parameters such as permeability, mineralogy, activity, grain size distribution and plasticity index are still present. These effects are not investigated further in this paper.

11.6 Closure

Soil sampling and testing involves unavoidable stress relief. During testing of sensitive clay samples stress relief adversely affects the sample quality. In this paper, an attempt was made to understand the processes involved during stress relief. In doing so, a new test procedure was developed and discussed based on two representative tests. The testing procedure consisted of consolidating slurry to a desired stress state, unloading the sample and monitoring the pore pressure changes in it. This preliminary study confirms that there exists a connection between stress relief and sample quality.

The test setup and the methodology were verified by conducting tests. The results show that the residual effective stress in the unloaded sample is significantly lower than the theoretically expected value, similar to other studies reported in the literature. Moreover, swelling of the sample could not be avoided as the sample absorbed water during and after unloading of the total stress. The reduction of quality has been illustrated using two oedometer test results where one of the samples had access to water and swelled. However, this aspect needs to be studied in detail before any further conclusions can be made. In summary, despite all simplifications and assumptions, the test setup and the results are promising, as they contributed to increasing the knowledge related to the effects of stress relief on sample quality.

Acknowledgements Engineers P. Østensen, F. Stæhli and T. Westrum at NTNU are gratefully acknowledged for their skills and knowledge, without which the experimental work would have been impossible. The intergovernmental research program Natural hazards: Infrastructure, Floods & Slides (2012–2015) is acknowledged for their support. The first author partly supported by the OFFPHD program by the Research Council of Norway, Grant No. 246629. The authors gratefully acknowledge Dr. S. Degago from Norwegian Public Road Administration for reviewing this paper.

References

Adams JI, Radhakrishna HS (1971) Loss of strength due to sampling in a glacial Lake deposit. In: Sampling of soil and rock, vol 483. ASTM STP, Philadelphia, pp 109–120

Amundsen HA, Jønland J, Emdal A, Thakur V (2017) An attempt to monitor pore pressure changes in a block sample during and after sampling. Géotechnique Letters 7(2)

Amundsen HA, Emdal A, Thakur V (2017) A new approach to investigate the effect of stress relief in soft clay samples. To be submitted to Géotechnique

Bjerrum L (1967) Engineering geology of Norwegian normally-consolidated marine clays as related to settlements of buildings. Géotechnique 17(2):83–118

Carrubba P (2000) Stress relief disturbance and residual pore pressure in cohesive soils. Soils Found 40(1):57–72

Degago S, Grimstad G (2014) Significance of sample quality in settlement analysis of field cases. In: Numerical methods in geotechnical engineering. Informa UK Limited, London

Fredlund DG, Rahardjo H, Fredlund MD (2012) Compressibility and pore pressure parameters. In: Unsaturated soil mechanics; unsaturated soil mechanics in engineering practice. Wiley, Hoboken, pp 783–808

Gens A (1982) Stress-strain and strength characteristics of a low plasticity clay. PhD thesis, University of London

Graham J, Lau SL-K (1988) Influence of stress-release disturbance, storage, and reconsolidation procedures on the shear behaviour of reconstituted underwater clay. Géotechnique 38(2):279–300

Graham J, Kwok CK, Ambrosie RW (1987) Stress release, undrained storage, and reconsolidation in simulated underwater clay. Can Geotech J 24(2):279–288

Gylland A, Long M, Emdal A, Sandven R (2013) Characterisation and engineering properties of tiller clay. Eng Geol 164:86–100

Hight DW, Burland JB (1990) Review of Soil Sampling and Laboratory Testing for the Science and Engineering Research Council. Summary Report. SERC, England

Janbu N (1985) Soil models in offshore engineering. Géotechnique 35:241–281

Karlsrud K, Hernandez-Martinez FG (2013) Strength and deformation properties of Norwegian clays from laboratory tests on high-quality block samples. Can Geotech J 50(12):1273–1293

Kirkpatrick WM, Khan AJ (1984) The reaction of clays to sampling stress relief. Géotechnique 34(1):29–42

Ladd CC, DeGroot DJ (2003) Recommended practice for soft ground site characterization: Arthur Casagrande lecture. In: 12th PCSMGE, MIT, Cambridge, MA

Ladd CC, Lambe TW (1963) The strength of "undisturbed" clay determined from undrained tests. Symposium on Laboratory Shear Testing of Soils, ASTM STP 361:342–371

Leroueil S (2001) Natural slopes and cuts: movement and failure mechanisms. Géotechnique 51(3):197–243

Lunne T, Berre T, Strandvik S (1997) Sample disturbance effects in soft low plastic Norwegian clay. In: Proceedings of the symposium on recent developments in soil and pavement mechanics, Rio de Janeiro, Brazil, June 1997. pp 81–102

Okumara T (1971) The variation of mechanical properties of clay samples depending on its degree of disturbance. In: Proceedings of the 4th Regional Asian conference, Bangkok, July 1971. pp 73–81

Schjetne K (1971) The measurement of pore pressure during sampling. In: Proceedings of the 4th Regional Asian conference, Bangkok, July 1971. ISSMFE, pp 12–16

Skempton AW, Sowa VA (1963) The behaviour of saturated clays during sampling and testing. Géotechnique 13(4):269–290

Tanaka H, Tanaka M (2006) Main factors governing residual effective stress for cohesive soils sampled by tube sampling. Soils Found 46(2):209–219

Tanaka H, Ritoh F, Omukai N (2002) Quality of samples retrieved from great depth and its influence on consolidation properties. Can Geotech J 39(6):1288–1301

Chapter 12
Sample Disturbance in Deep Clay Samples

Anders Beijer Lundberg

Abstract A large part of the uncertainty in geotechnical design originates from the soil properties, which are assessed through the site investigation. The use of high-quality soil block sampling may reduce these uncertainties, but such methods are only available for comparably shallow soil layers. Deeper soil layers are of interest for analysis of large progressive landslides, where the slide surface can reach a significant depth (>20 m), and where the assessment of the stability requires information about the strength, and in some cases the compressibility, of the soil. A case study of sample disturbance in such deep layers of clay is therefore discussed to highlight how sample disturbance can be detected in different types of measurements from a site investigation.

12.1 Introduction

Recent advances in laboratory and numerical techniques offer the possibility of advanced modelling of the strength and compression properties of clay, e.g. Grimstad et al. (2012). These are however dependent on a reliable site investigation, and in any such program, the sample disturbance is a common source of uncertainty, (Lunne et al. 2006). The sample disturbance is also highly dependent on both the sample method as well as the soil type, (DeGroot et al. 2005, Lunne et al. 2008). The issue of sample disturbance therefore merits further study in order to assess the reliability resulting from both advanced and routine analysis of soil.

Soil sampling at larger depths (>20 m) has been shown to result in more extensive sample disturbance, but frequently in practical design no formal assessment of the resulting uncertainty is made, (DeGroot et al. 2005). An analysis of sample disturbance in high-quality block samples shows a clear correlation between the sample depth and the sample quality, with a higher level of disturbance in the deeper layers, (Amundsen et al. 2016). The possible sample depth of block samplers is relatively shallow, which means that samples from deeper layers are retrieved with

A.B. Lundberg (✉)
ELU Konsult AB, Stockholm, Sweden
e-mail: anders.beijer@elu.se

V. Thakur et al. (eds.), *Landslides in Sensitive Clays*, Advances in Natural and Technological Hazards Research 46, DOI 10.1007/978-3-319-56487-6_12

standard piston samplers. This may not be of large concern in low-risk projects, but the properties of deeper soil layer are significant in the analysis of large progressive landslides, in which the slide surface has been shown to reach deeper soil layers, (Bernander 2011). Such slides are also influenced by strain softening, and the validity of advanced modelling clearly depends on the soil properties, and consequently the sample quality, (Lunne et al. 2006; Thakur et al. 2014). Sample disturbance of such deep clay layers is discussed briefly in the scientific literature, (Amundsen et al. 2016; Andresen et al. 1979; Emrich 1971). DeGroot et al. (2005), Hight et al. (2002) and Lacasse and Nadim (1998) discuss sample disturbance and apparent underconsolidation of samples from depths deeper than 20 m for soft clay. General suggestions for site investigations, including triaxial tests of anisotropically reconsolidated clay samples are given in DeGroot et al. 2010. These methods are however often not available in low to moderate risk projects, following Lacasse and Nadim (1998). In such projects the assumptions about sample disturbance are often based on empirical experience.

A case study of sample disturbance of deep soil samples of clay from a site investigation program is discussed here. The case study is based on a site investigation on the east coast of Sweden. In-situ and laboratory tests of samples from the deeper layers are compared to the samples from the shallow layers. The shear strength and compressibility of clay soil are dependent on the soil anisotropy, the strain rate, temperature, as well as other parameters, (Löfroth 2012, Thakur et al. 2014). The aim of the current evaluation is limited to discuss the level of disturbance of the deep soil layers relative to the shallow layers, in order to assess the reliability of the soil parameters from the deeper layers resulting from the site investigation.

12.2 Site Investigation Program

12.2.1 Site Location and Geology

The 500 × 500 m^2 site is located in Uppsala, in the Eastern part of Sweden, as shown in Fig. 12.1. The aim of the site investigation was to assess the soil properties before planning and design of earthworks and foundations supporting buildings and infrastructure around a residential area. The area is flat and at an elevation of around 5 m compared to the Baltic Sea. The soil conditions in the area are characterized by Holocene soil deposits, resulting from deposition of sedimentary soil layers on top of the rock base in water with a salinity of around 0.5% at the end of the last ice age (around 10,000 years BCE). The frequently occurring overconsolidation ratio in the current area is around 1.2–1.3, resulting from creep as described by Bjerrum (1973). The area is located well below the highest sea level after the melting of the inland ice. Pore pressure measurements display almost hydrostatic conditions, with low excess pore pressure (< 5 kPa) in the top soil layers, possible as a result of

Fig. 12.1 Site location in Sweden

decomposing of organic soil or creep. The sedimentary soil layer extends to around 50–60 m depth at the site, and (from the ground surface) consists of blue-grey clay with sulphide content, grey varved clay and a bottom layer of moraine on top of the bedrock. The ground level arose from the sea around 7500 BCE, and the top layers of clay are mixed with organic material, resulting in an organic content of around 5% for the top 5 m layer, (Nilbrink and Hedberg 2014). The area is covered by 0.5–1 m fill.

12.2.2 Site Investigation

An overview of the site investigation program is shown in Table 12.1 and Fig. 12.2. The sampling was carried out with a Swedish standard St II piston sampler in a pre-drilled hole through the fill. The sampler is 1 m long and has a 50 mm inner diameter tubular container. The piston sampler has a cutting edge of 5°, with a 45° angle over a 0.3 mm end length at the edge. Five plastic tubes are placed inside the sampler, of which three are sample tubes with length 170 mm, (Löfroth 2012).

Table 12.1 In-situ and laboratory methods used in the site investigation

Method	Boreholes	Tests per borehole
FVT	2	14
CPTu	12	1
Index	4	8–9
CRS	4	8–9
CAUC-triaxial	1	1
IL-Oedometer	1	2

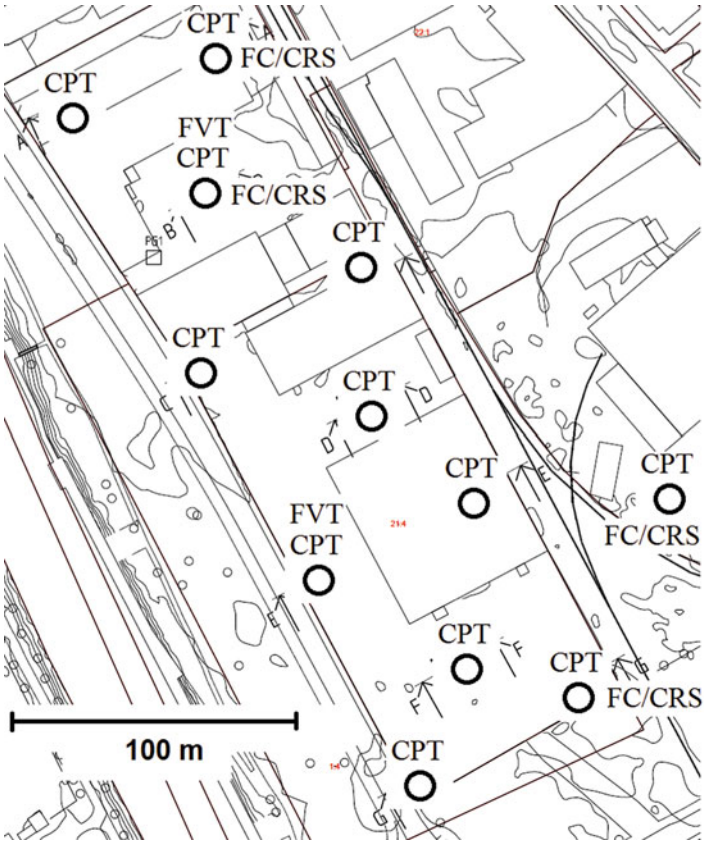

Fig. 12.2 Site investigation plan

12.2.2.1 Field Vane Test (FVT)

The field vane tests were conducted down to 29 m depth with a 65 x 130 mm field vane. The measured undrained shear strength in direct shear c_u^{DSS} of the vane was corrected according to Bjerrum (1973) to adjust for the strain rate effect, which is

assumed to increase with increasing plasticity index. The torsional shaft resistance increases with depth, and the measurements were therefore not possible to conduct in the glacial clay.

12.2.2.2 Cone Penetration Test (CPTu)

The CPTu tests were carried out with a 1000 mm^2 piezoelectric CPTu cone. The cone was penetrated into the soil until it reached the moraine or till layer, at around 50 to 60 m depth. The cone factor N_{kt} for the shear strength in direct shear ${c_u}^{DSS}$ of the CPTu was estimated from a site-specific correlation from the field vane tests following the procedure discussed in Lundberg and Li (2015).

12.2.2.3 Standard Laboratory and Index Tests

The bulk density and natural water content was measured in the laboratory. Sulphide-, root- and shell contents in the soil samples were estimated through visual observation. The liquid limit, shear strength, remolded shear strength and sensitivity were assessed through the fall cone test. The shear strength was corrected according to Bjerrum (1973) to adjust for the strain rate effect.

12.2.2.4 Constant Rate of Strain Tests (CRS)

The constant rate of strain (CRS) tests were conducted with a 0,7–0,75%/h vertical deformation rate on 20 mm samples with 50 mm diameter. The CRS tests were carried out on soil samples from 3 to 55 m depth. The preconsolidation pressure and consolidation characteristics were assessed from the tests, as well as conventional measurements of sample disturbance, (Lunne et al. 2008).

12.3 Site Investigation Results

The soil types and index properties of the soil samples are shown in Table 12.2 and follow the general form of the area, (Nilbrink and Hedberg 2014). The maximum and minimum values of the index properties are reported. The clay plasticity index is normally not reported in Swedish practice since most deposits found in the country contain high-plasticity clay. Empirical correlations between the liquid limit and the plasticity index of Swedish clays in Ahnberg and Larsson (2012) are shown for each layer in the table. The clay was not assessed in the current site investigation, but samples from a nearby site (<40 km away) displayed a clay content of 60–70% clay at a comparable liquid limit. The area is relatively large and located next to

Table 12.2 Soil strata and min-max values of index properties

Depth (m)	Soil type	ρ_{bulk} (t/m^3)	w_n (%)	w_L(%)	Empirical PI from Ahnberg and Larsson (2012)	S_t (−)
3	Grey – green silty clay with organic content	1.57–1.64	59–64	59–72	30–40	10–16
5	Grey clay	1.48–1.55	77–81	77–93	40–50	9–14
9	Black clay with sulphide content	1.46–1.53	79–90	93–105	50–60	9–14
14	Black – grey clay with sulphide content	1.43–1.56	75–89	88–107	50–60	8–10
21–25	Black grey clay	1.56–1.69	53–61	57–75	30–40	7–16
28–31	Brown – grey varved clay	1.66–1.76	48–66	53–74	25–40	8–11
38–42	Brown – grey varved clay	1.80–1.88	37–48	49–57	20–30	5–10
55	Brown – grey varved clay	1.85–1.91	31–40	45–53	20–25	3–11

a river, which can be assumed to have influenced the deposition pattern of the soil layers around the ground level. Some of the deeper samples were retrieved from somewhat different depths because of practical reasons during drilling, as well as to try to retrieve soil from a drained soil layer at 28–29 m depths for subsequent consolidation analysis.

12.3.1 Shear Strength

Figure 12.3 shows the estimated undrained shear strength in direct shear c_u^{DSS} from field vane tests (FV), fall cone tests, (FC), and a typical CPTu (representative for the area) with a cone factor $N_{kt} = 14$ (for the uncorrected shear strength), and then corrected according to Bjerrum (1973) for normal clay without sulphide content, and Larsson et al. 2007 for clay with sulphide content. Note that the undrained shear strength is significantly lower for the fall cone tests in comparison to the CPTu correlation, with a relatively large variation.

12.3.2 Compressibility

The compressibility of the clay and the preconsolidation pressure were measured in the CRS tests. Figure 12.4a and b show the CRS compression curves for CRS III from 3 m depth and 55 m depth. Figure 12.5 shows the measured preconsolidation

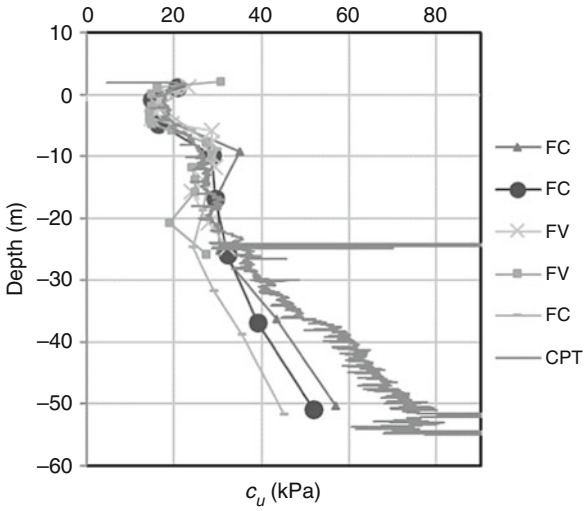

Fig. 12.3 Field vane, fall cone and CPTu measurements of the corrected c_u^{DSS}

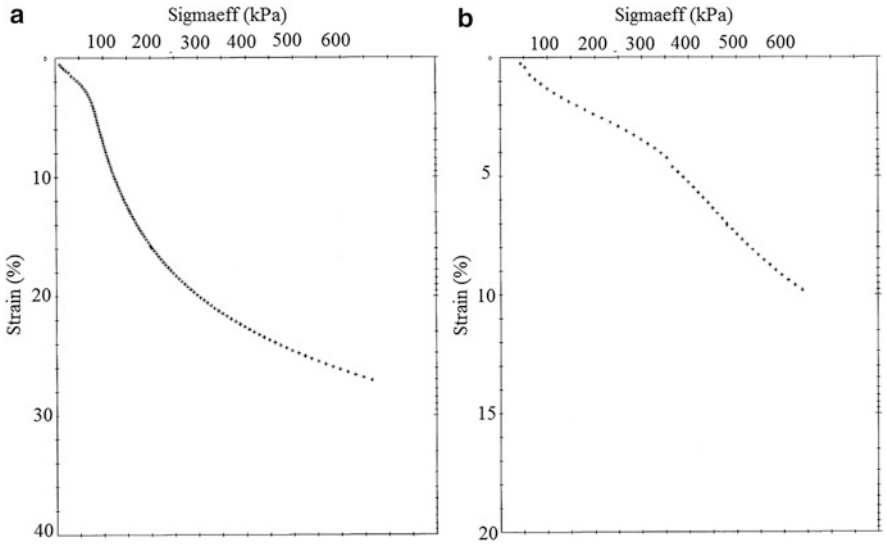

Fig. 12.4 (**a**) CRS-III (3 m depth) (**b**) CRS-III (55 m depth)

stress for CRS I – IV, as evaluated by conventional methods, e.g. as elaborated in Lunne et al. (2008). Figure 12.5 also shows the vertical effective stress, as evaluated from the index properties and from pore pressure measurements. The evaluated preconsolidation pressures in the lower part of the clay profile are lower than the vertical effective stress.

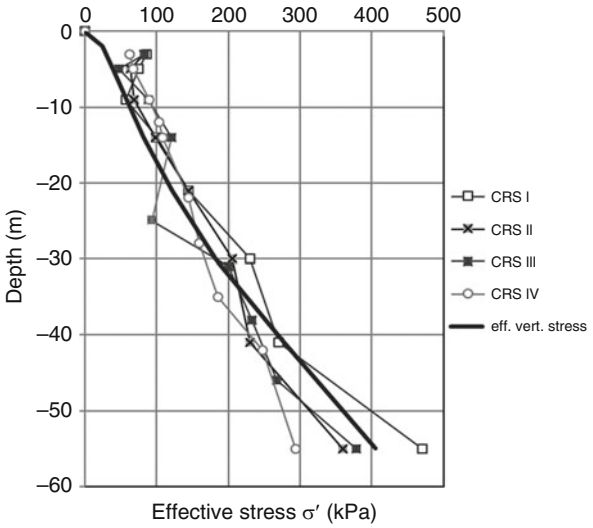

Fig. 12.5 Preconsolidation pressure evaluated from CRS I–IV and vertical effective stress

Table 12.3 CRS tests and sample disturbance indicators

Depth (m)	CRS I		CRS II		CRS III		CRS IV	
	$\Delta e/e_0$	M_0/M_L	$\Delta e/e_0$	M_0/M_L	$\Delta e/e_0$	M_0/M_L	$\Delta e/e_0$	M_0/M_L
3	0.021	5.5	0.039	2.7	0.035	3.9	0.028	3.8
5	0.035	3.1	0.028	5.8	0.031	2.4	0.031	4.4
9	0.055	2.7	0.043	3.5	0.081	3.7	0.029	4.3
14	0.079	1.9	0.083	1.3	0.062	2.2	0.040	3.6
21–25	0.075	2.7	0.078	2.7	0.113	1.4	0.062	3.4
28–31	0.086	2.6	0.069	3.8	0.067	2.5	0.065	2.1
38–42	0.120	1.9	0.096	2.6	0.107	1.6	0.088	3.2
55	0.114	2.1	0.150	2.3	0.114	1.7	0.110	2.1

12.3.3 Sample Disturbance

The conventional indicators for sample disturbance is the $\Delta e/e_0$ (where Δe is the change in void ratio and e_0 is the initial void ratio), after Lunne et al. (1997), and M_0/M_L (where M_0 is the initial confined modulus and M_L is the confined modulus after yield), after Karlsrud and Hernandez-Martinez (2013). These indicators are shown for the CRS I – IV in Table 12.3. The void ratio change indicator shows that the samples from the top layers are very good to excellent for the first 5 m depth, which agrees with tests conducted in Löfroth (2012).

The sample quality decreases after the top layer, and the quality of the samples from the varved clay is poor to very poor, following Lunne et al. (1997). The sample quality according to the modulus change M_0/M_L on the contrary shows that most

samples even in the varved clay layer are good to fair, and in most cases very good to excellent according to Karlsrud and Hernandez-Martinez (2013).

12.4 Discussion

The laboratory measurements of compressibility, as well as the index tests and in-situ tests of the soil, show that some sample disturbance has occurred in the deeper clay layers. The presence of clay samples from fairly deep layers that have a lower preconsolidation pressure than the vertical effective stress, shown in Fig. 12.5, contradicts the stress history and deposition mechanism of the soil. The top layers largely follow the behavior of normally consolidated soil set out in Bjerrum (1973), where secondary consolidation in the form of creep results in a slight overconsolidation ratio for the Holocene deposits. The apparent results showing underconsolidation in the deeper layers in the CRS tests are similar to other cases where sample disturbance has occurred, (DeGroot et al. 2005; Hight et al. 2002). The measurements of shear strength in direct shear $c_u{}^{DSS}$ from the CPTu are much larger than the fall cone tests. This confirms that index tests are more sensitive to sample disturbance compared to other tests, an issue which is discussed in DeGroot et al. (2010). The sample disturbance could originate in stress release after sampling, followed by swelling as a result of soil suction, as demonstrated by Amundsen et al. (2016). Sample disturbance and low shear strength has previously been observed in varved clay, (Lacasse et al. 1977). The varved clay which was subjected to the sample disturbance is not homogenous, and the more permeable layers should be able to access any fluid in the sampling tube relatively fast, which results in swelling. One set of samples were tested in the CRS apparatus almost immediately (around 1 day waiting time) after sampling was completed, but still displayed similar levels of sample disturbance. This suggests that the sample disturbance occurs rapidly in the soil directly after sampling.

12.5 Conclusions

The exhibited in-situ and laboratory measurements show that samples from deep clay layers are prone to show some sample disturbance, confirming other recorded site investigation results. The measurements show that especially CRS tests from varved clays should be assessed with some care for practical design purposes. The properties of the varved clay are somewhat different from those of very sensitive types of clay as discussed in Amundsen et al. (2016), and Thakur et al. (2014), but sample disturbance in deep layers, where the aid of block sampler is not possible, is however of general interest. The discussed results are therefore a modest step towards systematic assessment of the uncertainty in site investigation techniques.

Acknowledgements The very helpful review by Arnfinn Emdal is greatly appreciated, as well as the assistance and interesting discussions provided by Fredrik von Resare and Emil Davidsson in the preparation of the site investigation.

References

Ahnberg H, Larsson R (2012) Strength degradation of clay due to cyclic loadings and enforced deformation. Swedish Geotechnical Institute, Report, 75

Amundsen HA, Thakur V, Emdal A (2016) Sample disturbances in block samples on low plastic clay. NGM 2016 Reykjavik, Proceedings of the 17th Nordic Geotechnical Meeting

Andresen A, Berre T, Kleven A, Lunne T (1979) Procedures used to obtain soil parameters for foundation engineering in the North Sea. Mar Georesour Geotechnol 3(3):201–266

Bernander S (2011) Progressive landslides in long natural slopes, formation, potential extension and configuration of finished slides in strain-softening soils. Luleå tekniska universitet, Luleå

Bjerrum L (1973) Problems of soil mechanics and construction on soft clays. Proceedings of the 8th International Conference on Soil Mechanics and Foundation Engineering, Moscow

DeGroot DJ, Poirier SE, Landon MM (2005) Sample disturbance, soft clays. Studia Geotechnica et Mechanica 27(3–4):91–105

DeGroot D, Lunne T, Tjelta TI (2010) Recommended best practice for geotechnical site investigation of offshore cohesive sediments. In: Invited Keynote paper, Proceedings of the 2nd International Symposium on Frontiers in Offshore geotechnics, Perth, Western Australia

Emrich WJ (1971) Performance study of soil sampler for deep-penetration marine borings. In: Sampling of soil and rock. ASTM International, Trondheim

Grimstad G, Andresen L, Jostad HP (2012) NGI-ADP: anisotropic shear strength model for clay. Int J Numer Anal Methods Geomech 36(4):483–497

Hight DW, Hamza MM, El Sayed AS (2002) Engineering characteristics of the Nile Delta clays. In: Proceedings of the International Symposium, IS Yokohama, 200, AA Balkema, pp 149–162

Karlsrud K, Hernandez-Martinez FG (2013) Strength and deformation properties of Norwegian clays from laboratory tests on high-quality block samples. Can Geotech J 50(12):1273–1293

Lacasse SM, Ladd CC, Barsvary AK (1977) Undrained behavior of embankments on new Liskeard varved clay. Can Geotech J 14(3):367–388

Lacasse S, Nadim F (1998) Risk and reliability in geotechnical engineering. In: Proceedings of the fourth international conference on case histories in geotechnical engineering, St Louis, Missouri, March, pp 9–12

Larsson R, Westerberg B, Albing D, Knutsson S, Carlsson E (2007) Sulfidjord, geoteknisk klassificering och odränerad skjuvhållfasthet. SGI Rapport 69, (In Swedish)

Lundberg AB, Li Y (2015) Probabilistic characterization of a soft Scandinavian clay supporting a light quay structure. In: Geotechnical safety and risk V. IOS Press, Amsterdam, pp 170–175

Lunne T, Berre T, Strandvik S (1997) Sample disturbance effects in soft low plastic Norwegian clay. In: Symposium on recent developments in soil and pavement mechanics

Lunne T, Berre T, Andersen KH, Strandvik S, Sjursen M (2006) Effects of sample disturbance and consolidation procedures on measured shear strength of soft marine Norwegian clays. Can Geotech J 43(7):726–750

Lunne T, Berre T, Andersen KH, Sjursen M, Mortensen N (2008) Effects of sample disturbance on consolidation behaviour of soft marine Norwegian clays. In: Geotechnical and geophysical site characterization: proceedings of the third international conference on site characterization ISC, vol 3. Taylor & Francis, London, pp 1471–1479

Löfroth H (2012) Sampling in normal and high-sensitivity clay – a comparison of results from specimens taken with the SGI large diameter sampler and the standard piston sampler St II. SGI Varia 637, Linköping

Nilbrink D, Hedberg S (2014) Ground settlement in Uppsala, a comparison between calculated and actural outcome. Master's thesis

Thakur, V, Jostad HP, Koinbekke HA, Begago SA (2014) How well do we understand the undrained strain softening response in soft sensitive days? In Lanslides in Sensitive clays, Springer Netherlands, 291–303

Chapter 13
Effects of Sample Disturbance in the Determination of Soil Parameters for Advanced Finite Element Modelling of Sensitive Clays

Marco D'Ignazio, Hans Petter Jostad, Tim Länsivaara, Ville Lehtonen, Juho Mansikkamäki, and Christopher Meehan

Abstract The stress-strain response of sensitive clays tested in a laboratory setting can be significantly affected by disturbance effects caused by sampling, transport, storage and specimen preparation. Soil models for finite element analyses are commonly calibrated using the results from laboratory tests and, consequently, calibrated model parameters are likely to be affected by sample disturbance. For sensitive clays subjected to constant volume shearing, the stress-strain behavior is dependent on the direction of loading and, due to build-up of shear induced pore pressure, effective stresses will reduce with increasing strain in the post-peak regime. According to previous studies, peak strengths, strains at failure and post-peak behavior of sensitive clays are all significantly influenced by sample quality. Therefore, the relative quality of model predictions generated using a sensitive clay finite element model can also be expected to be notably affected by sample disturbance. In this study, the impact of sample disturbance on the determination of model input parameters for advanced finite element modelling of sensitive clays is addressed and critically discussed. Two advanced soil models are used for this purpose: the total stress based NGI-ADPSoft model, which is able to predict the anisotropic strain-softening behavior of saturated sensitive clays, and the effective

M. D'Ignazio (✉) • H.P. Jostad
Norwegian Geotechnical Institute (NGI), Oslo, Norway
e-mail: marco.dignazio@ngi.no; hans.petter.jostad@ngi.no

T. Länsivaara • J. Mansikkamäki
Tampere University of Technology (TUT), Tampere, Finland
e-mail: tim.lansivaara@tut.fi; juho.mansikkamaki@tut.fi

V. Lehtonen
Tampere University of Technology (TUT), Tampere, Finland

Ramboll Finland Oy, Tampere, Finland
e-mail: ville.lehtonen@tut.fi

C. Meehan
University of Delaware (UD), Newark, NJ, USA
e-mail: cmeehan@udel.edu

V. Thakur et al. (eds.), *Landslides in Sensitive Clays*, Advances in Natural and Technological Hazards Research 46, DOI 10.1007/978-3-319-56487-6_13

stress based S-CLAY1S model, which is characterized by an anisotropic yield surface and is able to simulate soil destructuration. The practical implications of a thoughtful selection of the input parameters are evaluated through FE stability analyses of a sensitive clay slope.

13.1 Introduction

The mechanical properties of soft sensitive clays determined from laboratory tests are highly dependent on the quality of the tested soil specimens (e.g. Lunne et al. 2006; Karlsrud and Hernandez-Martinez 2013). The main consequence of significant soil disturbance is that measured properties from poor quality samples may differ substantially from the in-situ values, especially with regard to undrained shear strength (s_u) and preconsolidation pressure (σ'_p), which may lead to conservative and costly design solutions (e.g. Powell and Lunne 2005).

Issues related to assessment of sample disturbance and its associated impacts on soft soil engineering have been studied extensively (e.g. Bjerrum 1954, 1973; Lunne et al. 1997, 2006, 2008; Hight and Leroueil 2003; Ladd and DeGroot 2003; Karlsrud and Hernandez-Martinez 2013). In Scandinavia, for practical projects, clay samples are commonly collected using the 50 mm diameter piston sampler ST2. It has been observed by various researchers (e.g. Lunne et al. 2006; Mataić 2016; Di Buò et al. 2016) that piston samples do not always provide high specimen quality.

Lunne et al. (2006) carried out parallel undrained triaxial and direct simple shear (DSS) tests on samples taken using a 250 mm diameter Sheerbrooke block sampler (Lefebvre and Poulin 1979) and piston tube samples (54, 76 and 95 mm diameter) from 11 clay sites from Norway. From these tests, it was observed that block samples of sensitive clays tended to maintain a more intact soil structure than the piston tube sample, making them generally of higher quality. The more disturbed piston samples were characterized by lower peak s_u and lower peak shear strain (γ_p) than the block samples (Lunne et al. 2006). This was attributed to the loss of clay structure and a breakdown of cementation bonds in the sensitive clays. At large strains, higher shear strengths were observed for the disturbed samples, which are characterized by lower water content than the block samples (Lunne et al. 2006). Lunne et al. (2008) suggest that σ'_p values determined from constant rate of strain (CRS) oedometer tests on 54 mm tube samples can be 20–30% lower than the values obtainable from block samples.

Soil parameters for Finite Element (FE) analyses are often directly determined from laboratory tests such as triaxial, DSS and oedometer tests. Therefore, poor sample quality may result in biased FE predictions and inaccurate estimate of the actual soil behavior. For instance, in short-term stability analyses of embankments or slopes, "disturbed" input parameters will result in low factors of safety (FOS) and incorrect predictions of displacements (soil stiffness is also affected by sample quality, e.g., Lunne et al. 2006).

In order to evaluate the implications of determining soil parameters for FE analyses from samples of varying quality, the undrained stability of a gently inclined sensitive clay slope was evaluated using two advanced FE soil models. The soil models studied are the NGI-ADPSoft (Grimstad et al. 2010) and the S-CLAY1S (Karstunen et al. 2005) models. The NGI-ADPSoft model is a total stress based model, which is capable of describing the anisotropic undrained response of saturated sensitive clays, including the strain-softening behavior in the post-peak regime. The S-CLAY1S model is an anisotropic effective stress based model, which is able to describe the anisotropic yielding behavior and soil destructuration of sensitive clays. Sample disturbance affects the two models differently – in the total stress model, sample disturbance directly influences the input strength, and in the effective stress model the strength parameters are not influenced, but the yielding and deformation properties are.

13.2 Description of the Finite Element Soil Models

13.2.1 NGI-ADPSoft

The NGI-ADPSoft soil model (Grimstad et al. 2010) is a special version of the elasto-plastic NGI-ADP model (Grimstad et al. 2012), which is based on an anisotropic Tresca failure criterion. The stress-path dependent behavior is based on the ADP framework proposed by Bjerrum (1973). The s_u profiles for active ($s_u{}^A$), direct simple shear ($s_u{}^{DSS}$) and passive ($s_u{}^P$) stress paths are given directly as input parameters. The non-linear hardening pre-peak behavior is described by input of the peak s_u ($s_u{}^A$, $s_u{}^{DSS}$, $s_u{}^P$) and corresponding shear strains ($\gamma_p{}^A$, $\gamma_p{}^{DSS}$, $\gamma_p{}^P$) in the three directions of loading, represented by triaxial compression (TXC), DSS and triaxial extension (TXE), as shown in Fig. 13.1. In general, $s_u{}^P < s_u{}^{DSS} < s_u{}^A$ for sensitive clays (e.g. Lunne et al. 2006; Karlsrud and Hernandez-Martinez 2013).

The NGI-ADPSoft model further accounts for the post-peak strain softening behavior typical of sensitive clays. The reduced shear stresses are described by input of the residual s_u values ($s_{ur}{}^A$, $s_{ur}{}^{DSS}$, $s_{ur}{}^P$) and corresponding shear strains ($\gamma_r{}^A$, $\gamma_r{}^{DSS}$, $\gamma_r{}^P$), as shown in Fig. 13.1. The shape of the stress-strain curve in the post peak regime can be modelled by means of two shape parameters, c_1 and c_2. By interpolation between the three input stress-strain curves, the model predicts the anisotropic behavior of the clay for a general 3D stress state.

The triaxial curves in Fig. 13.1 start from the initial shear stress τ_0, as undrained triaxial tests are consolidated to the in-situ stress conditions. The initial inclination of the curves is described by the shear modulus at small strain (G_0).

The model assumes linear variation of s_u with depth within a soil layer. The s_u profile is defined by a constant $s_u{}^A{}_{ref}$ at a reference depth y_{ref}, along with a strength increase parameter $s_u{}^A{}_{inc}$. For inclined layers, y_{ref} can be given by a reference point x_{ref} and an inclination $\Delta y_{ref}/\Delta x$. The input anisotropic s_u is defined by the anisotropy ratios $s_u{}^{DSS}/s_u{}^A$ and $s_u{}^P/s_u{}^A$. The residual anisotropic s_{ur} is given as a fraction of the active shear strength, through the parameters $s_{ur}{}^A/s_u{}^A$, $s_{ur}{}^{DSS}/s_u{}^A$, and $s_{ur}{}^P/s_u{}^A$.

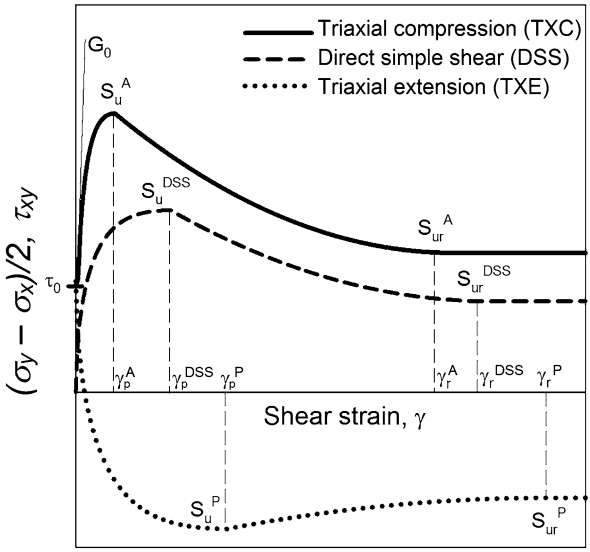

Fig. 13.1 Input parameters for NGI-ADPSoft model (After D'Ignazio 2016)

In order to avoid mesh dependency of the solution, the shear band thickness (t_{sb}) must also be provided as an input parameter. This thickness (t_{sb}) is directly proportional to an internal length parameter (l_{int}) and a parameter α for numerical integration (Brinkgreve 1994). For a more detailed description of the NGI-ADPSoft model, model parameters and their determination see Grimstad et al. (2010), Jostad and Grimstad (2011), D'Ignazio and Länsivaara (2015), D'Ignazio et al. (2017).

13.2.2 S-CLAY1S

The S-CLAY1S model (Karstunen et al. 2005) is an effective stress based model developed for soft clays. S-CLAY1S is characterized by an elliptical inclined yield surface (Fig. 13.2a), and is able to model both the initial and the plastic strain induced anisotropy. In addition, S-CLAY1S can account for strain softening caused by soil destructuration that occurs along with plastic straining (Karstunen et al. 2005).

The elasto-plastic formulation of S-CLAY1S includes volumetric and rotational hardening of the yield surface. The volumetric hardening law modifies the size of the yield surface during yielding and it is a function of the slope of the compression line in the e-ln$p$ space for the remoulded state (λ_i) and the slope of the swelling line in the e-ln$p$ space (κ) (Fig. 13.2b).

The rotational hardening law describes the change in structural anisotropy due to plastic straining, which is controlled by two parameters, μ and β. The effect of destructuration and degradation of bonds is described by an intrinsic yield surface, as shown in Fig. 13.2a. The link between the sizes of the two yield surfaces is a

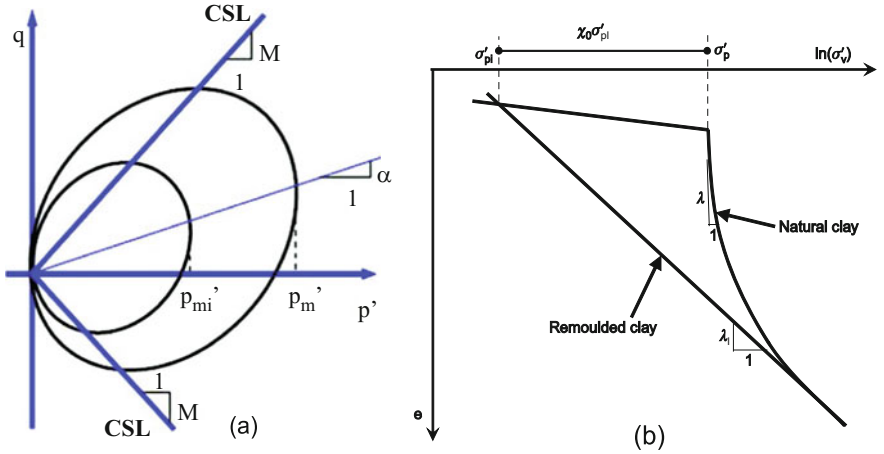

Fig. 13.2 (**a**) S-CLAY1S yield surfaces in a triaxial stress space (Karstunen et al. 2005, with permission from ASCE) and (**b**) normal compression lines for natural and reconstituted clay samples (Karstunen and Yin 2010, with permission from ICE Publishing)

function of the initial amount of bonds (χ_0), which is defined as shown in Fig. 13.2b. Two parameters, a and b, control the destructuration hardening after yielding. The initial anisotropy is defined by the parameter α_0, which gives the initial inclination of the yield surface. According to Wheeler et al. (2003), α_0 can be estimated based on the friction angle (ϕ'). μ can be calculated according to Leoni et al. (2008). The slope M of the critical state line (CLS) (Fig. 13.2a) is consequently solely a function of ϕ'.

13.3 Determination of Soil Parameters for Finite Element Analyses

For both the NGI-ADPSoft and S-CLAY1S models, soil parameters are chosen in order to compare different levels of disturbance. Lunne et al. (1997) proposed a criterion to assess sample disturbance based on the recompression volume of the sample during reconsolidation to the in-situ stress. Based on this criterion, sample quality is classified as "Very good to excellent", "Good to fair", "Poor" and "Very poor". However, such definitions are not directly linked to s_u or σ'_p. For this reason, assumptions are made in this study so that reference s_u or σ'_p values corresponding to "Very good to excellent" quality are reduced by factors equal to 1.15 and 1.30 to represent the idealized situations of "Poor" and "Very poor" sample quality, respectively. Therefore, three sets or parameters are derived for each model.

In practice, DSS and TXE tests are rarely carried out, while TXC are more common. For instance, when using the NGI-ADPSoft model for simple projects,

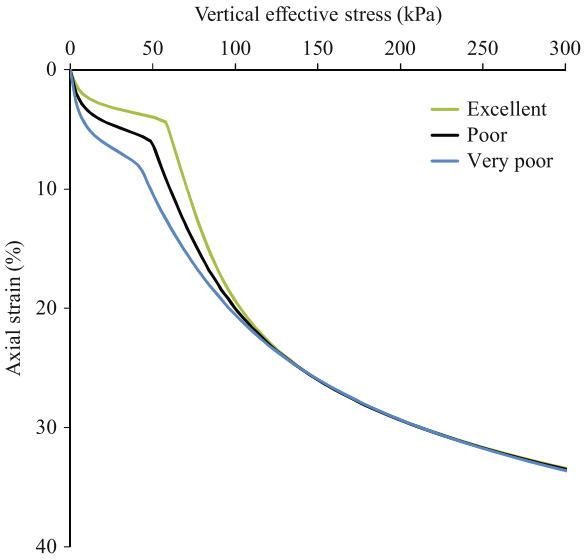

Fig. 13.3 Ideal CRS tests on samples of different quality simulated using S-CLAY1S model

the anisotropy ratios $s_u{}^{DSS}/s_u{}^{A}$ and $s_u{}^{P}/s_u{}^{A}$ could be evaluated as a function of the plasticity index (e.g. Thakur et al. 2014). The post-peak behavior can be modelled by fitting the model to TXC test results (e.g. D'Ignazio 2016; D'Ignazio et al. 2017). In this study, $s_u{}^{DSS}/s_u{}^{A} = 0.70$ and $s_u{}^{P}/s_u{}^{A} = 0.40$ are chosen following Thakur et al. (2014) for a clay of medium plasticity, and kept constant in all the calculations. $s_u{}^{A}{}_{ref} = 8$ kPa is assumed at the ground surface, corresponding to "Excellent" sample quality, linearly increasing with depth by $s_u{}^{A}{}_{inc} = 1.5$ kPa/m. The stress strain curves are selected according to D'Ignazio (2016).

The basic set of parameters for the S-CLAY1S model is chosen according to the study by Mansikkamäki (2015) on Perniö clay, from 50 mm piston samples of generally "Poor" quality. Perniö clay is a soft, slightly overconsolidated sensitive clay from Western Finland. The average sensitivity ($S_t = s_u/s_{ur}$) is equal to 40 with $\phi' = 25°$ (Mansikkamäki 2015). Parameters for the "Good" and "Very poor" sets are chosen so that curves from simulated CRS tests (Fig. 13.3) coincide at large strain. The parameters λ_i, α_0, β, M are independent of sample quality, being functions of intrinsic properties. On the other hand, a, b and μ are affected by the stress-strain behavior after yielding. Nevertheless, for the sake of simplicity, they are kept equal to their initial values for each calculation scenario. κ is however severely affected by the soil structure. Therefore, reasonable input values are selected for κ, corresponding to samples of different quality. Moreover, S_t is also affected by sample quality, being directly evaluated from the peak s_u. Therefore, as $\chi_0 = S_t - 1$ (Koskinen et al. 2002), χ_0 is modified accordingly. Fig. 13.3 shows the simulated CRS tests representing ideal tests on specimens of different quality. Input parameters for S-CLAY1S model, which differs from those derived by Mansikkamäki (2015), are summarized in Table 13.1.

Table 13.1 Input parameters for S-CLAY1S model affected by sample quality

Parameter	Description	Sample quality		
		Excellent	Poor	Very poor
κ	Slope of swelling line in e-ln$p$ plot	0.025	0.038[a]	0.055
χ_0	Initial bonding effect	45	38[a]	34
OCR	Overconsolidation ratio	1.50	1.30	1.15

[a]From Mansikkamäki (2015)

13.4 Finite Element Analyses

13.4.1 Methodology

The effect of sample disturbance on undrained FE simulations is studied by performing stability analyses of a natural sensitive clay slope. The study is carried out using the FE software PLAXIS 2D. The natural clay slope that was modelled is characterized by a slope angle of 9° (Fig. 13.4). The utilized FE geometry and mesh are shown in Fig. 13.4. A "fine" mesh is adopted for the calculations, consisting of 15-node triangular elements. Local mesh refinement is applied where the shear band develops. Full node fixities are applied at the base, while the lateral boundaries are set free to move only in the vertical direction. The ground water table is located 1 m below the ground level.

The initial stresses are generated from the combination of a "K_0" phase and a plastic nil phase (Plaxis 2012). The undrained stability is assessed by manually reducing the strength parameters until failure occurs, and evaluating the FOS as FOS $= {s_u}^A{}_{ref}/{s_u}^A{}_{min}$ for NGI-ADPSoft and FOS $= tan\phi'/tan\phi'_{min}$ for S-CLAY-1S.

In the total stress analyses, ${s_u}^A{}_{inc}$ is reduced along with ${s_u}^A$ by the same quantity. In the effective stress analyses, the reduction of ϕ' implies that α_0, M and β must be also updated, while the other parameters are kept equal to their initial values. A comparison between the two different methods is not straightforward, as the s_u reduction is carried out in different ways. Hence, the results obtained for the two models should be analyzed separately.

13.4.2 Results

Results from the FE analyses suggest that sample quality has a high impact on the undrained stability of the slope of Fig. 13.4. For clay samples of "Very poor" quality, the undrained FOS is underestimated, with respect to samples of "Excellent quality", by 15% and 25% using NGI-ADPSoft and S-CLAY1S, respectively. Calculation results are summarized in Table 13.2. The observed failure mechanism from the FE analyses resulted to be the same for both models.

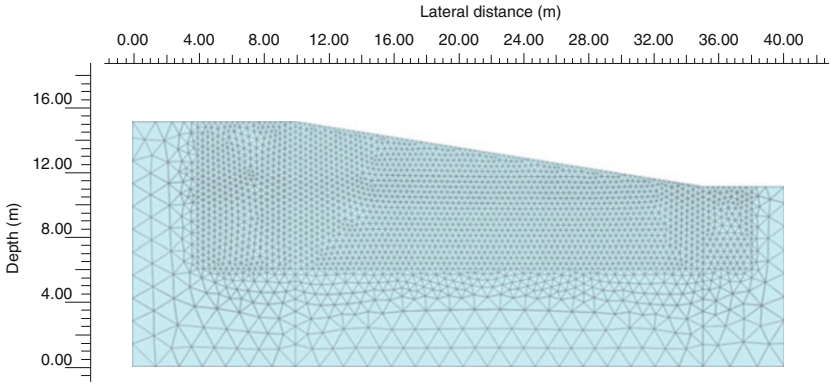

Fig. 13.4 Finite element mesh used in the calculations

Table 13.2 Undrained FOS for different calculation scenarios and calculation methods

	FOS = $s_u{}^A{}_{ref}/s_u{}^A{}_{min}$	FOS = $tan\phi'/tan\phi'_{min}$
Sample quality	NGI-ADPSoft	S-CLAY1S
Excellent	1.45	1.44
Poor	1.35	1.21
Very poor	1.26	1.10

13.5 Discussion

To counterbalance the disturbance effects, it can be observed that standard triaxial and CRS tests are normally carried out at relatively high strain rates, relative to the actual rates that occur in the field. In-situ failures may take several days or weeks, while in a laboratory test undrained failure occurs after only a few hours. Therefore, measured s_u and σ'_p should be reduced in order to account for strain rate effects, before being used for design purposes (ϕ' is rate independent). For instance, standard CRS oedometer tests may overestimate σ'_p of Finnish soft clays by 17–20% (Länsivaara 1999). This may suggest that sample disturbance would balance the higher effective stresses reached during a laboratory test resulting from high strain rate, without leading to an actual underprediction of soil properties.

13.6 Conclusions

Sample disturbance affects the determination of parameters for the two models analysed in this study, the NGI-ADPSoft and the S-CLAY1S soil models, in different ways. The outcome of this disturbance is, however, the same, as when input parameters are calibrated from disturbed samples, the undrained FOS of a natural

slope is underestimated. When using the anisotropic total stress NGI-ADPSoft model, the loss of soil structure due to disturbance effects will result in lower input peak s_u to the model. With regard to the S-CLAY1S model, disturbance effects are seen on yielding and deformation properties. While ϕ' is generally not affected by sample quality, stiffness may be severely underpredicted. Furthermore, the lower measured σ'_p will result in a smaller initial yield surface and, hence, s_u.

The FE analyses of a sensitive clay slope presented in this study have shown that when using the S-CLAY1S model, the calculated undrained FOS for "very poor" sample quality is about 25% lower than for "excellent" sample quality. Such a difference is about 15% for the NGI-ADPSoft model.

Acknowledgements The authors wish to express their gratitude to Dr. Siew Ann Tan from National University of Singapore for his valuable comments on the manuscript.

References

Bjerrum L (1954) Geotechnical properties of Norwegian marine clays. Géotechnique 4(2):49–69

Bjerrum L (1973) Problems of soil mechanics and construction on soft clays. State-of-the-art report. In: Proceedings of the 8th ICSMFE, Moscow, 3, pp 111–159

Brinkgreve RBJ (1994) Geomaterial models and numerical analysis of softening. PhD thesis, TU Delft, Delft University of Technology

D'Ignazio M (2016) Undrained shear strength of Finnish clays for stability analyses of embankments. PhD thesis, Tampere University of Technology, Tampere

D'Ignazio M, Länsivaara T (2015) Shear bands in soft clays: strain-softening behavior in finite element method. Rakenteiden Mekaniikka J Struct Mech 48(1):83–98

D'Ignazio M, Länsivaara T, Jostad HP (2017) Failure in anisotropic sensitive clays: a finite element study of the Perniö failure test. Can Geotech J 10.1139/cgj-2015-0313

Di Buò B, D'Ignazio M, Selänpää J, Länsivaara T (2016) Preliminary results from a study aiming to improve ground investigation data. In: Proceedings of the 17th Nordic Geotechnical Meeting, Reykjavik, 25–28 May 2016, 1, pp 187–197

Grimstad G, Jostad HP, Andresen L (2010) Undrained capacity analyses of sensitive clays using the nonlocal strain approach. In: Proceedings of the 9th HSTAM international congress on mechanics, Vardoulakis mini-symposia, Limassol, Kypros, 12–14 July. pp 153–160

Grimstad G, Andresen L, Jostad HP (2012) NGI-ADP: anisotropic shear strength model for clay. Int J Numer Anal Methods Geomech 36(4):483–497

Hight DW, Leroueil S (2003) Characterisation of soils for engineering purposes. In: Proceedings of the international workshop characterisation and engineering properties of natural soils, Singapore, 2–4 December 2002, 1, pp 255–360

Jostad HP, Grimstad G (2011) Comparison of distribution functions for the nonlocal strain approach. In: Proceedings of the 2nd international symposium on computational Geomechanics, Cavtat-Dubrovnik, Croatia. pp 212–223

Karlsrud K, Hernandez-Martinez FG (2013) Strength and deformation properties of Norwegian clays from laboratory tests on high-quality block samples 1. Can Geotech J 50(12):1273–1293

Karstunen M, Yin ZY (2010) Modelling time-dependent behaviour of Murro test embankment. Géotechnique 60(10):735–749

Karstunen M, Krenn H, Wheeler SJ, Koskinen M, Zentar R (2005) Effect of anisotropy and destructuration on the behavior of Murro test embankment. Int J Geomech 5(2):87–97

Koskinen M, Karstunen M, Wheeler SJ (2002) Modelling destructuration and anisotropy of a natural soft clay. Proceedings of the 5th European conference on numerical methods in geotechnical engineering, Paris, pp 11–20

Ladd CC, DeGroot, DJ (2003) Recommended practice for soft ground site characterization: arthur Casagrande Lecture. Proceedings of the 12th Panamerican conference on soil mechanics and geotechnical engineering, 22–26 June 2003, 1, pp 1–57

Länsivaara TT (1999) A study of the mechanical behavior of soft clay. PhD thesis, Norwegian University of Science and Technology, Trondheim

Lefebvre G, Poulin C (1979) A new method of sampling in sensitive clay. Can Geotech J 16(1):226–233

Leoni M, Karstunen M, Vermeer P (2008) Anisotropic creep model for soft soils. Géotechnique 58(3):215–226

Lunne T, Berre T, Strandvik S (1997) Sample disturbance effects in soft low plastic Norwegian clay. Proceedings of the conference on recent developments in soil and pavement mechanics, Rio De Janeiro, 25–27 June 1997, pp 81–102

Lunne T, Berre T, Andersen KH, Strandvik S, Sjursen M (2006) Effects of sample disturbance and consolidation procedures on measured shear strength of soft marine Norwegian clays. Can Geotech J 43(7):726–750

Lunne T, Berre T, Andersen KH, Sjursen M, Mortensen N (2008) Effects of sample disturbance on consolidation behaviour of soft marine Norwegian clays. Proceedings of the third International Conference on Site Characterization ISC: geotechnical and geophysical site characterization, 3, pp 1471–1479

Mansikkamäki J (2015) Effective stress finite element stability analysis of an old railway embankment on soft clay. PhD thesis, Tampere University of Technology, Tampere

Mataić I (2016) On structure and rate dependence of Perniö clay. PhD Thesis, Aalto University, Helsinki

Plaxis BV (2012) User's manual of PLAXIS, The Netherlands

Powell JJ, Lunne T (2005) Use of CPTU data in clays/fine grained soils. Studia Geotechnica et Mechanica 27(3–4):29–66

Thakur V, Oset F, Viklund M, Strand SA, Gjeskiv V, Christensen S, Fauskerud OA (2014). En omforent anbefaling for bruk av anisotropifaktorer i prosjektering i norske leirer. Report no. 1/2014. ISBN n. 978–82–410-0962-4

Wheeler SJ, Näätänen A, Karstunen M, Lojander M (2003) An anisotropic elastoplastic model for soft clays. Can Geotech J 40(2):403–418

Chapter 14
Viscometric Tests of Sensitive Clay from Byneset, Norway, and Fit to the Herschel–Bulkley Model

Ragnhild Håøy Grue, Dieter Issler, Jean-Sébastien L'Heureux, and Vikas Thakur

Abstract The flow behaviour of fully remoulded sensitive clay from Esp, near Trondheim, Norway, is investigated using a wide-gap concentric-cylinder viscometer. The salinity S and liquidity index I_L are varied over a wide range. The Esp clay shows shear thinning flow behaviour, similar to Canadian sensitive clays. The Herschel–Bulkley (H-B) model allows a better fit to the measured flow curves than the Bingham model for the Norwegian as well as Canadian clays. All model parameters depend strongly on the liquidity index and the salinity. The H-B exponent n was found to vary from 0.36 at high S and low I_L to 0.97 at low S and high I_L. The onset of turbulence in the rheometer is detected at Reynolds numbers of 50–100.

14.1 Introduction

Quick clay slides are a serious natural hazard in parts of the Scandinavian countries, eastern Canada, Alaska and Russia. Mapping of potential quick clay slide areas has made significant progress in the past decades and is carried out nation-wide, e.g., in

R.H. Grue (✉)
Multiconsult ASA, Oslo, Norway
e-mail: ragnhild.haoy.grue@multiconsult.no

D. Issler
Natural Hazards Division, Norwegian Geotechnical Institute, Oslo, Norway
e-mail: di@ngi.no

J.-S. L'Heureux
Trondheim Division, Norwegian Geotechnical Institute (NGI), Trondheim, Norway
e-mail: jsl@ngi.no

V. Thakur
Department of Civil and Environmental Engineering, Norwegian University of Science and Technology (NTNU), Trondheim, Norway
e-mail: vikas.thakur@ntnu.no

V. Thakur et al. (eds.), *Landslides in Sensitive Clays*, Advances in Natural and Technological Hazards Research 46, DOI 10.1007/978-3-319-56487-6_14

Norway. In contrast to all other gravitational hazards like snow avalanches or debris flows, adequate tools for mapping the potential run-out areas are presently missing, even though these areas may be large. The recently initiated development of such numerical models (Issler et al., 2014) has raised the question how the flow behaviour of quick clay can be described in adequate mathematical terms. The problem has two complementary aspects, namely (i) the rheology of fully remoulded quick clay, and (ii) the dynamics of the remoulding. Locat and Demers (1988) did pioneering work on the first problem through rheometric tests of Canadian quick clays. Later work confirmed their findings and provided some insight into the second problem, even though the latter has not been solved comprehensively yet (Locat, 1997; Locat et al., 2008).

This paper focuses on the first problem. We measure the flow curve of a Norwegian sensitive clay to investigate whether or not the Canadian findings can be applied to it as well. Locat and Demers (1988) analysed their results in terms of Bingham rheology, but remarked that their samples showed shear-thinning behaviour. Locat (1997) presented data that showed the more general Herschel–Bulkley (H-B) rheology and the bilinear or Worrall–Tuliani (1964) rheologies to provide superior fits. The Bingham rheology is the special case $n = 1$ of the H-B rheology, which reads

$$\tau = \mathrm{sgn}(\dot{\gamma}) \left(\tau_y + K|\dot{\gamma}|^n\right) \tag{14.1}$$

Here, $\dot{\gamma}$ is the shear rate, τ is the shear stress, τ_y is the yield stress below which the material behaves as a solid, K is the consistency parameter (which becomes the viscosity coefficient in a Bingham fluid) with units $\mathrm{Pa\,s}^n$, and n is the flow index. For shear thinning fluids, $n < 1$. The Worrall–Tuliani rheology is given by

$$\tau = \mathrm{sgn}(\dot{\gamma}) \left[\tau_y + \left(\mu_\infty + \frac{\mu_0 - \mu_\infty}{1 + \dfrac{\mu_0 - \mu_\infty}{\tau_\infty - \tau_y}|\dot{\gamma}|}\right)|\dot{\gamma}|\right] \tag{14.2}$$

τ_y is the true yield stress, τ_∞ the apparent yield stress at high shear rate, μ_0 the viscosity at vanishing shear rate, and μ_∞ the asymptotic (Bingham) viscosity. In the limits $\dot{\gamma} \to 0$ and $\dot{\gamma} \to \infty$, τ tends to $\tau_y + \mu_0\dot{\gamma}$ and $\tau_\infty + \mu_\infty\dot{\gamma}$, respectively. For simplicity, we analysed our measurements in terms of H-B rheology. Experimental procedures along with detailed information about the tested clay can be found in Grue (2015).

14.2 Materials and Methods

14.2.1 Test Materials

The tested Norwegian sample is from Esp near Trondheim, Trøndelag county. It is a low-activity clay ($A_c = 0.17$) with a sensitivity of 42. At clay-size fraction of 35–50%, salinity of 1.1 g/l, and water content of 35%, its plasticity index was 6.4% and its liquid limit, 29%. With a remoulded undrained shear strength of 590 Pa, our sample cannot be considered quick, but in the immediate vicinity, where a substantial quick clay slide occurred in 2012, shear strengths around 200 Pa have been measured in the same layer.

The properties of Canadian sensitive clays from several locations that we have re-analysed, as well as the measurement procedures, are described by Locat and Demers (1988) and Locat (1997).

14.2.2 Instrument

A Bohlin Visco 88BV coaxial-cylinder viscometer (CCV) was used. The stationary outer cylinder has a closed bottom, the inner cylinder rotates. Different combinations of inner and outer cylinder radius (R_i, R_o) can be used, see Table 14.1. The apparatus features eight rotation speed settings from 20 to 1000 min^{-1}. It measures torque (mN m^{-1}) applied to the inner cylinder, rotation speed, and temperature.

14.2.3 Rheological Testing Procedures

Procedures followed those described by Bentley (1979) and Torrance (1987). The same methods were also applied by Locat and Demers (1988), whose data on Canadian clays we re-analysed. First, index tests were performed to find the natural

Table 14.1 Dimensions of the coaxial-cylinder viscometer used in the tests

System	Inner cylinder Radius R_i (mm)	Height h (mm)	Outer cylinder Radius R_o (mm)	R_o/R_i
1	7.0	21.1	13.75	1.97
2	7.0	21.1	22.75	3.26
3	12.5	37.6	22.75	1.82

clay properties. Samples were prepared for viscometric testing by adding the desired amount of NaCl and brine (consisting of NaCl added to deionized water) to obtain salinities in the range 0.9–4.6 g/l and liquidity indices in the range 2.3–4.9. The mixtures were always fully remoulded before testing. Between any two measurements, the sample was sheared at the highest rotation speed until a stable torque was reached. This was done to have the same start conditions for every new rotation speed in the dynamic test.

14.2.4 Processing of Viscometric Data

In all the tests, the ratio of the radii, R_o/R_i, was 1.8 or larger so that the shear rate was not uniform across the gap. For a H-B fluid, no analytic solution is known for the associated inverse Couette problem, i.e., for obtaining n, τ_y and K from the torque and rotation speed. Following Grue (2015), we used the approximation that Heirman et al. (2008) have proposed and tested on concrete slurries in a rheometer with $R_o/R_i = 1.45$. The torque at the inner cylinder is divided into a flow resistance, G_{HB}, independent of the rotation speed N, and a flow dependent part $H_{\mathrm{HB}}N^J$ with H_{HB} the viscosity factor and J the flow index:

$$T \approx G_{\mathrm{HB}} + H_{\mathrm{HB}}N^J \tag{14.3}$$

Heirman et al. (2008) give the following formulas for the approximate values of the H-B parameters (h is the height of the inner cylinder, see Table 14.1):

$$n \approx J \tag{14.4}$$

$$\tau_y \approx \frac{G_{\mathrm{HB}}}{4\pi h}\left(\frac{1}{R_i^2} - \frac{1}{R_o^2}\right)\frac{1}{\ln(R_o/R_i)} \tag{14.5}$$

$$K \approx \frac{H_{\mathrm{HB}}}{2^{2J+1}\pi^{J+1}h}J^J\left(R_i^{-2/J} - R_o^{-2/J}\right)^J \tag{14.6}$$

For each test consisting of measurements at eight different speeds, seven separate fits of Eq. 14.3 were performed using 5, 6, 7 or 8 consecutive measurement points to study the stability of the fitted values. Strictly speaking, Eqs. 14.4, 14.5 and 14.6 apply only if there is no plug region at the outer cylinder. A posteriori one finds that most of our measurements do not meet this condition. However, fitting only to the data points with the highest torque values did not change the results much; hence, we assume this method to yield an acceptable approximation.

14.2.5 Detection of Turbulence

One of the basic assumptions in the tests is that the flow in the annular gap is laminar. Turbulent flow has much higher resistance and would give an unrealistically large H-B exponent n if not detected. Andereck et al (1986) studied the flow regimes of a Newtonian fluid in a circular Couette system and found a threshold Reynolds number of $\mathrm{Re_N} \sim 120$ (with the outer cylinder stationary) for the transition to turbulence (Taylor cells). In our measurements, onset of turbulence will manifest itself through an inflection point in the flow curve, i.e., transition from shear thinning to shear hardening behaviour ($\tau \propto \dot{\gamma}^2$) at high rotation speeds.

The usual definition of the Reynolds number applies only to Newtonian fluids. However, its physical essence as the ratio of inertial to viscous forces can be captured also for non-Newtonian fluids by defining the generalized Reynolds number as $\mathrm{Re_{nN}} = \rho U^2/\tau$. This expression was successfully used by Zakeri et al. (2008) for flows of clayey slurries impinging on pipelines. It reduces to the usual expression in the case of Newtonian fluids. For the CCV, we set $U = 2\pi R_i N$ and $\tau \approx \frac{1}{\pi}\frac{T}{h(R_o^2-R_i^2)}\ln(R_o/R_i)$ (the mass-weighted average shear stress across the cell) and obtain

$$\mathrm{Re_{CCV}} = 4\pi^3(R_o^2 - R_i^2)R_i^2 h\frac{\rho N^2}{T\ln(R_o/R_i)} \tag{14.7}$$

14.3 Results

14.3.1 Fit to the Herschel–Bulkley Rheology

The laboratory measurements show that the samples of the tested clay exhibit yield stress (τ_y) and shear thinning behaviour ($0 < n < 1$), see Eq. 14.1 and Fig. 14.1. This agrees with the findings of Locat and Demers (1988) for Canadian clays, although these authors fitted their measurements to the Bingham model. The discrepancies between the data and the Bingham model are most pronounced at low shear rates. The H-B model fits our data very well, with the resulting τ_y, K and n being functions of the liquidity index and the salinity. For all fits, $r^2 > 0.97$ (where r^2 is the coefficient of determination). Note that one data set was excluded because of technical problems during its acquisition. Some data points at high shear rate affected by turbulence were also excluded in the curve fitting process. The onset of turbulence is discussed below.

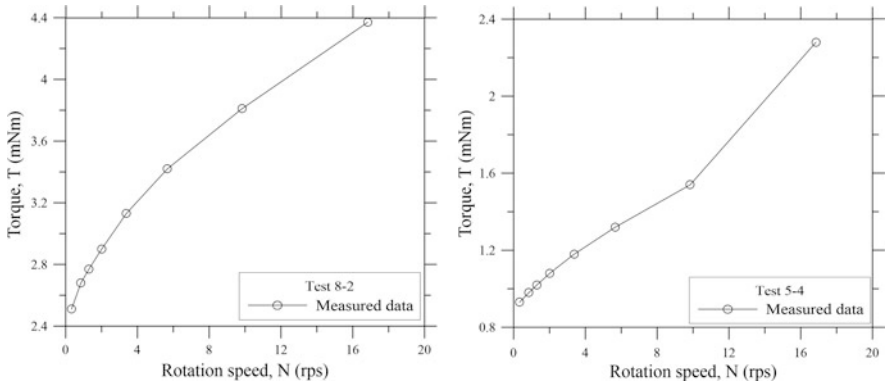

Fig. 14.1 Torque vs. rotational speed for two different samples of Esp clay. *Left panel:* A sample with salinity 2.1 g/l and $I_L = 3.3$. *Right panel:* The sample with salinity 1.4 g/l and $I_L = 3.8$ (test 5–4 in Table 14.4) shows onset of turbulence at the highest rotation speed

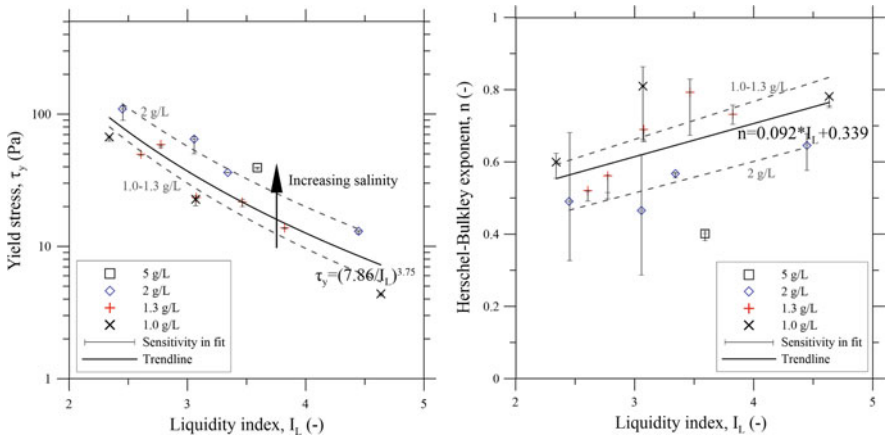

Fig. 14.2 Yield stress τ_y (*left-hand side panel*) and H-B exponent n (*right-hand side panel*) versus liquidity index I_L for Esp clay. Samples with different salinities are shown with different symbols

14.3.2 The Effect of Liquidity Index and Salinity on the Rheological Parameters

In Figs. 14.2 and 14.3, the H-B parameters τ_y, n and K^* found for Esp clay are plotted against the liquidity index (I_L). Note that the consistencies of clays with different exponents n have different physical units Pa s^n so that they cannot be compared with each other. In an attempt to discern trends nevertheless, we choose an arbitrary reference shear rate, $\dot{\gamma}_0 = 1\,s^{-1}$, and rewrite the shear stress as $\tau = \tau_y + K^*(\dot{\gamma}/\dot{\gamma}_0)^n$, where all K^* have the dimension of Pa. The salinity and

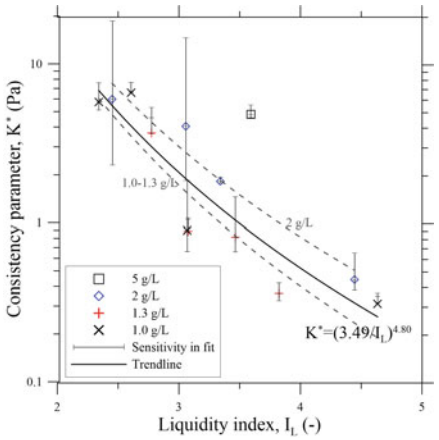

Fig. 14.3 Normalized consistency K^* versus I_L for Esp clay. Samples with different salinities are shown with different symbols

Table 14.2 Parameters of power-law fits of τ_y and K^* and linear fits of n vs. I_L for Esp clay with salinity 1.3 g/l and 2 g/l. K^* is defined by the relation $K\dot{\gamma}^n = K^*(\dot{\gamma}/\dot{\gamma}_0)^n$, where $\dot{\gamma}_0 = 1\,\mathrm{s}^{-1}$

Salinity (g/l)	$\tau_y(I_L)$	r^2	K^*	r^2	$n(I_L)$	r^2
1.0–1.3	$2300\,\mathrm{Pa}\,I_L^{-3.95}$	0.936	$445\,\mathrm{Pa}\,I_L^{-5.07}$	0.856	$0.105I_L + 0.347$	0.481
2.0	$3170\,\mathrm{Pa}\,I_L^{-3.66}$	0.979	$444\,\mathrm{Pa}\,I_L^{-4.54}$	0.945	$0.087I_L + 0.253$	0.795
All	$2279\,\mathrm{Pa}\,I_L^{-3.75}$	0.823	$403\,\mathrm{Pa}\,I_L^{-4.80}$	0.819	$0.092I_L + 0.339$	0.308

the liquidity index vary in the ranges 1–5 g/l and 2.4–4.6, respectively. We found τ_y to range from 4 Pa to 109 Pa, K^* from 0.3 Pa to 6.6 Pa, and n from 0.36 to 0.81.

Figure 14.2 shows that τ_y decreases with increasing I_L and decreasing S. A similar trend is observed for K^*, see Fig. 14.3. Figure 14.2 shows that n increases with increasing I_L and decreasing S. n is found to be less than 1 in all tests, which means that Esp clay does not behave as a Bingham fluid for the tested values of S and I_L. Table 14.2 shows preliminary parametrisations of the I_L-dependence of τ_y, K^* and n, using power-law fits for τ_y and K^*, and a linear approximation for n.

We have re-analysed some of the data from Locat (1997) with the H-B rheology. In most of these tests the gap between the inner and outer cylinder was fairly narrow ($R_o/R_i \leq 1.14$), and flow curves $\tau(\dot{\gamma})$ were deduced using the narrow-gap approximation. Therefore, we used the provided flow curves $\tau(\dot{\gamma})$ directly in the fitting procedure. Some of the results are shown in Table 14.3. In all cases, one obtains a better fit with the H-B model than with the Bingham model, the improvement being most pronounced at low shear rates. For example, the differences between these two models are small and irrelevant for run-out modelling in the case of St. Alban clay with low salinity (Fig. 14.4, left panel), but more pronounced for the clay at high salinity, despite its high liquidity index (Fig. 14.4, right panel). As in the case of Esp clay, the exponent n tends towards 1 at high liquidity index and low salinity.

Table 14.3 Results from the re-analysis of the flow curves of selected Canadian clays in terms of the H-B model and comparison with the original results, which assume Bingham rheology

	Salinity	I_L	Bingham		Herschel–Bulkley		
Clay	(g/l)	(—)	τ_y (Pa)	μ (mPa s)	τ_y (Pa)	K^* (Pa)	n (—)
St. Alban 1	0.7	1.72	128.6	79.0	123.3	0.24	0.84
St. Alban 1	0.7	2.86	15.6	28.8	14.7	0.067	0.87
St. Alban 2	1.0	2.22	96.8	78.6	93.31	0.24	0.83
St. Alban 2	1.0	3.06	27.3	23.7	25.7	0.099	0.79
St. Alban 2	4.0	3.03	49.7	31.0	43.7	0.702	0.55
Saguenay Fjord	30.0	2.00	146.3	87.7	122.4	3.47	0.47
Saguenay Fjord	30.0	3.01	46.7	23.0	41.6	0.186	0.73

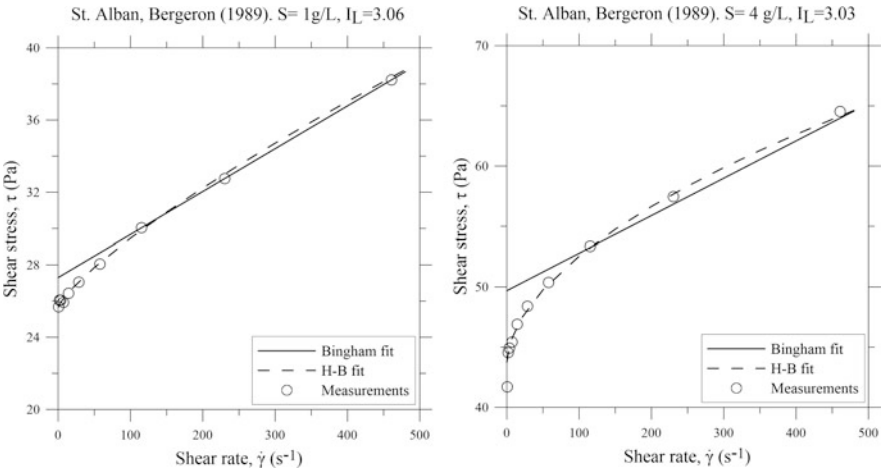

Fig. 14.4 Flow curves of Canadian clays from St. Alban. The *dots* represent measurements, the *dashed line* is the best fit with the H-B model, and the *full line* is the best fit with the Bingham model

14.3.3 Onset of Turbulence

In three measurement series with Esp clay, the curve $T(N)$ showed a clear inflection point and shear thickening behaviour at the highest rotation speeds. Table 14.4 lists the relevant parameters of those measurements and the generalized Reynolds number inferred from Eq. 14.7; see Fig. 14.1, right panel for an example of a corresponding torque–rotation-speed curve. Given the limited set of available rotation speeds (see Fig. 14.1), we cannot determine the critical Reynolds number better than to a factor 2. Our measurements exhibit signs of turbulence at somewhat lower Reynolds numbers than found by Andereck et al (1986)—the test runs 9–2 and 9–4 indicate that turbulence may set in as early as Re $\approx$ 50. We caution, however, that our set-up does not allow us to apply the same methods as Andereck et al (1986)

Table 14.4 Measurement series of Esp clay that indicate onset of turbulence. For all concerned measurements, $R_i = 12.5\,\text{mm}$, $R_o = 22.75\,\text{mm}$, and $h = 37.6\,\text{mm}$

Test	ρ (kg m^{-3})	N (s^{-1})	T (mN m)	Re (–)
5–4	1630	16.9	2.29	89
8–1	1550	16.9	1.97	99
9–2	1710	16.9	2.25	95
9–2	1710	9.8	1.23	59
9–4	1730	16.9	5.17	42

for determining the critical Reynolds number. It is therefore conceivable that part of the discrepancy is due to differences in the criteria.

14.4 Discussion and Future Work

Our tests of the rheological properties of sensitive clay from Esp, Norway, revealed similar patterns as for the Canadian clays tested by Locat (1997): (i) Fully remoulded Esp clay is a yield stress fluid with shear thinning behaviour before turbulence sets in. (ii) The yield stress and the consistency decrease with increasing liquidity index and with decreasing salt content, as is expected. (iii) The H-B exponent n depends strongly on both the liquidity index and the salinity. n increases from low values—presumably below 0.3–0.4—at low I_L (and thus outside the range accessible to our rheometer) to values close to 1 at high I_L. It is reassuring that even the approximate relation $\tau_y(I_L)$ for Esp clay is close to the one found by Locat and Demers (1988) and Locat (1997).

In view of practical applications of a run-out model based on the Herschel–Bulkley (H-B) rheology, it is important to test a considerable number of Norwegian quick clays in order to obtain support for our preliminary conclusions, to refine the approximations for $\tau_y(I_L)$ and $n(I_L)$ and finally to develop a workable relation $K(I_L, n)$. It will be interesting to quantify the clay fraction of the samples to see which role this parameter plays in these relations.

However, before carrying out further measurements, it is desirable to establish an analysis method that does not require a priori knowledge about the shape of the flow curve and also works reliably if there is a plug region in the specimen. Yeow et al. (2000) developed an approach that formulates the inverse problem as a Volterra integral equation of the first kind for the unknown function $\dot{\gamma}(\tau)$:

$$\omega = -\int_{R_o}^{R_i} \frac{\dot{\gamma}(r)}{r}\mathrm{d}r = \int_{\max(\tau_o,\tau_y)}^{\tau_i} \frac{\dot{\gamma}(\tau)}{\tau}\mathrm{d}\tau \tag{14.8}$$

The input is the data set of angular velocities and torques, $\{(\omega_1, T_1), \ldots, (\omega_m, T_m)\}$, the output consists of the function $\dot{\gamma}(\tau)$. However, with only a few experimental points $\tau(N)$ available to determine a function, i.e., an infinite number of unknowns,

this is an ill-posed problem. It can only be solved in a weak sense by minimizing a suitable functional of $\dot{\gamma}$, in this case the sum of the squares of the relative errors in Eq. 14.8. In addition, it requires regularization in the sense of Tikhonov by imposing a penalty on strongly curved functions $\dot{\gamma}(\tau)$ (Yeow et al., 2000). The yield stress is found iteratively by trying to fulfil the condition $\dot{\gamma}(\tau_y) = 0$. Once $\dot{\gamma}(\tau)$ has been determined, it can be fitted to the H-B rheology (14.1) or any other model using the non-linear least-squares method. Preliminary tests showed that the method is promising, but further work is needed to obtain better estimates of τ_y and to optimize the choice of the regularisation parameter.

If the water content of the quick clay is raised far beyond the liquid limit, w_L, the sample behaves increasingly like a Newtonian liquid, and one may argue that this should also be the case for lower water content if only the shear rate is high enough (disregarding the transition to turbulence here). This suggests that the Worrall–Tuliani (1964) rheology (14.2) might describe the behaviour of remoulded quick clay even better than the H-B model. Once appropriate analysis methods for wide-gap rheometers are developed, a number of avenues to explore open up: (i) In contrast to the Herschel–Bulkley consistencies K at different values of n, the Worrall–Tuliani viscosities μ_0 and μ_∞ of different clays or of a given clay at different values of I_L and S can be easily and unambiguously compared. (ii) Are the ratios τ_∞/τ_y and μ_∞/μ_0 similar for all quick clays, or is there some trend depending on the clay fraction? (iii) Can similar universal trends for the dependence of τ_∞ and μ_0 on liquidity index and salinity be found as Locat and Demers (1988) established for τ_y and μ_∞?

Locat and Demers (1988) established that their clays are thixotropic, and Grue (2015) also saw signs of such behaviour at time scales of 1–10 s in Esp clay. With such time scales, this effect can in principle be relevant to quick clay slides, even though its magnitude is limited. In this context, it is interesting that the Worrall–Tuliani rheology can be obtained as the equilibrium flow curve of a simple structural kinetic model applied to the Bingham rheology and that data on the transient behaviour of the material allows one to determine the agglomeration and break-up coefficients of the structural kinetic model (Toorman, 1997).

A major challenge remains, however: How can one reliably measure and quantitatively describe the *remoulding* behaviour of quick clays? This question is of paramount importance for assessing whether a disturbed quick clay mass develops into a flow with long run-out or not. L'Heureux (2012) summarizes existing measurements and modelling attempts. Most earlier work on this topic considers the degree of remoulding as a function of the applied shear work. The product of the undrained unremoulded shear stress and the plasticity index of the clay has emerged as a candidate scale through which the remoulding work can be made dimensionless and the remoulding curves approximately collapsed to a universal line (Locat et al., 2008). More data on remoulding is urgently needed, but there are substantial experimental challenges, e.g., recovering undisturbed samples, preventing shear bands from forming, and covering several orders of magnitude of shear stress and shear rate in a single experiment (Thakur and Degago, 2013; Thakur et al., 2015). On the theoretical side, structural kinetic theory is a candidate

framework for describing remoulding as the progressive break-down of flocculated clay particles to clay platelets, as already suggested by Toorman (1997).

Acknowledgements We thank Jacques Locat and Denis Demers for sharing the raw data of their tests on Canadian quick clays; Jacques Locat and Dominique Turmel also provided much appreciated information about their experimental procedures. We are grateful to Kjell Karlsrud for his constructive review of the paper. RHG acknowledges the support by Multiconsult ASA during the write-up. The work of DI and JSL was supported by the Research Council of Norway through its general research grant to NGI.

References

Andereck CD, Liu SS, Swinney HL (1986) Flow regimes in a circular Couette system with independently rotating cylinders. J Fluid Mech 164:155–183. doi:10.1017/S0022112086002513

Bentley SP (1979) Viscometric assessment of remoulded sensitive clays. Can Geotech J 16(2):414–419. doi:10.1139/t79-043

Grue RH (2015) Rheological parameters of Norwegian sensitive clays, focusing on the Herschel–Bulkley model. Master's thesis, Department of Civil and Transport Engineering, Norwegian University of Science and Technology (NTNU). http://hdl.handle.net/11250/2349972

Heirman G, Vandewalle L, Van Gemert D, Wallevik O (2008) Integration approach of the Couette inverse problem of powder type self-compacting concrete in a wide-gap concentric cylinder rheometer. J Non-Newtonian Fluid Mech 150(2):93–103. doi:10.1016/j.jnnfm.2007.10.003

Issler D, L'Heureux J, Cepeda JM, Quan Luna B (2014) Towards a numerical run-out model for quick-clay slides. In: Proceedings of INTERPRAEVENT, Nara, 23–27 Nov 2014

L'Heureux JS (2012) Characterisation of historical quick clay landslides and input parameters for Q-Bing. NGI Report 20120753-02-R, Norwegian Geotechnical Institute, Oslo, Norway, also published in Norwegian by Norwegian Water Resources and Energy Directorate in collaboration with Norwegian Public Roads Administration and Norwegian National Railways Administration as NIFS-report nr. 8/2013

Locat J (1997) Normalized rheological behaviour of fine muds and their flow properties in a pseudoplastic regime. In: Chen CL (ed) Debris-flow hazards mitigation: mechanics, prediction, and assessment. Proceedings of first international conference, San Francisco, 7–9 Aug 1997, pp XVI, 817 s

Locat J, Demers D (1988) Viscosity, yield stress, remolded strength, and liquidity index relationships for sensitive clays. Can Geotech J 25(4):799–806. doi:10.1139/t88-088

Locat P, Leroueil S, Locat J (2008) Remaniement et mobilité des débris de glissements de terrain dans les argiles sensibles de l'est du Canada. In: Proceedings of the 4th Canadian conference on Geohazards: from causes to management, presse de l'Université Laval, Québec, pp 97–106 (in French)

Thakur V, Degago SA (2013) Disintegration energy of sensitive clays. Géotech Lett 3:20–25. doi:10.1680/geolett.12.00062

Thakur V, Gylland AS, Degago SA, Oset F, Sandven R (2015) In-situ determination of disintegration energy for soft sensitive clays. In: Proceedings of GEOQuébec2015 – challenges from North to South, Canadian Geotechnical Society

Toorman EA (1997) Modelling the thixotropic behaviour of dense cohesive sediment suspensions. Rheol Acta 36(1):56–65

Torrance JK (1987) Shear resistance of remoulded soils by viscometric and fall-cone methods: a comparison for the Canadian sensitive marine clays. Can Geotech J 24(2):318–322. doi:10.1139/t87-037

Worrall WE, Tuliani S (1964) Viscosity changes during the ageing of clay–water suspensions. Trans Br Ceram Soc 63:167–185

Yeow YL, Ko WC, Tang PPP (2000) Solving the inverse problem of Couette viscometry by Tikhonov regularization. J Rheol 44:1335–1351. doi:10.1122/1.1308520

Zakeri A, Høeg K, Nadim F (2008) Submarine debris flow impact on pipelines – Part I: experimental investigation. Coast Eng 55(12):1209–1218. doi:10.1016/j.coastaleng.2008.06.003

Chapter 15
Dynamic Properties of a Sensitive Clay Deposit

Sarah Bouchard, H. Ali, D. LeBoeuf, Serge Leroueil, and G. Cascante

Abstract This paper describes a detailed geotechnical site investigation carried out to study the static and dynamic properties of a post-glacial Goldthwait Sea sensitive clay deposit. The focus is on the evaluation of the small-strain shear modulus of the sensitive clay. The site is located on the North Shore of the St-Lawrence Gulf (Province of Quebec) and it is selected as it is the location of a major landslide triggered by rock blasting operations in 2009. The investigations involved both in-situ and laboratory tests (resonant column and bender element testing). The laboratory tests were carried out on high quality large diameter clay samples from three different depths. The objective of this paper is to compare the laboratory small-strain shear modulus obtained with resonant column and bender elements with the small-strain shear modulus obtained in the field using the seismic piezocone (SCPTu) and ambient vibrations.

15.1 Introduction

A rock blasting activity carried out for the construction of a road triggered a large landslide in the Province of Québec in 2009 (Fig. 15.1). The landslide occurred in a sensitive clay deposit shortly after blasting (Locat et al. 2010; Bouchard et al. 2015). The failure mechanism of the landslide is still not well understood and

S. Bouchard (✉) • D. LeBoeuf
Department of Civil Engineering and Water Engineering, Laval University, Québec City, QC, Canada
e-mail: sarah.bouchard.3@ulaval.ca; Denis.LeBoeuf@gci.ulaval.ca

H. Ali
GHD Ltd, 140 Bathurst Dr, Waterloo, ON, Canada
e-mail: hassan.ali.1@uwaterloo.ca

S. Leroueil
Département de génie civil et de génie de eaux, Université Laval, Québec City, QC, Canada
e-mail: serge.leroueil@gci.ulaval.ca

G. Cascante
Civil Engineering Department, Waterloo University, Waterloo, ON, Canada
e-mail: gcascante@uwaterloo.ca

V. Thakur et al. (eds.), *Landslides in Sensitive Clays*, Advances in Natural and Technological Hazards Research 46, DOI 10.1007/978-3-319-56487-6_15

is under study. The characterization of the dynamic properties of this material is relevant to understand the mechanism of this failure. The goal of this study is to determine the soil model profile that will be used for dynamic analysis of the site. This paper focuses on studying the dynamic properties (V_s) of this highly sensitive clay obtained with different in situ and laboratory tests. The field tests include seismic cone penetration method (SCPTu) and microtremor recordings (H/V ambient vibrations method). The laboratory tests involved resonant column (RC) and bender element (BE) tests. Those tests were performed on three high quality samples extracted from the field with the Laval sampler (Rochelle et al. 1981). The damping (ξ) is also measured during RC tests. The field investigation is explained in the next section. Then, the samples are described, followed by the description of the experimental program. The shear wave velocity, V_s measured in the field and in laboratory by the different methods are presented and compared.

15.2 Field Investigations

The field investigations presented in this paper were carried out in 2009 and 2012 and involved one SCPTu, two CPTu, four dynamic cone penetrometer (DCP) tests, one borehole (with 200 mm diameter sampling) and three H/V ambient vibration recordings. Other field tests were performed but are not described herein and can be referred to Bouchard et al. (2015). The DCP tests were carried out to reach a denser layer or refusal. Refusal is considered to be reached when it takes more than 100 blow counts for 60 consecutive cm depth (50 each 30 cm). The location of the tests is shown in Fig. 15.1 with symbol abbreviations and profile number of the road. The

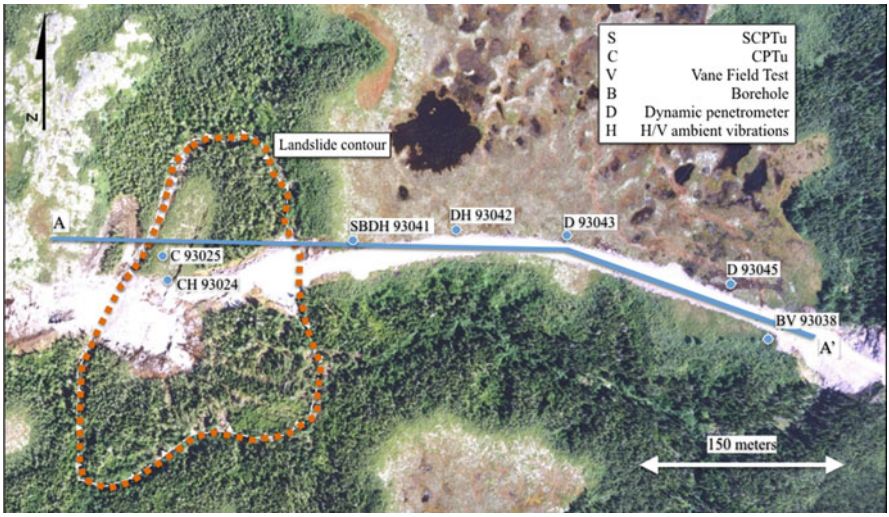

Fig. 15.1 Aerial view of La Romaine landslide and localization of the field tests. The *blue line* is the cross-section presented in Fig. 15.2

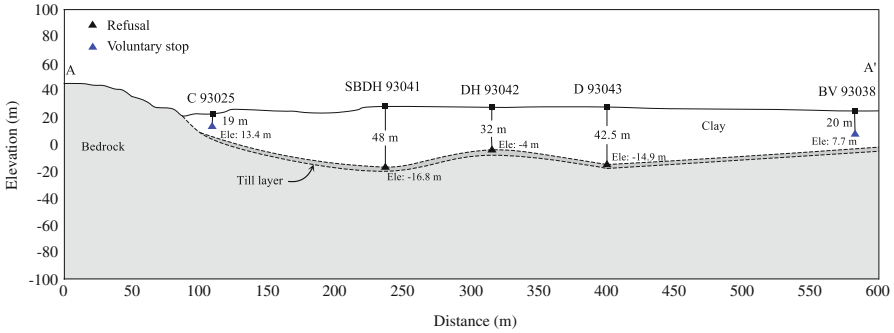

Fig. 15.2 General stratigraphy of the site (Cross section AA′ in Fig. 15.1)

cross-section in blue in Fig. 15.1 is presented in Fig. 15.2. The results from the DCP and CPTu were used to produce the general stratigraphy of the site in this cross-section. There is a thick deposit of homogeneous sensitive clay overlaid by 2–3 m of peat (Locat et al. 2010). The thickness of the clay deposit varies in the area from 0 m to 50 m, and the bedrock outcrops at some locations. The bedrock is massive granitic gneiss. A 3 m thick layer of till is considered to be located between the rock and the clay.

The H/V ambient vibrations method is a non-invasive method used in geotechnical engineering and in seismology to estimate dynamic characteristics of soils. This apparatus is used since 1950 (Nakamura 2000) and is efficient to determine the natural frequency of a sedimentary deposit. Three accelerometers record at the same time ambient vibrations (two horizontal components and one vertical). In the present study, all the ambient vibrations recordings were performed close to a penetrometer test. The Horizontal/Vertical (H/V) spectral ratio technique shows the amplification characteristics by the multiple reflections of the surface waves (Nakamura 2008). On the soft ground, the horizontal motion is larger than the vertical one, whereas on hard ground, both components are similar. The ratio permits to remove the Rayleigh waves effect on the sediments response. Special attention should be taken during the installation of the device. It is important to avoid recording near structures, to protect the device from the wind, rain, temperature and other meteorological perturbations (SESAME 2004). Furthermore, it is critical to obtain a good coupling with the soil and assure that the apparatus is levelled. Those recommendations were respected during the investigation.

The seismic cone penetrometer test (SCPTu) has a velocity geophone located inside the penetrometer (Mayne 2000). A steel beam is installed under the rig parallel to the axis of the geophone inside the cone. Generally, an operator hits the beam with a hammer to produce a shear wave that propagates into the soils until it reaches the geophone. The shear wave velocity V_s is determined by the time interval between the hit and the signal reception. In this study, one SCPTu was carried out (site S93041) and V_s was measured at every meter from 5 to 30 m depth. The small strain shear modulus is estimated by the following equation:

$$G_{\max} = \rho \cdot V_s^2 \tag{15.1}$$

15.3 Laboratory Testing

In the present study, three high quality samples (200 mm diameter) were tested in the laboratory with resonant column (ASTM D4015 2007) and bender element tests. These tests were carried out using the RC device at University of Waterloo. In RC tests, the specimen is excited at small strains (10^{-6} to 10^{-1}) in torsional mode. The dynamic properties of the soil are evaluated at its resonant frequency. The shear wave velocity is calculated from the dominant frequency and the damping ratio is evaluated with the half-band width method. BE tests (Shirley and Hampton 1978) provide shear wave velocity of the soils and can be performed simultaneously with RC tests. Piezoelectric elements are installed at both ends of the sample: one of them transmits a pulse while the other one receives it. Both methodologies and laboratory setups from Waterloo University are detailed in Ali et al. (2016).

Atterberg limits, fall cone, and consolidations tests were carried out at Université Laval. The soil specimens used for classification tests are from the same borehole and located very close to the samples used for RC and BE tests. The classification tests results and main properties of the soils are presented in Table 15.1.

The calculated stresses in situ and the applied stresses in the laboratory are presented in Table 15.2. The diameter and the height of the samples for RC and BE tests are 7 cm and 13 cm respectively.

The consolidation of the samples before performing RC and BE tests was done isotropically: $\sigma'_{vo} = \sigma'_{ho}$. Those conditions do not reflect the stress state in the clay deposit, which is anisotropic. In its natural state, the horizontal stresses of a soft clay deposit are lower that the vertical ones (Leroueil and Hight 2003). In order to estimate σ'_h, a K_o ($=\sigma'_h/\sigma'_v$) of 0.6 has been used which is a typical value for a lightly overconsolidated natural clay with a typical OCR of 1.2. The objective is to study the material behavior in its natural state, i.e. in the overconsolidated domain. As the device used did not permit anisotropic consolidation, it has been decided to use a certain percentage (60%) of vertical in situ stresses to stay inside the limit state curve, as shown in Fig. 15.3.

Table 15.1 Selected engineering properties of Goldthwait Sea clay

No	Depth (m)	γ (kN/m^3)	w (%)	S_u (kPa)	I_p (%)	I_L (%)	σ'_p (kPa)	σ'_v[a] (kPa)
TM2-B	17.87	17.6	56	22	6.2	5.1	100	124
TM5-B	20.31	16.5	58	26	3.6	7.6	210	141
TM7-B	22.27	16.5	61	34	8.1	4.8	210	154

[a]σ'_v (in situ stresses) calculated with an average unit weight of 16 kN/m^3 for the clay with 3 m of peat at the top (unit weight of 11 kN/m^3) and water table located at 2.9 m below surface. No is the sample number, γ is the unit weight, w is the natural water content, Su is the undrained shear strength obtained from swedish fall cone, PI is the plasticity index, LI is the liquidity index and σ'_p is the preconsolidation test obtained with consolidation tests.

Table 15.2 Principal characteristics, in situ and laboratory stresses of the samples used for RC and BE tests

No	Depth (m)	γ ($\kappa N/\mu^3$)	H_i (cm)	w_i (%)	σ_{vo} (kPa)	u (kPa)	σ'_{vo} (kPa) [a]	σ'_{ho} (kPa)	*Lab* σ'_c (kPa)
TM2-C	18.02	16.5	13.3	53	273	149	124	74	48
TM5-A	20.17	14.8	13.3	59	308	169	139	83	80
TM7-A	22.15	14.9	13.0	59	339	189	150	90	80
	22.15	14.9	13.0	59	339	189	150	90	160

[a] σ'_{vo} (in situ effective vertical stress) calculated with an average unit weight of 16 kN/m^3 for the clay with 3 m of peat at the top (unit weight of 11 kN/m^3) and water table located at 2.9 m below surface. No is the sample number, γ is unit weight, H_i is the initial height of the sample, w_i is the initial natural water content, σ_{vo} is the total vertical stress, u is the pore pressure, σ'_{ho} is the estimate effective horizontal stress and σ'_c is the confinement pressure applied in the laboratory.

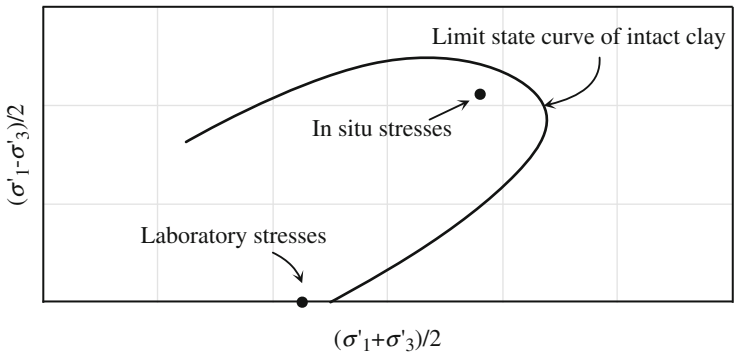

Fig. 15.3 Schematic representation of laboratory stresses used for RC and BE tests compared with in situ stresses and limit state curve of intact clay

15.4 Results

15.4.1 H/V Ambient Vibrations Method

Figures 15.4 and 15.5 show an example of ambient vibrations result obtained at site 93042. Figure 15.4 shows the three components recordings (N-S, E-W and Up-Down) of ambient vibrations, while Fig. 15.5 presents the average H/V spectral ratio. The amplitude of the ratio reaches a maximum value at the frequency of 1.7, which corresponds to the dominant frequency of the deposit. The quality of the data was validated with the criteria proposed in the SESAME (2004) report. It is important to mention that the peak in Fig. 15.5 is sharp and clear, which is an indication of an acceptable result. The fact that there is only one clear peak indicates that the deposit has a unique dominant frequency.

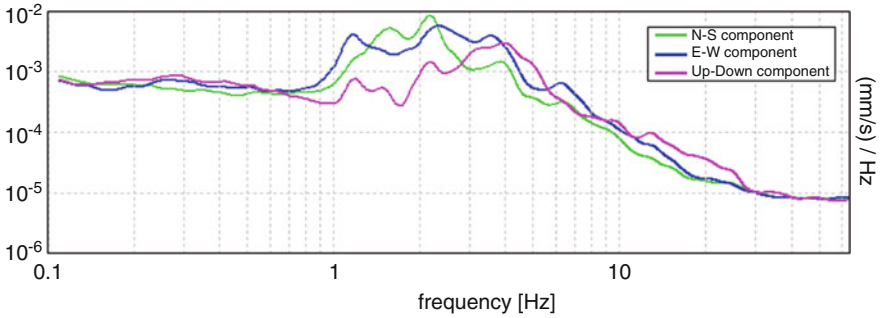

Fig. 15.4 Horizontal and vertical ambient vibrations recordings at site 93042

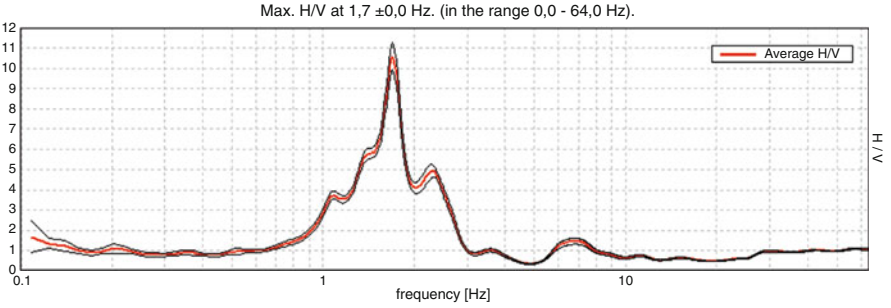

Fig. 15.5 Average H/V spectral ratio at site 93042

15.4.2 V_s from SCPTu and H/V Ambient Vibrations Method (Field Investigation)

Table 15.3 summarizes the results obtained from H/V ambient vibrations method, penetrometer tests and SCPTu. The Vs from the ambient vibrations records is calculated from the following equation:

$$V_s \approx 4H/T_o \tag{15.2}$$

where T_o is the natural period of the deposit ($T_o = 1/F_o$), H is the thickness of the sedimentary layer obtained with the penetrometer sounding. The same equation can be used to estimate T_o from V_s.

The site 93024 is located inside the landslide and part of the soils investigated is above the failure surface. The failure surface is located at around a 10 m depth at that location. The V_s obtained at this site from ambient vibrations is 145 m/s, which is lower than at the other stations. This is consistent with the fact that the remolded clay shows a lower strength than the intact soil. On the other hand, site 93041 permits to compare the V_s values from the seismic cone profile and ambient

Table 15.3 Field investigation results of V_s

Site	Depth to refusal (m)	Microtremor peak frequency F_o (period T_o)	Vs (≈4H/Vs)	Average $\overline{V_s}$ seismic cone	Remarks
93024	20 m	Pt 001: 1.8 Hz (0.55 s)	145 m/s	–	Inside the landslide[a]
93041	48 m	Pt 002: 1.33 Hz (0.75 s)	256 m/s	150 m/s	$\overline{V}_s$ (SCPTu) from 4 to 30 m depth
				200 m/s	$\overline{V}_s$ (SCPTu) extrapolated from 4 to 48 m depth
93042	32 m	Pt 003: 1.7 Hz (0.6 s)	213 m/s	–	No SCPTu

[a]From CPTu (part of the clay is remolded because it is above the failure surface)

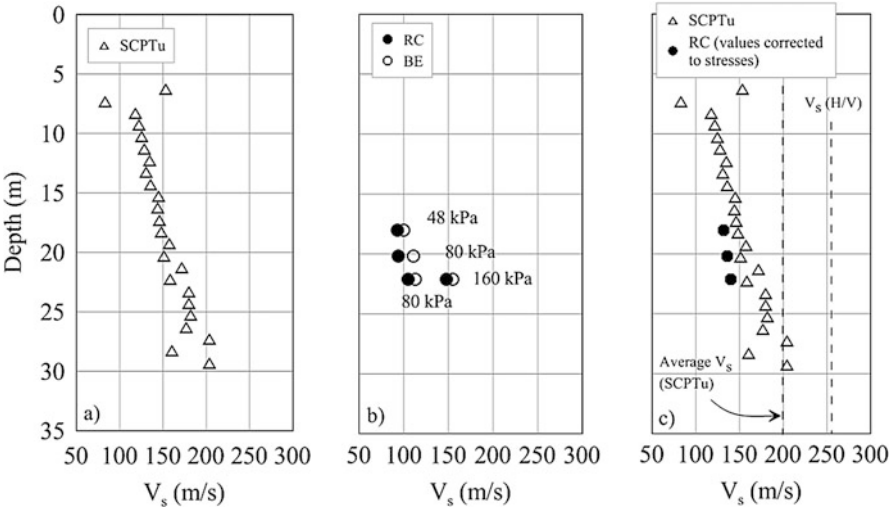

Fig. 15.6 (**a**) V_s from SCPTu, (**b**) V_s from RC and BE tests with the applied confinement stresses and (**c**) corrected V_s values (RC) to in situ stresses, V_s from SPCTu, average V_s from SCPTu extrapolated to 48 m and V_s from H/V method

vibrations recordings. The complete V_s profile from SCPTu is shown in Fig. 15.6a. The first 5 meters were not investigated because of the presence of peat and fill layers. At 6 m depth, it is possible to notice the presence of a clayey crust layer with high values of V_s. V_s decreases rapidly when the cone reaches the sensitive clay deposit at 7 m depth and then increases gradually with depth.

There is a difference between V_s results from SCPTu and H/V ambient vibrations: 150 m/s (4 – 30 m depth) for SCPTu and 256 m/s for the H/V ambient vibrations (0–48 m). In Fig. 15.6, the average Vs from H/V ambient vibrations is shown until 30 m. If the results of V_s from SCPTu are extrapolated to 48 m, the

Table 15.4 Laboratory test results from RC and BE tests

Sample	σ'_c (kPa)	V_s (RC) (m/s)	V_s (RC)[a] (m/s)	ξ (%)	V_s (BE) (m/s)
TM2-C	48	93.1	131.9	1.4	99.9
TM5-A	80	93.4	136.2	1.8	111.2
TM7-A	80	104.5	140	1.4	113
TM7-A	160	147.7	140	0.9	155.1

[a]Corrected values to in situ stresses with $V_s = \alpha(\sigma'_v)^{\beta}$, where $\alpha = 28.13$ and $\beta = 0.32$ from Ali et al. (2016), σ'_c is the confining pressure in laboratory, ξ is the damping measured in RC test.

average V_s would be around 200 m/s if the soil is homogeneous. V_s from SCPTu is smaller than H/V ambient vibrations method. It is important to mention that ambient vibrations are recorded at lower strains than SCPTu. A difference between both tests was also observed in Molnar et al. (2007), where 12 SCPTu and ambient vibrations were carried out in different soil types (mainly clays). In general, ambient vibrations showed shorter fundamental period than SCPTu (i.e. larger V_s). The site 93042 is consistent with site 93041 with a V_s of 213 m/s.

15.4.3 V_s from RC and BE Tests (Laboratory Results)

The V_s values obtained in the laboratory with RC and BE tests are presented in Table 15.4. They were measured at very small strains, e.g. 10^{-4}.

There is a good agreement between the RC and BE tests with 10% difference at low confinement and 5% difference at higher confinement (Ali et al. 2016). However, the V_s obtained with BE are in general higher than those obtained with RC. The sample TM7-A was submitted to two different confining pressures, 80 kPa and 160 kPa. It is clear that the applied confining pressure has an impact on V_s. This is observed for RC test as well as BE test and this effect was shown in previous research (e.g. Lefebvre et al. 1994). For both tests, the values of V_s have increased, reflecting the direct effect of confining pressure on G_{max} value (Ali et al. 2016).

15.4.4 Comparison Between Test Results

RC values are corrected to field stresses and compared with the seismic cone profile in Fig. 15.6. The correction for field stresses reduces the gap between the laboratory and in situ results. The difference between laboratory (RC) and in situ V_s values is about 10%. This is possibly due to frequency effects and light remolding of samples during extraction, cutting and installation.

15.5 Conclusion

In this paper, the dynamic properties of a very sensitive clay from Canada were studied. The goal was to determine the V_s profile that will be used in dynamic analysis of La Romaine landslide site. Shear wave velocity was estimated from various field and laboratory methods.

It has been observed that V_s obtained in situ is slightly larger than the one obtained in the laboratory. This observation was also shown in previous research on the small shear strain modulus of sensitive clays (Lefebvre et al. 1994).

Also, it was shown that confining pressure has an important effect on V_s. The applied confining pressure in the laboratory was 0.6 of in situ vertical stresses. This explains the main difference observed in situ versus laboratory. Shear wave velocity values from RC test were corrected to the field stresses reducing the gap between the results (10% difference). The effect of confining pressure on V_s was also shown with sample TM7-A: two tests were carried out at different confining pressure (80 and 160 kPa). The 160 kPa confinement is close to the in situ stresses (150 kPa) and both V_s (lab vs *in situ*) were very close, i.e. 148 m/s (RC), 155 m/s (BE) and 158 m/s (SCPTu).

Acknowledgements The authors would like to thank the Ministère des Transports du Québec, Ministère de la Sécurité publique and Natural Sciences and Engineering Research Council of Canada (NSERC) for their financial support. Didier Perret (commission géologique du Canada) is also thanked for his help with microtremor ambient vibrations measurements. Dr. Samson Degago at the Norwegian Public Road Administration (NPRA) is acknowledged for reviewing this paper.

References

Ali H, Bouchard S, Cascante G, LeBoeuf D, Leroueil S 2016 Measurement of shear wave velocity in sensitive clays using resonant column, bender element and seismic cone penetration tests (under press). In: 69th Canadian Geotechnical Conference, Vancouver

Bouchard S, Leroueil S, LeBoeuf D, Deschênes P.-L, Dorval P (2015) Analysis of a blast loading near sensitive clay slope in La Romaine village, Quebec. In: 68th Canadian Geotechnical conference, GEOQuébec 2015, Québec city, Canada. p 8

D4015, A (2007) Standard test methods for modulus and damping of soils by resonant-column method

Lefebvre G, Leboeuf D, Rahhal ME, Lacroix A, Warde J, Stokoe KH II (1994) Laboratory and field determinations of small-strain shear modulus for a structured Champlain clay. Can Geotech J 31(1):61–70

Leroueil S, Hight DW (2003) Behaviour and properties of natural soils and soft rocks. In: Proceedings of international workshop on characterisation and engineering properties of natural soils, Singapore. pp 29–254

Locat P, Delisle M.-C, Demers D, Robitaille D, Grondin G (2010) Cas d'un glissement dans les argiles sensibles provoqué à la suite d'un sautage à La Romaine, Basse-Côte Nord, Québec, Canada. Calgary, p 7

Mayne PW 2000 Enhanced geotechnical site characterization by seismic piezocone penetration tests. In: Invited lecture, fourth geotechnical conference, Cairo University, pp 95–120
Molnar S, Cassidy JF, Monahan PA, Dosso SE (2007) Comparison of geophysical shear-wave velocity methods. In: Ninth Canadian conference on earthquake engineering, Ottawa, Ontario, Canada, pp 390–400
Nakamura Y (2000) Clear identification of fundamental idea of Nakamura's technique and its applications. In: 12th world conference on Earthquake Engineering, New Zealand
Nakamura Y (2008) On the H/V spectrum. In: The 14th world conference on earthquake engineering, Beijing, China
Rochelle PL, Sarrailh J, Tavenas F, Roy M, Leroueil S (1981) Causes of sampling disturbance and design of a new sampler for sensitive soils. Can Geotech J 18(1):52–66
SESAME (2004) Guideline for the implementation of the H/V spectral ratio technique on ambient vibrations, SESAME European research project
Shirley DJ, Hampton LD (1978) Shear wave measurements in laboratory sediments. J Acoust Soc Am 63(2):607–613

Part II
Pre-failure and Failure Stages

Chapter 16
The Role of Instability and Shear Band Localisation in Triggering Landslides in Sensitive Clays

Lars Andresen and Hans Petter Jostad

Abstract The mechanism of initiation or triggering of landslides in soft sensitive clays is governed by strain softening and localization of deformation into thin shear bands. The triggering load and the extent of the initial part of the landslide depend upon the formation and propagation of these shear bands and in particular upon their thickness. The role of local pore water drainage and rate dependency in the formation and propagation of these shear bands is not fully understood. This paper reviews some of the research carried out during the last decades within this field, discuss the results and points to some recommendations for further research in order to reach a conclusion.

16.1 Introduction

The processes and mechanisms governing the triggering of landslides in slopes of sensitive clay are very complex. In spite of a large research effort over several decades they are not fully understood and can still not be analysed properly. This paper addresses the triggering process and mechanism. It is noted that other important issues have to be dealt with as part of a proper risk assessment, such as the consequences of the evolving post-triggering failure mechanism which typically includes large deformations and geometry changes caused by retrogression and run-out. Instability and strain softening are associated with the localisation of deformations into shear bands while the clay adjacent to these bands is elastically unloaded. The formation, propagation and in particular the thickness of these bands have a major effect on the triggering load and are in many ways the key to the understanding of instabilities and failures in sensitive clays. A total stress approach gives no information of the shear band thickness. Theoretically the thickness is undefined, but in finite element analyses restricted by the discretization. This is clearly not physical and not according to observations. Through research carried

L. Andresen (✉) • H.P. Jostad
Norwegian Geotechnical Institute (NGI), Oslo, Norway
e-mail: lars.andresen@ngi.no; Hans.Petter.Jostad@ngi.no

V. Thakur et al. (eds.), *Landslides in Sensitive Clays*, Advances in Natural and Technological Hazards Research 46, DOI 10.1007/978-3-319-56487-6_16

out over the last two decades, whereas a large part has been carried out at NTNU and NGI (Jostad and Andresen 2002; Andresen and Jostad 2004; Jostad et al. 2006, 2013; Grimstad et al. 2010; Thakur 2011, 2014; Gylland et al. 2014). Much insight and understanding have been gained into the process of shear band formation in sensitive clays, however there are still missing links and fundamental questions remain. In particular in verifying the hypothesis that the shear band formation and thickness are governed by local pore water drainage and strain rate dependency. This past work is revisited, its potential for providing a proper framework for analysis is discussed and recommendations for further research are given.

16.2 Instability as a Triggering Mechanism

The traditional understanding of a slope failure in geotechnical engineering is when the driving forces, i.e. the external loads, exceeds the resisting forces given by the mobilization of a shear strength along a failure surface. However, soil slopes might become unstable and collapse, with a mechanism quite similar to the buckling problem, due to material instability. Within the framework of continuum mechanics, the stability of a body with volume V_0 can be assessed mathematically by disturbing the present displacement field $\mathbf{u}$ by an infinitesimal small displacement perturbation $\mathrm{d}\mathbf{u}$ (this could have been a small external load $\mathrm{d}\mathbf{E}$ as well). The resulting strain increments $\mathrm{d}\boldsymbol{\varepsilon}$ are given by the displacement gradients, $\mathrm{d}\boldsymbol{\varepsilon} = 1/2[\nabla \mathrm{d}\mathbf{u} + \nabla^{\mathrm{T}}\mathrm{d}\mathbf{u}]$, and the resulting stress increments are obtained from the incremental constitutive relationship $\mathrm{d}\boldsymbol{\sigma} = \mathbf{D} \cdot \mathrm{d}\boldsymbol{\varepsilon}$ where $\mathrm{d}\boldsymbol{\sigma}$ is the stress increment, $\mathbf{D}$ is the constitutive matrix and a linear relationship between stress and strain on incremental form is assumed. The second order internal work within the body V_0 caused by this incremental displacement field $\mathrm{d}\mathbf{u}$ is:

$$dW_{int} = \int_{V_0} d\boldsymbol{\sigma} \cdot d\boldsymbol{\varepsilon}\, dV \tag{16.1}$$

Then, according to Hill (1958), the equilibrium state of the body V_0 may be considered *stable* if $\mathrm{dW} > 0$ for any $\mathrm{d}\mathbf{u}$ and *unstable* if $\mathrm{dW} < 0$ for at least one $\mathrm{d}\mathbf{u}$. Here a stable equilibrium state is one where the response of a vanishingly small disturbance also remains vanishingly small. If we consider a material with a constitutive relationship where $\mathrm{dw} = \mathrm{d}\boldsymbol{\sigma} \cdot \mathrm{d}\boldsymbol{\varepsilon} > 0$ for all points within the body for all loading paths it is obvious that stability is guaranteed. However, for soil materials which exhibit non-associated plastic flow or strain softening, or both, the constitutive relationship is such that $\mathrm{dw} = \mathrm{d}\boldsymbol{\sigma} \cdot \mathrm{d}\boldsymbol{\varepsilon}$ might become negative (e.g. Jostad and Nordal 1995). The system V_0 is not necessary unstable when the second order work $\mathrm{d}\boldsymbol{\sigma} \cdot \mathrm{d}\boldsymbol{\varepsilon} < 0$ in some part of the system. However, for some loading paths one might encounter equilibrium states where the total integrated second order work dW becomes negative. This corresponds to a global instability point, i.e. a small perturbation or disturbance might lead to a situation where the system can't any

longer sustain its loads and collapse follows. Equilibrium at such a state can only be maintained by rapid unloading of the external loads or balanced by inertia from an accelerating soil mass. The field situation will be load controlled so removing the loads is not possible and the soil body will start accelerating and a failure or collapse of the soil body will follow. For sensitive clays the shear stress reduces with increasing plastic strain after a peak point, i.e. $d\tau \cdot d\gamma < 0$ and we might encounter local instability at the material point. The internal second order work might be decomposed into a shear term and a volume term: $d\boldsymbol{\sigma} \cdot d\boldsymbol{\varepsilon} = d\tau \cdot d\gamma + dp' \cdot d\varepsilon_{vol}$ and for the special case of undrained loading we have $dp' \cdot d\varepsilon_{vol} = 0$ and the instability is governed by the shear term alone. Here dp' denotes the effective mean stress and $d\varepsilon_{vol}$ is the volumetric strain. The triggering point represents a state of global instability where the rate of loss of strength $d\tau \cdot d\gamma < 0$ in one part of the slope can't any longer be balanced by the rate of strength gain or elastic unloading, which both gives $d\tau \cdot d\gamma > 0$, in other parts of the slope. It is noted that instability might be reached also for drained or partly drained loading paths by considering also the contribution from the volumetric work. The instability point might be reached without mobilizing the shear strength along any failure surface. Only small parts of the slope might have passed the peak stress, and as will be shown later, might not have formed a shear surface at this stage. The instability is therefore not associated with soil failure in the classical way. For slope instabilities or landslides involving strain-softening material this global instability phenomenon is referred to as progressive failure and early contributions considering softening of the friction angle from its peak value ϕ_p towards it residual value ϕ_r in over-consolidated clays are made by Skempton (1964) and Bjerrum (1967). The mechanism of progressive failure caused by strength reduction due to pore pressure build up in sensitive clays has however not until recently been fully appreciated. The mechanism is clearly demonstrated by the pioneering work of Bernander (1981, 2011). It is shown that, due to the progressive failure mechanism, the load bearing capacity of such slopes is lower than for slopes with perfectly-plastic clays with no or little softening, even if their peak strengths are the same. The loading of a clay slope inevitably imposes non-uniform strains and stresses. Figure 16.1 illustrates a slope where erosion in the toe area causes some parts of the slope to reach peak strength τ_p first. Further erosion causes the shear stresses to reduce from the peak strength τ_p towards the residual strength τ_r which expands the local zone of softening. The softening zone will typically localise into a shear band of thickness t_{sb} as will be shown later. This causes redistribution of stresses to other parts of the slope where the shear stress still increases towards the peak strength. At a certain critical value, the triggering point, the loss of strength by strain softening in the progressing zone can't any longer be balanced by the gain in strength outside this zone.

When the triggering load is reached a "point of no return" is passed and the subsequent failure process is self-driven. The residual strength of sensitive and quick clays will mostly be lower than the gravitational shear stress τ_0 which carries the weight of the slope, even for a very gently inclined (i.e. 3–5°) slopes. When parts of the slope reach the residual strengths, the component of the slope weight parallel to the failure surface can't anymore be resisted by the soil and equilibrium can be

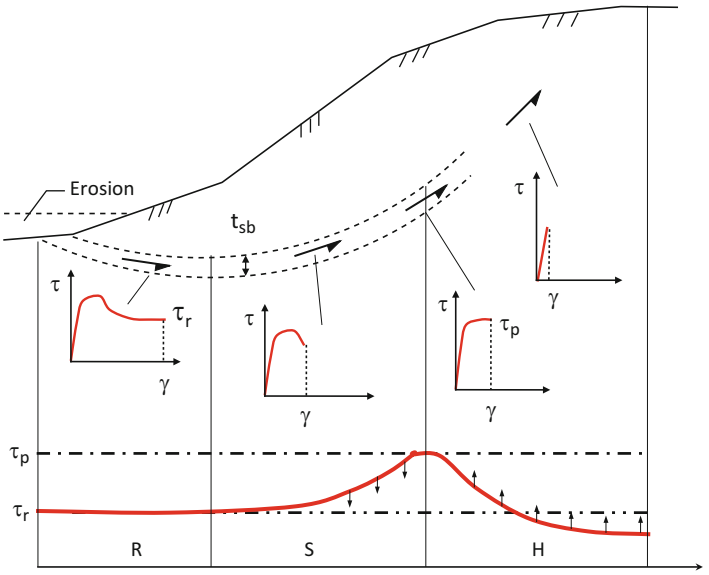

Fig. 16.1 Simplified illustration of a progressive failure mechanism in a slope with strain softening sensitive clay

sustained only by accelerating large soil masses. The progressive failure involves rapid stress and strain redistribution. Very large soil volumes are set into movement more or less simultaneously by this mechanism as shown by Bernander (2011). The initial progressive failure mechanism, i.e. the phase with stress redistribution, may not involve any large geometrical changes of the slope. However, when the slope starts accelerating, large deformations and changes in the slope geometry develop which again might initiate new progressive failures triggered by unloading from retrogression or loading from the weight of the runout debris. On the other hand, large deformations and changes in slope geometry might also stabilize the slope and arrest the progressive failure by counterweight added downslope from ploughing and heave (Puzrin 2016).

16.3 Stress-Strain Characteristics of Sensitive Clay

Sensitive and quick clays have an unstable microstructure and exhibit contracting behaviour and shear induced excess pore pressures u_e during undrained or partly drained shearing. This is shown in Fig. 16.2 which illustrates an undrained triaxial compression test on sensitive clay which has been consolidated to its in-situ effective stresses σ'_{v0} and $\sigma'_{h0} = K_0 \cdot \sigma'_{v0}$ prior to undrained shearing. The shear resistance, here illustrated by the maximum shear stress invariant $\tau_{max} = ½(\sigma_1 - \sigma_3)$, reach a

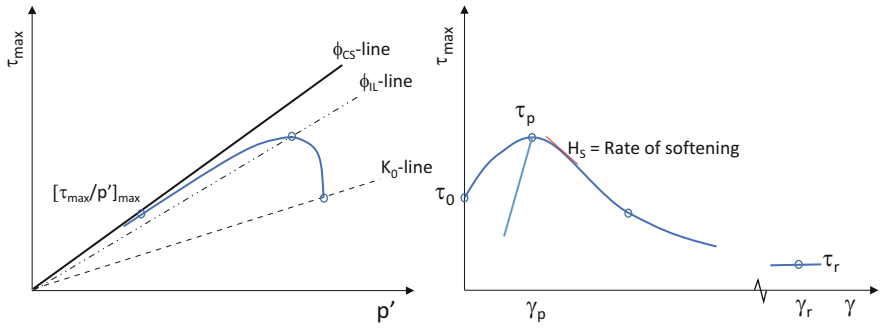

Fig. 16.2 Illustration of stress-strain behaviour of sensitive clay in a CK_0UTC test

peak value τ_p at a shear strain of γ_p followed by a post-peak reduction towards the residual or remoulded shear stress τ_r. The peak state is reached at a critical mobilized friction ϕ_{IL}, defining an instability line, inside the critical state Mohr-Coulomb (MC) failure surface. After passing the peak stress τ_p the shear resistance decreases with increasing plastic shear strain at a softening rate given by the negative modulus H_S as shown in the figure. This reduction of shear resistance is by the authors referred to as strain-softening, however some researchers are not referring to this as strain-softening since the mobilized friction, i.e. the stress ratio $\eta = \tau_{max}/p'$ still increases causing plastic hardening on effective stress basis until the stress path reaches the MC line at the point $\eta_{max} = [\tau_{max}/p']_{max}$. The peak state τ_p and the following post peak strain-softening are obtained without any reduction of the MC effective strength parameters ϕ and cohesion c'. However, it has been demonstrated (e.g. Lade 2002) that the pore pressure induced reduction in shear resistance might lead to instability and failure.

The critical mobilization ϕ_{IL} or stress ratio $\eta_{IL} = [\tau_p/p']$ defines an instability line whereas stress states below this line is stable and stress states above the line is potentially unstable. Stable loading above the instability line is clearly possible by drained loading. The soil will then be in a state where it is stable for drained loading but potentially unstable for an undrained or partly drained disturbance. Since slopes can be highly mobilized in drained loading this is of course of particular interest for landslide mechanisms. Conventional triaxial testing, as illustrated in Fig. 16.2, is carried out at an axial strain rate of about 1.0–2.0%/h. The stress-strain behaviour is however strain-rate dependent with the peak strength typically increasing with 8–17% for every order of magnitude of increase in the shear strain rate (Lunne et al. 2006). The slope of the instability line defined by the stress ratio η_{IL} also increases and move closer to the critical state failure line with higher rates as shown in Fig. 16.3.

Instability is therefore closely related to the rate of loading and for a given strain rate stable loading to a mobilization which is above the instability mobilization for a lower strain rate is possible. If such a state is reached, where after the strain rate

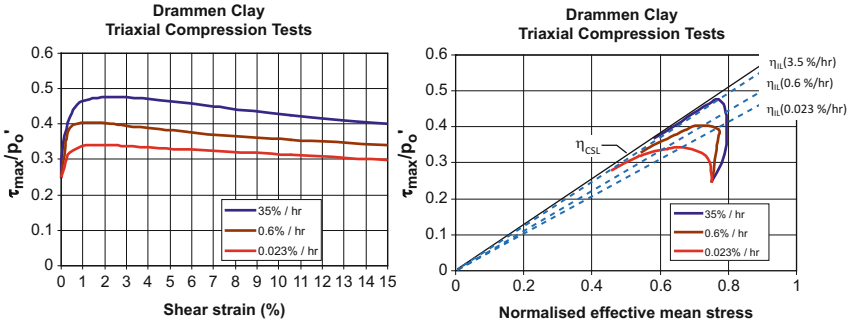

Fig. 16.3 Results from CK_0UTC tests on Drammen clay (w = 50%) from Berre (1973) replotted by Jostad et al. (2006)

decreases, one would expect instability to be reached as well. The rate dependency of the instability regime is thus an essential effect, which probably affects the local instability, strain localisation and also the undrained creep rupture phenomena (Mitchell 1964).

16.4 Localization of Deformation

The instability and progressive failure phenomenon are associated with plastic deformations localising into shear bands. Mechanically this is a consequence of strain softening and the solution of the static equilibrium stability problem becoming non-unique and can be proved mathematically within the framework of continuum mechanics (e.g. Rice and Rudnicki 1980; Nordal and Jostad 1995). The possibility of non-uniqueness and a localised solution can be explained by considering Fig. 16.4. Figure 16.4 illustrates a segment of a slope of thickness H of sensitive strain softening clay being disturbed with a downslope load ΔE in addition to the gravity component E_0. When the external loading causes the slope to reach the peak strength τ_p two solutions are possible. One possibility is a homogenous solution with the entire slope volume deforming uniformly and undergoing strain softening with stresses following points a-b-c in Fig. 16.4a. Another solution, which would also satisfy equilibrium and displacement compatibility, would be that the displacements localise in a zone or shear band of thickness t_{sb}. The clay within this band would strain soften according to points a-b-c′ of Fig. 16.4b, however the clay outside of this band would elastically unload and follow stress points a-b-d in the same figure. The soil within and just outside of the shear band carry the same shear stress, however, almost all the deformation and thus shear strain is concentrated within the shear band. Note that for the same downward slope displacement δ_t, the shear strains within the shear band of the localised solution will be much greater than

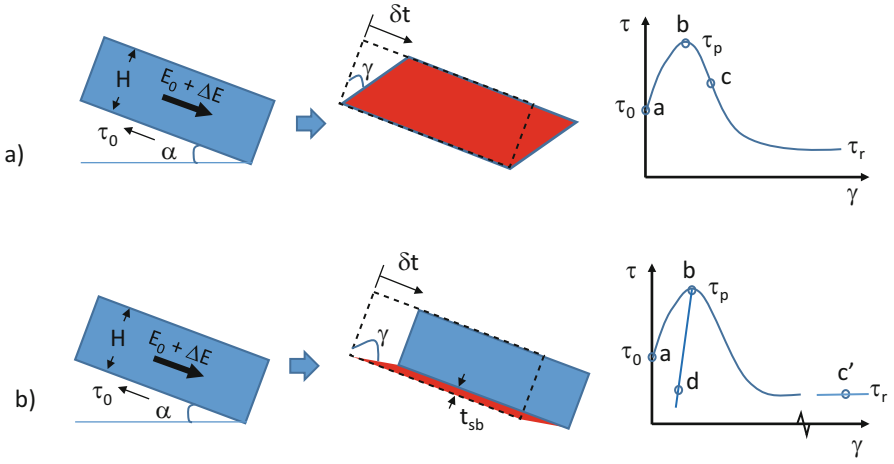

Fig. 16.4 Idealized slope failure (**a**) homogenous and (**b**) localised deformation

for the homogenous solution. The homogenous solution is theoretically possible, however we know that the localized solution is often observed in the field and in some laboratory tests.

The thickness t_{sb} of the shear band strongly affects how fast the strength decreases after the peak strength has been passed and also affects the triggering load ΔE. Figure 16.4b illustrates a situation where all the downward displacement δ_t of the slope is concentrated in a narrow shear band of thickness t_{sb}. The shear strain developing in the shear band becomes $\gamma = \delta_t/t_{sb}$. Let us assume that the slope moves downward at a rate $d\delta_t/dt$ caused by some external loading. It is seen that the rate of shear strain increases with a decreasing shear band thickness t_{sb}. If one, as an example, assumes a shear band thickness $t_{sb} = 1$ cm, a downward displacement of the slope of $\delta_t = 1$ cm would be sufficient to develop $\gamma = 100\%$ shear strain within the band. For such a deformation the clay would have reached it's residual strength as illustrated by point c in Fig. 16.4b. For the homogenous solution much less shear strains would develop for the same displacement. If one considers a slope of thickness H = 1.0 m the shear strain would be $\gamma = 1/100 = 1\%$ as illustrated by point c in Fig. 16.4a. The thickness t_{sb} of the evolving shear bands strongly affects the conditions for an instability state and therefore the triggering load of a potential landslide. Finite element analyses show that the external load, or the necessary triggering disturbance, decreases with decreasing shear band thickness (Jostad and Andresen 2002).

Referring to Fig. 16.5, the total integrated rate of negative second order work within a uniformly deforming shear band of unit length and thickness t_{sb} can be written as $dW = d\tau \cdot d\gamma \cdot t_{sb} \cdot 1$. The rate of strain can be written as $d\gamma = d(\delta t)/t_{sb}$ and the rate of stress $d\tau = H_S \cdot d\gamma$, where δt is the relative displacement across the shear band and H_s is the rate of softening. Hence, the second order work can be

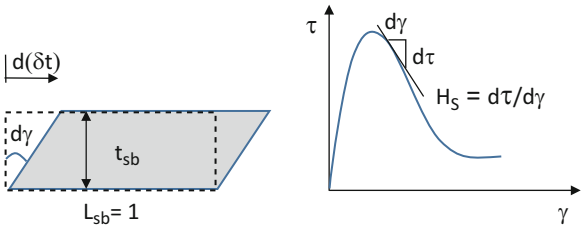

Fig. 16.5 Negative second order work within a shear band of thickness t_{sb} and unit length

written as $dW = H_S \cdot [d(\delta t)/t_{sb}]^2 \cdot t_{sb} = H_S \cdot d(\delta t)^2/t_{sb}$. It is seen that the total negative second order work within the shear band is inversely proportional to the shear band thickness and hence proves that the global instability load decreases linearly with decreasing shear band thickness. For the unrealistic case of a shear band thickness approaching zero the negative second order work goes to infinity and the global instability state will thus be reached when the first material point reaches the peak shear stress, i.e. when the local instability state is reached at one material point. This is clearly not physical and not according to observations.

16.5 Regularization

The formation and development of shear bands and their thickness are essential for understanding and analysing the instability or triggering of landslides of sensitive clays. However, the standard continuum framework does not provide any information on the thickness of the shear band t_{sb} which then theoretically might be reduced to zero or limited by the discretization in finite element analyses. A zero thickness shear band is clearly not physical and does not agree with field and laboratory observations. The shear band thickness t_{sb} of granular materials has been found to be about 10–20 times the mean grain size diameter d_{50} from laboratory testing (e.g. Vardoulakis et al. 1978) and by discrete element modelling (e.g. Gu et al. 2014). By cutting samples after testing, shear band thicknesses of 2–4 mm is reported by Thakur et al. (2006) and 2–8 mm by Gylland et al. (2014) with a decreasing thickness with increasing nominal strain rate. These observed post-test thicknesses are however probably not representative for the shear band thicknesses at onset of localisation at the peak instability point. With a known shear band thickness, methods have been proposed to enhance the continuum theory such that the thickness can be included in the formulation. Techniques to include a finite shear band thickness are called regularization and finite element analyses using such techniques have proved to give mesh independent and defined finite thickness shear bands for granular materials. A nice review of these methods is presented by de Borst et al. (1993) and the non-local strain method has been used by the NGI group (Grimstad et al. 2010). The mechanisms that govern the shear band thickness of sensitive clays are however not fully understood. A hypothesis is that

the thickness is regularized by time dependent effects caused by local pore pressure generation and dissipation in the vicinity of the shear and/or by the rate dependency of the instability state. This hypothesis has been studied by Jostad et al. (2006) and Thakur (2011). The fact that instability and post peak stress reduction is obtained in undrained triaxial testing without any shear band localisation and under more or less uniform deformations supports this view. Conventional undrained triaxial testing is performed at a rate of deformation (0.5–2.0%/h) which is slow enough for pore pressure equalization within the specimen even if global undrained conditions are preserved by the closed valves. It seems that with more or less equal pore pressures over the height of the specimen localisation is prevented. In this case one could argue that the dimensions of the specimen represents the shear band. The work by Jostad et al. (2006) also supports the hypothesis of a shear band being regularized by local pore water flow. The shear band formation in the direct simple shear (DSS) situation is studied using a fully coupled effective stress finite element analysis with a non associated elasto plastic mobilized friction model (MFM) (Nordal et al. 1989). As shown on Fig. 16.6a, this model allows a peak shear stress instability state and subsequent strain softening to be reached within the Mohr-Coulomb critical state line by input of plastic shear strain induced excess pore pressure.

Jostad et al. (2006) found that the local pore pressure flow regularizes the solution and a mesh independent post peak response was obtained. This is in accordance with the experimental findings of Gylland et al. (2014) and experimental and numerical observations by Oka et al. (2005). It can be explained by higher strain rates allowing less time for the pore pressures being generated in the shear band to dissipate into the adjacent soil and by that enlarging the band. It is also found that for a given constant nominal strain rate the thickness t_{sb} is not constant throughout the loading process. The shear band thickness decreases with increasing post peak strain. This can be qualitatively explained by considering that the rate of pore pressure

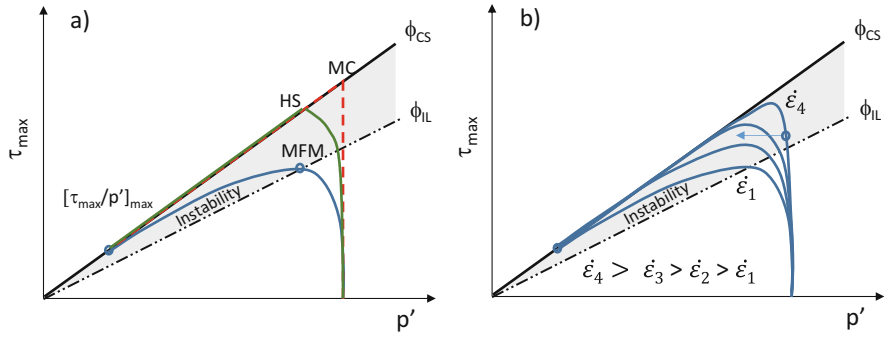

Fig. 16.6 Illustration of stress-strain behavior of the mobilized friction model (MFM) used by Jostad et al. (2006). (**a**) The MFM model compared to the Plaxis Mohr-Coulomb (MC) and Hardening soil (HS) models with negative dilatancy. (**b**) Illustration of the MFM model with rate dependent plastic shear strain

generation decreases with increasing strain and thus the regularization effect would diminish. A few simulations were also done by Jostad et al. (2006) where a strain rate dependency of the mobilized friction was included. The MFM model including strain rate dependency is illustrated on Fig. 16.6b. Localization causes an increasing local strain rate for a constant nominal applied rate of deformation. This local increased strain rate will, according to rate dependent model, reduce the pore pressure generation and allow for higher shear stresses without instability as shown in Fig. 16.6b. Experimental observations by Berre (1973) shown in Fig. 16.3 supports that the slope of the instability lines for clays increases with increasing strain rates. This is in line with the general knowledge that the peak shear stresses of clays increases with increasing strain rate. Thus it is possible to reach a state which is stable for a high strain rate but instable for a lower strain rate. This is shown by Jostad et al. (2006) to add regularization and prevent localization within the height of the specimen, i.e. a homogenous solution was obtained until the critical state line was reached. The hypothesis of shear band regularization by local pore pressure flow was also studied by Thakur (2011) using the Plaxis Mohr-Coulomb (MC) and Hardening soil (HS) models. Pore pressure generation was modelled by a negative dilatancy angle. The MC model was not able to regularize the shear band formation and the thickness t_{sb} clearly became mesh dependent. For the HS model the results indicate a mesh independent shear band thickness at the onset of localization which decreases to a single element size with increasing deformation. The shear band thickness seems however to be related to the size of the initial perturbation of weaker material used to trigger the localisation. It appears that the MC and the HS models are not as successful in regularizing the shear band formation. This is probably due to the fact that these models does not account for an instability point with decreasing shear stress within the MC failure surface. This is illustrated in Fig. 16.6a. Localization is not possible before a material point reach the MC line and the material points not reaching the MC line will undergo elastic unloading irrespective of the increasing pore pressure received from the shear band. This is also shown in Fig. 9 of Thakur (2011).

16.6 Conclusions and Recommendations for Further Research

The process of shear band formation and propagation in sensitive clays is related to local pore pressure generation and dissipation in the vicinity of the shear bands and probably also to the rate dependency of pore pressure generation and the instability states. A proper numerical modelling of the process requires an effective stress model and a fully coupled analysis. Promising results with a regularized shear band formation are obtained with a constitutive model which allows for a region of possible instability states within the MC critical state failure surface and by including rate dependency of the plastic strain and pore pressure generation. Most of

the ingredients for a proper modelling of the instability and shear band localisation associated with the triggering of landslides in sensitive clays seems to have been developed. Further research is however needed to reach a conclusion about the general applicability of the fully coupled analysis with a rate dependent mobilized friction model. The shear band regularization properties of the MFM model with rate dependency should by studied by more finite element analysis of laboratory experiments such as those presented by Gylland et al. (2014) and by boundary value problems such as the progressive landslide failure presented by Andresen and Jostad (2004). The instability region of sensitive clays should also be studied by more experimental and numerical work. One should study the effects of initial water content (void ratio), consolidation stresses, varying strain rates and stress paths.

Acknowledgements Professor Gustav Grimstad at NTNU, Norway is acknowledged for reviewing this paper.

References

Andresen L, Jostad HP (2004) Analyses of progressive failure in long natural slopes. Proc. Num. Models. Geomech.-NUMOG IX, Ottawa, Canada: 603:608

Bernander S (1981) On formation of progressive failures in slopes. Proc 10th ICSMFE, Stockholm 3:357–362

Bernander S (2011) Progressive landslides in long natural slopes. Doctoral Thesis, University of Luleå, Sweden

Berre T (1973) Effect of rate of strain on the stress-strain relationship for undrained triaxial tests on plastic Drammen clay. NGI report No. 50301–4

Bjerrum L (1967) Progressive failure in slopes of overconsolidated plastic clay and clay shales. J Soil Mech Found Eng 93:3–49

De Borst R, Sluys LJ, Mülhaus HB, Pamin J (1993) Fundamental issues in finite element analyses of localization of deformation. J Eng Comput 10:99–121

Grimstad G, Jostad HP, Andresen L (2010) Capacity analysis with the non-local strain approach as regularization technique for strain softening behavior. Proc. 9th HSTAM International Congress of Mechanics, At Limassol, Cyprus

Gu X, Huang M, Qian J (2014) Discrete element modeling of shear band in granular materials. Theor Appl Fract Mech 72(1):37–49

Gylland AS, Jostad HP, Nordal S (2014) Experimental study of strain localization in sensitive clays. Acta Geotech 9:227–240

Hill R (1958) A general theory of uniqueness and stability in elastic plastic solids. J Mech Phys Solids 6:236–249

Jostad HP, Andresen L (2002) Capacity analysis of anisotropic and strain-softeing clays. Proc. Num. Mod. Geomech. – NUMOG VIII, Rome, Italy, 2002

Jostad HP, Nordal S (1995) Bifurcation analysis of frictional materials. Proc. NUMOG V, Davos, Switzerland, 173:179

Jostad HP, Andresen L, Thakur V (2006) Calculation of shear band thickness in sensitive clays. In: Conference: 6th numerical methods in geotechnical engineering, At Graz, vol 1

Jostad HP, Fornes P, Thakur V (2013) Effect of strain-softening in design of fills in gently inclined areas with soft sensitive clays. First international workshop on landslide in sensitive clays. Quebec, Canada.

Lade PV (2002) Instability, shear banding and failure in granular materials. Int J Solids Struct 39:3337–3357

Lunne T, Berre T, Andersen KH, Strandvik S, Sjursen M (2006) Effects of sample disturbance and consolidation procedures on measured shear strength of soft marine Norwegian clays. Can Geotech J 43:726–750

Mitchell JK (1964) Shearing resistance of soils as a rate process. J Soil Mech Found Div, ASCE (90:1): 2961

Nordal S, Jostad HP, Kavli A (1989) A coulombian soil model offshore platform. Proc. 12th ICSMFE, Rio de Janeiro, Brazil.

Oka F, Kodaka T, Kimoto S, Ichinose T, Higo L (2005). Strain localization of rectangular clay specismen under undrained triaxial compression conditions. Research gate

Puzrin M (2016) Simple criteria for ploughing and runout in post-failure evolution of submarine landslides. Can Geotech J 53(8):1305–1314

Rice JR, Rudnicki JW (1980) A note on some features of the theory of localization of deformation. Int J Solids Struct 16:597–605

Skempton AW (1964) Long term stability of clay slopes. Geotechnique 45:321–333

Thakur V (2011) Numerically observed shear bands in soft sensitive clays. J Geomech Geoeng 6:131–146

Thakur V (2014) Experimentally observed shear bands in a Scandinavian soft clay subjected to an undrained shearing under the plane strain condition. Proc. 14th IACMAG Vol. 1, Kyoto, Japan

Thakur V, Grimstad G, Nordal S (2006). In: F Nadim, R Pöttler, H Einstein, H Klapperich, S Kramer (eds.). Instability in soft sensitive clays. Proc. ECI conference on Geohazrads, Lillehammer, Norway

Vardoulakis I, Goldscheider M, Gudehus G (1978) Formation of shear bands in sand bodies as a bifurcation problem. Int J Numer Anal Methods Geomech 2:99–128

Chapter 17
Vibratory Roller Influence Zone Near Slopes with Vibration Susceptible Soils

Jörgen Johansson, Sarah Bouchard, and Jean-Sébastien L'Heureux

Abstract Vibratory rollers transmit vibrations that may lead to pore pressure build up and soil failure in vibration susceptible soils. In a recent incident at Statland in mid Norway, a vibratory roller had compacted a shoreline embankment fill shortly before a submarine landslide was initiated. The landslide triggered a tsunami causing economic damages for several millions NOK. This incident shows the need for guidelines for controlling the effects of construction activity induced vibrations on slope stability. In a follow up study, the effect of vibratory roller compaction on soil degradation has been evaluated with a finite element model. The effect of vibrations varies with parameters such as soil stiffness, bedrock depth and geometry, and presence of thin soft layers. To develop a vibration measurement procedure, we suggest, based on a threshold shear strain of 0.025%, a 15 m wide and 5 m deep influence zone outside of which the soil strength is not reduced. A tentative vibration limit is set to 10 mm/s near slopes with vibration susceptible materials. We also provide some recommendations on how to account for vibratory compaction in slope stability analysis.

17.1 Introduction

A submarine-landslide-triggered tsunami caused economic damages for several millions NOK at Statland, in mid Norway in January 2014. The investigation report concluded that vibrations from a compaction roller likely contributed to the failure (NVE 2014). A vibratory roller is also believed to have caused a landslide in Sweden

J. Johansson
Norwegian Geotechnical Institute, Oslo, Norway
e-mail: Jorgen.Johansson@ngi.no

S. Bouchard (✉)
Department de génie civil et de génie des eaux, Université Laval, Québec, Canada
e-mail: sarah.bouchard.3@ulaval.ca

J.-S. L'Heureux
Trondheim Division, Norwegian Geotechnical Institute (NGI), Trondheim, Norway
e-mail: jsl@ngi.no

V. Thakur et al. (eds.), *Landslides in Sensitive Clays*, Advances in Natural and Technological Hazards Research 46, DOI 10.1007/978-3-319-56487-6_17

in 1990 (Bernander 2011). There are currently no regulations or guidelines for managing the hazard and risk of slope instabilities due to construction activity induced vibrations in Norway. To this end we propose a measurement procedure, a vibration limit, and an influence zone for vibratory compaction close to sensitive slopes. These recommendations are based on results from finite element analyses using Comsol Multiphysics (Comsol 2016). We have evaluated soil strains induced by a typical vibratory roller accounting for the effects of different soil profile characteristics. Based on the numerical result we propose a size of the influence zone and how it can be used in slope stability analysis.

17.2 Vibrations from Vibratory Compaction

Ground vibrations from vibratory rollers transmits large loads to the soil which can cause build-up of pore pressure and reduce soil strength in vibration susceptible soils such as loose silt and sand, and sensitive clays. This should be considered when carrying out construction work near slopes with such soils. The strength reduction is dependent on soil state, load amplitude and number of cycles.

Vibratory roller compaction is performed by passing over the same area up to eight times (NS 3458) which means a soil element is exposed to a large number of vibration cycles. The number of cycles depends on the speed of the roller and the vibration frequency. Vibratory rollers have vibration frequencies between 20 and 40 Hz and both the load amplitude and vibration frequency varies with the type of soil and the thickness of the compacted layer and the speed is usually between 0.5 and 1.5 m/s. E.g. for the case of the Statland landslide (NVE 2014; NGI 2014) a lower estimate was several hundred load cycles.

The vibration amplitude depends on the vibratory roller's dynamic behaviour during the compaction (see e.g. Adam and Kopf 2004; Susante and Mooney 2008). There are various vibration modes, varying from full contact between drum and the substrate, to a chaotically bouncing drum. Jumping is more common at larger load amplitudes and can cause increased vibration amplitudes. Automatic Feedback control systems (AFC) can help to avoid such jumping through changing drum vibration amplitude and/or frequency (TRB 2010).

17.3 Model and Analysis Description

To evaluate the effect of vibratory roller vibrations on sensitive soil deposits, we analysed different cases with a 2D FE-model using Comsol Multiphysics. The analyses are performed in the frequency domain for frequencies up to 40 Hz. To account for the reduction of vibration with distance from the vibratory roller (geometric spreading) the model is axi-symmetric.

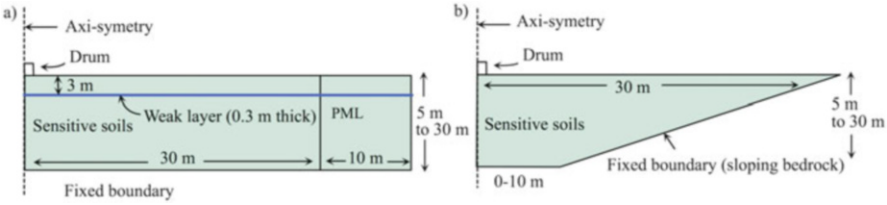

Fig. 17.1 Geometries used in the numerical model

Table 17.1 Overview of material properties used in the 2D axi-symmetric F-E analyses

Soils	Parameters	
Sensitive soils (soft clays or loose sands	Density, ρ	1800 kg/m^3
	Damping, ξ	0.04
	Young modulus, E	53.4 MPa (for constant modulus case), 53.4-z*8.06 MPa (for increasing modulus case)
	Shear wave velocity, V_s	100 m/s (for constant modulus case)
		100–200 m/s (for increasing modulus case)
	Poisson ratio, υ	0.49
Thin weak layer	Thickness	0.3 m
	Shear wave velocity, V_s	50 m/s

The geometries used in the numerical model are shown in Fig. 17.1a,b), while Table 17.1 gives an overview of the soil properties. The soil profile consists of a 30 m wide soil layer on top of a horizontal or sloping stiff bedrock. An absorbing boundary, so called perfectly matched layer (PML), is placed on the right-hand side of the model to avoid unphysical reflections of waves. The thickness of the soil layer was varied between 5 and 30 m.

Based on typical soil stiffness profiles for soft and sensitive Norwegian clays (c.f. (L'Heureux and Long 2016) a soil layer with a constant stiffness (shear wave velocity of 100 m/s) and a soil layer with linearly increasing stiffness with shear wave velocity of 100 m/s at the surface and 200 m/s at 20 m depth were used in the analysis.

Thin soft layers of silt and sand are often present in sensitive soil deposits. To evaluate the effect of such layers within the soil profile, a 0.3 m thick layer with a stiffness reduced to one fourth of the stiffness of the surrounding soil was included in some of cases.

The embankment materials to be compacted where only included in a few of the cases since it was considered a 20–30 cm layer of fill would only have a small effect on the results and that the compaction of the first fill layer would cause the highest strains in the layer with vibration sensitive soils.

The drum of the vibratory roller is modelled as an elastic block fully coupled to the soil, thus jumping cannot occur and the induced vibrations are sinusoidal for each frequency. The vibrations generated by the roller are applied as a boundary load at the bottom of the block. The block has a radius of 0.5 m, height of 1.0 m, and has a mass of 2827 kg.

The Comsol model was verified with the NGI in-house code Laysac (NGI) by comparison of vertical elastic stiffness of a massless plate on an elastic layer. The programs gave the identical stiffness values.

17.3.1 Influence Zone Based on Threshold Strain

Vibration susceptibility of soils can be defined in terms of a threshold cyclic shear strain amplitude necessary to cause a reduction in shear modulus and/or pore pressure build up in water saturated soils. This threshold has been related to the plasticity index of materials. In general, the shear modulus tends to decrease more rapidly with decreasing plasticity index (Vucetic 1994; ISO 2015). Seed (2003) and further work by Bray and Sancio (2006) have shown soils with ratio of water content, w_c, to liquid limit, LL, lower than 0.8 are not vibration susceptible.

The degree of mobilization of a soil element, which will be high in slopes with low factors of safety, affect the vibration susceptibility. The same amplitude of shear strain will for a higher mobilisation degree causes a larger permanent shear strain and pore pressure build-up (Andersen 2015).

Often the vibration susceptible slopes consist of layered soils. Layers with low permeability can prevent the drainage of built-up pore pressure which leads to weak zones in the slope. Case histories and laboratory experiment have shown such a mechanism have large effect on the slop stability (Fiegel and Kutter 1994; Kokusho 2003; Nordal et al. 2009; L'Heureux et al. 2012).

With the above in mind, considering that the plasticity index of Norwegian sensitive clay are often lower than 15% (Karlsrud et al. 2005) and have ratios of water content to liquid limit higher than one, a cyclic shear strain of 0.025% was chosen as threshold. For cyclic strain below the threshold, the soil stiffness is assumed to reduce on the order of 20% or less, and very little pore pressure increase occur. The influence zone is defined as the soil around the vibratory roller with shear strains above the threshold. The soil outside this zone is assumed not to be affected by the vibration. The influence zone is evaluated for the shear strain distribution at typical operating frequencies between 23 and 35 Hz.

17.4 Results

Figures 17.2 and 17.3 show the shear strain distributions induced by a 100 kN load at the top 10 m thick soil profile with constant and increasing soil stiffness with depth. There is a thin soft layer at 3 m depth. Zones in red are above the threshold cyclic shear strain of 0.025%.

17.4.1 Effect of Soil Stiffness, Depth to Bedrock and Thin Layers

The amplification effect due to reflections at the bedrock (resonance) is much smaller for the case of a soil profile having an increasing soil stiffness with depth. For this case, the shear strains also decrease faster with distance from the vibratory roller. The effect of bedrock depth is more pronounced for soil profiles with constant soil stiffness. The depth and width of the influence area is reduced 0.5 m and 1 m, respectively for soil with increasing stiffness compared to a soil layer with constant stiffness.

Results in Figs. 17.2 and 17.3 show that thin soft layers can amplify the strains. The amplification is equal to the ratio of shear moduli outside and inside the thin

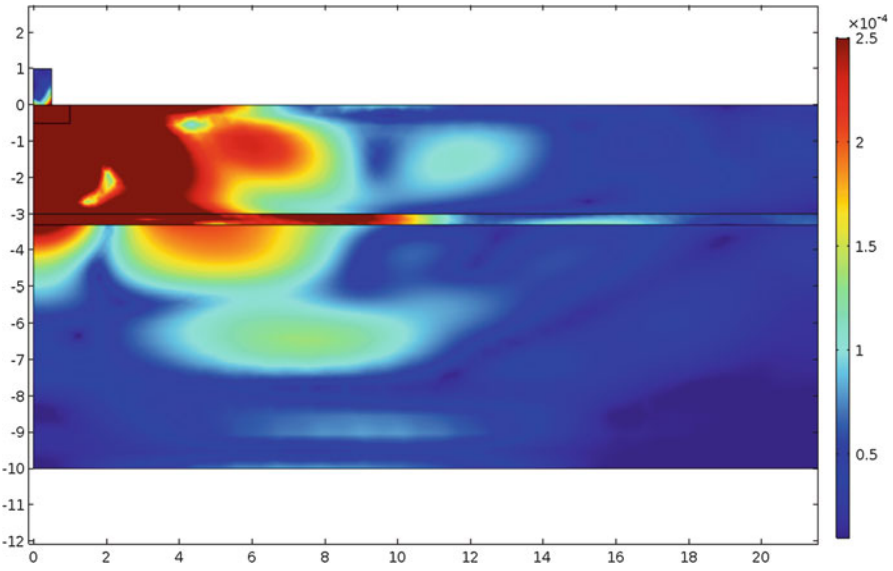

Fig. 17.2 Shear strain distribution induced by a 100 kN load in a 10 m thick soil profile with constant soil stiffness. Zones in *dark red* are above the threshold strain of 0.025%

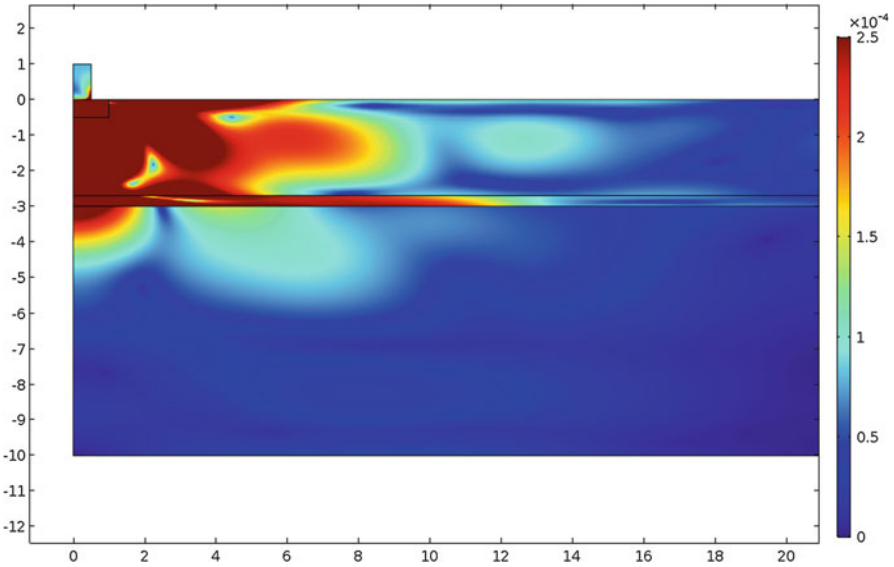

Fig. 17.3 Shear strain distribution induced by a 100 kN load in a 10 m thick soil profile with increasing soil stiffness with depth. Zones in *dark red* are above the threshold strain of 0.025%

layer. The presence of such thin layers has a large effect on the size of the influence zone. In our analyses with a thin layer stiffness of one fourth of the surrounding soil stiffness the width of the influenced zone was doubled.

17.4.2 Effect of Bedrock Morphology

The impact of bedrock morphology was analysed by changing the depth, geometry and slope of the soil/bedrock interface in the numerical simulations. Results show that bedrock morphology has little effect on the resulting size of the influence zone in the cases we have analysed. Bedrock morphology has a larger impact on the vibration amplitude for soil profiles with constant soil stiffness with depth. The vibration amplitudes increase near the areas where bedrock outcrops the model (i.e. ground surface). However, as the depth to bedrock increase, the vibration amplitudes obtained compared well with the horizontal bedrock scenario.

17.4.3 Equivalent Linear Analysis

Soil is a nonlinear material with its stiffness decreasing with increasing strain. Directly beneath the vibratory roller drum the strains are large. To evaluate the effect

of soil nonlinearity on the size of the influence zone, some preliminary analyses with a hyperbolic equivalent linear soil model were done with the same geometry as described above (Fig. 17.1). Typical parameter for the stiffness reduction was based on Darendeli (2001). Compared to the linear elastic models the results indicate a reduction of the vibration amplitude at the drum at resonance with a factor of about three. The frequencies of the resonance decrease due to the reduced soil stiffness. The response and shear strain distribution at typical operating frequencies of 30 Hz are reduced to some extent compared to the linear elastic model. Thus, the width of the influence area is 30% smaller than for the linear elastic models for the specific soil parameters used. Based on the equivalent linear analysis the influence zone was determined to be 15 m wide and 5 m thick.

17.4.4 Effect of a Stiff Layer Under the Drum or in a Wider Area

The confining pressure due to the static weight of the vibratory roller will lead to a temporary increase in soil stiffness under the location of the drum. The volume decrease due soil compaction leads to a permanent increase in stiffness across a wider area. To evaluate this effect, analyses were performed using a stiffer soil in 1–2 m deep and 1 m wide zone directly beneath the drum. The resulting effect on the influence zone size was small.

17.4.5 Effect of Threshold Strain on Influence Zone Size

Since a soil element is subject to very many loading cycles during vibratory compaction, it can be argued that a lower threshold strain should be used to evaluate the influence zone. However, results show that the strain amplitude reduces quickly with distance from vibratory roller and thus an influence zone based on a threshold strain of e.g. 0.01% instead of 0.025% would increase the influence zone with some 20%.

17.4.6 Effect of Vibratory Roller Operating Frequency

The numerical results indicate that the highest vibration amplitudes are in the frequency range of 15–20 Hz. Some vibratory compaction rollers can vary operating frequencies between 23 and 33 Hz in order to compact more efficiently (Volvo 2015; Wersäll 2016). While compaction become more efficient at lower frequencies it can also lead to higher shear strains induced further away from the roller. Results from

the analysis indicate an increase in the width of the influence zone of about 80% when reducing the frequency from 33 to 23 Hz for the same load amplitude. Further studies of the effect of vibration frequency on the induced shear strains are needed.

17.5 Vibration Monitoring and Slope Stability Evaluation

Based on the concept of a threshold strain and the results of the numerical analysis we suggest an influence zone with a width, W, smaller than 15 m and thickness, D, of 5 m with the vibratory roller drum in the center. Such influence zones are shown in Fig. 17.4.

When performing compaction near slopes with vibration sensitive soils we suggest to monitor the vibration amplitudes on the ground surface or at depth of known weak layers. In addition, pore pressure measurements will also be useful to monitor to detect any pore pressure build up, and assess any stability issues.

17.5.1 Vibration Limit

Shear strains decrease with depth and distance from a vibration source. However, due to e.g. irregular geometry of the underlying bedrock, wave reflection can occur which in turn can cause larger strain at certain depths or distances from a given source. Since the location of zones with higher straining also may coincide with weak layers and the number of cycles during compaction is large we suggest to use a vibration limit of 10 mm/s. The vibration amplitude should be measured at the ground surface.

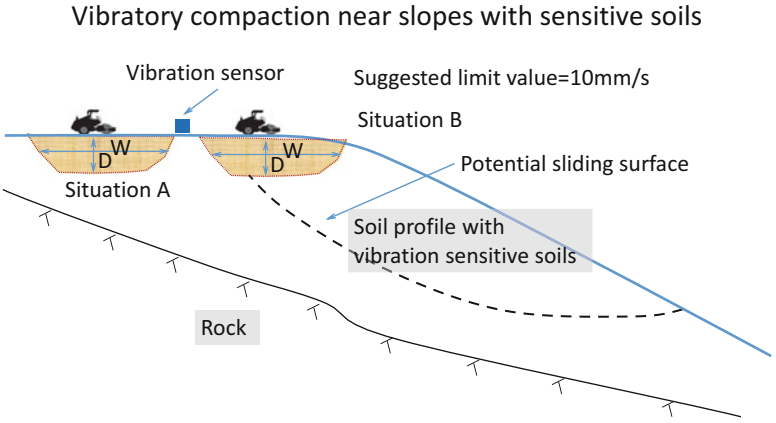

Fig. 17.4 Influence zone of compaction near slopes with vibration sensitive soil

A vibration velocity of 10 mm/s on the ground surface of a soil profile with a shear wave velocity of 100 m/s with a weak layer with a velocity of 70 m/s, induces 0.02% shear strain in the weak layer. For the same vibration velocity of 10 mm/s on the ground surface of a stiffer soil profile with a 150 m/s shear wave speed, the shear strain in the weak layer with 70 m/s shear wave speed would become around 0.03%. Thus a vibration velocity of 10 mm/s on the ground surface would give strains on the order of the threshold strain of 0.025% and we propose to use this as a vibration limit.

17.5.2 Implication for Slope Stability Analysis

It is recommended to reduce the strength of the soil within the influence area when evaluating the effect of vibratory compaction on the stability of a slope. The soil outside the influence area can be considered to have no strength reduction since the influence area is chosen based on cyclic threshold strains. Guidance on selecting a residual strength is available in NVE 2014.

Stability analysis using residual strengths will in many cases lead to very low factors of safety. In such cases it might be difficult to comply with regulations and national standards. This would hence result in unnecessary expensive measures to increase slope stability. As the dynamic loading is a short term effect (i.e. hours or maybe a day), we suggest that the factor of safety (FoS) during such loading case could be lowered to values below those presented in standards. This would be similar to regulations specified for earthquake loading of slopes in sensitive soil (NS-EN 1998-5). Another approach could be to accept a relative improvement of the FoS during the construction period. As for the above, the values of FoS should be decided in accordance with potential consequences and risks a slope failure. As a basis for such a change of regulations in Norway we recommend a parametric study to evaluate the effect of residual strengths on different types of slopes.

17.6 Conclusions and Recommendations

2D finite element analyses were performed to evaluate the volume of soil influenced by vibratory compaction near slopes containing sensitive clays. The zone of influence was defined using a threshold shear strain. Interpretation of the numerical results shows that the influence zone is about 15 m wide and 5 m deep. The soil strength in this zone should be reduced to account for vibratory compaction in slope stability analysis.

To ensure the stability of slopes during vibratory compaction works in sensitive clay terrain, a vibration limit of 10 mm/s is suggested.

Some vibratory rollers can vary the vibration frequency and thus come closer to resonance frequencies. The resonance frequencies are further affected by soil nonlinearity. There are several uncertainties related to the effect of vibration frequency and soil nonlinearity on the vibration amplitudes and thus on the size of the influence zone, and further studies are recommended.

Performing slope stability with residual soil strengths in the influence zone may lead to unnecessary expensive remedial measures. Further evaluation of design guidelines with respect to this is necessary. As basis for discussion a parametric study of the effect of residual strengths on different type of slopes are recommended.

Acknowledgments The cooperative research program «Natural hazards: Infrastructure for Floods and Slides (NIFS)» by the Norwegian Public Roads Administration, the Norwegian National Rail Administration and the Norwegian Water Resources and Energy Directorate is acknowledged for the support. The authors would like to thank Professor Gudmund Eiksund for reviewing this paper.

References

Adam D, Kopf F (2004) Operational devices for compaction optimization and quality control (continuous compaction control & light falling weight device). In: Proceedings of the international seminar on geotechnics in pavement and railway design and construction, Athens, Greece, pp 97–106

Andersen KH (2015) McLelland lecture, cyclic soil parameters for offshore foundation design, frontiers in offshore geotechnics III, Ed. Meyer V., ISBN: 978-1-138-02848-7

Bernander S (2011) Progressive landslides in long natural slopes: formation, potential extension and configuration of finished slides in strain-softening soils. 240 p. Doctoral thesis, Luleå University of Technology

Bray JD, Sancio RB (2006) Assessment of the liquefaction susceptibility of fine-grained soils. J Geotech Geoenviron Eng 132:1165–1177

Comsol Multiphysics (2016) www.comsol.no, version 5.2a

Darendeli MB (2001) Development of a new family of normalized modulus reduction and material damping curves, Ph.D. dissertation, The University of Texas at Austin, August, 2001

Dowding CH (2000) Construction vibrations. pp. 610

Fiegel GF, Kutter BL (1994) Liquefaction induced lateral spreading of mildly sloping ground. J Geotech Eng ASCE 120(12):2236–2243

ISO (2015) Standard, 14837-32, Mechanical vibration – Ground-borne noise and vibration arising from rail systems – Part 32: Measurement of dynamic properties of the ground

Karlsrud K, Lunne T, Kort DA, Strandvik S (2005) CPTU correlations for clays. In: Proceedings of 16th international conference on soil mechanics and geotechnical engineering, Osaka, September 2, pp 693–702

Kokusho T (2003) Current state of research on flow failure considering void redistribution in liquefied deposits. Soil Dyn Earthq Eng 23(7):585–603

L'Heureux J-S, Long M (n.d.) Correlations Between Shear Wave Velocity And Geotechnical Parameters In Norwegian Clays, NGI-report 20150030-04-R, Rev.No. 0/2015-11-02

L'Heureux JS, Long M (2016). Relationship between shear wave velocity and geotechnical parameters for Norwegian clays. J Geotech Geoenv Eng, ASCE. (Accepted for publication) NGI, Laysac code

L'Heureux JS, Longva O, Steiner A, Hansen L, Vardy ME, Vanneste M, Haflidason H, Brendryen J, Kvalstad TJ, Forsberg CF, Chand S, Kopf A (2012) Identification of weak layers and their role for the stability of slopes at Finneidfjord, northern Norway. In: Yamada Y et al (eds) Submarine mass movements and their consequences, advances in natural and technological hazards research, 29th edn. Springer, Dordrecht, pp 321–330

NGI (2014) Vurdering av innvirke av rystelser fra vibrokomprimering og sprengning på skråningsstabilitet. Technical Note 20140347-03-TN. Norwegian Geotechnical Institute, Oslo, Norway. (In Norwegian)

Nordal S, Alen C, Emdal A, Jendeby L, Lyche E, Madshus C (2009) Landslide in Kattamarkvegen in Namsos 13. March 2009. Oslo: Transportation Ministry, Oslo, Report ISBN 978-82-92506-71-4 and ISBN 978-82-92506-72-1

NVE (2014) The landslide at Nord-Statland. Investigation of technical causes. Report nr. 93-2014.ISBN-nr.978-82-410-1042-2, http://www.naturfare.no/_attachment/751994/binary/1007572, in Norwegian

Pistrol J, Kopf F, Adam D, Villwock S, Völkel W (2013) Ambient vibration of oscillating and vibrating rollers. In: Adam C, Heuer R, Lenhardt W, Schranz CH (eds) Proceedings – Vienna Congress on Recent Advances in Earthquake Engineering and Structural Dynamics 2013 (VEESD 2013). ISBN: 978-3-902749-04-8; Paper ID 167

Seed RB et al (2003) Recent advancesin soil liquefaction engineering: a unified and consistent framework. Keynote presentation, 26th annual ASCE Los Angeles Geotechnical Spring Seminar, Long Beach, Californie

Susante PJ, Mooney MA (2008) Capturing nonlinear vibratory roller compactor behavior through lumped parameter modeling. J Eng Mech 134(8):684–693

Transportation Research Boards 2010 Intelligent soil compaction systems, NCHRP report 676, http://www.trb.org/Publications/Blurbs/164279.aspx

Volvo Construction Equipment (2015) SD 115, Single drum compactor, Information brochure

Vucetic M (1994) Cyclic treshold shear strains in soils. J Geotech Eng 120(12):2208–2228

Wersäll C (2016) Frequency optimization of vibratory rollers and plates for compaction of granular soil. http://kth.diva-portal.org/smash/get/diva2:929931/FULLTEXT01.pdf

Chapter 18
Bayesian Updating of Uncertainties in the Stability Analysis of Natural Slopes in Sensitive Clays

Ivan Depina, Cecilia Ulmke, Djamalddine Boumezerane, and Vikas Thakur

Abstract Safety assessment of natural slopes in sensitive clays is subjected to uncertainty due to the natural variation of soil properties, measurement and modelling errors. In order to ensure acceptable safety levels, geotechnical design codes (e.g., Eurocode 7) commonly provide frameworks for a systematic treatment of uncertainties in the safety assessment of a slope. The treatment of uncertainties in the design codes is primarily focused on the parameters directly involved in the analysis of the mechanical stability of a slope (e.g., soil strength parameters). Additional valuable contributions to the safety assessments of slopes can be also provided by information that relates indirectly to the mechanical stability of a slope (e.g., past slope performance). However, there is often a lack of systematic integration of indirect information in the existing design codes. This paper examines the integration of indirect information based on the observed past slope performance in the safety assessment of a slope. The integration is facilitated through the Bayesian framework because it provides a basis to update uncertainties in the slope stability and safety assessment, such that they are consistent to the observed slope performance. The paper examines the effects of slope survival and failure events on uncertainties in the slope stability analysis.

18.1 Introduction

The stability of slopes in sensitive clays is a geotechnical problem of high importance due to the social and economic consequences commonly associated with the corresponding failures. A good appraisal of slope stability provides a basis for

I. Depina (✉)
SINTEF Building and Infrastructure, Rock and Geotechnical Engineering, Trondheim, Norway
e-mail: ivan.depina@gmail.com

C. Ulmke • D. Boumezerane • V. Thakur
Department of Civil and Transport Engineering, Norwegian University of Science and Technology (NTNU), Trondheim, Norway
e-mail: culmke@student.ethz.ch; djamalddine.boumezerane@ntnu.no; vikas.thakur@ntnu.no

V. Thakur et al. (eds.), *Landslides in Sensitive Clays*, Advances in Natural and Technological Hazards Research 46, DOI 10.1007/978-3-319-56487-6_18

the evaluation of hazards and consequences imposed by a potential slope failure. An appraisal of slope stability relies on a wide range of information provided by in-situ and laboratory soil tests, load predictions, engineer's experience, site geology, surveying, past slope performance etc. In order to ensure acceptable safety levels, geotechnical design codes (e.g., Eurocode 7 EU 2004; ISO 2010) commonly provide a systematic framework for the treatment of different information in the evaluation of a slope stability. The focus of the design codes is mainly on the information directly involved in the analysis of mechanical stability of a slope (e.g., soil strength parameters, loads). Conversely, there is often a lack of systematic treatment of information contributing indirectly to the analysis of mechanical stability of slopes, as for example past slope performance.

Despite the large number of international design codes, relatively few provide the necessary framework to integrate the indirect information obtained by past slope performance in the safety assessment of a slope (e.g., ISO 13822 (ISO 2010) and SIA 269/7 (e.g., Brühwiler et al. 2012). When it comes to the stability analysis of sensitive clays, significant efforts on the integration of information based on the past performance were conducted within the Natural hazards, infrastructure, floods and landslides (NIFS) project (e.g., Myrabø et al. 2016). The NIFS project introduced the percentage improvement method (e.g., Oset et al. 2014) to account for indirect information in the safety assessment of a slope. The percentage improvement method adjusts the safety assessment of a slope based on the observed slope performance by considering that a stable natural slope at a given location has a factor of safety of at least one (Oset et al. 2014). The uncertainties are updated implicitly by recalibrating the safety assessment of a slope in terms of the factor of safety. The required safety levels are achieved by implementing a relative (i.e., percentage) improvement to the initially estimated factor of safety. The level of the relative improvement decreases proportionally with the level of agreement between the initially estimated and the observed slope performance in terms of the factor of safety.

In addition to the recalibration of the safety assessment, the information on the observed slope performance can be valuable for risk management, upgrading analysis, repair design and post-failure analysis of slopes. This is based on the consideration that the observed performance of a slope (e.g., survival of a certain load) can be characterized as an outcome of a full-scale test on the slope. In contrast to the percentage improvement method, where the uncertainties in the safety assessment are implicitly accounted for, this paper provides an explicit updating of uncertainties. The explicit updating of the uncertainties is facilitated through the implementation of the probabilistic Bayesian framework. The Bayesian framework is highly flexible in updating uncertainties in engineering systems based on information of the system performance (e.g., Straub and Papaioannou 2014). The framework has a wide range of applications in geotechnical engineering. For example, the application of the Bayesian framework for updating of slope safety assessment based on observed performance was also considered in Gilbert et al. (1998), Luckman et al. (1987), and Zhang et al. (2010). The Bayesian framework

was applied to update uncertainties in the safety assessment and of deep excavations in Hsein Juang et al. (2012) and Papaioannou and Straub (2012). Depina et al. (2016) applied the Bayesian framework to integrate different sources of information in the classification of CPT data. The application of Bayesian updating to dike safety was examined in Schweckendiek et al. (2014).

This study employs the Bayesian framework to examine the effects of information provided by a survival and a failure event on uncertainties in the safety assessment of a slope. In comparison to the previous studies on slope safety assessment this study employs a relatively simple direct Bayesian updating approach, implemented in Schweckendiek et al. (2014). The advantages of the Bayesian framework for updating problems related to the safety assessment of slopes in sensitive clay are examined on numerical examples of a slope in drained and undrained conditions.

18.2 Problem Definition

The stability of a slope is evaluated by a model comprised of a set of equations and boundary conditions that specify material properties, geometry, and loads. Due to the various sources of uncertainty, the parameters of a slope stability model are often subjected to uncertainties (e.g., spatially variable soil properties). Consider an n-dimensional vector of random parameters, $\mathbf{X} = [X_1, \ldots, X_n]^{\mathrm{T}}$ that corresponds to the uncertain parameters in a slope stability model. $\mathbf{X}$ is distributed according to a joint probability density f unction (pdf), $f(\mathbf{x})$, where $\mathbf{x}$ is a realization of $\mathbf{X}$ in the corresponding outcome space, $\Omega_{\mathbf{x}}$. A slope stability model often includes a series of assumptions and simplifications that introduce additional uncertainties in a slope stability analysis. The model uncertainty is commonly modeled by introducing one or more additional random variables to $\mathbf{X}$ (e.g., Straub and Papaioannou 2014).

The aim of this study is to utilize observations of a slope performance to learn about the uncertain parameters in a slope stability analysis. The Bayesian framework can be applied in such problems, because it allows one to update a prior model of uncertainties, $f'(\mathbf{x})$, with observations to a posterior probability distribution, $f''(\mathbf{x})$, as follows:

$$f''(\mathbf{x}) = \frac{L(\mathbf{x}) f'(\mathbf{x})}{\int_{\Omega x} L(\mathbf{x}) f'(\mathbf{x}) \, d\mathbf{x}} \tag{18.1}$$

where $L(\mathbf{x})$ α Pr (Observation | $\mathbf{X}$=$\mathbf{x}$) is the likelihood function, proportional to the probability of observing a given value of model parameters. The evaluation of the likelihood function is one of the central elements in the Bayesian framework. In the case of the Bayesian updating of engineering models, the likelihood function relies on a link between an observed performance and the corresponding model prediction.

Let y denote the observed performance, while $h(\mathbf{X})$ represents the corresponding model prediction. Due to measurement or prediction errors, it is common to detect a certain deviation between the observation and the model prediction, $\varepsilon = y - h(\mathbf{X})$. The deviations are uncertain due to uncertain model predictions and distributed according to a pdf f_ε. The distribution of deviations provides a basis for the construction of the likelihood function as $L(\mathbf{x}) = f_\varepsilon[y - h(\mathbf{x})]$.

Depending on the type of an information provided by an observation, two classes of observations can be defined as follows (e.g., Straub and Papaioannou 2014):

Class 1: Observation providing inequality information (e.g., slope survival corresponds to a factor of safety of larger than one). A model response can be formulated such that the observation is defined as an event $Z = [\mathbf{x} \in \Omega_\mathbf{x} : h(\mathbf{x}) < 0]$. The corresponding likelihood function is $L(\mathbf{x}) = \Pr(Z|\,\mathbf{X} = \mathbf{x}) = I[h(\mathbf{x}) < 0]$, where I is the indicator function that takes the value of one if $h(\mathbf{x}) < 0$, and zero otherwise.

Class 2: Observation providing equality information (e.g., slope failure that corresponds to a factor of safety equal to one). The corresponding likelihood function is defined as $L(\mathbf{x}) = f_{Y|\mathbf{X}}(y|\,\mathbf{x})$, where $f_{Y|\mathbf{X}}(y|\,\mathbf{x})$ is the pdf of the observation given $\mathbf{X}=\mathbf{x}$. Usually, $f_{Y|\mathbf{X}}(y|\,\mathbf{x})$ is specified by f_ε and it is defined as a Gaussian distribution (e.g., Straub and Papaioannou 2014). Implementations of the equality information can be simplified by transforming it into an inequality information. Additional information on the transformation of equality into an inequality information and the proof can be found in Straub (2011).

The posterior distribution, $f''(\mathbf{x})$, is commonly evaluated numerically with the implementation of sampling methods as for example the Markov Chain Monte Carlo (MCMC) or the Bayesian Updating with Structural reliability methods (BUS) methods (Straub and Papaioannou 2014). However, given that the goal of this study is the evaluation of slope safety, the focus is on the effects updating on the slope reliability. The reliability of a slope is commonly evaluated based on its complement, the failure probability, P_F. P_F is calculated as an integral under the joint pdf in the region of the outcome space $\Omega_\mathbf{x}$ known as the failure domain, F:

$$P_F = \Pr(F) = \int_F f(\mathbf{x})\, d\mathbf{x} = \int_{g(\mathbf{x}) \le 0} f(\mathbf{x})\, d\mathbf{x} = \int_{\Omega\mathbf{x}} I[g(\mathbf{x}) \le 0] f(\mathbf{x})\, d\mathbf{x} \qquad (18.2)$$

where I is the indicator function, $g(\mathbf{x})$ is the performance function that has a positive value if the state of a slope is safe for a given realization of random parameters, $g(\mathbf{x}) > 0$, and a non-positive value if the state of a slope is unsafe, $g(\mathbf{x}) \le 0$. Consequently, the failure domain is commonly expressed by the performance function as $F = \{\mathbf{x} \in \Omega_\mathbf{x} : g(\mathbf{x}) \le 0\}$

The information on an observed slope performance can be employed to update P_F, from the initial value based on $f'(\mathbf{x})$, P'_F, to the updated one calculated with $f''(\mathbf{x})$, P''_F. This procedure corresponds to an indirect reliability updating (e.g., Schweckendiek et al. 2014). This paper implements an alternative and simpler approach, known as the direct reliability updating (Schweckendiek et al. 2014).

Given that both the inequality and equality information can be expressed as inequality information, the direct reliability updating utilizes the following relation:

$$P_F'' = P(F|Z) = \frac{P(F \cap Z)}{P(Z)} = \frac{P(\{g(\mathbf{X}) \leq 0\} \cap \{h(\mathbf{X}) < 0\})}{P(h(\mathbf{X}) < 0)} \tag{18.3}$$

where $P_F'' = P(F|Z)$ is the posterior failure probability given an event Z. The advantage of the direct reliability updating is that an estimate of P''_F can be evaluated on a set of samples from the prior distribution, $\mathbf{x}_k \sim f'(\mathbf{x}), k = 1, \ldots, N$ as follows:

$$\widehat{P}_F'' = \widehat{P}(F|Z) = \frac{\sum_{k=1}^{N} I[g(\mathbf{x}_k) \leq 0] \cdot I[h(\mathbf{x}_k) < 0]}{\sum_{k=1}^{N} I[h(\mathbf{x}_k) < 0]} \tag{18.4}$$

Although the effects of updating on $\mathbf{x}$ are not explicitly examined with the direct reliability updating method, $f''(\mathbf{x})$ can be examined empirically based on the subset of samples that satisfies the constraint specified by the observation, $h(\mathbf{x}) < 0$.

18.3 Reliability Updating of an Undrained Slope

Motivated by some recent slope failures in Norway (e.g., Nilsen 2010) this study examines reliability updating of an undrained and drained slopes. Consider a slope of height $H = 25$ m that extends for depth $D = 3$ m until bedrock, as illustrated in Fig. 18.1. The slope closes an angle of $\beta = 14°$ with the horizontal. The height of the water table above the toe, H_w, is a random variable with a beta prior distribution, specified by the mean of 9 m and standard deviation of 0.8 m on the interval [0, H]. An undrained loading condition is examined on the slope to correspond to a situation where a sudden increase in stresses on a soil element within the slope soil mass leads to an increase in pore pressures within the element, while the volume of the element as a whole remains unchanged. Undrained conditions in slope stability analyses occur in low permeable soils (e.g., clay) and after a rapid load application.

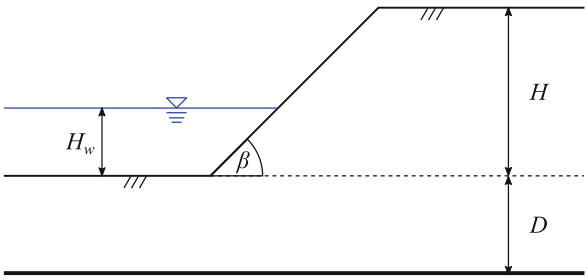

Fig. 18.1 Undrained slope stability analysis

The slope stability analyses in this paper are conducted with the Janbu's direct method (Janbu 1954) that evaluates the factor of safety of a slope based on the stability number, N_o, that is obtained from the Janbu's stability charts (e.g., Janbu 1954):

$$F_S = \frac{N_o s_u \mu_w}{\gamma H - \gamma_w H_w} \tag{18.5}$$

where s_u is the undrained shear strength, specified with a normal prior distribution with the mean of 40 kPa and standard deviation of 5 kPa, $\gamma = 19$ kN/m^3 is the saturated soil unit weight, $\gamma_w = 10$ kN/m^3 is the water unit weight, μ_w is the submergence factor, extracted from the stability charts (Janbu 1954). Uncertainties in the Janbu's method are modeled by an additive model error, ε, which is defined as a normal random variable with the mean of 0.01 and standard deviation of 0.049 (Duncan and Wright 1980).

The set of random variables is defined with mutually independent components as $\mathbf{X} = [s_u, H_w, \varepsilon]^T$. The uncertainties associated with s_u and H_w are subjected to updating as they are considered as reducible, while the uncertainties in ε are considered as unreducible. Based on the prior information, an estimate of the failure probability is calculated to be $\widehat{P}_F' = 0.2847$ with the Monte Carlo method on $5{\cdot}10^5$ samples. The following two cases of reliability updating are considered:

Case 1 Bayesian updating based on the observation of a stable slope with an uncertain measurement of H_w. It is assumed that a measurement of $H_w = 10$ m is made with zero-mean normally distributed measurement error, specified by the standard deviation of 0.2 m. This observation corresponds to an inequality information, as a stable slope implies the value of $F_S > 1$. The updated failure probability is evaluated according to Eq. 18.4 to be $\widehat{P}_F'' = 0.0657$. The observation of a stable slope under these conditions increases the reliability of the slope and favors higher values of s_u as observed from the posterior distributions in Fig. 18.2 and empirically estimated mean and standard deviations in Table 18.1.

Case 2 Bayesian updating based on the observation of a failed slope. This observation corresponds to an equality information as a failed slope implies the value of $F_S = 1$. The equality information is transformed into an inequality formulation. Given that the slope failed (i.e., $P''_F = 1$), the observation of a slope failure provides a valuable information on the most likely combinations of slope parameters that led to the failure. The effect of the observed slope performance on the posterior distribution of random parameters can be examined in Fig. 18.2 and Table 18.1. Given that the updating does not have a significant effect on the distribution of H_w, it can be concluded that the failure of the slope is likely to be associated with relatively low s_u values.

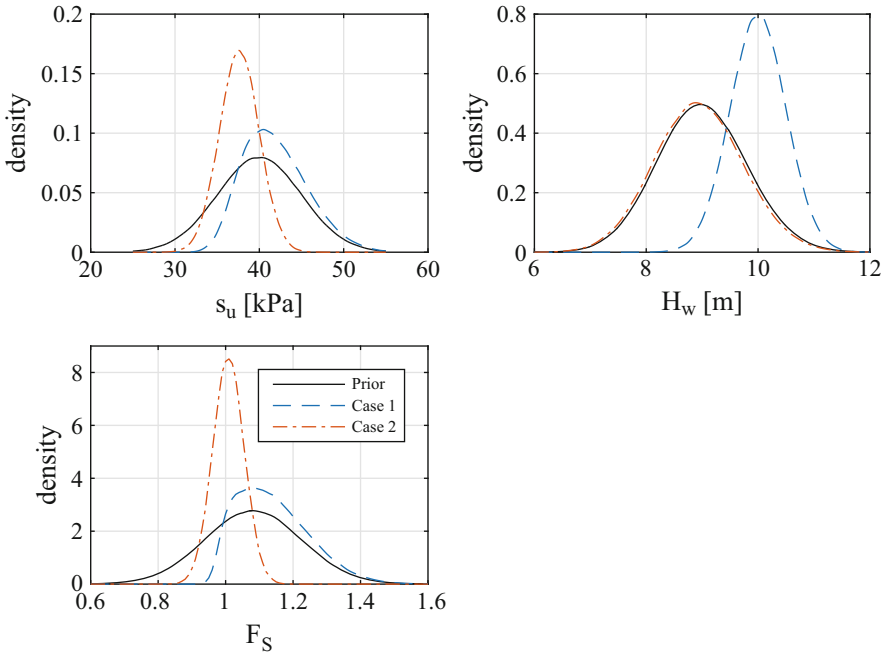

Fig. 18.2 Prior and posterior distributions for different updating cases of the undrained slope problem

Table 18.1 Empirically estimated means and standard deviations for the undrained slope stability updating problem

	Prior		Case 1		Case 2	
Variable	Mean	St. Dev.	Mean	St. Dev.	Mean	St. Dev.
s_u	40.0	5.0	41.90	3.869	37.636	2.353
H_w	9.0	0.8	10.0	0.2	8.945	0.791
F_S	1.082	0.144	1.140	0.107	1.01	0.049

18.4 Reliability Updating of a Drained Slope

Drained loading conditions occur in slopes after sufficient time has passed from a load application such that the generated excess pore pressures are dissipated. The analysis of slope stability in drained conditions is conducted with the Janbu's direct method (Janbu 1954). The geometry of the studied drained slope is illustrated in Fig. 18.3 with $H = 17$ m and $\beta = 20°$. When compared to the undrained slope stability analysis in Fig. 18.1, the drained analysis features a groundwater table at

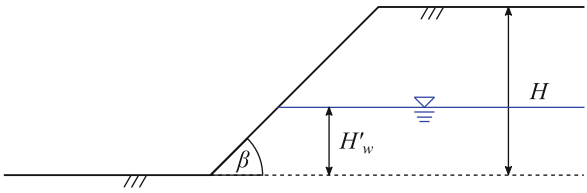

Fig. 18.3 Drained slope stability analysis

height H'_w above the toe instead of a general water Table. H'_w is specified with a prior beta distribution with the mean of 13 m and standard deviation of 1 m.

The direct Janbu's method (Janbu 1954) evaluates the factor of safety of a slope for drained conditions as follows:

$$F_S = \frac{N_{cf}\left(\lambda_{c\phi}\right) c}{\gamma H}; \quad \lambda_{c\phi} = \frac{\gamma H - \gamma_w H'_w}{\mu'_w c} \tan\phi \tag{18.6}$$

where N_{cf} is the stability number as a function of $\lambda_{c\phi}$, μ'_w is the water seepage factor. Both N_{cf} and μ'_w are extracted from the charts associated with the direct Janbu's method (Janbu 1954). c is cohesion, specified by a lognormal prior distribution with the mean of 10 kPa and standard deviation of 4 kPa, ϕ is the friction angle, distributed according to a normal prior with the mean of 20° and standard deviation of 5°, $\gamma = 19$ kN/m^3 is the saturated soil unit weight. Uncertainties in the Janbu's method are modeled by an additive model error, ε, which is defined as a normal random variable with the mean of 0.01 and standard deviation of 0.049. The set of mutually independent random variables is defined as $\mathbf{X} = \left[c, \phi, H'_w, \varepsilon\right]^T$. The uncertainties associated with c, ϕ, and H_w are subjected to updating as they are considered as reducible, while the uncertainties in ε are considered as unreducible.

Based on the prior information, an estimate of the failure probability is calculated to be $\widehat{P}'_F = 0.5036$ with the Monte Carlo method on $5{\cdot}10^5$ samples. As defined for the undrained slope stability analysis, the following two cases of Bayesian updating are considered:

Case 1 Bayesian updating of a drained slope based on the observation of a stable slope with an uncertain measurement of H'_w.

It is assumed that a measurement of $H'_w = 12$ m is made with a zero-mean normally distributed measurement error, specified by the standard deviation of 0.2 m. The updated failure probability is evaluated according to Eq. 18.4 to be $\widehat{P}''_F = 0.1874$. The observation of a stable slope increases the reliability of the slope and favors higher values of c and ϕ as observed from the posterior distributions in Fig. 18.4 and empirically estimated mean and standard deviations in Table 18.2.

Case 2 Bayesian updating based on the observation of a failed slope.

This observation corresponds to an equality information, as a failed slope implies the value of $F_S = 1$. From Fig. 18.4 it can be observed that the failure of the slope is likely to be associated with slightly lower c values, and ϕ values centered on the mean. The updating does not have a significant effect on the distribution of H'_w.

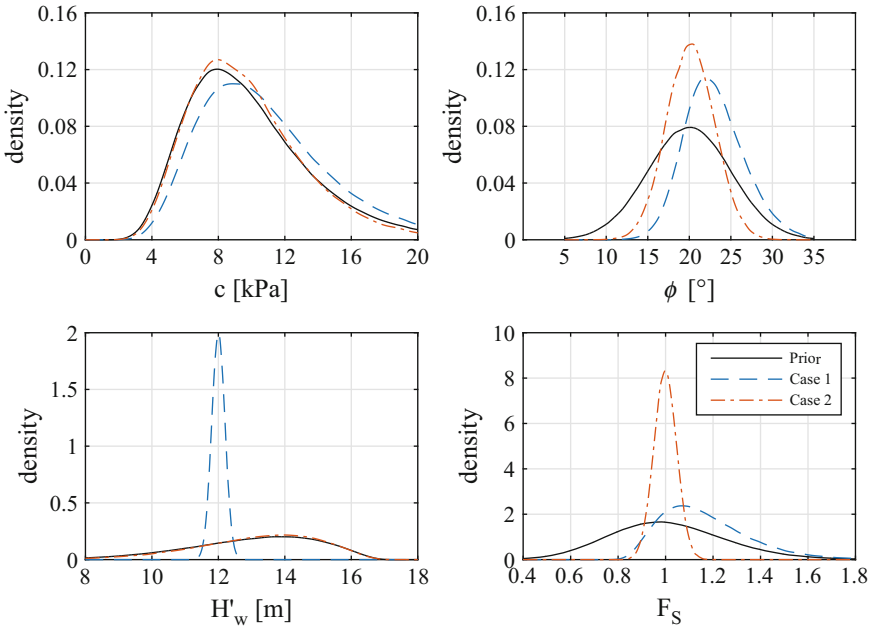

Fig. 18.4 Prior and posterior distributions for different updating cases of the drained slope problem

Table 18.2 Empirically estimated means and standard deviations for the drained slope stability updating problem

	Prior		Case 1		Case 2	
Variable	Mean	St. Dev.	Mean	St. Dev.	Mean	St. Dev.
c	10.0	4.0	10.994	4.252	9.775	3.529
ϕ	20.0	5.0	23.019	3.641	20.166	2.879
H'_w	13.0	2.0	12.0	0.2	13.145	1.868
F_S	1.012	0.249	1.167	0.188	1.01	0.049

18.5 Conclusion

The results of the conducted study demonstrated that the Bayesian framework can efficiently integrate information on observed slope performance in the safety assessment of a slope. The Bayesian framework provides a basis to explicitly update uncertainties in the safety assessment of a slope, such that they conform to the observed slope performance. The updating process is flexible and can be adapted to different types of observed information, as demonstrated by the analysis of slope survival and failure events. The application of the Bayesian framework can be further extended to consider different sources of uncertainty in slope stability

analysis, spatial variability of soil properties, upgrading and repair works, code calibration, and implications on the risk management of slopes.

Acknowledgments The authors gratefully acknowledge the valuable comments and suggestion provided by the reviewer Thi Minh Hue Le and the financial support by the Research Council of Norway and several partners through the research Centre SFI Klima 2050.

References

Brühwiler E, Vogel T, Lang T, Lüchinger P (2012) Swiss standards for existing structures. Struct Eng Int 22(2):275–280

Depina I, Le TMH, Eiksund G, Strøm P (2016) Cone penetration data classification with Bayesian mixture analysis. Georisk: AssessManag Risk Eng Syst Geohazards 10(1):27–41

Duncan J, Wright S (1980) The accuracy of equilibrium methods of slope stability analysis. Eng Geol 16(1–2):5–17

EU (2004) EN 1997-1 (2004): Eurocode 7: geotechnical design *Part 1: General rules* (Vol. Regulation 305/2011, Directive 98/34/EC, Directive 2004/18/EC)

Gilbert RB, Wright SG, Liedtke E (1998) Uncertainty in back analysis of slopes: Kettleman Hills case history. J Geotech Geoenviron 124(12):1167–1176

Hsein Juang C, Luo Z, Atamturktur S, Huang H (2012) Bayesian updating of soil parameters for braced excavations using field observations. J Geotech Geoenviron 139(3):395–406

ISO (2010) ISO 19822:2010 Bases for design of structures. Assessment of existing structures

Janbu N (1954) Stability analysis of slopes with dimensionless parameters. Harvard University, Division of Engineering and Applied Physics

Luckman P, Der Kiureghian A, Sitar N (1987) Use of stochastic stability analysis for Bayesian back calculation of pore pressures acting in a cut at failure. Paper presented at the Proc., 5th Int. Conf. on Application of Statistics and Probability in Soil and Struct Engr

Myrabø S, Viklund M, Øvrelid K, Øydvin EK, Petkovic G, Humstad T, Aunaas K, Thakur V, Dolva BK. (2016). *NIFS – sluttrapoprt*. Retrieved from http://www.naturfare.no/_attachment/1304535/binary/1101879

Nilsen T (2010) Ett år siden raset i Namsos. *NRK*. Retrieved from https://www.nrk.no/trondelag/ett-ar-siden-raset-i-namsos-1.7030089

Oset F, Thakur V, Dolva B, Aunaas K, Sæter M, Robsrud A,... Jensen O (2014) Regulatory framework for road and railway construction on the sensitive clays of Norway *Landslides in Sensitive Clays* (pp. 343–353): Springer.

Papaioannou I, Straub D (2012) Reliability updating in geotechnical engineering including spatial variability of soil. Comput Geotech 42:44–51

Schweckendiek T, Vrouwenvelder A, Calle E (2014) Updating piping reliability with field performance observations. Struct Saf 47:13–23

Straub D (2011) Reliability updating with equality information. Probab Eng Mech 26(2):254–258

Straub D, Papaioannou I (2014) Bayesian updating with structural reliability methods. J Eng Mech 141(3):04014134

Zhang J, Zhang L, Tang WH (2010) Slope reliability analysis considering site-specific performance information. J Geotech Geoenviron 137(3):227–238

Chapter 19
Potential Landsliding at the North Spur, Churchill River Valley

Denise Leahy, Régis Bouchard, and Serge Leroueil

Abstract The North Spur is a piece of land acting like a natural dam whose stability is crucial for the Muskrat Falls hydroelectric project. Stabilization measures have been designed to improve its stability taking into account the presence of sensitive clay. This paper discusses the potential landsliding at this site and presents the methodology used to study the progressive failure mechanisms which could impact the stability of the North Spur.

19.1 Introduction

Forming part of the Lower Churchill Project (LCP) in Newfoundland and Labrador, Canada, the Muskrat Falls Hydroelectric Development is located on the Churchill River. The installed capacity of the facility will be 824 MW. Presently, the water elevation in the river is about at 17 m on the upstream side and at 3 m on the downstream side of the Muskrat Falls. After impoundment at Full Supply Level (FSL), the upstream water level will be at 39 m in elevation.

The North Spur is a marine and estuarine sediments deposit which naturally provides a partial closure of the river at the Muskrat Falls site. This natural closure needs to be maintained and improved for the life of the project. It is about 1 km long between the Rock Knoll in the south and the Kettle Lakes in the north which represent natural boundaries in terms of both seepage and stability (Fig. 19.1).

The lower Churchill River valley shows numerous landslide scars and a major slide on the downstream face of the Spur, in November 1978 (see Fig. 19.1), revealed the fragility of this natural deposit and its susceptibility to toe erosion.

D. Leahy (✉) • R. Bouchard
SNC-Lavalin, Montréal, QC, Canada
e-mail: Denise.Leahy@snclavalin.com; Regis.Bouchard@snclavalin.com

S. Leroueil
Département de génie civil et de génie de eaux, Université Laval, Québec City, QC, Canada
e-mail: Serge.Leroueil@gci.ulaval.ca

V. Thakur et al. (eds.), *Landslides in Sensitive Clays*, Advances in Natural and Technological Hazards Research 46, DOI 10.1007/978-3-319-56487-6_19

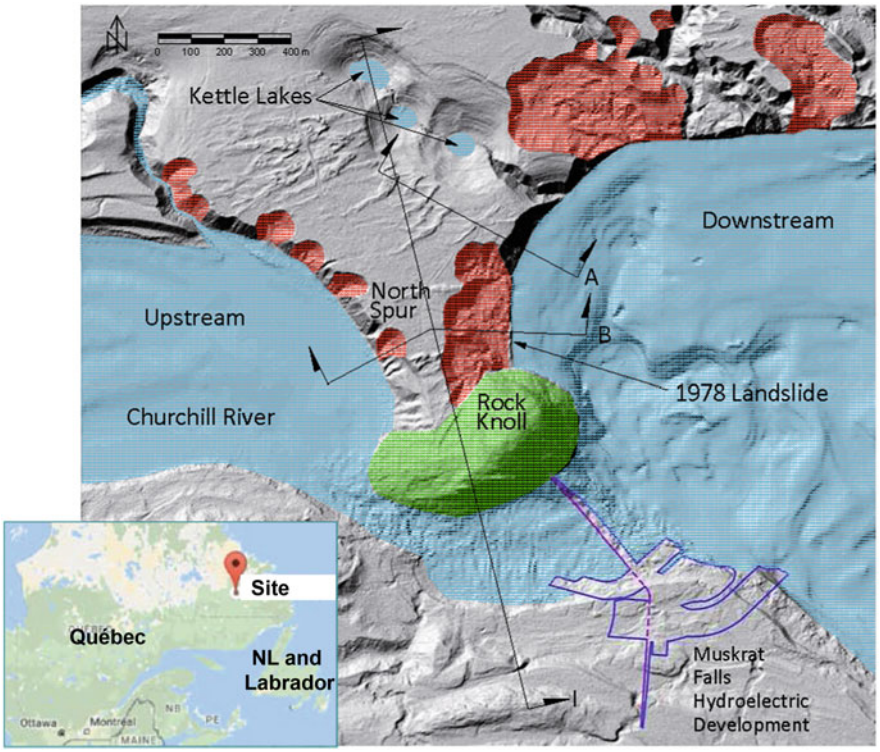

Fig. 19.1 Plan view of the North Spur Site

19.2 Geology and Geotechnical Characteristics

The Muskrat Falls site is underlain by Precambrian rock. Outcrops occur along both sides of the river in addition to the Rock Knoll.

As illustrated on Fig. 19.2, the present river channel has eroded a bedrock based channel, south and around the rock knoll, and about 1 km south of a buried preglacial valley which underlies the northern part of the Spur. In the Spur, about 140 m of glacial sands, gravels and boulders infill the lower part of the preglacial buried valley. Following deglaciation, sea level rose and submerged the Churchill River valley up to about elevation 80 m; abundant sediments carried into this estuary resulted in the deposition of thick marine clay and estuarine silty sand deposits. Isostatic rebound following deglaciation caused gradual recession of the sea and resulted in the deposition of fine sand deposits over the underlying marine clay sediments (SLI-AGRA 1998).

Most of the current knowledge of the Spur stratigraphy and the soil characteristics are derived from investigation campaigns carried out in 1979 and 2013. Hydrogeological information was obtained from pumping tests, piezometer

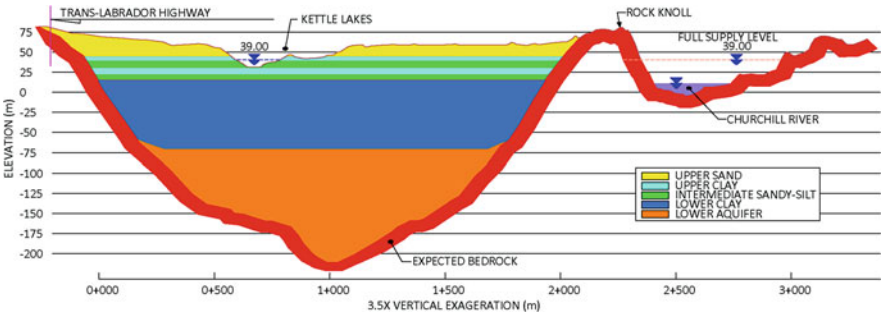

Fig. 19.2 North spur simplified stratigraphic longitudinal section (Section I-I of Fig. 19.1)

readings and in-situ permeability tests. A simplified stratigraphic interpretation (see Fig. 19.2) was developed (SLI 2016), from ground surface to the bedrock level:

- Upper sand, from elevation 60 m to elevation 45 m;
- Stratified drift, including two layers of silty sand/sandy silt and two layers (top and bottom) of clay material (Upper Clay), from elevation 45 to 15 m;
- Lower marine clay (Lower Clay), generally from elevation 15 m to −70 m;
- Lower aquifer (pervious sand and gravel layer), generally from elevation −70 m to bedrock (down to −210 m).

The Upper Clay is a low to medium plastic, sensitive, stiff to very stiff silty clay to clayey silt material observed within the stratified drift. The Liquidity Index (I_L) is generally above unity (average 1.4) and the in-situ undrained shear strength from vane shear tests (VST) of 40–120 kPa indicates clay material of firm to very stiff consistency in intact condition. Average shear strength parameters of $\phi' = 31°$ and $c' = 6$ kPa were interpreted from Triaxial test and Direct Shear Test (DST) results.

The Lower Clay layer is located below the stratified drift and above the lower aquifer (lower sand and gravel layer). This layer consists of clay of low to medium plasticity which exhibits values of I_L lower than the upper clay layer and can be classified as slightly sensitive. The consistency of clay is stiff to very stiff with in-situ undrained shear strength of 70–200 kPa.

Piezocone and VST tests performed at the North Spur indicate that the undrained shear strength (Su) at a given elevation is generally similar throughout the North Spur. Below the crest of the Spur, Su appears to be equal to or somewhat lower than 0.20 σ'_v where σ'_v is the effective vertical stress. It should be noted that some lower Su values were measured below the slide debris in areas subjected to previous slides. These are interpreted as an indication of local remolding due to unloading and plastification of the material below the toe.

The same information in terms of estimated preconsolidation pressure generally indicates normally consolidated conditions (OCR near 1.0) under the crest of the Spur and an OCR of about 3–15 at the toe of the slope, confirming that the upstream and downstream sides of the Spur have resulted from erosion.

19.3 Landslides and Stabilization Works for the North

A major landslide occurred in November 1978 on the downstream side of the North Spur (see Fig. 19.1); it involved about 1 million m^3 of soil. The maximum retrogression distance from the original slope crest was slightly less than 200 m. The slide involved movement of a block along weak layers within the stratified drift, followed by retrogressive flowslides. Limit Equilibrium slope stability analyses performed 2 years before the landslide had shown an effective stress safety factor close to unity. In 1982, considering that the North Spur was threatened by such potential landslides, a series of drainage wells were installed on its South side.

As part of the reservoir retention works at Muskrat Falls, stabilization works for the North Spur (SLI 2016) were projected as illustrated in plan view on Fig. 19.3 and for a typical upstream section on Fig. 19.4. These works include measures for (1) local unloading of the upper part of the Spur, (2) control of the groundwater (cement bentonite cut-off walls, till blanket barrier), (3) erosion protection on both sides of the Spur and (4) downstream finger drains. Due to the installation of cut-off walls, till blanket and finger drains, the normal water level below the crest on the upstream side of the Spur is expected to drop.

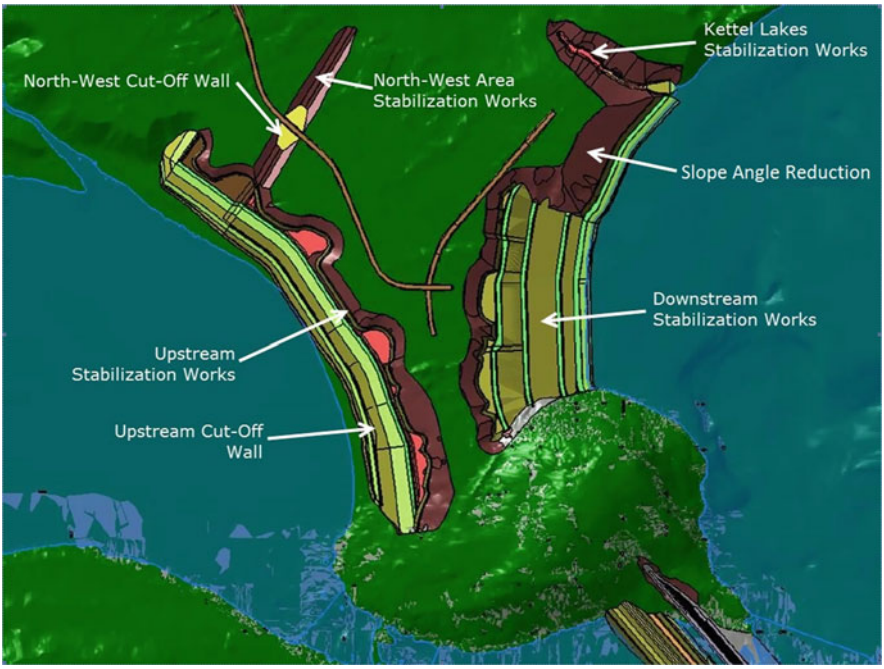

Fig. 19.3 Stabilization works of North Spur slopes (sketch)

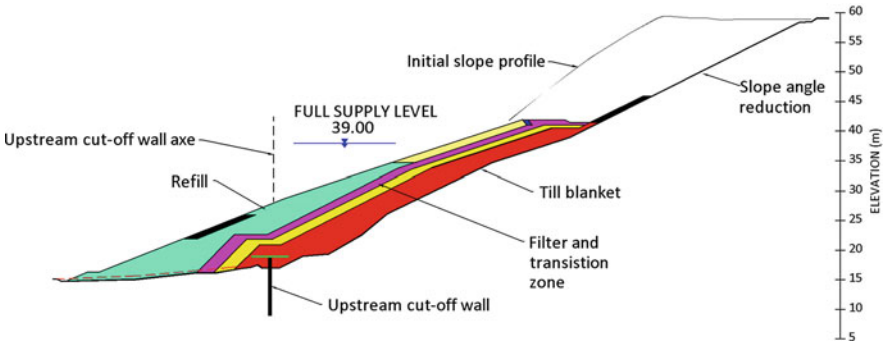

Fig. 19.4 Stabilization works – typical for upstream slope

19.4 General Considerations on Landsliding Potential

There are hundreds of landslides in sensitive clays every year in Eastern Canada, most of them, simple small size landslides. Most of the largest ones (>1 ha) are classified as flowslides and spreads. According to Demers et al. (2014), in the Province of Quebec, 58% of the large landslides are flowslides, 37% are spreads and the remaining 5% are of another type or intermediate.

Flowslides result from a succession of slides. If the backscarp of a slide is unstable either in undrained or partly drained conditions, there will be another failure. And the process may go on and on. To get a flowslide in sensitive clays, there are four requirements (Tavenas 1984; Leroueil et al. 1996):

- An initial slope failure: no first failure, no flowslide.
- Enough potential energy to remould the clay: experience shows that $\gamma H/S_u$ must be larger than a value that increases from about 3 in low plasticity clays to about 7 or 8 in clay with a plasticity index of 40, where γ is the unit weight of the material and H is the height of the slope.
- Once remoulded, the clay must be able to flow outside the crater. This is reached if $I_L > 1.2$ or $S_{ur} < 1$ kPa (Lebuis et al. 1983).
- A topography which permits the evacuation of the liquefied debris.

Spreads result from a different process, a progressive failure over a quasi-horizontal surface near the level of the toe of the slope. If there is a slope as that shown in pale grey in Fig. 19.5a, the shear stress τ_{0x} along such a surface may be as shown by the dashed line on Fig. 19.5b. If there is erosion or a small landslide at the toe of the slope (Case 1 in Fig. 19.5a), the shear stress along the horizontal surface may increase, as shown by τ_{1x}, and reach the peak undrained shear strength τ_p of the clay. If the clay is sensitive, the failure may then progress inward over a large distance, and the soil above dislocates in horsts and grabens. This is the most common case of spreads observed in Eastern Canada (Locat et al. 2011, 2015).

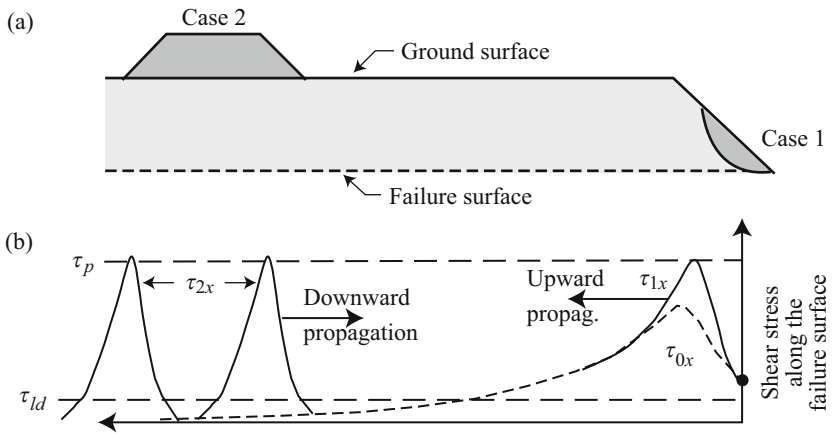

Fig. 19.5 Schematic representation of upward progressive failure (Case 1) and downward progressive failure (Case 2)

Another type of landslide resulting from progressive failure is the downward progressive failure observed in Scandinavia and described by Bernander (2000) and Locat et al. (2011). If loading or piling at the top of a slope is such that the undrained shear strength of the clay is reached (schematically represented by Case 2 in Fig. 19.5a), progressive failure may be triggered, and a failure surface may progress towards the toe of the slope and generate a landslide. In all cases, there is progressive failure because the peak strength has been reached somewhere.

So, avoidance of an initial slope failure in general and avoidance that the shear stress may reach somewhere in the slope the peak strength initiating progressive failure should eliminate the possibility of retrogressive landslides at the North Spur. It is these principles that have been followed for the design of the stabilization works.

19.5 Landslide Potential at North Spur

The lower Churchill River valley shows numerous landslides scarps on both river banks, upstream and downstream from the Muskrat Falls site. Most of these landslides show characteristics of flowslides. Yet, the stability of the slopes of the North Spur was examined for simple landslides and for the three types of large landslides (flowslide, upward and downward progressive failure).

Simple Landslide and Flowslide: For the Upper Clay top layer, typical characteristics are: S_u about 45 kPa; $\gamma H/S_u$ about 7; and I_L about 1.4. For the Upper Clay bottom layer, typical characteristics are: S_u about 60 kPa; $\gamma H/S_u$ about 10; and I_L average 1.4 (greater than 1.0). So, if a first-time failure occurs, there could be

retrogression and flowslide; the 1978 landslide confirms that possibility. The Lower Clay layer found below elevation 15 m has a typical I_L of 0.6. Thus, even if there would be a first failure in this unit, retrogression and flowslide are not expected.

Used with appropriate strength parameters, LEM (Limit Equilibrium Method) have been shown over the last 40 years or so to give representative factors of safety for simple landslides in Eastern Canada sensitive clays. For the North Spur, the stability of rotational landslides was examined through LEM stability analyses in terms of effective stresses (Lefebvre 1981; Tavenas and Leroueil 1981) for the most critical current conditions (Section A-A on Fig. 19.1) where the slope had a height of about 55 m at 1V:1,65H. The safety factor from LEM calculations is near the unity, confirming calculations done in 1976. Stabilization works for all the slopes of the Spur have been designed to achieve a factor of safety of at least 1.5 against a "first slide". In the critical area around Section A-A (Figs. 19.1 and 19.3), the stability of the slope has been improved due to improved drainage and a reduction of the slope inclination to 1V:2,5H.

Progressive Failure Landslide: The North Spur clays are sensitive and thus present strain softening behaviour that could generate progressive failures. However, there is no approved and standardized method to estimate in advance a safety factor against such a slide. Cases presented in literature are related to landslides that have already occurred and are examined through back calculation analyses.

A methodology for the numerical back analysis of progressive failures has been developed by Locat et al. (2013, 2015) and tested on different landslide events. For analyzing the pre-failure conditions, they compare the initial shear stress along a potential horizontal failure surface with the shear strength of the clay. The basic idea is to keep the shear stress far from the strength.

For the North Spur, planned stabilization works will increase the slope stability and thus reduce the initial shear stress that should become smaller compared to the soil shear strength. They will also reduce disturbance potential at the toe of the slopes. And, to avoid downward progressive failure, precautions will be taken to prevent any uphill disturbance (loading at the crest, piling, etc.). It is thus expected that stabilization works will eliminate the potential of progressive failure and failure in general. To quantify this improvement, specific stress distribution modeling was performed for the slopes of the North Spur. First, the steepest slope of the North Spur (Section A-A on Fig. 19.1) was analyzed to define the presently mobilized shear stress in the clay layers and thus a minimum strength for the soil that will be considered thereafter as a reference strength. Then, the conditions for stabilized sections at various locations were analyzed and compared with this reference strength. This is considered conservative since the reference strength may be smaller than the real strength of the soil.

Stress Distribution Analyses were performed using Sigma/W, the 2D Finite Element module of the GeoStudio Suite (GeoSlope International 1991–2014). Elastic-plastic behavior was assumed and Mohr-Coulomb yield criteria were used as yield functions. Four different stages were analyzed: flat ground conditions prior

to river erosion upstream and downstream the Spur, present conditions, conditions at the end of stabilization works and conditions after reservoir infilling.

The shear modulus, G, was selected mainly based on shear wave velocity, V_s, from seismo-piezocone tests performed on the North Spur. For the clay layers, the Poisson's ratio for the initial flat ground conditions was selected to produce a stress ratio, K_0 value equal to $(1 - \sin \phi')$ typical of normally-consolidated conditions. For the following stages, the Poisson's ratio was reduced to 0.25, a value used by Locat et al. (2015) for unloading.

Reference Case: The first analysis has been performed for the existing conditions at section A-A where the natural slope is the most abrupt but still stable. The results are presented in Fig. 19.6 for two horizontal shear surfaces, one in the Upper Clay at elevation 20 m and one in the Lower Clay at elevation −10 m. Assuming a safety factor at least 1.0 for the present conditions, the maximum mobilized shear stress before stabilization (shown in red on the shear stress profiles of Fig. 19.6) becomes the reference strength available along horizontal shear surfaces for the site: 162 kPa at elevation 20 m and 188 kPa at elevation −10 m. These values are significantly

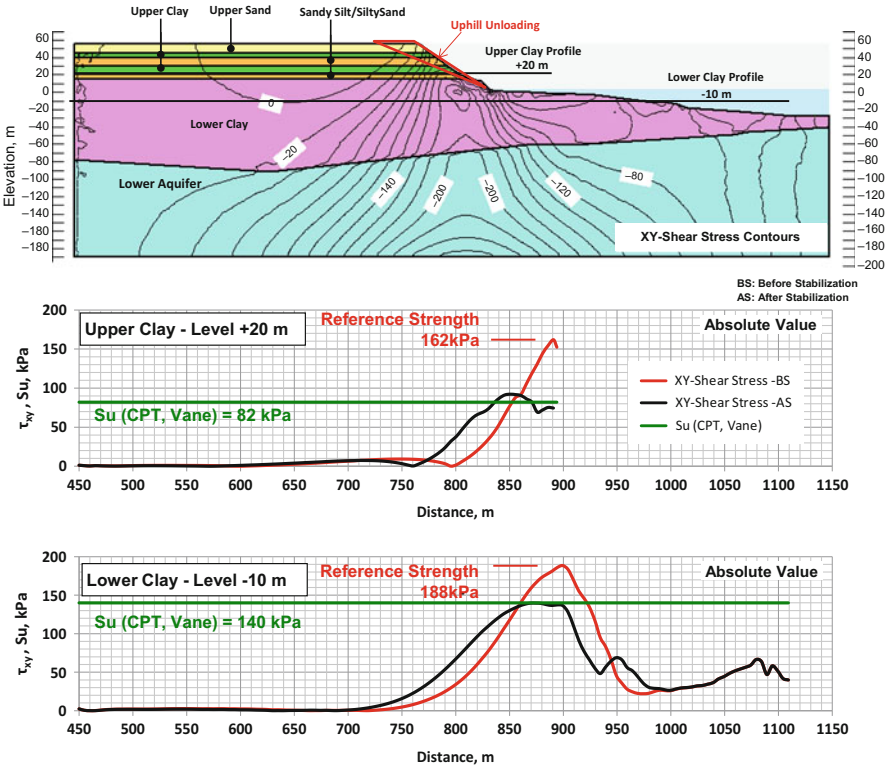

Fig. 19.6 Section A-A – shear stresses on horizontal surfaces

greater than the undrained shear strength measured in VST and estimated from piezocone at the same elevation (green lines on Fig. 19.6): 82 kPa at elevation 20 m and 140 kPa at elevation −10 m.

The slope at Section A-A will be stabilized by unloading the upper part (red triangle on the cross-section of Fig. 19.6). The shear stress profiles on horizontal surfaces after stabilization (shown in black on the shear stress profiles of Fig. 19.6) show a reduction of the maximum mobilized shear stress by 40–45% in the Upper Clay and by 20–30% in the Lower Clay, thus a significant improvement against the possibility of progressive failure.

Narrow Section: Similar analyses were then performed for various sections of the Spur. The results for the most narrow part of the Spur, Section B-B (see location on Fig. 19.1), are shown on Fig. 19.7. They show that the maximum shear stresses on horizontal surfaces are reduced due to stabilization works to less than 50% of the maximum shear stress mobilized in Section A-A before stabilization, thus very far from conditions that could trigger progressive failure.

It is worth noting that reservoir impounding at Full Supply Level (FSL) decreases the shear stresses on the upstream side of the North Spur (dashed blue line on Fig. 19.7) and does not change the stress level on the downstream side. It thus cannot be a triggering or aggravating factor for downhill progressive failure.

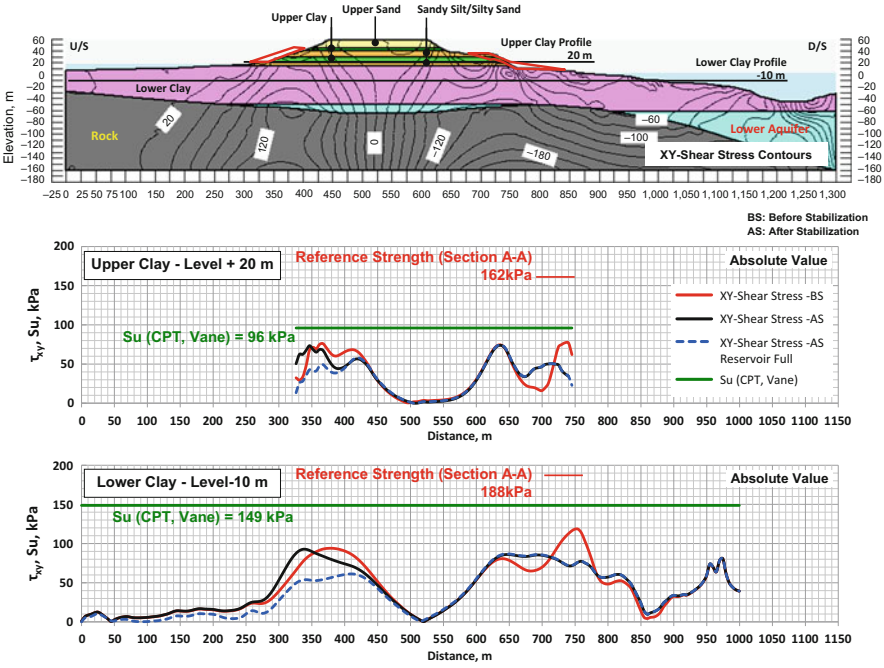

Fig. 19.7 Section B-B – shear stresses on horizontal surfaces

19.6 Conclusion

The objective of the analyses presented above was to assess the stability of the natural slopes of the North Spur against landslides in general and large retrogressive slides in particular, and to estimate the stability improvement provided by the projected stabilization works.

The possibility of occurrence of simple landslides, flowslides, upward and downward progressive landslides has been studied and the results show that with the mitigation measures taken, the stability of the North Spur regarding such events is adequate.

Flowslides are prevented by stabilization works designed for a LEM safety factor equal to or greater than 1.5 and which include protective measures against erosion as to prevent any "first slide" by unloading/erosion in the toe area. The effect of a potential surcharge in the uphill region of the Spur (not presented herein) has also been examined to specify acceptable maximum loading and minimum distance from the crest.

Regarding progressive failures, the paper presents a method specifically developed to address this specific case. As there is no recognized method already developed, an approach was developed based on observations, data and judgment, and also on the methodology developed by Locat et al. (2013) for back-analyses of such landslides. Using the actual conditions as the worst case scenario gives confidence to make engineering recommendations.

By reducing the maximum mobilized shear stress by 20–50% of the reference strength, the stabilization works should insure an adequate safety against a progressive failure initiation.

Acknowledgements The writers would like to acknowledge the contribution of the following individuals: Mr. Alvaro Ceballos (SNC-Lavalin) who conducted the LEM stability analyses, Mr. Amir Hossein Zamani (SNC-Lavalin) who performed the Stress Distribution analyses, Ms. Audrey Boucher (SNC-Lavalin) who produced the majority of the figures of the paper and Prof. Ariane Locat (Université Laval) who reviewed the paper. The writers would also like to thank Nalcor Lower Churchill Project Management for the permission to use their data and to publish this paper.

References

Bernander S (2000) Progressive landslides in long natural slopes, formation, potential extension and configuration of finished slides in strain-softening soils. MSc thesis, Luleå University

Demers D, Robitaille D, Locat P, Potvin J (2014) Inventory of large landslides in sensitive clays in the province of Québec, Canada: preliminary analysis. In: L'Heureux J-S et al (eds) Landslides in sensitive clays: from geosciences to risk management, advances in natural and technological hazards research 36. Springer, Dordrecht, pp 77–89

Lebuis J, Robert JM, Rissmann P (1983) Regional mapping of landslide hazard in Quebec. In: Proceedings of the symposium on slopes on soft clays. Swedish Geotechnical Institute Report no. 17, Linköping, Sweden, p 205–262

Lefebvre G (1981) Fourth Canadian geotechnical colloquium: strength and slope stability in Canadian soft clay deposits. Can Geotech J 18(3):420–442

Leroueil S, Vaunat J, Picarelli L, Locat J, Faure R, Lee H (1996) A geotechnical characterization of slope movements. In: Senneset K (ed) Proceedings of the 7th international symposium on landslides, Trondheim. Balkema, Rotterdam, pp 53–74

Locat A, Leroueil S, Bernander S, Demers D, Jostad HP, Ouehb L (2011) Progressive failures in eastern Canadian and Scandinavian sensitive clays. Can Geotech J 48(11):1696–1712

Locat A, Jostad HP, Leroueil S (2013) Numerical modeling of progressive failure and its implication to spreads in sensitive clays. Can Geotech J 50(9):961–978

Locat A, Leroueil S, Fortin A, Demers D, Jostad HP (2015) The 1994 landslide at Sainte-Monique, Quebec: geotechnical investigation and application of progressive failure analysis. Can Geotech J 52(4):490–504

SNC-Lavalin (SLI, 2016) Lower Churchill project – engineering report – North Spur Stabilization. Design Report no 505573-3281-4GER-0001

SNC-Lavalin and AGRA Monenco (SLI-AGRA 1998) (1998) Muskrat falls hydroelectric development final feasibility study report – volume I – engineering report

Tavenas F (1984) Landslides in Canadian sensitive clays – a state of the art. In: Proceedings of the 4th Intern. symposium on landslides. Canadian Geotechnical Society, vol 1, p 141–153

Tavenas F, Leroueil S (1981) Creep and failure in slopes in clays. Can Geotech J 18(1):106–120

Chapter 20
Correction Factors for Undrained LE Analyses of Sensitive Clays

Petter Fornes and Hans Petter Jostad

Abstract Correction factors to be used in conventional undrained stability calculations in order to account for post peak strain softening behaviour of sensitive clays, has been recommended based on an extensive sensitivity study with advanced finite element simulations. It is found that a correction of the material factor is preferred compared to a reduction of the shear strength. The input parameters to the sensitivity study that had the highest correlation with the required correction factor were the shear strength increase with depth and the brittleness, which is the rate of shear strength reduction with strain. In a large block sample database of sensitive Norwegian clays, there was no clear correlation between the brittleness and the sensitivity. Hence, classification of the clays based on the sensitivity is not recommended for evaluating the effect of strain softening on the capacity.

20.1 Introduction

In sensitive clays progressive failure mechanisms may develop due to strain softening behavior, i.e. where the undrained shear strength after a peak value reduces significantly with growing shear strain as shown in Fig. 20.1. In Norway, slope stability analyses are generally performed by limit equilibrium methods (LEM). However, these methods cannot directly account for the strain softening behaviour of sensitive clays, since the peak strength will not be fully mobilized along the shear surface. In the past, the peak undrained shear strengths used in LEM analyses were generally underestimated due to sample disturbance when using 54 mm soil sampler (also shown in Fig. 20.1). Today, the undrained shear strength is more often based on

P. Fornes (✉)
Norwegian Geotechnical Institute (NGI), Oslo, Norway

Norwegian University of Science and Technology (NTNU), Trondheim, Norway
e-mail: petter.fornes@ngi.no

H.P. Jostad
Norwegian Geotechnical Institute (NGI), Oslo, Norway
e-mail: hans.petter.jostad@ngi.no

V. Thakur et al. (eds.), *Landslides in Sensitive Clays*, Advances in Natural and Technological Hazards Research 46, DOI 10.1007/978-3-319-56487-6_20

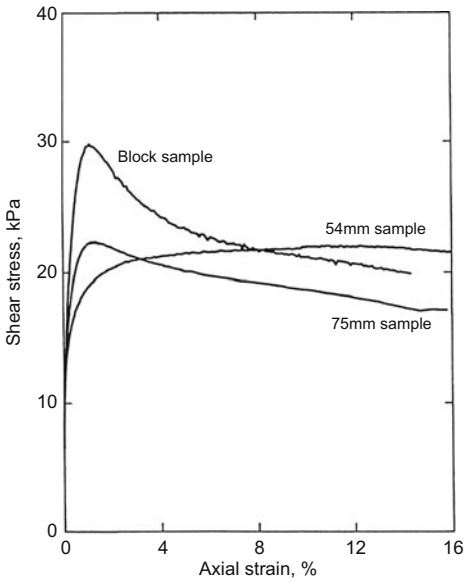

Fig. 20.1 Example of increased peak undrained shear strength and increased rate of softening from block samples on a soft low plastic Norwegian clay (Lunne et al. 1997)

triaxial tests on high quality block samples. Therefore, in order to not overestimate the safety margin when taking advantage of the higher peak shear strength, one need to also account for the effect of strain softening behaviour generally observed for these materials.

In a research and development project sponsored by NIFS (www.naturfare.no), an extensive Finite Element Method (FEM) sensitivity study was performed in order to quantify the effect of strain softening behaviour on the bearing capacity of sensitive Norwegian clays (Jostad et al. 2014). It is concluded that a pragmatic solution may be to use an increased material factor if conventional LEM is used on strain softening brittle clays (NGI 2014). The material factor increase should aim to maintain more or less the same average safety level compared to the current design practice based on 54 mm samples.

20.2 Correction of the Material Factor

The effect of strain softening when calculating the stability with conventional LEM, could either be accounted for by reducing the undrained shear strength or increasing the required material factor. However, based on results from the advanced finite element analyses, it is found that the failure mechanism is rather complex since the peak load corresponds to an instability condition. The effect of the reduced capacity is therefore difficult to capture by only reducing the shear strength of the strain softening material. Also the effect that the passive zone is not fully mobilized at this state reduces the capacity. An increase of the required material factor also agrees with the current practice proposed in NPRA (2014) where the material factor

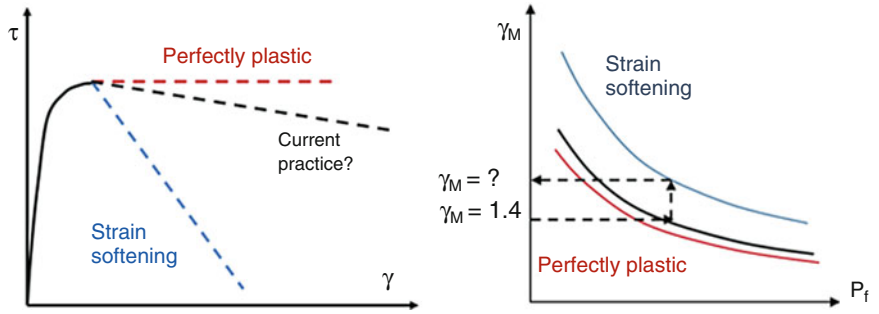

Fig. 20.2 Illustration of a perfectly plastic and a strain softening material behaviour. The current practice accepts some higher probability of failure P_f for materials that show a modest strain softening behavior

should be increased by about 7% in order to account for a brittle material response. Therefore, in this study the effect of strain softening is accounted for by:

$$\gamma_M^{\text{softening}} = \gamma_M \cdot F_{\text{softening}}$$

where γ_M is the material factor calculated by LEM based on the peak undrained shear strength, and $F_{\text{softening}}$ is the necessary correction in order to account for the reduced capacity obtained by a corresponding finite element analyses (FEA) using Plaxis (www.plaxis.nl) and the material model NGI-ADPSoft that includes the effect of post peak strain softening behaviour (Grimstad and Jostad 2010, 2011).

Ideally, the recommended design practice should give the same probability of failure for materials with or without strain softening behaviour. If a material factor γ_M results in an accepted safety level for a perfectly plastic material, the recommended material factor for a strain softening material should then be higher when the capacity is calculated with the same LEM. This is illustrated in Fig. 20.2.

20.3 Sensitivity Study

An extensive sensitivity study including about 500 finite element analyses including direct modelling of typical strain softening behaviour of Norwegian sensitive clays was performed in order to quantify the effect of strain softening on the calculated capacity. An embankment for a new road in a gently inclined very long slope of mainly sensitive clay covered by a non-sensitive clay (dry crust) was considered as an appropriate problem case (NGI 2012). A representative range of input parameters, including the post-peak behavior, was based on results from laboratory tests on high quality block samples from different locations with sensitive clays in Norway (Karlsrud and Hernandez-Martinez 2013). The parameter set for each simulation was then established by sampling randomly from the distributions by the Monte Carlo method.

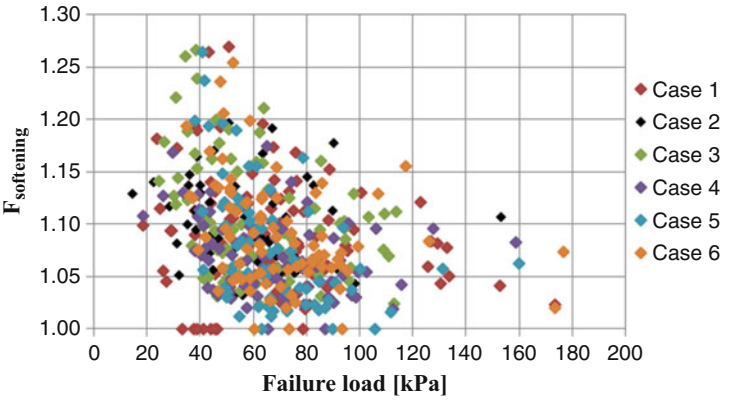

Fig. 20.3 Correction factor $F_{softening}$ to account for strain softening in a perfectly plastic stability calculation, versus failure load for different cases of input parameters. Cases 1–6 are based on different geometrical parameters (Jostad et al. 2014)

For each parameter set, the maximum height of the embankment was determined by applying a distributed vertical load representing the weight of the fill. The maximum load that could be applied is the load capacity. The correction factor $F_{softening}$ was found by a corresponding simulation without post-peak softening, where the peak undrained shear strength was reduced by a factor until the load capacity was equal to the simulation with softening. These analyses were described in a paper to IWLSC in 2013 (Jostad et al. 2014).

The calculated correction factors in this study varied between 1.0 and 1.3, with a mean value of 1.09 and a standard deviation of 0.06, as shown in Fig. 20.3. This means that in a stability analysis using conventional LEM (without the effect of softening) and an undrained shear strength based on the peak strength from high quality block samples, the capacity may be overestimated by as much as 30%. One simple way of accounting for this shortcoming is to increase the required material factor γ_M by 30%.

20.4 Correction Factor for Different Input Parameters

Increasing the required material factor for all cases involving sensitive clays by 30% will be very conservative, i.e. with a safety level higher than the present design practice. To avoid this, the large range of correction factors presented in Fig. 20.3 are divided into groups depending on the input data, so that the correction factor can be related to specific sets of material parameters.

20.4.1 Correlations with Input Parameters

In order to identify which parameters give the largest correction factor, the correlation between the correction factor and the different input parameters was studied, see NGI (2012) and Fornes and Jostad (2013). It was found that the parameters that govern the shear strength increase with depth had the largest effect on the magnitude of the correction factor. In this study, the undrained shear strength profile is defined by y_{ref} that gives the depth where the shear strength starts to increase significantly with depth, see Fig. 20.4. Then, the idealized linear increase in shear strength with depth is given by $s_u{}^A{}_{inc}$. The correction factor $F_{softening}$ increases with increasing y_{ref} and with decreasing $s_u{}^A{}_{inc}$.

The reason why the shear strength profile affects the effect of softening, is that the maximum load (capacity) in these cases occurs before a fully developed failure mechanism is obtained. At this point of instability, the reduction in resistance in the zones that experience softening (reduction in shear strength) is exactly balanced by the increase in resistance in the remaining soil volume upon further deformation. After this instability point, the propagation of the failure zone (also often called shear band) which generally starts from the loaded area, continue to propagate downwards however with a gradually reducing driving force, see Fig. 20.5. Therefore, a case with a shear strength that increases with depth will delay the point where the system becomes instable. This means that the shear band has propagated longer and the critical point is closer to the condition with a fully developed failure mechanism. If the failure mechanism is fully developed when the peak load is reached, the correction factor becomes equal to 1.0. A high correction factor is obtained if the instability point occurs close to the condition where the first point in the soil has reached the peak shear strength.

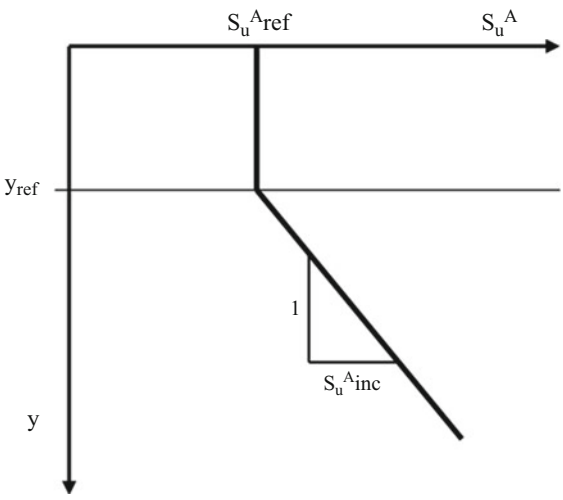

Fig. 20.4 Shear strength profile defined by y_{ref}, $s_u{}^A{}_{ref}$ and $s_u{}^A{}_{inc}$

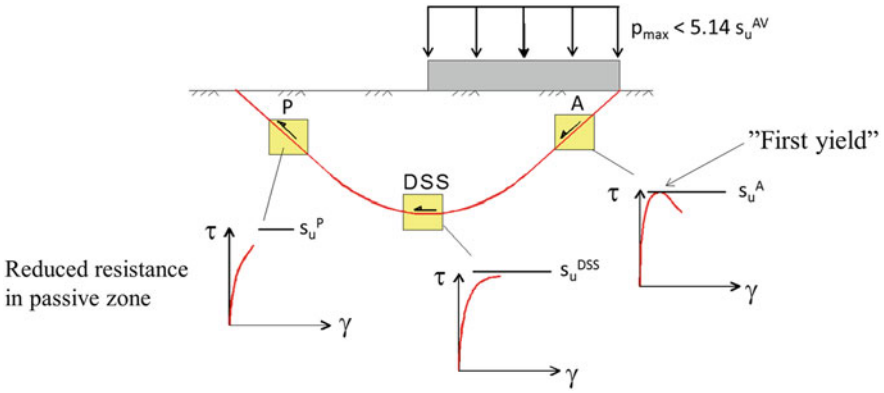

Fig. 20.5 Peak load at an instability point where the reduction in resistance due to softening is exactly equal to the increase in resistance in the remaining soil upon further deformation

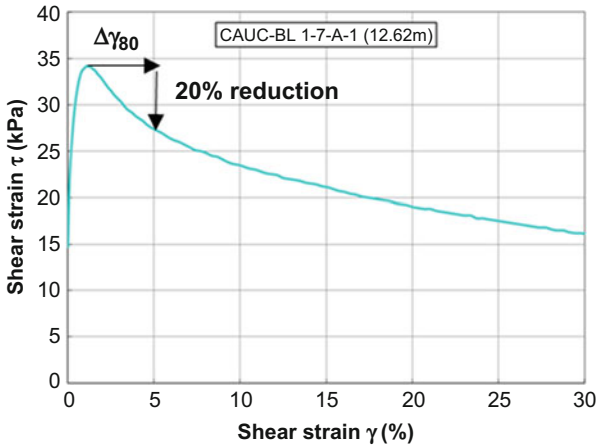

Fig. 20.6 The brittleness is here defined by the parameter $\Delta\gamma_{80}$, which is the additional shear strain necessary to reduce the active peak undrained shear strength by 20–80%

The brittleness of the clay may be defined by how much additional strain is necessary in order to reduce the peak shear strength by a given amount (percent). Since this parameter controls the post peak softening behaviour, it affects the correction factor. In this study, the brittleness is controlled by a parameter $\Delta\gamma_{80}$, defined as the additional shear strain necessary to apply in order to reduce the peak undrained shear strength in a triaxial CAUA-test by 20–80% as illustrated in Fig. 20.6. Low values of $\Delta\gamma_{80}$ corresponds to high brittleness, and thus a more rapid reduction in the resistance in the zones with softening. Thus, also an instability point closer to the point of "first yield". The selection of reduction to 80% of the

Table 20.1 Mean value and standard deviation of $F_{softening}$ for the 27 input parameter groups

$\Delta\gamma_{80}$	$s_u{}^A{}_{inc}$	Mean value and standard deviation of $F_{softening}$		
		y_{ref} = 0–2 m	y_{ref} = 2–4 m	y_{ref} > 4 m
0–2%	2–3.5 kPa/m	1.059 ± 0.020	1.125 ± 0.044	1.164 ± 0.055
	3.5–5 kPa/m	1.041 ± 0.021	1.083 ± 0.035	1.138 ± 0.038
	>5 kPa/m	1.021 ± 0.023	1.057 ± 0.023	1.107 ± 0.017
2–5%	2–3.5 kPa/m	1.062 ± 0.027	1.111 ± 0.041	1.167 ± 0.058
	3.5–5 kPa/m	1.041 ± 0.020	1.066 ± 0.029	1.110 ± 0.040
	>5 kPa/m	1.024 ± 0.006	1.046 ± 0.025	1.081 ± 0.026
> 5%	2–3.5 kPa/m	1.000[a]	1.070 ± 0.026	1.138 ± 0.046
	3.5–5 kPa/m	1.030 ± 0.021	1.045 ± 0.012	1.104 ± 0.052
	>5 kPa/m	1.019[a]	1.042 ± 0.013	1.045

[a]Only one data point

peak shear strength is based on the results from the finite element analyses, where this value is found to be typical when the peak load is reached.

20.4.2 Correction Factors Based on Ranges of the Most Important Input Parameters

In order to relate the correction factor to specific values of input parameters, the results from the sensitivity study were grouped based on the three most important parameters ($\Delta\gamma_{80}$, y_{ref} and $s_u{}^A{}_{inc}$). Brittleness parameter $\Delta\gamma_{80}$ was divided into values from [0–2%], [2–5%] and [>5%]. Reference depth y_{ref} was divided into values from [0–2 m], [2–4 m] and [>4 m]. Incremental shear strength $s_u{}^A{}_{inc}$ was divided into values from [2–3.5 kPa/m], [3.5–5 kPa/m] and [>5 kPa/m]. This gave in total 27 different groups of input parameters, further documented in NGI (2014). The mean value and standard deviation of $F_{softening}$ within each of these 27 groups are presented in Table 20.1. An example of the distribution of the correction factor $F_{softening}$ is shown in Fig. 20.7 for groups with high brittleness and low shear strength increase with depth.

20.4.3 Correlations Between Brittleness Parameter $\Delta\gamma_{80}$ and Index Data

To study possible correlations between standard index data and the brittleness parameter $\Delta\gamma_{80}$, in order to replace this parameter with a more common soil parameter, NGI's block sample data base (Karlsrud and Hernandez-Martinez

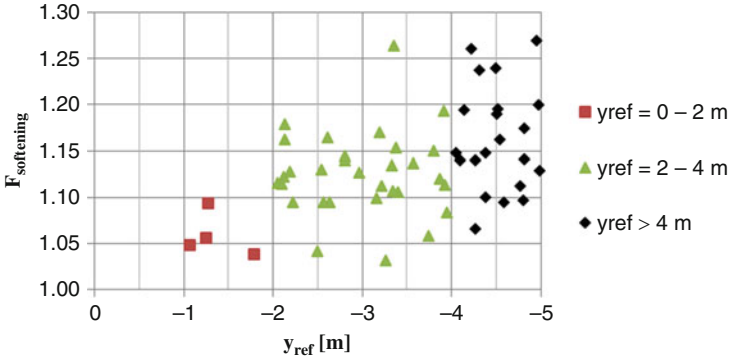

Fig. 20.7 Correction factor $F_{softening}$ versus reference depth y_{ref} for cases with high brittleness ($\Delta\gamma_{80}$ = 0–2%) and low shear strength increase with depth ($s_u{}^A{}_{inc}$ = 2–3.5 kPa/m) (NGI 2014).

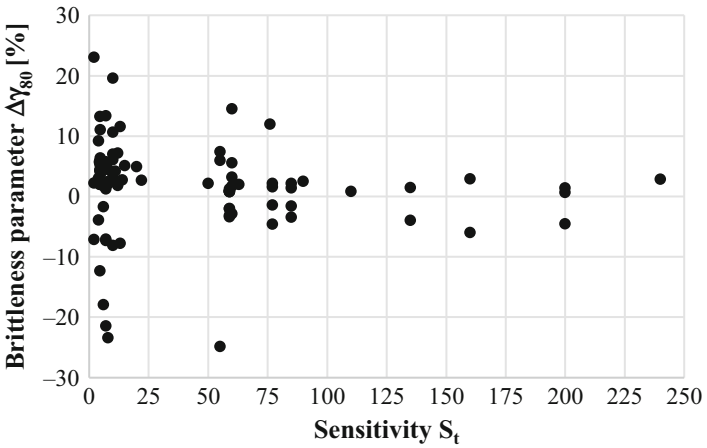

Fig. 20.8 Correlation between brittleness parameter $\Delta\gamma_{80}$ and sensitivity S_t. Negative values are from passive triaxial tests

2013) was investigated. The following parameters were considered: sensitivity S_t, remoulded undrained shear strength s_{ur}, over-consolidation ratio OCR, water content w, plasticity index I_p, liquidity index IL and sample depth.

No clear correlation was found between the brittleness parameter $\Delta\gamma_{80}$ and the index data. High sensitivity and high IL are clear indications of high brittleness. However, low values may still give high brittleness as shown for sensitivity S_t in Fig. 20.8.

Based on this study, it is therefore concluded that one should be very careful to use sensitivity or other index data to estimate the potential brittleness of sensitive

clays that effects the capacity. The only reliable information is results from CAUC tests on high quality block samples.

20.5 Adjustment Based on Current Design Practice

All Norwegian sensitive clays show some degree of strain softening behaviour, which means that the capacity is lower than for a perfectly plastic material. The current practice and regulations for sensitive clays in Norway are described by Oset et al. (2014). Based on recommendations in NPRA (2014) and NVE (2014), it is typically only the soils classified as brittle or with high sensitivity that are corrected due to this strain softening behavior. In NVE (2014), brittle clays are defined by $S_t > 15$. However, as shown in this study, less sensitive clays ($S_t < 15$) may still be brittle based on $\Delta\gamma_{80}$ (as shown in Fig. 20.8) and require a high correction factor. This means that some reduction in the capacity compared to a perfectly plastic material is accepted in the current design practice. Therefore, in order not to increase the safety level significantly (with a corresponding increase in costs during developments of new infrastructure), it is estimated how much of the correction factor has been included in the current practice.

A simple approach was to assume that sensitive clays which are in the lowest degree of brittleness category according to the definition used here ($\Delta\gamma_{80} > 5\%$), are accepted to not be adjusted (correction factor 1.0). Only the relative part of the calculated correction factor is then proposed to be used. Figure 20.9 illustrates this approach for the cases with high brittleness and low shear strength increase with depth.

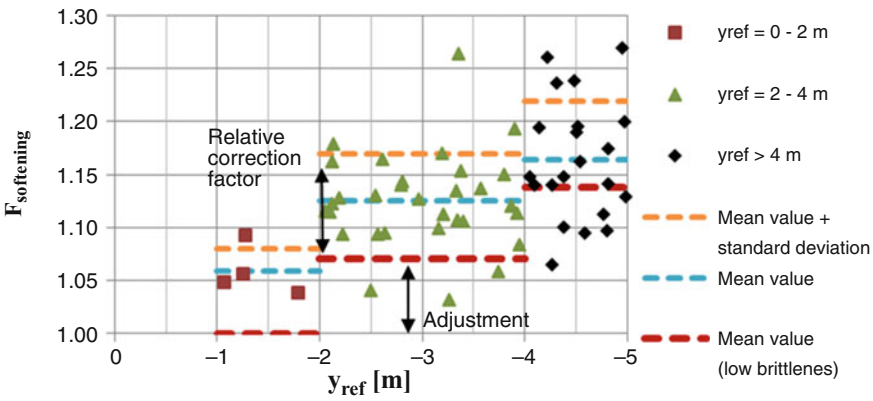

Fig. 20.9 Adjustment of correction factor, for high brittleness and low shear strength increase with depth. The *red dashed line* shows the mean value for the corresponding less brittle clays

Table 20.2 Recommended correction factor $F_{softening}$ for high and medium brittle clays

	$F_{softening}$ for high and medium brittleness ($\Delta\gamma_{80} = 0$–5%)		
${s_u}^A{}_{inc}$	$y_{ref} = 0$–2 m	$y_{ref} = 2$–4 m	$y_{ref} > 4$ m
2–3.5 kPa/m	1.10	1.10	1.15[a]
3.5–5 kPa/m	1.05	1.10	1.10
>5 kPa/m	1.05	1.05	1.10

[a]Increased from 1.10 in order to account for that current practice most likely give higher probability of failure for these cases

20.6 Recommended Correction Factors for Sensitive Clays

The sensitivity study shows some variations in the calculated correction factor. The actual value to use in order to give the accepted probability of failure depends therefore also on the uncertainties in the peak shear strength. If the uncertainty in the peak shear strength is high, the accepted probability of failure could be satisfied by using the mean value of the correction factor as shown in Fornes and Jostad (2015). For rather typical uncertainties in the peak undrained shear strength, a mean value plus one standard deviation of the correction factor can give approximately the same probability of failure.

Table 20.2 provides recommended correction factors for the high ($\Delta\gamma_{80} = 0$–2%) and medium ($\Delta\gamma_{80} = 2$–5%) brittle clays. The values are equal to the mean value plus one standard deviation from Table 20.1, minus the mean value for the less brittle clays ($\Delta\gamma_{80} > 5\%$) in the corresponding parameter groups, and then rounded up to the closest increment of 0.05. In this way, the same values were obtained for both high and medium brittle clays. The values in the [${s_u}^A{}_{inc} = 2$–3.5 kPa/m and $y_{ref} > 4$ m] group are further increased from 1.10 to 1.15, in order to account for that these shear strength profiles can be expected to have relatively large probability of failure in the current practice.

20.7 Conclusions

The effect of strain softening behaviour of typical Norwegian sensitive clays is quantified in an extensive sensitivity study by advanced finite element analyses. Based on this study, correction factors are proposed for increasing the required material factor when the stability analysis is performed by standard limit equilibrium methods (LEM). These factors are first of all meant for cases where the undrained shear strength is obtained from triaxial tests on high quality block samples and conditions with rapidly increasing driving loads. Different correction factors are proposed depending on the actual brittleness of the material and the shape of the idealized shear strength profile with depth. To use the index parameter sensitivity, S_t, to estimate the brittleness of sensitive clays is not recommended, since even

less sensitive clay ($S_t < 15$) also may show very brittle post peak strain softening behaviour. The recommended values are suggested in order to keep the safety level on the same level as used in the current design practice, to not increase the costs of new developments.

Acknowledgments This study was performed with funding from the Norwegian Geotechnical Institute (NGI) and NIFS (Natural hazards: Infrastructure for Floods and Slides), a cooperative research program by the Norwegian Public Roads Administration (NPRA), the Norwegian National Rail Administration (NNRA) and the Norwegian Water Resources and Energy Directorate (NVE). Thanks are given to Prof. Steinar Nordal for his helpful comments.

References

Fornes P, Jostad HP (2013) A probabilistic study of an inclined slope in sensitive clay using FEA. In: ComGeoIII 3rd international symposium computational geomechanics, Krakow, August 2013

Fornes P, Jostad HP (2015) Calibration of material factor to account for strain softening in undrained loading of sensitive clays. In: Proceedings of the 24th European Young Geotechnical Engineers Conference (EYGEC), Durham, UK Osman, A.S. & Toll, D.G. (Eds.) 2015 ISBN 978-0-9933836-01

Grimstad G, Jostad HP (2010) Undrained capacity analyses of sensitive clays using the nonlocal strain approach. In: 9th HSTAM international congress on mechanics Vardoulakis mini-symposia, Limassol, Cyprus

Jostad HP, Grimstad G (2011) Comparison of distribution functions for the nonlocal strain approach. In: Proceedings of 2nd international symposium on computational geomechanics, Cavtat-Dubrovnik, Croatia

Jostad HP, Fornes P, Thakur V (2014) Effect of strain-softening in design of fills in gently inclined areas with soft sensitive clays. In: 1st international workshop landslides in sensitive clays, Québec, October 2013

Karlsrud K, Hernandez-Martinez FG (2013) Strength and deformation properties of Norwegian clays from laboratory tests on high-quality block samples. Can Geotech J 50(12):1273

Lunne T, Berre T, Strandvik S (1997) Sample disturbance effects in soft low plastic Norwegian clay. In: Proceedings of the conference on recent developments in soil and pavement mechanics, Rio de Janeiro, Brazil, 25–27 June. Balkema, Rotterdam. p 81–102

NGI (2012) Effekt av progressiv bruddutvikling for utbygging i områder med kvikkleire, A3 Sensitivitetsanalyse. NGI report 20092128-00-6-R, available as NIFS report 40/2014 at http://www.naturfare.no/_attachment/650154/binary/970297

NGI (2014) NIFS N-6.5.2 Sikkerhet ifm utbygging i kvikkleireområder, Oppsummeringsrapport. NGI report 20140075-01-R, available as NIFS report 88/2014 at http://www.naturfare.no/_attachment/748815/binary/1006602

NPRA (2014) Håndbok V220 Geoteknikk i Vegbygging. http://www.vegvesen.no/Fag/Publikasjoner/Handboker

NVE (2014) Sikkerhet mot kvikkleireskred. Vurdering av områdestabilitet ved arealplanlegging og utbygging i områder med kvikkleire og andre jordarter med sprøbruddegenskaper. Veileder 2014_7

Oset F, Thakur V, Dolva BK, Aunaas K, Sæter MB, Robsrud A, Viklund M, Nyheim T, Lyche E, Jensen OA (2014) Regulatory framework for road and railway construction on the sensitive clays of Norway. In: 1st international workshop landslides in sensitive clays, Québec, October 2013

Chapter 21
Advances in Determining Δu and s_u for Limit Equilibrium Analyses

Ville Lehtonen and Tim Länsivaara

Abstract It is well known that in undrained stability calculations, total stress and effective stress analyses do not give the same calculated factor of safety when FOS >1. This is due to the fact that shear strength is defined differently in these two approaches: In total stress analyses, the mobilised shear stress is compared to undrained shear strength, i.e. strength at failure. In undrained effective stress analyses, the shear strength is defined as corresponding to the mobilised effective stress state. This causes an overestimation of FOS in undrained φ'-c' analyses. Modelling of excess pore pressure Δu has traditionally been source of most uncertainty in undrained effective stress analyses. Having the correct shear strength along the slip surface can be considered the most crucial detail in all stability analyses. It can be argued that in the context of Limit Equilibrium analyses where deformations are not considered, priority should be given to calculating the shear strength correctly, instead of attempting to obtain a "correct" mobilised Δu value. This paper gives a general introduction to the new HSU (Hybrid s_u) method. For the purposes of LEM analyses, Δu is calculated so that the resulting Mohr-Coulomb shear strength corresponds to the assumed failure state. This approach solves the inherent overestimation of FOS in undrained φ'-c' analyses. To predict the effective stress at failure, a constitutive effective stress soil model is employed. Also presented is a concept of deriving undrained shear strength s_u in LEM, based on an effective stress soil model. This makes it possible to conduct the LEM stability analysis in terms of total stresses, while deriving soil strength from effective strength parameters. The different approaches of calculating Δu and s_u with the HSU method are compared using a theoretical stability calculation example. The relative merits of the different approaches are discussed.

V. Lehtonen (✉)
Tampere University of Technology (TUT), Tampere, Finland

Ramboll Finland Oy, Tampere, Finland
e-mail: ville.lehtonen@tut.fi

T. Länsivaara
Tampere University of Technology (TUT), Tampere, Finland
e-mail: tim.lansivaara@tut.fi

V. Thakur et al. (eds.), *Landslides in Sensitive Clays*, Advances in Natural and Technological Hazards Research 46, DOI 10.1007/978-3-319-56487-6_21

21.1 Introduction

In the recent decade there has been increased interest in undrained effective stress stability analyses in Finland. The reason for this has been the discovery that many existing railway embankments on soft soils have a very low calculated factor of safety. Calculated factors of safety (FOS) may even be as low as FOS <1 with no partial factors applied. The reasons for such results lie mainly in the unreliable determination of undrained shear strength s_u. In typical Finnish design practise, strength determination is based on field vane testing, unfortunately of variable quality and reliability. While the in situ determination of s_u is constantly being refined, a parallel approach to the issue has been to improve the methods of undrained φ'-c' calculations.

Typically, undrained φ'-c' analyses would be used to provide a comparison result for $\varphi = 0$ calculation results that are based on s_u measurements of questionable quality. The determination of the effective strength parameters φ' and c' is quite reliable with proper triaxial testing. The uncertainty however lies in the determination of excess pore pressure Δu, which is quite complicated to model correctly especially in a LEM framework.

This paper discusses some commonly recognised issues related to undrained effective stress stability analyses using LEM and briefly presents a new calculation method that is intended to solve these issues. The method results are illustrated using a theoretical example of an external load on a horizontal clay deposit. The relative merits of total stress and effective stress analyses are discussed.

21.2 On Undrained Effective Stress Calculations and LEM

Probably the most important issue in undrained effective stress analyses is the calculation of shear strength. Pore pressure u has a direct influence on shear strength through the generally accepted Mohr-Coulomb equation:

$$\tau_f = c' + (\sigma - u) \cdot \tan \phi' \tag{21.1}$$

Undrained excess pore pressure (Δu) is a function of the change in mean total stress p (confining stress) as well as changes in deviatoric stress q. One expression of the pore pressure components is (Wood 1990):

$$\Delta u = \Delta p + A \Delta q \tag{21.2}$$

where A is a pore pressure parameter that controls the amount of shear-induced pore pressure.

Note that Eq. 21.2. assumes the Cambridge stress definition ($p' = (\sigma_1' + \sigma_2' + \sigma_3')/3$, $q = \sigma_1' - \sigma_3'$), which is assumed throughout this paper also.

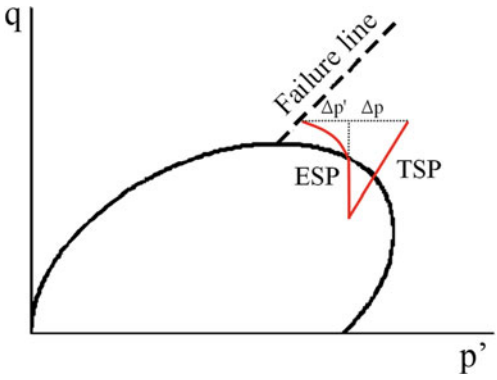

Fig. 21.1 Components of excess pore pressure illustrated in normalized p'-q stress space. *ESP* effective stress path, *TSP* total stress path (after Lehtonen and Länsivaara 2013)

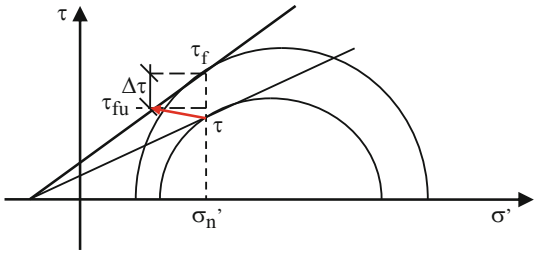

Fig. 21.2 Overestimation of shear strength τ_f for FOS >1 (Lehtonen and Länsivaara 2016)

Yet another, even more direct expression can be given as a direct result from the principle of effective stresses:

$$\Delta u = \Delta p - \Delta p' \tag{21.3}$$

In Eq. 21.3, the effective stress component $\Delta p'$ depends on the volumetric tendencies of the clay in undrained loading. When clay is sheared on the wet side of the critical state line, there is tendency for plastic compression. This tendency is offset by an elastic expansion tendency, i.e. a build-up of excess pore pressure to maintain constant volume. In p'-q stress space this is evidenced by a decrease of p' (i.e. the component $\Delta p'$) (Fig. 21.1).

The amount of $\Delta p'$ from the initial state to failure depends on several factors, such as anisotropy, consolidation state, rate of loading and temperature. The effects of these variables are quite well discussed in available literature (e.g. Wood 1990). The variability and complexity of excess pore pressure response makes accurate modelling of Δu a somewhat difficult proposition, especially in LEM framework.

Yet another crucial issue in undrained φ'-c' analyses (not restricted to LEM) is the inherent overestimation of shear strength when FOS >1. This happens because further pore pressure generation between the mobilised state and failure is not accounted for. This is illustrated in Fig. 21.2.

The strength in undrained φ'-c' analyses thus corresponds to the mobilised stress state, and is not the strength that can actually be mobilised at failure. This is in contrast to a corresponding $\varphi = 0$ analysis where the undrained shear strength

always corresponds to the strength at failure (but only for the given type of loading, e.g. direction, rate of loading etc. . . .).

Furthermore, it has been established (e.g. Krahn 2003) that the normal stress distribution in LEM may be quite inaccurate. The normal stress distribution is a product of a static equilibrium calculation only, and as such the analysis ignores much of the actual physics involved. As there is a connection between shear strength and total normal stress (coupled with pore pressure u), the resulting shear strength in LEM can be incorrect due to potentially inaccurate total stresses on the slip surface.

For example, when loading is increased in an undrained effective stress LEM analysis, the mobilised total stress all along the slip surface tends to increase so that equilibrium is maintained. This is typically not counteracted by a corresponding increase in excess pore pressure, which may lead to an increase of τ_f that is unrealistic for undrained conditions.

There are therefore several potential complications that affect the accuracy of undrained φ'-c' LEM analyses. Excess pore pressure should ideally be calculated so that relevant physical factors affecting the result are taken into account. This is somewhat difficult by itself. Even if the pore pressure is modelled "right", if the normal stress distribution along the slip surface is inaccurate, the resulting shear strength (and factor of safety) will not be realistic.

21.3 The Hybrid s_u Method

A new calculation method has been developed to facilitate undrained LEM stability analyses. The Hybrid s_u (HSU) method (Lehtonen 2015) is intended for use with soft, normally consolidated or slightly overconsolidated clays. HSU can be used either to calculate s_u values for $\varphi = 0$ analyses, or Δu_f values for undrained φ'-c'. The end results take into account anisotropy, consolidation state and volumetric hardening properties.

The HSU method is intended to be used as an engineering tool: It gives the user a reasonably accurate method of predicting essential strength-related parameters in LEM context without requiring complicated soil models with several input parameters. This is reflected in the basic premise that shear strength is the most essential factor in LEM. The main goal of a LEM stability analysis is to obtain the factor of safety as accurately as possible – not to analyse stress states with high accuracy.

HSU is based on the effective stress soil model S-CLAY1 (Wheeler et al. 2003). S-CLAY1 is a derivative of the Modified Cam Clay model (Roscoe and Burland 1968), with an inclined yield surface and the addition of rotational hardening of the yield surface. In HSU, the S-CLAY1 initial yield surface and volumetric hardening law are used to derive a closed form solution for the effective mean stress at failure p'_f (Eq. 21.4). The rotational hardening present in the S-CLAY1 model is omitted for simplicity. For a detailed derivation of the solution and explanations of assumptions made, see Lehtonen (2015).

$$p'_f = f\left(\phi', c', \sigma'_{v0}, OCR, \lambda/\kappa, C, D, b, \theta\right) \tag{21.4}$$

The model parameters of the HSU method are:

φ'	critical state friction angle (°)
c'	effective cohesion at critical state (kPa)
σ'_{vo}	initial vertical effective stress (kPa)
OCR	overconsolidation ratio
λ/κ	hardening control parameter
C	coefficient for K_{0NC}
D	coefficient for initial K_0 (overconsolidated)
b	intermediate principal stress parameter (assumed $b = 0.3$)
θ	principal stress rotation angle (°)

Undrained shear strength in HSU is defined simply as:

$$s_u = \frac{q_f}{2} = \frac{p'_f \cdot M}{2} \tag{21.5}$$

where q_f is the deviator stress at failure, and M is the inclination of the critical stress line in p'-q space, value for triaxial compression.

In LEM context, s_u is calculated separately for every slice bottom. As s_u is a function of the principal stress rotation angle θ (itself a function of slip surface inclination and friction angle φ'), strength anisotropy along the slip surface can be accounted for in an analytical manner. The LE calculation is conducted as a normal $\varphi = 0$ analysis, using the calculated s_u values as input for the given slip surface. The shear strength distribution along the slip surface is thus independent from the normal stress distribution along the slip surface.

In undrained effective stress applications, the HSU approach is quite different from traditional undrained φ'-c' analyses. Instead of attempting to predict pore pressure, focus is instead in obtaining the correct shear strength that can be mobilised at failure. No consideration is given to whether the predicted Δu is "correct". Instead, excess pore pressure at failure Δu_f is modelled so that the resulting shear strength is "correct" and corresponds to the actual failure state as accurately as possible.

There are two approaches to an undrained φ'-c' analysis with HSU. One is to force the values of Δu_f so that the resulting shear strength along the slip surface matches the s_u value predicted by the HSU method:

$$s_u = \tau_f = c' + \left(\sigma_n - u_0 - \Delta u_f\right) \cdot \tan\phi' \tag{21.6}$$

$$\Delta u_f = \sigma_n - u_0 - \frac{s_u - c'}{\tan\phi_c{}'} \tag{21.7}$$

The process is iterative, as the values of Δu_f are updated based on the output σ_n values. This type of analysis gives the exact same result as the corresponding HSU

total stress analysis using the predicted s_u values. In this paper it is used to obtain theoretical Δu_f values that would be required to match an undrained φ'-c' analysis with a corresponding $\varphi = 0$ analysis (see the following example).

Another method of conducting an HSU φ'-c' analysis is calculating Δu_f based on assumed stress changes from the initial state to failure. As the stress changes are calculated corresponding to the predicted failure state, the resulting shear strength also corresponds to the actual failure state. This in theory avoids the inherent overestimation of τ_f, when FOS>1. At failure it can be written that:

$$\Delta u_f = \Delta p_f - \Delta p'_f \tag{21.8}$$

The effective stress component $\Delta p'_f$ is obtained for each slice from the HSU closed form solution. The total stress component Δp_f is calculated based on vertical stress changes between the initial state and failure, the known relationship of principal effective stresses at failure, as well as iterative assumptions of Δu_f. The full solution (see Lehtonen 2015) cannot be given here due to space constraints.

The HSU method has been verified by various laboratory data fitting examples and back-calculations of documented embankment failures (Lehtonen and Länsivaara 2016; Lehtonen 2015). It has been shown to give quite good results (comparable to literature values of clay strength, e.g. Larsson et al. 2007) with reasonable parameter combinations.

21.4 Conceptual Example

A simple theoretical example is used to illustrate the differences between different methods of conducting an undrained stability analysis in LEM. The example consists of an external, 5 m wide strip load (e.g. a new embankment) placed on a horizontal soil deposit. The soil consists of a 0.5 m thick dry crust, below which lies a normally consolidated soft clay layer. The ground water table is at the border of the dry crust and clay layers.

The assumed soil properties are shown in Table 21.1. For predicting the HSU strengths, it was assumed that $K_{0NC} = 1 - \sin\varphi' = 0.5$. The parameter value $\lambda/\kappa = 3.0$ is somewhat "typical" of values that often are obtained in data fitting or back-calculation scenarios using HSU (Lehtonen 2015).

A predetermined circular slip surface of 20 slices was used (Fig. 21.3a). The method used was Bishop's Simplified (Bishop 1955). Bishop's Simplified was

Table 21.1 Soil parameters

	s_u (kPa)	φ'	c' (kPa)	γ (kN/m^3)	OCR	HSU parameter: λ/κ
Dry crust	30	n/a	n/a	17	n/a	n/a
Clay	n/a	30°	0	15	1	3.0

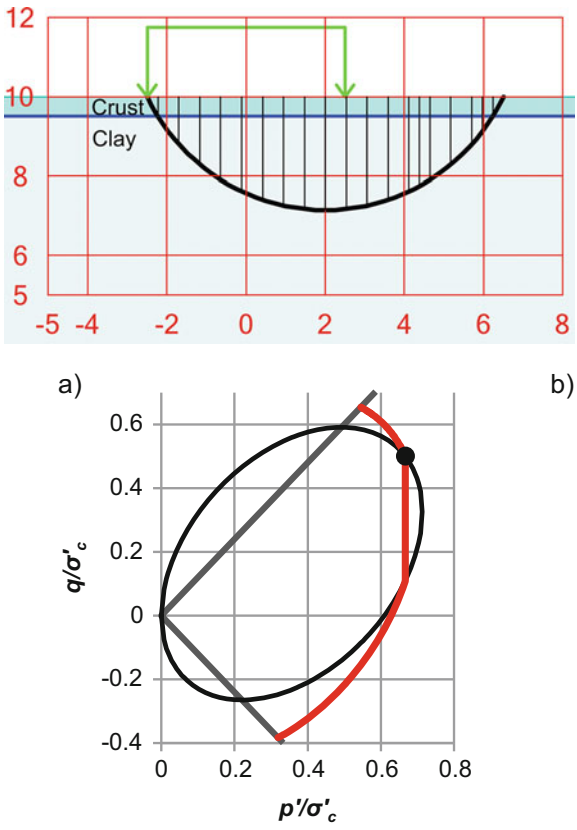

Fig. 21.3 **a** Slip surface geometry. **b** Initial yield surface and triaxial effective stress paths predicted by HSU with the given parameters

selected for convenience and simplicity. With the given circular slip surface, rigorous methods would have given nearly the same results. In the calculations, the applied external load q_{app} was varied. The HSU initial yield surface and triaxial effective stress paths are illustrated in Fig. 21.3b.

The calculations were carried out with the following options:

(A) "Simple traditional": Undrained φ'-c' analysis, $\Delta u = q_{app}$. This represents a typical "rough" calculation that corresponds to linear elastic behaviour (no shear-induced pore pressure). Isotropic strength.

(B) "Enhanced traditional": Undrained φ'-c' analysis, $\Delta u = q_{app} - \Delta p'_f$. For each slice, assumed shear-induced excess pore pressure Δu_s is calculated with the HSU method (prediction of $\Delta p'_f$), see Table 21.2. Anisotropic strength.

(C) HSU, $\varphi = 0$ analysis using the predicted s_u profile, see Table 21.2. In addition, the Δu values needed to obtain the same result (i.e. $\tau_f = s_u$) are calculated (with the method of "forcing" Δu, see previous section). Anisotropic strength. Used as the benchmark result.

(D) HSU, Undrained φ'-c' analysis. Δu at failure is calculated based on changes in vertical stress. Anisotropic strength.

Table 21.2 Initial effective vertical stress σ'_{v0}, HSU predicted s_u values and predicted shear-induced pore pressure Δu_s for the slices in the clay layer

Slice	2	3	4	5	6	7	8	9	10	11	12	13	14	15	16	17	18	19
x (m)	–1.97	−1.44	−0.91	−0.38	0.15	0.68	1.21	1.74	2.26	2.79	3.32	3.85	4.25	4.51	4.91	5.44	5.83	6.10
σ'_{v0} (kPa)	10.3	13.5	15.8	17.5	18.8	19.7	20.3	20.6	20.6	20.3	19.7	18.8	17.9	17.2	15.8	13.5	11.3	9.5
s_u (kPa)	3.3	4.1	4.6	4.8	4.9	4.8	4.8	4.6	4.5	4.3	4.1	3.8	3.6	3.5	3.2	2.7	2.3	1.9
s_u/σ'_{v0}	0.32	0.31	0.29	0.27	0.26	0.25	0.23	0.22	0.22	0.21	0.21	0.20	0.20	0.20	0.20	0.20	0.20	0.20
Δu_s (kPa)	1.4	2.1	2.9	3.7	4.4	5.1	5.6	6.0	6.3	6.4	6.4	6.2	5.9	5.7	5.2	4.5	3.7	3.1

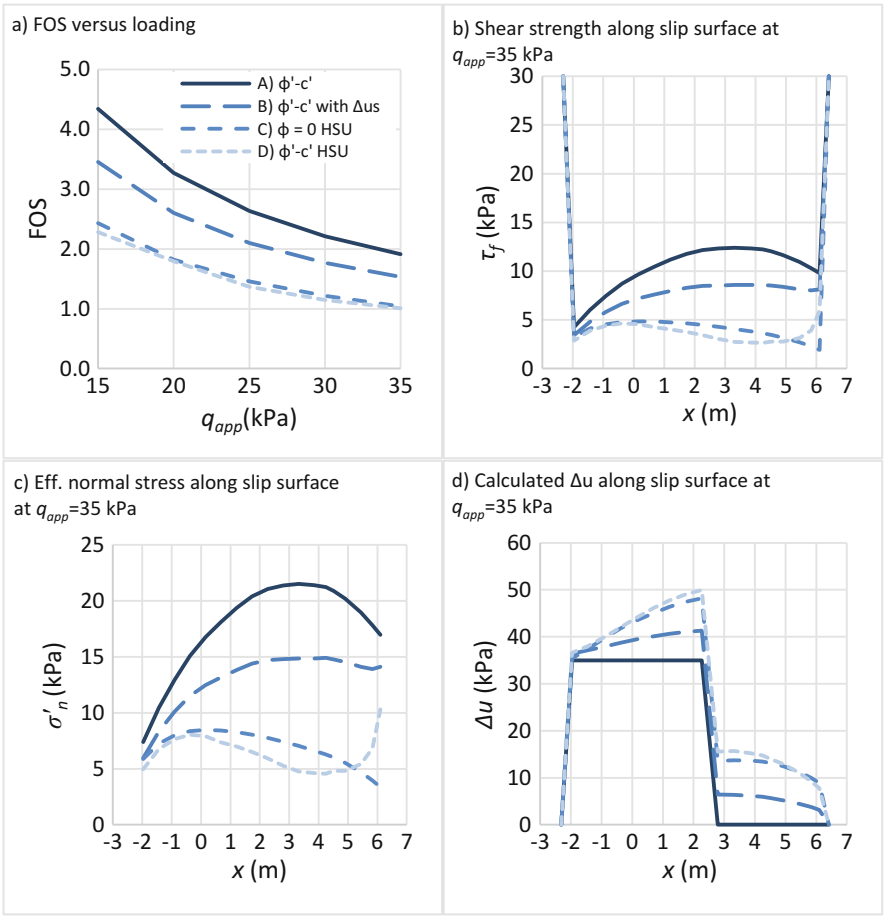

Fig. 21.4 Results of the different analyses. Note that the effective normal stress and pore pressure distributions of the $\varphi = 0$ HSU analysis (C) are obtained from an effective stress HSU analysis where the strength is set as $\tau_f = s_u$ (see Eq. 21.7)

The results for different analyses are shown in Fig. 21.4. Table 21.2 shows the s_u predicted by HSU for each slice bottom, as well as the corresponding shear-induced pore pressure $\Delta u_s = -\Delta p'_f$.

21.5 Discussion

There is a very high discrepancy between the more traditional undrained φ'-c' analyses (A and B), and the HSU analyses (C and D) where strength is fully predicted using an anisotropic effective stress soil model. If the $\varphi = 0$ analysis

is considered the benchmark (as the predicted shear strength distribution along the slip surface is close to available literature values, e.g. Larsson et al. 2007), all of the more "traditional" undrained effective stress analyses overestimate shear strength τ_f and FOS greatly. The strengths are comparable only in the active (left) part of the slip surface.

The results do not converge even when the HSU analyses give FOS values close to unity. This is likely due to unrealistically large total stress levels compared to the initial in situ stress state that is used to determine the HSU s_u values. As shear strength in "traditional" undrained effective stress analyses (A and B) is determined both by mobilised total normal stress and predicted Δu, an "incorrect" total normal stress value results in "incorrect" shear strength.

The HSU effective stress analysis based on stress changes (D) is capable of obtaining very similar results as the corresponding total stress analysis (C). There is however a discrepancy at the passive (right) end of the slip surface due to high total normal stresses there that the method cannot quite take into account.

The example shows that traditional undrained φ'-c' analyses are possibly incapable of giving accurate results. This is due to general difficulties in accurately predicting excess pore pressure in LEM; the overestimation of shear strength when FOS >1 (this may not be observed in the given example); and possible inaccuracies in the total stress distribution that affect the shear strength distribution unless excess pore pressure Δu values are adjusted accordingly.

The HSU method can be used to conduct an undrained effective stress analysis, the results of which are comparable to the corresponding total stress analysis. This requires an altogether different approach to the problem where instead of accurately predicting excess pore pressure Δu, the emphasis is on predicting shear strength τ_f. Excess pore pressure is deliberately calculated "wrongly" to obtain a "correct" shear strength. This however makes the complicated undrained φ'-c' analysis somewhat redundant, as the benchmark undrained shear strength s_u distribution is in any case needed. A much simpler total stress analysis can be done directly using the predicted s_u values.

21.6 Conclusions

This paper has discussed possible pitfalls of undrained effective stress stability analyses, especially in the framework of LEM. A new calculation method Hybrid s_u (HSU) has been developed partially to address these issues.

A theoretical example shows that traditional undrained effective stress analyses may be quite inaccurate when compared to a benchmark $\varphi = 0$ analysis. The HSU method can be used to conduct an undrained φ'-c' analysis that gives the same "correct" results as a total stress analysis. This is shown as a theoretical example.

While no broad conclusions should be made based on a single example, it can be stated that utmost care needs to be taken with undrained effective stress analyses. In

fact, they should likely be avoided if a corresponding short-term total stress analysis can be reasonably conducted. This of course requires either accurate laboratory measurements of s_u, or accurate s_u prediction based on effective strength parameters.

Acknowledgments The authors would like to gratefully thank the reviewer, Professor Leena Korkiala-Tanttu (Aalto University, Finland), for her essential input and comments. This research has been made possible by funding from Finnish Transport Agency.

References

Bishop AW (1955) The use of the slip circle in the stability analysis of slopes. Géotechnique 5(1):7–17

Krahn J (2003) The 2001 R.M. Hardy lecture: the limits of limit equilibrium analyses. Can Geotech J 40(3):643–660

Larsson R, Sällfors G, Bengtsson P-E, Alén C, Bergdahl U, Eriksson L (2007) Skjuvhållfasthet – utvärdering i kohesionsjord. Statens geotekniska institut (SGI), Linköping

Lehtonen V (2015) Modelling undrained shear strength and pore pressure based on an effective stress soil model in Limit Equilibrium Method. Dissertation, TUT Publication 1337, Tampere University of Technology

Lehtonen V, Länsivaara T (2013) Two methods for estimating excess pore pressure in LEM. In: Proceedings of the 18th international conference on soil mechanics and geotechnical engineering, 2–6 September 2013, Paris, p 755–758

Lehtonen V, Länsivaara T (2016) Back-calculation of the Saint-Alban A test embankment with a new modelling approach in LEM. In: Proceedings of the 17th Nordic geotechnical meeting, 25–28 May 2016, Reykjavik, p 691–699

Roscoe K, Burland, J B (1968) On the generalized stress-strain behaviour of wet clay. Engineering plasticity, p 535–609

Wheeler SJ, Näätänen A, Karstunen M, Lojander M (2003) An anisotropic elastoplastic model for soft clays. Can Geotech J 40(2):403–418

Wood DM (1990) Soil behaviour and critical state soil mechanics. Cambridge University, Cambridge

Chapter 22
Recommended Practice for the Use of Strength Anisotropy Factors in Stability Calculations

Vikas Thakur, Vidar Gjelsvik, Odd Arne Fauskerud, Stein Christensen, Frode Oset, Margareta Viklund, and Stein-Are Strand

Abstract This paper presents a recommended practice for the use of strength anisotropy in stability calculations. The recommendations are based on laboratory data from high quality block samples collected by NGI from more than 20 sites. The strength anisotropy was correlated against natural water content, OCR, sensitivity, plasticity index and clay contents. Despite some scatter in data, the paper presents correlations to estimate strength anisotropy for Norwegian clays. A benchmark stability calculation has been done to illustrate the overall impact of various anisotropy factors on the factor of safety.

V. Thakur (✉)
Department of Civil and Environmental Engineering, Norwegian University of Science and Technology (NTNU), Trondheim, Norway
e-mail: vikas.thakur@ntnu.no

V. Gjelsvik
Norwegian Geotechnical Institute (NGI), Oslo, Norway
e-mail: vidar.gjelsvik@ngi.no

O.A. Fauskerud
Multiconsult AS, Oslo, Norway
e-mail: odd.arne.fauskerud@multiconsult.no

S. Christensen
SINTEF Building and Infrastructure, Oslo, Norway
e-mail: stein.christensen@sintef.no

F. Oset
Norwegian Public Roads Administration (NPRA), Oslo, Norway
e-mail: frode.oset@vegvesen.no

M. Viklund
Norwegian National Rail Administration (NNRA), Oslo, Norway
e-mail: margareta.viklund@banenor.no

S.-A. Strand
Norwegian Water Resources and Energy Directorate, Oslo, Norway
e-mail: sas@nve.no

V. Thakur et al. (eds.), *Landslides in Sensitive Clays*, Advances in Natural and Technological Hazards Research 46, DOI 10.1007/978-3-319-56487-6_22

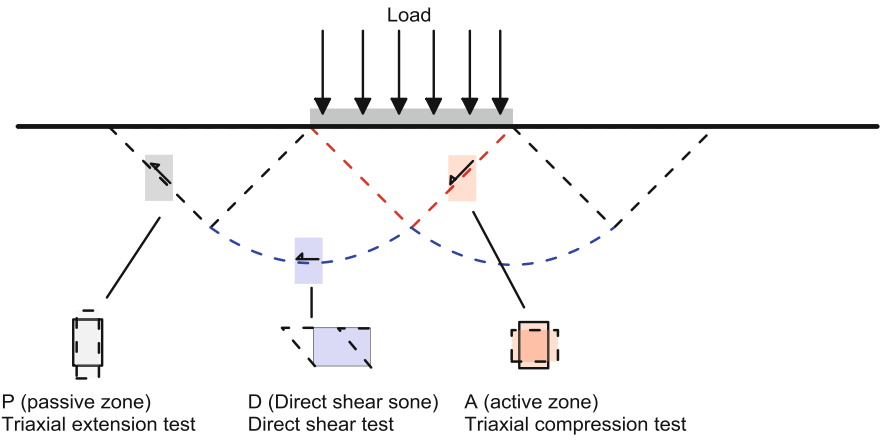

Fig. 22.1 An illustration of strength anisotropy in stability problems

22.1 Introduction

Scandinavian sensitive clays are highly anisotropic in nature. Therefore, their undrained shear strength (c_u) is not identical when they are subjected to a compression/active (A), direct shear (D) and extension/passive (P) loading, see Fig. 22.1. Strength anisotropy of sensitive clays plays a significant role in many geotechnical applications, including slope stability analysis and bearing capacity of shallow and deep foundations. In stability analysis of an undrained situation, the ADP-analysis has therefore become increasingly common to account for the strength anisotropy of sensitive clays. The selection of strength anisotropy factors (c_{uE}/c_{uC} and c_{uD}/c_{uC}) should be site-specific and deduced from high quality soil samples. Here c_{uC}, c_{uE} and c_{uD} refer to the undrained shear strength obtained from active/compression (C), passive/extension (E) and direct shear (D) tests. More than 40 years ago, Berre and Bjerrum (1973) reported a trend between strength anisotropy factors and plasticity index based on a field vane test. However, the development over the years has been such that empirical values for strength anisotropy is preferred, often with inadequate references to empirical correlations. An agreed code of practice for the use of strength anisotropy felt lacking. To overcome this issue, a practice has been developed by the authors of this paper on behalf of their respective organizations. Main findings and recommendations are comprehensively presented in this paper.

22.2 Data Collection and Correlations

NGI's database for block samples has been used as the basis for this study. The database contains samples from a total of 20 different locations in Norway. Overview of the tested material is well documented in the literature, e.g. Karlsrud

and Hernandez-Martinez (2013). In each individual sample, the anisotropy factors (c_{uD}/c_{uC} and c_{uE}/c_{uC}) are calculated using samples from the exact same depth and with the same consolidation pressure. High quality test results only, i.e. sample quality class 1 and 2, according to Lunne et al. (2006), were considered in this study. All values of c_{uD}, c_{uE} and c_{uC} used in this study refer to peak strength.

22.2.1 Correlations

The majority of block samples in the database had the natural water content (w) between 30 and 45% and the plasticity index (I_p) between 5 and 20%, which is the most typical area for Norwegian clays. The correlations parameters considered are the plasticity index (I_p), the natural water content (w), the over consolidation ratio (OCR), the clay content (<2 μ), the sensitivity (S_t) and the liquid limit (w_L) (see Fig. 22.2). There are relatively few datasets with higher w and I_p, and they are only represented by the Onsøy clay.

Figure 22.2 presents the anisotropy ratio (c_{uD}/c_{uC} and c_{uE}/c_{uC}) against these parameters. The relationship seems to be less dependent on the OCR, clay content and sensitivity. As described in the literature, I_p is affected (reduced) with increasing soil sensitivity (S_t) through leaching of salt. This may be part of the reason for the wide scatter in the data of clay with high sensitivity and low plasticity, namely, that some of these originally had a higher I_p and thus behave accordingly.

It is worth noticing that the dependencies between anisotropy factors and w and I_p show similar trends. The trend line for anisotropy factors and w seems to a greater extent controlled only by a few data points concerning the high values of w. Therefore, I_p has been selected as the main parameter for the correlation in the recommendation for the strength anisotropy ratio. However, other plots are also shown in Fig. 22.2 as the basis for the review.

22.3 Recommendations

Based on the correlations, recommendations are shown in Fig. 22.3 and Table 22.1. The following assumptions are the basis for these recommendations:

- Location-specific high-quality samples are not available.
- The undrained compression shear strength (c_{uC}) has been selected as a carefully estimated mean value.
- Recommendations are applicable to all Norwegian clays (sensitive and non-sensitive clays).

The importance of the strength anisotropy factors in the results of the stability calculation is considered to be relatively low (variation in the material factor of 4–8%). This aspect is discussed later. However, there is good reason to urge greater

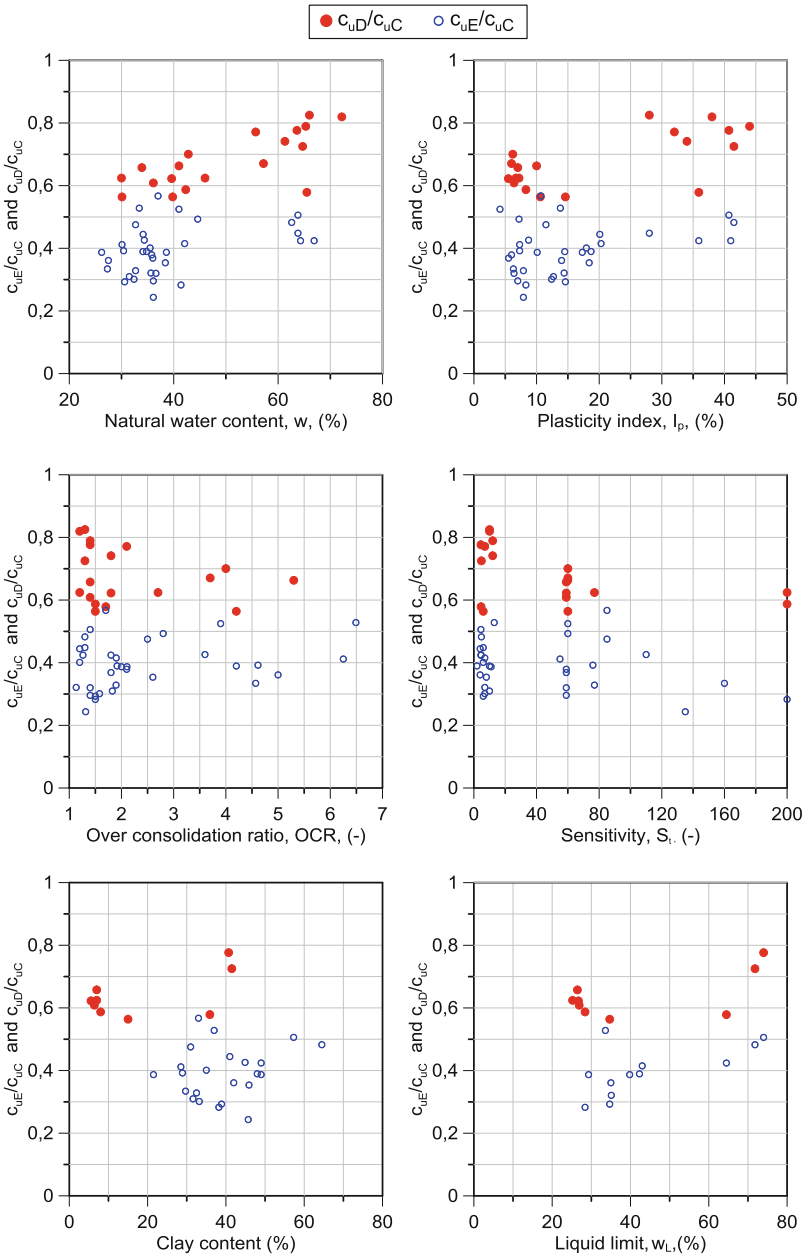

Fig. 22.2 Dependencies between the strength anisotropy parameters and: (**a**) natural water content, (**b**) plasticity index, (**c**) over consolidation ratio, (**d**) sensitivity, (**e**) clay content, and (**f**) liquid limit.

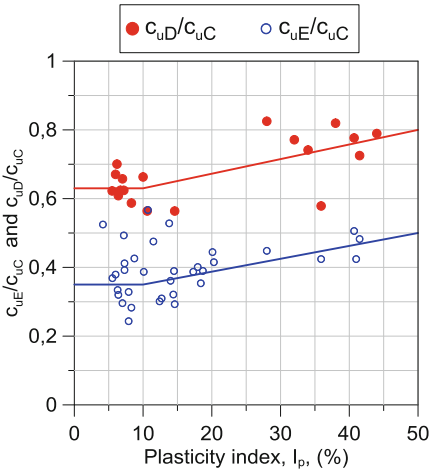

Fig. 22.3 Recommended trend lines to estimate the strength anisotropy factors. The *red* and *blue* trend lines are for estimate c_{uD}/c_{uC} and c_{uE}/c_{uC}, respectively. Equations for these lines are provided in Table 22.1

Table 22.1 Recommendation for the strength anisotropy factors

I_p	c_{uD}/c_{uC}	c_{uE}/c_{uC}
$I_p \leq 10\%$	*0.63*	*0.35*
$I_p > 10\%$	*0.63 + 0.00425 * (I_p−10)*	*0.35 + 0.00375 * (I_p−10)*

I_p is in % in these formulas

care in selecting the anisotropy factors. Normally, the characteristic value of c_{uC} has the greatest impact on the result and should therefore have the greatest focus. This aspect is highlighted in detail in the discussion chapter.

22.4 Discussions on the Recommended Practice

Norwegian clays are sensitive in nature. Accordingly, the soil characterisation of Norwegian clays is categorised based on their S_t values. The threshold S_t is set at 15 to define whether a Norwegian clay is sensitive ($S_t > 15$) or non-sensitive ($S_t \leq 15$) (Karlsrud et al. 2005). The c_{uD}/c_{uC} and c_{uE}/c_{uC} ratio is generally somewhat lower for clays having $S_t > 15$ than for those with low sensitivity for the OCR on 1–2, while other plots may indicate that there is little difference or that this is the appearance of different I_P. This study has not found the basis for distinguishing between sensitive and non-sensitive clays in connection with the c_{uD}/c_{uC} and c_{uE}/c_{uC} ratio, so this recommendation is valid in general.

The magnitude of the structural effects in natural clays is reflected by their sensitivity (e.g. Skempton and Northey 1952). On the one hand, there is a common belief, which is logical, that the c_{uD}/c_{uC} and c_{uE}/c_{uC} ratio should be dependent on soil structure. While this study finds no direct connection between soil sensitivity and

c_{uD}/c_{uC} and c_{uE}/c_{uC} ratio, it is possible that c_{uC}, c_{uD} and c_{uE} individually account for the soil structure. However, the ratio of these strength values, i.e. c_{uD}/c_{uC} and c_{uE}/c_{uC}, nullifies any noticeable effect.

Based on a limited number of test results, Berre and Bjerrum (1973) and Ladd et al. (1977) proved that soil strength anisotropy decreases with I_p. This study too supports their observation. The literature also advocates including other aspects such as clay fraction, clay structure, mineralogy, origin, etc. As mentioned earlier, the c_{uD}/c_{uC} and c_{uE}/c_{uC} ratio is independent of soil sensitivity; therefore, clay structure may have a small influence on the c_{uD}/c_{uC} and c_{uE}/c_{uC} ratio. Moreover, from Fig. 22.2 it can be noted that clay fractions show no correlation with the c_{uD}/c_{uC} and c_{uE}/c_{uC} ratio. On other hand, soil mineralogy may have some significant influence on the anisotropy. To check whether the recommendation made in this study holds true in Norway in general, an exhaustive study was carried out to map the mineralogy of Norwegian clays. Over 100 clay samples were collected from across Norway, and they were analysed for mineral content. This study was performed by Syversen (2013) with the help of Norwegian government agencies and the consulting firms that are involved in soil sampling and soil testing. Figure 22.4 shows that the mineralogical content is relatively uniform throughout Norway. The tested samples contained quartz, feldspar and amphibole, but they were dominated by illite and chlorite. Analyses of the clay fraction showed that it essentially consisted of illite and chlorite, with less amphibole and quartz content. In summary, it can be said that clay mineral composition differs very little for Norwegian clays in general. Hence, the recommended practice can be considered as applicable to all of Norwegian clays.

Some researchers, e.g. Won (2014), have shown their concern regarding correlating the c_{uD}/c_{uC} and c_{uE}/c_{uC} ratio with $I_{p.}$ They observe that the undrained shear strength is poorly correlated with I_p. However, they agree that a correlation between the c_{uD}/c_{uC} and c_{uE}/c_{uC} ratio and I_p exists for less plastic and more sensitive Scandinavian clays. Won (2014) gathered over 203 pairs of data for soils from 14 different countries. For the sake of comparison, our recommendation for c_{uE}/c_{uC} is

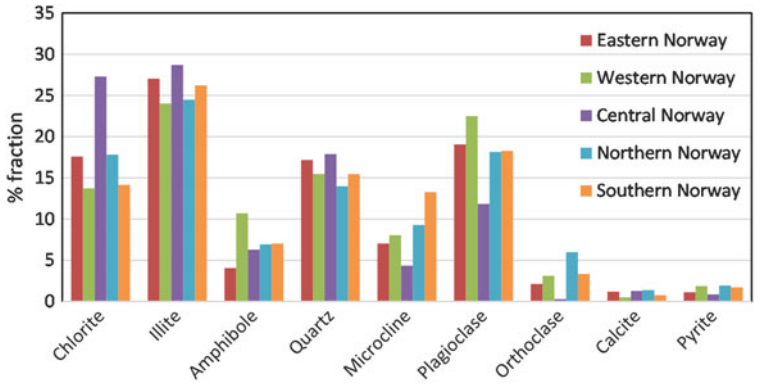

Fig. 22.4 Regional variation of minerology of Norwegian clays based on Syversen (2013)

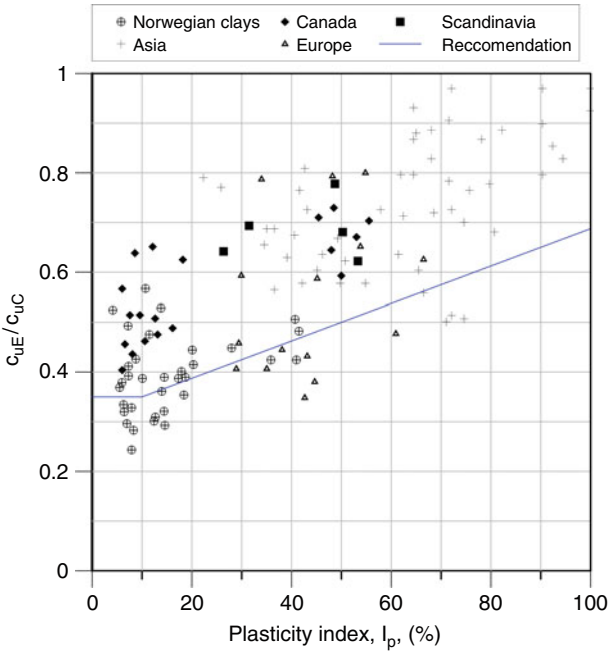

Fig. 22.5 A comparison between the recommendation for the Norwegian clays and other soils reported by Won (2014)

plotted against I_p together with these data. From Fig. 22.5 it can be noticed that the recommended values of c_{uE}/c_{uC} for Norwegian clays are rather conservative for other soils. Moreover, despite a large scatter, c_{uE}/c_{uC} seems to be positively correlated with I_p for all soils.

The recommendations are obtained by weighing several aspects against each other, such as statistical variation for non-site-specific samples, rewards for the site-specific sampling with high quality, importance of the strength anisotropy factors to the calculation results and experience with the current practice. Since the basis for the general recommendation is based on non-site-specific samples, it may be natural to implement some conservatism in the recommended values. The impact of the average undrained shear strength values (c_u) on a calculation depends on both the chosen c_{uC}, c_{uD}/c_{uC} and $c_{uE}/_{uC}$;

$$\overline{c_u} = c_{uC}\left(A\frac{c_{uC}}{c_{uC}} + D\frac{c_{uD}}{c_{uC}} + P\frac{c_{uE}}{c_{uC}}\right) \tag{22.1}$$

Where A, D and P are the portion of the surface: the active, direct and passive zone, respectively, c_{uC} is the single parameter that most affects the average undrained shear strength. Therefore, it is considered sensible to put resources into determining this correctly, if possible, and that incentive for high quality sampling

for triaxial testing to obtain c_{uC}. As in the block test, the data show a very large spread on the c_{uD}/c_{uC} and c_{uE}/c_{uC} ratio. However, the average strength has far less diversification. c_{uC} is first determined and used as a constant in equation.

22.5 Implications of the Variations in the Strength Anisotropy Ratio

It must be realised that there is a large scatter in the dataset selected for this study. The scatter is apparently the greatest for the low plastic clays. To assess the implication of the recommended trend line for c_{uD}/c_{uC} and c_{uE}/c_{uC}, a simple stability analysis for an idealized case was conducted. A 15 m high homogeneous slope with an inclination of 1: 4.5 was considered. The c_{uD}/c_{uC} and c_{uE}/c_{uC} factors varied as shown in Fig. 22.6 along with the slope geometry and the active undrained shear strength profile. Three composite sliding surfaces (SS1, SS2 and SS3) and a circular slip surface (SS4) were investigated. The results of the calculations are compiled in Table 22.2.

The simple calculations show that the variation of the strength anisotropy factors in the range ($c_{uD}/c_{uC} = 0.65$ $c_{uE}/c_{uC} = 0.33$) and ($c_{uD}/c_{uC} = 0.60$ $c_{uE}/c_{uC} = 0.30$)

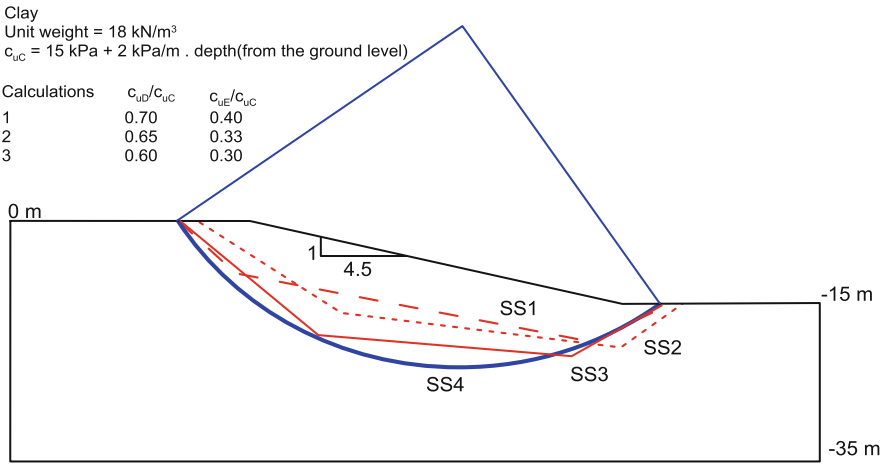

Fig. 22.6 Slope geometry and the input parameters used in the calculations

Table 22.2 Partial factors (γ_M) for calculation 1–3

Calculation	SS1 γ_M	SS2 γ_M	SS3 γ_M	SS4 γ_M
1	1.56	1.48	1.38	1.34
2	1.50	1.42	1.32	1.29
3	1.44	1.37	1.27	1.24

Table 22.3 Change ($\Delta\gamma_M$) in the partial factors between the calculations

	SS1	SS2	SS3	SS4
Between	$\Delta\gamma_M$	$\Delta\gamma_M$	$\Delta\gamma_M$	$\Delta\gamma_M$
1–2	3.8%	4.1%	4,3%	3.7%
1–3	7.7%	7.4%	8%	7.5%
2–3	4.2%	3.6%	3.9%	4%

leads to a 4% change in the calculated partial factor (**γM**). The size of the change is a direct result of the relative distribution between the active, direct and passive zone for the sliding surfaces. For the stability analysis of slopes, the passive zone normally constitute a small percentage of the sliding surface. For the infinite slopes, the share of the shear surface that is located in the area of the direct shear could constitute the main part of the shear surface. For most practical purposes, as illustrated here, the variation range of the calculated partial factor with the ADP factors that are selected for the calculation for two and three falls within the 4–8% (Table 22.3).

22.6 Conclusions

This paper presents a recommended practice for the use of strength anisotropy factors as a function of plasticity index. The recommendations were deduced from high quality block samples. The dependency of strength anisotropy was investigated against natural water content, OCR, sensitivity, plasticity index and clay contents. Despite some scattered in data, the paper presents correlations, based on plasticity index, to estimate strength anisotropy for Norwegian clays. This work strongly recommends local sampling and laboratory testing with quality to obtained the c_{uE}/c_{uC} and c_{uD}/c_{uC} ratio. In absence of this one shall opt for an empirical solution. The work further suggests that c_{uE}/c_{uC} and c_{uD}/c_{uC} ratio shall be 0.63 and 0.35 for low plastic Norwegian clays. Empirical equations to obtained c_{uE}/c_{uC} and c_{uD}/c_{uC} is proposed for medium and high plastic Norwegian clays. Based on the mineralogical investigations, the recommendations are found to be valid for all types of Norwegian clays regardless of their location and sensitivity. A benchmark stability calculation has been done to illustrate the overall impact of various anisotropy factors on the factor of safety. The choice of the c_{uD}/c_{uC} and c_{uE}/c_{uC} ratio within reasonable values has relatively little effect (4–8%) on the calculation result. Thus, it is recommended that the c_{uD}/c_{uC} and c_{uE}/c_{uC} ratio give an average trend line, i.e. a conservative estimate.

Acknowledgements The cooperative research program «Natural hazards: Infrastructure for Floods and Slides (NIFS)» by the Norwegian Public Roads Administration, the Norwegian National Rail Administration and the Norwegian Water Resources and Energy Directorate is acknowledged for the support. The authors also wish to express their gratitude to the reviewer Dr. Ivan Depina for his valuable comments.

References

Berre T, Bjerrum L (1973) Shear strength of normally consolidated clays. In: Proceedings 8th ICSMFE, Moscow 1. pp 39–49

Karlsrud K, Hernandez-Martinez FG (2013) Strength and deformation properties of Norwegian clays from laboratory tests on high-quality block samples. Can Geotech J 50(12):1273–1293

Karlsrud K, Lunne T, Kort DA et al (2005) CPTU correlations for clays. In: 16th ICSMFE 16, 2. pp 693–702

Ladd CC, Foott R, Ishihara K et al (1977) Stress deformation and strength characteristics. In: 9th ICSMFE, Tokyo, 2. pp 421–424

Lunne T, Berre T, Andersen KH et al (2006) Effects of sample disturbance and consolidation procedures on measured shear strength of soft marine Norwegian clays. Can Geotech J 43: 726–750

Skempton AW, Northey RD (1952) Sensitivity of clays. Geotechnique 3(1):40–51

Syversen FS (2013) Et studie av den mineralogiske sammensetningen i norske sensitive leirer. Mater thesis. UiO

Won JY (2014) Anisotropic strength ratio and plasticity index of natural clays. In: Proceedings 18th ICSMGE, Paris, 1. pp 445–448

Chapter 23
On the Benefits of Incorporating Anisotropy in Stability Analyses in Sensitive Clays

Mats Karlsson and Minna Karstunen

Abstract During construction of E45 – Norge/Vänerbanan, analyses of an area located in Agnesberg, just north of Gothenburg, showed an evaluated factor of safety significantly less than prescribed in the codes for both the new main road E45 and the new railway Norge/Vänerbanan. The road and railway are situated very close to each other, just next to the Göta River that complicates the evaluation of the safety factor. The empiricism commonly used was questioned due to an unfamiliar change in undrained shear strength in the profile. Consequently, an extensive field and laboratory campaign was conducted to establish a more accurate and reliable strength profile. The extensive laboratory programme contained a number of direct simple shear tests, as well as triaxial tests in both compression and extension to be able to determine the strength anisotropy in the area. The laboratory study showed that the soft clay in the area was more anisotropic than anticipated, which was more favourable in the studied case regarding the stability. This lead to a new anisotropic function to be used in evaluation of the safety factor. This combined with a general increase in undrained shear strength for the entire profile highlights the potential cost savings resulting from extensive site investigation that incorporates evaluation the magnitude of strength anisotropy.

23.1 Introduction

In the Göta River valley in the Western part of Sweden, 80 km of a new motorway and a new high speed railway was constructed between Göteborg and Trollhättan during the period 2007–2012, at a cost of approximately €1.1 billion. The ground condition consists mainly of deep layers of soft, highly plastic clay, which was deposited in marine conditions some 5,000–10,000 years ago. Slope stability is a major challenge in all infrastructure projects, when building on soft sensitive clays. During construction of E45 – Norge/Vänerbanan, analyses of an area located in

M. Karlsson (✉) • M. Karstunen
Department of Civil and Environmental Engineering, Chalmers University of Technology, Gothenburg, Sweden
e-mail: mats.karlsson@chalmers.se; minna.karstunen@chalmers.se

V. Thakur et al. (eds.), *Landslides in Sensitive Clays*, Advances in Natural and Technological Hazards Research 46, DOI 10.1007/978-3-319-56487-6_23

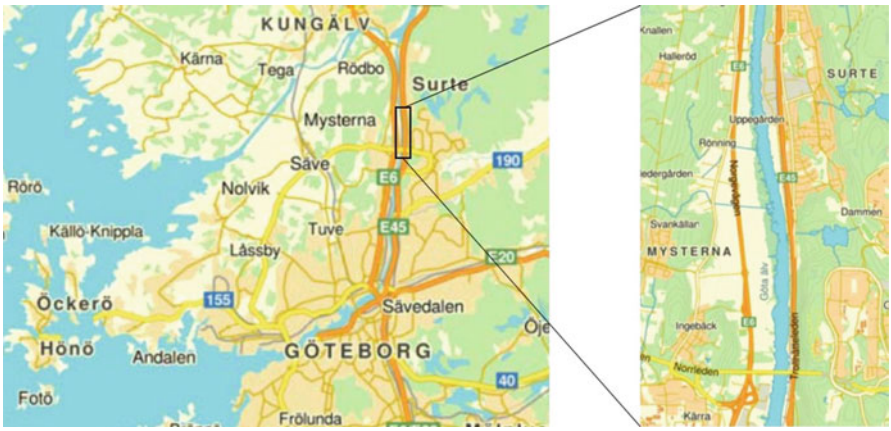

Fig. 23.1 Overview of the area (www.hitta.se)

Agnesberg, just north of Gothenburg see Fig. 23.1, showed an evaluated factor of safety significantly less than prescribed by the Swedish authorities for both the new main road E45 and the new railway Norge/Vänerbanan. The road and railway are located very close to each other, just next to the Göta River that complicates the evaluation of the safety factor. After the initial laboratory and field investigations the empiricism commonly used, see e.g. Larsson et al. (2007), was questioned due to an unfamiliar change in undrained shear strength in the profile. Approximately between 15 and 20 m depth in the soil profile the increase in the undrained shear strength suddenly dropped, to come regain the increase after about 20 m, see Fig. 23.2.

During the design process of the road E45 and railway Norge/Vänerbanan, part Agnesberg-Bohus, substantial field and laboratory work was undertaken to determine the geotechnical properties. Parallel with this, an additional investigation of the stability in the area was undertaken due to the low safety factor for the stability in the area, especially close to the river. This investigation included additional field and laboratory investigations that resulted in the appreciation of the anisotropic behavior of the clay. It also included an in-depth investigation of the pore pressure profile in the area, and the mapping of quick clay areas that resulted in a measure against secondary landslides initiating from an underwater landslide in the river.

23.2 Ground Conditions

The geology of the area is characterized by outcropping bedrock with deep deposits of soft, slightly overconsolidated, clay. Below the clay there is generally a few metres thick layer of frictional material. The clay is made of glacial and post glacial clays. The unit weight varies between 14.5 and 17.0 kN/m^3. The water content is about 100% in top, with a decrease to around 70% at a depth of 30 m. The liquid limit is of same order, but slightly smaller in the upper 5–10 m. The

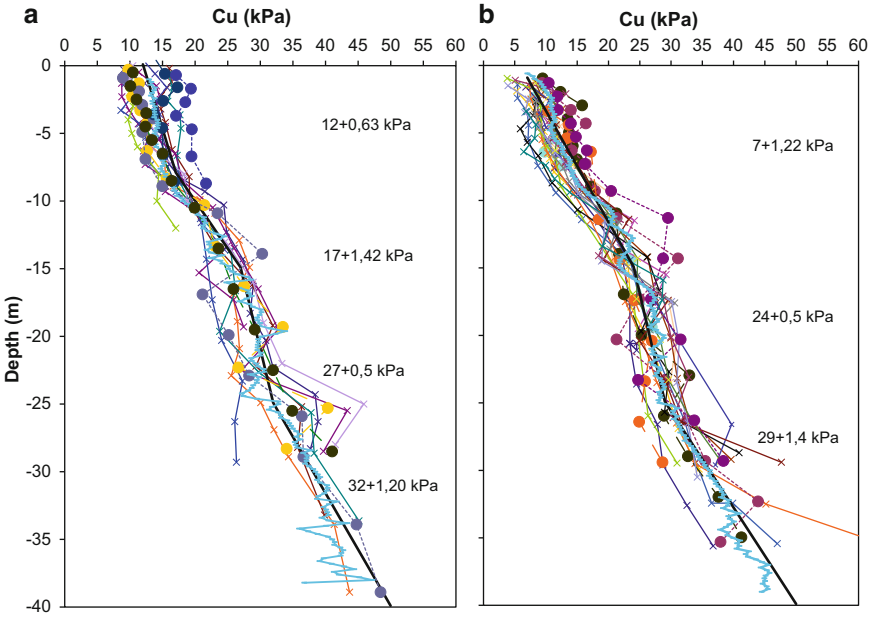

Fig. 23.2 Undrained shear strength, c_u, versus depth in (**a**) around the road and railway embankments and in (**b**) close to the river from CPT (*solid line*), field vane (*solid line* with ×) and fall-cone (*dotted line* with •). *Solid black line* is the evaluated undrained shear strength

clay-sized particle content is in most cases above 50%. The ground water table is approximately 0.5–1 m below the ground surface, and the pore pressure profile is more or less hydrostatic. The hydraulic conductivity is about $5–10 \bullet 10^{-10}$ m/s. In terms of the undrained shear strength, the area was divided into to two different regions, namely close to the river and at the road and rail embankments. The area studied is approximately 500 m long and 50 m wide. The undrained shear strength profiles for the area close to the river and around the road and railway embankments are shown in Fig. 23.2.

Based on Fig. 23.2, the undrained shear strength is quite different for the two cases, especially in the top part in the area close to the river where the undrained shear strength is about 7 kPa in the top, compared to 12 kPa for the area around the embankments. However, the relative differences between the two reduce with depth.

23.2.1 Evaluation of Initial Safety Factor of Slopes in the Studied Area

During the early stage of the design process, the safety factor for slope stability of both the embankments and slopes close to the river were calculated to be too low. This was based on what one could call the classical approach, i.e. no anisotropy

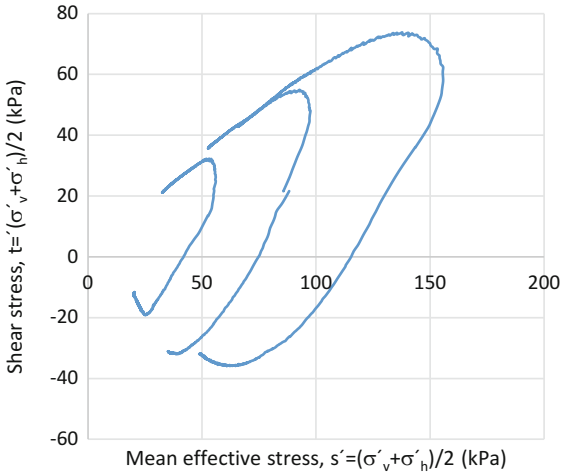

Fig. 23.3 Results from some of the K_0-consolidated undrained triaxial tests in s′-t stress space for three different depths

is included in the calculation of slope stability. In this case the result was that the ground improvement by lime cement technique that had been used around this area, see Alén et al. (2005, 2006) and Olsson et al. (2008), seemed to be insufficient, and perhaps not even feasible in safety aspects. If reinforcement with lime cement columns was deemed insufficient, pre-cast concrete piles would most likely have been the alternative, and hence a much more expensive solution. This lead to an additional study of the slope stability with focus on studying the anisotropic behaviour of the clay in the area.

23.2.2 Additional Laboratory Experiments

The supplementary laboratory tests were carried out at Chalmers University of Technology in a climate controlled geotechnical laboratory with a constant temperature of 7 °C. The additional laboratory tests consisted of eight direct simple shear (DSS) tests and 24 K_0-consolidated undrained triaxial (K_0CU) tests, 12 in compression and 12 in extension. The K_0-consolidation is done by ramping the stresses to a defined stress ratio K_0 from where the undrained shearing starts. In Fig. 23.3 three compression and three extension tests are presented, highlighting the strongly anisotropic behaviour of the clay.

23.2.3 Results from the Additional Laboratory Experiments

The evaluated undrained shear strength from all laboratory tests, i.e. DSS and K_0CU tests, conducted in this additional investigation is summarized in Fig. 23.4. The

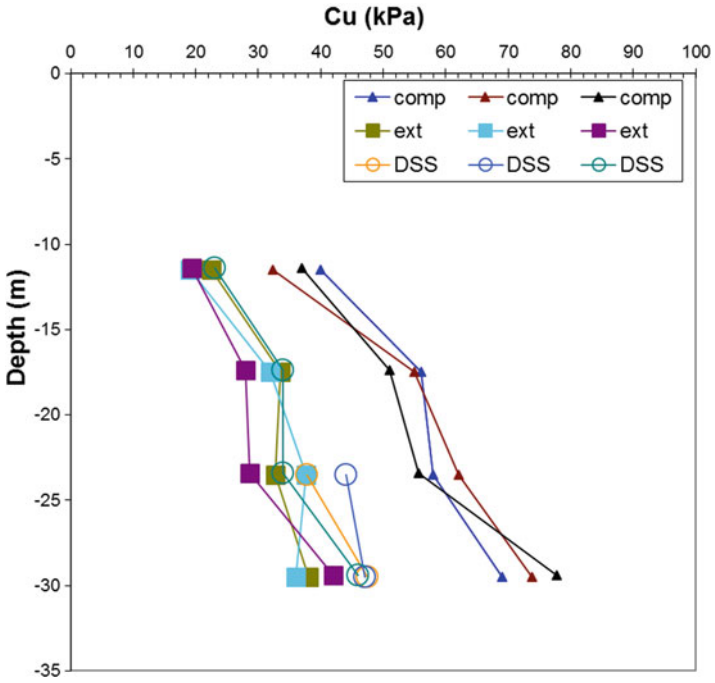

Fig. 23.4 Evaluated results from DSS and K_0CU tests in this additional investigation

proposed anisotropic function that was used in this area was evaluated, mainly based on these laboratory tests and is presented in Fig. 23.5. As shown in Fig. 23.4, the anisotropy in the clay is quite distinct, especially between the compression test and the other two (extension and DSS test). It is also somewhat surprising that the DSS and extension tests has more or less the same magnitude of the undrained shear strength, and in about half the cases the undrained shear strength from extension tests is larger than the DSS tests. The anisotropic function was carefully evaluated and compared with a $K_0{}^{nc} = 0.6$ relation based on the function from (Skredkommissionen 1995). As could be seen in Fig. 23.5, the new anisotropic function is higher at the compression side, but falls in line with the $K_0{}^{nc} = 0.6$ relation according to (Skredkommissionen 1995). The $K_0{}^{nc} = 0.6$ value is assumed from (Skredkommissionen 1995).

The reason for not using a higher value from the anisotropic function is not over estimating the effect of the anisotropy in the soft clay, since this anisotropic function is used as a factor multiplied with the evaluated undrained shear strength, normally representing the DSS value.

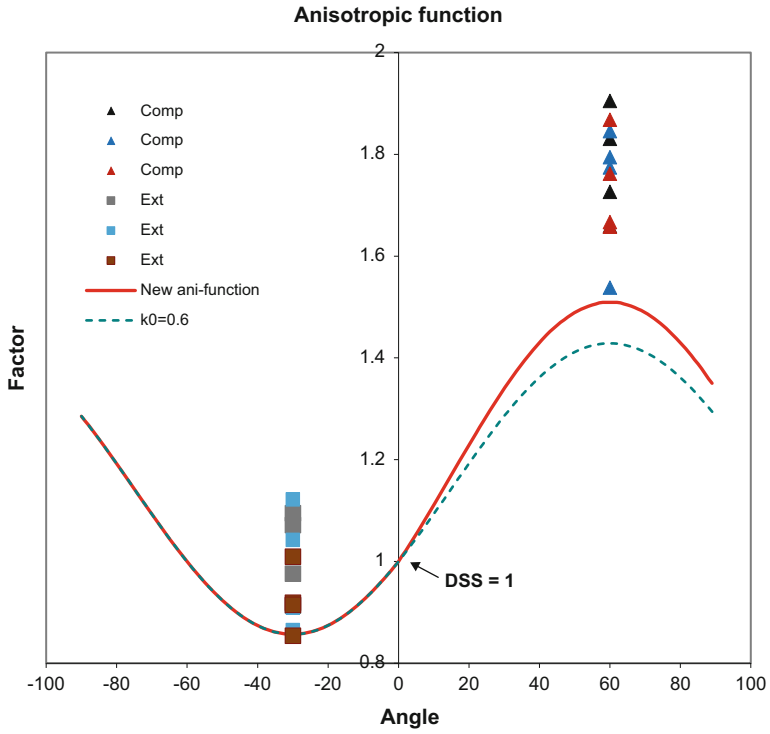

Fig. 23.5 Anisotropic function evaluated from compression and extension tests w.r.t. direct simple shear tests. The *solid line* is the new anisotropic function and the *dotted* is based on $K_0{}^{nc} = 0.6$ relation according to Skredkommissionen (1995)

23.3 Evaluation of Slope Stability Including Anisotropy

In the beginning of the design process the use of lime cement columns was considered to be insufficient for an acceptable safety factor for the slopes close to the river and the road and railway embankments. After this additional investigation, the proposed new anisotropic function was used together with an evaluation of possible secondary landslide due to a possible underwater landslide in the river (Johansson 2010). The influence area from a secondary landslide due to a possible underwater landslide in the river is evaluated from a factor, n, times the height of the underwater slope (h), see Fig. 23.6. For sensitivity higher than 100 a factor n = 15 is used.

With the new anisotropic function together with reinforcement of lime cement columns, the safety factor for the new road and railway was evaluated to be in acceptable range with respect of the slope stability. For the use of lime cement columns as reinforcement in the soil, it was required that they should be installed in continues walls with a predefined distance apart perpendicular to the embankment, depending on load from embankments and initial safety factor of the slopes. For the

Sensitivity	Factor n
10	2
20	5
50	10
100	15

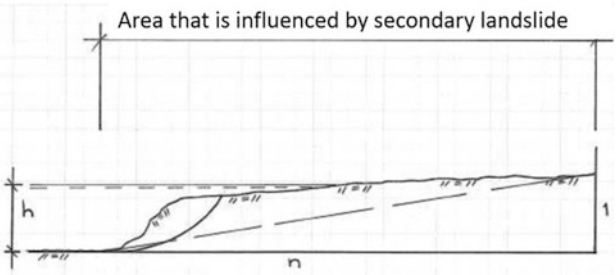

Fig. 23.6 Influence area due to secondary landslide (Johansson 2010)

area where the lime cement columns where installed, a volume average technique is used to establish a mean value of the soil strength. However, the safety factors for the underwater slopes was accepted to be lower, as long as the possible secondary landslide did not influence the new road and railway constructions (Johansson 2010).

23.4 Conclusions

With a slightly more field and laboratory investigation together with an appropriate analyses of the data in this project, the reinforcement with lime cement column instead of pre-cast concrete piles could be used, resulting in significant savings in terms of money and embodied CO_2. This paper demonstrates that if anisotropy is included in assessing and modelling the soil strength in the stability assessment of natural slopes, large cost savings could be achieved. Ideally, considering any future scenarios such as the possible change in pore pressure due to e.g. climate change, it would be advisable to perform the analyses with an anisotropic stress based model, using e.g. finite elements.

Acknowledgements The financial support by Trafikverket (TrV) is greatly acknowledged. The authors would acknowledge the contribution from Jan Ekström and Anders Hallingberg from TrV, Per-Evert Bengtsson from Swedish Geotechnical Institute and Göran Sällfors and Claes Alén from Chalmers University of Technology. Finally, we would like to thank Prof. Tim Länsivaara for his valuable input to improve this paper.

References

Alén C, Baker S, Ekström J, Hallingberg A, Svahn V, Sällfors G (2005) Test embankments on lime/cement stabilized clay. In: Proceedings of deep mixing '05. Stockholm, pp 213–219

Alén C, Sällfors G, Bengtsson P-E, Baker S (2006) Test embankments Rv 45/Nordlänken, Embankments on lime/cement stabilized soil. The Swedish Deep stabilization Research Centre, Linköping

Johansson L (2010) E45 – Norge/Vänerbanan delen Agnesberg – Bohus Totalstabilitetsutredning delen 1/800–3/000. Bana Väg i Väst, Göteborg

Larsson R, Sällfors G, Bengtsson P-E, Alén C, Bergdahl U, Eriksson L (2007) Shear strength – evaluation of cohesion soil. Swedish Geotechnical Institute, Linköping

Olsson M, Edstam T, Alén C (2008) Some experiences from full-scale test embankments on floating lime-cement columns. In: Karstunen M, Leoni M (eds) Proceedings of the second international workshop on geotechnics of soft soils. Glasgow, pp 77–85

Skredkommissionen (1995) Anvisningar för släntstabilitetsutredningar. Rapport 3:95. Linköping

Chapter 24
Development and Application of a Regional Slope Stability Assessment Screening Tool

Brian D. Carlton, Katherine Price, Maarten Vanneste, and Carl Fredrik Forsberg

Abstract This article describes the development of a screening tool to estimate factors of safety and probabilities against slope failure for static and pseudo-static analyses, as well as seismically induced permanent displacements, for both onshore and offshore slopes. The screening tool combines geophysical and geotechnical data to rapidly assess and identify potentially unstable regions over large areas. The results allow a quick, objective, and logical rationale for selecting regions to perform more in-depth and detailed slope stability analyses, and/or areas to avoid when selecting locations or paths for future infrastructure development. We apply the screening tool to part of the continental slope offshore the Lofoten islands, Norway.

24.1 Introduction

Landslides are a major threat to human life and infrastructure in many regions of the world. However, due to time and budget constraints, it is not practical to conduct advanced numerical analyses for every possible slope within a given study area. Therefore, it is important to select the most critical slope(s) based on the project criteria. In some cases, the most critical slopes are obvious; however, in many cases they are not and some sort of screening is necessary to select them. This screening usually consists of selecting the steepest slopes closest to the development area. However, this approach does not take into account sediment thickness, soil strength, excess pore pressure, or other geomechanical parameters that could affect slope stability.

B.D. Carlton (✉) • M. Vanneste • C.F. Forsberg
Norwegia Geotechnical Institute (NGI), Oslo, Norway
e-mail: brian.carlton@ngi.no; maarten.vanneste@ngi.no; carl.fredrik.forsberg@ngi.no

K. Price
University of Washington (UW), Seattle, USA
e-mail: katherine.price@uw.edu

V. Thakur et al. (eds.), *Landslides in Sensitive Clays*, Advances in Natural and Technological Hazards Research 46, DOI 10.1007/978-3-319-56487-6_24

Lee and Edwards (1986) were one of the first to suggest a method for regional evaluation of slope stability for offshore slopes. They used a modified version of the pseudo-static infinite slope method (Morgenstern 1967) to estimate the critical earthquake accelerations or wave heights to initiate failure for slopes offshore Alaska and California. Lee et al. (1999) employed a similar methodology within a Geographic Information System (GIS) framework to evaluate the seismic stability of Eel margin offshore California.

The screening tool developed in this study uses a similar infinite slope methodology to estimate static and pseudo-static factors of safety against slope failure. However, it is unique in that it also predicts the probability of failure for both static and dynamic loading, calculates seismically induced permanent displacements, and includes excess pore pressure as an input parameter allowing for parametric studies. In addition, the screening tool is applicable to both onshore and offshore sites under drained and undrained conditions. This paper describes the development of the screening tool and its application to part of the continental slope offshore the Lofoten Islands, Norway.

24.2 Formulation of the Screening Tool

The screening tool combines geophysical and geotechnical data to quickly assess potentially unstable areas. It discretises the three-dimensional topographic and soil properties data into equally sized blocks. For blocks on the soil surface, the program calculates the slope angle as the angle between the highest and lowest edge points of the surface face. Blocks below the surface take the slope angle of the block directly above. The user can define the block widths and depths independently. The minimum block width depends on the resolution of the topographic data. The maximum block depth is limited by the depth to bedrock. The program allows the user to import the soil thickness as a grid file and automatically calculate the maximum block depth.

The user defines the soil properties with depth and can include several soil layers. Each soil layer can have uniform or depth-varying soil properties. To represent soil variation in the horizontal direction the user can define soil provinces with different soil properties. In this way, soil properties can vary in three dimensions.

The program performs one-dimensional infinite static and pseudo-static slope stability analyses, First Order Second Moment (FOSM) probabilistic analyses, and simplified seismic displacement analyses to estimate the factor of safety, probability of failure, and seismically induced permanent displacements for each soil block. The following sections give more detail on each analysis type.

24.2.1 Static and Pseudo-static Slope Stability Analyses

The screening tool conducts static and pseudo-static slope stability analyses using the infinite slope method (Morgenstern 1967). The main assumptions of the method are: (1) the thickness of the failing soil mass is much less than the length of the slope;

(2) the slip plane is parallel to the surface; (3) and the failing soil mass acts as a rigid block. The infinite slope method calculates the factor of safety against landslide failure (FS) as the ratio of the resisting shear strength of the soil on the failure plane (τ_R) to the driving shear stress (τ_D) due to the weight of the slope ($FS = \tau_R/\tau_D$). In addition, the screening tool assumes fully saturated soil with seepage parallel to the slope for slopes on land and hydrostatic conditions for offshore slopes.

Pseudo-static analyses are similar to static analyses except they add an inertial force, $k * W$, acting in the horizontal direction to represent the effect of earthquake shaking on the slope, where k is the pseudo-static coefficient and W is the total weight of the failing soil mass. The magnitude of k is commonly taken as a fraction of the peak ground acceleration (PGA) expected at the site, and is in units of gravity.

For drained conditions, the screening tool assumes Mohr-Coulomb failure criteria:

$$\tau_R = c + \sigma'_N * \tan\varphi = c + \sigma'_v * \cos^2\vartheta * \tan\varphi \tag{24.1}$$

where σ'_N is the normal effective stress acting on the failure plane, σ'_v is the vertical effective stress, c is the soil cohesion, φ is the soil friction angle, and ϑ is the slope angle.

For undrained conditions, τ_R is equivalent to the undrained shear strength s_u. However, extensive laboratory testing has shown that cohesive soils sheared at earthquake strain rates can have undrained shear strength values greater than their static shear strength. Therefore, the screening tool also includes a dynamic strength factor (S_D) that allows the user to adjust the undrained shear strength for rate effects.

Excess pore pressures (Δu) can exist in some soil layers due to underconsolidation, gas migration from deeper layers, and after sudden dynamic loading such as earthquakes or blasting. Excess pore pressures reduce the effective stress, which in turn reduces the shear strength of soils. Therefore, it has a direct effect on slope stability. To model excess pore pressure, we include the pore pressure ratio (r_u), which is defined as $r_u = \Delta u/\sigma'_v$.

24.2.2 Probabilistic Analyses

The screening tool calculates the probability of failure for both static and pseudo-static cases using the First Order Second Moment (FOSM) method. Assuming c, tan φ, s_u, and k are independent random variables and follow a normal distribution, the mean (μ_{FS}) and standard deviation (σ_{FS}) of the factor of safety for a pseudo-static analysis are calculated as:

$$\mu_{FS} \approx \frac{\mu_{\tau_R}}{\mu_{\tau_D}} \tag{24.2}$$

$$\mu_{\tau_R} = \begin{cases} \mu_c + \left(\sigma_v'^* \left(\cos^2\vartheta - r_u\right) - \sigma_v{}^* \mu_k{}^* \cos\vartheta^* \sin\vartheta\right)^* \mu_{\tan\varphi} & \text{drained} \\ S_D{}^* \mu_{s_u}{}^* \left(1 - r_u\right) & \text{undrained} \end{cases} \tag{24.3}$$

$$\mu_{\tau_D} = \begin{cases} \sigma_v{}^* \left(\cos\vartheta^* \sin\vartheta + \mu_k{}^* cos^2\vartheta\right) & \text{onshore} \\ \sigma_v'^* \cos\vartheta^* \sin\vartheta + \sigma_v{}^* \mu_k{}^* cos^2\vartheta & \text{submerged} \end{cases} \tag{24.4}$$

$$\sigma_{FS} \approx \begin{cases} \sqrt{\left(\frac{\partial \mu_{FS}}{\partial c}\right)^2 \sigma_c^2 + \left(\frac{\partial \mu_{FS}}{\partial k}\right)^2 \sigma_k^2 + \left(\frac{\partial \mu_{FS}}{\partial \tan\varphi}\right)^2 \sigma_{\tan\varphi}{}^2} & \text{drained} \\ \sqrt{\left(\frac{\partial \mu_{FS}}{\partial s_u}\right)^2 \sigma_{s_u}^2 + \left(\frac{\partial \mu_{FS}}{\partial k}\right)^2 \sigma_k^2} & \text{undrained} \end{cases} \tag{24.5}$$

where σ_v is the vertical total stress, μ_x is the mean value of parameter x and σ_x is the standard deviation of parameter x. For static analyses $\mu_k = \sigma_k = 0$, and $S_D = 1$.

The reliability index β and probability of failure P_f are calculated as:

$$\beta = \left(\mu_{FS} - 1\right) / \sigma_{FS} \tag{24.6}$$

$$P_f\left(FS < 1\right) \approx \Phi\left(-\beta\right) \tag{24.7}$$

where $\Phi(\cdot)$ is the cumulative standard normal function. For non-probabilistic analyses, FS is calculated the same as μ_{FS} using Eqs. 24.2, 24.3 and 24.4.

24.2.3 Seismically Induced Permanent Displacements

Probabilities and factors of safety give an estimate of how close a slope is to failure, whereas seismically induced permanent displacements provide an estimate of the magnitude of the failure. This is useful because maximum allowed displacements are different for different structures. In this study, we implemented the model of Rathje and Saygili (2009), which requires as inputs the yield acceleration coefficient (k_y), the peak ground acceleration (*PGA*) and earthquake magnitude (*M*). The yield acceleration coefficient is the value of k that gives $FS = 1$ in a pseudo-static slope stability analysis and is calculated internally by the screening tool. The advantages of using the Rathje and Saygili (2009) model are that the input parameters *PGA* and *M* are readily available for many areas of the world, the values of *PGA* can vary in space, and the model is computationally fast and easy to implement.

24.3 Application of the Screening Tool

24.3.1 Site Characterization

We apply the screening tool to part of the continental slope offshore the Lofoten islands, Norway. The study area is approximately 560 km^2 in size, located 100 km west of the Lofoten islands, and in water depths of 750–2,000 m. Figure 24.1 shows the bathymetry and slope angles of the study area. RV Jan Mayen (Helmer Hansen, Univ. Tromsø) collected the bathymetry data in June 2010 with additional data provided through the Norwegian Seep-Water project SEABED. Figure 24.1 shows evidence of past slides, with slope angles of up to 25° at the headwalls, sidewalls, and secondary escarpments. In general, however, the slopes vary from about 1 to 3°.

In June of 2010, the RV G.O. Sars collected a 16 m long giant piston core sample in 1,178 m water depth. Table 24.1 lists the geotechnical parameters established from this core sample, where clay, silt, and sand are the percentages of each soil type, γ is the soil total unit weight, I_p is the plasticity index, S_t is the soil sensitivity, s_u/σ'_{v0} is the undrained shear strength divided by the vertical effective stress, and

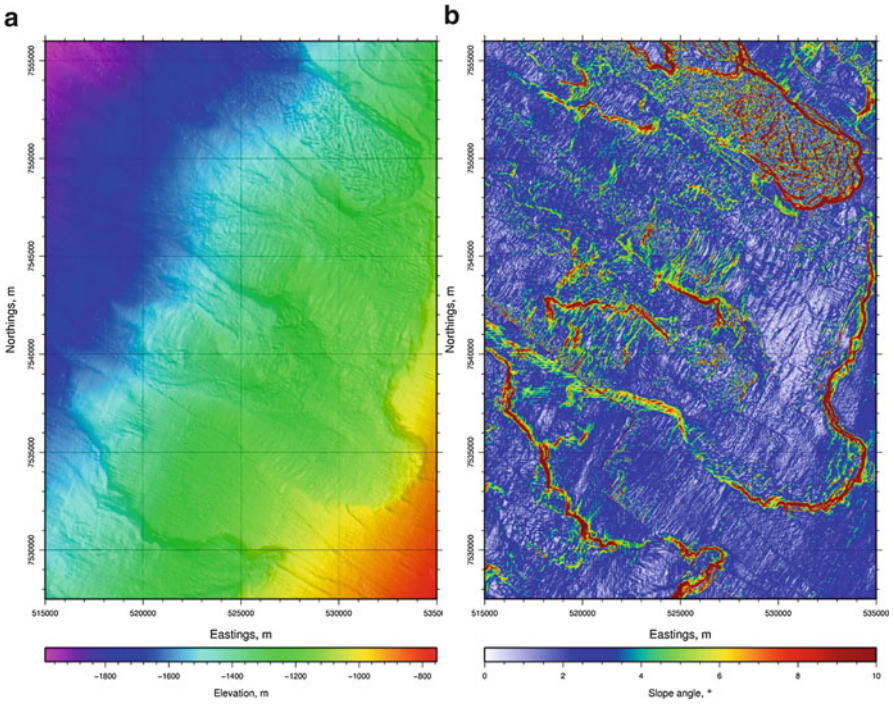

Fig. 24.1 (**a**) Bathymetry and (**b**) slope map of the study area

Table 24.1 Geotechnical parameters

Clay	Silt	Sand	γ	I_p	S_t	s_u/σ'_{v0}	OCR
%	%	%	(kN/m^3)	%	–	–	–
40–60	20–40	5–40	15.7–18.6	20–40	2–6	0.2–0.3	1–1.3

From Baeten et al. (2014)

Table 24.2 General input parameters to the screening tool

z_{max}	k	COV_k	M_w	PGA
mbsf	g	–	–	g
12	0.04	0.1	6	0.08

Table 24.3 Soil parameters

	Soil province 1	Soil province 2	Soil province 3
γ (kN/m^3)	17.5	15.5	17.5
s_u (kPa)	2 + 2.25*z	1 + 0.3*z	1 + 1.5*z
S_D	1.3	1.3	1.3
r_u	0	0.1	0
COV_{su}	0.2	0.3	0.1

OCR is the overconsolidation ratio. The soil is mainly normally consolidated marine clay with layers of glacigenic debris flows and plumites (Baeten et al. 2014).

Seismicity in Norway is relatively low, however, earthquakes are thought to be the main triggers that caused the Storegga slide (Kvalstad et al. 2005), the Trænadjupet slide (Laberg and Vorren 2000), and several smaller slides seen on the continental margin off Vesterålen (L'Heureux et al. 2013), which is just north of the study area in this paper. Gruenthal et al. (1999) estimate *PGA* values for the Lofoten islands of 0.06–0.08 g with a return period of 475 years.

24.3.2 Input Parameters

Tables 24.2 and 24.3 list the input parameters to the screening tool for the study area investigated in this paper. Table 24.2 gives the maximum depth (z_{max}) in meters below seafloor (mbsf) of the analyses, the pseudo-static coefficient (k), the coefficient of variation of k (COV_k), the moment magnitude (M_w), and the peak ground acceleration (*PGA*). The values of k and *PGA* can be varied in space, however, for this example we applied the same values everywhere. We chose 12 meters as the maximum analysis depth consistent with Baeten et al. (2014).

Table 24.3 presents the soil properties for each of the soil provinces, where γ is the total soil unit weight, s_u is the undrained shear strength, z is depth in meters below seafloor, S_D is the dynamic strength factor, r_u is the pore pressure ratio, and COV_{su} is the coefficient of variation of s_u.

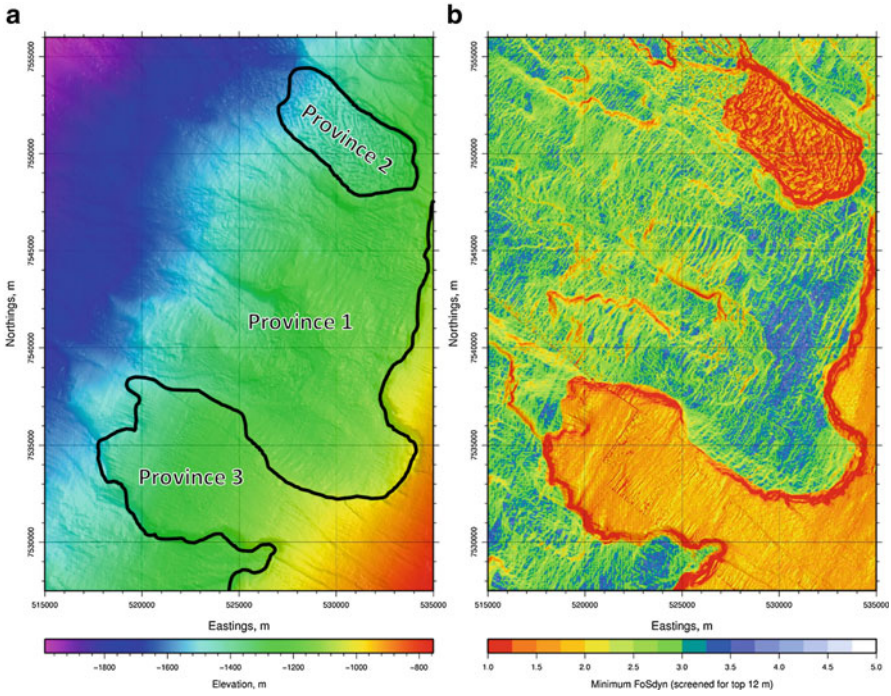

Fig. 24.2 (**a**) Soil provinces and (**b**) pseudo-static factor of safety for z = 12 mbsf

Figure 24.2a shows the soil provinces. We modelled soil province 1 to represent the exposed soil downslope of the shelf, soil province 2 to represent the mass movement complex in the northeast part of the study area and soil province 3 to represent the shelf in the southeast part of the study area. The parameters for soil province 3 are based on the data from the giant piston core sample, which was taken in this region. We increased the s_u values for soil province 1 because the soil is likely overconsolidated as a result of the removal of sediments due to past landslides. Soil province 2 we modelled as a sensitive soil that has been disturbed due to a past landslide. We increased the value of COV_{su} for soil province 2 and 3 because of the greater uncertainty in these assumptions.

24.3.3 Results and Discussion

Figure 24.2b shows the pseudo-static factor of safety for a depth of 12 mbsf. Soil province 2 has the lowest values of *FS*, between 1 and 1.5, followed by soil province 3 and then soil province 1. These differences are expected due to the different undrained shear strength profiles. Figure 24.2b also shows low values of *FS* along the steep edges of the old landslide scarps. However, there is likely little sediment

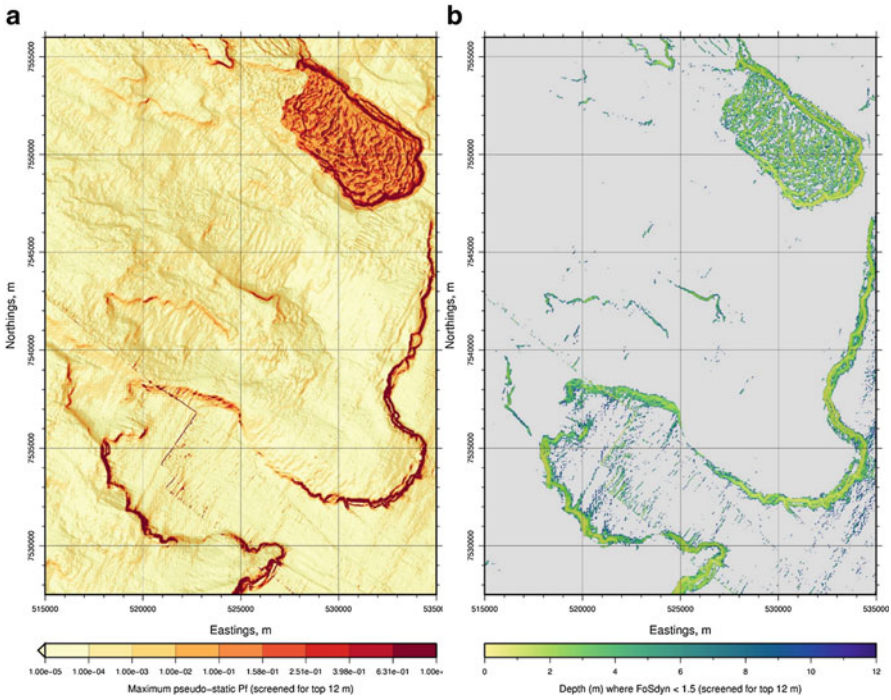

Fig. 24.3 (**a**) Probability of FS < 1 for pseudo-static analysis and (**b**) smallest depth where FS < 1.5 for pseudo-static analysis

left on these slopes precisely because they are so steep. If soil thickness data was available, this could be incorporated directly in the analyses to remove this type of issue. If soil thickness data is not available, as in this case, then the results for steep slopes should be used with caution.

Figure 24.3a shows the probability of the pseudo-static factor of safety being less than 1. In Fig. 24.3a province 2 has the highest probability of failure, however, soil provinces 1 and 3 have similar probabilities even though soil province 3 has a weaker undrained shear strength profile. This is due to the larger uncertainty in the undrained shear strength expressed through the coefficient of variation COV_{su}. Figure 24.3b presents the smallest depth where $FS < 1.5$ for the pseudo-static analyses. Most of the depths are between 1 and 4 mbsf, indicating shallow failures.

Figure 24.4a is a plot of the k_y values for when z = 12 mbsf. Figures 24.2b and 24.4a correlate well because k_y is the value of k that gives FS = 1 in a pseudo-static analysis. Therefore, if FS is lower in the pseudo-static analysis, k_y will also be lower. If FS is one, then k_y is zero. Hynes-Griffin and Franklin (1984) recommend to estimate k as $k = 0.5 * PGA$, which is what was done in this study. Using this method, to reduce the value of FS to one for province 1, an earthquake with PGA

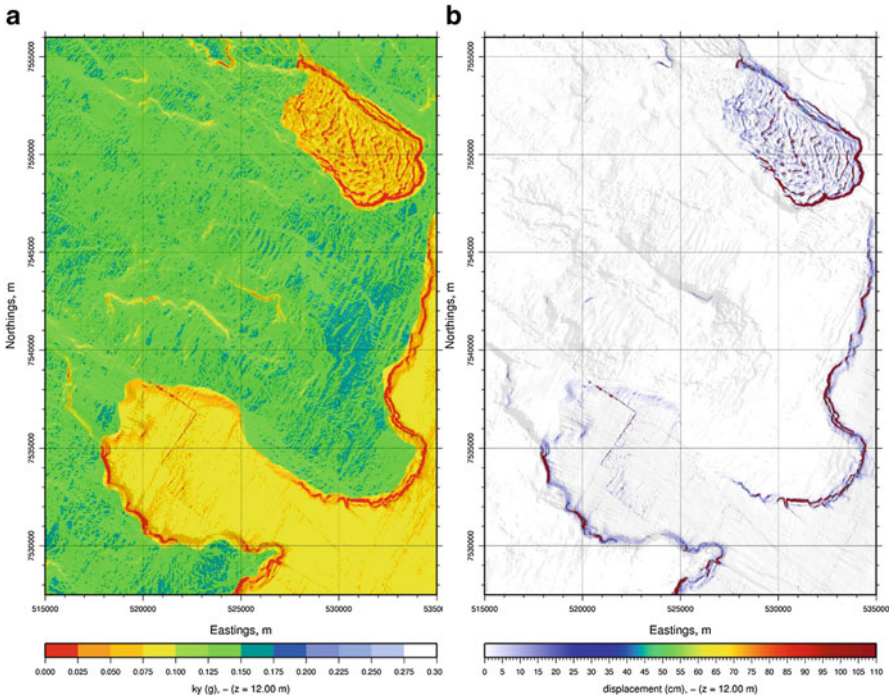

Fig. 24.4 (**a**) k_y values for z = 12 mbsf and (**b**) median plus one standard deviation seismically induced permanent displacements for z = 12 mbsf

>0.25 g would have to occur. This value of PGA corresponds to a return period of about 10,000 years for this location (NORSAR and NGI 1998).

Figure 24.4b displays the median plus one standard deviation of the seismically induced permanent displacements for when z = 12 mbsf. Figure 24.4b shows that if an earthquake with $PGA = 0.08$ g and $M_w = 6$ occurred, most of the study area would have displacements less than 5 cm. Only on the steep slopes bordering soil province 3 and in soil province 2 are there displacements of up to 1 m. The Rathje and Saygili (2009) method is a simplified model that was developed for onshore applications and does not consider retrogressive failures. Therefore, there is a large amount of uncertainty.

24.4 Summary and Conclusions

This article described the development of a screening tool to rapidly assess and identify potentially unstable regions over large areas. The results allow a quick and objective way to select regions to perform more in-depth and detailed slope

stability analyses. In addition, it provides a basic understanding of the stability of the entire study area that can be used to select routes or locations for future infrastructure development that avoid the most hazardous regions. However, the user must remember that it is only a screening tool and should not replace more detailed slope stability analyses. We applied the screening tool to part of the continental slope offshore the Lofoten islands, Norway, which have normally consolidated sensitive marine clays. The results include static and pseudo-static factors of safety, probability of failure, seismically induced permanent displacements, and depths to given threshold values of factors of safety and probabilities. The results show the importance of including geomechanical parameters such as sediment thickness, soil unit weight, soil strength, and excess pore pressure in slope stability analyses.

Acknowledgements The authors would like to acknowledge Prof. Jacques Locat and Dr. Farrokh Nadim for their helpful comments and insights during the review process. This work was performed with the support of NGI's internal research funding, the EU MIDAS project (grant 603418, FP7). Thanks also to Prof. J.S. Laberg, Univ. Tromsø, for permission to use the bathymetry data.

References

Baeten NJ, Laberg JS, Vanneste M, Forsberg CF, Kvalstad TJ, Forwick M, Vorren TO, Haflidason H (2014) Origin of shallow submarine mass movements and their glide planes—sedimentological and geotechnical analyses from the continental slope off northern Norway. J Geophys Res Earth Surf 119:2335–2360

Gruenthal G, Bosse C, Camelbeek T, de Crook T, Gariel JC, Gregersen S, Guterch B, Halldorsson P, Labak P, Lindholm C, Lenhardt W, Mantyniemi P, Mayer-Rosa D, Musson RMW, Schenk V, Schenkova Z, Slejko D, Verbeiren R, Wahlstrom R, Zabukovec B, Ziros T (1999) Seismic hazard assessment for central, north and northwest Europe: GSHAP region 3. Ann Geofis 42(6):999–1011

Hynes-Griffin ME, Franklin AG (1984) Rationalizing the seismic coefficient method. U.S. Army Corps of Engineers Waterways Experiment Station, Vicksburg. GL-84-13:21

Kvalstad TJ, Nadim F, Kaynia AM, Mokkelbost KH, Bryn P (2005) Soil conditions and slope stability in the Ormen Lange area. Mar Pet Geol 22:245–256

L'Heureux JS, Vanneste M, Rise L, Brendryen J, Forsberg CF, Nadim F, Longva O, Chand S, Kvalstad TJ, Haflidason H (2013) Stability, mobility and failure mechanism for landslides at the upper continental slope off Vesterålen, Norway. Mar Geol 346:192–207

Laberg JS, Vorren TO (2000) The Trænadjupet slide, offshore Norway — morphology, evacuation and triggering mechanisms. Mar Geol 171:95–114

Lee HJ, Edwards BD (1986) Regional method to assess offshore slope stability. J Geotech Geoenviron Eng 112(5):489–509

Lee HJ, Locat J, Dartnell P, Israel K, Wong F (1999) Regional variability of slope stability: application to the Eel margin, California. Mar Geol 154:305–321

Morgenstern NR (1967) Submarine slumping and the initiation of turbidity currents. In: Richards AF (ed) Marine geotechnique. University of Illinois Press, Urbana, pp 189–210

NORSAR and NGI (1998) Seismic Zonation for Norway; report prepared for the Norwegian Council for Building Standardization (NBR). Oslo, p 190

Rathje EM, Saygili G (2009) Probabilistic assessment of earthquake-induced sliding displacements of natural slopes. Bull N Z Soc Earthq Eng 42(1):18–27

Part III
Post-failure Stage

Chapter 25
The Use of LiDAR Airborne Data for Retrogressive Landslides Inventory in Sensitive Clays, Québec, Canada

Denis Demers, Denis Robitaille, Alexandre Lavoie, Stéphane Paradis, Alexis Fortin, and Daniel Ouellet

Abstract Since 2003, the Québec Government uses airborne lidar surveys to map landslide-prone areas. Hillshade maps greatly helped in obtaining a detailed inventory of old scars of retrogressive landslides in sensitive glacio-marine clays. This technique allowed a much better identification of scars than with conventional air photo interpretation. It has also made possible to distinguish different types of landslide, even when scars are very old and forested. Although only 66% of the area has been covered by lidar so far, about 3,500 scars of retrogressive landslides have already been counted in post-glacial Champlain, Laflamme and Goldthwait seas. The 50 largest scars identified so far were split into three groups of dimensions. The seven cases included in the first group have surface areas comprised between 6.5 and 20 km^2, and most were triggered by earthquakes. The second group is characterized by landslide scars with a surface area between 2.5 and 5.3 km^2. The only event of this group documented in historical records is the St. Alban landslide, with a surface area of 4.5 km^2. The third group includes the last 23 cases that have surface areas comprised between 1.0 and 1.9 km^2. The second largest event in recorded history is the 1896 spread of Grandes-Bergeronnes, with a surface area of 0.54 km^2.

25.1 Introduction

The majority of the Quebec population is settled in the southern part of the province, within the limits of post-glacial seas, which include extensive deposits of sensitive clay (Fig. 25.1). These deposits are prone to very large retrogressive landslides which can reach dimensions of a few to several hundred hectares

D. Demers (✉) • D. Robitaille • A. Lavoie • S. Paradis • A. Fortin • D. Ouellet
Ministère des Transports, de la Mobilité durable et de l'électrification des transports du Québec, Quebec City, QC, Canada
e-mail: denis.demers@transports.gouv.qc.ca; alexandre.lavoie@transports.gouv.qc.ca; stephane.paradis@transports.gouv.qc.ca; alexis.fortin@transports.gouv.qc.ca; daniel-a.ouellet@transports.gouv.qc.ca

V. Thakur et al. (eds.), *Landslides in Sensitive Clays*, Advances in Natural and Technological Hazards Research 46, DOI 10.1007/978-3-319-56487-6_25

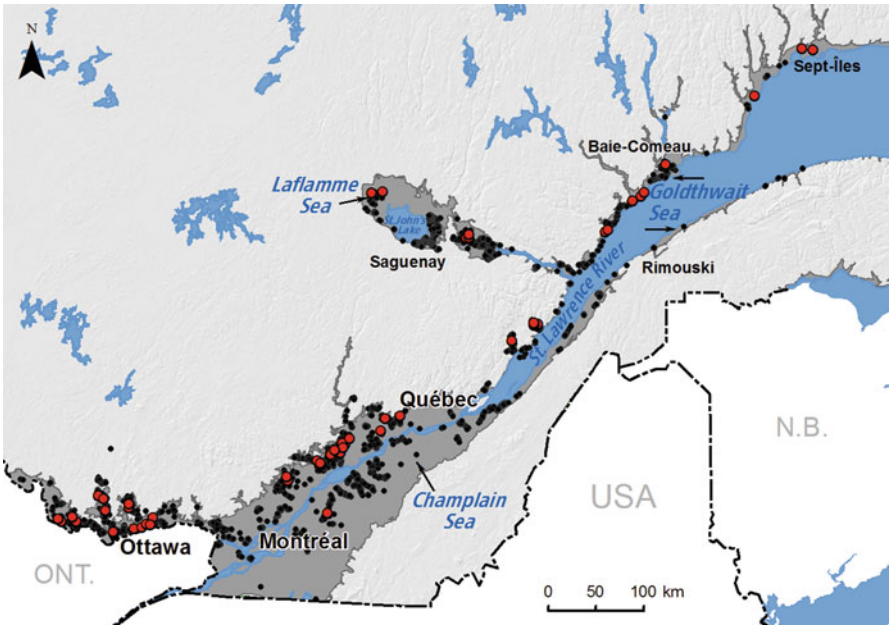

Fig. 25.1 Location of post-glacial seas in Southern Quebec (*dark grey area*). *Black dots* refer to retrogressive landslide scars identified with lidar. The 50 largest landslides are shown with *red dots*

(Demers et al. 2014). In a first inventory made by Chagnon (1968) using air photos, 678 scars of large retrogressive landslides were identified in the Champlain, Laflamme and Goldthwait seas deposits. The observation by Lebuis et al. (1983) and Quinn et al. (2007) that new retrogressive landslides tend to occur near clusters of existing scars highlights the paramount importance of detailed and reliable landslide inventories in hazard mapping. The first government mapping program in Quebec, which was initiated in 1972 (Lebuis et al. 1983), showed that the number of scars was much larger than first estimated by Chagnon (1968), even though no detailed inventory was yet available. Landslide scars identification was still performed using air photos.

Since 2003, the Quebec Government uses airborne lidar surveys to map landslide-prone areas (Potvin et al. 2014). These surveys helped generate a detailed inventory of retrogressive landslides in sensitive glacio-marine clays. Interpretation of hillshade images allowed the identification of many unrecorded scars, some being extremely large. It has also made it possible to distinguish different types of retrogressive landslides, even for very old and densely forested scars. Although only 66% of the area of the Champlain, Laflamme and Goldthwait seas has been covered by lidar so far, about 3,500 scars of old retrogressive landslides have already been identified in post-glacial deposits using this approach, about five times more than the initial inventory established with air photos by Chagnon (1968). The purpose of this paper is to summarize the results of the inventory carried out since 2003 and illustrate how this information can improve hazard assessment.

25.2 Some Aspects of Lidar Technology Used

The lidar data used for the present inventory was obtained from airborne surveys, with a point density of 2–8 points per m^2 and an absolute ground precision in elevation of approximately 25 cm. Digital terrain models generated for this study are made with a resolution of 1 m/pixel. In order to remove anomalous points and to smooth the model topography, a 3×3 m median filter is applied prior to generating the hillshade images.

As a part of the mapping of landslides-prone areas, the most favourable periods in Quebec to perform optimal lidar surveys are relatively limited, partly because of the heavy snow cover obscuring the land topography and that can last several months. In addition, for several weeks in the spring, freshets (high water levels due to rapid snowmelt) do not allow the determination of the maximum height of watercourse banks. Rainy periods in autumn can also cause similar constraints. Finally, the presence of deciduous trees in summer does not allow for an optimal amount of points on the ground, especially in steep, wooded banks. Therefore, for mapping purposes, the most suitable periods for lidar surveys are in the fall, after leaves have fallen and before snow has accumulated, or in the spring, during a short period of time after the spring freshets and before there are too many leaves in trees. It is important to take these constraints into account because the topographical setting in which large retrogressive landslides occur in Quebec shows no major differences in elevation. Indeed, the height of the watercourse banks cutting the immense clay plains is rarely more than 30 m, and often between 10 and 20 m.

The inventory of large retrogressive landslide scars was made by visual identification on hillshade images and with the help of contour levels. In some cases, the use of air photo from the 1970s or earlier helped complete the identification of landforms that have since been strongly altered by agricultural ploughing and surfacing works.

25.3 Advantages of Using Lidar for Landslide Inventories

Jaboyedoff et al. (2012) made a good review of the use of lidar data in landslide investigations. Several papers have reported recent experiences of the use of lidar for the purposes of landslides inventory and mapping (e.g. McKean and Roering 2004; Van Den Eeckhaut et al. 2005; Ardizonne et al. 2007; Mora et al. 2014). In some cases, landslide recognition was based on automated procedures (e.g. Booth et al. 2009; Leshchinsky 2016).

Lidar data provides many advantages over other inventory techniques. By providing a detailed overview of the topography of the bare ground surface, an overall picture is obtained that would otherwise be impossible to get from conventional approaches. For example, it is often very difficult to recognize landslide scars

from air photos. In a heavily wooded area in Vancouver, Canada, Brardioni et al. (2003) reported that 85% of landslides inventoried through field inspections were not visible on air photos.

Scars of large retrogressive landslides in Quebec may sometimes have only minor relief along their rims, which makes for difficult detection by air photo analysis. In some cases, only lidar data can provide sufficiently good information to properly analyze the shape of landslide scars, to differentiate them from other landforms and to locate where they were initiated. Moreover, as pointed out by McKean and Roering (2004), most inventories made from air photos only delineate the edge of the scars and do not provide information on the failure mechanisms, which can be deducted from internal deformations. The high resolution of lidar data can help distinguish the type of large retrogressive landslide because it reveals details and minor landforms found therein. The following section provides examples illustrating the many benefits mentioned previously.

25.4 Some Examples of Landslides Inventoried with Lidar

25.4.1 Colombier Site

The Colombier site, located near Baie-Comeau (Fig. 25.1), shows a very large scar of an undated landslide (Fig. 25.2). The retrogression of the landslide is 900 m and its maximum width is 1,300 m. It covers a surface area of approximately 97 ha. The right part of the figure shows rock outcrops (R) near which many beach ridges

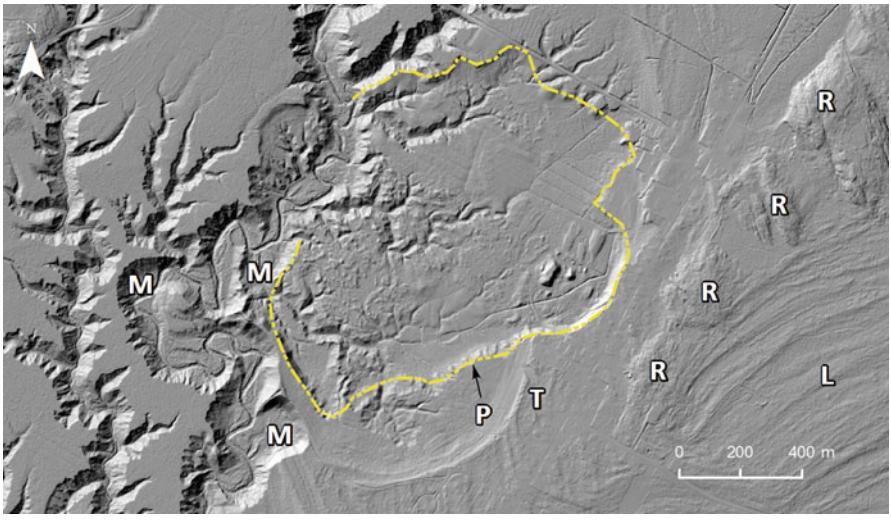

Fig. 25.2 Hillshade image of the Colombier site. The main river banks are about 26 m high. The *yellow dotted line* delineates the landslide scar. Signification of the letters is in the text

(L) were built. In the lower part, the edges of the scar cross the escarpment of an ancient marine terrace (T), which was confused in a previous analysis with the landslide lateral scarp (P) due to the presence of a dense vegetation cover on air photos. Moreover, the arced nature of some topographical forms (M) can be clearly identified as former banks of the meandering Colombier River and not as scars of large landslides.

25.4.2 Salvail River Site

The Salvail River site is located about 50 km east of Montreal (Fig. 25.1) and includes the 2010 St. Jude landslide which resulted in four casualties (Locat et al. 2012). This example shows large landslide scars in a densely forested area on both sides of the river. These scars are clearly visible on the hillshade image but not on the air photo (red dots on Fig. 25.3). The ribbed morphology within these scars

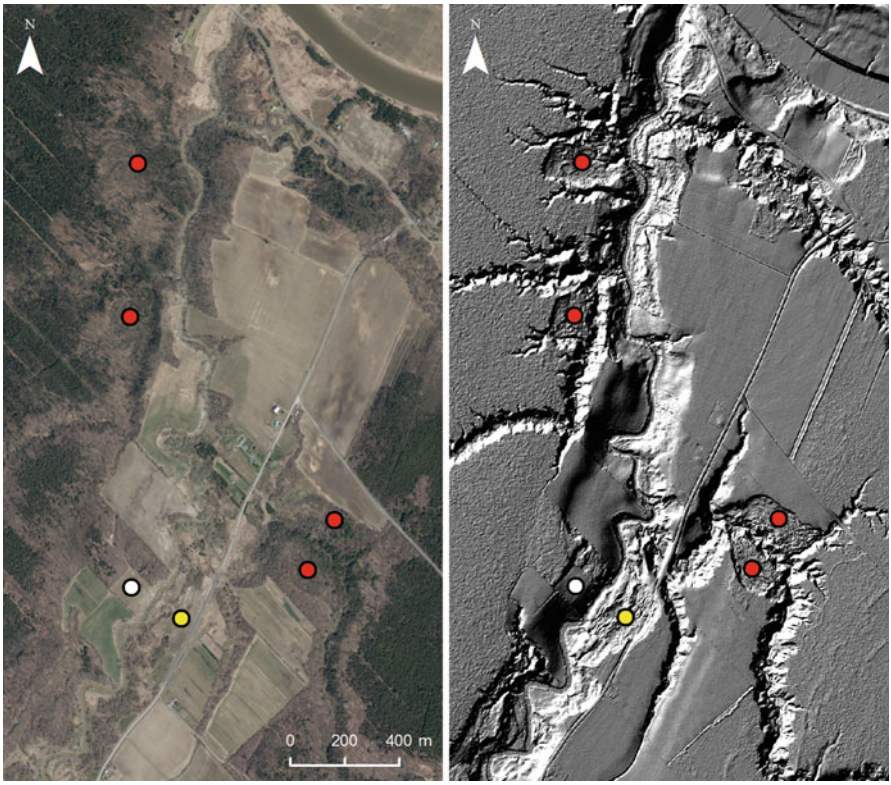

Fig. 25.3 Air photo (2009) and hillshade image (2010) of the Salvail River site. The main river banks are about 22 m high. The *yellow dot* locates the 2010 St-Jude landslide (not visible on the air photo). *Red dots*: scars in densely forested areas. *White dot*: altered spread scar

is identical to the succession of parallel ridges visible in the 2010 landslide scar (yellow dot on Fig. 25.3). This latter event was a lateral spread (4.2 ha) and showed a horst-and-graben pattern. The high resolution of lidar images allows the easy identification of the typical morphology of lateral spreads with respect to other types of large retrogressive landslides (Demers et al. 2014). These shapes can remain visible for centuries and millennia, even if they are affected by weathering and climatic events, as long as they are not altered by agricultural activities or other human interventions. A good example of human modification of the morphology of an old and undated spread is visible just to the right of the white dot on Fig. 25.3, where ridges are sharply cut on both sides along the margin of the agricultural lots (Fig. 25.3).

25.4.3 Bristol Site

The Bristol site is located about 60 km northwest of Ottawa (Fig. 25.1). The hillshade image of the Fig. 25.4 shows the scar of a large translational landslide (flakeslide) in sensitive clay (Fournier et al. 2017). The landslide is 780 m in length and 520 m across, and it covers an area of about 34 ha. The hillshade image clearly shows a wide graben (G) on the right side of the scar, and a bulge (B) at the other end, near the watercourse. Except for a small area with horsts and grabens in the northern part of the slide (H), the rest of the mobilized mass is practically intact. These features characterize a third kind of large retrogressive landslides in sensitive clay in Eastern Canada, showing a pattern different to the two previous examples. Only a few other scars of this type were identified on lidar hillshades.

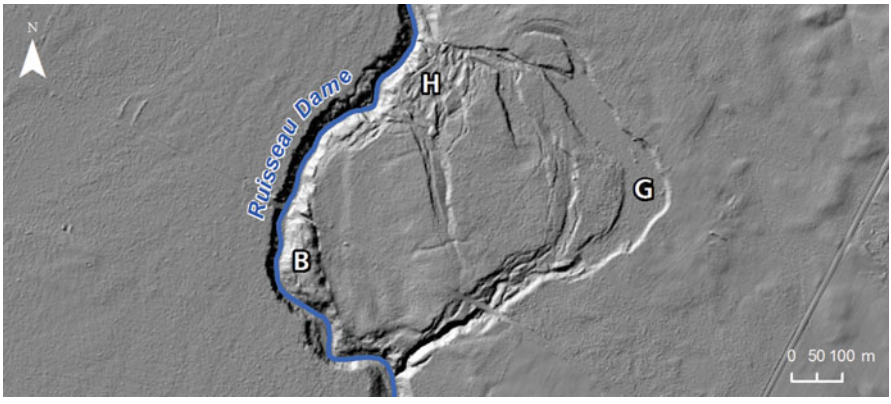

Fig. 25.4 Hillshade image of the Bristol site. The river banks are about 12 m high. Signification of the letters is in the text

25.5 The 50 Largest Scars of the Lidar Inventory

A list of the 50 largest scars identified up to now from lidar surveys was established. The scars are relatively well distributed throughout postglacial marine deposits, but are located almost exclusively on the north shore of the St. Lawrence River (Fig. 25.1).

Surface areas of these scars are separated into three groups in Fig. 25.5. The seven cases included in the first group have surface areas comprised between 6.5 and 20 km^2, and are associated with historical and prehistorical earthquakes. The largest event is located in Quyon, about 45 km west of Ottawa (Fig. 25.1). Its surface area is estimated at 19.9 km^2 and was most probably triggered by an earthquake about 1,000 years ago (Brooks 2013). This earthquake probably triggered many others large landslides in the Ottawa region (Brooks 2014), including one with an area of about 5.3 km^2 and ranked eighth in the list (in the second group). The St. Jean-Vianney landslide that occurred in 1663 is the second largest event identified and has a surface area of 13.5 km^2. It was also triggered by an earthquake (Lasalle and Chagnon 1968). Four others landslides in the first group are associated with this 1663 earthquake: three in the Shawinigan area (Desjardins 1980) and one in Colombier (Cauchon-Voyer et al. 2011).

The second group include 20 cases with surface areas comprised between 2.5 and 5.3 km^2. Most of these landslides are either associated with the aforementioned earthquakes or located near morainic deposits, in a marine environment. The only event of the list described in historical records is the landslide of St. Alban, occurred in 1894 (Laflamme 1894). With a surface area of 4.5 km^2, it belongs to this second group, and is ranked 11th (Fig. 25.5). Lebuis and Rissmann (1979) mentioned that

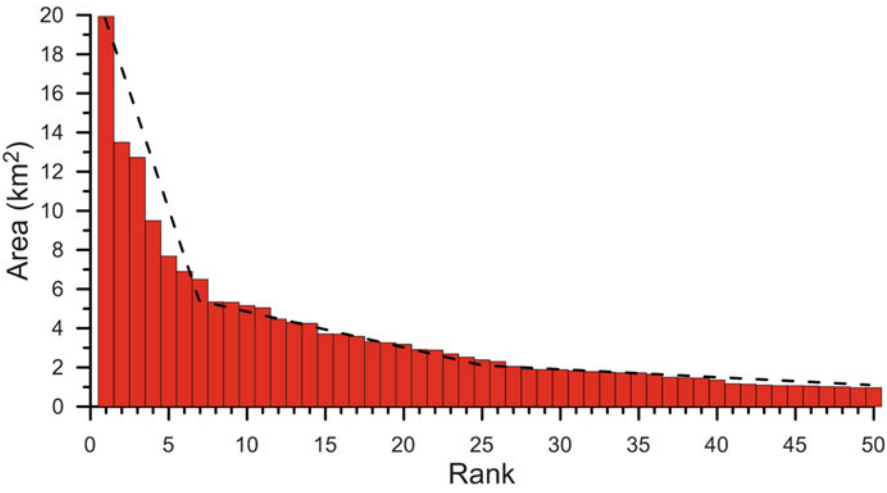

Fig. 25.5 Distribution of the 50 largest retrogressive landslides in the province of Québec

this case was probably triggered by the erosion of the banks, but was influenced by seepage coming from the St. Narcisse morainic segment located along the north side of the scar.

The third group includes the last 23 cases, whose areas are comprised between 1.0 and 1.9 km^2. Many of them are also located near glacial deposits in marine environments, which are more frequent on the north shore of the St. Lawrence River.

Surface areas of smaller scars inventoried by lidar are not shown in Fig. 25.5. It is noteworthy, however, that the second largest historical event is the spread of Grandes-Bergeronnes which occurred in 1896 (Tremblay 1945). Its surface area (0.54 km^2) is only half of the last scar on the list of the 50 largest ones. The 1971 St-Jean-Vianney flowslide, which resulted in 30 casualties (Potvin et al. 2001), has a surface area of 0.32 km^2 and is thus not included in the list either.

25.6 Concluding Remarks

The results presented in this paper show that lidar surveys may provide much more reliable inventories and a far more detailed knowledge of hazards in an area. When landforms within landslide scars have not been too altered by natural processes or human activities, it is even possible to distinguish between different types of large retrogressive landslides. The general shape of scars can also be a good indicator to determine if the landslide is probably associated with a flowslide or a spread, as mentioned by Demers et al. (2014). In these cases, the ability to delineate contour scars more accurately with lidar surveys is an additional asset.

The spatial distribution of the 50 largest scars confirmed the significant influence of morainic and fluvio-glacial deposits in marine environments, as already observed by Lebuis et al. (1983). This geological context influenced the stratigraphy, the composition and the properties of the nearby sensitive clay deposits, predisposing the leaching of the soils, which are generally more silty, less plastic and as a consequence more sensitive. Since morainic and fluvio-glacial are more frequent on the north shore of the St. Lawrence River, we find a higher concentration of large landslide scars there.

Based on our new lidar inventory and considering that, with a few exceptions, the oldest landslides dated in Quebec are about 5,000 years old according to C^{14} dating (Lebuis et al. 1983; Aylsworth et al. 2000; Brooks 2014), the frequency of retrogressive landslides in sensitive clay is approximatively one event every 1.4 year. Although only one of the 108 historical large retrogressive landslides inventoried since 1840 in Quebec (Demers et al. 2014) is part of the 50 largest identified scars, one cannot ignore that huge landslides could still occur in the future, for example in the event of a major earthquake. For this reason, this inventory of old events helps us better define this hazard and provides a database on which to base our reflection on risk management for exceptionally large cases.

Acknowledgements The authors would like to thank the Ministère des Transports, de la Mobilité durable et de l'Électrification des transports du Québec for the permission to use and present the results of this landslide inventory. The authors wish to express their gratitude to Didier Perret and Thomas Fournier for their valuable comments and to Mélissa Raymond for the preparation of the figures.

References

Ardizzone F, Cardinali M, Galli M, Guzzetti F, Reichenbach P (2007) Identification and mapping of recent rainfall-induced landslides using elevation data collected by airborne Lidar. Nat Hazards Earth Syst Sci 7:637–650

Aylsworth JM, Lawrence DE, Guertin J (2000) Did two massive earthquakes in the Holocene induce widespread landsliding and near-surface deformation in part of the Ottawa Valley, Canada? Geology 28:903–906

Booth AM, Roering JJ, Perron JT (2009) Automated landslide mapping using spectral analysis and high-resolution topographic data: Puget Sound lowlands, Washington, and Portland Hills, Oregon. Geomorphology 109:132–147

Brardinoni F, Slaymaker O, Hassan MA (2003) Landslide inventory in a rugged forested watershed: a comparison between air-photo and field survey data. Geomorphology 54:179–196

Brooks GR (2013) A massive sensitive clay landslide, Quyon Valley, southwestern Quebec, Canada, and evidence for a paleoearthquake triggering mechanism. Quat Res 80:425–434

Brooks GR (2014) Prehistoric sensitive clay landslides and paleoseismicity in the Ottawa valley, Canada. In: L'Heureux JS et al (eds) Landslides in sensitive clays: from geosciences to risk management, Advances in natural and technological hazards research, vol 36. Springer, Dordrecht, pp 119–131

Cauchon-Voyer G, Locat J, Leroueil S, St-Onge G, Demers D (2011) Large-scale subaerial and submarine Holocene and recent mass movements in the Betsiamites area, Quebec, Canada. Eng Geol 121:28–45

Chagnon J-Y (1968) Les coulées d'argile dans la province de Québec. Nat Can 95:1327–1343

Demers D, Robitaille D, Locat P, Potvin J (2014) Inventory of large landslides in sensitive clay in the province of Québec, Canada: preliminary analysis. In: L'Heureux JS et al (eds) Landslides in sensitive clays: from geosciences to risk management, advances in natural and technological hazards research, vol 36. Springer, Dordrecht, pp 77–89

Desjardins R (1980) Tremblements de terre et glissements de terrain: corrélation entre des datations au 14C et des données historiques à Shawinigan, Québec. Géog Phys Quatern 34:359–362

Fournier T., Demers D., Perret D., Robitaille D., Locat P. (2017) Large translational landslides in marine sensitive clay of Bristol area, Quebec. Submitted to the 70th Can. Conf. of Geotech., Ottawa, Canada, Sept 2017

Jaboyedoff M, Oppikofer T, Abellán A, Derron M-H, Loye A, Metzger R, Pedrazzini A (2012) Use of LIDAR in landslide investigations: a review. Nat Hazards 61:5–28

Laflamme JC-K (1894) L'éboulis de St-Alban. Trans R Soc Can 12(Section IV):63–70

Lasalle P, Chagnon JY (1968) An ancient landslide along the Saguenay River. Québec Can J Earth Sci 5:548–549

Lebuis J, Rissmann P (1979) Earthflows in the Quebec and Shawinigan area. Geol. Ass. of Canada, Quebec Congress, Field-trip B-11. pp 18–38

Lebuis J, Robert J-M, Rissmann P (1983) Regional mapping of landslide hazard in Quebec. In: Proceedings of the symposium on slopes on soft clays. Swedish Geotechnical Institute Report No. 17. Linköping, Sweden, pp 205–262

Leshchinsky B (2016) Contour connection method: a semi-automated method for hazard mapping using lidar. Proc. of the 12th international symposium on landslides, Naples. 2:1267–1273

Locat P, Demers D, Robitaille D, Fournier T, Noël F, Locat A, Leroueil S, Lefebvre G (2012) The Saint-Jude landslide of May 10, 2010, Québec, Canada. In: Eberhardt et al (eds) Landslides and engineered slopes: protecting society through improved understanding. Taylor & Francis Group, London, pp 635–640

McKean J, Roering J (2004) Objective landslide detection and surface morphology mapping using high-resolution airbone laser altimetry. Geomorphology 57:331–351

Mora OE, Liu JK, Lenzano MG, Toth CK, Grejner-Brzezinska DA (2014) Small landslide susceptibility and hazard assessment based on airbone lidar data. Photogramm Eng Remote Sens 81:239–247

Potvin J, Pellerin F, Demers D, Robitaille D, La Rochelle P, Chagnon JY (2001) Revue et investigation complémentaire du site du glissement de St-Jean-Vianney. In: Proceeding of the 54th Canadian geotechnical conference, pp 792–800.

Potvin J, Thibault C, Demers D, Bilodeau C (2014) An overview of the mapping landslide-prone area and risk management strategies in the province of Québec, Canada. In: L'Heureux JS et al (eds) Landslides in sensitive clays: from geosciences to risk management, Advances in natural and technological hazards research, vol 36. Springer, Dordrecht, pp 331–342

Quinn PE, Hutchinson DJ, Rowe RK (2007) Toward a risk management framework: sensitive clay landslide hazards affecting linear infrastructure in eastern Canada. In: 1st North American landslide conference, Vail, Colorado, pp 102–114

Tremblay V (1945) Bon Désir – Un coin de la paroisse des Bergeronnes. Publication de la Société historique du Saguenay, no 7.

Van Den Eeckhaut M, Poesen J, Verstraeten G, Vanacker V, Moeyerson J, Nyssen J, van Beek LPH (2005) The effectiveness of hillshade maps and expert knowledge in mapping old deep-seated landslides. Geomorphology 67:351–363

Chapter 26
Runout of Landslides in Sensitive Clays

Stein-Are Strand, Vikas Thakur, Jean-Sébastien L'Heureux, Suzanne Lacasse, Kjell Karlsrud, Trude Nyheim, Kristian Aunaas, Hanne Bratlie Ottesen, Vidar Gjelsvik, Odd Arne Fauskerud, Rolf Sandven, and Anders Rosenquist af Åkershult

Abstract An essential part of landslide hazard and risk assessment is the estimate of the runout distance of the landslide masses. There is, however, little guidance available today on the estimation of the landslide runout in sensitive clays and no suitable model exists for predicting runout in sensitive clays. A new empirical model for the runout estimation is presented in this paper. The new model is based on empirical data, and is recommended for use in Norway until further research on analytical models becomes available. The recommended empirical procedure is based on the historical landslides in sensitive clays in Norway. The paper discusses the implementation of the proposed empirical models in a calculation tool called *GeoSuite Toolbox* as a part an ongoing R&D project *GeoFuture II*.

S.-A. Strand (✉) • T. Nyheim
Norwegian Water Resources and Energy Directorate, Oslo, Norway
e-mail: sas@nve.no; tny@nve.no

V. Thakur
Department of Civil and Environmental Engineering, Norwegian University of Science and Technology (NTNU), Trondheim, Norway
e-mail: vikas.thakur@ntnu.no

J.-S. L'Heureux
Trondheim Division, Norwegian Geotechnical Institute (NGI), Trondheim, Norway
e-mail: jsl@ngi.no

S. Lacasse • K. Karlsrud • V. Gjelsvik
Norwegian Geotechnical Institute (NGI), Oslo, Norway
e-mail: suzanne.lacasse@ngi.no; kjell.karlsrud@ngi.no; vidar.gjelsvik@ngi.no

K. Aunaas • H.B. Ottesen
Norwegian Public Roads Administration (NPRA), Oslo, Norway
e-mail: Kristian.Aunaas@norconsult.com; hanne.ottesen@vegvesen.no

O.A. Fauskerud • R. Sandven (deceased)
Multiconsult AS, Oslo, Norway
e-mail: odd.arne.fauskerud@multiconsult.no; rolf.sandven@multiconsult.no

A. Rosenquist af Åkershult
Trimble, Sunnyvale, CA, USA
e-mail: anders_rosenquist@trimble.com

V. Thakur et al. (eds.), *Landslides in Sensitive Clays*, Advances in Natural and Technological Hazards Research 46, DOI 10.1007/978-3-319-56487-6_26

26.1 Introduction

Rapid debris flows, debris avalanches, earth flows, sensitive clay landslides, rock avalanches and failures of loose fill and mining waste are among the most dangerous and most damaging of all landslide phenomena. Their runout determines a large portion of the consequences and the risk associated with the landslides. Runout parameters include the maximum distance reached, flow velocities, thickness and distribution of deposits, as well as the behaviour in bends and at obstacles in the flow path (Crosta et al. 2003; Rickenmann 2005; Hungr 2005, 2016; Lacasse 2013).

Retrogression distance and runout distance of sensitive clay debris, which are occasionally fast moving, may involve massive soil volumes of the order of millions of cubic metres (Bjerrum 1955; Lebuis et al. 1983; Karlsrud et al. 1985; Tavenas et al. 1983; Leroueil et al. 1996; Locat et al. 2008, 2011; L'Heureux 2012; Lacasse 2013, 2016; Thakur et al. 2014). As illustrated in Fig. 26.1, retrogression distance (L) refers to the total horizonal length of a slope that is involved in a landslide. The runout distance (Lu) is the depositional part or terminal flow path downstream from the toe. The entire length ($L + Lu$) affected by a landslide is often referred to as travel distance. In the literature, the assessment of L of sensitive clay landslides has received more attention than the estimation of Lu.

The guidelines for hazard mapping and construction on sensitive clay deposits by the Norwegian Water Resources and Energy Directorate (NVE 2014) require an assessment of *Lu.* However, in absence of an appropriate method, the assessment of *Lu* has so far been based on the experience of the individual geotechnical engineer in Norway. An agreed code of practice for the assessment of the runout distance *Lu* is lacking. An empirical procedure to determine runout distance together with main findings and recommendations are presented in this paper. This paper also presents initial ideas for the implementation of the recommendations in *GeoSuite Toolbox* (www.vianovasystems.no) which is being developed further as a part of an ongoing R&D project called GeoFuture-II (www.geofuture.no).

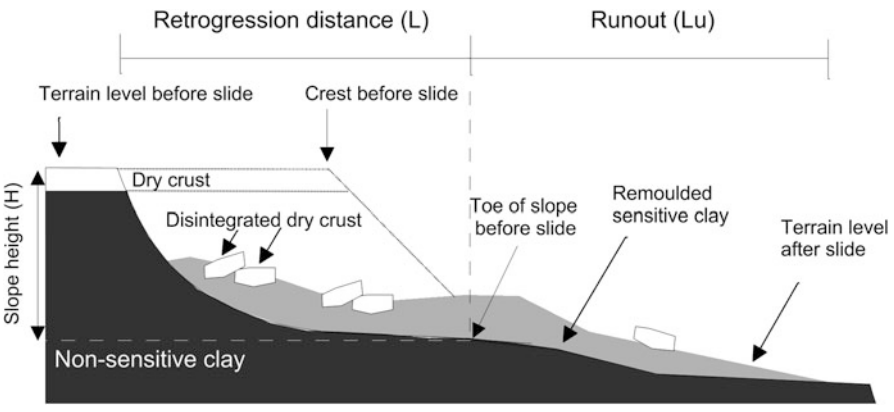

Fig. 26.1 Schematic illustration of landslide in sensitive clays

26.2 State of Knowledge on Landslide Runout

Several authors, e.g. Mitchell and Markell (1974), Corominas (1996), Rickenmann (1999), Fell et al. (2000), Fannin and Wise (2001), Legros (2002), Vaunat and Leroueil (2002), Bathurst et al. (2003), Crosta et al. (2003), Hungr (2005), Locat and Lee (2005), L'Heureux (2012), Thakur and Degago (2013), Haugen et al. (2017) proposed different analytical and empirical models to estimate L and Lu. These prediction methods are based on travel distance ($L + Lu$) and event magnitude, volume balance, mass point methods, remoulding energy, or some limiting criteria such as critical slope angle. However, continuum based simulation models to calculate Lu have so far received limited focus. Some approaches and methods have been developed in the past for a quantitative risk analysis using dynamic runout models for debris flows and avalanches such as BING (Imran et al. 2001) and NIS (Norem et al. 1990), and quasi-three-dimensional models such as DAN3D (Hungr 1995; McDougall and Hungr 2005), MassMov2D (Begueria et al. 2009), LS-RAIPD (Sassa 1988) and RAMMS (Christen et al. 2002). Depending on the characteristics of landslide debris, Bingham, plastic, frictional or Voellmy rheology is used. It is worth mentioning that none of these models are specifically developed for sensitive clay landslides. However, efforts are being made in this direction by Grue et al. (2017), Tran et al. (2017), Yifru et al. (2017), and Turmel et al. (2017), but a lot of research still needs to be done.

26.3 Factors Influencing the Runout of Sensitive Clay Debris

Historical landslides in sensitive clays in Norway form the basis for the recommendation made in this paper. Geotechnical and morphological information of these historical landslides can be obtained in L'Heureux (2012), Thakur et al. (2014), and NIFS (2016). The Norwegian landslide catalogue suggests that a combination of several factors, e.g. topography, geotechnical properties of the clay, landslide type, flow behaviour of sensitive clays, energy required to remould the sensitive clay and landslides retrogression, determine the extent of runout of sensitive clay debris. These factors are briefly summarized below.

26.3.1 Topography

Large landslides are often the result of initial failure under a favourable topographic situation, in which the remoulded materials have the possibility to flow out from the landslide pit. Hence, the downhill topography is a vital aspect for the occurrence of large runout. A downward sloping terrain will assist sensitive clay debris to flow a longer distance. However, in the absences of a suitable numerical tool, topographical aspects empirically predict the retrogression of landslides (Thakur et al. 2014).

26.3.2 Flow Behaviour

The flow behaviour of sensitive clays is usually described using remoulded shear strength (c_{ur}), liquidity index (I_L) and viscosity or quickness (Q). These parameters, which are interrelated, control the ability of sensitive clay debris to flow. The historical Norwegian landslides, as reported in the literature, show that flow slides in sensitive clays occur when the remoulded shear strength (c_{ur}) is less than 1 kPa. Demers et al. (2014) confirmed this observation with the data from 108 landslides in Canadian sensitive clays.

L'Heureux (2012) and Thakur et al. (2014) presented a comprehensive overview of several parameters that may influence the extent of landslides, and suggested that a large landslide with a retrogression greater than 100 m is only possible when $c_{ur} < 1.0$ kPa or $I_L > 1.2$ or $Q > 15\%$. Thakur and Degago (2012) explained this by using a so-called quickness test. The test shows that a material having $c_{ur} > 1.0$ kPa (or $Q < 15\%$) could not potentially cause a flow slide, because such material is very viscous and is more or less semi-solid in its remoulded state, as shown in Fig. 26.2.

26.3.3 Landslide Types

Landslides in sensitive clays can be categorized into four major types; flow slide, spreads, flake slide and rotational slide. Based on the landslide data, criteria to differentiate flow slide, flake slide and rotation slide in sensitive clay are established

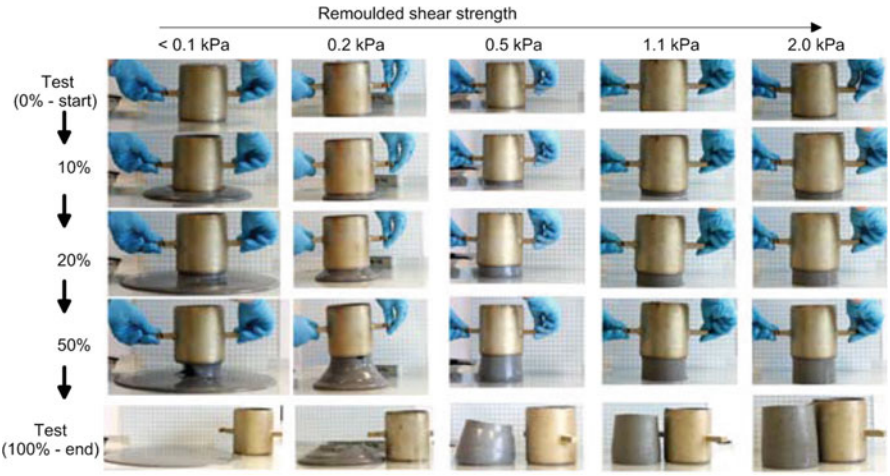

Fig. 26.2 Behaviour of remoulded sensitive clay in quickness test. The flow of the sensitive clay is illustrated from the start (0%) to the end (100%) of the test (After Thakur and Degago 2014)

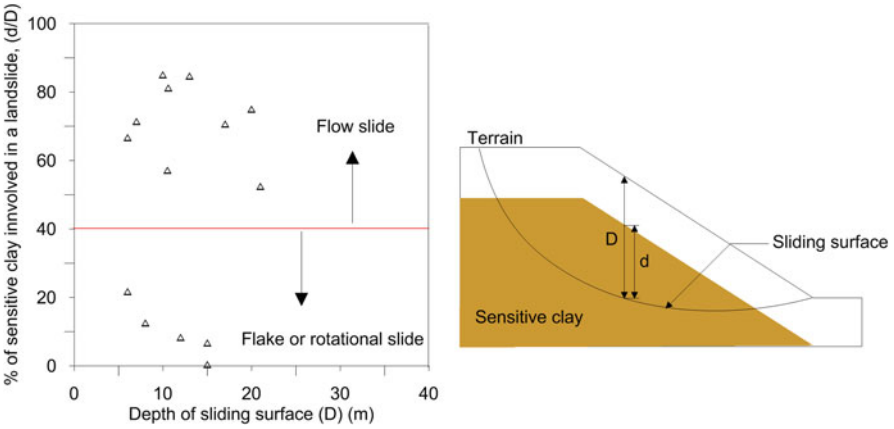

Fig. 26.3 Ratio of sensitive clay thickness (d) over depth of critical failure surface (D) for Norwegian landslides. A schematic visualization of parameters d and D

and discussed in the next paragraphs. Spread type landslides in sensitive clays are uncommon in Norway. This landslide type is not considered in this paper.

Flow slides, also known as retrogressive landslide, occur only when $d/D \geq 40\%$ according to historical data in Norway (Fig. 26.3). As illustrated in same Fig. 26.3, d is the average thickness of the sensitive clay layer having $c_{ur} < 1$ kPa over an area involved in a slide, and D is the average depth to the sliding surface from the terrain level over an area involved in a slide.

Flake slides may occur when the thickness of sensitive clay layer involved in a landslide relative to the depth to the sliding surface is under 40% ($d/D < 40\%$). Typically, flake slides occur when the sensitive clay lies in a layer approximately parallel to the ground surface. The landslide data suggest that d/D is found to be relatively low for flake slides, typically less than 10–20%. However, the Baastad flake slide in 1974 had an exceptionally high d/D ratio of 52%.

Rotational slides occur when the d/D ratio is less than 40% and there is no retrogression involved in the landslide.

26.3.4 Energy Aspects

Material involved in a landslide utilises a part of its potential energy in the disintegration of sensitive clays. The remaining energy, i.e. kinetic energy, is available for the runout of slide debris. Longer runout can be observed if less energy is utilised in the remoulding of the sensitive clay debris. By incorporating energy aspects for five identical sensitive clay landslides in characterising the post-failure movements, Thakur and Degago (2013) made a preliminary suggestion to calculate runout. Recently, Thakur et al. (2015, 2017) proposed a method to determine the remoulding energy of soft sensitive clays based on in-situ vane shear testing.

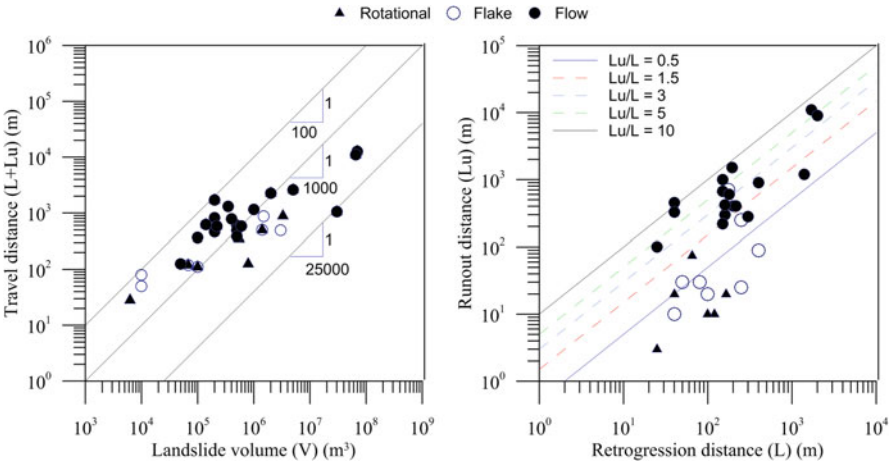

Fig. 26.4 Relationships between (*left*) travel distance ($L + Lu$) and landslide volume and (*right*) runout distance (Lu) and retrogression distance (L), landslides in Norwegian sensitive clays

26.3.5 Landslide Volume and Retrogression

Retrogression distance (L) and the total volume of landslides are positively correlated with runout distance (Lu), as shown in Fig. 26.4. The left-hand side Fig. 26.4 indicates that the ratio ($Lu + L$)/(Slide volume) is between 1/100 and 1/25,000. The retrogression distance L and runout distance Lu are also strongly correlated with the landslide type (rotational, flake or flow slides), as illustrated by Fig. 26.4 on the right. The Norwegian landslides along the shorelines have the largest Lu/L ratio with $Lu/L = 10$, whereas the ratio Lu/L seems to be much lower than 0.5 for many rotational and flake landslides in Norway. The majority of Norwegian onshore flow slides have a Lu/L ratio between 1 and 5, depending on the terrain characteristics, i.e. channelized or open terrain topography.

26.4 Recommendations and Procedure for the Assessment of Runout

The new recommendation for runout of sensitive clays is one of the products of the large inter-Govt. R&D project NIFS[1]. The approach uses geomorphological and geotechnical information from Norwegian landslides.

[1]NIFS is a large Inter Government R&D project by the Norwegian Public Roads Administration, the Norwegian National Rail Administration and the Norwegian Water Resources and Energy Directorate (Dolva and Pektovic 2017).

26.4.1 Retrogression and Runout Distances, Lu and L

Retrogression distance (L) is first determined. The current practice in Norway suggests that L should be between 15 and 20H, where H is the slope height (NVE 2014). Should one want to assess L more rigorously, stability analyses should be performed. In case of a flow slide, one needs to consider a backward cascading landslide development based on the stability number and/or assessments related to the remoulding energy (Thakur and Degago 2013). For flake and rotational slides, L should be based on stability calculations.

A recent semi-empirical methodology to assess L was recently proposed in NIFS (2016). In this approach one considers the geometry of the sensitive clay pocket and the potential for the sensitive clay to evacuate the landslide scar. Typical indicators necessary to evaluate L in this method includes: *b/D* ratio, topography in the runout zone, information from historical clay slides in the near area, and the stability number. Once a reasonable evaluation of L is obtained, one can evaluate *Lu* based on the relationships presented in Fig. 26.4 as follow:

$$\text{Flow slide in channelized terrain} : Lu = 3.0^{*}L \tag{26.1}$$

$$\text{Flow slide in open terrain} : Lu = 1.5^{*}L \tag{26.2}$$

$$\text{Flakes or rotational landslides} : Lu = 0.5^{*}L \tag{26.3}$$

26.4.2 Runout Zone and Width of Deposited Slide Debris, Bu

The recommended empirical relationships are based on topography, landslide types and *L.* They are considered suitable for onshore and coastal landslides in sensitive clays. Once the *Lu* is calculated, the possible run-out zone should be drawn on a map.

A conceptual example of this procedure for a 20 m high (H) and 280 m wide (B) slope is illustrated hereafter. The retrogression distance was calculated to be $15{\cdot}H = 300$ m. Assuming that more than 40% of the landslide debris is sensitive clay with $c_{ur} < 1$ kPa and that the runout takes place on a channelized terrain, one may expect a flow slide. Accordingly, *Lu* becomes 900 m (Fig. 26.5). The example is inspired by the region close to the Byneset 2012 flow slide. More information on the Byneset flow slide can be obtained from Thakur et al. (2013).

Equations 26.1, 26.2, and 26.3 provide one-dimensional information only. To estimate the width of deposited debris, *Bu,* it is necessary to estimate the potential runout area on a map. The runout zone and width of deposited slide debris are illustrated in Fig. 26.6 for three types of landslides.

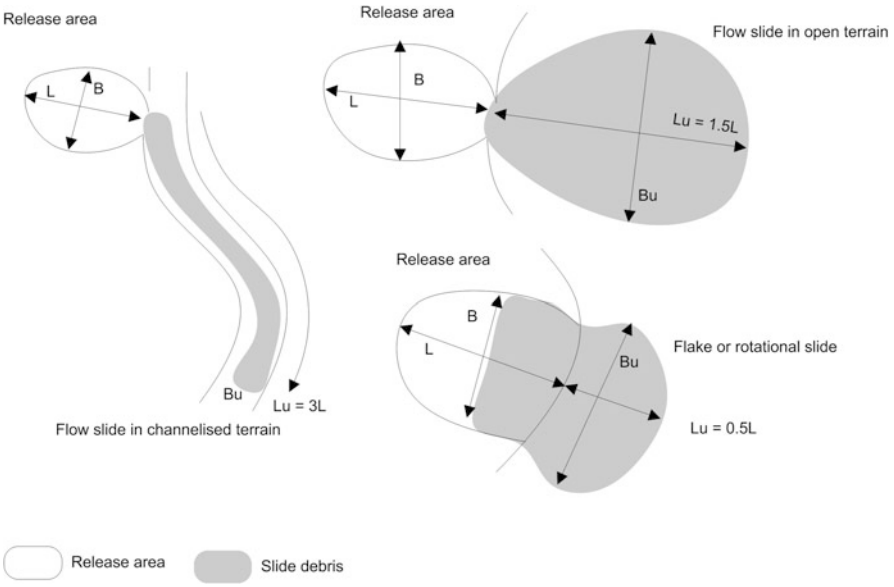

Fig. 26.5 Conceptual release area and runout zone for three landslide types

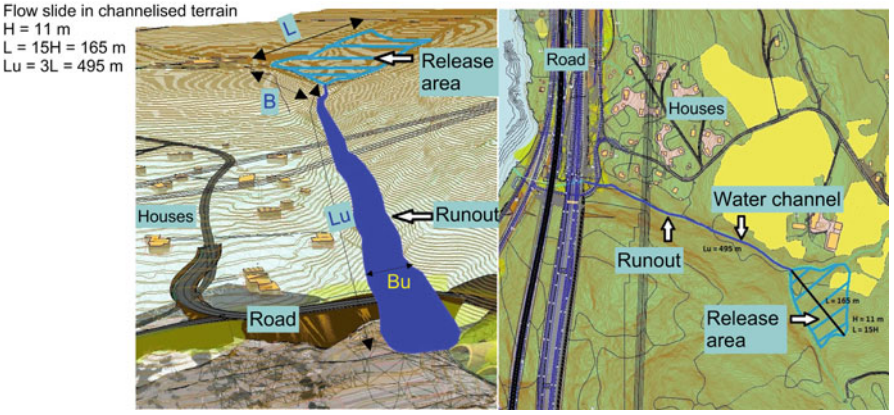

Fig. 26.6 Illustration of the release area and the runout path in 3D (*left*) and in 2D (*right*)

For flow slides, Bu can be estimated by assuming that $V = Vu$, where V is the volume of material involved in the landslide and Vu is the volume of slide debris along the runout path (outside the toe of the slope). The width of deposited debris Bu can be calculated from Eqs. 26.4 and 26.5. For flow slides in channelized terrain:

$$B_u = \frac{1}{3} \times \frac{D}{D_u} \times B \tag{26.4}$$

For flow slides in open terrain, *Bu* becomes:

$$B_u = \frac{2}{3} \times \frac{D}{D_u} \times B \tag{26.5}$$

where *D* is the depth of the sliding surface from the terrain (Fig. 26.3) and *Du* is the average thickness of slide debris deposited along the runout path. Equations 26.4 and 26.5 say that *Bu* and *Du* are interrelated. While *B* and *D* are known, *Bu* should be obtained incrementally for a representative value of *Du* such that the condition $V = Vu$ is achieved. The resulting value of *Du* and *Bu* will be greatly influenced by the characteristics of the terrain along and across the runout area. Information from the historical landslides should be utilised to get an idea over typical values of *D*/*Du* to use in Eqs. 26.4 and 26.5. It is important to mention that Eqs. 26.4 and 26.5 neglect the fact that the values of *Bu* and *Du* also depend on the shape of the release area (*B*/*L*), the inclination of the terrain, and the flow characteristics and behaviour of the remoulded slide debris. However, these aspects are implicitly included in Eqs. 26.1, 26.2, and 26.3.

For flake and rotational slides, a large part of the slide debris remains inside the release area. Based on the landslide data and Eq. 26.3, it is assumed that for this type of landslide 50% of the landslide volume leaves the release area. With $Vu = 0.5\ V$, the values *Du*/*D* become 0.5 and 1 for *Bu*/*B* equal to 2 and 1. Recent landslides, such as Leistad (2004) and the Skjeggestad bridge (2015), suggest that the *Bu*/*B* values were close to 1. Runout in a channelized terrain means that the slide debris are confined. On the other hand, slide debris are unconfined when the runout takes place in open terrain. For the latter case, the *Du* can theoretically set to not exceed $2{\cdot}c_{ur}/\gamma_s$, where c_{ur} and γ_s are the remoulded undrained shear strength and the total unit weight of the slide debris, respectively material.

26.5 Implementation Strategies and Future Developments

The above recommendation is being implemented in a new 'Slide runout' module in the software *GeoSuite Toolbox* as a part of the GeoFuture II R&D project (www.geofuture.no). This R&D project aims at integrating geotechnical design calculations with the management of in situ and laboratory geotechnical data, selection of input parameters for analysis, online assistance to the user and 3D visualisation. The 'Slide runout' module will assist in the assessment of the retrogression and runout distances with the above empirical relationships and will illustrate the runout over an area in three dimensions. This is conceptually illustrated in the Fig. 26.6 for a channelized flow slide from an 11 m high slope. The resulting distances were $L = 165$ m and $Lu = 495$ m. The figure illustrates that the debris flow downhill along the water channel and across a road sections.

Through landslide experience indicates that the empirical relationships usually fall short of a reliable prediction because of simplifications and approximations, the GeoSuite "Slide runout' module also aims to develop and implement in addition a continuum based model suitable for Scandinavian sensitive clays. Grue et al. (2017) suggests that a Herchel-Belkley rheology model (Locat and Demers 1988) may be representative to the behaviour of remoulded Norwegian sensitive clays. As part of the implementation, the new model will be validated possibly for both Norwegian landslides and selected landslides from landslides abroad.

26.6 Summary and Conclusions

Runout distance is of great significance for landslide hazard and risk assessment, particularly the identification of the elements at risk. The runout is usually predicted by one of two approaches: either empirical/statistical methods or analytical dynamic methods. A reliable estimation requires a detailed rheology model and material parameters that are rarely, if ever, available in practice. Until this becomes available for sensitive clays, it is recommended to perform estimate the runout and likely landslide impact with empirical methods.

This paper recommends a review of available and newly developed empirical approach to estimate landslide runout in for sensitive clays. The recommendations are based on a detailed catalogue of historical landslides in sensitive clays in Norway, and are now under implementation in the geotechnical calculation software *GeoSuite Toolbox*. These recommendations will be complemented with more advanced analytical model when more research results become available. For the time being, the recommendation in this paper can be used for an approximate estimation for landslides in sensitive clays.

Acknowledgements The cooperative research program (Natural Hazards: Infrastructure for Floods and Slides (NIFS)) and the partners in the GeoFuture II research program, and The Research Council of Norway are gratefully acknowledged for their support. The authors also wish to express their gratitude to the reviewer Dr. Samson Abate Degago, from Norwegian Public Roads Administration, for his valuable comments.

References

Bathurst JC, Burton A, Ward TJ (2003) Debris flow run-out and landslide sediment delivery model tests. J Hydraul Eng 123(5):410–419

Begueria S, Van Asch TWJ, Malet JP, Gröndhal S (2009) A GIS-based numerical model for simulating the kinematics of mud and debris flows over complex terrain. Nat Hazards Earth Syst Sci 9:1897–1909

Bjerrum L (1955) Stability of natural slopes in quick clay. Geotechnique 5(1):101–119

Christen M, Bartelt P, Gruber U (2002) AVAL-1D: an avalanche dynamics program for the practice. In: International congress interpraevent 2002 in the Pacific Rim – Matsumo, Japan, congress publication. 2, pp 715–725

Corominas J (1996) The angle of reach as a mobility index for small and large landslides. Can Geotech J 33(2):260–271

Crosta GB, Cucchiaro S, Frattini P (2003) Validation of semi-empirical relationships for the definition of debris-flow behavior in granular materials. In: Rickenmann D, Chen C (eds) 3rd international conference on debris-flow hazards mitigation. Millpress, Davos, pp 821–831

Demers D, Robitaille D, Locat P, Potvin J (2014) Inventory of large landslides in sensitive clays in the province of Quebec, Canada: preliminary analysis. Natural hazards book: advances in natural and technological hazards research. ISSN: 1878–9897 (Print) 2213–6959 (Online). pp 77–89

Dolva BK, Petkovic G (2017) Natural hazards in changing climate. Second international workshop on landslides in sensitive clays. Springer book series advances on natural and technological hazards research. This volume

Fannin RJ, Wise MP (2001) An empirical–statistical model for debris flow travel distance. Can Geotech J 38:982–994

Fell R, Hungr O, Leroueil S, Reimer W (2000) Keynote lecture – geotechnical engineering of the stability of natural slopes, and cuts and fills in soil. GeoEng 2000, issue 1, pp 21–120

Grue R, Issler D, L'Heureux JS, Thakur V (2017) Viscometric tests of sensitive clay from Byneset, Norway, and fit to the Herschel–Bulkley model Second International Workshop on landslides in sensitive clays. June 2017. Springer book series Advances on natural and technological hazards research

Haugen ED, Tveit M, Heyerdahl H. (2017) Mapping quick clay hazard zones: a new method for the estimation of the retrogression distance applied to existing zones. Second international workshop on landslides in sensitive clays. June 2017. Springer book series Advances on natural and technological hazards research. This volume

Hungr O (1995) A model for the runout analysis of rapid flow slides, Debris flows, and avalanches. Can Geotech J 32(4):610–623

Hungr O (2005) Classification and terminology. Debris-flow hazards and related phenomena. Springer. ISBN 3–540–20726-0. pp 9–24

Hungr O (2016) A review of landslide hazard and risk assessment methodology. Landslides and engineered slopes. Experience, theory and practice. Proceedings of the 12th international symposium on landslides (Napoli, Italy)

Imran J, Parker G, Locat J, Lee H (2001) 1D numerical model of muddy subaqueous and subaerial debris flows. J Hydraul Eng 127(11):959–968

Karlsrud K, Aas G, Gregersen O (1985) Can we predict landslide hazards in soft sensitive clays? Summary of Norwegian practice and experience. NGI Publication 158

L'Heureux JS (2012) A study of the retrogressive behaviour and mobility of Norwegian quick clay landslides. Proc. 11th INASL, Banff, Canada, vol 1. pp 981–988

Lacasse S (2013) 8th Terzaghi Oration. Protecting society from landslides – the role of the geotechnical engineer. 18th international conference on soil mechanics and geotechnical engineering. Paris. 20p

Lacasse S (2016) 55th rankine lecture hazard, risk and reliability in geotechnical practice. Geotechnique

Lebuis J, Robert JM, Rissmann P (1983) Regional mapping of landslide hazard in Quebec. In Proceedings of the symposium slopes on soft clays. SGI Report 17. pp 205–262

Lefebvre G (1981) Strength and slope stability in Canadian soft clay deposits. Can Geotech J 18:420–442

Legros F (2002) The mobility of long-runout landslides. Eng Geol 63:301–331

Leroueil S, Locat J, Vaunat J et al. (1996) Geotechnical characterization of slope movements. In: Senneset K (ed) Proceedings of the 7th international symposium on landslides. pp 53–74

Locat J, Demers D (1988) Viscosity, yield stress, remolded strength, and liquidity index relationships for sensitive clays. Can Geotech J 25:799–806

Locat J, Lee HJ (2005) Subaqueous debris flow. Debris-flow hazards and related phenomena. Springer, pp 203–246. ISBN 3–540–20726-0

Locat P, Leroueil S, Locat J (2008) Remaniement et mobilité des débris de glissements de terrain dans les argiles sensible de l'est du Canada, Proceedings of the 4th Canadian conference on geohazards: from causes to management. Presse de l'Université Laval, Québec, pp 97–106

Locat A, Leroueil S, Bernander S et al (2011) Progressive failures in eastern Canadian and Scandinavian sensitive clays. Can Geotech J 48:1696–1712

McDougall S, Hungr O (2005) Modeling of landslides which entrain material from the path. Can Geotech J 42:1437–1448

Mitchell RJ, Markell AR (1974) Flow slides in sensitive soils. Can Geotech J 11(1):11–31

NIFS (2016) Metode for vurdering av løsne – og utløpsområder for områdeskred Report 14/2016. ISBN: 978-82-410-1204-4

Norem H, Locat J, Schieldrop B (1990) An approach to the physics and the modeling of submarine flowslides. Mar Geotechnol 9:93–111

NVE (2014) Construction on brittle clays. Guidelines by NVE, Norway

Rickenmann D (1999) Empirical relationships for debris flows. Nat Hazards 19(1):47–77

Rickenmann D (2005) Run-out prediction methods. In: Jakob M, Hungr O (eds) Debris-flow hazards and related phenomena. Springer, Berlin, pp 305–324

Sassa K (1988) Special lecture: geotechnical model for the motion of landslides. In: Bonnard C (ed) Proc. of 5th symp. on landslides. Balkema, Rotterdam, pp 37–55

Tavenas F, Flon P, Lerouil S et al (1983) Remolding energy and risk of slide retrogression in sensitive clays. Proc. of the Symp. slopes on soft clays, Linköping, Sweden. pp 423–454

Thakur V, Degago SA (2012) Quickness of sensitive clays. Géotech Lett 2(3):87–95

Thakur V, Degago SA (2013) Disintegration of sensitive clays. Géotech Lett 3(1):20–25

Thakur V, Degago SA (2014) Quickness approach for assessment of flow slide potential. Int J SEAGS AGSSEA 45(1):85–94

Thakur V, Degago S, Oset F, Dolva BK, Aabøe R, Aunaas K, Nyheim T, Lyche E, Jensen OA, Viklund M, Sæter MB, Robsrud A, Nigguise D, L'Heureux JS (2013) Characterization of post-failure movements of landslides in soft sensitive clays. Natural hazards book: advances in natural and technological hazards research. ISSN: 1878-9897 (Print) 2213-6959 (Online). pp 91–104

Thakur V, Degago S A, Oset F, Aabøe R, Dolva BK, Aunaas K, Nyheim T, Lyche E, Jensen OA, Sæter MB, Robsrud A, Viklund M, Nigussie D (2014) Characterization of post-failure 242 movements of landslides in soft sensitive clays. First international workshop on landslide in 243 sensitive clays. Advances in natural and technological hazards research 36, Chapter: 24, 244. Springer, pp 91–103

Thakur V, Degago SA, Oset F, Gylland SA, Sandven R (2015) In-situ measurement of remolding energy of sensitive clay. 68th Canadian Geotechnical Conference, GeoQuebec, Quebec

Thakur V, Degago SA, J. Selänpää, Länsivaara T (2017) Determination of remoulding energy of sensitive clays. Second international workshop on landslides in sensitive clays. June 2017. Springer book series Advances on natural and technological hazards research. This volume

Tran QA, Solowski W, Thakur V, Karstunen M (2017) Modelling of the quickness test of sensitive clays using the generalized interpolation material point method. Second International Workshop on landslides in sensitive clays. June 2017. Springer book series Advances on natural and technological hazards research

Turmel D, Locat J, Locat P, Demers D (2017) Parametric analysis of the mobility of debris from flow slides in sensitive clays. Second International Workshop on landslides in sensitive clays. June 2017. Springer book series Advances on natural and technological hazards research

Vaunat J, Leroueil S (2002) Analysis of post-failure slope movements within the framework of hazard and risk analysis. Nat Hazards 26:83–102

Yifru A, Degago S, Thakur V (2017) Back-calculation of the Byneset sensitive clay slide using the modified Voellmy rheology. Second International Workshop on landslides in sensitive clays. June 2017. Springer book series Advances on natural and technological hazards research

Chapter 27
Parametric Analysis of the Mobility of Debris from Flow Slides in Sensitive Clays

Dominique Turmel, Jacques Locat, Pascal Locat, and Denis Demers

Abstract Sensitive clays are prone to various types of landslides. Among these are flow slides that are able to affect hectares of land. Moreover, debris from these flow slides has a high mobility with run out distance of hundreds of meters, even in relatively flat areas, are quite common. In the context of hazard mapping, mobility of the debris is also an important factors to consider. In this context, a parametric analysis using simplified geometries is undertaken in order to evaluate the run out characteristics of these flows (such has the length of the run out area and the lateral spread of the debris) as a function of the rheological parameters such as the yield stress and viscosity. In order to proceed with the parametric analysis, a newly developed 3D numerical model was used.

27.1 Introduction

For an accurate assessment of landslide hazards in sensitive clays, two different parameters must be determined. The first one is the retrogressive distance of the landslide, and the other the run-out distance. Most rotational landslide in sensitive clays shows relatively low run-out distance. However, multiple retrogressive slides, in particular flow slides, have a high mobility and these landslides are able to affects lands on hundreds of meters and in relatively flat areas. In Canada, the Saint-Jean Vianney landslide is a well-known multiple retrogressive landslide, which showed run-out of over 2.8 km under channel condition (Tavenas et al. 1971). In Norway, the Verdal slide, which is the largest known quick clay slide in Norway, had a run-out of 9 km and a thickness of over 8 m (L'Heureux 2012). Numerical models able to estimate the run-out distance of sensitive clays flow slides are not commercially available (Grue 2015). According to Thakur et al. (2014), this

D. Turmel (✉) • J. Locat
Laboratoire d'études sur les risques naturels (LERN), Université Laval, Québec, QC, Canada
e-mail: dominique.turmel.1@ulaval.ca; jacques.locat@ggl.ulaval.ca

P. Locat • D. Demers
Ministère des Transports, de la Mobilité durable et de l'électrification des transports, Québec, QC, Canada
e-mail: Pascal.Locat@transports.gouv.qc.ca; Denis.Demers@transports.gouv.qc.ca

V. Thakur et al. (eds.), *Landslides in Sensitive Clays*, Advances in Natural and Technological Hazards Research 46, DOI 10.1007/978-3-319-56487-6_27

absence of models may be caused by, among others, insufficient knowledge about the complex rheological behaviour of sensitive clays. Therefore, the assessment of retrogression distance and runout are calculated using some empirical approaches. In this paper, a new numerical model is introduced. The model shall be able, in a near future, to estimate the areal runout extent of flow slides in sensitive clays. The reader is referred to Locat et al. (2017), where this model is used to model a real landslide. In this paper, a parametric analysis showing the effect of different rheological parameters on the run-out extent of debris will be presented. In the sections below, following the presentation of empirical relationships, the numerical model used, i.e. OpenFOAM will be presented. The different scenarios for the parametric analysis will then be describe, with the results of the modeling. These results will finally be discussed and compared with empirical relationships.

27.2 Empirical Relationships

Using 22 landslides in Quebec province, with debris not channelized, Locat et al. (2008) established different relations between the run-out distance (D) and volume mobilized (Vol) by width unit (W_M) and between the run-out distance and retrogression distance (R) (Figs. 27.1 and 27.2). In these relations, the run-out distance is measured from the toe of the slope where the retrogression distance is measured from the crest of the slope. The terminology used here is from Locat et al. (2008). They did establish mean values and maximum values for these relationships. The maximum values are:

$$D = 1.3\left(\frac{Vol}{W_M}\right)^{0.73} \tag{27.1}$$

$$D = 8.8R^{0.8} \tag{27.2}$$

L'Heureux (2012), using Norwegian landslides, established a similar relationship as (27.1) (Fig. 27.1), using not only subaerial landslides, but also submarine and channelized landslides. He found that the maximum value would be:

$$D = 9\left(\frac{Vol}{W_M}\right)^{0.73} \tag{27.3}$$

Finally, Strand et al. (2017) proposed another empirical approach to estimate the runout distance. This approach derives from a large inter-ministry research project in Norway called NIFS (Dolva and Petkovic 2017). They propose to use these relationships for flow slide in channelized terrain and in open terrain. It must be mentioned here that Strand et al. relationships do not use the same definition for retrogression distance, they consider it to be calculated from the toe of slope before slide and not from the crest of slope before slide.

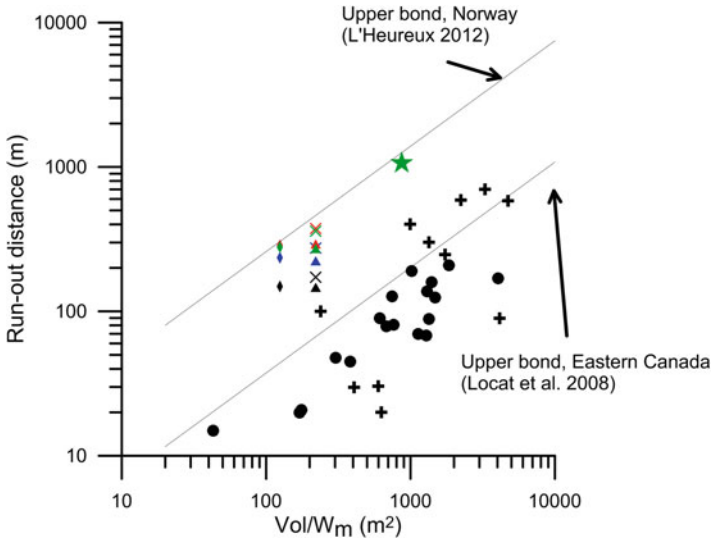

Fig. 27.1 Run-out distance as a function of the volume mobilized, normalized by the landslide width. Dark circles are data from Locat et al. (2008) where crosses are from L'Heureux (2012). Results from this study are also presented. *X* marks are for geometry 1, *triangle* for geometry 2, *diamond* for geometry 3 and *star* for geometry 4. *Black* is for $I_L = 1.2$, *blue* for $I_L = 2$, *red* for $I_L = 3$ and *green* for $I_L = 4$.

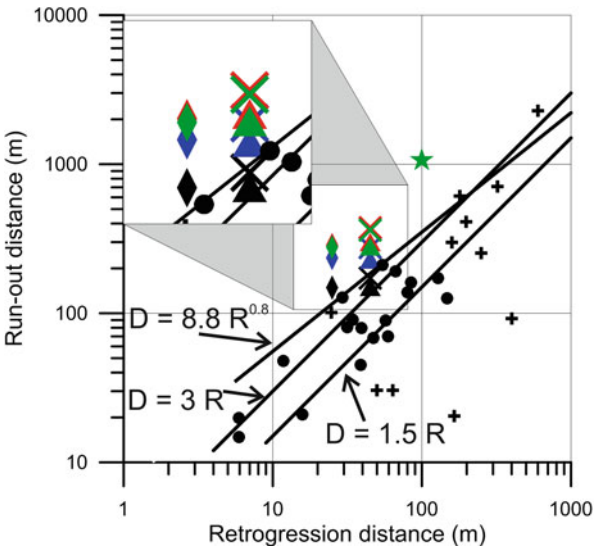

Fig. 27.2 Run-out distance as a function of the retrogression distance. Same color and symbol legend as in Fig. 27.1

$$\text{For flowslide in channelized terrain}: \quad D = 3.0^{*}R \tag{27.4}$$

$$\text{For flowslide in open terrain}: \quad D = 1.5^{*}R \tag{27.5}$$

It is possible to see in Fig. 27.1 that if only the terrestrial events are taken into account, the propagation distance is still higher than for Eastern Canada landslides. L'Heureux (2012) attributes the higher run-out distance showed by Norwegian landslides by difference in geotechnical properties between Eastern Canada and Norwegian clays.

27.3 Numerical Model

The software used to do the numerical modeling is called OpenFOAM (Open Field and Manipulation), which is a set of C++ modules used to build solvers to simulate specific problems in engineering mechanics (Weller et al. 1998). For this specific analysis, the solver called "interFoam" was used. This module is available as part of the OpenFOAM software. This is a solver for 2 incompressible fluids, that tracks the interface Γ between the fluids and includes dynamic meshing. This solver uses the Volume of Fluid (*VoF*) method to resolve Navier-Stokes equations over a finite-volume mesh. For a complete description of the interFoam solver, the reader is referred to Deshpande et al. (2012).

Considering a computational volume Ω that is composed of two phases, air and remoulded clay, one may map which portion of Ω is composed of each phase. A value of $\alpha = 0$ will be given for each elements that are composed of air, a value of $\alpha = 1$ for each elements composed of remoulded clay, and a value between 0 and 1 at the interface. This value will be equal to the portion of clay in this element. The first equation resolved by interFoam is equivalent to the conservation of mass equation solved in flows involving one fluid. This equation can be written:

$$\frac{\partial \alpha}{\partial t} + \nabla \cdot (\mathrm{U}\alpha) = 0 \tag{27.6}$$

Where U is the velocity. In practice, Eq. 27.6 implies that the transport of the liquid fraction has to be accomplished by a velocity field that corresponds to the liquid (Deshpande et al. 2012).

The second equation resolved is the momentum equation. For a two-phase flow, the following equation is applied (Deshpande et al. 2012).

$$\begin{aligned}\frac{\partial \rho \mathrm{U}}{\partial t} + \nabla \cdot (\rho \mathrm{U} \otimes \mathrm{U}) = -\nabla p + [\nabla \cdot (\mu \nabla \mathrm{U}) + \nabla \mathrm{U} \cdot \nabla \mu] \\ + \rho \mathrm{g} + \int_{\Gamma} \sigma \kappa \delta \left(\mathrm{x} - \mathrm{x_s}\right) \mathrm{n} d\Gamma \left(\mathrm{x_s}\right)\end{aligned} \tag{27.7}$$

In this equation, σ refers to surface tension coefficient, g the gravitational acceleration and $\delta(x - x_s)$ is the 3D Dirac delta function. κ is the local interfacial curvature defined as.

$$\kappa = -\nabla \cdot n \tag{27.8}$$

where n is the face centered interface normal vector.

It must be noted that in Eq. 27.7, only one ρ value and only one μ value are present, where both fluids (air and remoulded clays) have different ρ and μ value. In cells where only one fluid is present, this fluid value of ρ and μ values will be used. In interfacial cells, fluid density and viscosity are obtained by:

$$\rho = \alpha\rho_{clay} + (1 - \gamma)\,\rho_{air}; \quad \mu = \alpha\mu_{clay} + (1 - \gamma)\,\mu_{air} \tag{27.9}$$

As will be presented in the following section, rheology of remoulded sensitive clays can be described as a Herschel-Bulkley fluid. For such a fluid, the viscosity is defined in the numerical model as:

$$\mu = \min\left(\mu_0, \frac{\tau_0}{\gamma} + k\gamma^{n-1}\right) \tag{27.10}$$

This means that, at very low shear rate, the viscosity is equal to μ_0 which is defined as very viscous, where at higher shear rate, the real equivalent viscosity is calculated. For more information on how this equation system is resolved, reader is referred to Deshpande et al. 2012.

27.4 Parametric Analysis

A parametric analysis was performed on four different geometries. Table 27.1 shows the different characteristics of the landslides modeled. For all the geometries, the angle of the rupture surface was set to be 4 °, the slope angle at around 45 ° and the natural terrain was parallel to the surface of rupture. On the downstream side, the terrain is flat. Geometries 1 and 2 are chosen to have the same retrogression distance, but not the same width, where the difference between geometry 1 and 3 is in the retrogression distance Geometry 4 has a greater volume by a magnitude 10. This choice in the modeled geometries will allow looking at the mobilized volume vs landslide width relationship previously described. For the first three geometries, four different rheology were tested, which corresponds to liquidity index of 1.2, 2, 3 and 4. For the fourth geometry, only one liquidity index was used, i.e. 4. The rheological properties used in the analysis are given in Table 27.2, using relationships developed for eastern Canada clays (Eqs. 27.11 and 27.12). Locat and Demers (1988) showed that a good correlation exist between the liquidity index, the viscosity and remolded

Table 27.1 Geometric properties of the release area

Geometry	Width (m)	Retrogression distance (m)	Depth (m)	Volume (m^3)	Symbol
1.	40	45	5	8800	X
2.	20	45	5	4400	▲
3.	40	25	5	5000	♦
4.	100	100	8,7	87,000	★

Table 27.2 Rheological properties used in the numerical modeling

I_L	Yield strength (Pa)	Viscosity (mPa.s)
1,2	935	905
2	268	165
3	100	43
4	50	16

shear strength, for liquidity index between 1.5 and 6. Later, Locat (1997) showed that most sensitive clays behave as a Bingham or a Herschel-Bulkley fluid.

Locat (1997) proposed, using results from multiple experiments, relationships between viscosity (in mPa.s) and liquidity index, and between yield strength and liquidity index:

$$\mu = \left(\frac{9.27}{I_L}\right)^{3.3} \tag{27.11}$$

$$\tau_0 = \left(\frac{5.81}{I_L}\right)^{4.55} \tag{27.12}$$

For all the simulations, as a simplification, a constant total density of 2000 kg/m^3 was used for the remoulded clay. Some tests made by the authors showed that the total density have a little influence in the runout extent. Finally, the boundary condition on the run-out surface was set as a zero velocity boundary condition.

27.5 Results

In all the simulations, debris were allowed to spread freely on a flat terrain, which was large and wide enough to accommodate all the material. Two main parameters are reported here: the maximum width that was reached by at least 5 cm of debris and the maximal length that was reached by at least 5 cm of debris. Results from the different geometries, and from the different rheology, are reported in Table 27.3. They are also reported in Figs. 27.1 and 27.2, which allow a direct comparison with the previous case history data reported by Locat et al. (2008) and L'Heureux (2012). Figure 27.3 shows the maximum run-out length and width as a function of the volume of the slide, for all the simulations.

Table 27.3 Simulation results

	1.2		2		3		4	
IL	Width (m)	Length (m)	Width (m)	Length (m)	Width (m)	Length (m)	Width (m)	Length (m)
Geometry 1	116	172	200	275	300	374	300	360
Geometry 2	88	143	160	219	212	286	204	267
Geometry 3	94	149	150	235	202	286	180	277
Geometry 4							748	1060

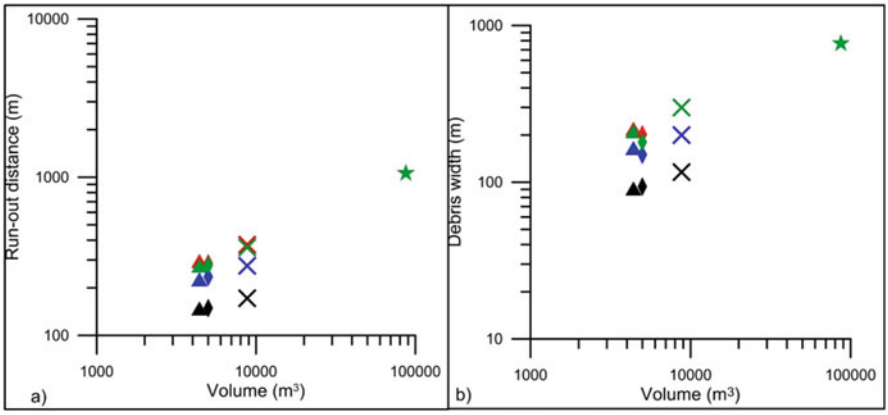

Fig. 27.3 (**a**) Run-out distance as a function of the mobilized volume and (**b**) Maximum debris width as a function of the volume. *Symbols* and *colors* are the same as in Fig. 27.1

27.6 Discussion

In these numerical experiments, two main parameters were varied: rheological parameters and geometry. It must be remembered here that, for all these experiments, the material was considered remolded from the beginning of the movement. This would say that, if remolding energy was taken into account, the run-out distance would be lower. These are then maximal values of run-out distance, considering a rheology and geometry. It is interesting to note that, in Fig. 27.1, all the results are lower than the upper bond described by L'Heureux (2012). However, in Fig. 27.2, almost all the results shows longer distance of propagation than the relationships described by Locat et al. (2008) and the guidelines from Strand et al. (2017). However, results of the simulations shows that the relation between the run-out distance and retrogression distance will be a linear relationship, as described in Strand et al. (2017) and not a power relationship as proposed by Locat et al. (2008).

27.6.1 Effect of Rheology

Up to a certain point, the rheology plays an important role in the run-out behaviour of the landslide. This is illustrated in Fig. 27.1 and 27.3a, where the run-out distance is plotted against the volume of the volume mobilized by width unit and with the volume. As expected, for a rheology that corresponds to a low liquidity index, the propagation distance will be lower than for a rheology corresponding to a higher liquidity index. This result from the fact that at low liquidity index, a plug flow will form since the yield strength of the material is high. When the shear stress at the base of this plug flow is below the yield strength, the volume will stop moving. Using Johnson (1984) relationship (13) between the final thickness of the deposit (H_f), which will be approximated as the plug flow height, the unit weight (γ') and the deposition slope (β_f), it can be calculated that for I_L of 1.2, 2, 3 and 4, the plug flow height will be of, for a slope of 1 °, of 2.8, 0.8, 0.3 and 0.15 m respectively. These values consider a static case, and since the flowing mass is moving at a certain velocity, the plug flow height should be lower than these values.

$$\tau_{ya} = H_f \gamma' \sin \beta_f \tag{27.13}$$

27.6.2 Effect of Geometry

Four different geometry were tested, with four different volumes. This effect can be seen on Figs. 27.1 and 27.2, where the propagation distance is compared to the volume mobilized as a function of the width and where the run-out distance is compared with the retrogression distance. When using the volume mobilized as a function of the landslide width, we can see that, for a same ratio and for the same rheological parameters, there will be a difference in the propagation distance if the width is not the same. Figure 27.2 shows that, for the same rheological parameters and the same retrogression distance, the run-out distance will not be the same, depending of the width of the landslide. It appears from Fig. 27.3 that the most important parameter to take into account for the propagation length is not the geometry of the landslide itself, but its total volume. However, for the maximum width of the debris, the geometry plays an important role, as this maximum width is a function of the initial width of the landslide (Fig. 27.3b). As an example, for the geometry 3, the maximum width is lower than with geometry 2, even if the volume is slightly higher. Finally, it is interesting to note that the upper bond for Norwegian slides defined by L'Heureux (2012) (Fig. 27.1) was never reached in our simulations, but all the simulations with the highest liquidity index are very close to this bond. This verification was the purpose of the simulation with the highest volume.

27.6.3 Remolding Energy

Results from the simulations shows that the maximum run-out distance, if we consider that there is no energy required to remold the samples, are higher than the field observations, which is expected. The next step in the modeling process will be to try to take into account the remolding energy, in order to be able to do a better modeling of the flow slides. With the OpenFOAM software, two different avenues are possible. The first one will be to limit the available potential energy, in order to simulate the energy lost in the remolding. The other avenue would be to find equivalent rheological parameters that take into account the remolding energy. In order to be able to develop one or the other option, multiple back-analyses will be needed, as well as geotechnical investigations and rheological investigations on the sites where flow slides happened. It will then be possible with such a data set to integrate the destructuration index, as defined by Vaunat and Leroueil (2002) in the modeling. This index is the ratio between the potential energy of a landslide and the energy required to remould a sample. According to Thakur et al. (2014), as low as only 5% of the total potential energy would be sufficient to remould Norwegian sensitive clays.

27.7 Conclusion

In this paper, we have described a numerical model able to simulate the propagation of flow slides in a full 3D frame. Using four different geometries, as well as four different rheology, their role in the post-failure behaviour was illustrated. For the geometry, it was shown that the most important parameter for the run-out distance was the volume displaced, and not the geometry itself. However, the width of the debris will be dependant of the width of the scar. The rheology will also play a role in the distance reached by the debris. For rheology equivalent to material with liquidity index under 3, there will be a difference in the run-out distance. However, at liquidity index over 3, difference in rheological won't anymore influence the movement, and the propagation distance will be approximately the same, i.e. independent of the rheology. All the simulations presented in this paper were done with completely remolded material, i.e. it represents a maximum run-out distance. It does not take into account the energy needed to remold the material. Future research will be needed in order to be able to take into account, in the numerical simulations, the energy lost in this process.

Acknowledgments The research presented in this paper has been financially supported by the Ministère de la Sécurité Publique du Québec, the Ministère des Transports, de la mobilité durable, et de l'électrification des transports, and by the Plan d'actions sur les changements climatiques (PACC). The authors also wish to express their gratitude to Vikas Thakur, NTNU, for his review of the manuscript.

References

Deshpande SS, Anumolu L, Trujillo MF (2012) Evaluating the performance of the two-phase flow solver interFoam. Comput Sci Discov 5:1–36. 37 p

Dolva BK, Petkovic G (2017) Natural hazards in changing climate. Second international workshop on landslides in sensitive clays. In: Thakur V, L'Heureux J-S, Locat A (eds) Landslides in sensitive clays. From research to implementation, Advances on natural and technological hazards research. Springer, Dordrecht, pp 539–547

Grue RH (2015) Rheological parameters of Norwegian Sensitive Clays, focusing on the Herschel-Bulkley model. Master thesis, Institute of Civil and Transport Engineering, NTNU Trondheim, 128 p

Johnson AM (1984) Debris flow. In: Brunsden D, Prior D (eds) Slope instability. Wiley, New York, pp 257–361

L'Heureux J-S (2012) Characterization of historical quick clay landslides and input parameters for Q-Bing. Report no. 39/2013, Norwegian Geotechnical Institute, 46 p

Locat J (1997) Normalized rheological behaviour of fine muds and their flow properties in a pseudoplastic regime. In: Proceedings of the 1st international conference on debris-flow hazards mitigation. ASCE, San Francisco/New-York, pp 260–269

Locat J, Demers D (1988) Viscosity, yield stress, remolded strength, and liquidity index relationships for sensitive clays. Can Geotech J 25:799–806

Locat P, Leroueil S, Locat J (2008) Remaniement et mobilité des débris de glissements de terrain dans les argiles sensibles de l'est du Canada. In: Proceedings of the 4th Canadian conference on Geohazards: from causes to management, 10 p

Locat J, Turmel D, Locat P, Therrien J, Létourneau M (2017) The 1908 disaster of Notre-Dame-de-la-Salette: analysis of the landslide and tsunami. Second international workshop on landslides in sensitive clays. In: Thakur V, L'Heureux J-S, Locat A (eds) Landslides in sensitive clays. From research to implementation, Advances on natural and technological hazards research. Springer, Dordrecht, pp 361–371

Strand SA, Thakur V, L'Heureux J-S, Lacasse S, Karlsrud K, Nyheim T, Aunaas K, Ottesen H, Gjelsvik V, Fauskerud OA, Sandven R, Rosenquist A (2017) Runout of landslide in sensitive clays. Second international workshop on landslides in sensitive clays. In: Thakur V, L'Heureux J-S, Locat A (eds) Landslides in sensitive clays. From research to implementation, Advances on natural and technological hazards research. Springer, Dordrecht, pp 289–300

Tavenas F, Chagnon J-Y, La Rochelle P (1971) The Saint-Jean Vianney landslide: observations and eyewitnesses accounts. Can Geotech J 8:463–478

Thakur V, Nigussie D, Degago SA (2014) A preliminary study of rheological models for run-out distance modelling of sensitive clay debris. Numerical methods in Geotechnical Engineering, 7 p

Vaunat J, Leroueil S (2002) Analysis of post-failure slope movements within the framework of hazard and risk analysis. Nat Hazards 26:83–109

Weller JG, Tabor G, Jasak J, Fureby C (1998) A tensorial approach to computational continuum mechanics using object-oriented techniques. Comput Phys 12:620–631

Chapter 28
Mapping Quick Clay Hazard Zones: Comparison of Methods for the Estimation of the Retrogression Distance

Ellen D. Haugen, Morten Tveit, and Håkon. Heyerdahl

Abstract The Norwegian regional mapping of quick clay hazard zones uses a 1:15 inclined line from the foot of the slope to decide the maximal retrogression distance of a quick clay slide. When the hazard zones are subjected to a more detailed examination, the site investigations give a better picture of the location of the quick clay, which is decisive for what type of slide that may occur. Based on this, a method was developed through the research project "Natural hazards – infrastructure for floods and slides (NIFS)". This has been applied to an existing hazard zone and compared with other existing methods to draw the depletion zone. The implementation shows the importance of first deciding the slide mechanism. If the extent of the quick clay is well mapped, the NIFS-method can be a useful tool to evaluate the retrogression distance, but it must be used with careful consideration of the geotechnical conditions.

28.1 Introduction

After the large quick clay slide in Rissa in 1978, national mapping of hazard zones was initiated by the Norwegian state (NVE 2011). Per 2016 over 1900 hazard zones have been mapped. These fulfil the criteria where large quick clay slides could occur (cf. Gregersen 2004, 2008). The hazard zones are taken into to land-use plans of each municipality to secure safe building plots. In the zones there are strict regulations to construction work and urban development, and for new

E.D. Haugen (✉)
Norwegian Water Resources and Energy Directorate (NVE), Tønsberg, Norway
e-mail: edha@nve.no

M. Tveit
Rambøll Norge AS, Kristiansand, Norway
e-mail: morten.tveit@ramboll.no

H. Heyerdahl
Norwegian Geotechnical Institute (NGI), Oslo, Norway
e-mail: Hakon.Heyerdahl@ngi.no

V. Thakur et al. (eds.), *Landslides in Sensitive Clays*, Advances in Natural and Technological Hazards Research 46, DOI 10.1007/978-3-319-56487-6_28

houses geotechnical investigations and stabilizing measures must be done before new projects are permitted (NVE 2014; Kalsnes et al. 2014; Oset et al. 2014).

To decide the maximum retrogression distance of a potential quick clay slide, a length to height ratio from the toe of the slope to the top of the back scarp (perpendicular on the contour lines) was decided empirically. Karlsrud et al. (1985) compared the L/H-ratio of landslides in clay investigated by NGI over 15 years (six of them in quick clay) and concluded that a maximum for quick clay slides was L/H = 15. Based on this study the 1:15-line from the toe of the slope defines the retrogression distance. This ratio is used to decide the size of the quick clay hazard zones mapped in the national mapping. The ratio does not take into account the location and thickness of the quick clay, which may reduce the size of a potential slide. It is therefore generally assumed that the extent of the hazard zones resulting from the national mapping is on the conservative side, although a few landslides have been larger (L'Heureux 2012). Usually it is only where ground investigations reveal shallow bedrock, bedrock outcrops, or no quick clay, that the zone size is reduced. In some projects NGI has used a different ratio in non-sensitive material over the quick clay (Gregersen 2010), which decreases the size of hazard zones with a limited quick clay layer, this is named the NGI-method in the present work.

The recent Norwegian national R&D project *Natural Hazards: Infrastructure for Flood and Landslides* ("NIFS") has suggested a new method for evaluating the retrogression distance of quick clay hazard zones by considering the geometry of the quick clay pocket and the potential for the remoulded clay to evacuate the landslide scar (NIFS 2016, NGI 2016a). The aim of this paper is to apply the NIFS-method to the hazard zone Myrahaugen and compare the extension of the zones to the 1:15-method and the NGI-method.

28.2 Case: Myrahaugen, Hvittingfoss

The quick clay hazard zone Myrahaugen in Kongsberg municipality consists of a plateau of sand situated over marine clay, which is quick clay at 15–20 m. The slope heights are up to 30 m high. The zone contains a school, more than 40 residential houses, a kindergarten, three farms and a church, which gives the consequence class "Highly severe". In 2012 a more thorough geotechnical investigation of the zone was initiated by NVE to evaluate the need for mitigation and find a more detailed extension of the zone. The consultant's report (Rambøll 2014) concluded in a much larger extent of quick clay than previously assumed, which resulted in an expansion of the hazard zone, see Fig. 28.1.

The new extent of the zone was drawn using the 1:15-method and did not take into account the depth of the quick clay layer under the sand. The large extent of the new zone would make development of the area around Myrahaugen difficult, as it is difficult to increase the safety factors in all profiles for such a large area.

The consultant (Rambøll 2016) and the external reviewer (NGI 2016b) agreed that the new zone (Fig. 28.1) could not possibly be the depletion area of one single quick clay slide, but because a slide initiation from the south or the north (using

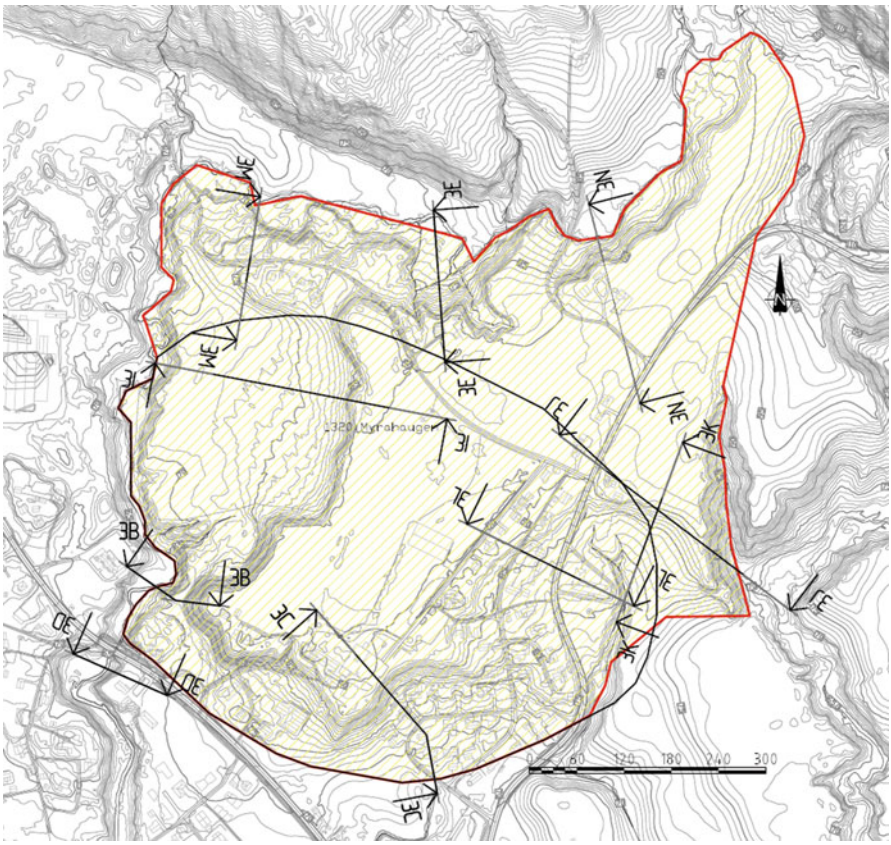

Fig. 28.1 The hazard zone Myrahaugen orginal extent (*black line*) and new extent (*red line*) after quick clay was discovered north of the existing zone (Rambøll 2014). The profiles indicate where the 1:15 line is drawn to estimate the new zone size

L/H = 15) would overlap in the middle of the zone, the zone had to be drawn as one. The quick clay layer lies 15–20 m under the plateau, below a 10 m thick layer of sand and a layer of non-sensitive clay, see Fig. 28.2. The methodology used for regional mapping, however did not take the layering and depth to quick clay into account when evaluating the extent of the quick clay zone.

28.3 Application of Methods

28.3.1 NIFS-Method

The new method suggested in NIFS (2016) was applied in the geotechnical evaluation of the Myrahaugen hazard zone. The method proposes that a retrogressive quick clay slide will only occur if more than 40% of the soil over the critical slip

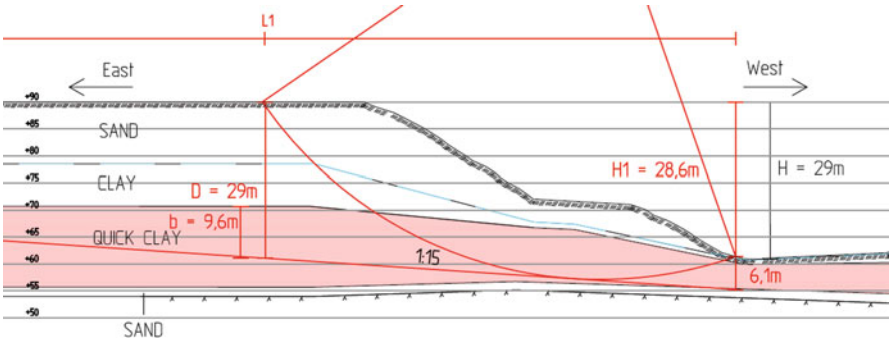

Fig. 28.2 Profile 3B in the south-west of the Myrahaugen hazard zone shows a top layer of 10 m sand over non-sensitive clay followed by quick clay (in *pink*) at 20 m depth (Rambøll 2016)

Table 28.1 Indicators used to calculate the zone of depletion for Myrahaugen hazard zone

		Profile					
Indicators which give 0–3 points	Weight	3B	3C	3E	3 J	3 K	3I
b/D[a] at L1 from the toe of slope	1	2	1	0	2	0	0
b/D[a] at L2 from toe of slope	2	1	0	0	0	0	0
x_1[b]	1	3	3	1	3	3	1
Topography of the run-out area	2	2	3	3	2	2	3
Historic slide sizes[c]	1	2	2	2	2	2	2
$c_{ui}/(\gamma H)$[d]	1	3	1	2	2	2	2
Sum		16	13	11	13	11	11
Resulting L/H-ratio		15	10	10	10	10	10

See NIFS (2016) for details about the indicators
[a]Ratio between thickness of quick clay and total depth over the 1:15-line
[b]Distance from toe to where the 1:15-line encounters quick clay
[c]L/H-ratio of depletion area of known quick clay slides in the vicinity
[d]Inverse stability number $1/N_c$

surface is quick and $c_{u,r} < 1$ kPa. The NIFS-method may be applied on these slopes, by assessing certain indicators (see Table 28.1), which decide the retrogression distance.

The quick clay layer in several of the Myrahaugen-profiles is deeper than the bottom of the slope, and approximately horizontal. The 40%-criteria was applied, and it showed that for profile 3I (lower part), 3L and 3M the quick clay was too deep for a retrogressive slide to occur. The remaining profiles had approximately 40% or more quick clay over the critical slip surface (measured from the top of the slope to the lowest part of the slip surface), because of deep critical slip surfaces. This result was compared to a criterion which has been used sporadically in quick clay hazard mapping to decide if a retrogressive slide may occur: Quick clay layer

deeper than 0.5H under the slope toe should not be included in the evaluation (H = slope height). The depth of 0.5H under the slope toe was recommended as the maximum investigation depth by Gregersen (2008), and seems a conservative limit for to what depth the quick clay will be included in a potential retrogressive landslide. This criterion resulted in omitting the same profiles as the NIFS-method.

Table 28.1 shows the evaluation according to the NIFS-method for seven profiles in Myrahaugen hazard zone. The sum of points is used to select the L/H-ratio for the zone of depletion for each profile calculated. As seen, all of the profiles end up with L/H = 10, except the steepest profile 3B, which gets L/H = 15 by one point. Figure 28.3 shows the new extent of hazard zones (depletion areas). The boundaries

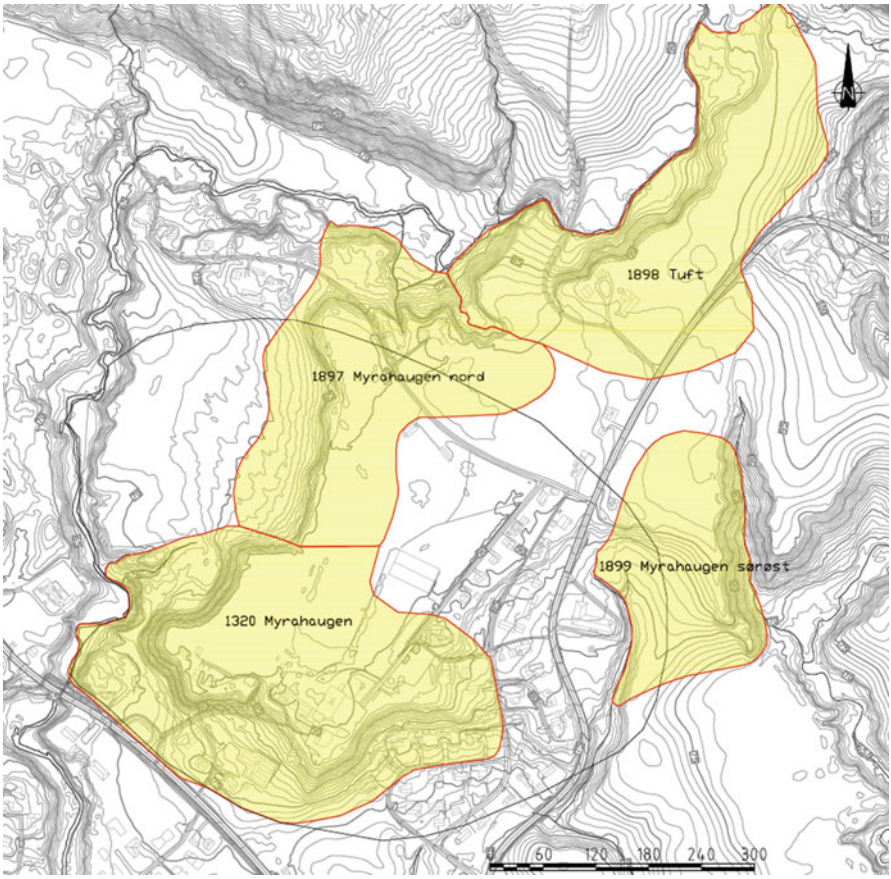

Fig. 28.3 Hazard zones Myrahaugen, Myrahugen nord and Myrahaugen sørøst were proposed using the NIFS-method (Rambøll 2016). Zone Tuft is based on the 1:15-method due to insufficient geotechnical investigations

are drawn according to the calculated L/H-ratio and areas with deep quick clay are removed (less than 40% over critical slip surface).

28.3.2 1:15-Method

To compare the result of the NIFS-method, hazard zones were also drawn with the national mapping criteria L/H = 15, but leaving out the areas where the quick clay was only found deeper than 0.5H. The extent of the hazard zones using this method is seen in Fig. 28.4. Table 28.2 shows the comparison of the methods.

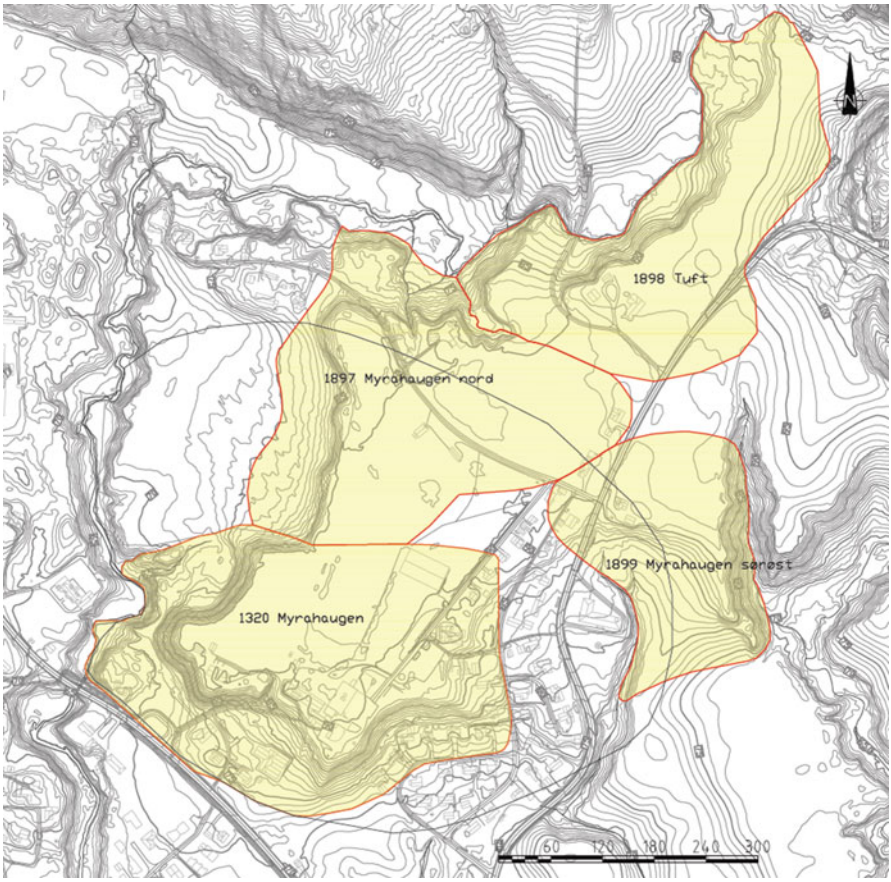

Fig. 28.4 Hazard zone limits in Myrahaugen using the 1:15-method (Rambøll 2016)

Table 28.2 Comparison of depletion zone lengths using different evaluation methods

Profile	Height (H)	Methods			
		NIFS 2016	1:15	NGI[a,b]	Simplified NGI[a,b]
3B	29 m	15H = 435 m	15H = 435 m	10H = 290 m	As NGI
3C	15 m	10H = 150 m	15H = 225 m	15.7H = 235 m	14.3H = 213 m
3E	19 m	10H = 190 m	15H = 285 m	20.3H = 385 m	13H = 248 m
3I	16 m	10H = 160 m	15H = 240 m	21.2H = 340 m	10.8H = 172 m
3 J	19 m	10H = 190 m	15H = 285 m	12.9 H = 245 m	As NGI
3 K	17 m	10H = 170 m	15H = 255 m	15.3H = 260 m	As NGI

[a] 1:3-inclination used over quick clay
[b] Max length of zone restricted to 15H

28.3.3 NGI-Method

NGI has used the calculated critical slip surface as a basis for drawing the zone of depletion in cases where the thickness of the quick clay layer is limited, or drops downward away from the slope (Gregersen 2010). From the bottom of the critical slip surface a 1:15-line is drawn in the quick clay, and in the higher non-sensitive material a steeper inclination is used, from 1:3–1:2 depending on the soil properties and groundwater/pore pressure conditions. The maximum extent is restricted to 15H. Table 28.2 and Fig. 28.5 show the extent of this method, with 1:3 inclination over the quick clay. It is similar to the 1:15-method in Fig. 28.4, due to the deep calculated critical slip surfaces. Also, the top of the quick clay layer often climbs upward from the foot of the slope, reducing the effect of the method. It is only for slopes with thin and/or deeply positioned quick clay layers (e.g. profile 3B, Fig. 28.2) that the NGI-method gives a shorter retrogression distance than the NIFS-method, because the latter does not use a steeper inclination in the non-sensitive materials in the present work.

28.3.4 Simplified NGI-Method

If the assumption is made that a critical slip surface has a maximum depth 0.5H under the slope toe, a simplified method may be used to draw a hazard zone without a detailed calculation of a critical slip surface. The horizontal position of the critical surface still has to be assumed, in order to construct the1:15-line from the bottom point. If quick clay does not reach as deep as 0.5H, the maximum depth of the critical slip surface may be assumed at the bottom of the quick clay layer. In the non-sensitive material above the quick clay a 1:3-inclination is used, as in the NGI-method, see Table 28.2 shows the comparison of the methods. The Simplified NGI-method results in smaller depletion areas than the NGI-method for profiles with critical slip surfaces deeper than 0.5H, but still is larger than the NIFS-method.

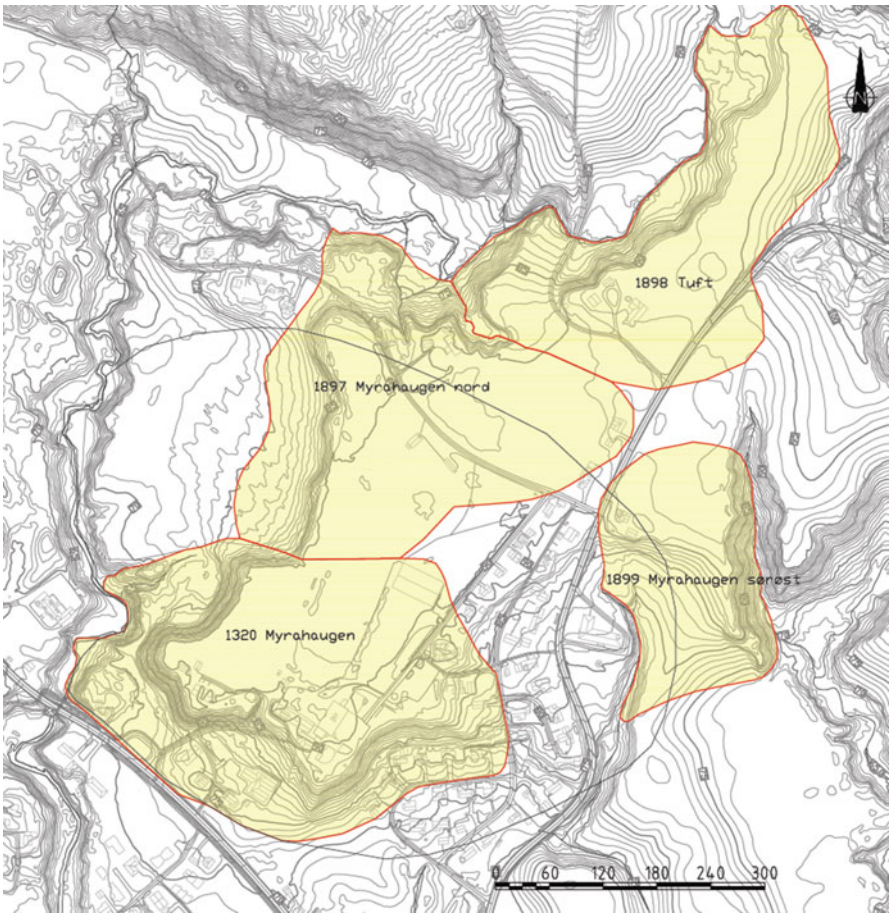

Fig. 28.5 Hazard zone limits in Myrahaugen using the NGI-method (Rambøll 2016)

28.4 Discussion of Methods for Estimation of Depletion Zones

As Figs. 28.3, 28.4 and 28.5 show, the NIFS-method results in notably smaller evaluated depletion areas. The NGI-method exceeds the length applied in the national mapping in many of the slopes, because of deeply calculated critical slip surfaces. The Simplified NGI-method is also not widely different from 1:15-method, because the limited depth of the slip surfaces (0.5H) has little effect. The advantage of the Simplified NGI-method is that it does not need the calculation of a critical slip surface, so this method may be used for quick assessments in zones where the shear strength profile is not investigated.

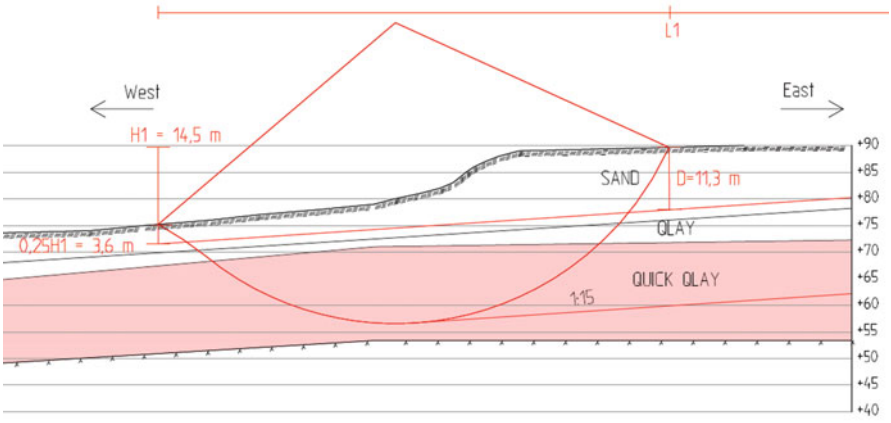

Fig. 28.6 The NIFS-method gives a retrogression distance of 160 m for Profile 3I, while the NGI- and Simple NGI-method give respectively 340 m and 170 m

Both the NIFS-method and the NGI-method rely on the calculation of reliable critical slip surface. In several of the profiles in Myrahaugen the critical slip surface was calculated very deep, e.g. Profile 3I (Fig. 28.6), and the NGI-method exceeds the 1:15-distance. But the NIFS-method also gives 10H as the retrogression distance, since the slope fulfils the 40% criteria for retrogressive slide, which for this slope seems unlikely.

The advantage of the NGI-method is that it principally visualises the actual development of a quick clay slide, with an initiating rotational slide and 1:15-inclination in the quick clay from there, which seem logical with a correctly drawn initial slide. The NIFS-method does not have this direct link, but NIFS (2016) does state that where the top of the quick clay layer is situated deep below the toe of the slope and under the 1:15-line, a large slide is less likely. But it is not clear in NIFS (2016) how deep below the quick clay should be situated for a retrogressive slide not to occur. Because of this the depth 0.5H under the slope toe was used in Myrahaugen as a conservative limit.

NIFS (2016) may be interpreted to that a retrogressive landslide cannot occur if there is no quick clay over the 1:15 line, which for deep slip surfaces uses 0,25H1 as the starting depth under the toe. If this is applied to Myrahaugen profiles 3E, 3I and 3 K are ruled out, see Fig. 28.1. This would mean the hazard zone Myrahaugen Nord would not be drawn, and neither the southern part of Myrahaugen sørøst. This shows the importance of assessing first whether a retrogressive slide actually can develop from an initial slide, given the location of the quick clay. Once this is concluded, the retrogression distance may be estimated using the indicators in Table 28.1. But whether a landslide can reach to 10H or 15H may not be the main issue, but rather to determine if a retrogressive landslide may occur.

28.5 Conclusions

The NIFS-method for evaluation of the quick clay slide retrogression distance has been applied to Myrahaugen hazard zone. The aim has been to decide whether it is an applicable method to draw realistic zones of depletion. Three other methods were applied for comparison with the NIFS-method. For the Myrahaugen case the NIFS-method gives the smallest depletion area and varies more from the conventional 1:15-method than the NGI- and Simple NGI-method. The use of the methods show that the primary task when assessing a quick clay area, is to determine whether a retrogressive slide can occur. The NIFS-method proposes using the 40% ratio of quick clay over the critical shear surface, but because of deep calculated shear surfaces there is need of additional criteria, for instance the depth of the quick clay under the toe of the slope or whether the 1:15-line intersects quick clay.

In any case the most important factor for detailed evaluation of the extent of a hazard zone is still the extent and depth of quick clay within the zone. Thorough mapping of soil layering and lateral distribution of quick clay, including classical geotechnical soundings as well as geophysical methods such as ERT, should be the main priority. Based on this a consideration of possible release and slide mechanisms must be done, bearing in mind that catastrophic slides can happen even for slopes with relatively thin layers of quick clay if buildings or other values are hit e.g. the Skjeggestad slide in February 2015 (NVE 2015). Following this the possibility for retrogression can be determine, followed by an estimation of the retrogression distance. A good method for deciding the retrogression distance must build upon a large database of old and new quick clay slides, which hopefully will lead to less uncertainties in the future.

Acknowledgements The authors wish to thank Dr. Jean-Sébastien L'Heureux of NGI for reviewing the manuscript and giving valuable feedback. Thanks also to NVE Region Sør and Anne Cathrine Sverdrup who see the value of developing new and better methods for landslide hazard zonation.

References

Gregersen O (2004) Program for økt sikkerhet mot leirskred. Evaluering av risiko for kvikkleireskred i Ullensaker kommune, NGI-rapport 20001008-8. Vedlegg A: Veiledning ved bruk av faregrad-, konsekvens og risikokart

Gregersen O (2008) Program for økt sikkerhet mot leirskred. Metode for kartlegging og klassifisering av faresoner, kvikkleire, NGI-rapport 20001008-2, rev. 3

Gregersen O (2010) Sande, Gunnestad. Utstrekning av eventuelt kvikkleireskred, NGI-teknisk notat 20091655-00-16-TN

Kalsnes B, Gjelsvik V, Jostad HP et al. (2014) Risk assesment for quick clay slides – the Norwegian practice. In: Landslides in sensitive clays. From geosciences to risk management, ISBN 978-94-007-7079-9, p 355–367

Karlsrud K, Aas G, Gregersen O (1985) Can we predict landslide hazards in soft sensitive clays? Summary of Norwegian practice and experiences. NGI pub.no 158. ISBN 82-546-0119-4

L'Heureux JS (2012) A study of the retrogressive behaviour and mobility of Norwegian quick clay slides. Proceedings of the 11th International & 2nd North American Symposium on Landslides, Banff, Canada

NGI (2016a) Teknisk notat 20140848-01-TN rev.2 Beskrivelse av L/H tabellen for vurdering av løsneområdet for områdeskred, 01.02.2016

NGI (2016b) Teknisk notat 20120427-06-TN Gjennomgang av "Geoteknisk rapport – 1320 Myrahaugen" (Rambøll AS). 02.08.2016

NIFS: Natural Hazards – Infrastructure for flood and landslides (2016) Metode for vurdering av løsne- og utløpsområder for områdeskred. Naturfareprosjektet: Delprosjekt 6 Kvikkleire. NVE-rapport 14/2016. ISSN: 1501-2832

NVE: Norwegian Water Resources and Energy Directorate (2011) Plan for skredfarekartlegging Status og prioriteringer innen oversiktskartlegging og detaljert skredfarekartlegging i NVEs regi. Rapport no. 14/2011, ISSN: 1501-2832

NVE: Norwegian Water Resources and Energy Directorate (2014) Sikkerhet mot kvikkleireskred. Vurdering av områdestabilitet ved arealplanlegging og utbygging i områder med kvikkleire og andre jordarter med sprøbruddegenskaper. Rapport no. 7/2014, ISSN: 1501-0678

NVE: Norwegian Water Resources and Energy Directorate (2015) Skredet ved Mofjellbekken bruer (Skjeggestadskredet): utredning av teknisk årsakssammenheng. Rapport no. 53/2015, ISBN: 978-82-410-1100-9

Oset F, Thakur V, Dolva BK et al. (2014) Regulatory framework for road and railway construction on the sensitive clays of Norway. In: Landslides in sensitive clays. From geosciences to risk management, ISBN 978-94-007-7079-9, p 343–353

Rambøll AS (2014) Report 6120285-03 Hvittingfoss – Kvikkleireutredning 1320 Myrahaugen, rev. 01, 23.05.2014

Rambøll AS (2016) Report 6120285-03 Hvittingfoss – Kvikkleireutredning 1320 Myrahaugen, rev. 02, 23.05.2016. Preliminary report

Chapter 29
Modelling of the Quickness Test of Sensitive Clays Using the Generalized Interpolation Material Point Method

Quoc Anh Tran, Wojciech Solowski, Vikas Thakur, and Minna Karstunen

Abstract The presence of the sensitive clays in Scandinavia and Canada creates quick clay landslide hazards. The ability to predict the likelihood of such landslides occurrence, as well as their outreach would reduce the damage to the infrastructures and loss of life. Recently, a simple experimental technique named a quickness test (Thakur V, Degago S, Geotech Lett 2:87–95, 2012) has been employed to investigate the susceptibility of the clay to create large retrogression landslides. In this paper, we applied Generalized Interpolation Material Point Method (a numerical method suitable for large displacement dynamic problems) to replicate the quickness test experiment. The primary goal of the presented simulations is to further validate the modelling technique and the constitutive model used. In particular, the computations suggest the importance of the strain rates for the prediction of the run-out distance of the remoulded sensitive clays.

29.1 Introduction

The collapse of a granular column is well investigated by both experimental (Lube et al. 2005), and numerical studies using methods such as Discrete Element Method (DEM) (Utili et al. 2015), Smooth Particle Hydro-dynamics (SPH) (Bui et al. 2008) or Material Point Method (Solowski and Sloan 2015; Fern and Soga 2016). The failure of the granular column is dominated by the localized failure characterized by discontinuous shear localized bands. On the other hand, the failure of the soft

Q.A. Tran (✉) • W. Solowski
Department of Civil Engineering, Aalto University, Espoo, Finland
e-mail: tran.quocanh@aalto.fi

V. Thakur
Department of Civil and Environmental Engineering, Norwegian University of Science and Technology (NTNU), Trondheim, Norway

M. Karstunen
Department of Civil and Environmental Engineering, Chalmers University of Technology, Gothenburg, Sweden

V. Thakur et al. (eds.), *Landslides in Sensitive Clays*, Advances in Natural and Technological Hazards Research 46, DOI 10.1007/978-3-319-56487-6_29

sensitive clays may sometimes be classified as a diffuse failure (Nicot and Darve 2011) as visible localization is not always observed such as the flow failure of remoulded clays. The failure characteristics of a sensitive clays column (such as the run-out distance and the final height) are dependent on the mechanical properties of the material. In particular, the experiments point out towards strain rate effects as important in the soft clays in general and in the sensitive clays in particular (Leroueil et al. 1985; Lefebvre and LeBoeuf 1987). However, the influence of strain rate effects on the run-out and spreading distance of the sensitive clays has not been well investigated.

This paper presents simulations of quickness tests for sensitive clays. Shown research builds over investigations of fall cone tests (Tran et al. 2017). In particular, this study investigates the strain rate effects in greater detail. The research aims to validate the constitutive model and the material point method for sensitive clay modelling. Those will be used to analyse the failure and post-failure of slopes in sensitive clays.

29.2 The Generalized Interpolation Material Point Method

The Material Point Method (MPM) is a numerical method based on continuous mechanics especially well-suited to solve the dynamic large deformation problems. Sulsky et al. (1995) introduced the MPM for the first time and applied this method to the solid mechanics for history-dependent materials. Later, Badenhagen and Kober (2004) proposed Generalized Interpolation Material Point method (GIMP) which improves greatly the robustness and the accuracy of the original MPM. In this paper, GIMP version of material point method is used exclusively as coded in the Uintah software (http://uintah.utah.edu).

GIMP, to solve the problems, uses material points and a background grid. The material points represent the current state of the modelled material. Each material point has a constant mass leading to automatic mass conservation in the solution. The method employs explicit time stepping. In each time step, the material points interpolate information to the background grid nodes. After solving conservation of momentum equation, the information is mapped back to the material points. At the end of the time step, the background grid resets to the initial configuration while the material points' positions and velocities are updated.

29.3 Validation of the Constitutive Model: Mohr-Coulomb Extended with Strain Rate Effects

The Mohr-Coulomb model is commonly used to predict failure of geo-materials. As the quickness test takes only a few seconds, the soil behaves in undrained manner with the cohesion equal to the undrained shear strength. The strain rate effects

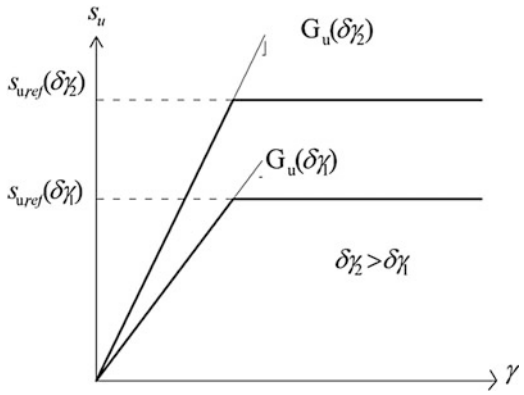

Fig. 29.1 Mohr-Coulomb enhanced with strain rate effects

and the degradation of shear strength are well recognized experimentally in the sensitive clays (Leroueil et al. 1985; Lefebvre and LeBoeuf 1987). These effects could be significant in case of large displacement problems such as quickness tests. To capture the strain rate dependency on the simulations of the quickness tests, it is essential to extend Mohr-Coulomb model with strain rate effects. In this study, we make use of the power law (Einav and Randolph 2006). Figure 29.1 describes the schematic of the constitutive model at different strain rates ($\delta\gamma_2 > \delta\gamma_1$).

The undrained shear strength at a shear strain $\delta\gamma$ could be described as follows:

$$s_u(\delta\gamma) = a_1 * w^{-b_1} \left(\frac{\delta\gamma}{\delta\gamma_{ref}}\right)\beta \tag{29.1}$$

where a_1 (kPa) is the reference undrained shear strength at a water content of 100% and a reference strain rate $\delta\gamma_{ref}$, b_1 is an influence of water content parameter in the power law, w is the water content, β is the strain rate parameter in the power law, $\delta\gamma_{ref}$ is the reference shear strain rate and $\delta\gamma$ is the shear strain rate computed from the strain rate tensor as:

$$\delta\gamma = \frac{3}{2}\sqrt{2\left(\delta\varepsilon_{ii} - \delta\varepsilon_{jj}\right)^2 + 3\delta\varepsilon_{ij}{}^2} \tag{29.2}$$

In order to validate the GIMP and the above constitutive model for the soft clays, a series of fall cone tests simulations were carried out and is reported in Tran et al. (2017). Apart of the comparison to laboratory data (Hazell 2008) (see Figs. 29.3 and 29.4), the theoretical undrained shear strength as proposed by Koumoto and Houlsby (2001) was selected as a benchmark for the numerical solutions (see Fig. 29.2). The numerical material parameters were extracted from the experimental results of kaolin clays (Boukpeti et al. 2012). Table 29.1 shows the material parameters in the numerical models. The water content parameters (a_1 and b_1) were determined from the series of tests with different water contents and the strain rate parameters ($\delta\gamma_{ref}$, β) based on the vane shear tests. In particular, this

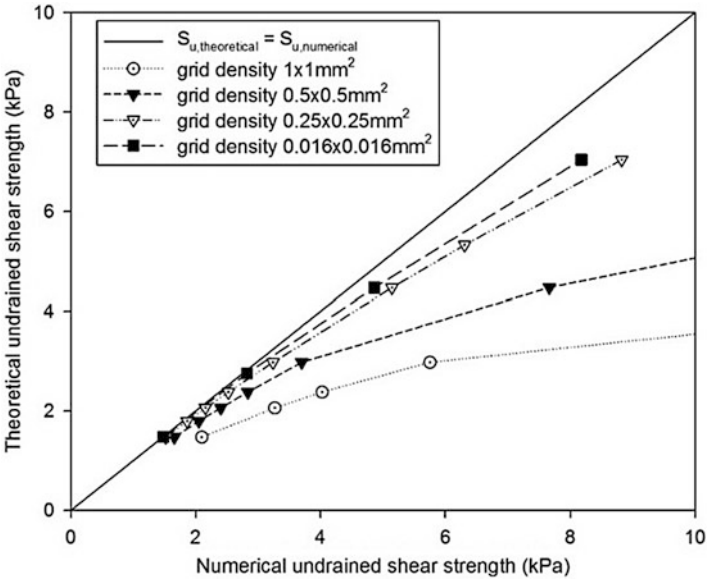

Fig. 29.2 Numerical error investigation of fall cone tests (Tran et al. 2017)

Table 29.1 Parameters in the numerical simulations of the fall cone tests (Tran et al. 2017)

a_1 (kPa)	b_1	W	$\delta\gamma_{ref}$ (s^{-1})	β	$E_{u,ref.}$ (kPa)	υ_u
0.205	3.86	0.4–0.6	0.5	0.06	$500s_{u,ref}$	0.49

reference strain rate ($\delta\gamma_{ref} = 0.5\ s^{-1}$) was calculated from the rotation rate of 1% of the vane shear test. The numerical results have shown excellent time-displacement and time-velocity agreement with the experiment (Figs. 29.3 and 29.4) as well as very good convergence for the increasing grid density to the theoretical results for a wide range of undrained shear strengths (Fig. 29.2). Despite coping with different materials, in this study, the same parameters ($\delta\gamma_{ref}$, β, $E_{u,ref.}$, υ_u) were used for the sensitive clays as in the previous fall cone simulations.

29.4 Application to the Quickness Test

29.4.1 Quickness Test Approach

The stability of sensitive clays slopes depends on the topography, hydrological conditions and chemical and mechanical properties of sensitive clays. For large flow-slides where the retrogression distance could reach more than hundreds metres, geotechnical parameters of soil are critical in the estimation of the possibility of the

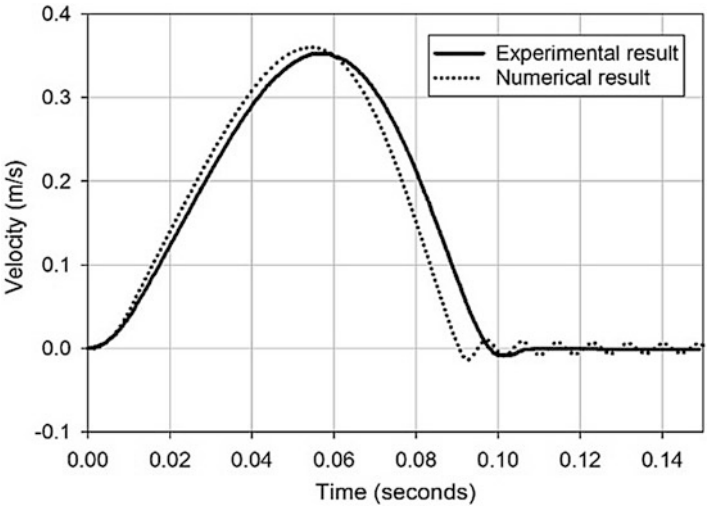

Fig. 29.3 Validation of the penetration velocity vs. time

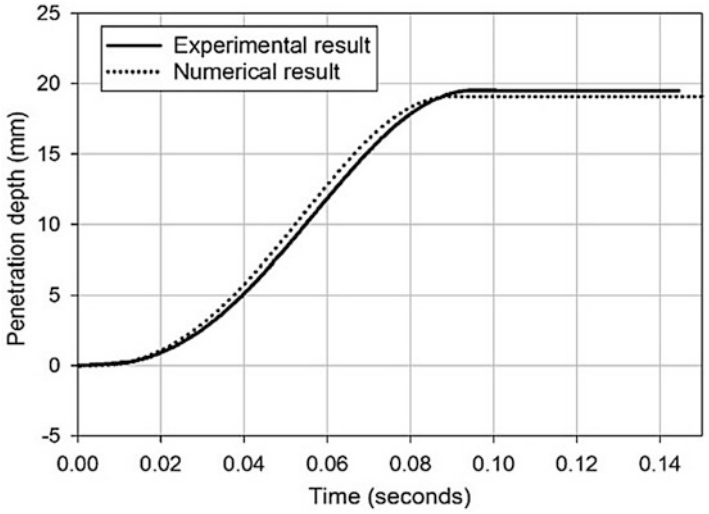

Fig. 29.4 Validation of the penetration depth vs. time

sensitive clays landslides. Mitchell and Markell (1974) suggested that continous flow-slides occur only when the stability number ($N_s = \gamma H/s_u$) exceeds 6. Also, statistically, large flow-slides in Canadian and Norway occur with the sensitive clays $s_{ur} < 1$ kPa. Those typically correspond to high liquidity index $I_L > 1.2$ (Leroueil et al. 1983; Locat and Demers 1988).

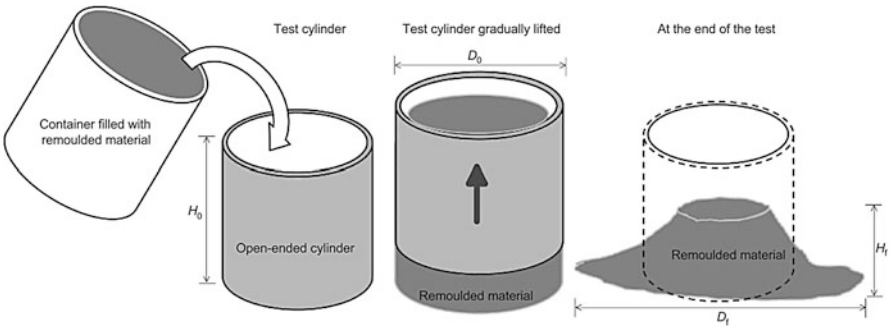

Fig. 29.5 Quickness test procedure (Thakur and Degago 2012)

Recently, Thakur and Degago (2012) proposed a new laboratory procedure called a quickness test for study the flow susceptibility of sensitive clays. Fig. 29.5 presents the schematic of the quickness test. A cylinder ($H_0 \times D_0 = 120$ mm $\times$ 100 mm) is filled with a remoulded sensitive clay. Then, the cylinder is slowly lift upward and the clays column is deformed by its own weight. The final height of the remoulded material H_f is recorded and the quickness value Q is computed as:

$$Q = \frac{H_o - H_f}{H_o} \tag{29.3}$$

Thakur and Degago suggested that Q < 15% could be the threshold limit where the landslides are limited to the initial slide. In this paper, the quickness values and the run-out distance of the sensitive clay columns (Thakur and Degago 2014) are used as data for the numerical analyses.

29.4.2 Geometry and Sensitive Clay Parameters

Figure 29.6 shows the geometry of the axi-symmetric numerical model. The clay cylinder column has the dimensions ($H_0 \times D_0 = 120$ mm $\times$ 50 mm) with the axis of symmetry on the left side. The soil is modelled with Mohr-Coulomb model extended with strain rate effects, as discussed in the previous section. The soil parameters were based on the laboratory tests of the sensitive clays near Lersbakken landslides area (Thakur and Degago 2012).

The sensitive clays deform under undrained conditions, therefore, Poisson's ratio is set to be 0.49. The other elastic parameter should not be significant as the plastic strains are expected to be pre-dominant. As such, for the soft clay, the elastic modulus is set to be 500 times of the undrained shear strength. Figure 29.7 presents

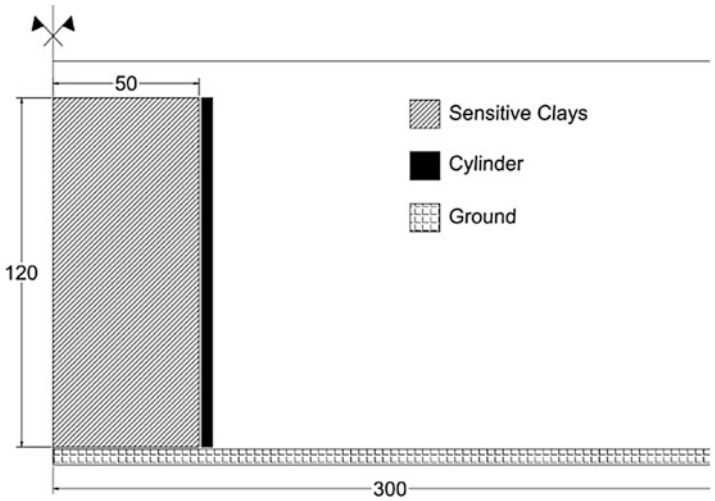

Fig. 29.6 Numerical model of the quickness test

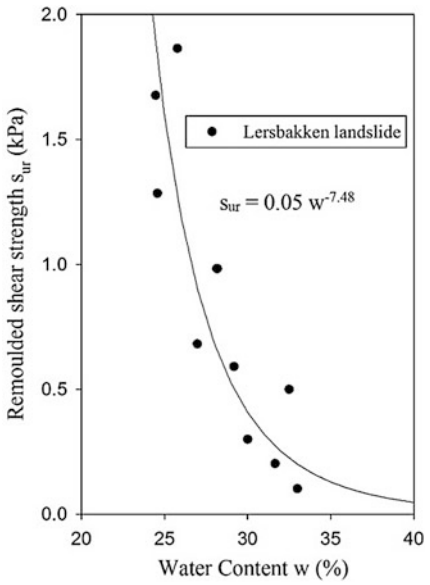

Fig. 29.7 Empirical relationship between water content and remoulded shear strength

the relationship between water content and remoulded undrained shear strength which provides parameters of the influence of the water content (a_1 and b_1). In the simulation, the clay density was one of the critical parameters for the failure which changes as a function of water content.

Table 29.2 Geotechnical parameters in the numerical simulation

γ (T/m3)	a_1 (Pa)	b_1	W (%)	$\delta\gamma_{ref}$ (s^{-1})	β	$E_{u,ref.}$ (kPa)	υ_u
1.85–2.0	0.05	7.48	24–35	0.5	0.06	$500s_{u,ref}$	0.49

After the remoulding, the saturated the bulk density was calculated as (Lee and Chough 1987):

$$\gamma = \frac{w+1}{w/\gamma_w + {}^{1}\!/_{G_s}} \tag{29.4}$$

If w = 0 then the bulk density is equal to the grain particle density ($\gamma = G_s = 2.65$ T/m^3 for clays) and if w approaches infinity, the bulk density is equal to the water density ($\gamma = \gamma_w = 1$ T/m^3). These computed density values are similar to the total unit weight of Norwegian sensitive clays Lersbakken slide (w = 25–35% and γ = 1.9–2.0 T/m^3) (Thakur and Degago 2014).

Because, at least in the authors' knowledge, there are currently no tests available which could allow for the calibration of the strain rate parameters for the sensitive clays near the Lersbakken, the strain rate parameters ($\beta = 0.06$) were chosen based on the investigation of the Scandinavian clays (Lansivaara 1999) with $\beta = 0.052$ for Norwegian Eberg clay and $\beta = 0.072$ for Soft Finnish clays. β was assumed to be 0.06 also based on the investigation of fall cone tests on the remoulded kaolin clay (Tran et al. 2017) under the reference strain rate $\delta\gamma_{ref}$ of 0.5 s^{-1}. The selected parameter ($\beta = 0.06$) is an intermediate measure – ideally the model should be calibrated for the given clay which is simulated. Table 29.2 summarizes the parameters for the remoulded sensitive clays.

In the experiment, the surface is assumed to be the perfectly smooth (i.e. the friction coefficient is 0). In the simulation, the rigid cylinder was lifted up with a constant velocity of 0.06 m/s. With that velocity, it took 2 s to totally lift up the cylinder, replicating roughly the lifting time in the experiments.

29.4.3 Investigation of the Grid-Dependency in the Quickness Test

Similar to the fall cone tests (see Fig. 29.2), the accuracy of the numerical solutions of quickness tests (quickness value, run-out distance) also depends significantly on the grid density. The required grid density is different for various numerical problems. Therefore, we investigated the grid-dependancy in the quickness tests of the sensitive clays with the remoulded undrained shear strength of 0.2 kPa. The numerical investigations consist of seven types of grid density with four material points per grid cell. The total number of material points for the sensitive clay

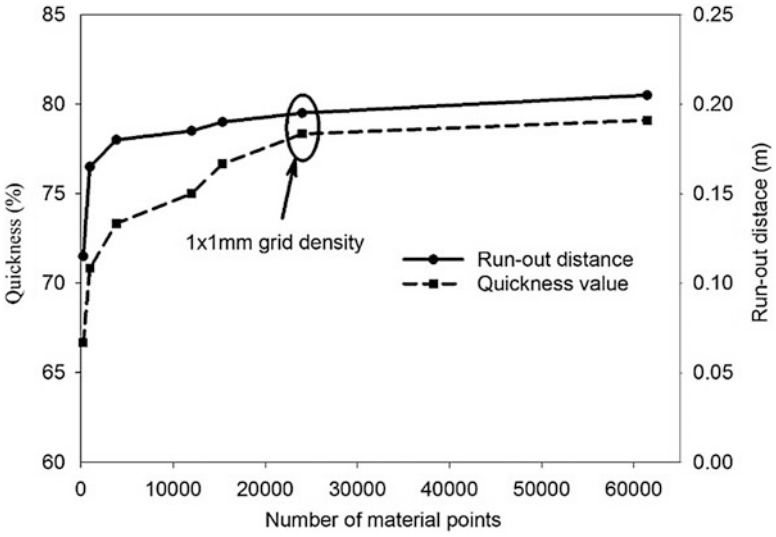

Fig. 29.8 Influence of grid density

columns are 240, 960, 3,840, 6,000, 15,360, 24,000 and 61,440 materials points respectively. Figure 29.8 presents the influence of the grid density. The denser grid density simulations gave more deformations and that leaded to higher quickness values and higher run-out distances. The numerical simulations became more stable at grid density of 1 × 1 mm (24,000 materials points) as relatively little difference was observed upon increasing it to 0.625 × .625 mm (61,440 materials points). As it appears that grid density 1 × 1 mm gives reasonable results, it was selected for the quickness test simulations.

29.4.4 Numerical Results

Series of numerical simulations were performed with varying the water content of clay from 24% to 35% so that the remoulded undrained shear strength was between 0 and 2 kPa. Figure 29.9 presents the comparison between the numerical and experimental results. The obtained results fell acceptably well within those obtained experimentally for remouded sensitive clays in three different landslide areas in Norway, that is Lersbakken, Byneset and Ols∅y. The fit is worse for stiffer clays with quickness lower than 20% or those with remoulded undrained shear strength $s_{ur} > 1$ kPa. In those cases, the deformations were negligible and it resulted in low quickness values ($Q < 15\%$). The reason for that discrepancy is being investigated. Nonetheless the small deformations in both numerical and experimental results for

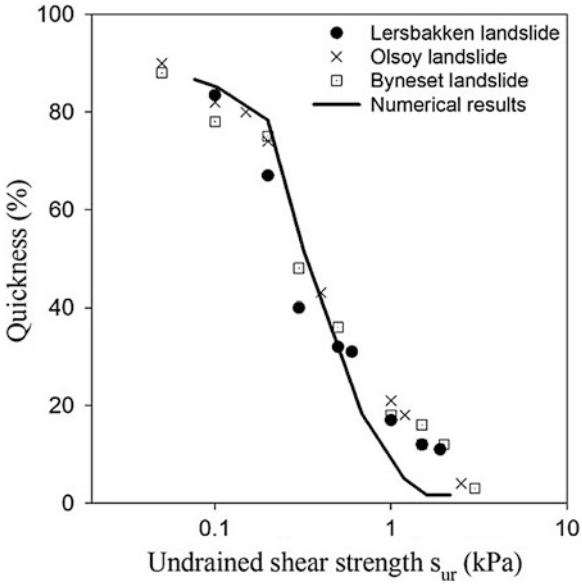

Fig. 29.9 Numerical results of the quickness test (Thakur and Degago 2014)

$s_{ur} > 1$ kPa perhaps could give some insights on why no large retrogresion landslides occurred with $s_{ur} > 1$ kPa. For the clays with undrained shear strength $s_{ur} < 1$ kPa, the quickness value increased sharply with the decrease of the undrained shear strength and that is well captured in the numerical results (Fig. 29.9).

In the range of 0.5–1.0 kPa, such as the sensitive clays with the remoulded undrained shear strength 0.7 kPa (Fig. 29.10) behaved like semi-solid as observed in the experiments. In contrast, the sensitive clays with the remoulded undrained shear strength under 0.2 kPa (Fig. 29.11) exhibited fluid-like behaviour. Simulations replicated both experimentally observed regimes of behaviour well.

In the constitutive model used, the power law coefficient β links the undrained shear strength with the strain rates (see Eq. 29.1). Several authors investigated the influence factors in the undrained strain rate parameters for the clayey soils. For instance, Quinn (2013) shows that β slightly increases with water content (0.003 per 10% of water content) for strains of magnitude of approximately 2%. However, other factors such as strain magnitude (Robinson and Brown 2013), over-consolidation ratio OCR (Mitchell and Soga 2005; Lehane et al. 2009) and initial stress (Quinn 2013) also influence the strain rate effects in the pre-failure and failure conditions of clays. For large retrogression landslides, a post-failure condition occurs and the flow-slide is similar to a fluid flow. In the fluid mechanics framework, the strain rate parameters could also link to the viscosity effects of a non-Newtonian flow (Boukpeti et al. 2012) and it influences considerably the run-out distance of such materials. To check whether those effects are captured

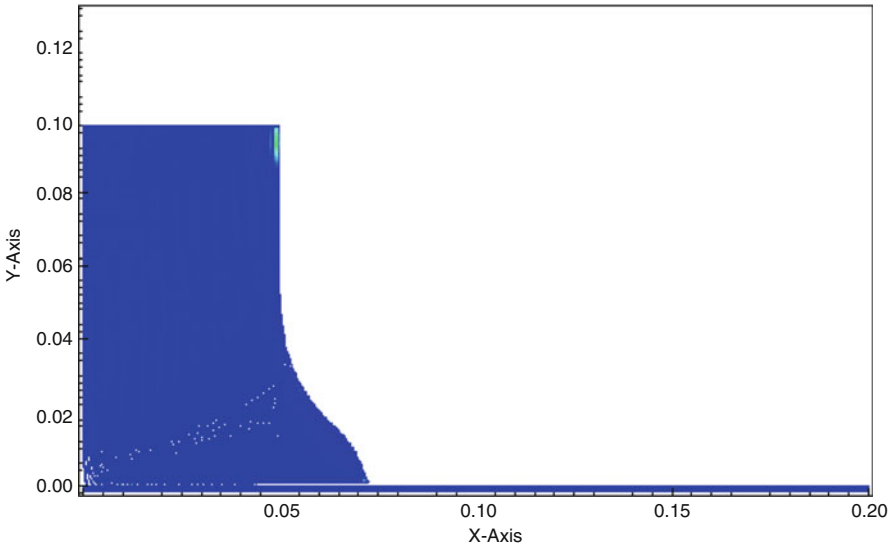

Fig. 29.10 Sample with w = 28% (s_{ur} = 0.7 kPa)

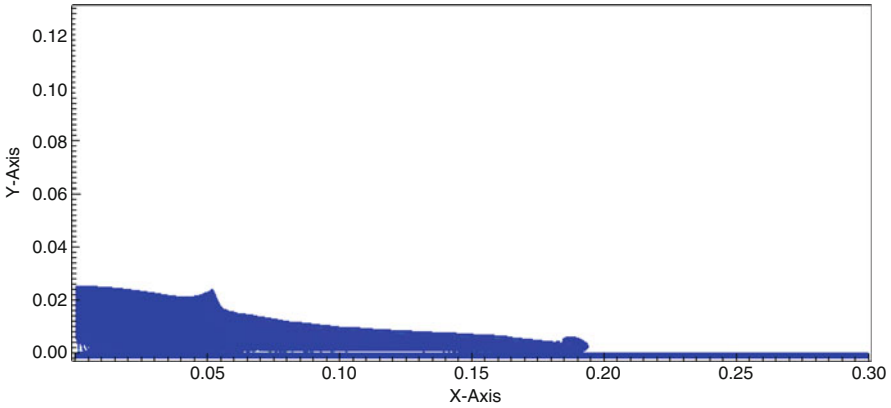

Fig. 29.11 Sample with w = 33% (s_{ur} = 0.2 kPa)

numerically, the paper investigated some effects of strain rate on run-out distance of the sensitive clays, see Fig. 29.12. Parameter $\beta = 0$ describes no strain rate effects and it significantly overestimates the run-out distance. Increasing β results in shorter spreading distance. Thus, the strain rates affect the prediction of the run-out distance significantly and should be considered in the landslides prediction.

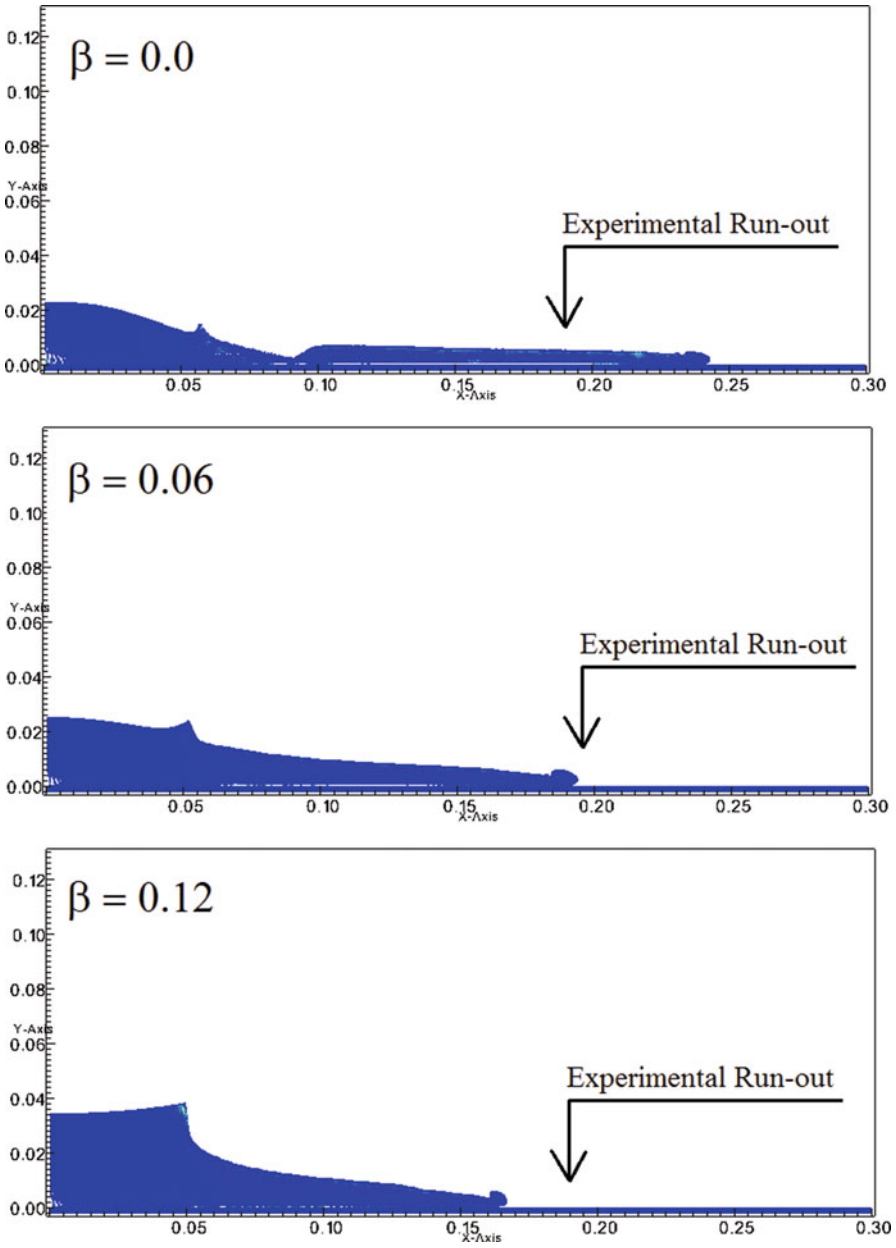

Fig. 29.12 Influence of the strain rate on the run-out distance (Experimental from Thakur et al. 2013)

29.5 Conclusion

The quickness test is a simple alternative approach to evaluate the possibility of the occurance of the large retrogression landslides. In this paper, the quickness test is modelled using the GIMP and the Mohr Coulomb enhanced strain rate effects. The results show a very good agreement between simulations and experimental data for the case of large deformation simulations in terms of the quickness values and the spreading distances. The numerical simulations replicate experimental results well. For clays with the remoulded undrained shear strength sur > 1 kPa, deformations of the remoulded sensitive clay column are generally limited. In contrast, the sensitive clays with low remoulded undrained shear strength ($s_{ur} \leq 0.5$ kPa) deform significantly perhaps pointing towards large retrogression flow trigger mechanism.

The study also suggests that the influence of the strain rate effects on the run-out distance are significant. Therefore, in order to predict the sensitive clay landslides, the strain rate effects should be taken into account to predict accurately the failure and post-failure mechanism as well as the retrogression distance of the sensitive clay landslides.

Acknowledgements The authors gratefully acknowledge constructive reviewing on the paper by Mr. Lars Andresen. The work has been funded by the Academy of Finland under the project 'Progressive failure and post-failure modelling of slopes with Generalized Interpolation Material Point Method (GIMP)' under decision number 286628.

References

Badenhagen SG, Kober EM (2004) The generalized interpolation material point method. Comput Model Eng Sci 5:477–495

Boukpeti N, White DJ, Randolph MF et al (2012) Strength of fined-grained soils at the solid-fluid transition. Geotechnique 62(3):213–226

Bui HH, Fukagawa R, Sako K et al (2008) Lagrangian meshfree particles method (SPH) for large deformation and failure flows of geomaterial using elastic-plastic soil constitutive model. Int J Numer Anal Methods Geomech 32:1537–1570

Einav I, Randolph M (2006) Effect of strain rate on mobilized strength and thickness of curved shear bands. Geotechnique 56(7):501–504

Fern EJ, Soga K (2016) The role of constitutive models in MPM simulations of granular column collapses. Acta Geotech 11(3):659–678

Hazell E (2008) Numerical and experimental studies of shallow cone penetration in clay. Dissertation, University of Oxford, UK

Koumoto T, Houlsby GT (2001) Theory and practice of the fall cone test. Geotechnique 51(8): 701–712

Lansivaara T (1999) A study of the mechanical behaviour of soft clay. Dissertatioon, Norwegian University of Science and Technology, Norway

Lee H, Chough SK (1987) Bulk density, void ratio, and porosity determined from average grain density and water content: an evaluation of errors. Mar Geol 7(1):53–62

Lefebvre G, LeBoeuf D (1987) Rate effects and cyclic loading of sensitive clays. J Geotech Eng 113(5):476–489

Lehane BM, Loughlin CD, Gaudin C, Randolph MF (2009) Rate effects on penetrometer resistance in kaolin. Geotechnique 59(1):41–52

Leroueil S, Tavenas F, Le Bihan J (1983) Propriétés caracteristiqués des argiles de l'est du Canada. Can Geotech J 20:681–705

Leroueil S, Kabbaj M, Tavenas F et al (1985) Stress-strain-strain rate relation for the compressibility of sensitive natural clays. Geotechnique 35(2):159–180

Locat J, Demers D (1988) Viscosity, yield stress, remolded strength, and liquidity index relationships for sensitive clays. Can Geotech J 25:799–806

Lube G, Huppert HE, Sparks RS (2005) Collapses of two dimensional granular columns. Phys Rev E 72(041301)

Mitchell RJ, Markell AR (1974) Flowsliding in sensitive soils. Can Geotech J 11(1):11–31

Mitchell JK, Soga K (2005) Fundamentals of soil behaviour, 3rd edn. Wiley, New York/Chichester

Nicot F, Darve F (2011) Diffuse and localized failure modes: two competing mechanisms. Int J Numer Anal Methods Geomech 35:586–601

Quinn T (2013) Rate effects in fine grained soils. Dissertation, University of Dundee, UK

Robinson S, Brown MJ (2013) Rate effects at varying strain levels in fine grained soils. 18th conference on soil mechanics and geotechnical engineering, Paris, France, 2013

Solowski W, Sloan S (2015) Evaluation of material point method for use in geotechnics. Int J Numer Anal Methods Geomech 39:685–701

Sulsky D, Zhou SJ, Schreyer HL (1995) Application of a particle-in-cell method to solid mechanics. Comput Phys Commun 87:236–252

Thakur V, Degago S (2012) Quickness of sensitive clays. Geotech Lett 2:87–95

Thakur V, Degago S (2014) Quickness test approach for assessment of flow slide potentials. Geotech Eng J SEAGS & AGSSEA 45(1):85–94

Thakur V, Degago A, Oset F et al. (2013) A new approach to assess the potential for flow slide in sensitive clays. 18th international conference on soil mechanics and geotechnical engineering. France, September 2013

Tran QA, Solowski W, Karstunen M et al. (2017) Modelling of fall-cone tests with strain-rate effects. 1st international conference on the material point method, Delft, January 2017

Utili S, Zhao T, Houlsby GT (2015) 3D DEM investigation of granular column collapse: evaluation of debris motion and its destructive power. Eng Geol 186:3–16

Chapter 30
Back-calculation of the Byneset Flow Slide Using the Voellmy Rheology

Ashenafi Lulseged Yifru, Samson Abate Degago, and Vikas Thakur

Abstract This work presents a back-calculation of run-out of Byneset flow slide that took place in Norway in 2012. The flow slide involved about 350,000 m^3 of sensitive clay. The Voellmy rheology is selected for this back-calculation. An attempt is made to verify whether this rheology can capture the actual run-out distance. The numerically obtained flow depth and flow velocity were evaluated. The results indicate that, this rheology was able to simulate the run-out distance for some range of values of the key input parameters, i.e. friction coefficient and turbulence factor. However, these parameters are not easy to relate to the well-established geotechnical parameters of sensitive clays e.g., liquidity index, remolded shear strength, quickness and viscosity. Therefore, more research is needed to understand the input parameters in terms of the geotechnical parameters. This is the key to explain how the Voellmy rheology works for sensitive clays.

30.1 Introduction

Rock and snow avalanches, rockslides and rock falls, debris and earth flows and sensitive clay flow slides are few kinds of Landslides. Out of these, sensitive clay flow slides, snow avalanches and rock falls are the most frequent events in Norway. Flow slide in highly sensitive clays is a typical geo-hazard that its retrogression and run-out of debris pose a serious risk to human lives and infrastructures. Retrogressive landslides in sensitive clays are historically known for their ability to cause varying degrees of destruction (Thakur et al. 2015). Such landslides near urban areas and infrastructure can be more catastrophic and deadly in nature. Delineation of possible areas that can be affected should a landslide occur are important aspect towards reduction of undesired consequences. Part of this phase,

A.L. Yifru (✉) • V. Thakur
Norwegian University of Science and Technology (NTNU), Trondheim, Norway
e-mail: ashenafi.yifru@ntnu.no; vikas.thakur@ntnu.no

S.A. Degago
Norwegian Public Roads Administration (NPRA), Trondheim, Norway
e-mail: samson.degago@vegvesen.no

V. Thakur et al. (eds.), *Landslides in Sensitive Clays*, Advances in Natural and Technological Hazards Research 46, DOI 10.1007/978-3-319-56487-6_30

that is particularly important for flow slides in sensitive clays, is estimating flow velocities and associated energies. This implies that one has to make a good prediction of the extent of the landslide run-out distance.

Several empirical approaches have been used to predict these post-failure movements and their flow extents e.g. (Mitchel and Markell 1974; L'Heureux 2012; Thakur et al. 2012, 2014a; Scheidl et al. 2013; Thakur and Degago 2014; Strand et al. 2017). On the other side, in the recent years, numerical approaches have been developed to simulate post-failure movements of flow slides e.g. (Hungr 1995; Imran et al. 2001; McDougall and Hungr 2004; Begueria et al. 2009; Christen et al. 2010; Mergili et al. 2012). These numerical models are primarily useful for estimating the extent of a potential rapid landslide as well as its associated velocity, pressure and flow depth, which are important for planning mitigation measures (McDougall and Hungr 2005).

Some attempts were made earlier to back analyze some sensitive clay flow slides using some numerical tools like DAN3D, MassMove2D and BING with different rheological models by Thakur et al. (2014b) and Issler et al. (2012). This work continues the attempt and assess the applicability and validity of a numerical mass flow model referred to as Rapid Mass Movement Simulation (RAMMS::Debris Flow V1.6 – here after referred as RAMMS (Christen et al. 2010)) for flow slides. Currently, RAMMS is the only quasi-3D commercially available debris flow software. In this work, a modified Voellmy rheology in RAMMS is examined for its potential to model post-failure movements of sensitive clay flow slides. The numerical study is illustrated using the Byneset sensitive clay flow slide happened in Norway in 2012.

The main objective is to simulate the real condition and evaluate the applicability of the modified Voellmy rheology by checking the consistency and the sensitivity of input parameters for use in simulating the run-out distance of sensitive clay flow slides. This study also focuses on determining the governing parameters for the Byneset clay flow slide according to the run-out distance, flow velocity and deposition depth. The numerical study is presented after a brief presentation of the case study that is used as a benchmark for the numerical study.

30.2 Case Study: The Byneset Clay Flow Slide

The Byneset clay flow slide happened few hours after the New Year day of 2012 due to natural causes. The Byneset area is located in Sør-Trøndelag province, 10 km west of Trondheim, Norway. The landslide area (the area designated as 'A' in Fig. 30.1d) has an approximate width of 150 m and retrogression distance of 350 m from the toe of the first slide. This landslide scar has an average depth of 8–10 m and a mobilized volume of slide mass estimated to be between $3{\cdot}10^5$ and $3.5{\cdot}10^5$ m^3. Measured from the toe of the slope, the slide volume has a total run-out distance of around 870 m along a low discharge stream with an average slope angle (θ) of 3°.

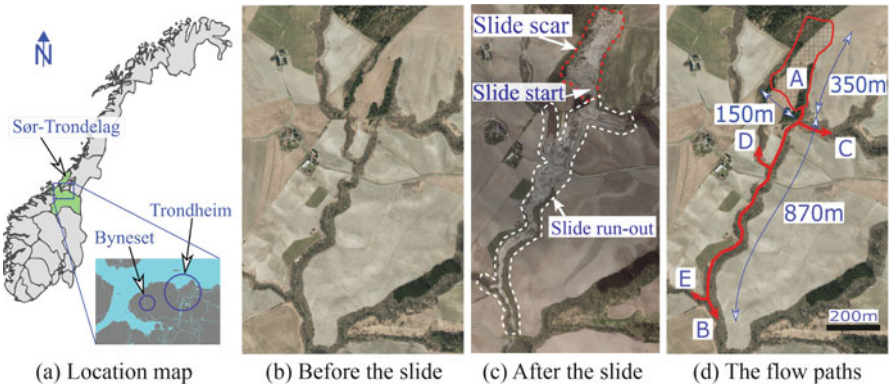

Fig. 30.1 Location map and topography of the Byneset clay flow slide area before and after the slide as well as the flow paths

Table 30.1 Soil properties of the Byneset clay flow slide area (Thakur 2012)

Sample depth	Water content	Undrained shear strength	Remolded shear strength	Sensitivity	Salt content	Cohesion	Friction angle
H [m]	w [%]	c_u [kPa]	c_{ur} [kPa]	S_t [−]	[g/l]	c [kPa]	θ [°]
4–10	27–48	5.2–72	0–0.5	3–403	0.5–13	3–7	27–35

The location map and the aerial photo before slide are given in Fig. 30.1a, b respectively. The actual observed flow slide is then presented in Fig. 30.1c. Figure 30.1d shows the main flow path in the direction of B covering a rough distance of 870 m. Relatively short flow slides were also observed in the secondary stream channels in the directions of C, D and E. However, the run-out distance along path B is measured to be 1000 m. This measure will be used as a reference run-out distance to compare the simulation run-out results. Immediately after the flow slide occurred, the area was extensively investigated with field and laboratory tests to characterize the engineering soil properties and parameters and given in Thakur (2012). The result of this extensive soil investigation shows that the area is rich in highly sensitive clay called quick clay, i.e. sensitive clay with $c_{ur} \leq 0.5$ kPa. Some of the soil properties are given in Table 30.1.

30.3 Back Analysis of the Byneset Clay Flow Slide

In the past, some attempts were made by Thakur et al. (2014b) and Issler et al. (2012) to back-calculate the Byneset clay flow slide using numerical tools referred to as DAN3D, Bing and MassMov2D. Different rheological models that are implemented

in these numerical tools, such as plastic and friction have been used and promising results were obtained. In this work, a quasi-3D numerical tool developed for debris flow simulation called RAMMS with the modified Voellmy rheological model is used. Brief description of the model is presented in the next section before presenting the numerical study.

30.3.1 The Voellmy Rheology and the Calculation Procedure

The version of RAMMS used in this study employs a modified version of the Voellmy rheology (Voellmy 1955). To obtain complete description of the Voellmy rheology, readers are encouraged to refer to Voellmy (1955) and Perla et al. (1980). The basal resistance, τ, as described by Voellmy rheology is given in Eq. 30.1.

$$\tau = \left(\mu\sigma + \frac{\gamma v^2}{\xi}\right) \tag{30.1}$$

where μ is the friction coefficient, σ is the total normal stress at the bed, γ is the unit weight of the flowing material, v is the flow velocity, and ξ is the turbulence factor. Equation 30.1 gives all the shear resistance offered by the fluid-channel friction and the dynamic drag that is inversely proportional to the turbulent factor and directly proportional to the square of flow velocity. However, in the modified Voellmy rheological model, the basal resistance equation is implemented as given in Eq. 30.2.

$$\tau = \mu\sigma + (1-\mu)\,c - (1-\mu)\,c\exp\left(-\sigma \Big/ c\right) + \frac{\gamma v^2}{\xi} \tag{30.2}$$

where c is the cohesion of the flowing material. Additional explanation about the modification can be found in Platzer et al. (2007a, b) and in the user's manual, WSL-SLF (2014). The model needs the three basal resistance parameters (c, μ, and ξ) as main inputs. In addition, digital terrain model (DTM) of the study area with good resolution is required.

The calculation procedure involves the following steps:

- Preparing a single 2×2 m grid DTM of the area from two pre- and post-slide topographies of the area (Fig. 30.1b, c) in such a way that the resulting DTM will have a post-slide topography at the slide source area and a pre-slide topography on the rest of the area.
- Defining the flow source by a method called block-release in which the total release volume was kept equal to the landslide volume, i.e. $3.5{\cdot}10^5$ m^3. This is done by drawing release area in the source location and specifying corresponding flow height to get same volume in each simulation.

Table 30.2 Ranges of values of governing input parameters in RAMMS (WSL-SLF 2014)

Parameters	Symbol	Unit	Value range
Cohesion	c	*kPa*	0–2
Friction coefficient	μ	–	0–0.4
Turbulence factor	ξ	m/s^2	1–10,000

- Selecting input parameters according to the field investigation results (Table 30.1) and the ranges of values suggested in literatures and the software manuals WSL-SLF (2013, 2014) as given in Table 30.2.
- Before an analysis commenced, the calculation domain area has to be defined and values of the three basal resistance parameters should be specified. As a simulation stopping criteria, 5% momentum is used, as it is suggested by the tool developers, in order not to have numerical diffusion problems. After running each analysis, the corresponding run-out distance is measured along the stream and compared with the actual observed run-out distance (1000 m). In addition, deposition depth and flow velocity are also assessed.

30.3.2 Back-calculation Results

Different combinations of the input parameters, Table 30.2, were used to simulate the actual run-out distance for the Byneset sensitive clay flow slide. A typical back-calculation of the flow run-out result is shown in Fig. 30.2 as a series of real time-lapse images. This result was obtained by one of the few equifinal combinations of the governing parameters that gave close run-out distance to what actually observed. This combination is found to be; $\xi = 2000$ m/s^2, $\mu = 0.005$ and $c = 0.1$ kPa. More can be seen in Yifru (2014). The simulation result shows that the flow source material evacuated completely from the slide scar and flowed along the main and secondary paths as it was actually observed in the field (Fig. 30.1c). The entire flow took around 288 s (approx. 5 min) and the maximum velocity of flow reached around 20 m/s. Note that his maximum velocity was only observed around the beginning of the flow (Fig. 30.3b). However, the estimated or conjectured flow velocity on site was around 10 m/s (Issler et al. 2012).

Figure 30.3 shows the maximum flow height and maximum velocity during the run-out and the final deposition depth of the simulation by the same parameters combination ($\xi = 2000$ m/s^2, $\mu = 0.005$ and $c = 0.1$ kPa).

30.3.3 Discussion

Before varying the two original friction parameters (μ and ξ), a thorough check on the cohesion, c, parameter implemented in the modified version (Eq. 30.2)

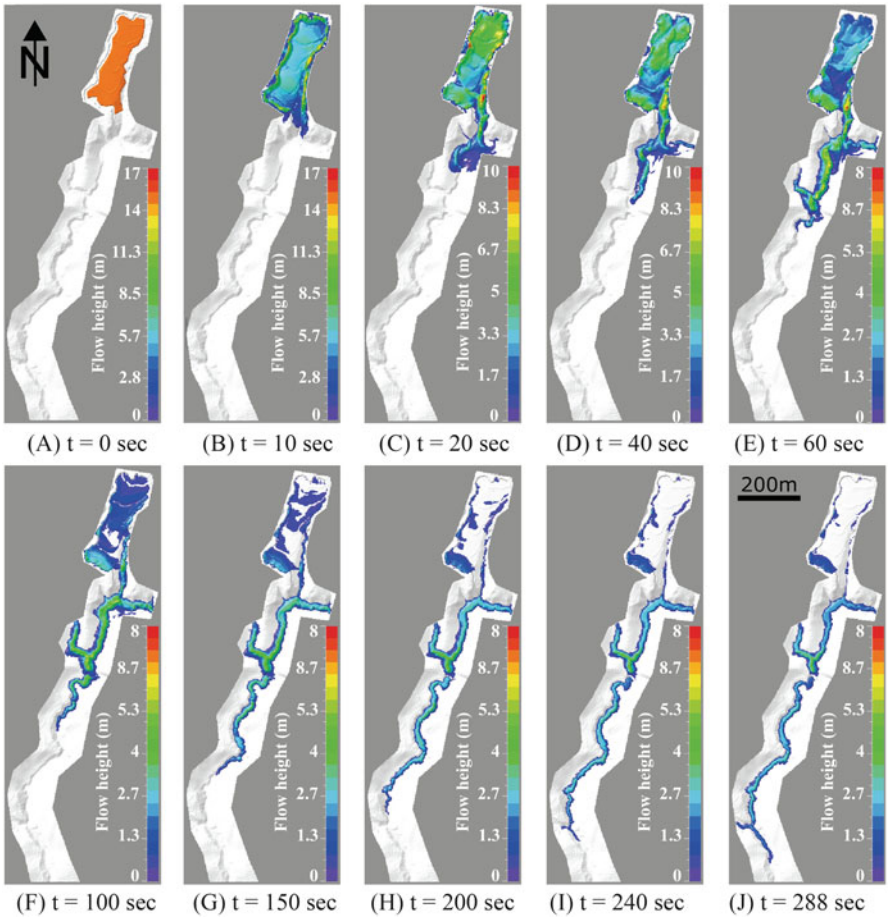

Fig. 30.2 Simulation of the Byneset landslide in real time with parameters $\xi = 2000$ m/s^2, $\mu = 0.005$ and $c = 0.1$ kPa

was made. The cohesion value given in Table 30.1 is for the intact soil while the remolded shear strength, c_{ur}, governs the situation during the flow slide. Therefore, the remolded shear strength is used to investigate the cohesion term given in Eq. 30.2. In addition, the c_{ur} value (0–0.5 kPa) given in Table 30.1 is found to fall into the recommended cohesion value given in Table 30.2 (0–2 kPa). This is in line with Thakur and Degago (2012) who suggested that Norwegian sensitive clays having remolded shear strength larger than 1.0 kPa shall not flow and thereby no run-out should be observed. A sensitivity analysis was also done to investigate the impact of cohesion parameter on the run-out distance when compared to the other two Voellmy friction parameters (μ and ξ). Figure 30.4 shows that an increase in c will result in a relatively significant decrease in the run-out distance only when one makes the other input parameters basal resistance contributions minimum.

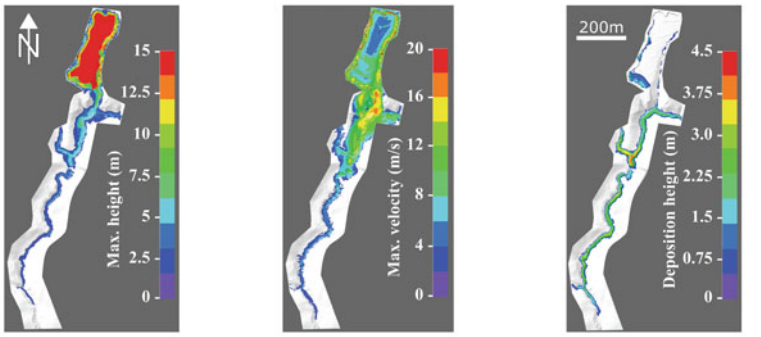

(a) Maximum flow height (b) Maximum flow velocity (c) Final deposition depth

Fig. 30.3 Maximum flow height, maximum flow velocity and final deposition depth of the flow with $\xi = 2000$ m/s^2, $\mu = 0.005$ and $c = 0.1$ kPa

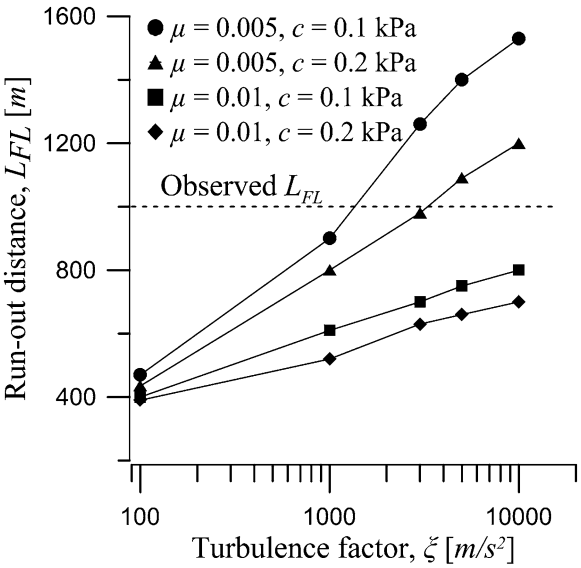

Fig. 30.4 Run-out distance as a function of μ and ξ for two selected cohesion values

It is worth noticing that the impact of cohesion on the run-out distance is non-linear and is dependent on the value of μ and ξ. Because of the above parameter check on c and the given remolded shear strength value in Table 30.1, a fixed value of cohesion parameter, $c = 0.1$ kPa, is chosen.

Friction coefficient values were varied to be $\mu = 0.005$, 0.01, 0.1 and 0.2 which can be considered to correspond to flow slope angles, $\theta = 0.29°$, 0.57°, 5.71° and 11.31° (with $\mu \approx \tan(\theta)$ according to Chen and Lee (2003)) respectively. Turbulence factor values, on the other hand, were varied to be $\xi = 100$, 1000, 3000, 5000 and 10,000 m/s^2. The obtained run-out distances corresponding to these values are presented in Fig. 30.5. A simulation with $\mu = 0.01$ along with a very high value

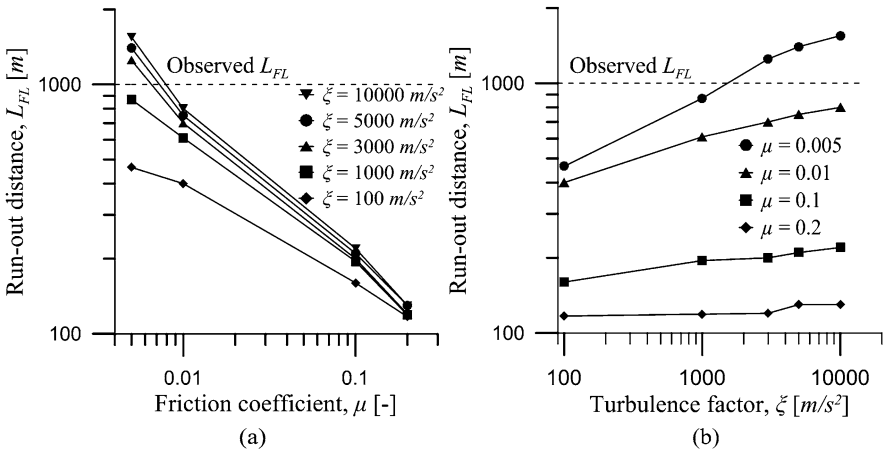

Fig. 30.5 Run-out distance as a function of **a** μ and **b** ξ for $c = 0.1$ kPa

of $\xi = 10{,}000$ m/s^2 is seen to give a result close to the actual run-out distance. However, by using smaller friction coefficient value like $\mu = 0.005$, it is possible to obtain a close run-out distance in combination with turbulence factor value as low as $\xi = 1000$ m/s^2. For $\mu = 0.1$ and $\mu = 0.2$, irrespective of the value of ξ, the flow is seen to come to stop very early before reaching half way of the observed run-out distance. According to the results found, applying the actual value of slope of flow, $\mu = 0.052 \approx \tan(3°)$, will not give the required run-out distance even if it is combined with the highest turbulence factor, $\xi = 10{,}000$ m/s^2.

It is suggested by WSL-SLF (2013) that relatively large values of turbulence factor can sometimes be associated with muddy type flows. This large value significantly decreases the resistance contribution from the velocity term and let the other parameters (cohesion and friction coefficient) govern the flow. If the resistance contribution from cohesion and friction coefficient is made to be low, the material will remain flowing even with a very slow speed. However, all simulations were made to stop when the momentum sum reaches 5% of the maximum momentum sum to avoid numerical diffusion problems. This is also to avoid minor internal movements and rearrangements that do not contribute for the total run-out at the supposed end of the flow. Generally, one should note that a fully remolded sensitive clay with such low remolded shear strength and viscosity could easily flow until it reaches a new equilibrium.

The typical simulation result presented in Fig. 30.3c gives final deposition height varied from 1.5 to 4.5 m in different locations. The approximate deposition depth on site was around 3 m with exception at the upstream area having 7 m depth (Issler et al. 2012). In addition, Fig. 30.3b gives maximum flow velocity of 10–20 m/s around the initial part and drops to 5 m/s during the final part of the simulation. The simulation result is seen to roughly replicating the deposition depth while the maximum velocity of flow obtained is found to be exceeding the value conjectured

to occur at the site, which is 10 m/s. For this Byneset clay flow slide case, ξ ranging between 2000 and 5000 m/s^2 with μ ranging between 0.005 and 0.01 and $c = 0.1$ kPa are back-calculated to simulate the actual run-out distance observed.

30.4 Conclusion

In this work, attempts were made to back-calculate the run-out distance of a real clay flow slide using the Voellmy rheology. A fundamental assumption in the material modelling is that the highly sensitive clay has attained its fully remolded state. Accordingly, the material is able to flow over a certain terrain topography as mainly governed by friction coefficient and cohesion value. The cohesion parameter defined in the modified Voellmy model was found to have minor impact in controlling the flow and barely represents the remolded shear strength of such clay flow slides. The friction coefficient is found to be the main parameter providing to the basal resistance. However, the estimation suggested in literatures to use tangent of the slope angle of the flow topography could not replicate the observed case as it results in larger basal resistance to the flow. The turbulence factor, however, is more responsible for describing the turbulent behavior of the flow where larger values result in turbulent and relatively rapid flows. It is also worth noting that Voellmy rheology is a single-phase rheology whereas flow slides in sensitive clays may be governed by the interaction between water and the clay particles resulting in excess pore pressure development behavior during the flow. Despite this, the Voellmy rheology reproduced the field observation results reasonably well. The major challenge lies in relating the governing parameters of this rheology with geotechnical parameters of sensitive clays.

Acknowledgments The authors of this paper would like to acknowledge the Natural Hazards program (NIFS) and the GeoFutue II project. The Authors would also like to acknowledge Professor Gustav Grimstad, NTNU, for his valuable review feedback.

References

Begueria S, Van Asch TWJ, Malet JP, Grondahl S (2009) A GIS-based numerical model for simulating the kinematics of mud and debris flows over complex terrain. Nat Hazards Earth Syst Sci 9(6):1897–1909

Chen H, Lee CF (2003) A dynamic model for rainfall-induced landslides on natural slopes. Geomorphology 51(4):269–288. doi:10.1016/S0169-555x(02)00224-6

Christen M, Kowalski J, Bartelt P (2010) RAMMS: numerical simulation of dense snow avalanches in three-dimensional terrain. Cold Reg Sci Technol 63:1–14

Hungr O (1995) A model for the runout analysis of rapid flow slides, debris flows, and avalanches. Can Geotech J 32(4):610–623

Imran J, Harff P, Parker G (2001) A numerical model of submarine debris flow with graphical user interface. Comp Geosci UK 27(6):717–729

Issler D, Cepeda JM, Luna BQ, Venditti V (2012) Back-analyses of run-out for Norwegian quick-clay landslides. NIFS report . Norwegian Geotechnical Institute (NGI) & Statens Vegvesen, Veidirektoratet, NorwayAvailable at www.naturfare.no

L'Heureux J-S (2012) A study of the retrogressive behaviour and mobility of Norwegian quick clay landslides. In: Proceedings of the 11th international & 2nd North American symposium on landslides, Banff, Canada

McDougall S, Hungr O (2004) A model for the analysis of rapid landslide motion across three-dimensional terrain. Can Geotech J 41(6):1084–1097

McDougall S, Hungr O (2005) Dynamic modelling of entrainment in rapid landslides. Can Geotech J 42(5):1437–1448

Mergili M, Schratz K, Ostermann A, Fellin W (2012) Physically-based modelling of granular flows with open source GIS. Nat Hazards Earth Syst Sci 12(1):187–200

Mitchel RJ, Markell AR (1974) Flow slides in sensitive soils. Can Geotech J 11:11–31

Perla R, Cheng TT, Mcclung DM (1980) A 2-parameter model of snow-avalanche motion. J Glaciol 26(94):197–207

Platzer K, Bartelt P, Jaedicke C (2007a) Basal shear and normal stresses of dry and wet snow avalanches after a slope deviation. Cold Reg Sci Technol 49(1):11–25

Platzer K, Bartelt P, Kern M (2007b) Measurements of dense snow avalanche basal shear to normal stress ratios (S/N). Geophys Res Lett 34(7)

Scheidl C, Rickenmann D, McArdell BW (2013) Runout prediction of debris flows and similar mass movements. Landslide Sci Pract 3:221–229

Strand SA, Thakur V, L'Heureux JS, Lacasse S, Karlsrud K, Nyheim T, Aunaas K, Ottesen H, Gjelsvik V, Fauskerud OA, Sandven R (2017) Runout of landslide in sensitive clays. In: Thakur V, L'Heureux J-S, Locat A (eds) Landslides in sensitive clays. From research to implementation. Springer, Dordrecht, pp 289–300. Paper presented at the 2nd international workshop on landslides in sensitive clays, Trondheim

Thakur V (2012) Datarapport for Kvikkleireskred ved Esp i Byneset i januar 2012. Statens vegvesen, Vegdirektoratet. 2012

Thakur V, Degago SA (2012) Quickness of sensitive clays. Geotech Lett 2:87–95

Thakur V, Degago S (2014) Quickness test approach for assessment of flow slide potentials. Geotech Eng J SEAGS & AGSSEA 45(1):85–94

Thakur V, Oset F, Aaboe R (2012) A critical appraisal of the definition of Brittle clays (Sprøbruddmateriale). In: Taylor, Francis (ed) Proceedings of the 16th Nordic geotechnical meeting, Copenhagen Vol 1: pp. 451–462

Thakur V, Degago SA, Oset F, Aaboe R, Dolva BK, Aunaas K, Nyheim T, Lyche E, Jensen OA, Saeter MB, Robsrud A, Viklund M, Nigussie D, L'Heureux JS (2014a) Characterization of post-failure movements of landslides in soft sensitive clays. Landslide Sensitive Clays Geosci Risk Manag 36:91–103

Thakur V, Nigussie D, Degago SA (2014b) A preliminary study of rheological models for run-out distance modeling of sensitive clay debris. In: 8th European conference on numerical methods in geotechnical engineering

Thakur V, Gylland AS, Degago SA, Oset F, Sandven F (2015) In-situ determination of disintegration energy for soft sensitive clays. Paper presented at the GeoQuebec 2015

Voellmy A (1955) Uber die Zerstorungskraft von Lawinen. Schweiz Bauzeitung 73:212–285

WSL-SLF (2013) RAMMS user manual v1.5 debris flow. http://ramms.slf.ch/ramms/downloads/RAMMS_DBF_Manual.pdf. Accessed 26 Aug 2016

WSL-SLF (2014) RAMMS user manual v1.6 debris flow. http://ramms.slf.ch/ramms/downloads/RAMMS_Version_1.6.pdf. Accessed 26 Aug 2016

Yifru AL (2014) Assessment of rheological models for run-out distance modeling of sensitive clay slides, focusing on Voellmy Rheology. Master Master, NTNU

Chapter 31
Effect of Strain Softening Behaviours on Run-Out Distance of a Sensitive Clay Landslide

Petter Fornes and Huynh D. V. Khoa

Abstract Reliable prediction of landslide triggering threshold and landslide run-out distance is essential for hazard risk assessment. The paper focuses on studying slides in sensitive clays, which represent a major geohazard in many countries including Norway, Sweden and eastern Canada. Large deformation finite element (FE) analyses were performed using the Coupled Eulerian-Lagrangian (CEL) method in Abaqus, which allows for capturing of the full progressive failure mechanism (initiation, propagation and breakoff) involved in a sensitive clay slide. The 1984 slide in Vestfossen, Norway, was chosen as problem case of progressive failure in sensitive clay to be back-calculated by using the CEL FE-model. It is found that the failure mechanism predicted by the FE-analysis agrees reasonably well with the historical failure mode observed at Vestfossen. A parametric study has been performed on the remoulded shear strength as well as the rate of strain softening of the sensitive clay in order to evaluate their effects on the landslide run-out distance.

31.1 Introduction

Most natural sensitive clays exhibit strain-softening behaviour which is generally a governing material property for progressive failure mechanisms. It is especially important for Scandinavian sensitive clays, which under large strains turns into a liquid with almost zero remoulded shear strength (Thakur and Degago 2012). Due to the progressive type of failure, a small local bearing capacity type of instability may potentially become a failure threshold triggering large devastating slides. The failure

P. Fornes (✉)
Norwegian Geotechnical Institute (NGI), Oslo, Norway

Norwegian University of Science and Technology (NTNU), Trondheim, Norway
e-mail: petter.fornes@ngi.no

H.D.V. Khoa
Norwegian Geotechnical Institute (NGI), Oslo, Norway
e-mail: khoa.d.v.huynh@ngi.no

V. Thakur et al. (eds.), *Landslides in Sensitive Clays*, Advances in Natural and Technological Hazards Research 46, DOI 10.1007/978-3-319-56487-6_31

can occur quite rapidly, essentially in undrained conditions (Locat et al. 2013). This type of hazard can cause significant damage to infrastructure, like the collapse of the Skjeggestad bridge in Norway in 2015, and loss of life.

Numerous methods have been developed, however, not many are capable of predicting the complete process of progressive failure involving its initiation, propagation and breakoff in sensitive clays. The main objective of the present study is to perform large deformation analysis of undrained slope stability in sensitive clays by using the Coupled Eulerian-Lagrangian (CEL) method available in the commercial finite element (FE) program Abaqus (2014). Many researchers have demonstrated that the CEL method is suitable for solving slope stability problem involving large deformations (Wang et al. 2013; Dey et al. 2015; Trapper et al. 2015). In this paper the CEL method is applied to simulate both the landslide triggering threshold and the landslide run-out distance.

The paper is organized in three main parts. In the first part, the CEL method is briefly introduced and the problem case of the 1984 slide in Vestfossen, which was chosen for the FE back-analysis, is described. The second part of the paper is devoted to provide some details about the CEL FE-model of the Vestfossen slide, the material inputs to the FE-model as well as a parametric study of the effect of strain-softening rate on the run-out distance of the failure. Finally, in the third part, the calculated FE-results are discussed and some concluding remarks are drawn from the present study.

31.2 Method: CEL

To calculate the full progressive failure mechanism involved in a quick clay slide, a numerical method that can handle large deformations is essential. In the standard Lagrangian FE method, excessively distorted elements during large deformation analysis can introduce error into the analysis results, and, in the worst case, they can cause the analysis to terminate prematurely.

The Coupled Eulerian-Lagrangian method is available in the Abaqus/Explicit program (Abaqus 2014), in which the element mesh is fixed in space and does not change with time while the material points (Gauss points) can flow freely across the mesh. In a CEL FE-model, the Lagrangian body and Eulerian body are discretized differently in separate (or with some overlap) regions of the problem domain. The Eulerian material can interact with Lagrangian elements through Eulerian-Lagrangian contact formulated based on an enhanced immersed boundary method. In this method the Lagrangian structure occupies void regions inside the Eulerian mesh. The contact algorithm automatically computes and tracks the interface between the Lagrangian structure and the Eulerian materials. Hence, the CEL method is suited for numerical problems involving large deformations due to the fact that there is no distorted element as illustrated in Fig. 31.1. The CEL method has been successfully used to model backward progressive sensitive clay slides, capturing the characteristic horsts and grabens modes of deformation (Dey et al. 2013, 2015).

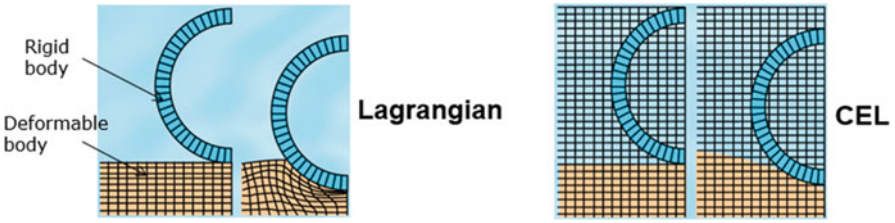

Fig. 31.1 Illustration of deformed mesh obtained from Lagrangian analysis and CEL analysis

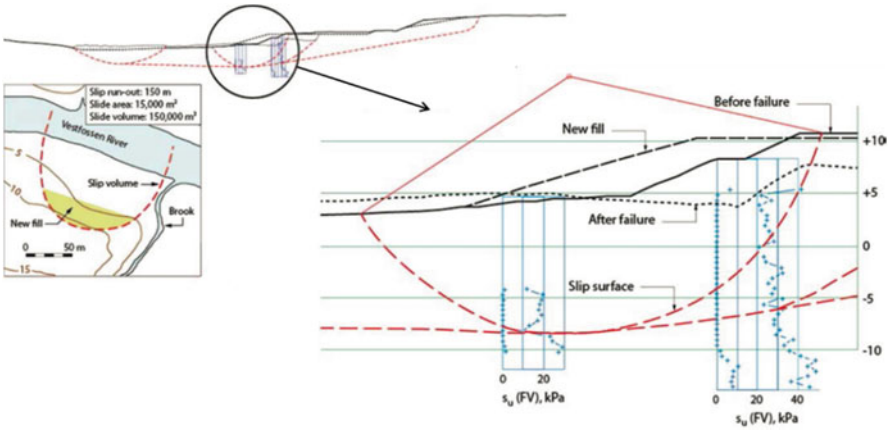

Fig. 31.2 Extent of the 1984 slide at Vestfossen (Modified from Kalsnes et al. 2013)

31.3 Problem Case: Vestfossen

The 1984 slide in Vestfossen, Norway, was chosen as problem case to investigate the effect of post peak stress strain behaviour on run-out distance of a quick clay landslide. The slide comprised an area of approximately 100×150 m, with roughly 10 m depth (Karlsrud 1984). The failure mechanism propagated horizontally quite far over a flat area, crossing the Vestfossen river, see Fig. 31.2.

The Vestfossen slide was most likely triggered by the construction of a new fill in a slope next to the Vestfossen river (NGI 1984), when a new soccer field was to be built. The very sensitive clay underneath the fill was thus mobilized past its peak undrained shear strength, which due to strain softening reduced the soil strength. This caused a downward progressive failure mechanism, where the local failure propagated almost horizontally over a larger distance. Soil investigations were performed after the slide, and the shearing plane was localized in the layer where the remoulded shear strength was close to zero in vane shear tests as shown in the cross section in Fig. 31.2.

The initiation of the slide was back calculated in a previous study (NGI 2012), using the (small strain) FE software Plaxis 2D (2015) with the user defined material

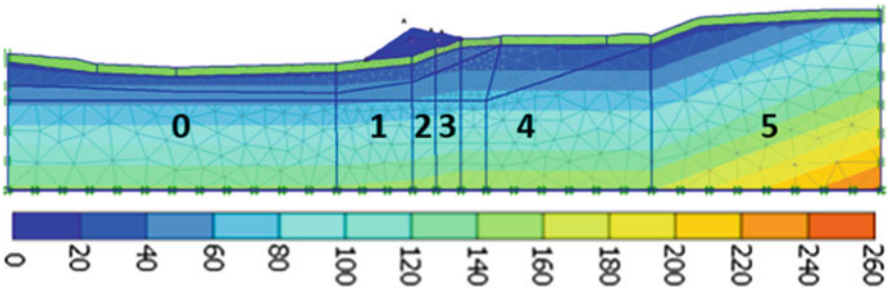

Fig. 31.3 Plaxis 2D model, undrained shear strength $s_u{}^A$ [kPa] contours (Adapted from NGI 2012)

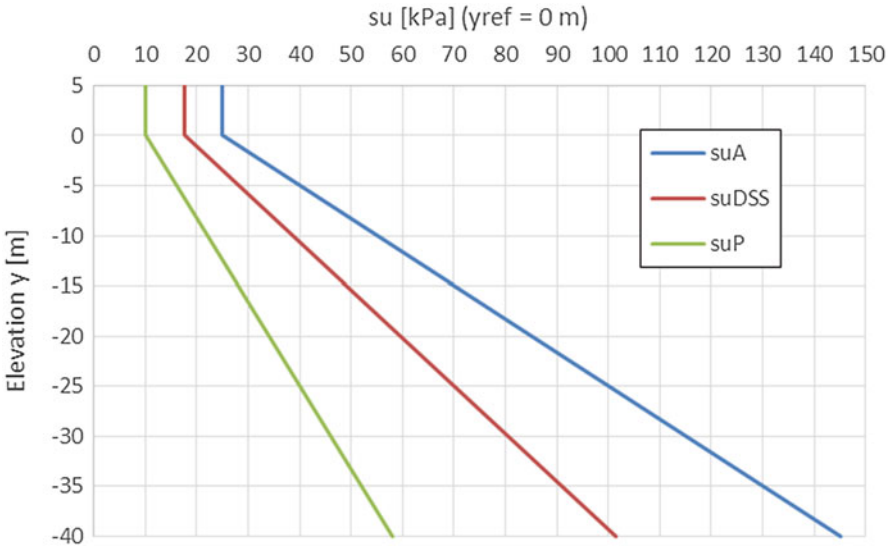

Fig. 31.4 Example of undrained shear strength profile, showing peak s_u values versus elevation in Section 0 ($y_{ref} = 0$ m). For isotropic strength, $s_u{}^{ave} = s_u{}^{DSS}$ was used

model NGI-ADPSoft, which could account for strain softening and anisotropy (Grimstad et al. 2010; Grimstad and Jostad 2010; Jostad and Grimstad 2011). The peak undrained shear strength profile was based on the available site data, and calibrated through back-calculation.

In a vertical cross section, the peak undrained shear strength increases linearly with depth from reference elevation y_{ref}. This parameter varies linearly in the horizontal direction within the sections 0–5 in Fig. 31.3, providing compatible strength contours for the different slope angles. The undrained shear strength profile is illustrated in Fig. 31.4, for Section 0 where the reference elevation $y_{ref} = 0$ m.

31.4 Abaqus CEL Modelling

In the current study, the Vestfossen cross section in Fig. 31.3 was modelled with Abaqus CEL as a 3D profile with 1 m unit thickness in the plane direction. The soil profile composed of a continuous layer of sensitive clay, with a dry crust material in the top 3 m and a fill that was applied to initiate failure. To apply the soil self-weight as the load gravity loading was used with acceleration 10 m/s^2 in negative y-direction (vertically) for simplicity. The respective unit densities then provides the volume mass. Each CEL FE-analysis is run as an explicit calculation, and a time interval for each calculation phase is given so that the velocities and kinetic energy become very small at the end of the phases. In the first phase the gravity was applied to the initial soil profile and the void, but not the fill, to provide the initial stresses. In the second phase, the gravity was also applied to the fill to initiate slope failure. In order to avoid unwanted numerical dynamic issues, the gravity loads were applied gradually over 10 seconds with the 'smooth step' function.

The CEL mesh size had (roughly) element size of 1 m, and thus only one element in the plane direction. The total number of elements was 22,755. A mesh sensitivity study was performed to see the effect of mesh fineness, where the length of the elements was reduced to 0.5 m. When using strain softening material behavior without any form of regularization, localization of shear bands and mesh size dependent results are expected. The user defined model in the small strain FE study (NGI 2012) used a non-local strain technique (Brinkgreve 1994), but the Mohr Coulomb material model in Abaqus does not include any regularization technique. However, the deformations with the finer mesh were comparable to the deformations with the original mesh. Hence, the original mesh was considered fine enough for this study.

31.4.1 Material Properties

31.4.1.1 Dry Crust

The 3 m dry crust in the top of the profile was described by the Mohr-Coulomb constitutive model with friction angle $\phi = 30°$, cohesion c = 5 kPa, Young's modulus E = 10,000 kPa, Poisson's ratio $\nu = 0.495$ and density $\rho = 1{,}800$ kg/m^3.

31.4.1.2 Fill Material

The fill behaviour was described by the Mohr-Coulomb material model with friction angle $\phi = 30°$, cohesion c = 1 kPa, Young's modulus E = 10,000 kPa and Poisson's ratio $\nu = 0.495$. The weight of the fill material was applied in the CEL calculations to initiate a local bearing capacity failure, and density $\rho = 1{,}800$–$2{,}000$ kg/m^3 was used. The necessary density depends on the degree of strain softening, and was initially determined from the Plaxis 2D FE-analysis.

31.4.1.3 Sensitive Clay Layers

The sensitive clays behaved undrained and were described by the Mohr-Coulomb constitutive model. For the elastic properties Young's modulus E = 30,000 kPa at elevation y_{ref} and increasing with depth 3,600 kPa/m, Poisson's ratio $\nu = 0.495$ and density $\rho = 1{,}800$ kg/m^3 were considered.

The standard Mohr Coulomb model in Abaqus was used to specify the variation of the cohesion (i.e. undrained shear strength) of the clays as a function of the plastic shear strain. For better comparison with possible future work, curve points of the cohesion and the corresponding plastic shear strain were specified so that the stress-strain softening curve has the same shape as in the NGI-ADPSoft model. The stress strain curves in the NGI-ADPSoft model are determined by the two state variables κ_1 and κ_2, respectively pre and post peak hardening functions. The functions are chosen so that the slope (first derivative) is zero at peak and residual strength

$$\begin{aligned}\kappa_1 &= 2\cdot\left(\gamma^p/\gamma_p{}^p\right)^{0.5}/\left(1+\gamma^p/\gamma_p{}^p\right), \kappa_2 \\ &= \left(\left[\gamma^p-\gamma_p{}^p\right]/\left[\gamma_r{}^p-\gamma_p{}^p\right]\right)^{C1}\cdot\left(2-\left[\gamma^p-\gamma_p{}^p\right]/\left[\gamma_r{}^p-\gamma_p{}^p\right]\right)^{C2}\end{aligned}$$

where γ^p is the plastic shear strain, $\gamma_p{}^p$ is the peak strength plastic shear strain, $\gamma_r{}^p$ is the residual strength plastic shear strain, and $1.0 \le C2 \le C1 \le 2.0$ are constant to control the shape of the post peak softening curve. For this study the parameter set $C1 = C2 = 1.5$ was chosen.

In order to define increasing undrained shear strength with depth, the cohesion was given as a function of temperature. The temperature parameter was only used as a variable to provide different strength gradients corresponding with Fig. 31.3. Anisotropic strength and stiffness properties can be specified with the NGI-ADPSoft model, but isotropic is required with the Mohr Coulomb model in Abaqus. Thus, isotropic properties were used for this study, with peak undrained shear strength $s_{u,p} = s_u{}^{ave} = s_u{}^{DSS} = 0.7{\cdot}s_u{}^C$, according to Fig. 31.4.

Normalized residual undrained shear strength $s_{u,r}/s_{u,p} = 0.1$ was considered as the base case. The plastic shear strain at peak strength $\gamma_p{}^p = 3\%$ and the plastic shear strain at residual strength $\gamma_r{}^p = 30\%$ were used as the base case. The corresponding shear stress-strain curve is indicated with a black line in Fig. 31.5. To prevent the volume upslope from the fill from sliding out in the CEL calculation, the normalized residual strength $s_{u,r}/s_{u,p}$ in Section 4 and 5 of Fig. 31.3 was increased to 0.3 and 0.5, respectively.

31.4.2 Parametric Study

A parametric study was performed where the potential effect of strain-softening rate on the run-out distance was investigated. Only the properties of the sensitive clay layers downslope (in Section 0–3, Fig. 31.3) were varied. The normalized residual

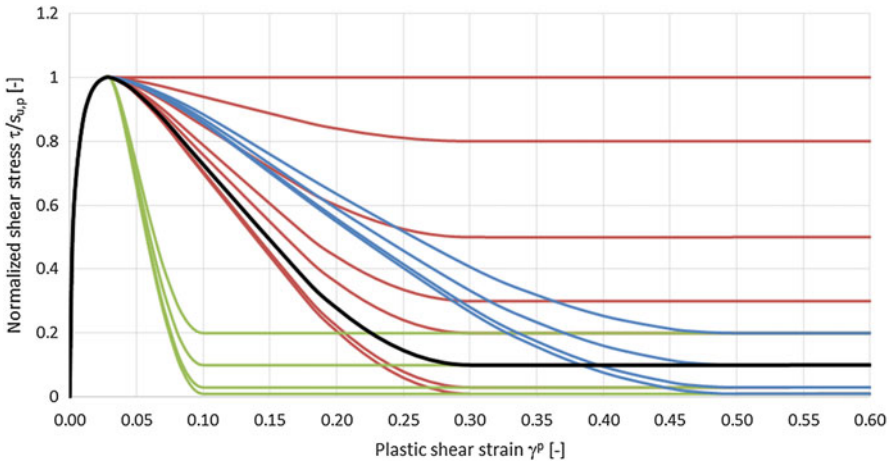

Fig. 31.5 Different normalized stress-strain curves considered in parametric study. *Black solid curve* corresponding to base case with $s_{u,r}/s_{u,p} = 0.1$, $\gamma_p{}^p = 3\%$, $\gamma_r{}^p = 30\%$

strength $s_{u,r}/s_{u,p}$ of these sensitive clay layers was varied between 0.01 and 1.0. The parameter controlling the rate of strain softening, the shear strain at residual strength $\gamma_r{}^p$, was varied from 10% to 50%. Note that a lower value of $\gamma_r{}^p$ results in a more brittle behavior. The stress-strain curves considered are illustrated in Fig. 31.5.

31.5 Results

The calculated results from the Abaqus CEL simulation of the base case strain-softening parameters are discussed here. The weight of the fill was applied from time T = 20 s to T = 30 s and the fill started to move after the full load had been applied. The only forces acting on the soil were the gravity and inertial loads. The kinetic energy of the whole system is a useful indicator to check if the soil failure mechanism has been stabilized. It can be seen in Fig. 31.6 that the kinetic energy increases as the local bearing capacity failure is initiated, and the peak kinetic energy appears at roughly T = 35 s. The motion slows down and the kinetic energy in the whole system is reduced to zero at roughly time T = 50 s.

The calculated average plastic shear strains and the velocity during the propagation of soil failures are illustrated in Fig. 31.7. The shading contours of plots with 5 s intervals are shown from time T = 30 s when the full fill weight has been applied to T = 50 s when the soil failure surface has stopped propagating.

A local failure is first initiated by the fill, and shear strains are developed in front of the slide as it is moving. The fill itself is not moving very far, but the downward progressive mechanism propagating is pushing material in front of the fill and is causing heave in the downstream area. After the main movement of the

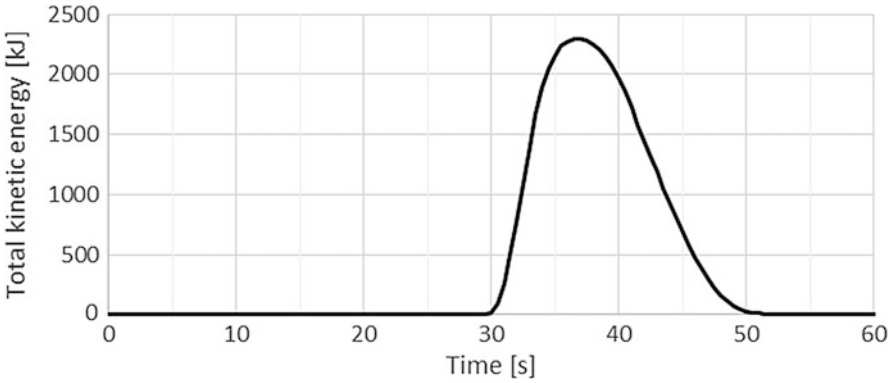

Fig. 31.6 Kinetic energy versus time. Peak when the slide is moving, goes down to zero

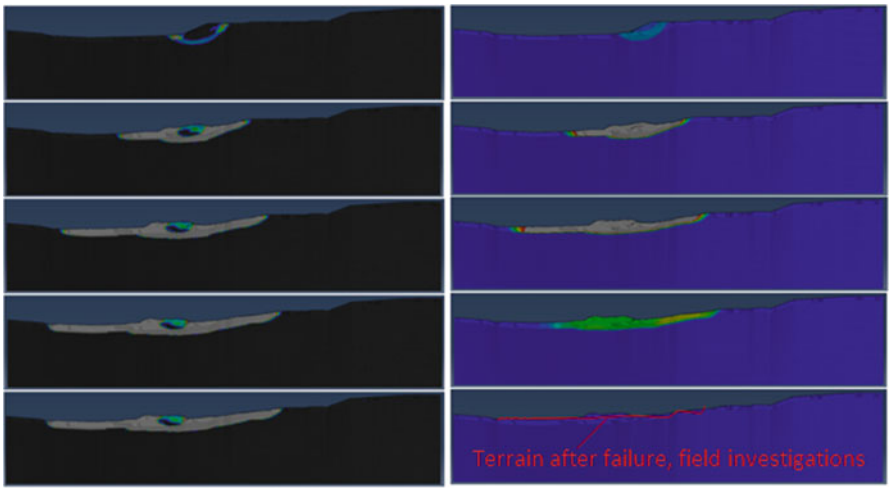

Fig. 31.7 Contours of (*left*) average plastic shear strain PEEQAVG (3–30%, i.e. peak to residual strength) and (*right*) velocity V (0–1 m/s) for time T = 30–50 s for the base case. The red line indicates the profile after failure that was recorded in the field investigation (Fig. 31.2)

fill, shear strains develop backwards, causing the slope to become gradually less inclined. It can be seen from the velocity contours that first the fill moves, followed by movement upslope after the fill volume has stopped.

31.5.1 Comparison with Field Data

The profile recorded in the field investigation after the Vestfossen landslide in 1984 is shown Fig. 31.2. The fill volume appears to have ended up completely flat

horizontally, and one retrogressive failure surface appears behind the local fill failure surface. There was registered heave as far as 90 m from the toe of the fill, on the other side of the river.

The large deformation shape of the Abaqus CEL model calculation in Fig. 31.7 is comparable to the historical failure mode. In the calculations the fill volume is moving a distance from the toe and its contours remains in the terrain when the deformations stops. The terrain behind the fill also deforms, but not directly as a retrogressive failure surface. The authors believe that by refining the layer modelling to better match the in-situ conditions, a realistic upslope deformation pattern could be obtained, as demonstrated by Dey et al. (2015). The base case calculations include heave roughly 90 m from the toe of the fill, as observed.

The calculated deformation patterns seems to mainly take place in the top of the clay layers, right below the dry crust. In the historical slide, the propagating failure surface was most likely deeper indicated by in-situ vane shear tests. This could possibly be replicated by introducing anisotropy and constant residual strength with depth. The residual strength increased with depth since constant $s_{u,r}/s_{u,p}$ ratio and peak strength increasing with depth was used in the calculations. By introducing sensitive clay layers of different strengths instead of a homogenous layer, the CEL FE-analysis can provide better prediction of the identified failure surface.

31.5.2 Parametric Study

In the parametric study the effect of the post peak strength reduction curve parameters on the run-out distance was investigated. Due to the distinct mode of deformation, there is not a unique way to define the run-out distance. Two measures describing the run-out distance are reported; one is the extent of downstream heave due to the propagation of shear strains, distance measured from the toe of the applied fill, and the second is the crest movement of the fill.

The results from the parametric study are plotted in Fig. 31.8 showing run-out distance for different values of normalized residual undrained shear strength $s_{u,r}/s_{u,p}$ and the residual strength plastic shear strain $\gamma_r{}^p$. Due to model boundaries, 120 m was the maximum run-out distance.

31.6 Conclusions

The 1984 Vestfossen landslide has been back-analyzed using the CEL FE-model. It is found that the calculated failure pattern is in reasonable agreement with the historical failure mode observed at Vestfossen. A parametric study has been performed on the remoulded shear strength and the rate of strain softening of the sensitive clay in order to evaluate their effects on the landslide run-out distance. It appears that low residual strength values have a bigger effect than the degree of brittleness.

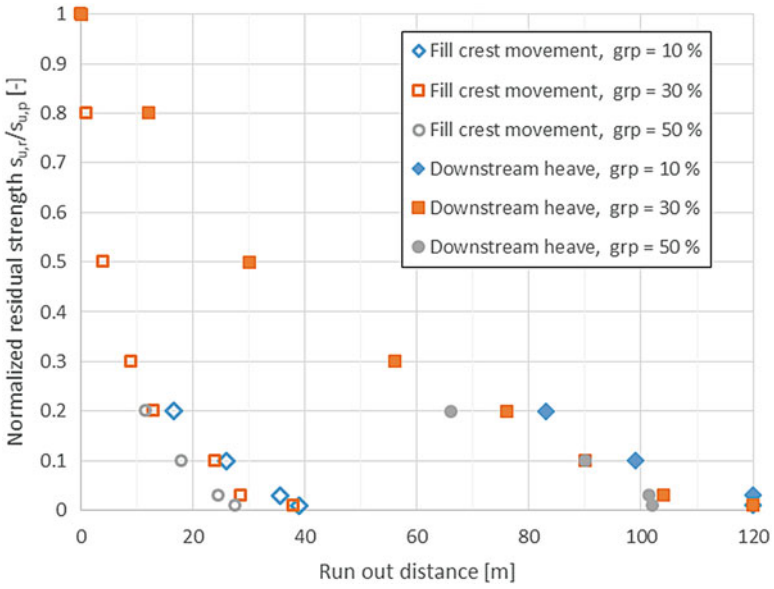

Fig. 31.8 Run-out distance (downstream heave and fill crest movement) versus normalized residual strength, with curves for different plastic shear strain at residual strength

Combining the CEL FE-model and an advanced constitutive model, which can account for the strain-softening behaviour and the anisotropic strengths in soils, provides a robust and suitable numerical tool for not only predicting landslide triggering threshold but also estimating landslide run-out distance in sensitive clays. However, applying different loads was not as easy as in a Lagrangian method due to the material deforming within the mesh, and the results can be mesh dependent due to no regularization with strain-softening.

Further work planned includes implementing the anisotropic NGI-ADPSoft model into the Abaqus/Explicit. This will enable the use of more realistic soil properties and better prediction of trigger load and run-out distance.

Acknowledgments The research has been supported by the Norwegian Geotechnical Institute. The authors also express their sincere thanks to Dr. Hans Petter Jostad for his assistance. Many thanks are given to Dr. Ha H. Bui for good feedback.

References

Abaqus (2014) Users' manual – version 6.14. Providence: Dassault Systems Simulia Corp., http://www.3ds.com/

Brinkgreve RBJ (1994) Geomaterial models and numerical analysis of softening. PhD thesis, TU Delft, Delft, The Netherlands

Dey R, Hawlader B, Phillips R, Soga K (2013) Progressive failure of slopes with sensitive clay layers. In: Proceedings of the 18th International Conference on Soil Mechanics and Geotechnical Engineering, Paris

Dey R, Hawlader B, Phillips R, Soga K (2015) Large deformation finite-element modelling of progressive failure leading to spread in sensitive clay slopes. Géotechnique 65(8):657–668. doi:10.1680/geot.14.P.193

Grimstad G, Jostad HP (2010) Undrained capacity analyses of sensitive clays using the nonlocal strain approach. In: 9th HSTAM International Congress on Mechanics Vardoulakis mini-symposia, Limassol, Cyprus

Grimstad G, Andresen L, Jostad HP (2010) NGI ADP: anisotropic shear strength model for clay. Int J Numer Anal Methods Geomech 36(4):483–497

Jostad HP, Grimstad G (2011) Comparison of distribution functions for the nonlocal strain approach. In: Proceedings of 2nd international symposium on computational geomechanics, Kroatia

Kalsnes BG, Gjelsvik V, Jostad HP, Lacasse S, Nadim F (2013) Risk assessment for quick clay slides – the Norwegian practice. In: 1st international workshop landslides in sensitive clays. Québec, Oct 2013

Karlsrud K (1984) Progressive failure in stiff overconsolidated and soft sensitive clays. Contribution to discussion session 9A – "Geologic aspects of slope stability problems", ICSMFE

Locat A, Jostad HP, Leroueil S (2013) Numerical modeling of progressive failure and its implications for spreads in sensitive clays. Can Geotech J 50(9):961–978

NGI (1984) Strandajordet, Vestfossen, Utredning vedrørende utglidningen den 11. september 1984, samt de stabilitetsmessige konsekvenser for idrettsanlegget. NGI report 82032–3

NGI (2012) Effekt av progressiv bruddutvikling for utbygging i områder med kvikkleire, A2 Tilbakeregning av skred. NGI report 20092128-00-5-R, available as NIFS report 56/2014 at http://www.naturfare.no/_attachment/668507/binary/976962

Plaxis (2015) Plaxis 2D, www.plaxis.nl

Thakur V, Degago S (2012) Quickness of sensitive clays. Géotech Lett 2(3):87–95. doi:10.1680/geolett.12.0008

Trapper PA, Puzrin AM, Germanovich LN (2015) Effects of shear band propagation on early waves generated by initial breakoff of tsunamigenic landslides. Mar Geol 370:99–112

Wang D, Randolph MF, White DJ (2013) A dynamic large deformation finite element method based on mesh regeneration. Comput Geotech 54:192–201

Part IV
Case Records, Slides in Sensitive Sediments Including Offshore and Nearshore Slides

Chapter 32
The 1908 Disaster of Notre-Dame-de-la-Salette, Québec, Canada: Analysis of the Landslide and Tsunami

Jacques Locat, Dominique Turmel, Pascal Locat, Julie Therrien, and M. Létourneau

Abstract The landslide of 1908 in Notre-Dame-de-la-Salette, Québec, was the deadliest event occurring in sensitive clays of Eastern Canada, causing 33 deaths. Of these, 26 are associated with the tsunami generated impact of water and ice on the opposite bank. A LiDAR survey of the sector, and a geotechnical investigation were carried out respectively in 2009 and 2010 to characterize this landslide. Covering an area of 6.5 ha, the soil mass carried is estimated at nearly 1.2 million m^3. The paper describes the event, reports the results of the investigation and discusses the tsunami caused by the debris of the landslide. The tsunami approach includes modeling both the kinematics of the slide and the wave.

32.1 Introduction

Landslides in sensitive clays are well known for their damaging effects resulting from retrogression phenomena, the propagation of the debris or both (Demers et al. 2008). Tsunamis generated by coastal slides have been well documented in the past (Chiocci et al. 2008; Poncet et al. 2009) but only recently for the case of slides in quick clays (L'Heureux et al. 2012). In Québec, recent research dealing with potential landslide-tsunamis in reservoir (Leblanc et al. in preparation) has raised an interest on this process. As a result, quite a few cases of landslides were found which, although not recognized as such, have generated a significant tsunami wave. The most recent took place in 2015 at Lac des Seize-Îles about 75 km North of

J. Locat (✉) • D. Turmel
Laboratoire d'études sur les risques naturels (LERN), Université Laval, Québec, QC, Canada
e-mail: jacques.locat@ggl.ulaval.ca; dominique.turmel.1@ulaval.ca

P. Locat • J. Therrien • M. Létourneau
Ministère des Transports, de la Mobilité durable et de l'Électrification des transports (MTMDET), Québec, QC, Canada
e-mail: Pascal.Locat@transports.gouv.qc.ca; Julie.Therrien@transports.gouv.qc.ca; Maryse.Letourneau@transports.gouv.qc.ca

V. Thakur et al. (eds.), *Landslides in Sensitive Clays*, Advances in Natural and Technological Hazards Research 46, DOI 10.1007/978-3-319-56487-6_32

Montréal (Locat et al. 2016; Leblanc et al. 2015). We will here focus on the April 6th 1908 Notre-Dame-de-la-Salette (NDLS) slide, which is the deadliest landslide in quick clays in Canada. Here, most of the fatalities were caused by the tsunami wave carrying the ice cover which was still on the river at that time of the year.

The objectives of the paper are the following: (1) present the case of the NDLS slide and tsunami event and its geotechnical characteristics, (2) propose a simulation of the observed tsunami and its inundation, and (3) comment on the integration of tsunami hazard in the process of developing hazard maps related to slide in sensitive clays.

In the Notre-Dame-de-la-Salette region, the Lièvre River valley is a narrow clay plain, having a width of about 1 km, which is flanked by Precambrian hills about 120 m or more above the valley floor. Locally, intact river banks can be as high as 18–20 m and consists mostly of Champlain Sea clays (Ochietti 1989). The underlying bedrock topography is quite variable and the thickness of the marine deposit can be as high as 20–40 m. Around the main scarp of the 1908 slide, ground elevation is between 148 and 150 m as it can be seen on Fig. 32.2.

According to the LiDAR based landslide inventory made by Demers et al. (2017), the region presents many highly retrogressive landslide scars which results either from flow slides or spreads. According to Fransham and Gadd (1977) many of them occurred soon after the retreat of the Champlain Sea. Some are more recent and of greater dimensions such as the Poupore spread of 1903 (Ells 1903) with an area of 47 ha and the flow slide of 2010 with an area of 5.6 ha (Perret et al. 2013).

The Notre-Dame-de-la-Salette slide took place on April 6th 1908 at the end of a long winter season. It was initiated on the right side of the river. It is the landslide in clays with the largest number of casualties at 33. According to Ells (1908, see also Buckingham Post 1908), it took place in two phases which remnants are still visible on the 1964 aerial photographs and on the 2009 LiDAR survey (see Fig. 32.1). According to the terminology proposed by Locat et al. (2008), the first failure generated a retrogression of 85 m over a width of 460 m. A few days later, a second smaller slide moved the head scarp back by another 38 m over a width of 330 m for a total retrogression of 123 m. The head scarp now has a height varying between 6 and 12 m. The total slide area is 6.5 ha, with 5.4 ha and 0.9 ha for phases 1 and 2 respectively. The debris accumulated over an area of about 13 ha, an estimation based on the fact that observations by Ells in 1908 indicate that the debris reached an elevation of 135.5 m. From the analysis of a bathymetry survey carried out in 2016, the debris spread by 250 m upstream and 200 m downstream and according to Ells (1908) they restrained the flow of the river.

From the records of the damages, it is possible to have an estimate of the extent of the tsunami wave and of the damages (Fig. 32.1). The houses were only moved a little which indicates that the ice and water came quite rapidly at their base. More considerations on this aspect are provided below in the section considering the modeling of the tsunami wave.

From the design plans of a bridge 240 m upstream from the site, the level of the water in the river would vary between 131 and 134 m. The 2016 bathymetry and 2009 LiDAR surveys indicate a level at 131.9 m and 131.1 m respectively. However,

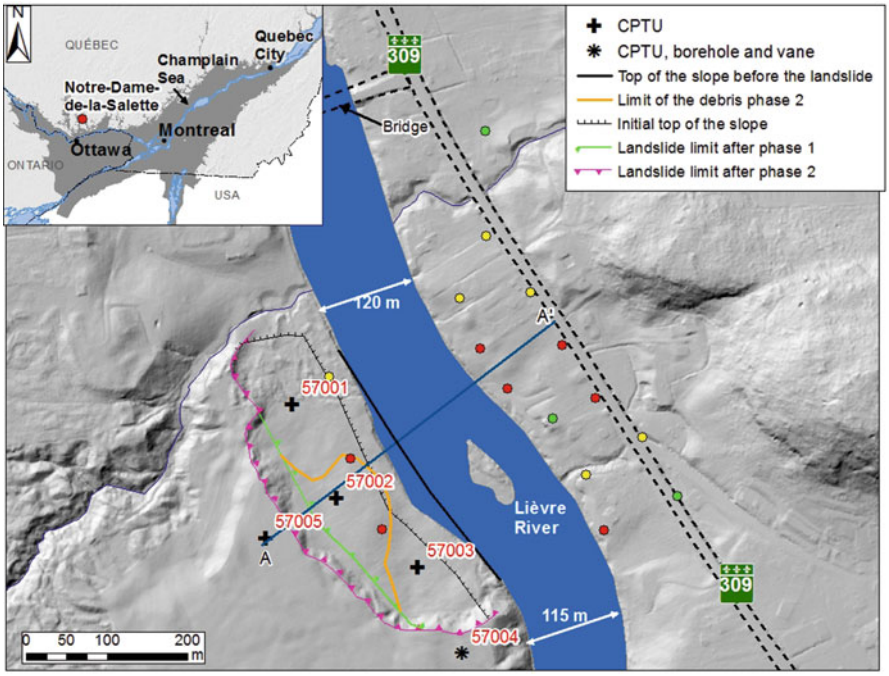

Fig. 32.1 General location and detailed extent of the Notre-Dame-de-la-Salette slide phases 1 and 2 showing also coring, testing, topographic section shown in Fig. 32.4, and damages caused by the tsunami wave on houses (*red*: destroyed, *yellow*: damaged, and *green*: no data). River flows towards the South, *Black line*: toe of slope before the slide with the island in the middle is made of the 1908 slide debris. LiDAR source is from MTMDET, May 2009

Ells (1908) noted that at the time of the slide, the river level was slightly higher than the summer level which could indicate a level between 131 and 132 m. For tsunami simulation presented later, a level of 132 m was used. The height of the river bank just south of the slide is about 18 m above the lowest river level with an average slope angle of 30°, which is believed to be the case here in 1908. According to the LiDAR survey, the river width is about 120 m which is taken to be the case in 1908.

According to the morphology of the terrain seen on 1926, 1950, and 1964 aerial photographs, and from ground photographs taken in 1908 just after the event, the slide is considered as a flow slide. In fact, most of the debris did evacuate the slide area and about 30% of those left after the event are evidenced by small buttes in the crater area (Fig. 32.1).

The slide generated a tsunami wave that moved the ice cover on the river across the river which acted as a significant aggravating factor responsible for the destruction of many houses which were inhabited (see Fig. 32.2b). As part of his report, Ells mentioned that:

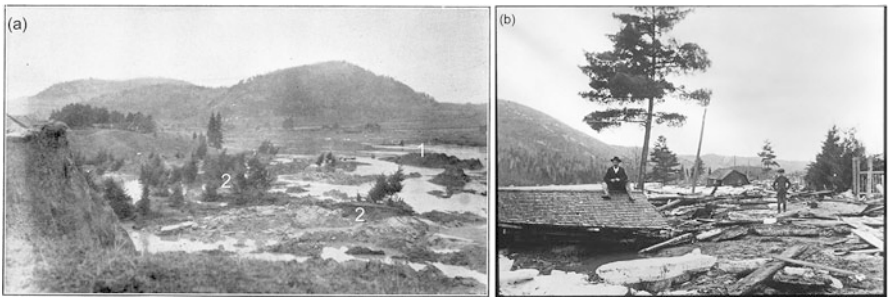

Fig. 32.2 The April 6th 1908 NDLS slide: **a** escarpment and debris; *1* may give the location of the actual island seen in Figs. 32.1 and 32.2 indicates debris displaced at the time of phase 2; **b** area across the river were some houses have been destroyed by the tsunami wave carrying the ice blocks. Note the very limited amount of mud on the ground

> . . . the ice in the river was apparently unbroken at the time, and was lifted and carried forward over the east bank on which Salette village is located, at an elevation not more than twelve to fifteen feet above the present level of the river, and which was some feet above the ordinary summer level. The rush of ice came with such force against the village as to completely demolish the greater portion of the village. In fact, everything within its course was destroyed: including twelve houses and some twenty five outbuildings, which were entirely destroyed to their foundation; while on the margin of the ice movement (see Fig. 32.1) several buildings were more or less damaged.

According to Ells (1908), the tsunami wave flooded up to an elevation of 15 m above the water level of the river at the time, which suggests a maximum elevation of about 146 m. The level of destruction varied, as mentioned by Ells (1908), but according to the available photographs, the roof of few houses survived the impact of the wave. The ice thickness is estimated to have been about 0.5 m (Ells 1908). The damages caused by the ice are illustrated in Fig. 32.2b where pieces of ice still remain but with no evidence of significant sediments from the slide itself, clearly indicating that ice and water were responsible for the destruction, not the debris.

32.2 Geotechnical Settings, Slide Modeling and Tsunami

The site investigation reported here was carried out in the fall of 2010 and included 5 CPTu and one borehole including sampling and in situ vane testing located just outside of the landslide scar (see location in Fig. 32.1). During the 2016 summer, a series of seismic ambient noise recordings were taken along the center of the slide and on either side of the river to ascertain the thickness of the clay deposit around the slide. Bathymetric data were also acquired in 2016 on both side of the landslide debris, in order to better define the pre-failure bathymetry. The site investigation aimed at defining both the stratigraphic conditions and the geometry of the surface of failure and also providing samples to determine the physico-chemical and geotechnical properties of the clay deposit (Fig. 32.3).

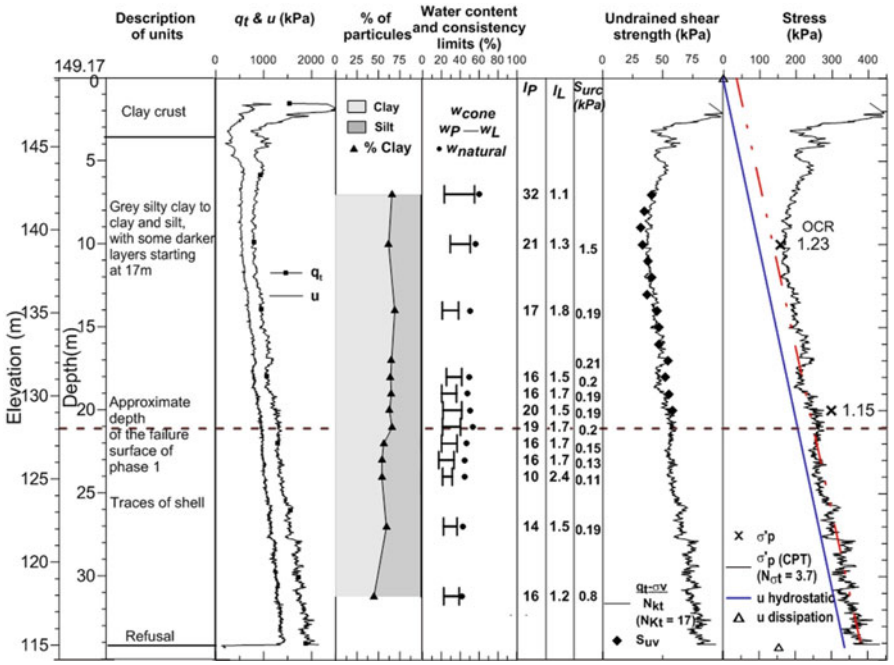

Fig. 32.3 Geotechnical profile for borehole 57,004 located on Fig. 32.1. The *red dashed line* estimates the amount of over consolidation due to erosion, which would be about 4 m

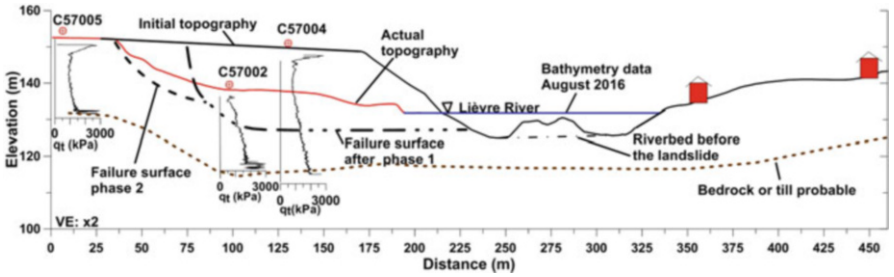

Fig. 32.4 Topographic section across the middle of the scar (see position in Fig. 32.1) showing the pre and post slide topography. In situ test used to help define the stratigraphy and the rupture surfaces are also shown. The *red line* shows the post slide topography and the *brown line* the bedrock topography. There is a *vertical* exaggeration of 2×

From CPTu tests C57004 and C57005 (Fig. 32.4) the stratigraphic setting is very similar all around the landslide scar except that the clay layer gets thinner away from the slide (to the West). At the base of the quaternary section, there is a layer of till (about 1 m) draping the bedrock. The till is overlain by a marine deposit which consists in a homogeneous silt and clay deposit with a thickness of 19 m at the C57005 site (i.e. between elevation 152 and 133 m) and of 34 m at site C57004 (between elevation 149 and 115 m). The upper part of this unit is weathered over

a thickness of about 4–7 m. The bedrock topography (Fig. 32.4) defines a small glacial valley with an elevation of about 120 m in the middle of the river to values around 135 m at 200 m away from the river banks.

The geotechnical properties were obtained from testing samples at borehole F57004, from CPTu and from in situ vane. Results are presented in Fig. 32.3. For the clay unit, the profile in Fig. 32.3 shows, below the clay crust, a fining upward sequence with a clay content increasing gradually from 42 to 69%, with a similar trend for the plasticity index (10–32%) and the Atterberg's limits (e.g. liquid limit from 31% to 50%). Such a change is also reflected in the stratification with banded clays (proglacial dark and gray alternating layers) in the lower part of the section, between 139 and 117.6 m becoming homogeneous above that latter elevation. The liquidity index tends to increase from 1.2 at the bottom to higher values above, with a maximum of 2.4 at an elevation of 125 m. The remoulded undrained shear strength varies accordingly. This suggests the whole section has been largely leached from the original interstitial salt. According to Fig. 32.4, the failure surface of the first phase of the slide would be at a depth of about 21 m.

The intact strength increases with depth showing a small overconsolidation corresponding to about 4 m of soil with a strength increase with depth from 32 kPa just below the crust to a maximum of about 80 kPa at the base of the section. Inversely, the water content decreases regularly with depth from 60% at the top to 40% at the base. The sensitivity varies between 19 and 1,220. Two oedometer tests yielded an OCR value of about 1.2.

For the slide analysis and tsunami modeling, the pre-slide topography (Fig. 32.4) was determined using the LiDAR topographic data of 2009 around the 1908 landslide scar and the river banks on either side of the river. The bathymetry before the slide is obtained by linking the existing upstream and downstream bathymetries relative to the landslide location. The three CPTu within the scar were used to locate the failure surface of phase 1 (CPTu C57002 and C57004, Figs. 32.1 and 32.4) and the depth to refusal, i.e. till or bedrock. These vertical profiles have been projected on the cross-section shown in Fig. 32.4.

Approximate location of phases 1 and 2 failure surfaces are shown in Fig. 32.4. Using the failure surface identified by CPTus for phase 1, the failure surface would be at an elevation of 128 m, i.e. about 4 m above the deepest part of the river. For phase 2, there is no in situ measurements of the rupture surface so it was interpreted from the analysis of aerial photographs and the observations made by Ells (1908). From this, the elevation of the failure surface for phase 2 would be about 10 m above that of phase 1 (Fig. 32.4). In addition, considering also that the debris from phase 2 are overlying those of phase 1 (see Fig. 32.2a) and did not left the scar (Fig. 32.1) they were likely less remolded than those of phase 1. The lower degree of remolding for phase 2 also reflects the fact that this portion of the section, above an elevation of about 138 m, has a lower liquidity index (less than 1.2, Fig. 32.3) and a lower remolding energy available due to the lower escarpment height.

The numerical model used to look at the landslide kinematic and tsunami generated is the solver multiphaseinterfoam, which is included in the OpenFOAM Suite. OpenFOAM is a set of C++ modules used to build solvers to simulate

specific problems in engineering mechanics (Weller et al. 1998). As explained in more details in Turmel et al. (2017), the solver tracks the interface Γ between fluids, and solves, using the Volume of Fluid method, the Navier-Stokes equations over a finite-volume mesh. The mesh size for this analysis varied in the domain: near the ground the mesh size was approximately of $0.25 \times 0.25 \times 0.25$ m, where in the portion not affected by the landslide or the tsunami, the mesh size was approximately $2 \times 2 \times 2$ m. The time step was also not constant, and was varied automatically in order to have a maximum Courant number (Co), in every cells of the domain, lower than 0.5, i.e. the magnitude of the velocity cannot be more than one half of the cell size (Δx) in one time step (Δt).

$$Co = \Delta t \frac{|U|}{\Delta x} \leq 0.5 \tag{32.1}$$

In this particular case, three fluids were modeled in the simulation: the clay from the landslide, the water in the river and finally the ambient air. Rheological properties for the water and air were set as constant, and the rheological properties of the clay were modified in order to simulate the run-out extent described previously. The density of the clay (ρ) was set as 1600 kg/m^3.

In order to best reproduce the observed and deduced run-out distances from the landslide (Fig. 32.5), the material was considered as a Bingham fluid, with a yield stress of 1.7 kPa, and a viscosity of 1.7 Pa.s. The 1:1,000 ratio between plastic viscosity and yield stress observed in laboratory by Locat (1997) was maintained

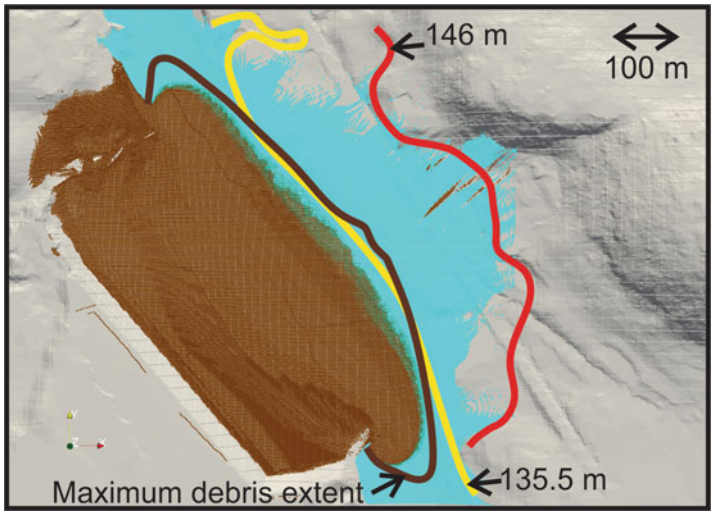

Fig. 32.5 Results of the numerical simulation: displaced water in *blue*, debris in *brown*. Maximum extent of the debris as a *brown line*, water is hiding some debris (*pale brown*). 135.5 m and 146 m isocontours; maximum elevations reached by the debris and of water respectively according to Ells (1908). North is up

in the analysis. These values correspond to rheological parameters equivalent to a liquidity index of approximately 1. Results from the modeling show that the debris reaches the opposite bank of the river, and did inundate part of the coast, up to an elevation of 137 m. This is slightly higher than the observations that showed debris up to an elevation of 135.5 m. However, in the river, the observations showed that debris spread by 250 m upstream and 200 m downstream, where the numerical simulation showed that the debris spread approximately 150 m upstream and 150 m downstream. In the direction perpendicular to the river, the elevation reached by the debris is higher than the one deduced from observations, and in the distance along the river, the travel distance is lower than the one showed by the bathymetric survey. The maximum velocity reached by the landslide is 15 m/s, and the total displacement took less than 20 s. However, it must be noted here that the whole volume is considered to have been mobilized at the same time, which is not the case. This difference may have had an influence on the debris extent, as well as the presence of ice.

Figure 32.5 shows the maximum run-out of the tsunami produced by this landslide. Due to the mesh size, the maximum resolution for the run-out is 10 cm of water. The extent of the modeled tsunami is slightly higher than the extent of the damages caused by the tsunami. However, it has to be mentioned that the ice coverage was not taken into account in the analysis, and this may have influenced the maximal tsunami run-up.

Simulation shows that when the tsunami generated wave reaches the destroyed houses nearest to the river, the maximum flow height (h) was approximately 1.5–2 m with a horizontal velocity (u) between 10 and 15 m/s. When the wave reaches the farthest houses destroyed, the flow height was 1 m with horizontal velocities around 10 m/s. Finally, for the northeast house, that was damaged but not destroyed by the tsunami, the water height when the wave reached the house was of 30–40 cm, with a velocity of 8–10 m/s.

32.3 Discussion and Concluding Remarks

The NDLS slide represents an interesting case supporting the need for furthering research in the field of river banks generated tsunamis. Using a model that was used for the first time here to model such type of landslide and tsunami interaction, we have been able to satisfactorily reproduce the extent of the landslide debris. As mentioned, the rheological properties used in this analysis are not the same as the rheological properties that could have been obtained in laboratory on a totally remoulded material. The liquidity index of the material involved in the landslide is between 1.2 and 2.4, and to obtain the best results, the rheological parameters were set for an equivalent liquidity index of 1.0. This difference can be explained by the energy lost in remolding the material that is not yet taken into account in the numerical model, as well as by the fact that the whole volume is considered to be mobilised at the same time in the numerical model. As it can be seen in Fig. 32.2a, the presence of large blocks is indicative that not all the displaced mass has been remoulded.

The numerical model also reproduces quite well the extent of the generated tsunami wave. Furthermore, the wave height seen at location of houses agrees with the observation that, for some buildings, the second floor was not damaged, meaning that the water level was less than one-story high. However, some factors were not taken into account into the simulation, such as the presence of an ice cover on the river. This ice could have attenuated the wave, leading to a shortest propagation.

Historical pictures also reveal that when ice is present on the river it can be seen as an aggravating factor regarding the consequences of a tsunami. Most of the buildings were made of wood so that their resistance to the impact by the ice or water was very limited. In order to look at the effect of the wave on the destruction of the houses, we may look at the wave pressure acting on the structures. This pressure (p) can be obtained as a sum of the hydrostatic pressure for the equivalent inundation depth (h) and pressure based on the conservation of momentum, as shown in Eq. 32.2 (Arimitsu et al. 2013), where g refers to gravitational acceleration.

$$p = \rho g h + \rho u^2 \tag{32.2}$$

According to Barbolini et al. (2004), for partly reinforced houses that were hit by snow avalanches, when the impact pressure exceed 20 kPa, houses are most of the time completely destroyed. Using Eq. 32.1, it can be considered that, for a flow depth of 1 m, such a dynamic pressure will be reached when the flow velocity is 10 m/s. For the houses completely destroyed near the river, this flow velocity was reached and the impact pressure was sufficient to destroy the houses. For the farthest houses that were destroyed, the impact pressure was almost 20 kPa. According to the type of construction, this may have been sufficient to destroy the houses. Finally, for the northeast house that was damaged, the impact pressure would have been, according to the simulation, of 13 kPa, which is lower than the threshold.

If for the Lac-des-Seize-Îles tsunami there were convincing arguments that the ice was the main aggravating factor, here it is not clear what would have been the level of damage if there had been no ice, but simulations shows that, if there were only water, the houses could have been destroyed. What is evidenced in this review of the NDLS slide and tsunami events is the need to introduce the hazard posed by such type of tsunamis in the establishment of hazard maps in sensitive clays. Further research is required to establish morphological and geotechnical criteria indicative of requirements for a specific tsunami analysis. As part of the same research, mitigation methods could be designed to protect infrastructures and inhabited areas against such a hazard.

Acknowledgments The research presented in this paper has been financially supported by the Ministère des Transports, de la Mobilité durable et de l'Électrification des transports du Québec, and in part funded by the Plan d'actions sur les changements climatiques (PACC). The authors also wish to thank Serge Leroueil for his review of the manuscript.

References

Arimitsu T, Ooe K, Kawasaki K (2013) Evaluation method of tsunami wave pressure acting on land structure using 2D depth-integrated flow simulation. Coast Dyn 2013:105–114

Barbolini M, Cappabianca F, Sailer R (2004) Empirical estimate of vulnerability relations for use in snow avalanche risk assessment. Risk Anal IV:533–542

Buckingham Post (1908) Appaling disaster at Notre Dame de la Salette, stories of eyewitness. Source: https://news.google.com/newspapers?nid=LWqeokA2EBkC&dat=19080424&printsec=frontpage&hl=fr

Chiocci FL, Romagnoli C, Tommasi P, Bosman A (2008) The Stromboli 2002 tsunamigenic submarine slide: characteristics of possible failure mechanisms. J Geophys Res 113:B10102. doi:10.1029/2007JB005172

Demers D, Robitaille D, Potvin J, Bilodeau C, Dupuis C (2008) La gestion des risques de glissements de terrain dans les sols argileux au Québec. In: 4th Canadian Conference on Geohazards, Université Laval, Université Laval Press, Québec, QC, 519–526

Demers D, Robitaille D, Paradis S, Fortin A, Ouellet D, Lavoie M (2017) The use LiDAR airbone data for retrogressive landslide inventory in sensitive clays, Québec, Canada. In: Thakur V, L'Heureux J-S, Locat A (eds) Landslides in sensitive clays. From research to implementation. Springer, Dordrecht, pp 279–288

Ells RW (1903) The recent landslide on the Lièvre River, P.Q. Canada Department of Mincs, Geological Survey Branch, Annual Report, V.15, Report A, p. 136A–139A

Ells RW (1908) Report on the landslide at Notre-Dame de la Salette, Lièvre River, Québec. Canada Department of mines, Geological Survey Branch, Report No. 1030, p. 1–16

Fransham PB, Gadd NR (1977) Geological and geomorphological controls of landslides in Ottawa valley, Ontario. Can Geotech J 14:531–539

L'Heureux J-S, Eilertsen RS, Glimsdal S, Issler D, Solberg I-L, Harbitz CB (2012) Chapter 45: the 1978 quick clay landslide at Rissa, Mid Norway: subaqueous morphology and tsunami simulations. In: Yamada et al. (eds) Submarine mass movements and their consequences. Advances in Natural and Technological Hazards Research, 31: 507–516. Springer Science.

Leblanc J, Turmel D, Therrien J, Locat J (2015) Observations of coastal landslide-generated tsunami under an ice cover: the case of Lac-des-Seize-Îles, Québec, Canada. In: Lamarche G et al. (eds) Submarine mass movements and their consequences, Advances in Natural and Technological Hazards Research, 41: 607–614

Leblanc J, Turmel D, Locat J, Harbitz C B, Grenon M, Locat A, in preparation Tsunami generation by potential rockslides in an abandoned open-pit mine: the case of Black Lake, Quebec, Canada. Submitted to the Canadian Geotechnical J

Locat J (1997) Normalized rheological behaviour of fine muds and their flow properties in a pseudoplastic regime. In: Proceedings of the 1st international conference on debris-flow hazards mitigation, San Francisco, ASCE, New York, p 260–269

Locat J, Turmel D, Leblanc J (2016) Tsunamigenic landslides in Quebec. In: Aversa et al. (ed) Landslides and engineered slopes. Experience, theory and practice. Associazione Geotecnica Italiana, Rome, pp 1305–1312. ISBN 978-1-138-02988-0

Ochietti S (1989) Quaternary geology of St. Lawrence Valley and adjacent Appalachian subregion. In: Fulton RT (ed) Quaternary geology of Canada and Green-land, Geological survey of Canada (Ottawa, Canada), Paper 1, pp 350–379

Perret D, Mompin R, Bossé F, Demers D (2013) Stop 2-5B: the Binette Road earth flow induced by the June 23, 2010 Val-des-Bois earthquake. In: Deglacial history of the Champlain Sea basin and implications for urbanization, Joint Annual Meeting GCMAC-SEG-SGA, Ottawa, ON, 25–27 May 2011, Field guide book, Geological Survey of Canada, Open File 6947, p 72–74

Poncet R, Campbell C, Dias F, Locat J, Mosher D (2009) A study of the tsunami effects of two landslides in the St. Lawrence estuary. In: Mosher DC, Shipp RC, Moscardelli L (eds) Submarine mass movements and their consequences. Advances in Natural and Technological Hazards Research, 28: 755–764

Turmel D, Locat J, Locat P, Demers D (2017) Parametric analysis of the mobility of debris from flow slides in sensitive clays. In: Thakur V, L'Heureux J-S, Locat A (eds) Landslides in sensitive clays. From research to implementation. Springer, Dordrecht, pp 301–310

Weller JG, Tabor G, Jasak J, Fureby C (1998) A tensorial approach to computational continuum mechanics using object-oriented techniques. Compr Physiol 12:620–631

Chapter 33
Fv. 287 Strandgata: Kjøreplass bru. Road Construction in Quick Clay

Ernst Pytten, Trine Flobak, and Hanne Bratlie Ottesen

Abstract Rambøll was responsible for the geotechnical design of a pedestrian road through an area with quick clay in Modum municipality Norway. This paper reviews the ground conditions and soil parameters, describes stability calculations and describes the design solution, including protection against erosion and the implementation of each construction phase. The design was done according to guidelines given by the Norwegian Public Roads Administration (NPRA) and The Norwegian Water Resources and Energy Directorate (NVE). The pedestrian road was considered to be an important project to improve the traffic safety for the pedestrians and cyclists in the area and the project was designed as a K1-project according to NVE guidelines. For K1-projects the design must ensure no reduction of the current factor of safety in any of the construction phases.

To determine the soil parameters comprehensive field and laboratory tests were performed. Interpretation of CPTUs and laboratory data indicated a weak layer in the slope, approximately coinciding with the critical shear surface. 3D–effects of the slope were taken into account and the soil parameters were increased to the level where a safety factor of ca. 1,0 was attained. The pedestrian road was located half way up the slope and stability calculations were performed both for the slope above the road and for the slope between the road and the river Simoa below. The design solution included lightweight material for the new road filling to avoid increased loads. Movements in the slope and the pore pressure were monitored throughout the project.

E. Pytten
Rambøll Norge AS, Kristiansand, Norway
e-mail: ernst.pytten@ramboll.no

T. Flobak (✉)
Rambøll Norge AS, Oslo, Norway
e-mail: trine.flobak@ramboll.no

H.B. Ottesen
Norwegian Public Roads Administration (NPRA), Oslo, Norway
e-mail: hanne.ottesen@vegvesen.no

V. Thakur et al. (eds.), *Landslides in Sensitive Clays*, Advances in Natural and Technological Hazards Research 46, DOI 10.1007/978-3-319-56487-6_33

33.1 Introduction

Rambøll was engaged by the Norwegian Public Roads Administration (NPRA) for the geotechnical design, and assistance in the construction phase, of a pedestrian road. The pedestrian road was built to improve traffic safety on the stretch of road "fv. 287 Strandgata – Kjøreplass bru" in Modum municipality in Norway. The project also included improvement and reinforcement of the existing road which was in poor condition. The road is located in a steep slope with the river Simoa below, and crosses an already mapped zone of quick clay, 848 Haugfoss.

The construction works on the pedestrian road started in summer 2015, and was completed in summer 2016.

33.2 Soil Conditions and Material Properties

The road is placed in a steep slope with the river Simoa below, and is located below the old marine sea level. The landscape has been eroded by streams and rivers, and the terrain has ravines towards the river. There are no registered previous landslides in the area except some small local slides in the riverside further south.

Several ground investigations have been performed in the area. The most relevant investigations were performed in 2012 by Multiconsult and by the NPRA.

According to the soil investigations, the soil consists essentially of a top layer of dry crust clay, above silty, partly quick clay. Below the silty clay layer, the investigations indicate sand and moraine down to solid rock. Figure 33.2 shows the interpreted layering of soils in the slope and measured pore pressure, including the road and the river Simoa.

To determine the soil parameters comprehensive field and laboratory tests were performed. We consider samples from borehole 131 to be representative for probe 4. The samples indicated sensitive silty clay down to about 13 m depth. Samples from probe 37 showed quick clay from about 8,5 to 13,5 m depth.

The samples from borehole 130 and 131 indicate dry crust clay above clay down to about 6 m depth. Below 6 m the soil is classified as quick clay, silty quick clay and sandy, silty quick clay. The clay appears to contain more silt and sand with depth. The deepest sample in borehole 131 was taken from a depth of about 12 to 13 m below terrain level (Table 33.1).

Results from grain size distribution curves in borehole 130 and 131 showed that the sensitive materials from about 6 m depth is characterised as silty quick clay and sandy, silty quick clay. The content of sand and silt made it more difficult to identify quick clay from the soundings. The identification of sensitive clay in the upper part of the slope was based on interpretations from CPTUs. The pore pressure was considered to be hydrostatic in level with bottom of the slope, and below hydrostatic upwards the slope according to measured values in the piezometers.

Table 33.1 Typical measured values from boreholes 37, 130 and 131

Borehole	37	130/131
Sensitivity (St)	83–224 (very sensitive)	12–270 (medium to very sensitive)
Remoulded shear strength from cone test (cr)	0,1–0,3 kPa	0,2–1,6 kPa
Water content (w)	25–40%	25–40%
Liquid limit (wL)	21–30%	20–35%
Plasticity index (Ip)	4–8 (low plasticity)	5–13 (medium to low plasticity)

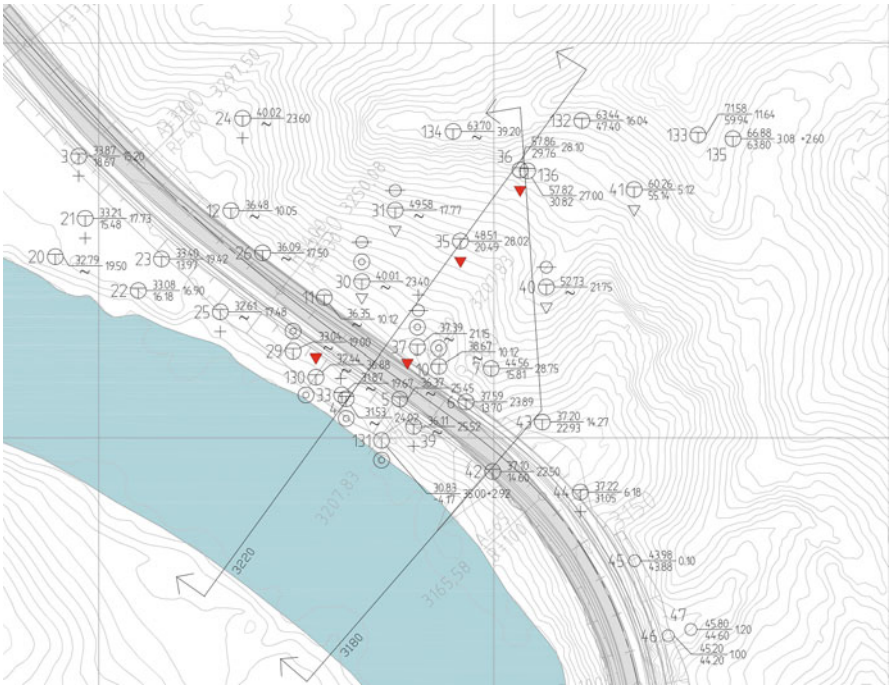

Fig. 33.1 Plan drawing showing boreholes and profiles

33.2.1 Design Parameters

Design parameters were based on field investigations and laboratory tests performed on 54 mm samples. Interpretation of CPTU's and laboratory data indicated quick clay and also a weak layer in the slope, coinciding with the critical shear surface. The red marked CPTUs in Fig. 33.1 showed signs of the possible weak layer. In Fig. 33.3, the presumed weaker layer is shown interpreted from CPTUs.

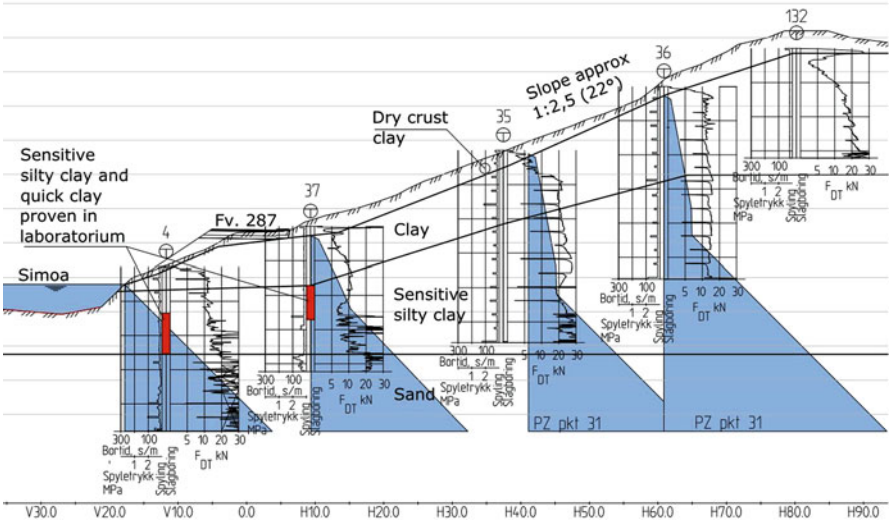

Fig. 33.2 Layering of soils and pore pressure in the critical profile of the slope

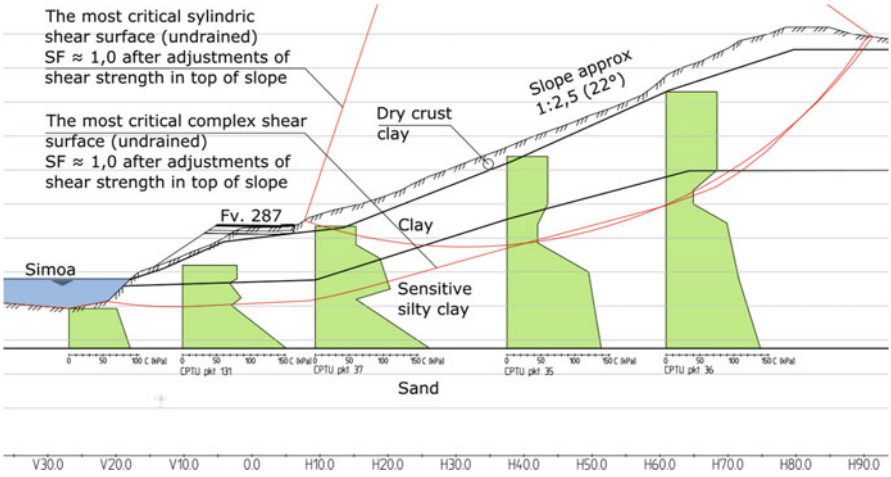

Fig. 33.3 Shows interpreted CPTUs and calculated critical shear surfaces in undrained situation

The possible weak zones interpreted from CPTUs seem to be near the presumed most critical shear surfaces in the slope in undrained situation. The complex shear surface is placed in the weak zone, and the factor of safety is calculated to be approximately the same as the most critical cylindrical shear surface.

Initial calculations performed with soil parameters directly interpreted from CPTUs and laboratory tests resulted in an unstable slope with safety factors less than 1.0. To level the safety factor up to 1.0, 3D effects were taken into account.

Table 33.2 Effective strength parameters and ADP ratio used in stability calculations

Soil	c (kPa)	Φ_k	Aa	Ad	Ap
Dry crust clay	0	30°	–	–	–
Quick clay, global stability (Ip≤15)	2,6	28°	0,85	0,63	0,35
Quick clay, local stability (Ip≤15)	3,2	33°	0,85	0,63	0,35
Clay (Ip>15)	3,2	33°	1,00	0,65	0,37

To avoid overestimation of the slope stability in the lower part of the slope, with typically short shear surfaces in the area by the road and the river, the strength of the soil was increased only for the upper part. It was found that to obtain a factor of safety of 1,0 for the slope in the initial situation, it was required to increase the soil properties in the upper slope by approximately 40%.

33.2.1.1 Effective Strength Parameters

To determine effective strength parameters active triaxial tests were performed. The results of triaxial tests showed relatively high effective friction angles for the quick clay, especially in the bottom of the slope, in the area by the road and the river. For calculations of the local stability in the lower parts of the slope, we therefor used effective friction angle as shown in Table 33.2 above.

33.2.1.2 Total Strength Parameters and ADP Ratio

Total strength parameters are shown in Table 33.2. In our calculations we used the ADP ratio according to publication, which describes an agreed recommendation for the use of anisotropy factor in design involving Norwegian clay. The active shear strength was also reduced for quick clay, to take into account that the correlations used in the CPTU interpretation are based on tests performed on block samples.

33.3 Design Rules

The following design rules were used in the project:

- NS-EN 1997-1:2004 + NA:2008, Eurocode 7, Geotechnical design
- NPRA Handbook V220, (Geoteknikk i vegbygging)
- NVE Guidelines 7 2014, (Sikkerhet mot kvikkleireskred)

Consequence class and reliability class in the project was set to class 3, which gives geotechnical category 3. The control class was set to extended control, and the NPRA completed this control.

In general the NPRA Handbook requires a factor of safety of 1,6 for stability calculations in sensitive clay, however since the project was considered to be an improvement of traffic safety, "tiltaksklasse" (construction classification) K1 according to NVE guidelines 7 was chosen. For K1-projects the road construction can be built if the global stability is not at any time reduced, and river erosion leading to reduced stability in the future is prevented. The safety requirements for this category are based on the prerequisite that the gained safety improvement for pedestrians and cyclists is higher than the risk of triggering a slide. For the local stability a low factor of safety was accepted by the client. This was treated by an application to deviate from the regulatory requirements.

33.4 Designed Solution

The new pedestrian road is located in a slope above the river Simoa. Filling for the new road will improve the stability above the road, but decrease the stability below the road. Lightweight materials were used in the filling to get sufficient safety for the lower part of the slope, a photo of the filling is shown in Fig. 33.4. The excavation for the lightweight filling was done in sections to reduce the destabilising effect on the upper part of the slope. It was considered that river erosion could possibly cause destabilisation in the long term situation. To prevent this, erosion protection was designed and built as shown in Fig. 33.5. The filling along the river gave an

Fig. 33.4 Filling with lightweight material (Photo: T. Flobak, Rambøll)

Fig. 33.5 Building of erosion protection (Photo: T. Flobak, Rambøll)

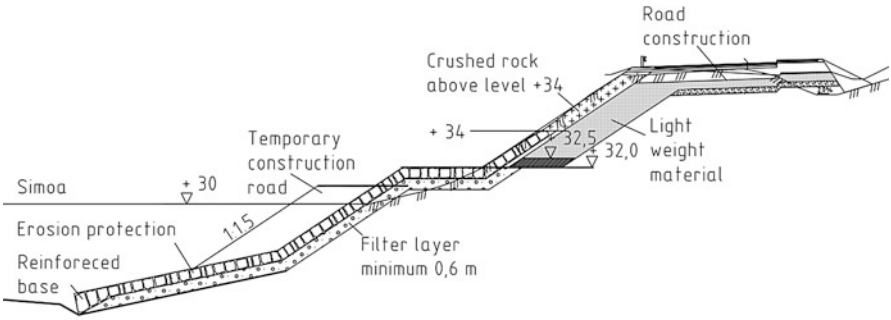

Fig. 33.6 A typical section showing the erosion protection and the lightweight fill

improvement of the stability for the lower part of the slope and a slight improvement of the overall stability. The extent of the filling was restricted due to requirements given by The Norwegian Water and Resources and Energy Directorate (NVE) regarding minimum flow area in the river. The filling was also used as temporary construction road for the further excavation works for the pedestrian road with applied traffic loads.

A section of the designed solution for erosion protection is shown in Fig. 33.6.

Stability calculations were performed for all construction phases and for both the lower part of the slope, the upper part of the slope and also for the overall slope. The first phase was today's situation and consideration of 3D–effects. The second phase

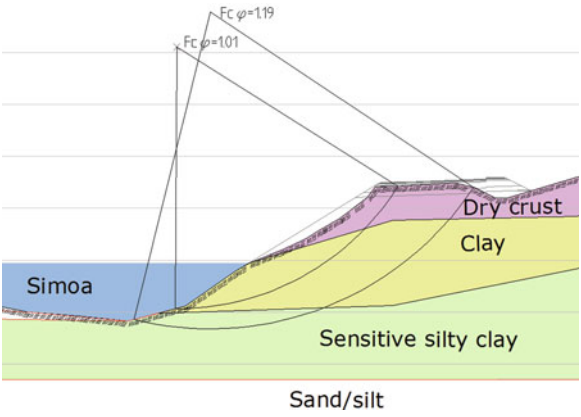

Fig. 33.7 Effective stress analysis for section 3180

Table 33.3 Effective stress analysis for section 3180

Phase	Factor of safety
Initial situation	1,01
Erotion protection	1,17
Excavation for filling	1,23
Completed road	1,21
Initial situation with traffic load	1,01
Completed road with traffic load	1,19

was a filling along the river to prevent erosion. The third phase was the sectionwise excavation of the road. Finally the stability of the complete road construction was checked. Since traffic load on the road would be stabilising for the upper part of the slope a separate calculation was done to check the lower part of the road.

Stability calculations were performed for two profiles, Profile 3180 and Profile 3220 shown in Fig. 33.1. Both profiles were located in the area where the ground investigations showed softer materials. Profile 3180 was drawn with a kink due to geometry and ground conditions. Drained analysis for the lower part of the slope indicated that the factor of stability was 1,0–1,2. The most critical shear surfaces from the calculations in Profile 3180 is shown in Fig. 33.7 and results from the calculations are summarized in Table 33.3.

33.5 Monitoring and Inspection

As part of the design, a control plan of critical points was developed. The plan gave instructions on how the project was to be followed up by a geotechnical engineer and what measurements had to be done. The plan also gave instruction to the contractor about daily routines and things to be aware of. The control plan was discussed with the contractor before the construction works started.

The following monitoring was performed before and during the construction period.

1. Three pore pressure gauges were installed in two boreholes to monitor the variation in pore pressure.
2. Two inclinometer channels were installed to register movements in the ground. The two channels had sensors both over and under the critical surface.
3. Three vibration gauges were installed to register vibrations due to rock blasting south of the area with quick clay.

Measurements of the pore pressure, the vibrations and the ground movement were automatically logged to websites. Rambøll performed daily checks of these measurements during the critical parts of the project. The measurements did not show significant deviation from predicted values, and the construction works were never stopped due to measured values. The river was scanned after about half the filling was established (Fig. 33.8a).

In the final stretch of filling the steepness of the river bank prevented the establishment of the filling from the riverside. Rambøll recommended that the filling works be done from a raft, or alternatively that a construction road be created down the slope with a safe platform for the excavator on bedrock (blasting necessary). The contractor suggested a third alternative; to fill from a crane standing on top of the slope (on bedrock). The contractor's alternative was chosen and the fill material was lifted in a container and tipped into the river from the water surface. A new scanning of the river bed was performed after the filling was done, to check the soil volumes and the slope of the embankment (Fig. 33.8b).

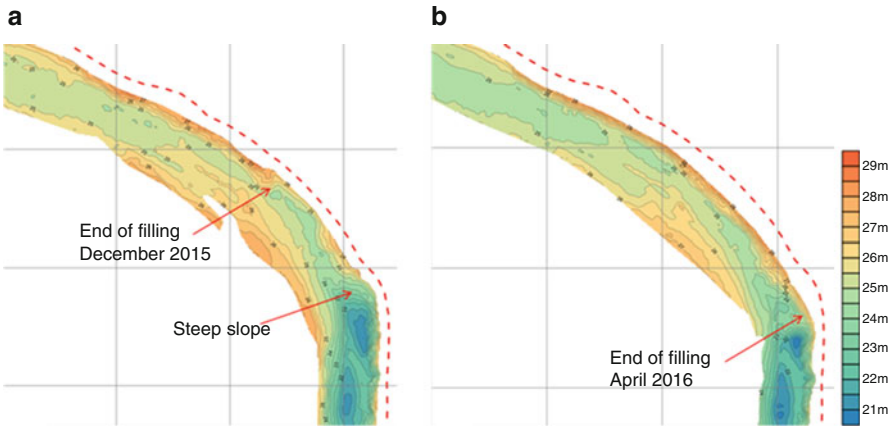

Fig. 33.8 Scanning of the river bank (**a**) after about half the erosion protection was built (**b**) after completed erosion protection

33.6 Experiences and Recommendations

- The accuracy of the monitoring needs to be taken into account. The two inclinometer channels varied +/−1 cm. The pore pressure showed natural variation within 5 kPa in periods without ongoing construction works.
- The location of the vibration gauges should be determined by the geotechnical engineer. The critical shear surfaces must be taken into account.
- It is especially important that the design of road constructions in quick clay includes setting up a plan for the control and monitoring during the construction phase.
- A geotechnical engineer should follow up the project according to the control plan. Good communication between the control engineer and the contractor is important to keep good progress.
- Competence requirements should be set when contracting entrepreneurs for work in quick clay areas. This is especially important for work involving drilling of piles and blasting. It is important that the contractor understands the importance of how the work affects the ground and that they have a system for quality assurance. It's recommended that requirements are set both for machine operators and project managers.

33.7 Conclusion

The project had a low factor of safety and was conducted successfully due to a detailed design, monitoring and close supervision by geotechnical engineer.

Acknowledgements We thank the Norwegian Public Roads Administration for good cooperation throughout the whole project and Frode Oset and Ariane Locat for reviewing the paper.

References

Multiconsult (2012) Geoteknisk utredning av kvikkleiresone 848 Haugfoss, Modum kommune, Report 813424/1-2

NPRA: Norwegian Public Roads Administration (2012) Fv287 Strandgata-Kjøreplass bru. Datarapport, Report 2010152432-8

NPRA: Norwegian Public Roads Administration (n.d.-b) Handbook V220

NS-EN 1997-1:2004+NA:2008, Eurocode 7, Geotechnical design

NVE: Norwegian Water Resources and Energy Directorate (2014) Guidelines 7

Chapter 34
Case Study: Characterization of a Thick Sensitive Clay Deposit in the St. Lawrence River Valley, Slope Stability Analysis and Preliminary Assessment of Permanent Deformations

M. Limoges, M. Demers Bonin, N. Pépin, and M. Lemieux

Abstract This case study presents the results of geotechnical investigations and desktop studies carried out on a site characterized by the presence of a 55 m thick sensitive Champlain sea clay deposit, in the Province of Quebec (Canada). The main objective was to determine an iron ore stockpile configuration that meets the design factor of safety (FoS). The site is located in the St. Lawrence River lowlands. It is adjacent to the river and extends 200 m south of the shore line. For decades, the site has been subjected to temporary loadings which induced vertical settlement and small lateral deformations towards the River. This paper presents the inferred site stratigraphy, including geotechnical properties of the units encountered, presents the results of a 1D wave propagation analysis, stability analyses and preliminary deformation assessment with regard to site conditions. Field works performed involved seismic piezocone penetration tests (SCPTu) with the recording of pore water pressure, and geotechnical boreholes.

34.1 Introduction and Background

The site is located in Sorel-Tracy, on the South shore of the St. Lawrence River in the Province of Quebec, Canada (Fig. 34.1). The site lies near the confluence of the St. Lawrence and Richelieu Rivers, within the St. Lawrence lowlands. It covers an area of 41.5 hectares, which contains several sectors. The sector studied in more detail covers an area of 3.3 hectares.

Since the mid-1950s, the site has been used for stockpiling heavy materials such as iron ore and smelting wastes, namely slag. For decades, the site was subjected to temporary loadings close to the river bank, where the surcharge induced vertical

M. Limoges (✉) • M. Demers Bonin • N. Pépin • M. Lemieux
Golder Associés Ltée, Montréal, QC, Canada
e-mail: marielle_limoges@golder.com; michael_demersbonin@golder.com; nicolas_pepin@golder.com; michel_lemieux@golder.com

V. Thakur et al. (eds.), *Landslides in Sensitive Clays*, Advances in Natural and Technological Hazards Research 46, DOI 10.1007/978-3-319-56487-6_34

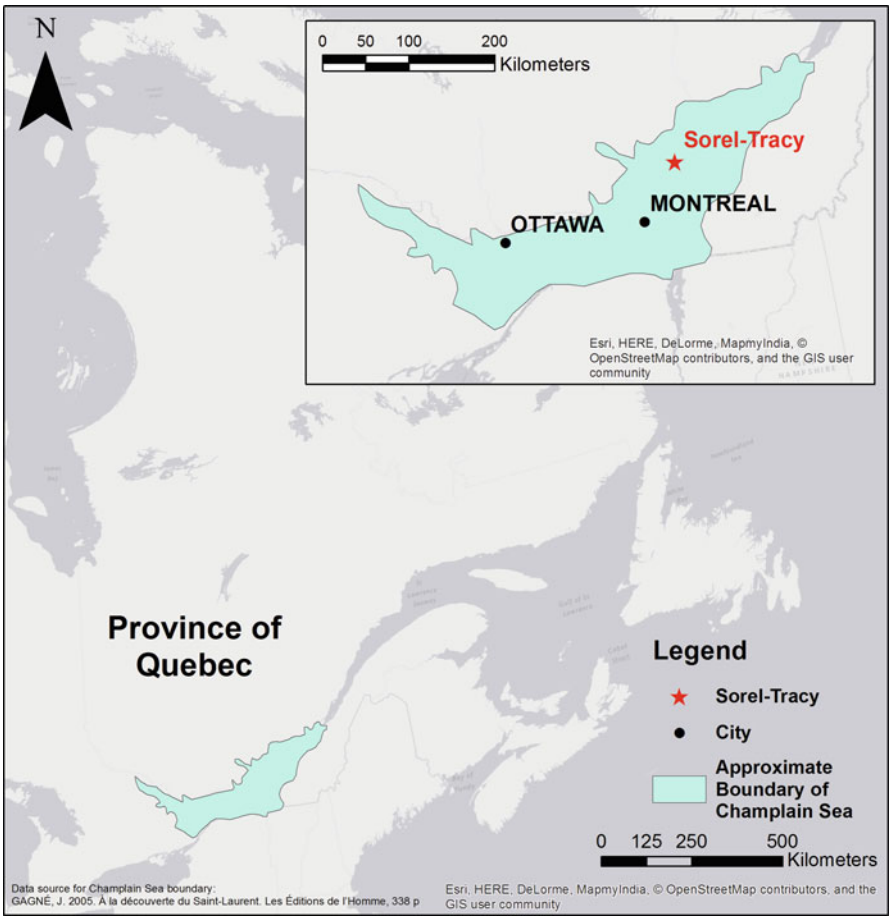

Fig. 34.1 Site location and approximate boundary of Champlain Sea adapted from Gagné (2005)

settlement and small lateral deformations towards the River. The main stockpile had surcharges varying from 0.3 to 1.72 Mt over the years.

The Eastern Canada clayey soils originate from proglacial and postglacial activities and sedimentation that occurred in water bodies formed by the retreat of the Wisconsin ice sheet that took place between 18,000 and 6000 BP (Quigley 1980). The site is located in the footprint of the former Champlain Sea (Fig. 34.1) that existed between 12,500 and 8500 BP (Leroueil et al. 1983). The stratigraphy at the site includes a thick and deep homogenous massive clay deposit which is characteristic of the distal regions of the ancient sea. As reported by Leroueil et al. (1983), the material located in proximity of the Laurentian Plateau shows a clay fraction (<2 μm) varying between 20% and 60% whereas the material within the center of the basin shows a clay fraction (<2 μm) varying between 60% and 85%. At the site, the grain size distributions performed on samples collected in the deep

clay (below elevation −27.5 m a.s.l.) show a clay fraction comprised between 56% and 82%. The Champlain sea clay is known for its high sensitivity.

Geotechnical investigations performed at the site since the mid-twentieth century allowed gathering in situ data and laboratory test results, including the installation of two inclinometers to monitor displacements induced by the main ore stockpile. A geotechnical study was performed in 2014–2015 with the following main objectives: *(i)* get more information about the soils stratigraphy; *(ii)* carry out a site-specific seismic wave propagation analysis; *(iii)* evaluate the static slope stability in order to determine the geometry of an iron ore stockpile that meets a FoS of 1.5; and (iv) assess preliminary soils displacements under seismic conditions based on the seismic wave propagation. Slope stability analyses were also carried out under pseudostatic loading conditions and the results meet the design factors of safety for certain return periods, although the FoS is below that for other return periods. The results from those analyses are not presented in this paper but they warranted the preliminary deformation analyses presented herein. This case study focuses on previous and recent results obtained in the area of the main ore stockpile.

34.2 Geotechnical Investigation

The 2014 geotechnical investigation involved seven piezocone penetration tests (CPTu) carried out with a 25 ton truck. The CPTu's were advanced at a steady rate of 20 mm/s. Three readings were collected during the soundings including *(i)* the cone tip resistance, q_c; *(ii)* the sleeve friction, f_s; and *(iii)* the penetration pore pressure behind the tip, u_2. The cone used had a tip correction factor a_{net} of 0.80 and equal end area friction sleeves. It is noted that all CPTu soundings, except for one (SCPT-15-02), were located in areas where no significant surcharge existed. The piezocone soundings were pushed down to refusal at depths ranging between 82.00 and 86.95 m.

Fifteen dissipation tests were realized in different geotechnical units. Shear wave velocity (V_s) measurements at 1 m intervals were performed in three soundings. The shear waves were generated using an impact hammer that horizontally stroke a beam held on the surface by a normal load.

A borehole was also advanced 49.6 m deep. Some samples were collected from the borehole using a 76 mm-ID thin wall sampler. Grain size distribution curves, Atterberg limits and lab vane shear tests were carried out on the samples retrieved.

A summary of the results of these in situ tests is presented in the next section.

34.3 Subsurface Conditions

Figure 34.2 presents the soil classification index (Ic) (Been and Jefferies 1992, 2006), the cone tip resistance (q_c), the sleeve friction (f_s) and the penetration pore water pressure (u_2) for CPT-15-01 and SCPT-15-02 from the recent geotechnical

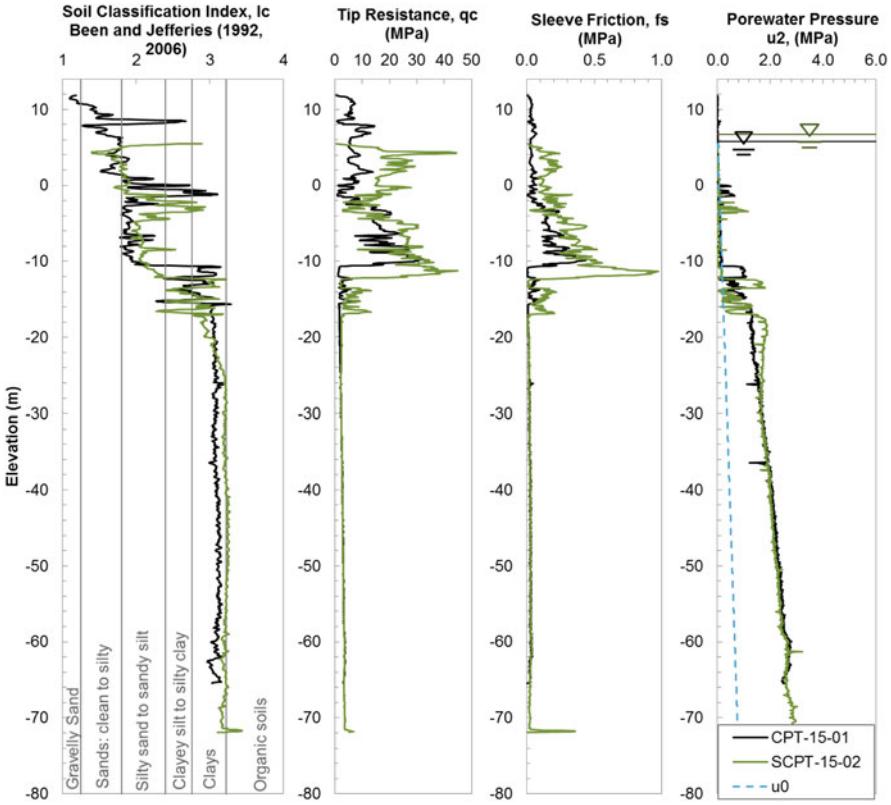

Fig. 34.2 Basic CPTu results from CPT-15-01 and SCPT-15-02

investigation. The soil classification proposed by Been and Jefferies (1992, 2006) had a better correlation with the lab results than the one proposed by Robertson and Wride (1998), which might be due to the integration of the measured pore water pressure readings within the classification.

Despite that several results may be interpreted from various empirical relationships and CPTu data, this paper focuses on the most relevant CPTu parameters with regards to the thick clay deposit. The two CPTu presented herein were very representative of all the tests performed at the site. However, SCPT-15-02 is particularly interesting since it was performed in the footprint of a cyclic stockpiling area. The impact of the stockpile can be observed in Fig. 34.2 between approximate elevations −14 m a.s.l. and −26 m a.s.l. Tip resistance and sleeve friction from SCPT-15-02 show a slight soil improvement which is believed to be resulting from densification of granular units and consolidation of cohesive units.

The inferred stratigraphy at CPT-15-01 and SCPT-15-02 is shown by the *Ic* in Fig. 34.2. Based on the soil classification chart of Been and Jefferies (1992, 2006), the inferred stratigraphy consists, from top to bottom, of *(i)* a granular layer of

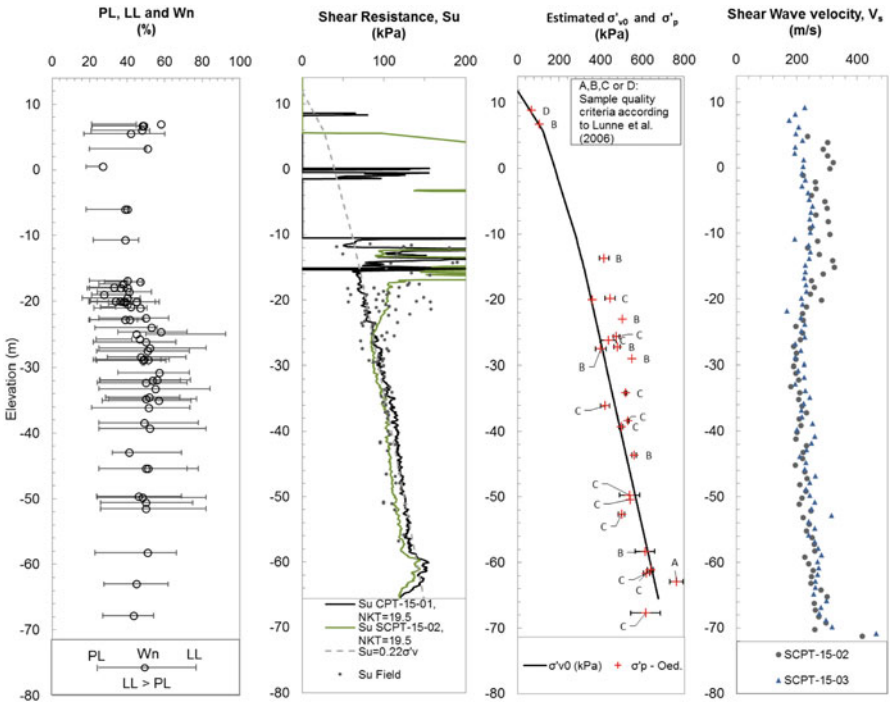

Fig. 34.3 w_n, *LL*, plastic limit (PL), *Su*, estimated σ'_{v0}, σ'_p and V_s

gravelly sand to silty sand; *(ii)* a first cohesive layer of silty clay to clay; *(iii)* a layer of sand to silty sand; *(iv)* a layer of clayey silt to silty clay; and *(v)* a thick marine clay deposit. The most variable units, in term of thickness, are the two granular layers and the first cohesive unit. Some geotechnical boreholes located west of CPT-15-01 and SCPT-15-02 showed thinner granular units interbedded with a cohesive soil, however the thick marine clay deposit was inferred approximately at the same elevation throughout this site (i.e. elev. of −16 m a.s.l.). The water table was estimated to be at elevation 5.79 m a.s.l. at the location of CPT-15-01 and 6.79 m a.s.l. at the location of SCPT-15-02, which is representative of a drawdown towards the St. Lawrence River. Based on the results of the dissipation tests performed in the sand and in the upper clayey layers, the pore water pressure was assumed hydrostatic. However, dissipation tests carried out in the thick clay deposit were halted before they have reached a full dissipation condition.

The hydraulic conductivity estimated from the dissipation tests performed in the thick clay deposit varies between 1.7E-9 and 4.5E-10 m/s. The V_s measurements performed in this material varied between 167 and 315 m/s but were generally comprised of between 200 and 300 m/s (see Fig. 34.3).

The geotechnical subsurface conditions were inferred based on the most recent CPTu soundings as well as on the dataset from previous boreholes that were

advanced in the deep clay deposit. Geotechnical data from samples retrieved include grain size distribution curves, Atterberg limits, undrained shear strength (*Su*) and inferred results from incremental loading consolidation tests (preconsolidation pressure, $\sigma'p$ and overconsolidation ratio, *OCR*). Incremental loading consolidation tests involve sample quality ranging between 0.04 and 0.13 (excellent "A" to poor quality "D" criteria) according to Lunne et al. (2006). It should be noted that the sample depths range between 36 and 80 m, which is significantly deeper than the depth range suggested by Lunne et al. (2006). The initial void ratio values measured from the consolidation tests performed in the thick clay deposit vary between 1.18 and 1.67.

Figure 34.3 shows water contents (w_n) with Atterberg Limits, *Su*, estimated *in situ* vertical effective stress profile (σ'_{vo}) and σ'_p inferred from incremental loading consolidation tests. Tavenas et al. (1978) presented very similar results to the following for some sites located nearby.

Plastic limit varies from 16% to 50%, liquid limit (*LL*) from 34% to 92% and w_n from 28% to 58% in the thick clay deposit. The plasticity index (*PI*) ranges from 8% to 59% and can be sub-divided in three zones: *(i)* increasing *PI* between 10% and 50% from El. −16 m a.s.l. to −30 m a.s.l.; *(ii)* a fairly constant *PI* of 50% to 60% from El. −30 m a.s.l. to −50 m a.s.l.; *(iii)* decreasing *PI* to 25% from El. −50 m a.s.l. to bedrock. The liquidity index (I_L) is generally below 1.0 (52/62 values) with a maximum value of 2.0.

The in situ *Su* measured using a field vane shear test and corrected for plasticity using the Bjerrum method (Bjerrum 1972) is shown in Fig. 34.3. The profiles obtained from the interpretation of data collected at CPT-15-01 and SCPT-15-02 are also presented. The CPTu *Su* profiles were plotted using a tip cone factor (N_{kt}) of 19.5. The grey dashed line is the *Su* calculated from Mesri (1975) where $S_u = 0.22\ \sigma'_p$ assuming an *OCR* of 1 ($\sigma'_p = \sigma'_{v0}$). SCPT-15-02 was performed under the stockpile footprint and shows an improvement of the S_u between elevation −14 m. a.s.l and −26 m. a.s.l. A graph of σ'_{v0} p'_{v0} and the σ'_p is presented in Fig. 34.3. The *OCR* is close to 1.4 at the surface of the thick marine clay deposit and tends to be around 1.0 at greater depth. Values of σ'_p lower than σ'_{v0} are assumed to be underestimated due to sample disturbance (poor sample quality) or due to the estimated σ'_{v0}.

The sensitivity of the clay deposit varies between 3 and 10 (a clay is considered sensitive for a value higher than 4 as per the *Canadian Manual of Foundation Engineering* Canadian Geotechnical Society (2013)). The sensitivity was obtained using the field vane tests, the laboratory Swedish Cone tests and estimated from empirical relationship derived from CPTu results (Robertson and Cabal 2012). Tavenas et al. (1978) reported sensitivity between 10 and 15 as measured by field vane on the Champlain sea clay at some sites located nearby Sorel-Tracy.

Despite the fact that the clay is sensitive, the effect of progressive failure was not addressed in this study because: *(i)* the topography is generally flat with no ravine or abruptly sloping terrain; *(ii)* the river banks slopes gently with a maximum difference in elevation of 10 m and a wharf exists along a part of the shoreline *(iii)*

except under the river, the sensitive marine deposit is overlaid by layers of gravelly sand to silty sand*; (iv)* the destructuration index (I_D) (Locat et al. 2008) shows values below unity in the marine clay deposit; *(v)* I_L is generally below 1.0.

34.4 Analyses

Seismic wave propagation: A 1D ground response analysis was carried out using SHAKE2000 (Ordonez 2012) to evaluate the potential effects of earthquakes. Each soil unit was characterized by the following parameters: unit weight (γ), shear modulus (G) and damping ratio (β). These were varied as a function of shear strain and static properties (PI and effective confining pressure, σ'_m according to Darendeli (2001). The small-strain shear modulus (G_{max}) was calculated based on measured shear wave velocities and the relationship $G_{max} = \rho v_s^2$, where ρ and v_s are respectively the bulk density and the shear wave velocity of each horizontal sub-unit defined in the model's column.

Results are related to the 1988 Chicoutimi-Nord, Saguenay (Quebec) seismic event for return periods of 2475 years, 1000 years and 475 years. Based on the 2010 National Building Code Seismic Hazard calculation (Canadian commission on Building and Fire Codes 2010), Peak Ground Accelerations (PGA's) at the site are 0.316 g, 0.188 g and 0.116 g, respectively, for a class C soil for these three return periods. The Saguenay earthquake time history was thus scaled down to maximum peak rock accelerations of 0.234 g, 0.312 g and 0.081 g for a class A material located at the base of the SHAKE column. The stratigraphy was inferred from CPT-15-01 whereas shear wave velocities were taken from another test (SCPT-15-03) located near CPT-15-01. The shear wave velocity profile used is presented on Fig. 34.3. The SCPT-15-02 shear wave velocities profile was also considered but the related results are not presented in this paper.

Profiles of maximum acceleration (AM) and maximum shear strain (τ_{max}) with elevation are presented in Fig. 34.4 for the three return periods selected. For instance, a surficial peak ground acceleration of 0.2 g and a maximum shear strain of 0.04% were calculated by SHAKE2000 for a 2475 year return period. The shear strain value confirmed that the use of an equivalent-linear approach was a fair assumption as it is generally admitted that such type of analysis is adequate as long as this parameter does not exceed 2%. Figure 34.4 also shows that there is no amplification of the acceleration until it reaches the upper portion of the granular unit, which might be due to surface effects.

Slope stability: Stability analyses in 2D were carried out under a static loading condition with Slope/W (version 2007 by GeoStudio). *Su* parameters were used for the low permeability units. The *Su* profile was defined from the values shown in Fig. 34.3 with improved shear strength parameters applied to cohesive layers underneath the stockpile as suggested by SCPT-15-02. The *Su* profile was assumed to be isotropic with no variation along the slip surface angle. For the granular units,

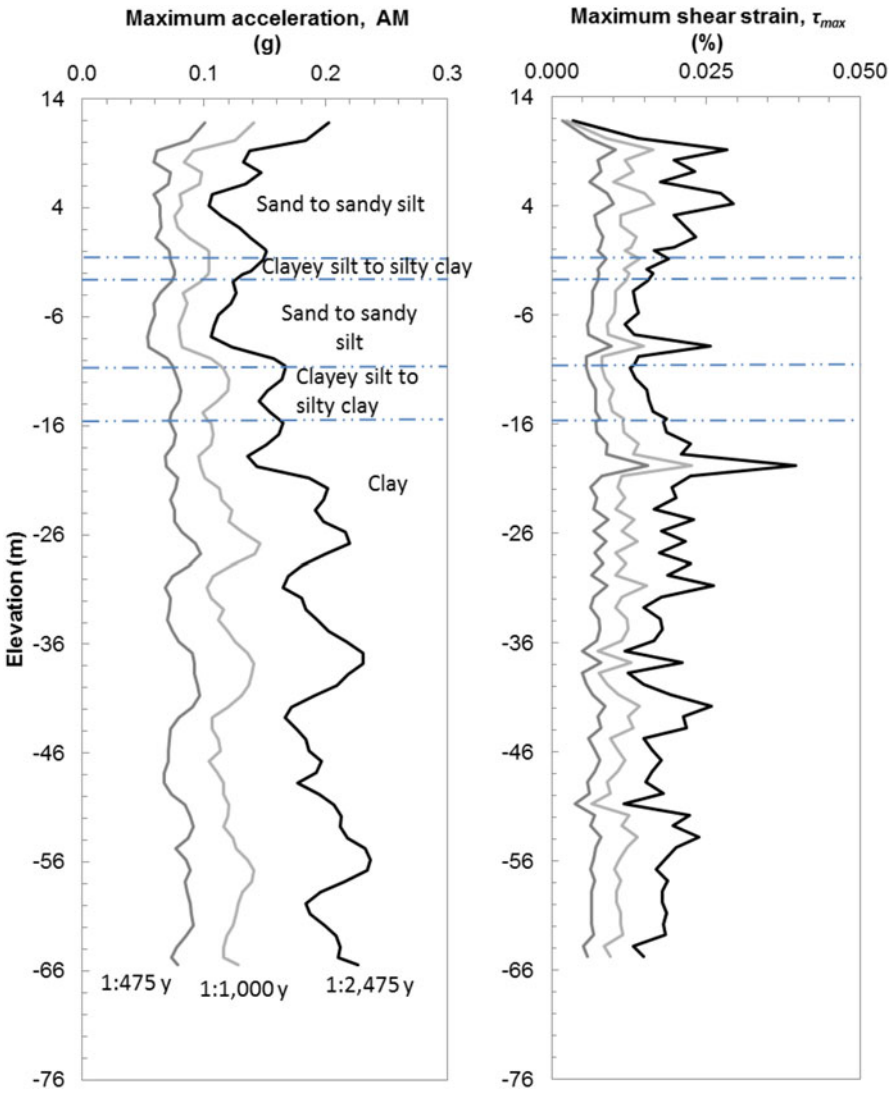

Fig. 34.4 Maximum soil acceleration and maximum shear strain vs elevation

typical values of effective friction angle (ϕ') were used. A summary of the properties used in the model is presented in Fig. 34.5.

The cross-section subsurface stratigraphy was established based on the available geotechnical data. The depth of the water table was estimated from the CPTu's dissipation tests. Hydrostatic pore water pressures were assumed throughout the model. Slip surfaces were analyzed for circular and non circular failure modes.

Unit #	Unit ID	Unit weight (kN/m³)	Su (kPa)	φ' (°)	Unit #	Unit ID	Unit weight (kN/m³)	Su (kPa)	φ' (°)
1	Sand to sandy silt	20.0	--	30	6	Clay	16.9	70 to 150, (1.42 kPa/m)	--
2	Clayey Silt to silty clay (1)	19.4	42	--	7	Clay (improved)	16.9	85	--
3	Clayey Silt to silty clay (1-improved)	19.4	130	--	8	Bedrock		Impenetrable	
4	Clayey Silt to silty clay (2)	19.4	70	--	9	Ore	31.4	--	37
5	Clayey Silt to silty clay (2-improved)	19.4	85	--	10	Wharf	18.1	--	30

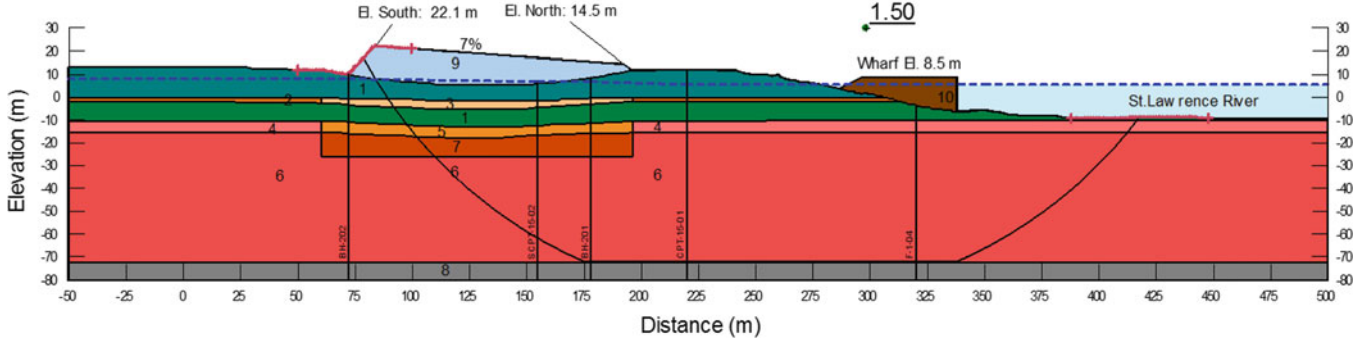

Fig. 34.5 Critical failure surface for static stability analysis

Table 34.1 Input parameters used in the preliminary displacement evaluation

Return Period	k_y (g)	H (m)	T_s (s)	Sa ($1.5T_s$) (g)	Magnitude, M_w
2475 years	0.054	65	1.15	0.049	6.94
1000 years	0.068	60	1.08	0.040	7.38
475 years	0.052	60	1.08	0.029	7.34

Figure 34.5 presents the critical slip surface and the optimized ore stockpile configuration for a static FoS of 1.5. The slip surface is deep-seated (approximately 80 m deep) and passes through the normally consolidated marine clay deposit. It was also noted that the improved cohesive layers under the main ore stockpile do not significantly increase the FoS. Stability analyses were also carried out under pseudostatic loading conditions and some of the FoS obtained were below the design criteria for some return periods. The results are not discussed herein but the slip surfaces obtained were also deep-seated.

Permanent deformations evaluation: Preliminary seismic slope displacements were evaluated using the method proposed by Bray and Travasarou (2007) for three return periods. Table 34.1 presents the input parameters used in the probabilistic model where *ky* is the yield coefficient of the sliding mass (i.e., the seismic horizontal coefficient which results in a factor of safety of unity), *H* is average depth of the sliding mass, *Ts* is the initial fundamental period of the sliding mass, *Sa* is the spectral acceleration of the site's design ground motion at a period of 1.5 *Ts*. and *Mw* is the magnitude.

The estimated displacements are 0.71 cm, 0.30 cm and 0.11 cm, respectively for return periods of 2475 years, 1000 years and 475 years. The probabilities for a negligible displacement are 90.6, 99.3 and 100%, respectively for the same return periods. The calculated displacements values are low and the probability for a negligible displacement are high for all return periods which may be due to the frequency content that does not generate amplification of the seismic acceleration.

34.5 Conclusion

The compilation of the datasets made possible the definition of sub-surface conditions which appeared homogeneous throughout the site with some unique conditions under the cyclic loading area. Standard geotechnical sounding methods were used to collect data and conventional laboratory tests were performed. Despite the great depths of the Champlain sea clay deposit intercepted at the site and despite all the difficulties associated with deep in situ testing and sampling, the results of the in situ and laboratory tests are of fairly good quality and correlate quite well.

The 1D wave propagation analysis results show that there is no amplification of the acceleration in the thick clay deposit. Preliminary seismic slope displacements were evaluated using the method proposed by Bray and Travasarou (2007) and

the results of the seismic wave propagation analysis. Despite some FoS are below the design criteria in pseudostatic conditions, low displacement values and high probabilities of negligible displacements were obtained from this preliminary assessment.

The effective stress profile was estimated based on hydrostatic pore water pressure profile. The installation of vibrating wire piezometers underneath the stockpile would help determining the pore water pressure profile and could have an impact on the effective stress profile.

The stability analyses were performed in 2-D which is somewhat simplistic and the authors recognize that a 3-D analysis would be beneficial to assess the stability of the stockpile at this site. Indeed, the finite geometry of the iron ore stockpile and the site topography would likely improve the factors of safety. A characterization of the strain-softening behavior of clay should also be performed at the site and the results should be implemented in stability analyses. Finally, a 2-D dynamic analysis would also be beneficial to increase the level of precision on the FoS and displacements anticipated in case of an earthquake.

Acknowledgments The authors would like to thank the site owner and their contribution and for accepting the publication of this case study and Prof. Vikas Thakur for his kind review of the paper.

References

Been K, Jefferies MG (1992) Towards systematic CPT interpretation. In: Proceeding of wroth memorial symposium, Thomas Telford Limited, London

Been K, Jefferies MG (2006) Soil liquefaction-a critical state approach. Taylor and Francis, New York

Bjerrum L (1972) Embankments on soft ground. In: Proceedings of the earth and earth-supported structures, Lafayette, June 11–14 1972

Bray JD, Travasarou T (2007) Simplified procedure for estimating earthquake-induced deviatoric slope displacements. J Geotech Geoenviron Eng 133(4):381–392

Canadian commission on Building and Fire Codes (2010) National building code of Canada 2010, National research council

Canadian Geotechnical Society (2013) Canadian foundation engineering manual, 4th edn. Canadian Geotechnical Society c/o BiTech Publisher Ltd, Richmond

Darendeli MB (2001) Development of a new family of normalized modulus reduction and material damping curves. Dissertation, The University of Texas at Austin

Gagné J (2005) À la découverte du Saint-Laurent. Les Éditions de l'Homme, Montréal

Leroueil S, Tavenas F, Le Bihan J-P (1983) Propriétés caractéristiques des argiles de l'est du Canada. Can Geotech J 20:681–705

Locat P, Leroueil S, Locat J (2008) Remaniement et mobilité des débris de glissements de terrains dans les argiles sensibles de l'Est du Canada. In: Proceedings of the 4th Canadian conference on Geohazards: from causes to management, Presse de l'Université Laval, Québec

Lunne T et al (2006) Effects of sample disturbance and consolidation procedures on measured shear strength of soft marine Norwegian clays. Can Geotech J 43:726–750

Mesri G (1975) Discussion on "New design procedure for stability of soft clay". J GED 101: 409–412

Ordonez GA (2012) SHAKE2000 A computer program for the 1-D analysis of geotechnical earthquake engineering problems. GeoMotions, LLC, Lacey

Quigley RM (1980) Geology, mineralogy, and geochemistry of Canadian soft soils: a geotechnical perspective. Can Geotech J 17:261–285

Robertson PK, Cabal KL (2012) Guide to cone penetration testing for geotechnical engineering. Gregg Drilling & Testing Inc., 5th edn., November 2012, 131p

Robertson PK, Wride CE (1998) Evaluating cyclic liquefaction potential using the cone penetration test. Can Geotech J 35:442–459

Tavenas F, Blanchet R, Garneau R, Leroueil S (1978) The stability of stage-constructed embankments on soft clays. Can Geotech J 15:283–305

Chapter 35
Revisiting the 1959 Quick Clay Landslide at Sokkelvik, Norway

Jean-Sébastien L'Heureux, Steinar Nordal, and Synnøve W. Austefjord

Abstract The Sokkelvik landslide and associated tsunami led to nine casualties and is considered one of the most devastating Norwegian quick clay landslide of the past century. In this paper we review the potential causes for this landslide based on an integrated study of eye witness testimony, swath bathymetry data and stability analyses. Results show that the Sokkelvik landslide was most likely triggered by intense rainfall and snowmelt, but that the main cause is associated to the load of an up to 7.5 m high embankment fill. This fill was placed at the shoreline for road construction 6 months before the landslide. Results presented herein show the importance of accounting for extreme rainfall events and groundwater flow when planning construction activity in sensitive near shore areas.

35.1 Introduction

Landslides along Norwegian fjords occur periodically and are a threat to coastal communities. Analysis of past landslide events give important information on factors contributing to failure, the mechanisms of sliding, and the links between mass-wasting processes and their tsunamigenic potential. The increasing need for urbanization in such areas calls for a better understanding of these types of processes.

This 1959 Sokkelvik landslide is the most devastating quick clay landslide of the last century in Norway. It resulted in nine casualties, in the destruction of many farms and offshore structures, and in the initiation of a tsunami wave. However, the causes for this landslide have until today been poorly documented. In this paper, the 1959 Sokkelvik landslide is revisited using an integrated data set of swath bathymetry data, borehole data, stability analyses and eyewitness testimony. The

J.-S. L'Heureux (✉)
Trondheim Division, Norwegian Geotechnical Institute (NGI), Trondheim, Norway
e-mail: jsl@ngi.no

S. Nordal • S.W. Austefjord
Norwegian University of Science and Technology (NTNU), Trondheim, Norway
e-mail: steinar.nordal@ntnu.no; synnove.austefjord@ramboll.no

V. Thakur et al. (eds.), *Landslides in Sensitive Clays*, Advances in Natural and Technological Hazards Research 46, DOI 10.1007/978-3-319-56487-6_35

submarine/subaerial landslide mechanism is reconstructed and factors that might have undermined slope stability over time in the bay of Sokkelvik are discussed.

The motivation for revisiting the 1959 Sokkelvik landslide came after a new landslide in May 2015 in Sørkjosen 3 km south of Sokkelvik (Nordal et al. 2016). The 2015 landslide involved more than 1 mill m^3 of soils under water, closed the main road, E6, and destroyed a breakwater. During the 2015 investigations similarities between the two landslides were identified. Further studies later confirmed similarities in soil conditions, destabilizing factors and potential causes of the two slides.

35.2 Review of the 1959 Landslide at Sokkelvik

The bay of Sokkelvik is located in the county of Troms in Northern Norway. The bay faces east onto Reisafjord. Before 1959 Sokkelvik consisted of a hamlet with 5 farms and c. 70 acres of farmlands (Fig. 35.1). From the high-water mark at the shoreline the terrain rose by 4–5° in the first 50 m, then at 15° up to the forest edge about 25 m above the shoreline. Further backwards there was a steep forest hill up to

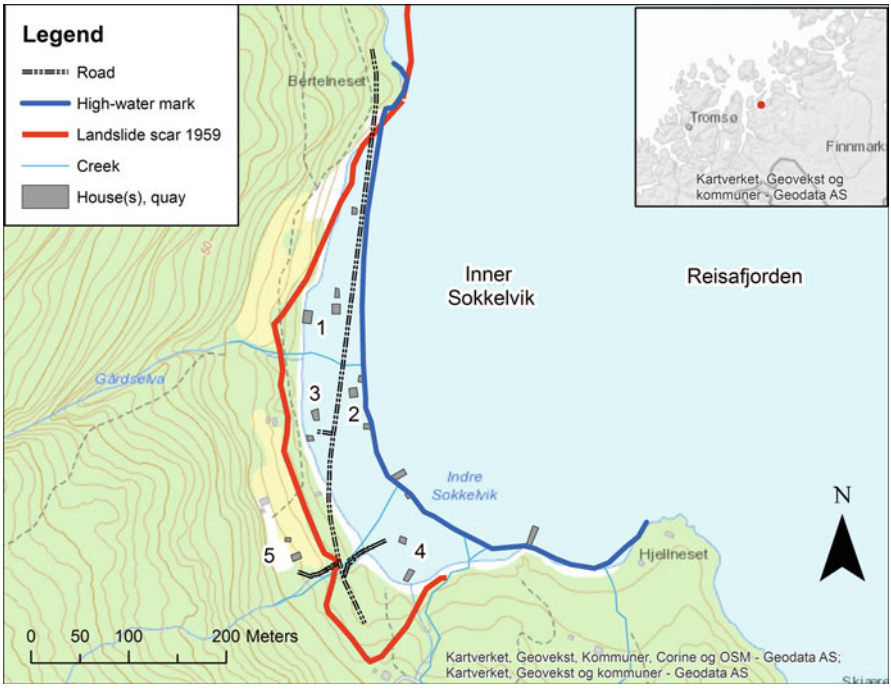

Fig. 35.1 Overview of the bay of Sokkelvik showing the location of the shoreline before 1959 and the resulting landslide scar. See text for details

200 m above sea-level. Figure 35.1 shows the approximate location of the shoreline until 1959 based on aerial photographs and earlier maps of the area.

The slope of the fjord bottom outside the shoreline was very gentle (c. 4–5°) prior to the event in 1959. At low tide the beach felt dry for over 50 m from the high-water mark.

The landslide at Sokkelvik occurred at around 20 o'clock on May 7th 1959. Spring low tide was registered 30 min before and there was intense rainfall at the time of the event. According to several eyewitnesses the landslide started in the northern part of the bay at Sokkelvik (Jørstad 1959). The two northernmost houses (see no. 1 and 2 on Fig. 35.1) were first observed moving into the fjord. Another house (no. 3) came sailing on top of the soil masses and soon after the southernmost house was also moving towards the fjord (house no. 4). Cracks were observed forming in the soil masses before slumping into the water. A large wave was also observed in the bay in the early stage of the landslide. Of the 29 persons living along the bay of Sokkelvik, 17 were taken by the landslide; 8 survived and 9 perished (Brænd 1961).

Onshore, the landslide scar was up to 12 m high and 600 m long (Figs. 35.1 and 35.2). Depth soundings in the fjord showed water depths of 15–20 m at the location where the shoreline was prior to the landslide (Brænd 1961).

Fig. 35.2 Picture of the landslide scar in the northernmost part of Sokkelvik following the landslide in 1959 (Courtesy NGI)

35.3 Site Characterization and Geotechnical Properties

Site surveys and some geotechnical soundings were performed in the aftermath of the 1959 landslide by the NGI (1959). A study of the fresh landslide escarpment showed that an up to 3 m thick layer of sand and gravel lay upon the clay. Shallow samples taken within and outside the landslide area showed clay material with an undrained shear strength of 10–20 kPa (from fall cone tests) and a sensitivity of about 100. The water content (w) in the clay was measured to about 40%, the liquid limit (w_L) at 35% and plastic limit (w_P) at 20%. The NGI performed further ground investigations in 1960 in the neighbouring bay called Outer Sokkelvik where similar and representative ground conditions are found (NGI 1960). Results showed a 0.5 m thick layer of sand and gravel on top a sensitive silty clay (Fig. 35.3). Thin layers of sand and gravel were also documented in the clay. From 2 to 12 m depth the water content slightly decreases in the clay from 52% to 40%. The water content was generally 12% above the liquid limit and the plasticity index more or less constant at approximately 9%. The salinity of the pore fluid in the clay was less than 1 g/l.

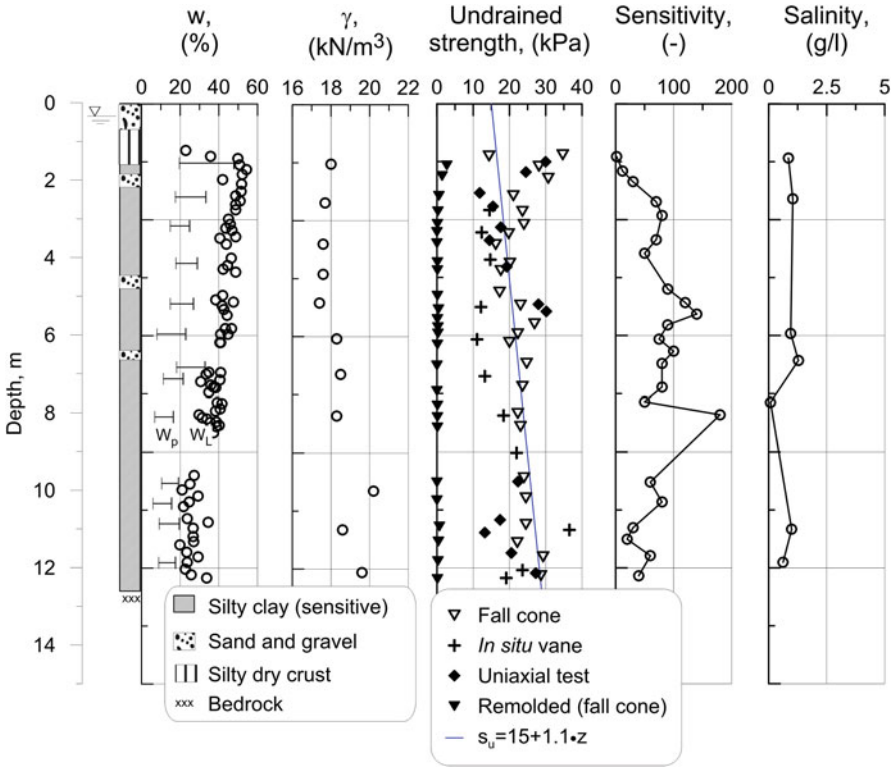

Fig. 35.3 Geotechnical borehole from Ytre Sokkelvik (Modified from NGI 1960)

35.4 Morphology and Landslide Mechanism

In 2006 the Geological Survey of Norway (NGU) performed a bathymetric survey in the bay of Sokkelvik. The survey was carried out using a 250 kHz interferometric sonar system (GeoAcoustics). Positioning was performed by means of differential GPS with an accuracy of ±1 m.

Figure 35.4 presents a 3D submarine view of the Sokkelvik landslide. The bathymetry data clearly reveals that a large portion of the fjord bottom was affected by the 1959 landslide. The largest observed feature is the emptied, pear-shaped, landslide crater immediately outside Sokkelvik. The scarp along the landslide crater is up to 15 m high. Within the landslide crater one can observe a thin veneer of sediment and blocks. The bathymetry image also shows a hummocky fjord bottom at larger water depths with flow lines towards the east/southeast. The source of this sediment and debris is interpreted as a sediment flow from the main landslide stage. North of the main landslide scar, a 2–3 m high escarpment (first stage) is observed on the bathymetry data (Fig. 35.4). Below the evacuated scar one can observe some landslide debris on the intact fjord-bottom slope. At greater depths these debris seems to be covered by landslide debris sourcing from the main landslide scar.

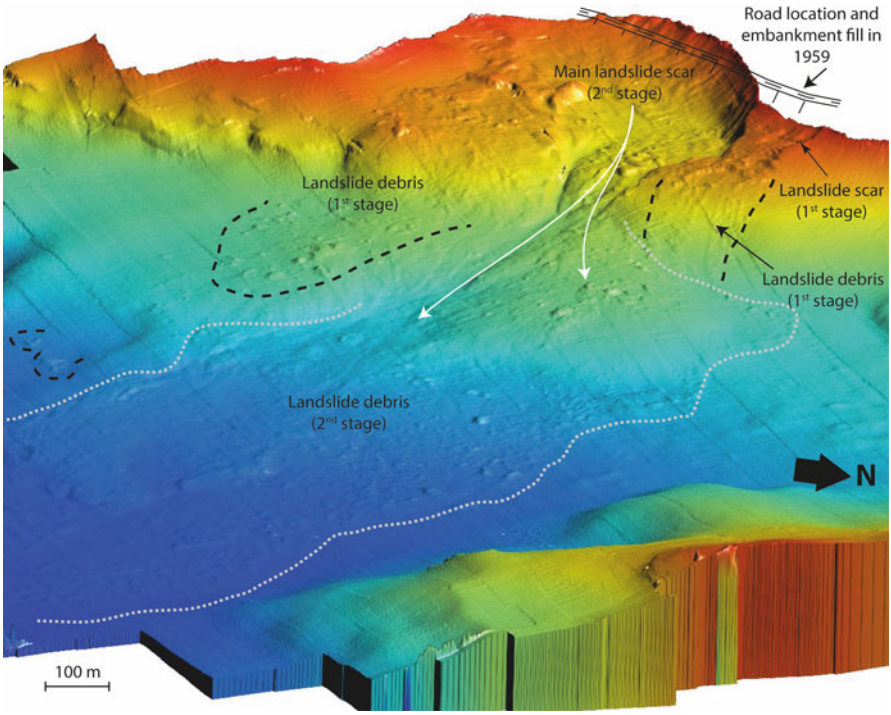

Fig. 35.4 3D submarine view of the 1959 Sokkelvik landslide with morphological interpretation

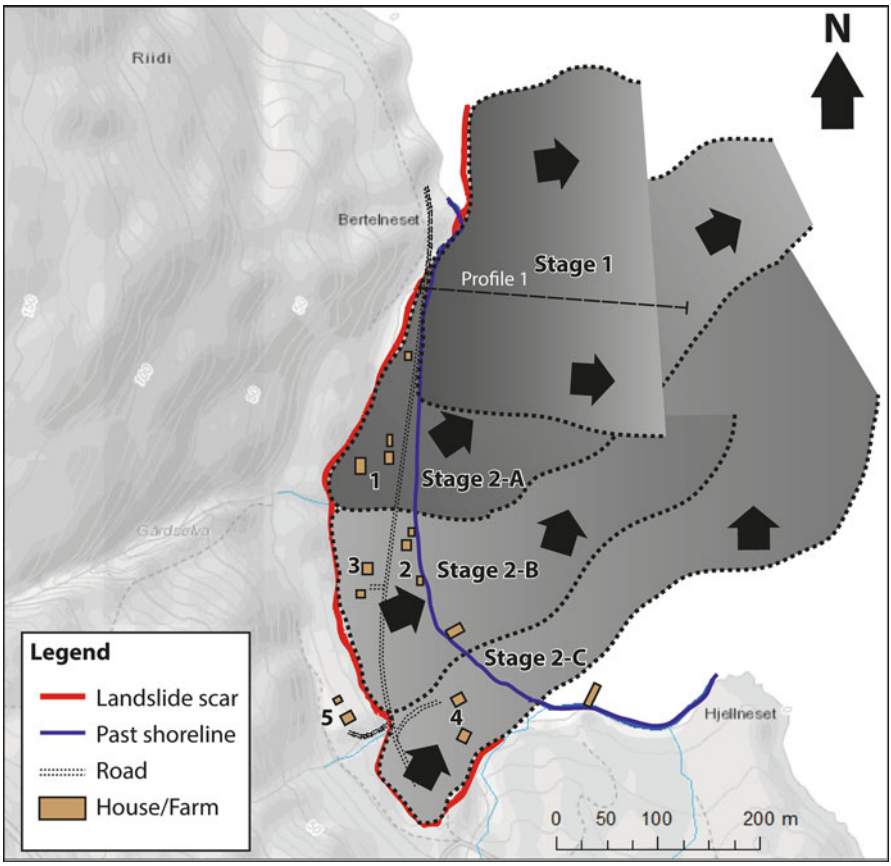

Fig. 35.5 Interpretation of the landslide mechanism at Sokkelvik based on eyewitness testimony and morphological fjord-bottom analysis

Based on morphological evidence and eye witness testimony, the chronology of the Sokkelvik landslide can be divided into two main stages (i.e. Stages 1 and 2; Figs. 35.4 and 35.5). In the first stage a shallower landslide seems to have occurred in the northern part of the bay.

Landslide debris from this stage are covered by debris from the main landslide stage (second stage). The size of the landslide in the first stage is difficult to evaluate, but based on the amount of debris on the fjord-bottom, this landslide may have been up to c. 250 m wide. The mass failure in the first stage likely opened the gate for subsequent landsliding in stage 2. The opening of the gate could explain why the witnesses saw the houses flowing in a north-eastern direction. The retrogressive landslide mechanism and flow pattern in the second stage is represented by subdividing stage 2 in sub-stages (i.e. 2A, 2B and 2C) in Fig. 35.5.

35.5 Preconditioning and Triggering Mechanism

The cause(s) for the Sokkelvik landslide are difficult to pinpoint and several factors may have led to a reduction of slope stability over time. During the field investigation in 1959, clear signs of wave erosion were documented along the shoreline of the neighbouring bay in Outer Sokkelvik (Rosenqvist 1959). Here, the landowner argued that during his time wave erosion had removed several meters of soil. According to Rosenqvist (1959) wave erosion must have been more accentuated in the study area at Sokkelvik than in the outer part of the bay. Satellite imagery shows that such processes are still active in the area (NGI 2016).

Creek erosion may have been a destabilizing factor over time in the nearshore area. Three small creeks run through the bay at Sokkelvik (Fig. 35.5), and satellite imagery shows signs of erosion at the shoreline (NGI 2016). It is conceivable that such erosion was also active before 1959.

Rapid changes in water–level associated to tidal variation (e.g. spring low tide) is known to reduce the stability of nearshore slopes (c.f. Kramer 1988). Low tide at Sokkelvik was registered at 20:20 on May 7th 1959 (i.e. c. 20 min after the landslide occurred). At that time the sea–level was −127 cm below mean sea–level, but 60 cm above the lowest astronomical tide. As shown in Fig. 35.6, lower sea–level was registered in this area earlier in April 1959. In sum, low–tide likely reduced the stability of the near-shore slope in 1959, but cannot be seen as the main triggering mechanism.

Rainfall and snowmelt are recognized as pre–conditioning and triggering mechanisms for landslides. The 1959 winter at Sokkelvik had been mild with little frost in the ground (Jørstad 1959). On May 5th and 6th 1959 intense rainfall and snow melt were registered and on May 7th the meteorological station at Storslett (c. 2 km west of the study area) registered 47 mm of rain (Fig. 35.7). Altogether the station recorded 57 mm of rain in the last 36 h before the landslide. This most likely led

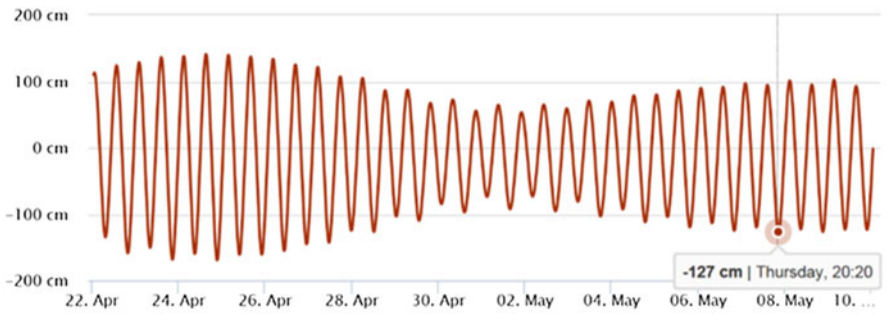

Fig. 35.6 Tidal variation diagram at Sokkelvik for the period 22 April-10 May 1959 (Data from Norwegian Mapping Authorities)

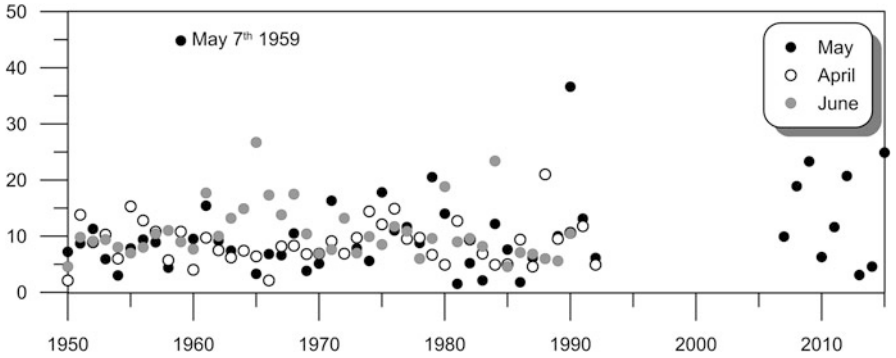

Fig. 35.7 Rainfall data from the meteorological station at Storslett (c. 2 km to the west) for spring months (i.e. April, May and June) during the period 1950–2015 (Data from Meteorological Institute)

to an increase in the soil unit weight (especially the embankment fill) and driving forces, and an increase in pore pressures. As shown in Fig. 35.7, the rainfall event registered on May 7th 1959 is the most intense spring rainfall ever registered in the study area. Clear signs of upward water groundwater flow were reported in the bay area before the slide. Fault zones identified in the uphill bedrock supports these statements and may have amplified the effect of precipitation and snow melt.

A few years before the landslide, a local fisherman witnessed a large sound and boils forming in the fjord water while rowing north in the bay (Jørstad 1959). It is possible to speculate that the sound and swirls the fisherman witnessed were caused by an underwater landslide. How large such a landslide may have been is difficult to know. However, such an observation may indicate that the nearshore slopes in the north of the bay had a low margin of safety against sliding.

Quick clay landslides often are linked to human activities. However, little focus has previously been given to human activity in the surrounding of the Sokkelvik landslide. Recent interviews with habitants in the region and results from an archive study has revealed that there was ongoing road construction in the area before the landslide event. The road in the inner part of Sokkelvik (close to houses no. 2–5) was primarily build from 1951 to 1953, and was resumed in 1957. The work progressed northwards and included placement of an embankment fill on top of the natural soil along the shoreline. The embankment would ensure that the road climbed slightly towards the basement rock at Bertelneset (8 m.a.s.l.; Fig. 35.1). The road was 4 m wide and its location back in 1959 is shown on Figs. 35.1, 35.4, and 35.5. North in the bay, the embankment must have been approximately 7.5 m thick (Fig. 35.7; see also Austefjord 2016). This reconstruction is based

on construction plans from 1957 and recent pictures taken along the shoreline. It is worth mentioning that the road construction at Bertelneset also included rock blasting, and that there was undergoing activity until November 1958 (Austefjord 2016). This is less than 6 months before the Sokkelvik landslide. It is therefore tempting to assume that the road construction contributed, at least to some extent, to destabilizing the near-shore slope through an increase in driving forces. It is also worth noting that more than 300 m of the road was destroyed by the landslide in stages 1 and 2a (c.f. Fig. 35.5).

To evaluate the impact of the road on the stability of the slope, numerical analyses were performed with Plaxis in 2016 (Fig. 35.8, Austefjord 2016). Drained and undrained analyses were performed, and different pore-pressure scenarios were evaluated in the drained analyses. The input undrained shear strength of the clay follows the data presented in Fig. 35.3, while the friction angle and cohesion in the clay were assumed to 25° and 5 kPa, respectively. For undrained situation, results show a factor of safety (FoS) of 1.57 prior to embankment construction and a FoS of 1.05 immediately after. For drained and hydrostatic pore-pressure situation, results show a FoS of 1.78 and 1.39 prior to and after construction of the embankment fill, respectively. Several layers of coarser soils were identified in the sub-surface at Sokkelvik (c.f. Fig. 35.3), and such layers might have experienced excess pore-pressures during the intense rainfall in 1959. The resulting failure mechanism in such case is shown in Fig. 35.9. Here, an excess pore-pressure of 19 kPa was necessary to bring the FoS down to 1.0 (i.e. slope failure).

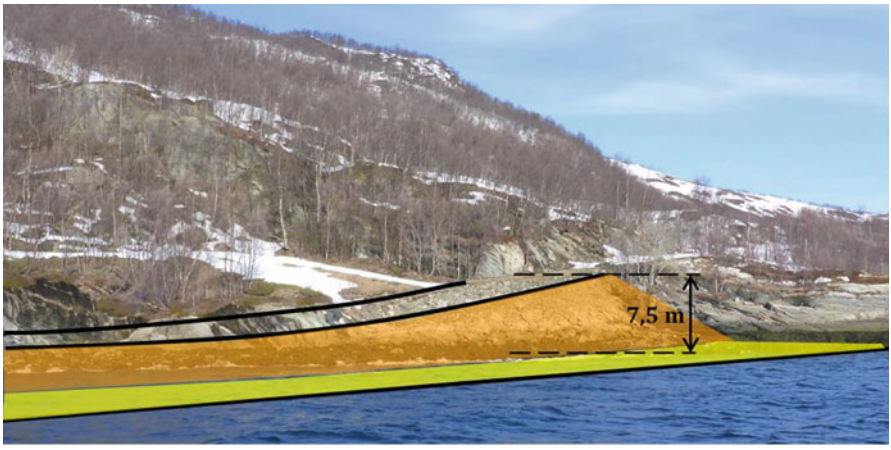

Fig. 35.8 Reconstruction of the embankment fill for the road along the shoreline of Sokkelvik prior to the landslide in 1959 (Modified from Austefjord 2015)

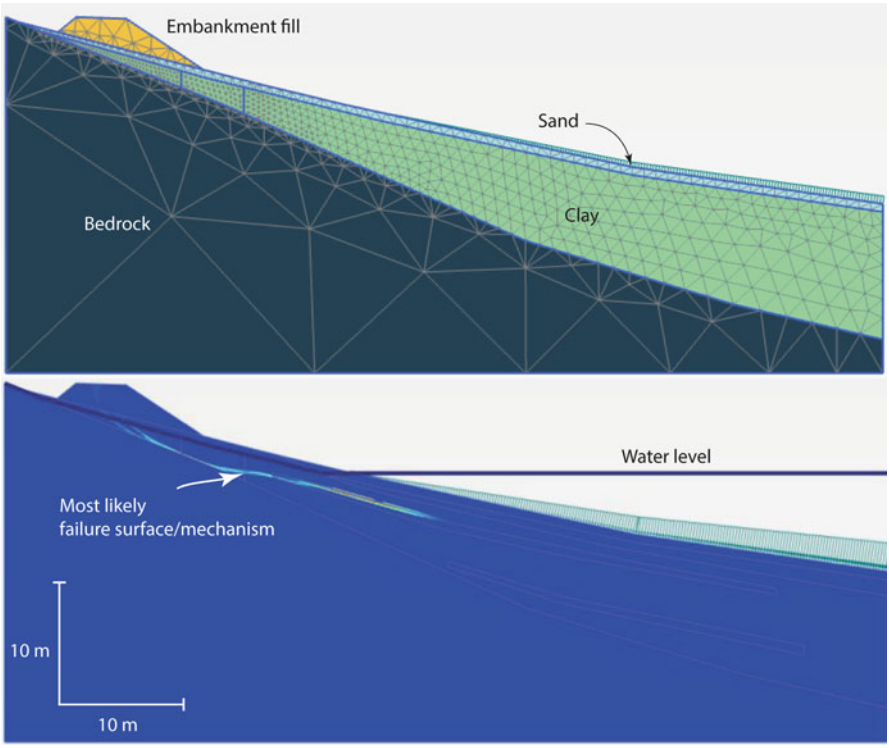

Fig. 35.9 (*Upper panel*) Geometry and layers used in the Plaxis numerical model. (*Lower panel*) Results from Plaxix simulation showing the most likely failure mechanism for a drained situation. See text for further details

35.6 Summary and Conclusions

The combined results of morphological analysis, stability analyses and eye witness testimony show that the Sokkelvik landslide initiated north in the bay where a large embankment fill had been placed 6 months earlier. The Sokkelvik landslide was most likely triggered by intense rainfall and snowmelt in on May 7th 1959, but the main cause of the landslide is associated to the load of the embankment fill that was recently placed at the shoreline. Neither rainfall, snowmelt, tidewater variation nor coastal erosion would have triggered such a landslide if the embankment have had sufficient stability.

The Sokkelvik landslide has since 1959 often been referred to as a catastrophic event with no clear cause leading to failure. This has created an uncertainty and raised questions like which village will randomly be hit next time? The new investigations herein removes a lot of the uncertainty by clarifying the extent of the road construction and identifying the most probable triggers for the slide.

It is concluded that the Sokkelvik landslide compares well to many other cases of nearshore landslides triggered by a combination human activities and intense rainfall events. Examples of such landslide events were reported in Norway at Trondheim in 1990 (L'Heureux et al. 2007), in 1996 at Finneidfjord (Longva et al. 2003) and more recently at Sørkjosen in 2015 (Nordal et al. 2016) and in France along the Nice airport in 1979 (Dan et al. 2007). It is therefore vital to assess the impact of exterme intense rainfall events, snow melt and regional groundwater flow when planning construction work in nearshore areas.

Acknowledgments The authors would like to thank Raymond Eilertsen from NGU for acquiring and processing the bathymetry data. We thank also A. Emdal, S. Christensen, A. Skotheim, E.r Lyche and V. Gjelsvik for input and discussion about the Sokkelvik landslide. They were, together with the authors of this paper, members of the investigation group established in 2015 by the Norwegian Public Roads Administration (NPRA) to study the cause of the Sørkjosen slide. We are grateful to NPRA for financing the investigation of the Sørkjosen slide and for initiating the reinvestigation of the 1959 Sokkelvik slide.

References

Austefjord SW (2016) Skred I strandsonen: Studie av skredet I Indre Sokkelvik 1959. MSc. Thesis. Norwegian University of Science and Technology (NNTU). pp. 91

Brænd T (1961) Landslide catastrophe at Sokkelvik, Nord Reisa May 7th 1959. Norwegian Geotechnical Institute (NGI) publication no. 40, pp 11–13. (In Norwegian)

Dan G, Sultan N, Savoye B (2007) The 1979 nice harbour catastrophe revisited: Trigger mechanism inferred from geotechnical measurements and numerical modelling. Mar Geol 245:40–64

Kramer SL (1988) Triggering of liquefaction flow slides in coastal soil deposits. Eng Geol 26:17–31

Jørstad F (1959) Notat fra befaring 9. til 12. mai 1959 i Sokkelvik, Nordreisa, i anledning leirskredet den 7. mai 1959. Norwegian Geotechnical Institute (NGI) Internal report F. 174.3. (In Norwegian)

L'Heureux JS, Longva O, Hansen L, Vingerhagen G (2007) The 1990 submarine slide outside the Nidelva River mouth, Trondheim, Norway. In: V Lykousis, D Sakellariou, J Locat (eds) Submarine mass movements and their consequences, Kluwer series on advances in natural and technological hazards research, vol. 27, 259–267

Longva O, Janbu N, Blikra LH, Bøe R (2003) The 1996 Finneidfjord slide; seafloor failure and slide dynamics. In: Submarine Mass movements and their consequences. Springer, Dordretcht.

NGI (1959) Orienterende undersøkelser i forbindelse med skredet i Indre Sokkelvik, 7. mai 1959. Report no. O.805-1. Norwegian Geotechnical Insititute. (In Norwegian)

NGI (1960) Grunnundersøkelser i Ytre Sokkelvik, Nordreisa. Report no. O.805-3 Norwegian Geotechnical Institute. (In Norwegian)

NGI (2016) Skredet i Sokkelvik i Nord-Reisa, 7. mai 1959. Norwegian Geotechnical Institute (NGI), Technical Note no. 20150562-01-TN. (In Norwegian)

Nordal S, L'Heureux JS, Skotheim A, Emdal A, Lyche E, Christensen S (2016) Skredet i Sørkjosen 10. mai 2015. Utredning om skredårsak fra undersøkelsesgruppa. Rapport no. SBF20160043. SINTEF Byggforsk

Rosenqvist IT (1959) Befaring av Indre og Ytre Sokkelvik 11. og 12 juli 1959. NGI Note F.174-02. (In Norwegian)

Chapter 36
Geotechnical Evaluation of a Quick Clay Area in Trondheim, Norway

Rolf Sandven, Konstantinos Kalomoiris, Tone Furuberg, and Anders Samstad Gylland

Abstract In geotechnical engineering, the presence of sensitive clays poses a major challenge. The landslides at Rissa in 1978, and more recently at the Skjeggestad bridge in Norway, are reminders of the potential devastating threats related to such soils. Norway has several sets of regulations to handle construction work in sensitive soils. This paper exemplifies the implementation of the regulations for a densely populated area on a quick clay area. The city area of Trondheim in central Norway has several zones of quick and sensitive clays which cause severe challenges for urban planning and development. One of these areas is the Gløshaugen – Bakklandet quick clay zone. The project partners consulted the company Multiconsult ASA to undertake the geotechnical evaluation of the area in the period 2012–2014. This work helped assessing areas where special geotechnical investigations and evaluations must be carried out to allow further development of infrastructure and erection of new buildings. The results from this work have been further developed into hazard maps, revealing several major deposits of quick clay within the quick clay zone. The results may be used as a basis for general planning by the local authorities, but are particularly helpful as a background for further development of the NTNU university campus at Gløshaugen.

36.1 Introduction

Large areas in Norway are prone to landslides in sensitive or quick marine clays, however with varying size and consequences. Examples of well-known major landslides are those in Verdal (1893), Rissa (1979) and Kattmarka (2009), see

R. Sandven (deceased) • A.S. Gylland (✉)
Multiconsult ASA, Trondheim, Norway
e-mail: anders.gylland@multiconsult.no

K. Kalomoiris
Multiconsult ASA, Oslo, Norway
e-mail: konstantinos.kalomoiris@multiconsult.no

T. Furuberg
Municipality of Trondheim, Trondheim, Norway
e-mail: tone.furuberg@trondheim.kommune.no

V. Thakur et al. (eds.), *Landslides in Sensitive Clays*, Advances in Natural and Technological Hazards Research 46, DOI 10.1007/978-3-319-56487-6_36

Fig. 36.1 Quick clay landslide in Kattmarka, Namsos, September 2009

Fig. 36.1. A summary of facts on Norwegian quick clay landslides is given in NIFS (2013). Fortunately, landslide disasters involving quick clay occur very rarely. Within the framework of landslides in sensitive clays, the Norwegian governmental agencies NPRA,[1] NNRA[2] and NVE[3] present regulatory frameworks to enable a decision making process regarding construction on sensitive clay deposits. These regulatory frameworks (NVE 2011; SVV 2014; JBV 2016) are focused on site investigations, design procedures and safety precautions for construction works. In addition, design principles for securing natural slopes also are addressed in the regulatory framework.

This paper exemplifies how the regulatory frameworks for quick clay in Norway is applied and implemented in a densely populated area.

The project of evaluating the stability in the Gløshaugen – Bakklandet quick clay area was a cooperation between the Municipality of Trondheim, the Student Society and the University of Science and Technology (NTNU). The partners consulted the company Multiconsult ASA to undertake the geotechnical evaluation of the area. This included primarily:

- A systematic review of all available information on soil conditions
- Classification of all previous drilling results with respect to presence of brittle materials (sensitive and quick clays)
- Supplementary borings in sub-areas where previous information of the soil conditions was deficient
- New stability analyses in selected profiles for evaluation of slide risk, including identification of slide susceptible sub-areas
- Proposed revision of hazard zonation

The scope of the project was primarily to evaluate the extension of sensitive and quick clays and how that influenced the stability. A total number of 16 profiles where

[1]Norwegian Public Roads Administration

[2]Norwegian National Railway Administration

[3]The Norwegian Water Resources and Energy Directorate

the safety factor is critically low are identified. Further analyses evaluating possible remedial measures are recommended for these profiles. The results from previous and new stability evaluations are summarized in this paper.

36.2 Description of the Project Area

The area is urbanized and heavily populated and covers a total area of about 2 km^2, see Fig. 36.2 The river Nidelven flows north-east of the area, but the embankment is protected against erosion.

The area contains the NTNU university campus at Gløshaugen and also various sites for student facilities. The use of the area is now in focus, motivated by the political decision to localize other parts of the university on the Gløshaugen campus. The project partners and local authorities hence had a strong motivation to clarify the potential for further development of the area.

To get a better overview of the project area, it was divided into eight sub-areas, see Fig. 36.2:

- **Sub-area 1**: Duedalen – Lillegårdsbakken
- **Sub-area 2**: Øvre Bakklandet – Nedre Singsaker N
- **Sub-area 3**: Øvre Bakklandet – Nedre Singsaker S
- **Sub-area 4**: Gløshaugen W - Hesthagen
- **Sub-area 5**: Gløshaugen E – valley Høgskoledalen
- **Sub-area 6**: Tidemanns gate
- **Sub-area 7**: Prestegårdsjordet
- **Sub-area 8**: Singsaker-Tyholt

This separation was based on topography, previously mapped quick clay deposits, boundaries such as roads and railway lines, together with natural barriers or terrain formations.

36.3 Topography

In the southern part of the project area, the terrain slopes upwards from the river Nidelven to the glacial deposit at Gløshaugen. The Gløshaugen-plateau is relatively flat in central areas, with very steep hills towards west and the partly filled ravine Høgskoledalen north-east of campus.

In the northern parts, the terrain rises eastwards from the river. Steep step hill up towards Tyholt defines the eastern boundary of the project area. Further to the south, the terrain falls from the southern side of the road Jonsvannsvegen down towards the southern parts of the campus.

The river Nidelven is a dominating element near the western boundary of the project area.

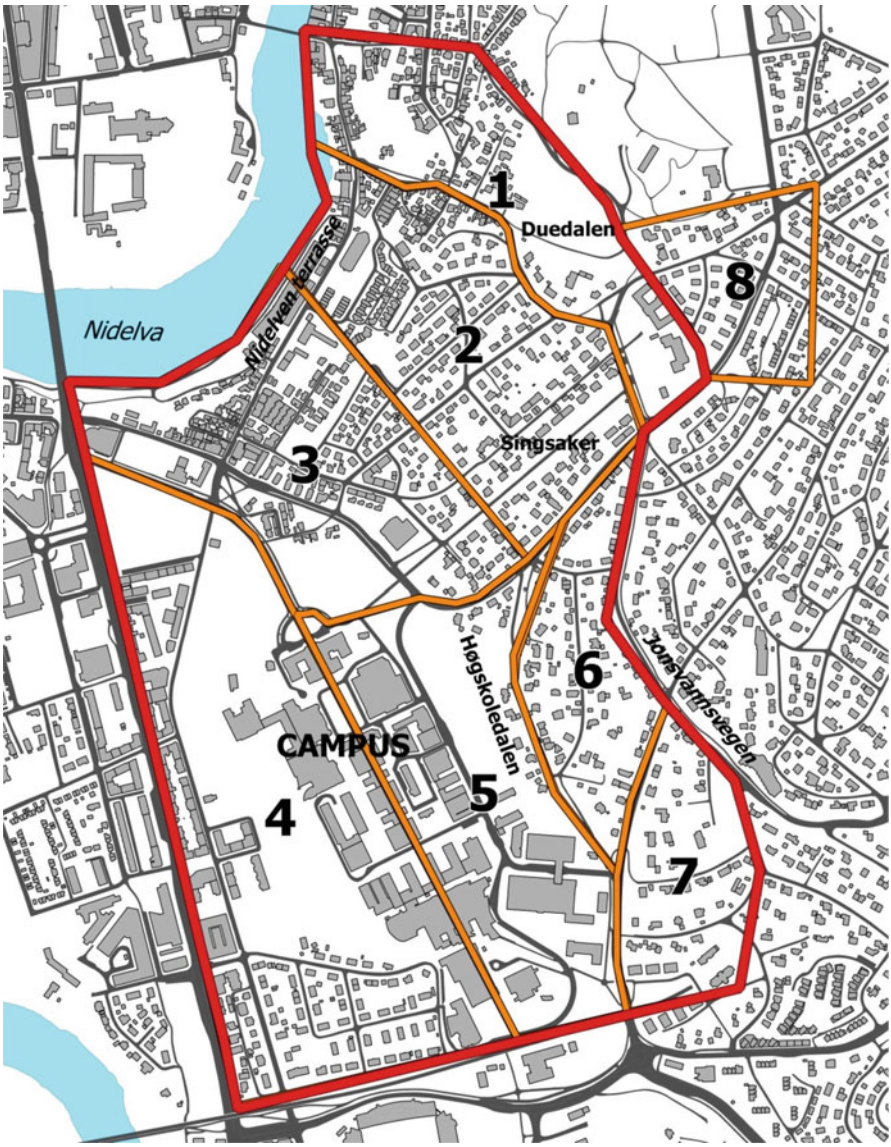

Fig. 36.2 The project area (*red line*) with division into sub-areas (*orange lines*)

In the area around an old brick factory south east of Nidelven Terrasse, several depressions with relatively steep slopes can be seen in the terrain. These depressions are due to a major slide in this area taking place in 1906.

Duedalen below the fortress (sub-area 1) is an example of a bulb-shaped slide pit from a quick clay slide in 1625.

36.4 Quick Clay Zones in the Area

Two quick clay zones have previously been mapped within the project area:

- Zone 188 Berg student village (studentby)
- Zone 183 Øvre Bakklandet – Singsaker

In addition, the western part of quick clay zone 184 Singsaker-Tyholt adjacent to the project area is considered (sub-area 8).

36.5 Ground Investigations in the Area

An extensive amount of site investigations has been carried out in the project area over the years. In the project, a total number of 1230 boreholes were systematically organized in a database, the only one of its kind in Norway.

The introductory evaluation of the local and global stability in the project area showed the need for supplementary soil investigations. New borings were hence carried out to obtain a more reliable mapping of the extension and thickness of sensitive materials. Results from these supplementary investigations contributed to improved stability calculations and better size estimates of release areas and run-out from potential slides.

The data collection was classified according to the definitions of quick clay, sensitive clay and brittle materials defined by NVE (2014).

Red status: Quick clay (K) with remoulded shear strength c_r <0,5 kPa or sensitive clay (S) with remoulded shear strength 0,5 < c_r < 2,0 kPa and sensitivity S_t >15, verified in the laboratory on retrieved samples or by in situ vane tests. These materials are defined as brittle materials.

Orange status: Assumed (A) or uncertain (U) evaluation of the presence of brittle materials, based on interpretation of sounding results or other non-verified information. No verified determination of brittle materials hence exists in the borehole.

Green status: Brittle materials not detected or assumed from field or laboratory tests. Sensitive/quick clays may be encountered in thin, discontinuous layers.

36.6 Ground Conditions and Extent of Quick Clay in the Project Area

Figures 36.3 and 36.4 shows the distribution of brittle materials within the project area, colored according to the scheme presented in the last section. Boring symbols marked with red color verify the presence of brittle materials of sufficient thickness and continuity. The classified borings have been used to revise the extension of

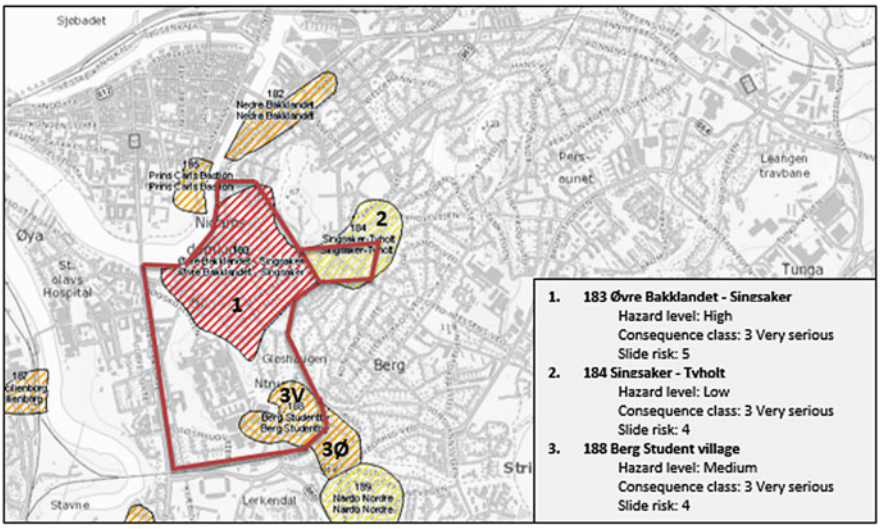

Fig. 36.3 Mapped quick clay zones in the project area (NVE, atlas.nve.no)

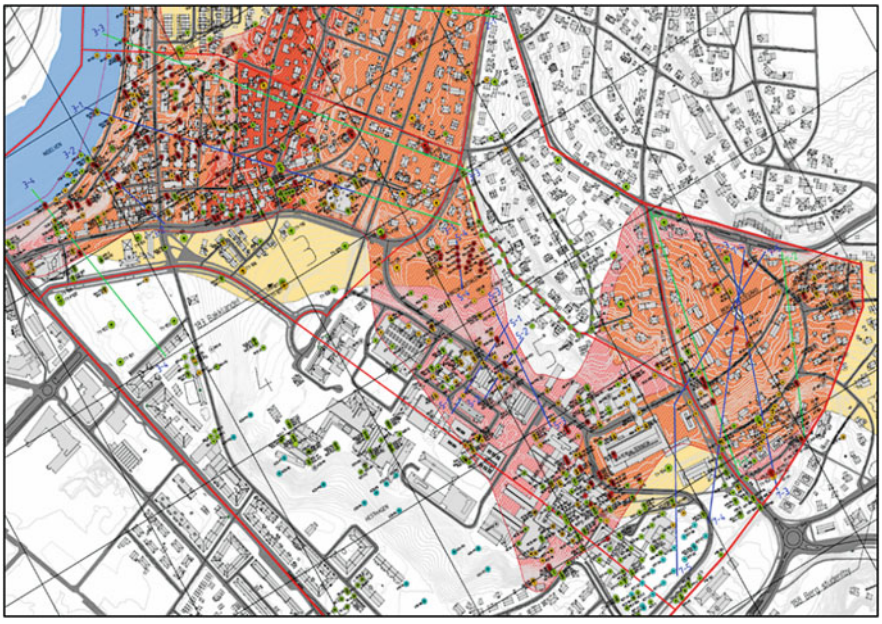

Fig. 36.4 Revised hazard map for the project area with classified boring symbols, from (Multiconsult 2014)

hazard zones in the project area as shown in figure below. The red shaded area indicates the revised hazard areas, whereas the yellow zones show the original hazard map.

Based on available results, a continuous zone with sensitive and quick clays is encountered between the sub-areas previous mapped shown in Fig. 36.3. This deposit is most likely connected with the quick clay areas in the northern parts up to Duedalen.

A corridor of quick and sensitive clays is also encountered at the NTNU campus at Gløshaugen (sub-area 5), possibly connected with the thick deposits of quick clay found south east in the area (sub-area 7).

Sub-areas without presence of quick or sensitive clays are also encountered within the hazard zone since the zonation also takes run-out of slide debris from adjacent areas into account. Sub-areas without brittle materials are mainly encountered at the western parts of the Gløshaugen plateau and the level areas in the vest (sub-area 4), the southern parts of the Gløshaugen plateau, and the north-west of campus. There is also an area with no sensitive materials near the former brick factory east of Nidelven Terrasse.

36.7 Evaluation of Slide Mechanisms and Triggering Factors

This project case is quite typical for the challenges and problems met when planning new development in urbanized areas containing quick clay. The societal needs for further development of new infrastructure and densification of buildings may easily be counteracted by strict regulations in local or national guidelines. Further development of the area may require local or global stabilization means, which may be practically difficult or even impossible to establish in an urbanized area.

Due to topographical and geological conditions, it is not likely that the project area can run-out in one slide. It may hence be practical to divide the area into sub-zones, where one such zone reflects the maximum release area for one single slide within this zone. Based on topography and soil conditions, the most likely slide mechanism is a retrogressive/progressive slide in quick clay layers, triggered by an initial slide in exposed areas. Further slide development, resembling a domino collapse mechanism, will then take place until a barrier is met preventing further sliding. Such a barrier may be a layer or a pocket of non-sensitive clay, changes in the slope or thickness of the sensitive layer or a rising rock surface.

An initial slide may be triggered by human action or by natural causes. Man-made landslides may be caused by overloading of the ground, following from terrain changes, construction work, blasting or pile driving and similar activities. Often, a combination of effects from such activities may be sufficient to trigger a landslide. The following assumptions have to be satisfied for such slides to take place:

- Important factors are the thickness and continuity of the brittle materials close to the triggering source.

- The location and slope of the layer with brittle materials within the sediments must qualify for a continuous, retrogressive or progressive failure mechanism.
- Where the terrain formations include terraces or other irregularities, the local stability of the surface layers may be poor. A progressive failure can hence be initiated by an initial slide in the terraces.

One particular area of interest is the terrain corridor between the river and eastwards to Høgskoledalen (sub-area 1). Theoretically, an initial slide released by the river may retrogressively develop from the river all the way up to Høgskoledalen, provided that a continuous layer of quick clay is present here.

The most likely landslide trigger is construction work. Natural causes may be:

- Erosion in or from the river Nidelven, particularly in the river bed
- Increased precipitation due to climate changes. Larger erosion risk due to increased water flow in Nidelven, but also from surface water
- Vibrations from earthquakes
- Creep or long-term deformations in soft and sensitive clays due to high shear mobilization.

36.8 Principles for Stability Calculations

Stability evaluations for new buildings and constructions in the area include local and global stability for new buildings and infrastructure. Both undrained, short-term and drained long-term stability evaluations are carried out (Table 36.1).

For undrained conditions, the NVE (2014) guidelines require a minimum factor of safety of $\gamma_m \geq 1{,}4$, or a documented percentual improvement of the safety factor.

Input data for stability analyses have mostly been based on results from index tests, oedometer and triaxial tests in the laboratory, in situ vane tests, and input parameters from recent CPTU soundings. The anisotropy coefficients have mostly been based on empirical relationships NIFS (2014).

Table 36.1 Partial safety factors for effective stress and total stress analyses according to Norwegian construction standards

	Failure mechanism		
Damage consequences	Dilatant	Perfectly plastic	Brittle and contractant
Less serious	1.2	1.3	1.4
Serious	1.3	1.4	1.5
Very serious	1.4	1.5	1.6

36.9 Identification of Possible Slide Areas

Particularly hazardous profiles with factor of safety γ_m <1,4 are found in the following sub-areas, see Fig. 36.2:

- **Sub-area 1 Duedalen – Lillegårdsbakken:** An initial slide triggered in the lower parts of the hill Lillegårdsbakken and spreads further in the direction of the valley Duedalen is the most dramatic scenario.
- **Sub-area 2 Singsaker - Nedre Bakklandet North:** Continuous layers of quick or sensitive clays are found between the street Jørgen Bjelkes gate and the Singsaker-area and may be subjected to sliding activity.
- **Sub-area 3 Singsaker - Nedre Bakklandet South:** Continuous layers of quick or sensitive clays may be found from the river Nidelven up towards the mouth of the valley Høgskoledalen and beyond. Quick or sensitive clays are also encountered in the terraces between the river and the area close to Studentersamfundet. A slide in this area may have dramatic consequences.
- **Sub-area 5 Gløshaugen East – Høgskoledalen:** Slide activity may take place in the thick deposits of quick and sensitive clay found in the terraces around the valley Høgskoledalen.
- **Sub-area 5 Gløshaugen East – Høgskoledalen:** Investigations at Prestegårdsjordet east of the NTNU campus reveal thick deposits of quick and sensitive clays in the central and southern parts of this sub-area. Slide debris from a slide in this area may threaten the NTNU campus.

36.10 Discussion

The scope of this project was primarily to evaluate the extension of sensitive and quick clays and how that influenced the stability.

A large amount of site investigations has been carried out in the project area over the years. In the project, a total number of 1230 boreholes were systematically organized in a database, the only one of its kind in Norway.

However, the introductory evaluation of the local and global stability in the project area showed the need for supplementary soil investigations. New borings were hence carried out to obtain a more reliable mapping of the extension and thickness of sensitive materials. With today's equipment it was possible to increase the depth of the site investigations and to obtain more reliable material parameters, something that contributed to improved stability calculations and better size estimates of release areas and run-out from potential slides. Cone penetration test with pore pressure measurements (CPTU) proved to be a field investigation method that contributed a lot to the scope of this project.

Furthermore, new and earlier site investigations were classified according to the definitions of quick clay, sensitive clay and brittle materials defined by NVE (2014).

Red status: Quick clay (K) with c_r <0,5 kPa or sensitive clay (S) with 0,5 < c_r <2,0 kPa and sensitivity S_t >15, verified in the laboratory on retrieved samples or by in situ vane tests. These materials are defined as brittle materials.

Orange status: Assumed (A) or uncertain (U) evaluation of the presence of brittle materials, based on interpretation of sounding results.

Green status: Brittle materials not detected or assumed from field or laboratory tests.

Results of the stability evaluations for new buildings and constructions in the area showed insufficient safety according to regulatory frameworks regarding construction on sensitive clay deposits. For an urbanized and heavily populated area like the project area it is not possible to document recommended improvement of the safety factor based on terrain changes (fills and/or cuts). Other ground improvement methods like lime/cement columns are not feasible most of the times, or too complicated to implement.

Insufficient safety factors may prevent further development of an urbanized area, and a challenge to the campus renewal project.

Acknowledgements The Municipality of Trondheim, the Student Society (SiT) and the Norwegian University of Science and Technology (NTNU) are greatly acknowledged for initiating the project and for excellent co-operation during the project work. The authors also wish to express their gratitude to the reviewer Dr. Denis Demers for his valuable comments.

This paper was written by Rolf Sandven before he all too early passed away in October 2016. The authors hope that his legacy and his focus on knowledge and quality in laboratory and field investigations will live on.

References

JBV (2016) The Norwegian railroad administration. Technical regulations http://trv.jbv.no/wiki/Hovedside

Multiconsult (2014) Gløshaugen-Bakklandet quick clay area. Main project Phase 1. Geotechnical evaluation – principles for further evaluation of area stability. Multiconsult report 415913-RIG-RAP-002 rev01, Trondheim April 2014 (in Norwegian)

NIFS (2013) Characterization of historical landslides and input parameters for Q-BING (in norwegian), Report 38–2013, ISBN: 978-82-410-0907-5

NIFS (2014) A unified recommendation for use of anisotropy factors in design in Norwegian clays. Report 14-2014

NVE (2011) Flooding and slide hazards in area planning. Norwegian Water Resources and Energy Directorate, Oslo. Guideline no. 2/2011 (in Norwegian), ISSN: 1501-9810

NVE (2014) Safety against quick clay landslides. Norwegian Water Resources and Energy Directorate, Oslo. Guideline no 7/2014 (in Norwegian), ISSN: 1501-0678

SVV (2014) Geotechnics in road construction. The Norwegian puclic Roads Administration, Handbook V220

Chapter 37
Saguenay Risk Management

Janelle Potvin, R. Mompin, Catherine Thibault, Denis Demers, Chantal Bilodeau, and L. Desbiens

Abstract The city of Saguenay, in the province of Quebec, is located in an area with a hilly topography and where sensitive marine clays are predominant. The slopes throughout the city are either former riverbanks or scarps of old large retrogressive landslides and their height can vary from a few meters to dozens of meters. Although the toe of these slopes is no longer subject to erosion, they can still be affected by shallow landslides. The spreading debris of such landslides is a threat to buildings located at the toe of slopes and thus a significant hazard for the safety of residents. This article presents the approach developed jointly by the Government of Quebec and the city of Saguenay to manage the risks associated with this hazard. Following the mapping of landslide prone areas, risk analyses allowed to bring out areas most exposed to shallow landslides. An annual inspection program was implemented in 2007 by the city of Saguenay and allowed on numerous occasions to detect early signs of landslides and take preventive action, in the form of stabilization work. This program has considerably reduced the risk to the population.

37.1 Introduction

In the early 2000s, the Government of Quebec reviewed its approach to risk management (Ministère de la Sécurité publique 2008; Potvin et al. 2014) after major disasters in the late 1990s (torrential rain in Saguenay–Lac-Saint-Jean and ice storm in Southern Quebec). The Government of Quebec recognized that landslides

J. Potvin (✉) • R. Mompin • C. Thibault • D. Demers
Ministère des Transports, de la Mobilité durable et de l'Électrification des transports, Quebec City, QC, Canada
e-mail: Janelle.Potvin@transports.gouv.qc.ca; remi.mompin@transports.gouv.qc.ca; catherine.thibault@transports.gouv.qc.ca; denis.demers@mtq.gouv.qc.ca

C. Bilodeau
Ministère de la Sécurité publique du Québec, Québec, QC, Canada
e-mail: chantal.bilodeau@msp.gouv.qc.ca

L. Desbiens
Ville de Saguenay, Quebec City, QC, Canada
e-mail: luc.desbiens@ville.saguenay.qc.ca

V. Thakur et al. (eds.), *Landslides in Sensitive Clays*, Advances in Natural and Technological Hazards Research 46, DOI 10.1007/978-3-319-56487-6_37

(particularly those occurring in sensitive clayey soils) pose a threat that must be considered a priority.

Different measures can be implemented to assist the municipal or government authorities to improve risk management in their territory, and thus reduce the risk level for the population and infrastructure (Demers et al. 2008; Thibault et al. 2008).

This article describes the problem of shallow landslides, the semi-quantitative analysis method and the treatment of the shallow landslide risk developed jointly by the Government of Quebec and the city of Saguenay. This historical case concern the La Baie borough located in the East part of the city.

37.2 Problems Related to Shallow Landslides

In Quebec Province, most landslides in clayey soils occur on the banks of watercourses where the toe is subjected to erosion. However, shallow landslides also occur along slopes without erosion. These slopes are the remains of old marine terraces or scarps of large retrogressive landslide scars (Fig. 37.1).

Hundreds of shallow landslides occur in Quebec per year. They can happen in all types of soil but are most common in clay. Shallow landslides are caused by saturation of the soil during heavy rains or spring snowmelt. This type of landslide is generally characterized by a shallow failure surface, usually less than 1.5 m deep. They occur essentially in the slope and rarely reach the crest. However, the debris may extend to the toe of the slope, sometimes over long distances. Although these landslides seem innocuous because they are relatively small, they can cause major damage to buildings located at the toe (Fig. 37.2) and, if there are people exposed even casualties.

Fig. 37.1 Typical example of a slopes without erosion formed by the scarp of a large retrogressive landslide scar

Fig. 37.2 Example of the consequences of a shallow landslide. The debris slammed into the house located at the toe of the slope

Many shallow landslides occur during extreme weather events. This was the case during the heavy rainstorm of July 19th and 20th, 1996, in the Saguenay – Lac-St-Jean area, where over 250 mm of rain fell within 36 h, causing more than 1,000 landslides (Demers et al. 1999). One of the landslides caused the death of two young children in Saguenay (Bouchard et al. 2008). In April 2005, in the Charlevoix region, heavy rains combined with snowmelt triggered about 50 landslides, forcing the evacuation of many residences (Locat et al. 2008). In June 2011, 260 mm of rain fell in the Outaouais region in western Quebec within 48 h, threatening over 50 homes. In view of the anticipated climate changes, extreme weather events should become more numerous, thus increasing the occurrence of landslides. Shallow landslides occur not only during extreme weather events but also during more regular and less significant events.

La Baie borough in the city of Saguenay is particularly exposed to this type of landslide. The very variable terrain and the large spread of clayey soils make this area prone to the development of shallow landslides.

37.3 Risk Analysis

Mapping of areas prone to landslides is the main step in risk identification. For the La Baie borough, it revealed that a large number of buildings at the toe of the slopes could be hit by shallow landslide debris. Due to the concerns expressed byt the municipal authorities, a risk analysis was performed.

For each building located in the restricted zone at the toe of a slope, the risk (R) is calculated by considering the following equation.

$$R = P_{site} \times C_{site}$$

Where

P_{site}: Probability of landslide occurrence for a site
C_{site}: Consequences for a site

The risk is assessed on the basis of the probability and the consequences associated with such an event in terms of the loss of lives for a given site. The value of the risk is not absolute; it serves to compare sites with each other. In a first stage, a general risk analysis is performed, which considers the predisposing factors of a slope (slope angle, height, etc.). This stage of the analysis is automated and uses geographic information systems. The buildings with a very high risk level are the object of a more specific analysis where the worsening and revealing factors, identified during site inspections, are then considered.

37.3.1 General Risk Analysis

At this stage, the probability that a shallow landslide will occur at a given site (P_{site}) is determined according to the slope angle and the height of the slope

$$P_{Site} = P_i \times K_h \times K_{ci}$$

Where

P_i: Probability of occurrence for slope class "i"
K_h: Weighting factor associated with the height of the slope
K_{ci}: Correction factor for each slope class

Clay slopes are divided into six classes according to the strongest slope section constituting them. Probability P_i is determined for each of these six classes (Levasseur 2003).

$$P_i = \frac{N_{gi}}{N_i}$$

Where

N_{gi}: Average number of landslides that occur each year in slope class "i"
N_i: Number of potential sites where a shallow landslide can occur for slope class "i"

N_{gi} is valued based on a non-exhaustive inventory produced from air photos that cover a period of nearly 50 years. The number of potential slope class "i" sites (N_i) is determined for each slope class, considering that the average width of a landslide is 10 m.

$$N_i = \frac{L_i}{L_g}$$

Table 37.1 Weighting factors associated with slope height

Height (in meters)	Weighting
5–10	0.8
10–15	1.0
15–25	1.5
25 and over	2.0

Where

L_i: Total length represented by each slope class throughout the territory
L_g: Average width of a landslide

The weighting factor (K_h) accounts for the possibility of having several steep segments in the same slope (Table 37.1). The higher a slope is, the greater is the probability of it being identified as a trigger zone.

The weighting factor (K_h) has the effect of stretching the variation range of the P_{site} probability values relative to the P_i probability of occurrence of a shallow landslide. Therefore, a correction factor (K_{ci}), varying according to slope class "i", must be applied to center the average probability assigned to each site in relation to probability P_i.

$$K_{ci} = \frac{P_i}{P_i \times K_h}$$

The potential severity of the consequences (C_{site}) can be assessed for each building according to the equation:

$$C_{site} = P_S \times V \times P_T \times E_V$$

Where

P_S: Spatial probability
V: Vulnerability of threatened elements
P_T: Temporal probability
E_V: Number of exposed elements

The spatial probability (P_s) depends on the principle that the closer a vulnerable element is to the toe of the slope, the greater is the probability for it to be affected by landslide debris. This probability is obtained from the landslide inventory carried out by Perret and Bégin (1997), in which 769 landsides were identified following the torrential rains that fell in July 1996 in the Saguenay – Lac-Saint-Jean area. This inventory made it possible to draw a graph of the frequency of landslides as a function of travel distance of the debris, factored by the height of the slope (D/H).

The portion of land located between the toe of the slope and a distance equal to twice the height of the slope is divided into four classes, as identified by the histogram in Fig. 37.3. The probability assigned to each class is obtained by taking

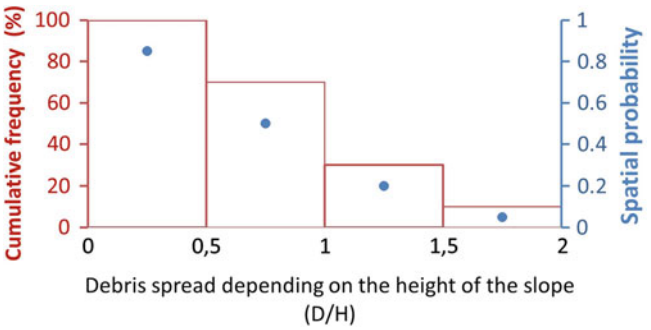

Fig. 37.3 Cumulative frequency relative to the travel distance of the debris (Modified from Perret and Bégin 1997 and Levasseur 2003). The blue dots represent the probability for each class (D/H)

the average probability of the limits of the class. Figure 37.3 shows that 100% of the debris reached or exceeded range 0–0.5H. The spatial probability for this zone is 0.85.

The vulnerability (**V**) represents the probability of mortality if people are found in a building hit by landslide debris. It is based on the damage from shallow landslides observed on different types of building.

The temporal probability (P_T) is associated with the exposure time of a person to danger. This probability varies according to the use of the building. It is admitted that residents remain in their home 16 h per day. In the case of a business or a farm, it is estimated that people work there 8 h per day.

The E_V factor corresponds to the number of vulnerable elements exposed to a shallow landslide hazard. As a preliminary estimate, an average of four people per residence, eight people per multiple-unit residential building, one person per farm building and five people per commercial building is considered in the analysis.

Mapping made it possible to target over 700 buildings directly exposed to various degrees to a shallow landslide debris hazard in the city of Saguenay only. The general risk analysis allowed quantification of the risk for each of these buildings, and thus target those with the highest risk level. Only the buildings most likely to be hit by debris were subjected to a more refined analysis. This specific analysis allowed the implementation of a risk management plan adapted to the territory studied.

37.3.2 Specific Risk Analysis

The specific risk analysis makes it possible to determine the risk level of each site, considering the worsening factors that could impair slope stability and considering the shallow landslide warning signs observed on the ground. Factors are added to the site probability (P_{Site}) determined by the general analysis.

$$P_{\text{Specific site}} = P_{Site} \times K_D \times K_E \times K_R \times K_V \times K_S \times K_c$$

Table 37.2 Weight assigned to the each factor

Factors	Ranges	Weight
Cutting (K_D)	D/H >1/3	2
	1/3 > D/H >1/5	1.5
	1/5 > D/H	1.2
	Nil	1
Water concentration (K_E)	Yes	1.5
	No	1
Height of the stiffest section (K_R)	Base	0.8
	Middle	1
	Top	1.5
Vegetation (K_V)	Denuded	1.5
	Shrubs	1
	Trees	0.8
Revealing signs of instability (K_S)	Nil	1
	Loss of plant cover	1.5
	Minor cracks	2
	Cracks with vertical shift	5

Where

K_D: Factor for the cut section
K_E: Water concentration factor
K_R: Factor for the position of the stiffest position in the slope
K_V: Factor for the type of vegetation found on the slope
K_S: Factor for the presence of revealing signs of instability
K_c: Correction factor

Weights were assigned to the different factors (Table 37.2). Their importance is based on field observations and expert judgement. As in the general analysis, a weight factor (K_P) was considered to recenter the probabilities on the average.

In the case of the risk analysis performed in the La Baie borough, a specific risk analysis was applied to approximately 350 buildings. The risk is presented in the form of a logarithmic graph based on the one produced by the Geotechnical Engineering Office (1998). The graph was divided into five risk classes, thus allowing each site to be classified according to a risk scale (Fig. 37.4a). The results shown in the graph are then transferred to the risk map (Fig. 37.4b).

37.4 Risk Treatment

In the territory of the La Baie borough of the city of Saguenay, the risk analysis revealed that several homes are exposed to shallow landslide hazard. As mitigation works could not be performed on all the sites, due to the high cost of such an

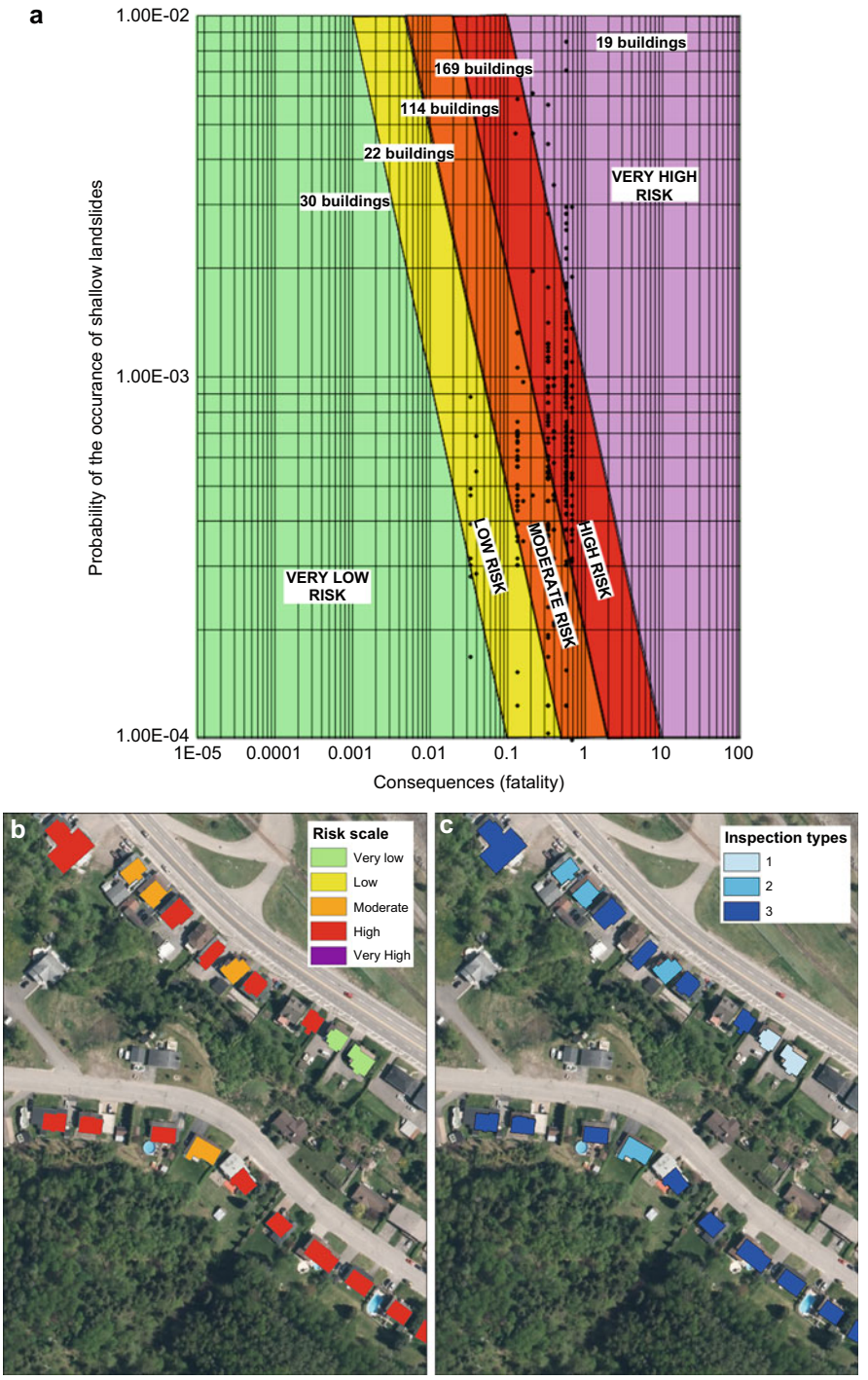

Fig. 37.4 (**a**) Graph of the specific risk analysis for the shallow landslide hazard; (**b**) Risk map example; (**c**) Inspection map example

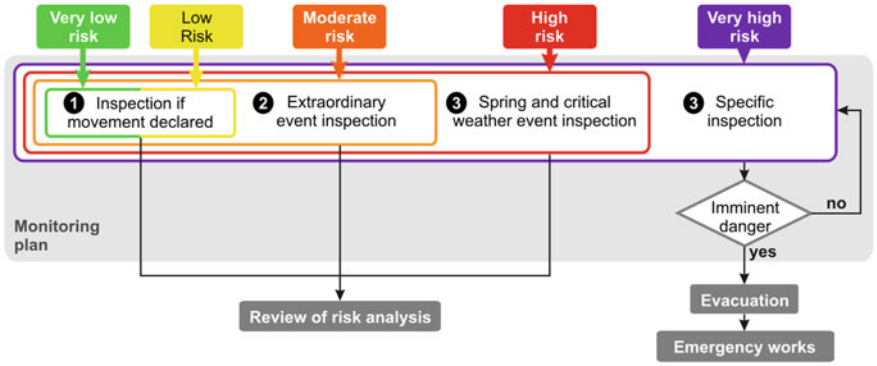

Fig. 37.5 Monitoring plan for areas exposed to shallow landslides

endeavor, preventive measures were therefore implemented. Thus, the municipal by-laws allow control of interventions that could impair slope stability. Moreover, the deployment of a slope monitoring plan makes it possible to reduce the likelyhood of disasters. Slope inspections are conducted at a certain frequency, based on the computed risk level, in order to identify early signs of instability (cracks in the slope or at its top, bulge in the ground at the foot of the slope, degradation of retaining walls, etc.) which have developed or worsened since the previous inspection. Figure 37.5 presents the monitoring plan for the areas exposed to shallow landslides in the city of Saguenay. Inspection maps can be drawn to facilitate the work of the municipal and government stakeholders (Fig. 37.4c). These maps take the information from the risk maps and transpose it into inspection types (1, 2 and 3) for each building. In the case of La Baie borough, 182 buildings are inspected annually. Over the past few years, the city of Saguenay has extended its monitoring plan to all its boroughs, using the same framework.

Since 2007, this innovative approach has allowed to detect about ten sites where danger became imminent. Interventions, totally or partially funded by the government, were carried out to avoid potential deaths and major property damage (Ministère de la Sécurité publique 2013a). Interventions made can seek to reduce the probability of occurence, by stabilizing the slope, for example, or to reduce the severity of the consequences, by building a protective wall, for example.

37.5 Conclusion

The approach described in this article is part of the Prevention Framework for Disasters adopted by the Government of Quebec in 2007 and renewed in 2013 (Ministère de la Sécurité publique 2013b). It allows implementation of management measures adapted to the magnitude of the risk and optimization of the preventive interventions to significantly reduce risks associated with shallow landslides. Its

success is linked to the political will and the cooperation of the authorities concerned, primarily on the municipal level. Communication and consultation among government authorities, geotechnical engineers, municipal authorities and the public is a key success factor in such an approach. This approach used by the city of Saguenay served as a model and remains to this day a reference in landslides risk management in Quebec Province.

Acknowledgements This publication was authorized by the departmental authorities of the authors concerned. They wish to thank their many colleagues who participated in the discussions and the development of this risk management process, as well as Paul Flon for the revision of the article.

References

Bouchard R, Michaud V, Demers D (2008) Le glissement de la rue McNicoll, 20 juillet 1996, Saguenay, Québec : causes et conséquences. In: Proceeding of the 4th Canadian Conference on Geohazards: from causes to management. Presse de l'université Laval, Québec 2008, p 503–510

Demers D, Potvin J, Robitaille D (1999) Gestion des risques de glissement de terrain liés aux pluies des 19 et 20 juillet 1996 au Saguenay – Lac-Saint-Jean. Rapport soumis au Bureau de reconstruction et de relance du Saguenay – Lac-Saint-Jean. Ministère des Transports du Québec.

Demers D, Robitaille D, Potvin J, Bilodeau C, Dupuis C (2008) La gestion des glissements de terrain dans les sols argileux au Québec. In: Proceeding of the 4th Canadian Conference on Geohazards : from causes to management. Presse de l'université Laval, Québec 2008, p 519–526

G eotechnical Engineering Office (1998) Landslides and boulder falls from natural terrain: interim risk guidelines. GEO Report No. 75, Geotechnical Engineering Office, The Government of the Hong Kong Special Administrative Region

Levasseur M (2003) Contribution des systèmes d'information géographique à l'analyse quantitative de l'aléa « glissement de terrain »- Exemple d'application au secteur de la ville de La Baie, Québec, Québec. Mémoire de maîtrise, INRS-E.T.E, Université du Québec, 213 p

Locat P, Demers D, Lessard D, Ouellet D (2008) Le sinistre d'avril 2005 à Petite-Rivière-Saint-François : des causes, à la gestion. In: Proceeding of the 4th Canadian Conference on Geohazards: from causes to management. Presse de l'université Laval, Québec 2008, p 559–567

Ministère de la Sécurité publique du Québec (2008) Gestion des risques en sécurité civile. Gouvernement du Québec, Available via http://www.securitepublique.gouv.qc.ca/securite-civile/publications-statistiques-civile.html. Accessed 10 Oct 2016

Ministère de la Sécurité publique (2013a) Programme général d'aide financière lors de sinistres réels ou imminent. Available via http://www.securitepublique.gouv.qc.ca/securite-civile/aide-financiere-sinistres/programmes-aide-sinistres/general/objet-general.html. Accessed 10 Oct 2016

Ministère de la Sécurité publique du Québec (2013b) Cadre de prévention des sinistres 2013–2020. Available via http://www.securitepublique.gouv.qc.ca/securite-civile/soutien-partenaires/soutien-aux-municipalites/cadre-pour-la-prevention-de-sinistres.html. Accessed 10 Oct 2016

Perret D, Bégin C (1997) Inventaire des glissements de terrain associés aux fortes pluies de la mi-juillet 1996: Région du Saguenay/Lac Saint-Jean. Rapport remis au Bureau régional de la reconstruction, ministère du Conseil exécutif du Québec – L'institut national de la recherche scientifique – INRS-Géoressources, 26 p

Potvin J, Thibault C, Demers D, Bilodeau C (2014) An overview of the mapping of landslide-prone areas and risk management strategies in the Province of Québec, Canada. In: Landslides in sensitive clays – from geosciences to risk management, vol 36. Springer

Thibault C, Potvin J, Demers D (2008) Development of a quantitative approach for evaluating and managing the risk associated with highly retrogressive slides. In: Proceedings of the 61th Canadian conference of geotechnique, Edmonton, pp 1055–1063

Part V
Sensitive Clays Mapping and Identification

Chapter 38
Development of a Methodology for Quick Clay Mapping

Hjördis Löfroth, Karin Lundström, Lena Persson, Mehrdad Bastani, J. Ekström, Colby A. Smith, J. Hedfors, and David Schälin

Abstract Quick clays involve considerable risks because small initial slips may evolve into large landslides involving the entire quick clay formation. Most large clay slides in Sweden, Norway and Canada have been in quick clay areas. It is therefore necessary to develop cost-effective methods for mapping the extent of quick clay formations and areas with probable quick clay. The most important areas are those with existing infrastructure and buildings as well as areas planned for exploitation. The methodology should be well-designed in proper steps with different levels of accuracy and include overview studies of topographical and geological methods, detailed geophysical and geotechnical ground investigations, as well as airborne geophysical methods with greater coverage but less accuracy. Three areas in southwest Sweden and one area in the northeast have been selected for this study. In these areas, locations with and without quick-clay have been identified by geotechnical sounding and sampling. Airborne electromagnetic (ATEM) measurements have been carried out in all four areas. The preliminary results from the first two areas, which are presented in this paper, show a reasonable correlation between the different methods used.

38.1 Introduction

Currently, the only reliable method for the detection of quick clay is to collect undisturbed samples and to perform laboratory fall-cone tests. Mapping of quick clays in this way requires extensive sampling at significant expense. There are

H. Löfroth (✉) • K. Lundström • J. Hedfors • D. Schälin
Swedish Geotechnical Institute (SGI), Linköping, Sweden
e-mail: hjordis.lofroth@swedgeo.se; karin.lundstrom@swedgeo.se; jim.hedfors@swedgeo.se; david.schalin@swedgeo.se

L. Persson • M. Bastani • C.A. Smith
Geological Survey of Sweden (SGU), Uppsala, Sweden
e-mail: lena.persson@sgu.se; mehrdad.bastani@sgu.se; colby.smith@sgu.se

J. Ekström
Swedish Transport Administration, Borlänge, Sweden
e-mail: jan.ekstrom@trafikverket.se

V. Thakur et al. (eds.), *Landslides in Sensitive Clays*, Advances in Natural and Technological Hazards Research 46, DOI 10.1007/978-3-319-56487-6_38

several indirect methods that have previously been used, for instance conventional sounding methods, cone penetration test (CPTU) with additional measurement of total penetration force, surface resistivity measurements (electrical resistivity tomography, ERT), down-hole measurements with resistivity probe (cone penetration test with resistivity module, CPTU-R) and vane testing. None of these methods detect quick clay, but they give information on the likelihood of quick clay occurrence. Therefore, they have to be supplemented by sampling, but if the indirect methods are performed and planned in a proper way, then the number of samples and associated expense may be reduced. Several authors have tested and compared different methods (Rankka et al. 2004; Solberg et al. 2008; Lundström et al. 2009; Rømoen et al. 2010; Löfroth et al. 2011; Dahlin et al. 2013, 2014; Pfaffhuber et al. 2014; Sandven et al. 2015). From these tests it can be concluded that: (1) the total penetration force is a useful tool for quick clay assessment and should be recorded when using CPTU and CPTU-R, (2) electrical resistivity (ERT and CPTU-R) can be used to differentiate between leached and unleached marine clays; and (3) that there is generally good agreement between the models derived from surface resistivity measurements and CPTU-Rs.

Recently, airborne electromagnetic measurements (ATEM) have been tested for quick clay mapping in a few places (Anschütz et al. 2014; Sandven et al. 2015). The method shows promising results, but the experiences are limited. Thus, the method requires further evaluation.

Different threshold values for resistivity of leached clays have been reported. Rankka et al. (2004) and Rømoen et al. (2010) introduce 5 Ωm as the lower threshold for resistivity of quick clays. Resistivity limits from other studies summarized by Solberg et al. (2010) ranges between 5 and 20 Ωm. The reason for the discrepancy in the lower limit value is not fully understood.

Most quick clays have been formed from glaciomarine sediments deposited during the last deglaciation. Information relating to the location of such sediments is therefore valuable in mapping quick clay. Other useful information about the occurrence of quick clay is the identification of areas where scarps from quick clay slides are present.

Different methods for quick clay mapping should be used and combined in a stepwise procedure. One example of such a procedure is presented in this paper together with results and evaluations of several methods, including airborne electromagnetic measurements acquired at test sites in Sweden.

38.2 Method

Based on the scale and extent of investigations, different levels of detail for mapping the possible presence of quick clay can be obtained by using different methods. Overview methods such as studies of topography and geology can cover broad areas but with limited detail. Geophysical surveys provide higher resolution data over

more limited areas. Geotechnical soundings and sampling provide the most accuracy but must be limited due to high costs.

Some of these methods used for mapping the possible presence of quick clay, e.g. sampling, are well established in Sweden. Other methods, for example airborne geophysical measurements, have only been tested to a limited extent outside Sweden. To develop guidelines for the use of different methods, their reliability and applicability must be examined both individually and in combination. This is done via comparison of the results of relatively unproven methods with results from the well-established ones, especially geotechnical sounding and sampling. Therefore, four test sites have been chosen for comparison of geological and geophysical methods with geotechnical methods, of which two are presented in this paper. Different geological conditions and the presence of both quick clay and non-quick clay are the main criteria for choosing the test sites. The test sites cover areas with different stratigraphies, for example clay layers of different thicknesses, clay with interbedded silt and sand layers, and clay layers close to bedrock outcrops. The test sites and the methods so far considered are described in this paper.

38.2.1 Visualization

The results from different methods together with background data have been integrated using GIS tools to allow for effective comparison and visualization. For the test sites, both the background data and the data collected in this study have been gathered in spatial databases for use in the evaluation of the different methods. Background data consists of surface elevation, position of the highest postglacial coast line, Quaternary deposits, bedrock outcrops, landslide scars and gullies (www.geodata.se). Both archived and present geotechnical soundings and sampling from the test sites have been compiled and utilized in the GIS application. From each sampling location, the highest sensitivity in each boring has been classified, see Fig. 38.1. Geotechnical investigations with borehole data have been geographically linked, hence providing instant and localized information via interactive maps. Figure 38.1 shows an example of such compilation.

38.2.2 Test Sites

The greatest occurrence of quick clay in Sweden is in the south-western part and therefore three test areas; Strömstad, Slumpån and Lödöse (see Fig. 38.2), have been selected in this region. A fourth test site, Torsåker, is situated in mid-Sweden along the east coast, where quick clays are rarer but still found in some places.

The Lödöse and Slumpån test sites are situated in the Göta River valley, about 30 km and 60 km north of Gothenburg, respectively. The valley has the highest frequency of landslides in Sweden, and most of them have occurred in quick clay.

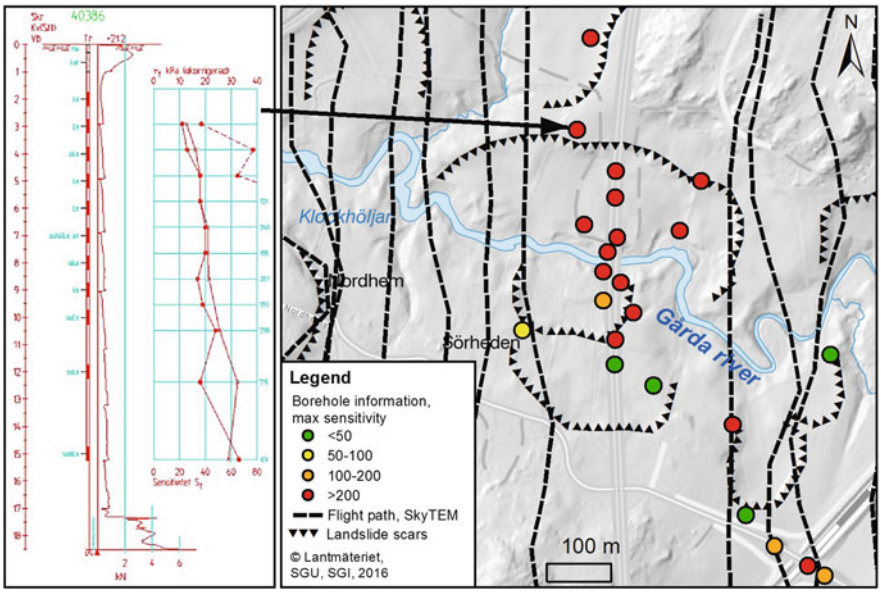

Fig. 38.1 Example of visualization of background data using the GIS application, including a shaded-relief background, the location of geotechnical boreholes, the estimated maximum sensitivities in each borehole and the results of soundings and laboratory tests in one borehole. The selected area is a part of the Lödöse test site

The northeastern part of the Lödöse test site is characterized by the stream Gårdaån (see Fig. 38.1 for location) along which scarps of minor landslides and erosional processes are found. The middle and southern parts consist of large, flat farmlands with some bedrock outcrops. The depth to firm bottom (till or bedrock) varies between 15 to over 45 m. The shear strength of the clay varies between 10 and 40 kPa. Highly sensitive clays are frequent and have previously been found in the northern and eastern parts of the area, while only clays with low sensitivities have been found in the western and southern parts (see Fig. 38.2).

The Slumpån study area is characterized by ravines and scarps of major and minor landslides. In the area, a 1–5 m thick layer of sand is interbedded between two clay layers. The depth to firm bottom varies between 15 and 45 m. Highly sensitive clays have previously been found on both sides of the stream Slumpån and the Göta River (Rankka et al. 2004; Löfroth et al. 2011; SGI 2012).

38.2.3 Geological and Topographical Methods

A map showing areas in Sweden that have been covered by salt- or brackish water during different periods has been produced (Schoning 2016). The map has been

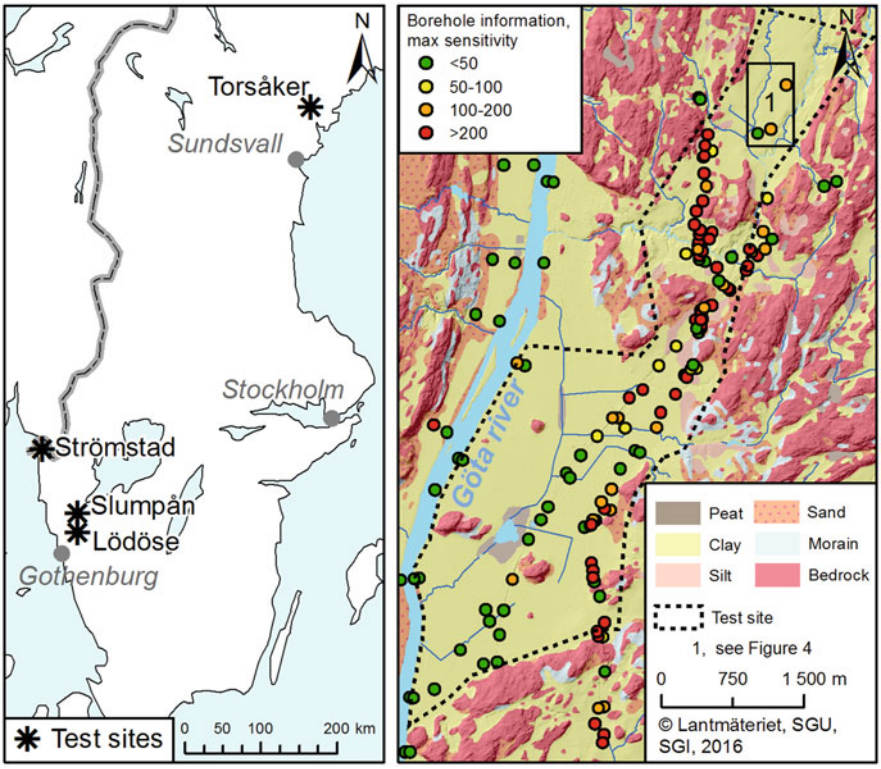

Fig. 38.2 Test sites (*left*). Lödöse test site including sampling points with sensitivity classification (*right*). The *small rectangle* marked (1) refers to the area described in the results section

modified so that only areas with a high sedimentation rate are included. Such sedimentation regimes are expected to be essential for quick clay formation. Also areas where the soil thickness is expected to be small, and thus the consequences of a potential slide are small, have been withdrawn from the map. Areas in Sweden with geological prerequisites for quick clay formation are given in Fig. 38.3.

A map showing probable quick clay slides has been produced (see Melchiorre et al. 2014) based on high resolution topographical data and a database with around 1,800 landslide scarps. Landslide scarps were classified in four types: wide, equidimensional, elongate, and bottle-neck, denominated by crater type 1, 2, 3, and 4, respectively. Based on the results, crater types 3 and 4 are suggested to be used as indicators of highly sensitive/quick clay and a majority of these scarps are located in the southwestern part of Sweden. Results from the classification in a part of the Slumpån test area are presented in Fig. 38.3.

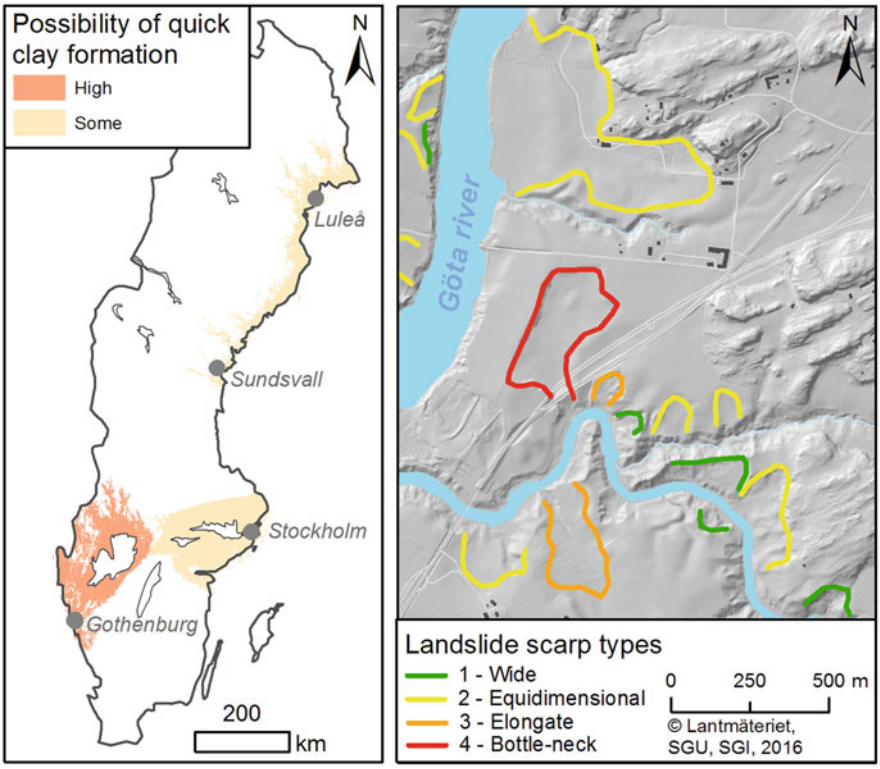

Fig. 38.3 Map (*left*), showing areas with geological prerequisites for quick clay formation (Schoning 2016). Classification of landslide scarps in the test area Slumpån (*right*)

38.2.4 Geophysical Methods

The ground based geophysical method that is most commonly used in Sweden for mapping of areas prone to quick clay is electrical resistivity tomography (ERT). At the Lödöse test site ERT measurements were carried out using an ABEM Terrameter LS instrument. The gradient electrode configuration with a minimum electrode separation of 5 m was used. At the Slumpån test site the ERT measurements were carried out in 2010 as a study within the Göta River investigation (Löfroth et al. 2011; Dahlin et al. 2013).

Measurements with ATEM were carried out covering all four test sites with a distance between flight lines of 75 m. The SkyTEM helicopter borne measurement system (Sørensen and Auken 2004) was used. The measurements are carried out 30–50 m above the ground with a transmitter loop and a receiver coil hanging below the helicopter. In the transmitting loop a strong current is sent out regularly. When the current in the transmitter is turned off, a current is induced in the ground and is spread downwards and outwards. The induced current generates a secondary

magnetic field that is measured by the receiver coil. The amplitude and decay rate of the magnetic field depends on the amplitude of the primary field and resistivity of the ground below the measurement point.

38.2.5 Geotechnical Methods

The relationship between the undisturbed and remoulded undrained shear strength is designated sensitivity. In Sweden, a quick clay is defined as a clay with a sensitivity St >50 and a remoulded undrained shear strength τ_R <0.4 kPa. The sensitivity is determined on undisturbed samples by fall-cone tests in the laboratory.

An indirect method for assessing the presence of quick clay is by measurement of the total penetration resistance with different types of geotechnical soundings (Möller and Bergdahl 1982; Rankka et al. 2004; Sandven et al. 2012). The principle is that the measured penetration resistance complemented by the weight of the rods and, for the CPTU, reduced by the tip resistance, corresponds to the rod friction (in kN). An almost vertical pushing force – depth curve generally indicates high sensitivity clay (Rankka et al. 2004). A correlation based on 1 kPa rod friction for mapping of quick clay has been verified for the two most widely used sounding methods in soft soil in Sweden; cone penetration test (CPTU) and static pressure sounding (Löfroth et al. 2012; SGI 2012; Åhnberg et al. 2014).

At the test sites, results from previous CPTU and static pressure soundings are used together with sampling for comparison to geophysical results. CPTU-R and sampling have so far been carried out at the Lödöse test site. At the Slumpån test site CPTU-R soundings were carried out in 2010 (Löfroth et al. 2012).

38.3 Results

All four test sites are located in areas with geological prerequisites for quick clay formation. Analysis of landslide scarps shows that landslides classified as crater types 3 and 4 (indicating highly sensitive or quick clay) only are found in one test area; Slumpån. Results from ATEM at Lödöse and Slumpån show that both leached clay (a prerequisite for quick clay formation) and unleached clay are present at both test sites. Results from geotechnical soundings and sampling reveal that high sensitive clay and quick clay as well as low sensitivity clay are present at all four test sites.

Comparisons between resistivity models from ATEM data and geotechnical data have been conducted at the Lödöse test site. Along eight flight lines the ATEM results are compared with the existing geotechnical samplings and soundings. Along four other flight lines new sampling and CPTU-R soundings were carried out for comparison. The agreement between ATEM models and geotechnical data is rather good. Soundings/samplings showing non-quick clay (St < 30) (example shown in

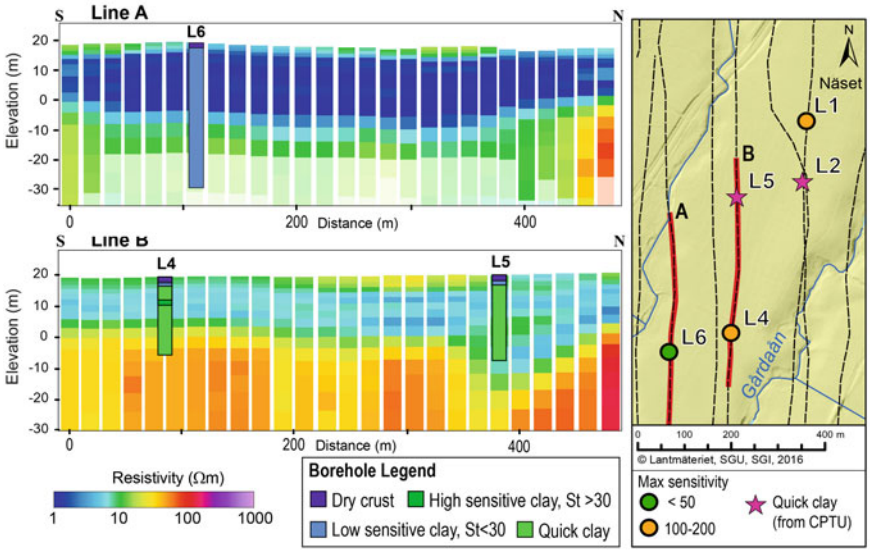

Fig. 38.4 Two examples of resistivity models from ATEM data. On *top* of the model the measured sensitivities from geotechnical data are shown for comparison. Locations of *flight lines* and geotechnical boreholes are shown in the *right* frame. The location of this area is presented in Fig. 38.2

the top frame in Fig. 38.4) are situated in areas with very low resistivity (<1 Ωm) and the soundings/samplings with quick and high sensitivity clay can be found in areas with higher resistivity (example shown in the bottom frame in Fig. 38.4). However, the depth sensing of the ATEM is limited in areas with thick sequences of very low resistivity clay (unleached clay). This can be seen as a successive increase in resistivity with depth, as shown in Fig. 38.4. This is not observed in the geotechnical data as increased sensitivity. Similarly, there is a successive increase in resistivity close to bedrock outcrops. The ERT measurements show a similar increase in the resistivity with depth as ATEM.

Resistivity measurements from ATEM, ERT and CPTU-R in the northern part of Lödöse show good agreement although ATEM and ERT show higher increases in resistivity with depth than CPTU-R. Results from sampling and penetration resistance from CPTU-R show that quick clay may be found in areas with resistivity even lower than 5 Ωm (see Fig. 38.5).

The results from three ATEM flight lines at the Slumpån test site have been compared with geotechnical data. Also at this test site there are areas with thick clay layers. However, the resistivity within these layers is more varied, which complicates the interpretation. A detailed analysis of these ATEM flight lines is presented in Bastani et al. (in preparation).

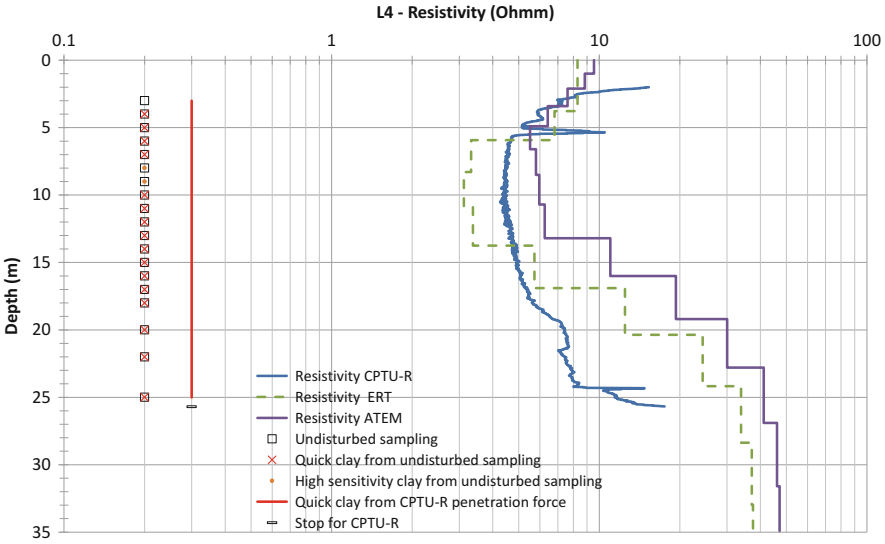

Fig. 38.5 Resistivity models by ATEM, ERT and CPTU-R at point L4 together with sensitivity determined by fall-cone tests and quick clay from CPTU penetration force

38.4 Discussion

Geological and topographical information used as layers in GIS maps (see Fig. 38.3) are important tools to identify areas where quick clay could be present. However, the results show that analysis of landslides by just using scarps may underestimate the occurrence of quick clay, as at the Lödöse test site. Landslide scarps indicating no quick clay are present adjacent to locations where quick clays are found by geotechnical sampling.

Geophysical models from ATEM and ERT measurements show reasonable agreement with geotechnical data, but there are limitations. The limited depth penetration in areas with thick layers of unleached, low resistivity clay, and limited resolution in areas adjacent to bedrock outcrops, makes evaluation of quick clay occurrence difficult. In Sweden, quick clay is often encountered close to bedrock outcrops. The quick clay layer with very low resistivity (<5 Ωm) found in the northern part of the Lödöse test site indicates that a lower limit in resistivity for possible quick clay has to be established locally rather than forming general rules.

38.5 Conclusions

A step-wise procedure to map quick clay should be based on topographical, geological, hydrological, geophysical and geotechnical prerequisites. The procedure will be adapted to different phases in the societal planning process. Initially, basic

geological information can rapidly give an indication if quick clay could be present in an area/region intended for development. In the early planning stages, use of more regional (smaller scale) geophysical methods can indicate if the prerequisites for the presence of quick clay exist in an area. In the later planning stages, quick clay occurrence should be verified by more detailed geotechnical investigations. The results from the early planning stage may reduce the costs of the detailed planning stage.

Acknowledgements The project is financed by the Swedish Civil Contingencies Agency (MSB) and it is carried out in cooperation between the Swedish Transport Administration (STA), the Swedish Geotechnical Institute (SGI) and the Geological Survey of Sweden (SGU). The reviewing of the manuscript by Kristian Aunaas, Norwegian Public Road Administration, is gratefully acknowledged.

References

Åhnberg H, Löfroth H, Lundström K (2014) Management of quick clay areas in slope stability investigations – the Göta River valley. Advances in Natural and Technological Hazards Research; 36. Landslides in sensitive clays. From geosciences to risk management, Springer, Dordrecht, pp 383–394

Anschütz H, Bazin S, Pfaffhuber, AA (2014) AEM method description & project examples. Norwegian Geotechnical Institute, Report 20130058-02-R_ENG. Oslo

Bastani M, Persson L, Löfroth H, Smith CA, Schälin D (in preparation) Analysis and comparison of ground geophysical, airborne TEM, and geotechnical data for recognition and modeling of quick clay areas in Sweden. IWLSC 2017

Dahlin T, Löfroth H, Schälin D, Suer P (2013) Mapping of quick clay using geoelectrical imaging and CPTU- resistivity. Near Surface Geophysics 11(6):659–670

Dahlin T, Schälin D, Tornborg J (2014) Mapping of quick clay by ERT and CPT-R in the Göta River Valley. Advances in Natural and Technological Hazards Research, vol 36. Landslides in sensitive clays. From geosciences to risk management. Springer

Löfroth H, Suer P, Dahlin T, Leroux V, Schälin D (2011) Quick clay mapping by resistivity – Surface resistivity, CPTU-R and chemistry to complement other geotechnical sounding and sampling. Swedish Geotechnical Institute, SGI. The Göta River Investigation. Subreport 30

Löfroth H, Suer P, Schälin D, Dahlin T, Leroux V (2012) Mapping of quick clay using sounding methods and resistivity in the Göta River valley. International conference on geotechnical and geophysical site characterization, 4, Porto de Galinhas, Brazil, 18–21 September, 2012. Proceedings, vol 2, pp 1001–1008

Lundström K, Larsson R, Dahlin T (2009) Mapping of quick clay formations using geotechnical and geophysical methods. Landslides 6:1

Melchiorre C, Smith C, Rodhe L (2014) Analysis of landslide scarp data, Sweden. Geological survey of Sweden, Report dnr: 315-1895/2014. Uppsala

Möller B, Bergdahl U (1982) Estimation of the sensitivity of soft clays from static and weight sounding tests. European symposium on penetration testing, 2, ESOPT2. Proceedings, vol 1, pp 291–295

Pfaffhuber A, Bazin S, Helle TE (2014) An integrated approach to quick-clay mapping based on resistivity measurements and geotechnical investigations. Advances m Natural and Technological Hazards Research, vol 36. Landslides in sensitive clays. From geosciences to risk management. Springer, Dordrecht

Rankka K, Andersson-Sköld Y, Hultén C, Larsson R, Leroux V, Dahlin T (2004). Quick clay in Sweden. Swedish Geotechnical Institute, SGI. Report 65. Linköping

Rømoen M, Pfaffhuber AA, Karlsrud K, Helle, T (2010). Resistivity on marine sediments retrieved from RCPTU-soundings: a Norwegian case study. International symposium on cone penetration testing, 2, CPT'10, Huntington Beach CA. PRO 2, pp 289–296

Sandven R, Montafia A, Gylland A, Kåsin K, Pfaffhuber A, Long M (2015) Detection of brittle materials. Summary report with recommendations. Final report. NPRA, NNRA, NWRED, doc code 415559-RIG-RAP-004. Report 126/2015

Sandven R,Vik A, Rønning S, Tørum E, Christensen S, Gylland A (2012) Detektering av kvikkleire fra ulike sonderingsmetoder. NIFS Report 46/2012. Oslo

Schoning K (2016) Saltvattenavsatta leror i Sverige med potential för att bilda kvicklera. Geological survey of Sweden. Report 2016:08. Uppsala

SGI (2012) Landslide risks in the Göta river valley in a changing climate. Swedish Geotechnical Institute, SGI. The Göta river investigation, GÄU. Final report. Part 2 – Mapping

Solberg IL, Hansen L, Rönning JS, Dalsegg E (2010) Veileder for bruk av resistivitetsmålinger i potentielle kvikkleireområder. Geological Survey of Norway. Report 2010.048

Solberg IL, Ronning JS, Dalsegg E, Hansen L, Rokoengen K, Sandven R (2008) Resistivity measurements as a tool for outlining quick clay extent and valley fill stratigraphy: a feasibility study from Buvik, Central Norway. Can Geotech J 45:210

Chapter 39
Helicopter Electromagnetic Scanning as a First Step in Regional Quick Clay Mapping

Asgeir Lysdahl, Andreas Aspmo Pfaffhuber, Helgard Anschütz, Kristoffer Kåsin, and Sara Bazin

Abstract Identification of sediment types and in particular delineation of leached, possibly sensitive marine clays is of crucial importance for geotechnical design of infrastructure projects in Norway. Since leached clays normally have a lower salt content than intact marine clays, the electrical resistivity is consequently higher, and thus clay characterization may be based on data from high-resolution airborne electromagnetics (AEM) collected from helicopter. However, the resistivity difference between leached and unleached clays is small compared to the transition to bedrock and may furthermore vary locally. Therefore, indication of leached clays based on resistivity data has so far been done by manual interpretation. Here, we present a new procedure to calculate the likelihood of possible sensitive clays directly from AEM data. Geotechnical ground investigations are used to locally determine the expected resistivity of sensitive clay. The computation results are compared with well-known quick clay zones. The procedure is not intended as a simple solution to delineate quick clay, but to evaluate an area's likelihood of sensitive clays that can be used as a cost-saving tool to efficiently place geotechnical investigations.

39.1 Introduction

Sensitive or quick clays are typically found in Norway, Sweden and Canada, and are characterized by a remoulded undrained shear strength that is considerably lower (less than 0.5 kPa by definition) than their undisturbed shear strength. Fresh water leaching of the marine clays has washed out the salt ions in the crystal structure, dramatically weakening the chemical bonds in the clay minerals. Consequently, a physical disturbance may initiate a breakdown of the crystal structures turning the clay into a fluid. As leached and possibly sensitive clays in general have a lower salt content than intact marine clays, they can be distinguished by measuring

A. Lysdahl • A.A. Pfaffhuber • H. Anschütz • K. Kåsin • S. Bazin (✉)
Norwegian Geotechnical Institute (NGI), Oslo, Norway
e-mail: Asgeir.Olaf.Kydland.Lysdahl@ngi.no; andreas.a.pfaffhuber@ngi.no; helgard.anschuetz@ngi.no; kristoffer.kaasin@ngi.no; sara.bazin@ngi.no

V. Thakur et al. (eds.), *Landslides in Sensitive Clays*, Advances in Natural and Technological Hazards Research 46, DOI 10.1007/978-3-319-56487-6_39

their electrical resistivity (the inverse of the electrical conductivity). This has been successfully done in several ground based geoelectrical (ERT/DC) surveys in the past years in especially Norway and Sweden (Bazin and Pfaffhuber 2013; Donohue et al. 2012, Lundström et al. 2009; Löfroth et al. 2012; Rømoen et al. 2010; Sauvin et al. 2013; Solberg et al. 2012). Using AEM data covering large areas would potentially be an outstanding planning tool (Pfaffhuber 2015). Since the resistivity is not only dependent on the pore fluid salt content, but also on other parameters such as the water saturation, the grain size distribution, the mineralogy and the pore fluid chemistry, it is firstly important to know the expected resistivity value of identified sensitive clay in the particular area, as it may vary both regionally and locally. This is achieved by performing in-situ R-CPTU soundings and/or laboratory resistivity measurement of quick clay samples. For example, quick clays in Trøndelag in Mid-Norway have a resistivity around 40 Ωm while quick clays in Vestfold, Southern Norway have values around 20 Ωm (both with large local variations). Unleached marine clays have normally resistivities between 1 and 10 Ωm. Secondly, one must ensure that the geophysical measurement is able to image resistivity with satisfactory accuracy (i.e. without systematic errors). For the latter, it has lately been demonstrated that both ground based ERT and AEM could quantify the electrical resistivity of a known sensitive clay body in south-eastern Norway with great accuracy (Anschütz et al. 2015). The AEM model was shown to resolve the resistivity values almost as good as the ERT model, given that AEM data were acquired with a modern, high resolution time-domain AEM system. Baranwal et al. (2015) reported opposite findings using a traditional frequency-domain AEM device. Recently, a time-domain system has been successfully used to map quick clay in the Lödöse area in western Sweden (Persson et al. 2016). Finally, it should be stressed that many different materials (rocks and soils) may have the same resistivity as that of quick clay. It is therefore important to have an understanding of what kind of geology and sediments are expected in the area and how they would respond to electromagnetic measurements.

39.2 Field Data

Two AEM-surveys from commercial infrastructure projects in Norway have been analysed during the method development, one from Trøndelag between Ranheim and Hommelvik, and one from Vestfold between Tønsberg and Larvik. Both datasets were acquired using the SkyTEM 304 system (Sørensen and Auken 2004). The line spacing was approximately 100 m and data processing and inversion was performed in Aarhus Workbench resulting in a 25-layer spatially constrained 3D resistivity model. A large number of total soundings was available for both projects, and a few R-CPTU-soundings were available for the Vestfold survey. Only the resistivity measurements of sediment layers should be considered for the analysis. It was therefore important to initially interpret a bedrock surface from AEM-data and geotechnical drillings and select only the AEM model cells situated above this surface (Anschütz et al. 2016), thereby resembling a soil resistivity model.

39.3 Method

The idea behind the methodology is to obtain the probability for the sediment being sensitive clay given a measured resistivity value. For that, a probability distribution for the expected resistivity of quick clay is needed. Figure 39.1 shows two examples of co-located total soundings and R-CPTU logs from Vestfold. Possible sensitive clay has been interpreted from the total sounding (black line) and is indicated with a brown background colour. The clay at location VSS13017 (left) is quick/very sensitive, whereas the clay in VSS16016 (right) is sensitive, possibly quick. The R-CPTU curve is composed of numerous single measurements (every 1 cm in depth) and shows the corresponding resistivity values. In Table 39.1, the values from the quick clay sections have been extracted and averaged for every borehole location. The corresponding standard deviation is also calculated. All the resulting resistivity means lie within the expected range for sensitive clays (10–80 Ωm), except for one location where the mean resistivity is 8.2 Ωm.

In order to assess the probability distribution of the resistivity of quick clay in the area, a histogram (Fig. 39.2) is generated from all the individual R-CPTU measurements (not averaged). The abscissa shows bins of the logarithm of the resistivity in steps of 0.025, and the ordinate shows number of measurements within

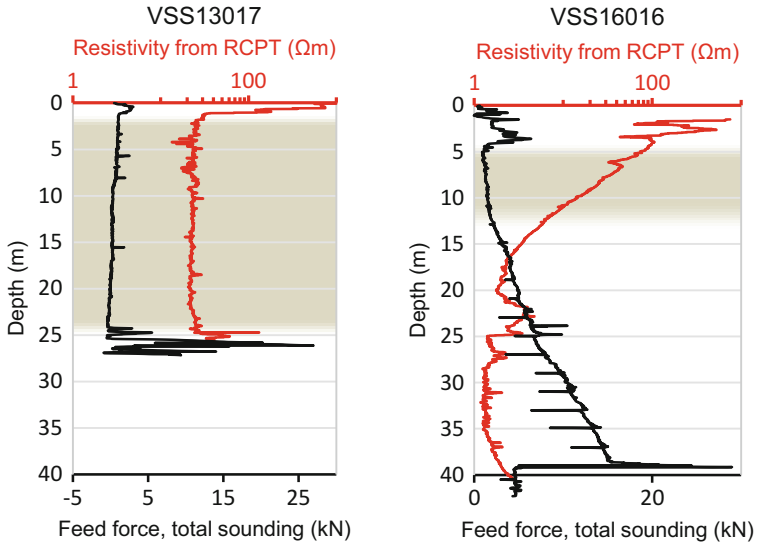

Fig. 39.1 Total sounding (*black*) and R-CPTU (*red*) logs at two locations in Vestfold. At VSS13017 (*left*), a top layer of dry crust covers a thick layer of very sensitive clay (*shaded layer*), until bedrock starts at 25 m depth. The resistivity values lie around 20 Ωm in the sensitive clay, and are higher in the crust and towards the bedrock. In VSS16016 (*right*), possibly sensitive clay is interpreted from 5 to 12 m depth, below that intact marine clay is found. Measured resistivity values within the sensitive clay layer ranges from 10 to 100 Ωm, which could indicate increasing water saturation and/or a gradual increase of the salt content with depth. The recorded values in the intact marine clay are very low, as expected

Table 39.1 Resistivity from R-CPTU measurements averaged over depth intervals interpreted as sensitive clay

Location-ID	Thickness sensitive clays (m)	Mean resistivity (Ωm)	Standard deviation (Ωm)
VSS11001	24.5	41.1	1.26
VSS11002	25.0	24.4	1.26
VSS11004	20.0	21.5	1.29
VSS11006	7.0	8.2	1.69
VSS11008	10.5	17.8	1.18
VSS11009	10.0	35.9	1.31
VSS13016	30.0	12.5	1.34
VSS13017	22.5	23.0	1.09
VSS13018	9.5	16.1	1.24
VSS16016	6.5	25.0	1.83

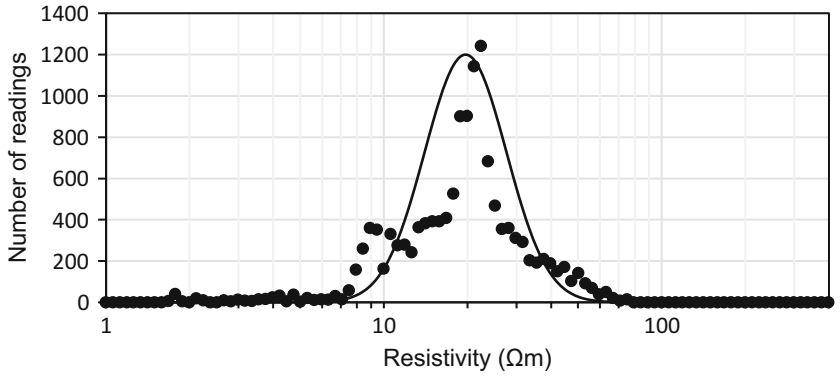

Fig. 39.2 Distribution of R-CPTU measurements in sensitive clays, Vestfold. The Gaussian curve fit has a mean of 19.7 Ωm and a standard deviation of 1.4 Ωm

each bin. The resistivity distribution is almost lognormal, with some discrepancies (the readings from VSS11006 stand out in the range 8–10 Ωm). This is as expected, since the readings are not independent events (many of them belong to a common borehole). The lognormal distribution was verified to be the best fitting probability distribution using the program EasyFit 5.2.

The resistivity means and standard deviations listed in Table 39.1 thus defines the expected resistivity of sensitive clay at the respective drilling locations. From these, inverse distance interpolation is used to assign an expectation value $\overline{\rho}$ and a standard deviation σ to each AEM sounding point in the survey area. The probability PN_l for a particular AEM-cell in an AEM-layer l to be sensitive clay based on its resistivity value is then assumed to be lognormal distributed around $\overline{\rho}$

$$PN_l = e^{-\frac{1}{2}\left(\frac{\log(\rho_l)-\log(\overline{\rho})}{\log(\sigma)}\right)^2}$$

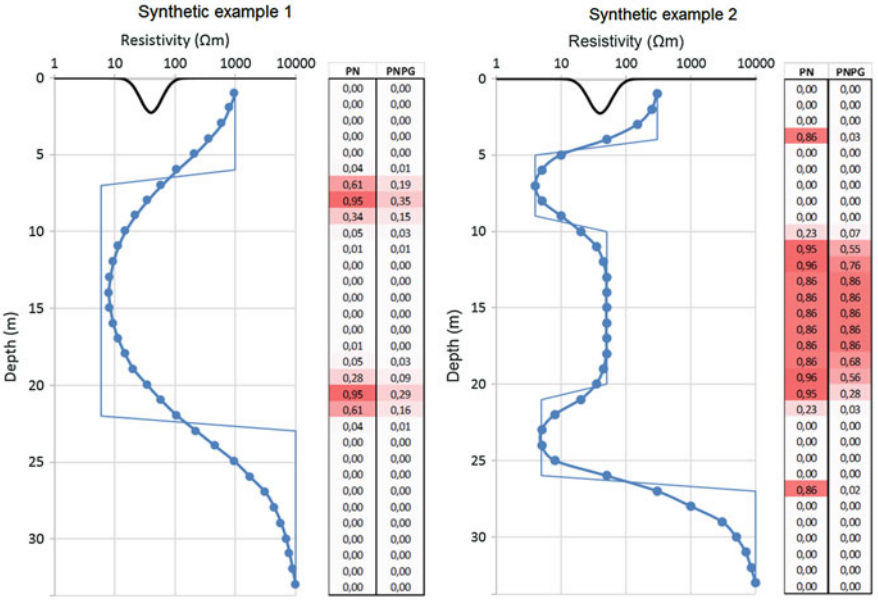

Fig. 39.3 Examples of two possible ground resistivity profiles and calculated probabilities. *Solid, blue line* represents the true resistivity values of an exemplary ground model. The *dotted line* shows a possible AEM model which smoothens out the boundaries. The table to the right shows calculated PN and PNPG respectively for each layer in the AEM model. The *black line* in the upper part of the graph shows a possible resistivity range for sensitive clay (for this curve only, the ordinate denotes probability)

Here, ρ_l is the resistivity of the AEM-cell. PN_l is not normalized and gives a number between 0 and 1.

AEM models are intrinsically smooth, which means that large discrete steps in resistivity values between layers are not allowed. As a consequence, an abrupt transition from high-resistive bedrock (∼1,000 Ωm) to conductive marine clay (∼1 Ωm) will be forced to pass through values that lie within the range for sensitive clays (20–40 Ohm). This is shown in a sketch in Fig. 39.3. The solid line represents the true resistivity profile of an exemplary ground model, whereas the dotted line represents the resistivity profile extracted from a typical AEM model obtained by inversion of the same ground model. The black line in the upper part of the graph shows a possible resistivity range for sensitive clay (This curve's vertical axis shows probability). According to the "true" resistivity model, no sensitive clay should be expected, but for the smoothened AEM model, several of the points lies within the range for sensitive clay. Assigning a high probability for sensitive clay for these points would be unjustified. Therefore, we calculate a correction factor PG_l that reduces the probability in case the gradient to the next AEM layer is large:

$$PG_l = e^{-g\left|\log\left(\rho_{l+1}\right)-\log\left(\rho_l\right)\right|}$$

Here, ρ_{l+1} og ρ_l are the resistivity values in layer $l+1$ and l respectively, and g is an experimentally found weighting factor. PG_l also gives a number between 0 and 1.

Lastly, the assumed probability for leached and possibly sensitive clay in layer l at a certain AEM sounding point becomes:

$$P_l = PN_l\, PG_l = e^{-\frac{1}{2}\left(\frac{\log(\rho_l)-\log(\bar{\rho})}{\log(\sigma)}\right)^2 - g\left|\log\left(\rho_{l+1}\right)-\log(\rho_l)\right|}$$

The effect of the gradient correction is shown in the table right of Fig. 39.3, where PN and P = PNPG is calculated for every layer. It can be seen that the points closest to a boundary are assigned a high probability with PN, but get a substantially lower probability with PNPG.

To the right in Fig. 39.3 another example is shown where the ground model also contains a layer of sensitive clay. The layer is ten meters thick, so that the AEM model can be assumed to give stable and consistent values throughout the layer. Consequently, PNPG gives meaningful probability values, and the "gradient effects" from PN are removed.

39.4 Results and Discussion

Figure 39.4 shows the results from PN and PNPG for one of the Vestfold flightlines crossing a well-studied quick clay zone. The model section is cropped at depth where the interpreted bedrock surface is situated. It should be noted that the method was developed and the weighting factor g was fixed before this particular profile was studied. The resistivity model is shown in the upper image. The relatively high resistivity values observed right below the surface indicate dry, drained soil on the field and fresh water in the river. Below the river bed there is likely marine clay. The smoothened transition to bedrock (increasing values) can be seen towards the bottom of the section. A relatively large zone of resistivity values around 10–20 Ωm is observed in the middle of the profile. This could indicate sensitive clay. The uncorrected automatic probability calculation PN classifies all cells with 10–20 Ωm as possible sensitive clay, while PNPG removes the gradient effects at the crust and the bedrock interface and correctly resembles the manual interpretation described above. Interestingly, sensitive clay is identified between 10 and 20 m in drillings and samples taken in the vicinity at the field (not seen in Fig. 39.3), supporting the interpretation. The two geotechnical soundings in the river (green bars in Fig. 39.3) show depth to bedrock and do not reveal any sensitive clay.

The method assigns a probability value to every cell in 3D. In case a map showing areas of possible sensitive clay zones is needed, every cell belonging to a certain AEM sounding point can be concatenated into a single value in various ways. One way would be to add together the probability values for all depth layers and scale the sum with a constant value of dimension meter in order to obtain a thickness

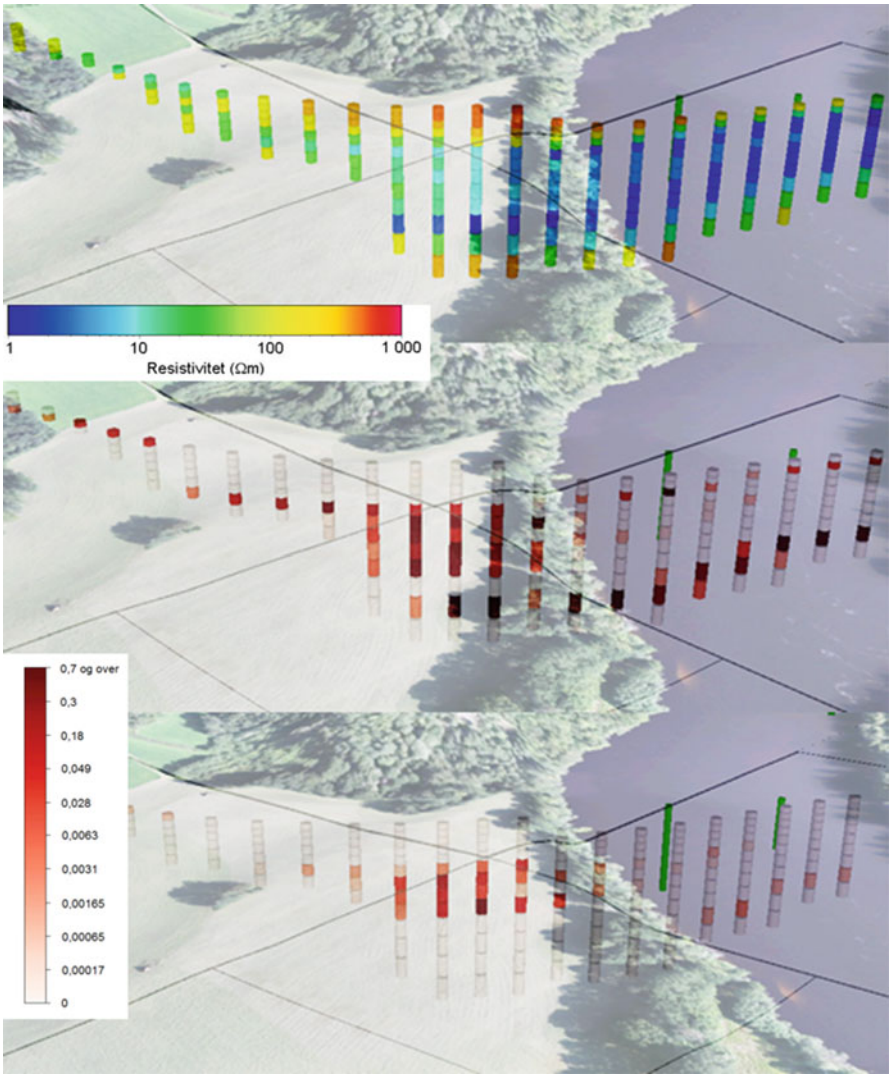

Fig. 39.4 One of the flightlines in the Vestfold area covering a known quick clay zone and a river towards the right side. Sensitive clay has previously been observed in the field between 10 and 20 m depth. The *upper* image shows the resistivity model which is cropped at depth at the interpreted bedrock surface. Here, 1–10 Ωm is interpreted as salty marine clay, 100–1,000 Ωm as dry crust or bedrock, whereas leached/sensitive clay is expected to lie right above 10 Ωm. The *middle* image shows PN calculated at every cell, and the *lower* image shows the gradient-corrected PNPG

estimation. An example of such an estimation is shown in Fig. 39.5. The background shows an elevation model, streams and lakes. The sea is situated directly south of the map. The estimation from AEM data fits well with existing zones and interpreted

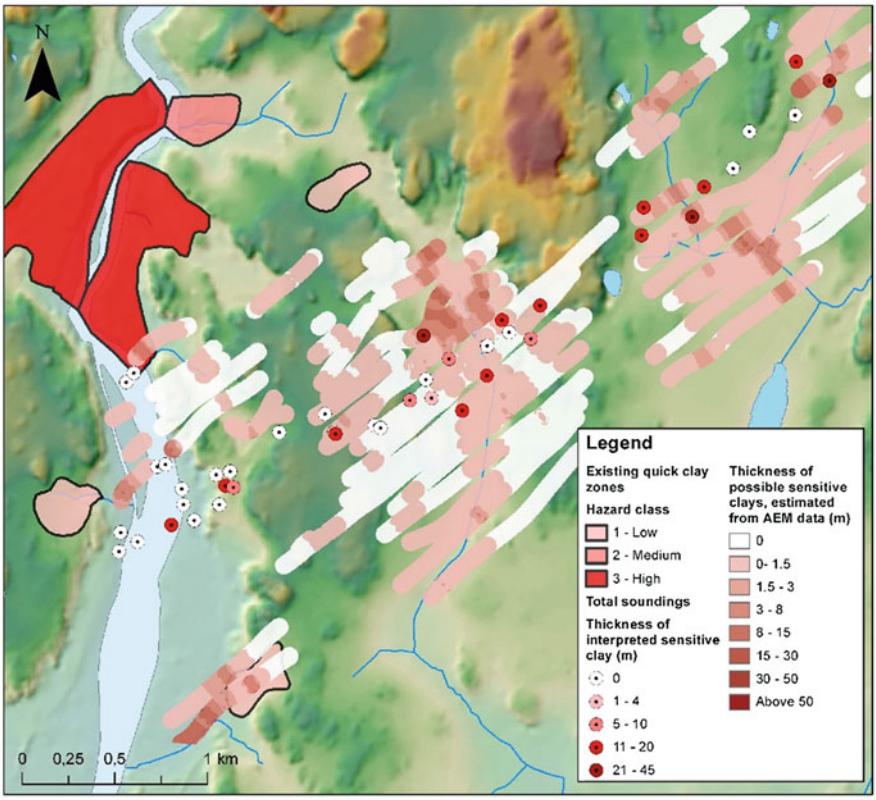

Fig. 39.5 Concatenation of 3D datapoints into a 2D map resulting in an estimate of the thickness of possible sensitive clays. Data is extrapolated up to 50 m away from AEM sounding points. The shown example area is in Vestfold. Note that the quick clay layer thicknesses given from the total soundings are only interpretations and are in general not verified by sampling. The one flightline crossing the tip of the north-western large quick clay zone is the one shown in Fig. 39.4

soundings with a few exceptions. Both AEM-data and boreholes suggests larger amounts of sensitive clay around the streams in the central and north-east area. The short flightline crossing the large quick clay zone in the north-west is the same as shown in Fig. 39.4.

Importing the 3D point cloud into a GIS environment enabled for 3D visualization offers great benefits: Firstly, the calculated values can be visually investigated in order to improve methods and optimize constants. Secondly, quaternary information can be used to further geo-code the resulting probabilities. For example, cells inside areas of fluvial deposits, which may have resistivity values in the same range as sensitive clays, can be assigned reduced or zero probability depending on the local conditions.

Finally, we would like to stress that although R-CPTU soundings have been used to locally specify the expected resistivity of sensitive clay, the spatial distribution

of probability values does solely come from the AEM model. The resulting 3D model and/or map should under no circumstances be considered as a detailed risk assessment but a planning base to refine the site investigation program. Resistivity remains only a proxy for the clay's mechanical properties.

39.5 Conclusions

Airborne EM data can be used to roughly evaluate possible sensitive clays on a regional scale given that the bedrock topography and the expected local resistivity of sensitive clay are known or can be reasonably well estimated. Total soundings and R-CPTU logs will greatly enhance the method's predictability. The proposed calculation procedure assumes a log-normal distribution of the clay's resistivity and applies an exponential gradient correction to reduce prediction errors caused by the smoothness-constrained inversion. Examples show that the obtained probability values are meaningful and agree with other ground investigation in many cases. We therefore consider the method as a cost-saving tool for early-phase regional project strategies and as a guideline for placing of more detailed ground investigations.

Acknowledgements The Norwegian National Rail Administration is acknowledged for the permission to publish the field data shown in this paper and for financing most of the reported developments. The authors would like to express their gratitude to Helge C. Smebye, Malte Vöge and Guillaume Sauvin for important contribution to the initial data processing phase, to Håkon Heyerdahl, Toril Wiig and Anne-Lise Berggren for valuable comments in the algorithm development phase and to the reviewer Thorleif Dahlin for his comments to this paper.

References

Anschütz H, Bazin S, Pfaffhuber A (2015) Towards using AEM for sensitive clay mapping-a case study from Norway. Paper presented at the First European Airborne Electromagnetics Conference, Torino, 6–10 September 2015

Anschütz H, Vöge M, Lysdahl AK, Bazin S, Sauvin G, Pfaffhuber AA, Berggren A-L (2016) From manual to automatic AEM bedrock mapping. J Environ Eng Geophy (in press)

Baranwal VC, Rønning JS, Solberg IL, Tønnesen JF (2015) Delineation of marine sediments in a landslide area in Norway using frequency domain helicopter-borne em and ground geophysical surveys. Symp Appl Geophys Eng Environ Probl 2015:90–94

Bazin S, Pfaffhuber AA (2013) Mapping of quick clay by electrical resistivity tomography under structural constraints. J Appl Geophys 98:280–287

Donohue S, Long M, O'Connor P, Helle TE, Pfaffhuber A, Rømoen M (2012) Multi-method geophysical mapping of quick clay. Near Surf Geophys 10(3):207–2019

Löfroth H, Suer P, Schälin D, Dahlin T, Leroux V (2012) Mapping of quick clay using sounding methods and resistivity in the Göta River valley. In: Proceedings of the 4th International Conference on Geotechnical and Geophysical Site Characterization (ISC'4), Porto de Galinhas, 15–18 September 2012

Lundström K, Larsson R, Dahlin T (2009) Mapping of quick clay formations by geotechnical and geophysical methods. Landslides 6:1–15

Persson L, Bastani M, Löfroth H, Smith CA (2016) Airborne TEM measurements used as reconnaissance tool for mapping areas with quick clay in Sweden. Presented at the 22nd European Meeting of Environmental and Engineering Geophysics, Barcelona, 4–8 September 2016

Pfaffhuber AA (2015) From colorful EM models to engineering facts: semi-automatic bedrock tracking and other geotechnical AEM challenges. Presented at the EAGE/DGG Workshop on Airborne Geophysics, Hannover, 27 March 2015

Rømoen M, Pfaffhuber AA, Karlsrud K, Helle TE (2010) Resistivity on marine sediments retrieved from R-CPTU soundings: a Norwegian case study. In: Abstracts of the 2nd International Symposium on Cone Penetration Testing (CPT'10), 5. September 2010

Sauvin G, Lecomte I, Bazin S, L'Heureux JS, Vanneste M, Solberg IL, Dalsegg E (2013) Towards geophysical and geotechnical integration for quick-clay mapping in Norway. Near Surf Geophys 11(6):613–623

Solberg IL, Hansen L, Rønning JS, Haugen ED, Dalsegg E, Tønnesen JF (2012) Combined geophysical and geotechnical approach to ground investigations and hazard zonation of a quick clay area, mid Norway. Bull Eng Geol Environ 71(1):119–133

Sørensen KI, Auken E (2004) SkyTEM – a new high-resolution helicopter transient electromagnetic system. Explor Geophys 35:191–199

Chapter 40
Developments in Mapping and Web Presentation of Fjord-Marine Deposit Distributions for Quick-Clay Related Work in Norway

Louise Hansen, Inger-Lise Solberg, A. Jarna, and Bo Nordahl

Abstract For several decades mapping of Quaternary geology has been the basis for quick-clay mapping in Norway. In this context it has been, and still is, of particular importance to define the distribution of fjord-marine deposits that commonly contain clays and silts where layers or pockets of quick clay may have developed. Quick clay may collapse under certain conditions and give rise to disastrous landsliding with severe consequences. It requires careful communication of Quaternary map information to get its full use for quick-clay mapping, landslide hazard assessment and other purposes. For this reason, there has been an increased focus in recent years at the Geological Survey of Norway (NGU) to improve existing web-based map services. This includes for example a National overview of the marine limit (ML) in Norway as the upper natural boundary for the occurrence of marine clays. In addition, a filtered version of Quaternary map information below ML has been added called clay-deposit susceptibility. This map service gives an overview over areas where clay deposits with some probability may be present even under other deposit types. The next step in the development of web services is to include information where the occurrence of fjord-marine clay deposits and quick clay are registered, for example, from drill-hole information. This is now made possible especially with the help of the newly established National Database of Ground investigations (NADAG) hosted by NGU.

40.1 Introduction

Sensitive clays, including quick clay, occur in many parts of Norway and comprise a serious threat to society, since quick-clay landslides happen almost on a yearly basis often with severe consequences (DSB 2013). To reduce this threat, a national quick-clay mapping program has been running since the early 1980s. The mapping, which

L. Hansen (✉) • I.-L. Solberg • A. Jarna • B. Nordahl
Geological Survey of Norway (NGU), Leiv Eirikssons vei 39, 7491, Trondheim, Norway
e-mail: louise.hansen@ngu.no; inger-lise.solberg@ngu.no; alexandra.jarna@ngu.no; bo.nordahl@ngu.no

V. Thakur et al. (eds.), *Landslides in Sensitive Clays*, Advances in Natural and Technological Hazards Research 46, DOI 10.1007/978-3-319-56487-6_40

is carried out by consultants, identifies zones where large, quick-clay landslides can potentially take place. These zones, in turn, are subjected to a hazard and risk classification as a basis for planning and mitigation work (Havnen et al. this volume). Public dissemination of hazard and risk zones is done through the web service https://atlas.nve.no hosted by the responsible governmental institution NVE (Norwegian Water Resource and Energy Directorate). Areas with quick-clay identified by the Norwegian Public Roads Administration have recently been included in the service. The information is crucial for planning purposes and to help protect life and property. The web presentations are accompanied by geological information provided by the web map services (WMS) by the Geological Survey of Norway. The Quaternary geological maps provide a general overview over where marine clays can be encountered in the Norwegian landscape. The map information is important because quick clay can be present also outside the identified quick-clay hazard zones, and even small landslides can be fatal. Several areas have not yet been mapped including scattered, marginal areas along fjords and coasts. Priorities for geological mapping are developed in collaboration with NVE who also provides financial support. The Quaternary geological maps from NGU are also used for other purposes in society from research to public planning and construction work. It is therefore important to communicate to decision-makers, engineers and other users about the full range of information that can be retrieved from geological maps from www.ngu.no. It is an important task for NGU to update and develop the geological, web-based services to maximize their use in society including quick-clay mapping and related work.

It is the purpose of the present paper to (1) present the Norwegian quick-clay problem in a geological perspective (2) give a brief overview over the main contents of Quaternary geological maps developed and produced by NGU, (3) explain their use for quick-clay mapping and issues associated to marine deposits, (4) present the most recent development of geological web services relevant for quick-clay issues, and (5) present suggestions for further development of web services and how to better include and make use of subsurface information (3D).

40.2 A Geological Perspective on the Quick-Clay Problem

The underlying cause for the presence of quick clay in Norway, Sweden and Canada is found in their recent geological histories. Scandinavia and North America were covered by thick ice sheets during the peak of the last Ice Age. When the glaciers melted back the glacially over-deepened fjords in Norway were flooded by the sea as the crust was still heavily suppressed by the load of glaciers. Melt water carried significant amounts of glacial rock flour that was deposited in the fjords as glacio-marine clays. Moraine material and glaciofluvial gravel were deposited under or at the margin of the glaciers (Fig. 40.1a). The highest level that the sea reached in any area following the Ice Age is called the marine limit (ML) and most often corresponds to the sea level right after deglaciation. The highest ML

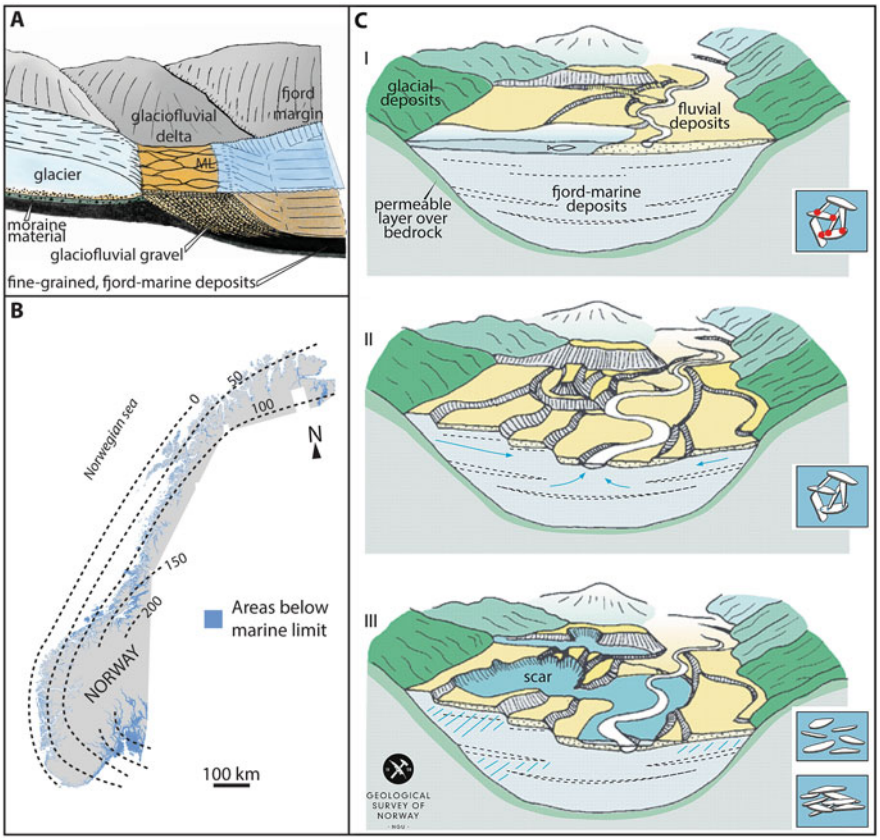

Fig. 40.1 (**a**) Sketch of a glaciofluvial delta deposited at the marine limit (ML) between a valley glacier and the fjord. (**b**) The ML isolines show generalized elevations of ML in Norway (shown numbers are in meters above present sea level). (**c**) Schematic landscape development after glacier retreat. (I) Fluvial deposition over fjord-marine clay deposits, locally with some coarser layers, (II) fluvial erosion during the emergence of land and leaching by groundwater (*blue arrows*) of salts from the clay, (III) quick-clay landsliding due to river erosion. Quick-clay pockets are hatched in *blue*. Changes in grain structure from the intact and leached clay to remolded clay are indicated. ((**a**, **b**) are modified from Hansen et al. (2014). (**c**) is modified from Sveian and Solli (1997))

values in Norway are around 220 m a.s.l. north of Oslo (Fig. 40.1b). As glaciers melted the land started to lift due to glacioisostatic unloading of the crust. In many parts of Norway the uplift was generally faster than the global eustatic sea level rise causing a net fall of relative sea level till the present sea level. The Holocene sea level trends vary throughout Norway (e.g. Vorren et al. 2006). Glacier retreat patterns and sea level trends have had a profound influence on the configuration of the present day landscapes below ML. Shallow marine and river processes, for example, have been important for both erosion and deposition of different deposit types above the emerging marine clays (Figs. 40.1c). Groundwater flow caused the leaching of salts from the pore water with local formation of sensitive clays and

quick clay (Rosenquist 1953). The geochemical processes are described in detail by Torrance (2014, this volume). Quick clay can collapse if disturbed and large landslides may be the result (Fig. 40.1c). The most common triggers in Norway are natural erosion processes or human activity (see e.g. L'Heureux 2013).

40.3 Quaternary Maps: A Basis for Quick-Clay Mapping in Norway

The landscape development is reflected in the geology as represented by the Quaternary geological maps produced at NGU (called Quaternary maps, Fig. 40.2a). The maps show color polygons representing the dominating deposit types at the land surface. Fine-grained fjord marine deposits, including marine clays, are shown in medium blue. Other deposit types comprise for example (glacio)fluvial deposits, beach deposits, peat, moraine deposits and various types of landslide debris. Line symbols show landforms such as river cut escarpments, ravines, abandoned channels, landslide scars and other features. Point symbols represent for example general grain sizes, sub-dominant deposit types and bedrock outcrops. Information on deposit types at depth includes, until now, only very local text-string registrations of layering (stratigraphy). Besides showing the distribution of fine-grained fjord marine deposits several other map features are relevant for quick-clay related work. Other deposit types potentially cover marine clays and some indicate that clays are likely absent. The latter includes barriers to quick-clay landsliding such as bedrock. Other features of special importance in a quick-clay context are signatures of erosion and processes creating relief and the occurrence of landslide scars. Grain size indications give a hint to the type of marine deposits present. The maps also give occasional indications of groundwater conditions such as springs.

An understanding of landscape development following deglaciation forms an important basis for Quaternary mapping in Norway. Mapping procedures consist of a combination of fieldwork and the analysis of LiDAR data, orthophotos and other data. The standardized maps were previously produced in an analogue way but are now produced in a fully digital workflow in a GIS environment from the field to the final product. The availability of LiDAR data has allowed for more detailed morphological analyses in association with geological mapping. Therefore, LiDAR data are also used for adjustment of some older Quaternary maps, which are produced in different scales. The digital products for superficial deposits are stored in the National database hosted by NGU. The map polygons are available to the public via web map services (WMS) for visualization, link and download from http://geo.ngu.no/kart/losmasse or /losmasse_mobil. The map service covers all of Norway and shows a combined product of maps in different scales (called 'best-of-NGU'). A simplified symbology for the polygons is used but a comprehensive list of all classes is linked. The scale and references are stored in the polygon boundaries and are accessed by clicking. For quick-clay mapping, and other practical purposes,

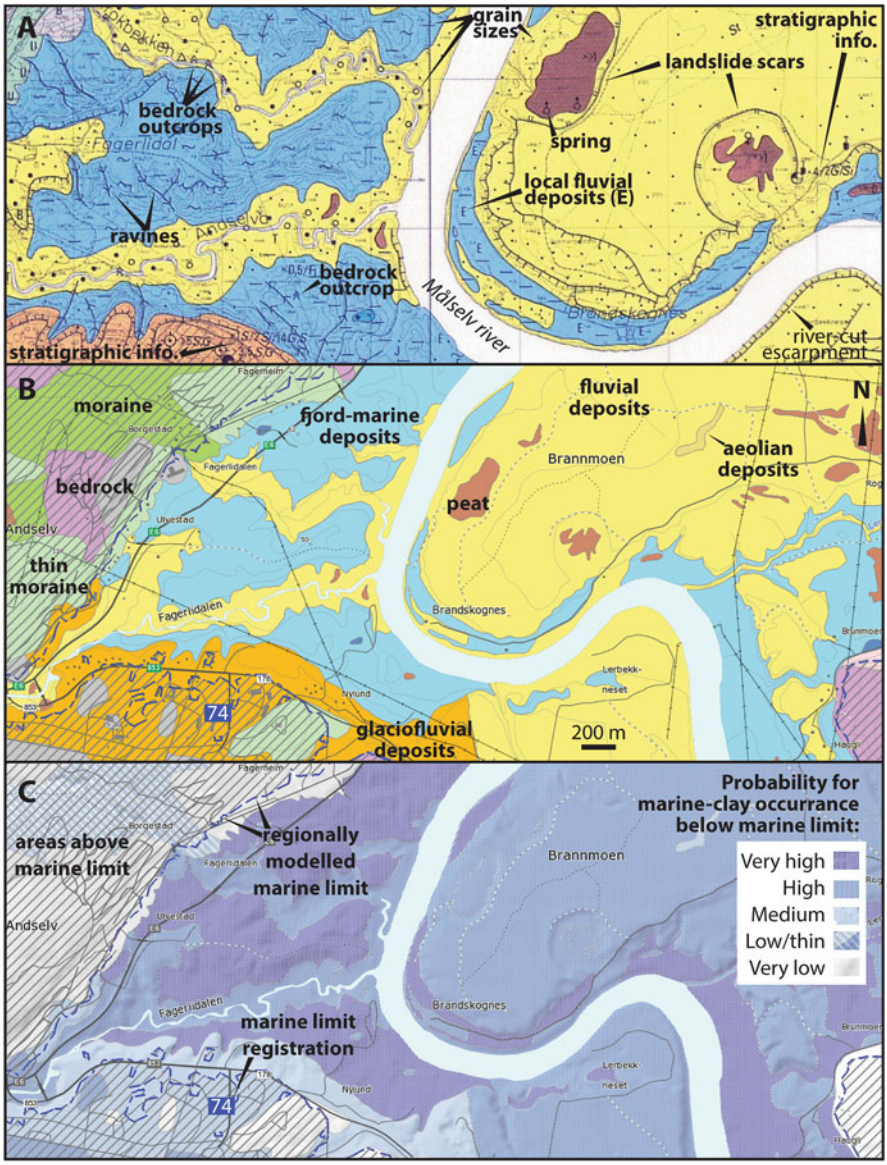

Fig. 40.2 (**a**) Detail from pdf of printed Quaternary map at 1:20.000 from near Bardufoss (Nålsund and Hamborg 1985). Selected *point* and *line* symbols are explained with *bold text*. (**b**) Quaternary map as displayed in http://geo.ngu.no/kart/losmasse or /losmasse_mobil where point and line symbols are now also available. Colours (also for (**a**)) are explained with *bold text*. No. 74 refers to the local marine limit, the *dashed blue line* is the modelled marine limit and the hatched areas are above marine limit as also explained in (**c**). (**c**) The bluish polygons show the probability for clay-deposit encounter as presented through the MML web-based map service (see text)

a scale of at least 1:50.000 is used. See www.ngu.no for more information and discussion below.

The Quaternary maps are used together with topographical data and geotechnical data for quick-clay mapping. Besides showing the distribution of marine deposits, the scars and erosion features are important parameters used directly in hazard assessment (Gregersen 2008).

40.4 Development of Geological Web Services

Web services communicating Quaternary map information have been improved recently to optimize their use for quick-clay mapping and other issues. All maps and associated descriptions are available from www.ngu.no. The direct link to the map services is http://geo.ngu.no/kart/losmasse_mobil or /losmasse.

Marine limit information is important as ML sets the uppermost level in the landscape for the possible occurrence of marine deposits (Fig. 40.2b). Nationwide registrations of ML have recently been systematically organized in the National database for superficial deposits at NGU (Hansen et al. 2012a, 2014; Høgaas et al. 2012). The ML registrations have been retrieved from numerous publications, reports and maps. Each point registration is stored with metadata on height, type, reference and general comments. The heights of ML registrations have been interpolated on a national basis. The modelled surface has been intersected with a national topographic grid at a resolution of 10 m. The resulting lines represent a modelled version of ML for all of Norway. The vertical accuracy is considered as generally within 10 m. A few exceptions are explained in the web service. ML point and line information in addition to polygons covering areas above and below ML are presented. The high-resolution information can be used for practical purposes and modelling. An example of the web service displaying high-resolution ML information is shown in Fig. 40.2b.

Below ML are scattered fine-grained, fjord marine deposits (blue) together with other deposit types and bedrock. An important challenge is that marine clays also occur underneath other deposit types such as beach and fluvial deposits. To address this challenge, a filtered version of Quaternary map information, called clay-deposit susceptibility has been added to the web services. This shows, based on Quaternary maps and knowledge of Norwegian landscapes, where marine clay deposits can potentially be encountered also below other deposit types according to probability (Hansen et al. 2014, In Norwegian: *Mulighet for marin leire*, MML, Fig. 40.2c). For more explanations about the different classes see Hansen et al. (2014) and Norwegian texts linked to the map services.

A recent development is that not only polygons but also most point and line symbols are now displayed on the web-based Quaternary maps. The complete point and line information is solely presented on the printed version of the Quaternary maps (Fig. 40.2a). Important options are the possibilities for users to link to the Quaternary maps from NGU through web maps services (WMS) and to download

the map data. Now only polygons are available but point and line symbols will be included in the future. The NGU web services also show other thematic maps and include links to various external map services. The web-based map services by NGU include a map catalogue with an overview over available Quaternary maps: http://geo.ngu.no/kart/kartkatalog_mobil or /kartkatalog. Scanned analogue maps in pdf format are linked. The overall goal is that all map information should be publically available in a digital format from the NGU website.

40.5 Toward the Third Dimension (3D) in Web Communication of Geological Information

The 2D Quaternary maps are used for quick-clay mapping mainly because they show where fine-grained, usually thick, fjord-marine deposits are exposed at the land surface. The maps are also predictive in the sense that they show areas where the fjord-marine deposits potentially occur below other deposit types. The MML web service described above can be regarded as a first step toward indirectly including the third dimension in web-based geological presentation. The next step in this development is to include actual information on layering (stratigraphy) in the services. Until now, only a few points with stratigraphic information are presented on the Quaternary maps as complicated text strings that are easily overlooked (e.g. 4/2G/Si, Fig. 40.2a). Extending the 2D geological map overviews with the third dimension is valuable for quick-clay related work and for other purposes in society.

The newly established national database for ground investigations (NADAG, http://geo.ngu.no/kart/nadag) and associated web application allow for a highly improved accessibility to data (see Solberg et al. this volume). Presently geotechnical data are in focus but other types of ground investigations will be included in the future. Numerous datasets are available and the database will gradually grow. The NADAG web service shows drill locations and various metadata. Attached are scanned drill reports and profile logs. Solutions for uploading geotechnical surveys and to freely download digital datasets are developed.

Drill data contain important geological information and the development of a database structure at NGU for the organization of stratigraphic information is at its infancy. A few test products presented here show the possibilities for extending the present-day 2D Quaternary map products with the third dimension (Fig. 40.3). Drill-hole information from NADAG and other sources are used, and lithology and other properties have been extracted from pdf reports.

There are several ways of filtering and presenting the stored stratigraphic information. For example, specific information can be presented in a 2D map for overview purposes (Fig. 40.3a). In this way clay/silt deposits and quick-clay occurrences can be verified even if occurring below other deposit types. A simple presentation of this information will improve the MML web service described above (Fig. 40.2a). A way of presenting more detailed stratigraphic information in

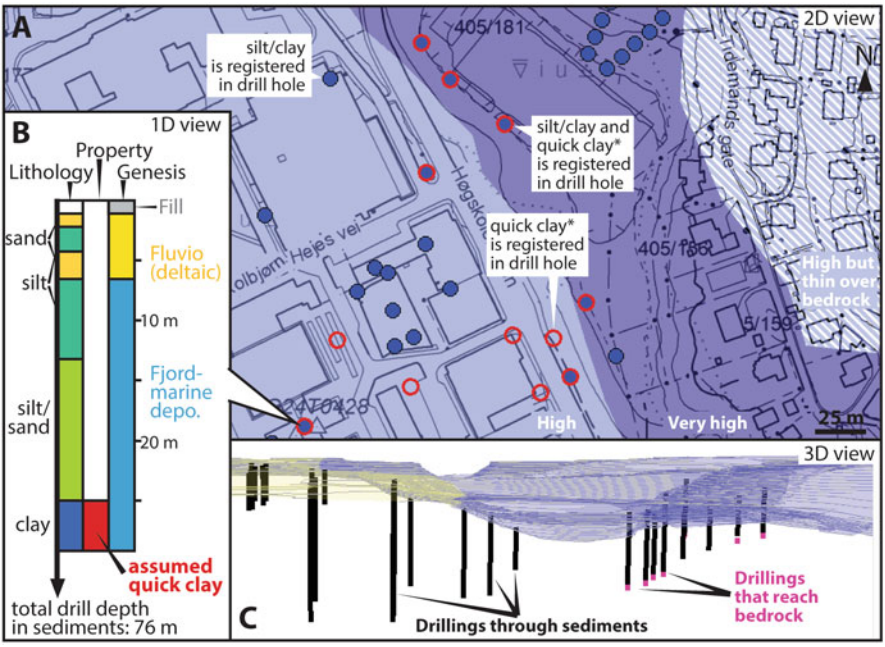

Fig. 40.3 Test products showing the possibilities for extending the present-day 2D Quaternary map. (**a**) 2D map showing the probability for encountering clay deposits (MML, *white text*) with drill hole information confirming the presence of clay/silt and/or assumed* quick clay. (**b**) Detailed stratigraphic log based on drill hole data. (**c**) 3D view of drill holes showing sediment thicknesses and depth to bedrock. The location is at NTNU in Trondheim

association to a 2D map is to show a log by clicking on the drill points as exemplified in Fig. 40.3b. An overview over e.g. lithological properties at various scales can be done through a 3D visualization of information from several drill holes (Fig. 40.3c). Genetic units (as on 2D maps) or simply the thickness of unconsolidated deposits and depth to bedrock may also be presented in this way. Animated, web-based 3D visualization will be possible in the future. As long as the stratigraphic information is stored in a database there are numerous options for analysis and web-based presentation. The digital registration and communication of reported but 'hidden' stratigraphic information is considered as cost effective and beneficial to the users.

40.6 Further Developments

Many clay areas in Norway border fjords and sounds and near-shore subaqueous conditions are therefore also important for quick-clay mapping. Ideally, landslide hazard zonation along the shoreline requires both on- and offshore information (e.g.

L'Heureux 2013; Hansen et al. 2012b, 2014). At present, geological information concerning near-shore subaqueous conditions appears via separate marine map services, see www.ngu.no and www.mareano.no. A combination of on- and offshore maps and stratigraphic data is however preferable. Marine maps are until now only available from a few near-shore areas but the number is expected to increase in the future.

Geophysical data also provide valuable information of importance for geological mapping and quick-clay related work. Such data give general information on soil properties and/or geometries of geological units. Ideally, all geological information and soil properties should be integrated in future web services.

Digital geological information provides possibilities for local to regional analysis of data and modelling. This can be done while including other datasets, for example, topography, hydrology, population and/or geotechnical information. Examples of 2D and 3D modelling for quick-clay related issues are: (1) regional identification of areas for quick-clay mapping (e.g. Wiig et al. 2011), (2) regional scale landslide susceptibility modelling (Quinn et al. 2010) and (3) three-dimensional quick-clay prediction modelling (Persson 2014). Improved availability of digital subsurface information allows for the creation of new types of thematic maps and modelling in the future.

40.7 Concluding Remarks

Quaternary geological maps display fjord-marine deposit distributions and various features of importance for quick-clay mapping and other purposes. The maps provide geological overviews and are often used for their predictive power and for setting local investigations into a geological context. Communication to users of the geological information is currently done through web-based map services by NGU and links are listed in this paper. The web services are continuously developed and stratigraphic information will be included in the future. The development of web-based map services and 3D visualization tools is aimed at maximizing the availability and use of geological information in society.

Acknowledgements A preliminary test version for organization of stratigraphic data was carried out during a project financially supported by the Norwegian Water Resource and Energy Directorate (NVE). We are grateful to Pete Quinn for reviewing the paper.

References

DSB (2013) Nasjonalt Risikobilde 2013. Direktoratet for samfunnssikkerhet og beredskap (Norwegian Directorate for Civil Protection) (In Norwegian)

Gregersen O (2008) Program for økt sikkerhet mot leirskred. Metode for kartlegging og klassifisering av faresoner, kvikkleire. NGI report 20001008-2, rev. 3, 2008.10.08. (In Norwegian)

Hansen L, Sveian H, Olsen L, Høgaas F, Rindstad BI, Wiig T, Lyche E (2012a) The marine limit as a basis for mapping of landslide susceptibility in fine-grained, fjord deposits, onshore Norway. In: Eberhardt E, Froese C, Turner AK, Leroueil S (eds) Landslides and engineered slopes: protecting society through improved understanding. Taylor Francis Gr, London, pp 1833–1838

Hansen L, L'Heureux, JS, Solberg, IL, Longva O, (2012b) Forebyggende kartlegging mot skred langs strandsonen i Norge. Oppsummering av erfaring og anbefalinger. NGU report 2012.046 (NIFS report 22/2013). (In Norwegian)

Hansen L, Høgaas F, Sveian H, Olsen L, Rindstad BI (2014) Quaternary geology as a basis for landslide susceptibility assessment in fine-grained, marine deposits, onshore Norway. In: L'Heureux et al (eds) Landslides in sensitive clays – from geosciences to risk management, Advances in Natural and Technological Hazard Research 36. Springer, Dordrecht, pp 369–381

Havnen I, Ottesen HB, Haugen ED, Frekhaug MH (this volume) Quick clay hazard mapping in Norway. In: Thakur V, L'Heureux J-S, Locat A (eds) Landslides in sensitive clays. From research to implementation. Springer, Dordrecht, chapter 50

Høgaas F, Hansen L, Rindstad BI, Sveian H, Olsen L (2012) Database for registrering av marine grense (MG) i Norge. NGU Report 2012.063. (In Norwegian)

L'Heureux, JS 2013: Vurdering av kartleggingsgrunnlaget for kvikkleire i strandsonen. NIFS report 26/2013. (In Norwegian)

Nålsund R, Hamborg M (1985) Bardufoss, kvartærgeologisk kart EYZ 257258–20, NGU. (With text in Norwegian)

Persson MA (2014) Three-dimensional quick-clay modelling of the Gothenburg Region, Sweden. In: L'Heureux et al (eds) Landslides in sensitive clays – from geosciences to tisk management, Advances in Natural and Technological Hazard Research 36. Springer, Dordrecht, pp 39–50

Quinn PE, Hutchinson DJ, Diederichs MS, Rowe RK (2010) Regional scale landslide susceptibility mapping using the weights of evidence approach: an example applied to linear infrastructure. Can Geotech J 47:905–927

Rosenqvist IT (1953) Considerations on the sensitivity of Norwegian clays. Géotechnique 3:195–200

Solberg IL, Nordahl B, Hansen L, Grøtan BO, Gulbrandsen S (this volume) The Norwegian National Database for Ground investigations (NADAG) – a tool to assist in landslide hazard zonation and other quick-clay related issues. In: Thakur V, L'Heureux J-S, Locat A (eds) Landslides in sensitive clays. From research to implementation. Springer, Dordrecht, chapter 43

Sveian H, Solli A (1997) Tid og form – geologisk historie. In: Dahl R, Sveian H, Thoresen M (eds) Nord-Trøndelag og Fosen – geologi og landskap. Geological Survey of Norway (NGU). (In Norwegian)

Torrance JK (2014) Chemistry, sensitivity and quick clay landslide amelioration. In: L'Heureux et al (eds) Landslides in sensitive clays – from geosciences to risk management, Advances in Natural and Technological Hazard Research 36. Springer, Dordrecht, pp 15–24

Torrance JK (this volume) Chemistry: an essential key to understand quick clays and addressing their landslide risk. In: Thakur V, L'Heureux J-S, Locat A (eds) Landslides in sensitive clays. From research to implementation. Springer, Dordrecht, chapter 3

Vorren TO, Mangerud J, Blikra L, Nesje A, Sveian H (2006) Norge av i dag trer frem. Kapitel 16 i Ramberg IB, Bryhni I, Nøttvedt A (Eds.) Landet blir til. Norges geologi. Norges geologiske forening. (In Norwegian)

Wiig T, Lyche E, Helle TE, Hansen L, Solberg IL, L'Heureux JS, Eilertsen R (2011) Plan for skredfarekartlegging. Delrapport kvikkleire. NVE rapport 17/2011. Norges vassdrags- og energidirektorat, Oslo

Chapter 41
Analysis of Ground Geophysical, Airborne TEM, and Geotechnical Data for Mapping Quick Clays in Sweden

Mehrdad Bastani, Lena Persson, Hjördis Löfroth, Colby A. Smith, and David Schälin

Abstract Airborne transient electromagnetic (ATEM) data for mapping clay areas are acquired in four areas in Sweden. The resistivity models from the inversions of ATEM data are compared to the existing geotechnical, geological and ground geophysical data in one of the areas at Slumpån located in the Göta River valley. The ATEM models reveal information about layering and thickness of the sediments, the river depth and bedrock undulations. The estimated resistivities at the known locations of quick clays are within the range of 8–40 Ωm. The variation is dependent on the type of the surrounding sediments and the leaching process. The resistivity models have a limited resolution and must always be integrated with geotechnical and geological information for a confident and precise interpretation that leads to a realistic model. The method can be utilized as an effective tool prior to planning of any detailed and costly ground geotechnical investigations.

41.1 Introduction

Most of the historical and disastrous landslides that have occurred in Sweden are related to the presence of the quick clay (QC) on relatively gentle slopes composed of glaciomarine silt and clay. Slopes that have a border with a river or a lake have shown higher risk for landslides (Nadim et al. 2008). The Tuve landslide in November 1977 (Nadim et al. 2008), the Vagnhärad landslide in May 1997 (Löfroth and Kjellberg 2003), and the Munkedal landslide in the December 2006 (Nadim et al. 2008) are some of recent quick clay landslides in Sweden.

M. Bastani (✉) • L. Persson • C.A. Smith
Geological Survey of Sweden (SGU), Uppsala, Sweden
e-mail: mehrdad.bastani@sgu.se; lena.persson@sgu.se; colby.smith@sgu.se

H. Löfroth • D. Schälin
Swedish Geotechnical Institute (SGI), Linköping, Sweden
e-mail: hjordis.lofroth@swedgeo.se; david.schalin@swedgeo.se

V. Thakur et al. (eds.), *Landslides in Sensitive Clays*, Advances in Natural and Technological Hazards Research 46, DOI 10.1007/978-3-319-56487-6_41

Study of the processes leading to the formation of QC dates back to the 1940s (Rosenqvist 1946). QC is mainly formed in the sediments that were deposited in the marine environment during the last deglaciation. After the ice retreated, the land underwent isostatic uplift, and areas of past glaciomarine sedimentation rose above the sea level. The uplifted marine clays have then been subjected to leaching by various processes such as infiltration of rainwater; artesian groundwater flow in underlying permeable layers or fractured rock; and by subsequent diffusion of ions in groundwater (Rankka et al. 2004). According to the Swedish classification, high sensitive clay has sensitivity >30. The quick clay has sensitivity >50 and remoulded, undrained shear strength <0.4 kPa. Traditionally, the only reliable method for detection and identification of QC is through laboratory tests on undisturbed samples taken from the investigated locations (Rankka et al. 2004). The laboratory tests include fall-cone tests on the samples. Mapping of QC using traditional methods requires extensive sampling that is not only economically infeasible but also time consuming and to some extent invasive. Geophysical methods are known to be reasonably fast, usually non-invasive and cost-effective for the mapping purposes. The leaching process usually increases the electrical resistivity. It is therefore expected that the QC should have higher electrical resistivities than the surrounding non-sensitive marine clays. If the contrast is large enough, use of the electrical and electromagnetic geophysical methods becomes a practical means to model and map the areas containing prerequisites for QC.

The use of ground geophysical methods to study QC areas in Sweden is reported by several researchers. Rankka et al. (2004), Löfroth et al. (2011), and Dahlin et al. (2013) presented examples of electrical resistivity tomography (ERT) close to the Göta River. A few years later radio magnetotelluric (RMT), ERT and reflection seismic measurements were carried out in the same area (Malehmir et al. 2013; Shan et al. 2014; Wang et al. 2016). Airborne geophysical measurements are considerably faster and more cost-effective when investigating large areas. The airborne geophysical data have less resolution and sensitivity to near surface variations compared to ground geophysical data. However, recent developments in the airborne transient electromagnetic (ATEM) data acquisition systems (Auken et al. 2009 and reference therein) have provided data with very high quality. Christensen et al. (2015) presented a successful application of the method for mapping depth to bedrock in Norway along the planned route of the new E16 located some 50 km NE of Oslo. Solberg et al. (2016) reported a comparison of results between frequency domain helicopter-borne electromagnetic (FHEM), various ground geophysical measurements and geotechnical data at a landslide site in Norway. They conclude that each data set reveals certain properties of the subsurface materials and there is no single method that can accurately define QC layers.

In 2015, a pilot project, in collaboration between the Swedish Transport Administration (TrV), the Swedish Geotechnical Institute (SGI) and the Geological Survey of Sweden (SGU), was initiated to develop a stepwise methodology for mapping quick clay in Sweden. One part of the project was to evaluate airborne transient electromagnetic data that were collected in four areas. Follow-up ground

geophysical surveys were carried out at a few locations in two areas to obtain more detailed information. In this study, we show examples of integration of ATEM, geotechnical data and ground geophysical data collected from one of these areas with known occurrences of QC and related landslides. The main objective is to evaluate the feasibility of using the ATEM method as a standard tool for mapping and modelling the areas with and without prerequisites for QCs. The ground geophysical and geotechnical data are mainly used as complementary information to validate the resistivity models from the ATEM data.

41.2 Airborne TEM Survey in Sweden

Figure 41.1 shows the location of areas in Sweden for the ATEM surveys. The areas are numbered as 1–4 from the south towards the north. The measurements took a total of 7 days including mobilization. Presence of QCs is known in all four areas from previous geotechnical, geological and geophysical studies. SkyTEM Surveys ApS carried out the ATEM data acquisition. The survey consists of 873 km flight lines in total with a nominal terrain clearance of 30–50 m and an average line spacing of 75 m. Based on the maximum target depth (the upper 50 m), the SkyTEM 301 system was used in order to provide high-accuracy data to resolve the near-surface resistivity structures (for more details see: http://skytem.com/tem-systems/). The system setup is a dual moment configuration containing a low moment (LM) and a high moment (HM). The former delivers 20 gates (8.7–553 μs) and the latter 25 gates (34–3525 μs). In the following section, we present a detailed comparison between the results of the ATEM investigations and the existing geotechnical and ground geophysical data from area 2.

41.3 Geological Description of Slumpån (Area 2)

Slumpån is located close to the Lilla Edet community in southwestern Sweden (shown as area 2 in Fig. 41.1) where previous extensive ground geophysical and geotechnical studies were conducted (Löfroth et al. 2011; Malehmir et al. 2013; Shan et al. 2014). Shan et al. (2014) give a detailed account of the geological settings and ground geophysical data in this area. The investigated area is located in the Göta River valley. According to Fredén (1984) the Quaternary deposits at the ground surface are mainly composed of glacial clays and postglacial silts (Fig. 41.1). The crystalline gneissic bedrock occasionally outcrops. Glacial clays with a maximum of approximately 60 m thickness are found in the area. The lowermost part of the sequences of the sediments consists of varved or laminated clays with layers of sands and silts (Fredén 1984). The sand layers often contain artesian water/aquifer (Rankka et al. 2004). The sequence is covered by fairly homogeneous blue-colored clay with varying silt content. Scars of older landslides and gullies with a clear

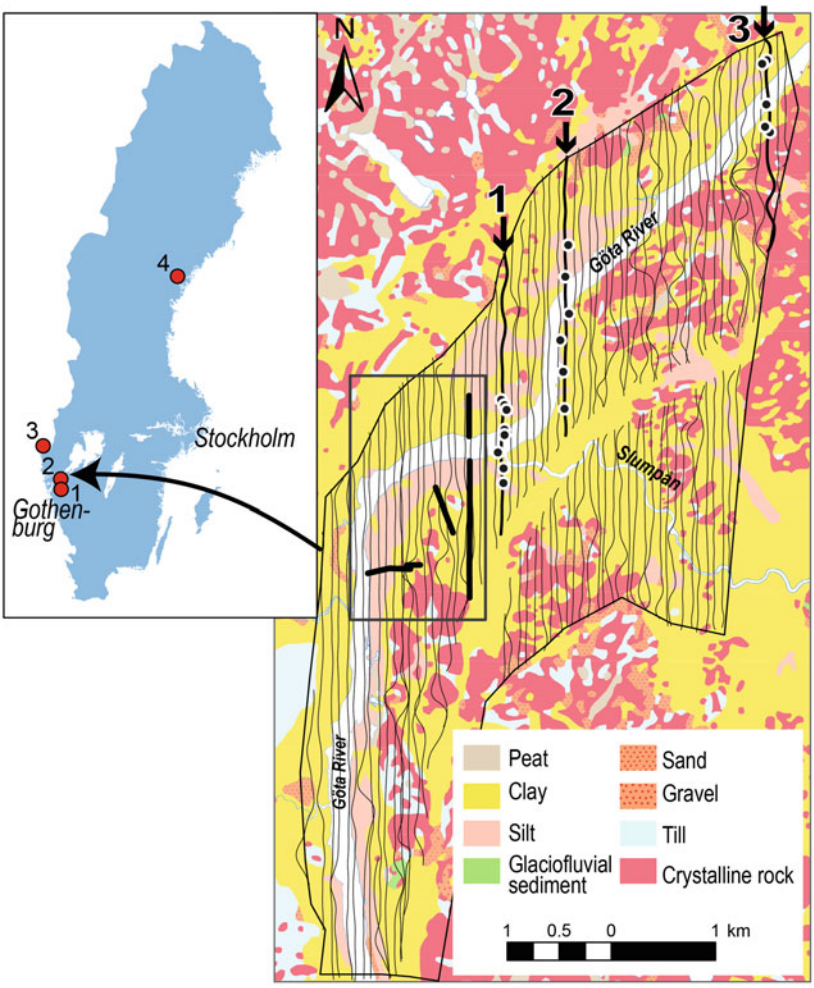

Fig. 41.1 Location of areas for ATEM measurements in Sweden (*top left* frame) and extent of ATEM survey in Slumpån area. The background is the simplified surficial deposits map from SGU's database. The *black rectangle* encloses smaller area chosen for comparison between ATEM and ground measurements. Locations of the ground RMT lines and the selected geotechnical boreholes are shown with *thicker black lines* and *black dots*, respectively. The *black arrows* indicate selected ATEM lines for comparison with geotechnical data

retrogressive signature are reported in the study area (Melchiorre et al. 2014). Salas-Romero et al. (2015) presented the results from reflection seismic measurements (Fig. 41.2a) from the same area together with detailed information on the geological and geophysical observations made in three boreholes where they had also taken undisturbed samples.

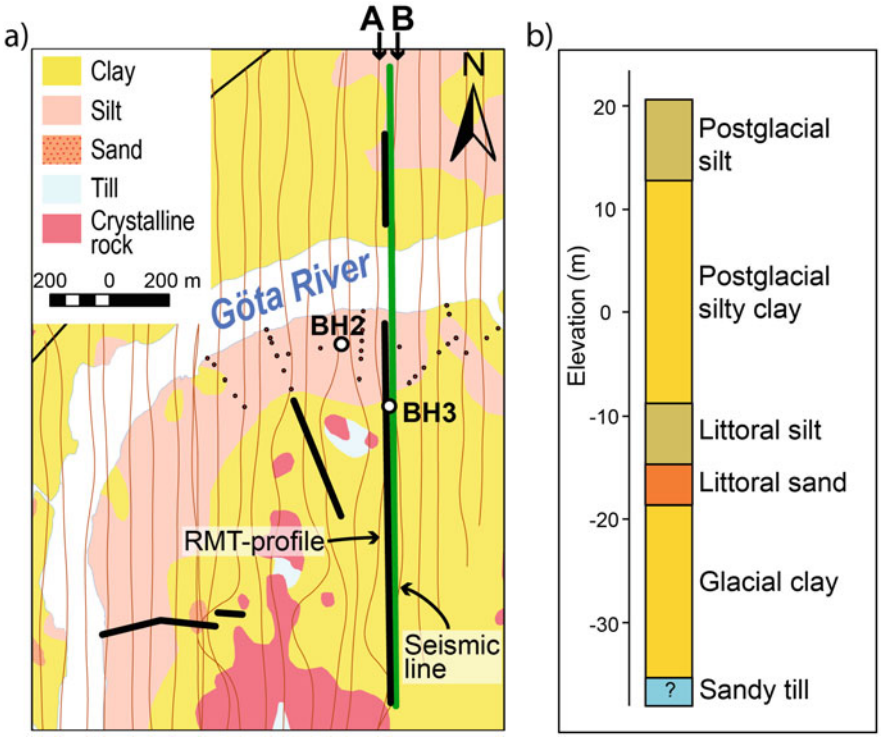

Fig. 41.2 (**a**) Selected area for comparison of ATEM and ground geophysical data. The *thick black lines* show the location of RMT lines and the *green line* the seismic line. The *black arrows* show selected flight lines (**a**, **b**) for comparison with ground geophysics. (**b**) Idealized stratigraphy of the Slumpån area adapted from borehole 2 of Salas-Romero et al. (2015)

Figure 41.2b shows an idealized stratigraphy of the Slumpån area adapted from borehole 3 of Salas-Romero et al. (2015). The sand and silt separating the glacial from postglacial clay are interpreted to be littoral sediments deposited during the early Holocene lowstand when local isostatic uplift outpaced global sea-level rise. The overlying postglacial silt and clay were deposited as global sea-level rose and local water depths became deeper.

41.4 Existing Geotechnical and Ground Geophysical Data

SGI has conducted intensive geotechnical investigations in area 2. TrV has also provided its geotechnical data which are used in this study. These include cone penetration test (CPT) and undisturbed sampling (US). Presence of QC is evaluated from CPT by an indirect method where an almost vertical pushing force vs.

depth curve generally indicates high sensitivity clay (Rankka et al. 2004). Ground geophysical data were acquired in area 2 in connection with various projects. Löfroth et al. (2011) and Dahlin et al. (2013) report the results from ERT measurements. Malehmir et al. (2013) carried out ERT, radio magnetotelluric (RMT), controlled source MT (CSMT) and reflection seismic measurements. The details on the methods, data acquisitions and processing can be found in the aforementioned references. Here, we solely use the results of investigations to compare them with ATEM results.

41.5 Comparison Between ATEM Models and Geotechnical Data

We used the Aarhus workbench software (Hydrogeophysics group at Aarhus University 2011) for the processing and inversion of the ATEM data. The data were modelled using the smooth spatially constrained inversion (SCI) developed by Viezzoli et al. (2008). The number of layers was set to 30 and a moderate horizontal/vertical smoothing constraint was applied. Figure 41.1 shows the location of three selected flight lines that are marked with black arrows and numbered as 1–3. Those geotechnical boreholes from SGI's earlier investigations in the area, located within a distance of 50 m from the flight lines 1–3, are selected for the comparison with the ATEM resistivity models (see Fig. 41.1). The results of SCI inversions together with the information from each geotechnical borehole are shown in Fig. 41.3a–c. These lines were flown over the Göta River and the modelled water resistivity is 200 to ca 300 Ωm that corresponds well with fresh water resistivity. The top few meters of the models have a resistivity less than 100 Ωm and they are attributed to the dry crust and more silty sediments. According to the geotechnical observations the high-resistivity layer does not contain any QC. Its thickness also correlates well with the first layer defined in the geotechnical boreholes as non-quick clay (see the borehole legend in Fig. 41.3). However, the detailed geotechnical information indicates that this layer often contains high sensitive clays. Such detailed information is not resolved in the ATEM models. A layer with lower resistivity (10–50 Ωm) underlies the dry crust (except at both ends of L3). This layer has a considerably more complex structure and contains the key features of this study which is reflected in both the ATEM models and the geotechnical boreholes. At the southern parts of L1 (0–500 m) the second layer is thicker and shows more resistivity variations compared to the northern parts of the line.

The presence of QC is confirmed in boreholes along line L1 at both sides of the Göta River (Fig. 41.3a). The QC at the southern parts of the river is found on top of a coarse-grained (CG) sandy layer (Löfroth et al. 2011; Shan et al. 2014) that was probably formed in a littoral environment whereas north of the river, no CG sand is reported. A second CG layer is observed at greater depths (∼45 m) in the first borehole along line L1 but not identified by ATEM. The smaller river called Slumpån located to the east of the line is likely the source of the coarse grained

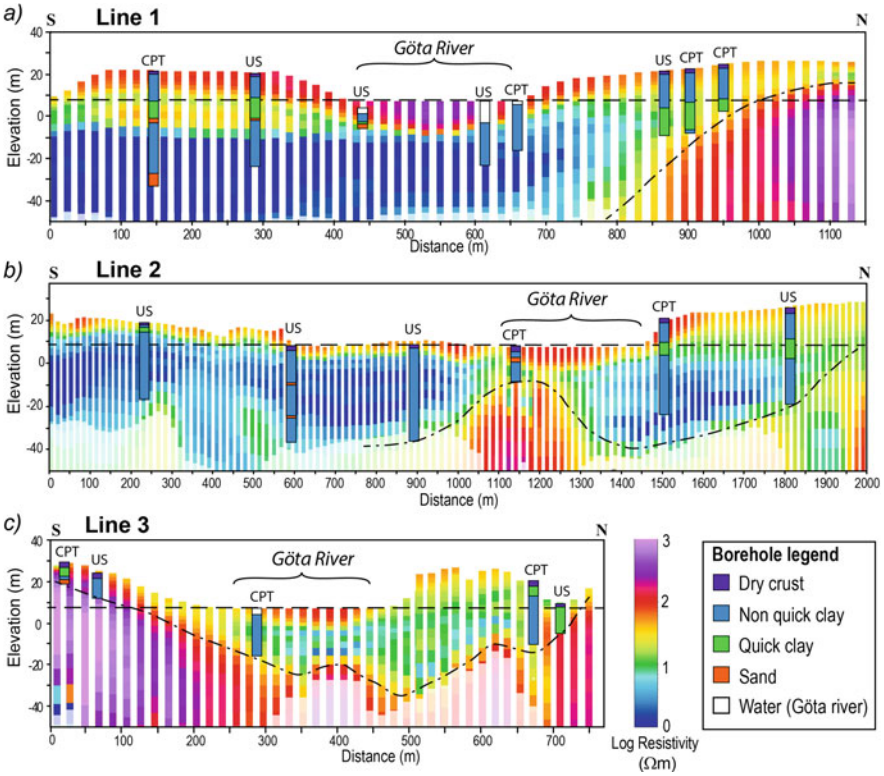

Fig. 41.3 Resistivity models from the inversion of ATEM data along three lines shown in Fig. 41.1. (**a**) Line 1, (**b**) Line 2, and (**c**) Line 3. Note that the lines are of different lengths. The geotechnical data from the boreholes are shown on *top* of the models. Note that the boreholes might be up to 50 m off the flight lines. The *dashed horizontal lines* indicate the level of Göta River extracted from LIDAR data. The *dashed-dotted lines* show interpreted upper surface of the resistive crystalline bedrock. Depth of investigation is shown by *faded color*

sediments (Fig. 41.1). A distinct layer with resistivity of 20–40 Ωm at elevations 7 to −5 m is well identified in north of the river along line L1 by ATEM model and correlates well with the occurrence of QC just above the bedrock in three boreholes (Fig. 41.3a). Possible location of the bedrock (marked by dashed-dotted line in north) is not resolved and could be deeper south of the Göta River along L1, because of attenuation of the TEM signal caused by very low resistivity clays. The ATEM model is smooth and does not resolve the upper boundary of the QC whereas the high resistivity feature at depth (possibly bedrock) marks the bottom of QC properly. The model has resistivity between 10 and 40 Ωm at the QC locations.

The geotechnical information along line L2 reveals the presence of CG sand layer in second borehole from south at −10 m and −28 m elevations and no evidence of QC above the CG sand layer. The ATEM model is also different (compared to L1) and shows a rather conductive layer with low resistivity material of around

5 Ωm and doesn't indicate any CG sand layers. On the north side of the Göta River, geotechnical observations in two boreholes indicate the presence of QC between 4 and 10 m elevation (Fig. 41.3b). The resistivity model in this interval has a resistivity of around 9 Ωm (low compared to L1) and shows a sharp drop to 5 Ωm at the bottom of QC and that is identified as non-QC clays from the borehole data. Note that in the southern part the bedrock is deeper in this model.

The resistivity model along line L3 interprets the bedrock (high resistivity feature at the bottom) at considerably shallower depth compared to lines L1 and L2. The QC is found at higher elevations (25 m and 20 m) in two CPT boreholes in north side of the line (Fig. 41.3c). QC in northernmost borehole is reported from 7 to −5 m elevation. It is of great importance to note that the QC is mostly found at the same elevations as the Göta River level is flowing today (see the dashed lines and QC interpreted from boreholes on the ATEM models in Fig. 41.3a–c). We will discuss it further in the discussion section.

41.6 Comparison with Ground Geophysics

Here, we compare the ATEM resistivity models (Fig. 41.4a, b) along two flight lines (marked with A and B in Fig. 41.2a) with the seismic velocity model (Fig. 41.4c) and the RMT resistivity model (Fig. 41.4d) along the same line reported by Wang et al. (2016). All the four models reflect the same structures with slight differences. A few characteristics of all the models are similar. For instance, the thicker low resistivity and low velocity zones at both ends of all the models (starting from 200 m for ATEM models) represent the glacial and post-glacial sediments (see Fig. 41.2 for details). The high resistivity and high velocity feature, marked by dashed-dotted line, in the interval 700–1,000 m (Fig. 41.4c, d) presumably reflects the crystalline bedrock (Wang et al. 2016). The estimated resistivity models from ATEM and RMT methods match well and show the same range of variation for similar structures (note that the colour scales are different). The models on the other hand also show different sensitivities and resolutions. For example, even though the seismic model (Fig. 41.4c) provides quite detailed information about the depth to the bedrock it is incapable of resolving the variations seen in the sediments especially in the southern parts. According to Wang et al. (2016), the RMT model (Fig. 41.4d) revealed the detailed variations in the uppermost 10 m of the sediments that correlate very well with observations in the geotechnical and the geophysical borehole (BH3) reported by Salas-Romero et al. (2015). The ATEM models provide a slightly smoother image of the topmost part of the ground (compared to RMT) and have a shallower penetration depth (compared to seismic) that is partly due to the system (SkyTEM 301) used in this survey and partly due to the screening effect of conductive sediments. The limitation in the ATEM and RMT models can be seen well on the northern side of the Göta River where the velocity model detects the bedrock at approximately −5 m elevation between 1,800 and 2,100 m distances whereas it is not seen at all in the ATEM and RMT models.

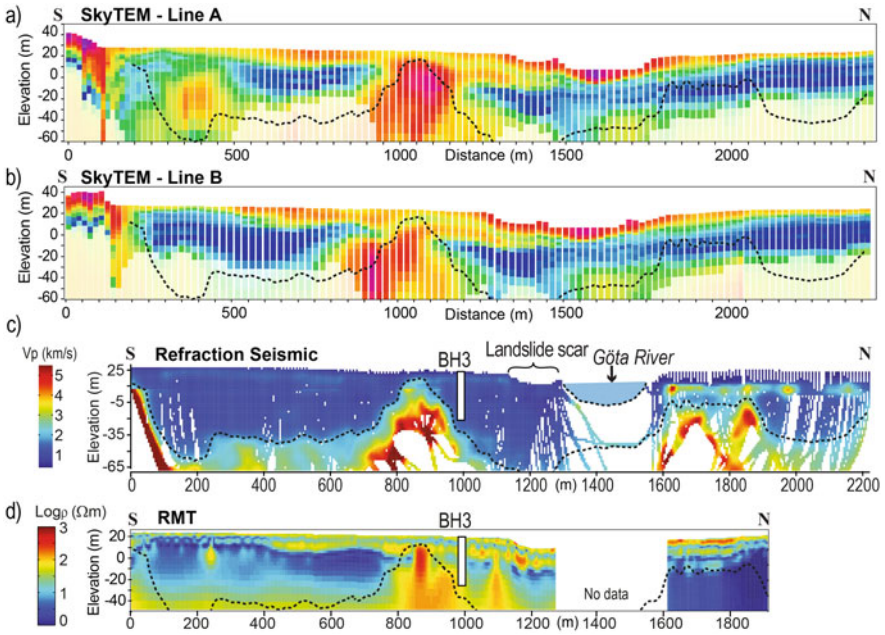

Fig. 41.4 Comparison between SkyTEM models along (**a**) Line A, (**b**) Line B, (**c**) refraction seismic tomography, and (**d**) the RMT models. Locations of flight lines are shown in Fig. 41.2a. The ground geophysical models are modified from Wang et al. (2016). BH3 shows the location of geophysical borehole reported by Sala-Romero et al. (2015). The *dotted line* indicates the *top* of bedrock interpreted from the velocity model in (**c**). Models in (**a**) and (**b**) have the same colour scale as in Fig. 41.3. Areas below depth of investigation are shown by *faded colors* in (**a**, **b**)

41.7 Discussions

The comparison between the ATEM, ground geotechnical and geophysical models showed a reasonably good correlation. By combining all the data, we have made a conceptual model as shown in Fig. 41.5 showing the processes leading to the formation of QC in the Slumpån area. In our model, the groundwater level (Göta River level) plays a key role in this process. The geotechnical information and to some extent the geophysical models (ground and airborne) reveal that the QC is mainly found below the river level. This implies that leaching must result either from groundwater flow within confined aquifers or from the seasonal fluctuations of the groundwater level during the past few thousand years. These might be the most dominant processes in north of the river (Fig. 41.5a). At locations close to bedrock outcrops where the clay is thin meteoric water may infiltrate beneath the clay (see boreholes in Fig. 41.3a, c). This groundwater flow through coarse-grained till at the sediment/bedrock interface may intensify the leaching and consequently the formation of QC close to the bedrock boundary (Fig. 41.5b). South of the river where the CG littoral layer is present, the scenario shown in Fig. 41.5b might occur

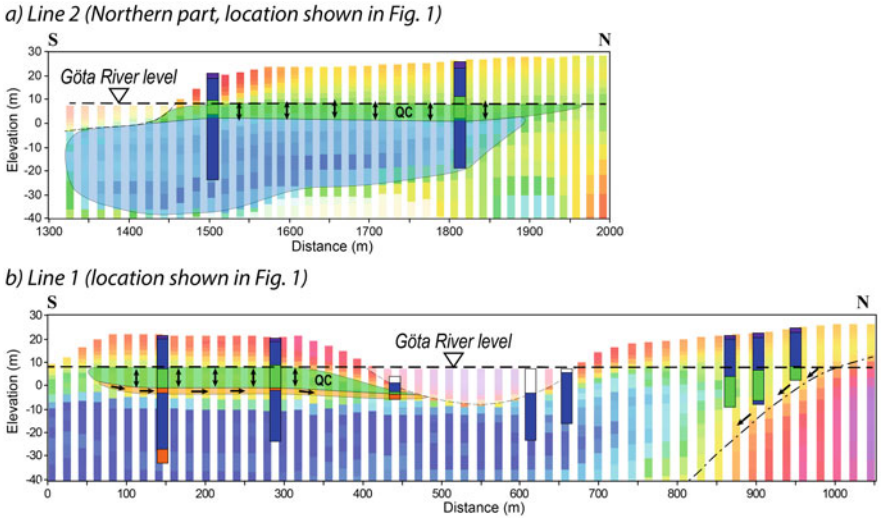

Fig. 41.5 Conceptual models showing different processes leading to formation of QC in the study area. (**a**) Seasonal fluctuations of the groundwater level through the Holocene. The *black arrows* indicate the range of fluctuations. (**b**) Variation of the groundwater level, confined water pressure in the coarse-grained layer under the marine clays, and bedrock undulations. The *smaller black arrows* show flow direction of groundwater in the CG layer

where the confined water in the CG layer may leach salt from the overlying marine clay. Overall, we suggest that leaching is controlled by a complex and variable combination of groundwater table fluctuations, the presence of CG sediments with high hydraulic conductivities and infiltration of the meteoric water near bedrock undulations.

41.8 Conclusions

The airborne TEM data from one of the four survey areas in Sweden are compared with the geotechnical and ground geophysical data to evaluate the accuracy of the method as well as its potential to use as a standard tool for mapping prerequisites for quick clays. The method is cost-effective, and it covers large areas in a short time. This study reveals that the ATEM results are comparable with the borehole and ground geophysical information. In this area the quick clay has a resistivity in the range 8–40 Ωm that is generally higher than resistivity of the surrounding clays. One must always remember that there are many controlling parameters involved in both ATEM data resolution and the inversion results. Some are method intrinsic (e. g., deeper penetration incorporates larger volumes and affects the average resistivity) and some are caused by the regularization used in the inversion. The ground-truthing with geotechnical data is always vital for the final interpretation of ATEM results.

There is no direct relationship between the resistivity range and identification of prerequisites for quick clays. ATEM data can be used as a powerful tool to identify potential areas as leached clay for further planning of more detailed ground geotechnical and geophysical investigations leading to much better management of resources and infrastructure developments.

Acknowledgements This study is a part of a pilot project financed by the Swedish Civil Contingencies Agency (MSB). The authors would like to thank Dr. Vikas C. Baranwal, Team leader Jan Steinar Rønning, and Dr. Inger-Lise Solberg from the Geological Survey of Norway (NGU) who kindly accepted to review this paper.

References

Auken E, Christiansen AV, Westergaard JA, Kirkegaard C, Foged N, Viezzoli A (2009) An integrated processing scheme for high-resolution airborne electromagnetic surveys, the SkyTEM system. Explor Geophys 40:184–192

Christensen CW, Pfaffhuber AA, Anschütz H, Smaavik TF (2015) Combining airborne electromagnetic and geotechnical data for automated depth to bedrock tracking. J Appl Geophys 119:178–191

Dahlin T, Löfroth H, Schälin D, Seur P (2013) Mapping of quick clay using geoelectrical imaging and CPTU-resistivity. Near Surf Geophys 11:659–670

Fredén C (1984) Beskrivning till jordartskartan. Sveriges Geologiska Undersökning, Vänersborg, p 48. (In Swedish)

HydroGeophysics Group, Dept. of Earth Sciences University of Aarhus (2011) Guideline and standards for SkyTEM measurements, processing and inversion, version 2.5, pp 51

Löfroth H, Kjellberg U (2003) The May 1997 landslide in soft clay at Vagnhärad, Sweden. Lessons learnt from landslide disasters in Europe. Report EUR20558EN, 33–40. European Commission Joint Research Centre

Löfroth H, Suer P, Dahlin T, Leroux V, Schälin D (2011) Quick-clay mapping by resistivity-surface resistivity, CPTU-R and chemistry to complement other geotechnical sounding and sampling, Report GÄU 30. Swedish Geotechnical Institute, Linköping

Malehmir A, Bastani M, Krawczyk C, Gurk M, Ismail N, Polom U, Persson L (2013) Geophysical assessment and geotechnical investigation of quick-clay landslides – a Swedish case study. Near Surf Geophys 11:341–350

Melchiorre C, Smith C, Rodhe L (2014) Analysis of landslide scarp data, Sweden, Report Dnr: 315–1895/2014. Geological Survey of Sweden, Uppsala

Nadim FS, Pedersen AS, Thomé PS, Sigmundsson F, Engdahl M (2008) Natural hazards in Nordic countries. Episodes 31:176–184

Rankka K, Sköld YA, Hultén C, Larsson R, Leroux V, Dahlin T (2004) Quick-clay in Sweden. Swed Geotech Inst, Tech Rep 65:145

Rosenqvist IT (1946) Om leirers kvikkagtighet. Statens Vegvesen. Veglaboratoriet. Meddelande Nr 4. Oslo. (In Norwegian)

Salas-Romero S, Malehmir A, Snowball I, Lougheed BC, Hellqvist M (2015) Identifying landslide preconditions in Swedish quick clays – insights from integration of surface geophysical, core sample- and downhole-property measurements. Landslides, 1–19, ISSN 1612–5118

Shan C, Bastani M, Malehmir A, Persson L, Engdahl M (2014) Integrated 2D modeling and interpretation of geophysical and geotechnical data to delineate quick clays at a landslide site in Southwest Sweden. Geophysics 79:EN61–EN75

Solberg IL, Long M, Baranwal VC, Gylland AS, Rønning JS (2016) Geophysical and geotechnical studies of geology and sediment properties at a quick-clay landslide site at Esp, Trondheim, Norway. Eng Geol 208:214–230. ISSN 0013-7952

Viezzoli A, Christiansen AV, Auken E, Sørensen KI (2008) Quasi-3D modelling of airborne TEM data by spatially constrained inversion. Geophysics 73:F105–F113

Wang S, Malehmir A, Bastani M (2016) Geophysical characterization of areas prone to quick-clay landslides using radio-magnetotelluric and seismic methods. Tectonophysics 677:248–260

Chapter 42
Investigation of a Sensitive Clay Landslide Area Using Frequency-Domain Helicopter-Borne EM and Ground Geophysical Methods

Vikas Chand Baranwal, Jan Steinar Rønning, Inger-Lise Solberg, Einar Dalsegg, Jan Fredrik Tønnesen, and Mike Long

Abstract Mapping of the distribution and properties of marine clay is important in Norway due to numerous landslides in sensitive clay. The degree of leaching of salt in marine clay may be reflected by its electrical resistivity. However, the degree of sensitivity of the clay needs to be confirmed by geotechnical studies. Electrical resistivity and various electromagnetic (EM) methods are common geophysical methods to investigate the resistivity of an area. Helicopter EM surveys are helpful to investigate a large area in rather shorter time compared to ground EM or resistivity surveys. Frequency domain helicopter-borne EM (FHEM), electrical resistivity tomography (ERT) and seismic refraction were performed in 2014 at Byneset outside of Trondheim, Norway where a landslide occurred in 2012. Geotechnical surveys were performed in the region before, but mainly after the landslide. There was a good correlation between the results from the different surveys. FHEM interpretation revealed that unleached marine clay was covered by varying thickness of leached clay in the survey area. At some places, bedrock was very shallow and even exposed at the surface. FHEM is proven to be a very good tool to get an overview of the leached and unleached clay zones and to map 3D resistivity of the region.

V.C. Baranwal (✉) • I.-L. Solberg • E. Dalsegg • J.F. Tønnesen
Geological Survey of Norway (NGU), Trondheim, Norway
e-mail: vikas.baranwal@ngu.no; Inger-Lise.Solberg@ngu.no; Einar.Dalsegg@ngu.no; Jan.Tonnesen@ngu.no

J.S. Rønning
Geological Survey of Norway (NGU), Trondheim, Norway

Norwegian University of Science and Technology (NTNU), Trondheim, Norway
e-mail: Jan.Ronning@ngu.no

M. Long
School of Civil Engineering, University College Dublin (UCD), Dublin, Ireland
e-mail: Mike.Long@ucd.ie

V. Thakur et al. (eds.), *Landslides in Sensitive Clays*, Advances in Natural and Technological Hazards Research 46, DOI 10.1007/978-3-319-56487-6_42

42.1 Introduction

A thorough investigation of ground conditions and quick-clay distribution is important to evaluate landslide hazards and for planning of land use and constructions. The ground truthing is generally carried out by drilling, which can be very extensive and expensive. Alternatively, geophysical techniques can be used together with the drilling to increase the efficiency and coverage of the larger areas to understand the geology and sediment properties.

Various geophysical methods have been used to investigate marine clay deposits (e.g. Solberg et al. 2008; Sauvin et al. 2014; Shan et al. 2016). Saline, unleached clay in Norway shows in general a resistivity less than 10 Ωm (Solberg et al. 2008). Leached clay that may be quick has a slightly higher resistivity that often ranges between 10 and 100 Ωm. This change in resistivity can be mapped by various resistivity and electromagnetic (EM) methods. Electrical resistivity tomography (ERT) provides a detailed subsurface resistivity down to about hundred meters depth, which can help in differentiating between areas containing leached and unleached clay. Airborne EM (AEM) surveys use various types of EM transmitter and receiver coils on fixed wing aircraft or helicopter. The measurements are done either in time domain or in frequency domain in different AEM systems (Siemon et al. 2009). Christensen et al. (2015) used time domain AEM data to map clay layers thickness and automated the bedrock depth estimation for a section of E16 highway northeast of Oslo, Norway. AEM survey can cover a large area in a rather short time compared to ERT. Frequency domain helicopter-borne EM (FHEM) provides high resolution subsurface resistivity though not as detailed as an ERT survey.

On January 1st 2012, there was a quick-clay landslide at Byneset, Trondheim (NVE 2012). The landslide area was surrounded mostly by agricultural lands and there were no injuries. The nearby farms were evacuated after the landslide. The landslide scar was 100 m wide and 400 m long, with a volume of ca. 350,000 m^3.

A lot of geotechnical and geophysical surveys were performed in Byneset just after the landslide in 2012 and in the following years. Details about all these investigations are documented in numerous reports, summarized in Baranwal et al. (2015) and Solberg et al. (2015, 2016). This paper presents detailed interpretation of geophysical surveys e.g. helicopter EM, seismic refraction and resistivity surveys and establishes the usefulness of airborne EM data for sensitive clay mapping. FHEM data provides a 3D subsurface resistivity image of the area which can be used in various aspects of the geological mapping.

42.2 Geology of the Area

Byneset is located in Trondheim municipality in Mid Norway. Figure 42.1 shows the Quaternary geological map of Byneset with locations of the various geophysical surveys. Most of the area is covered by marine sediments deposited during the

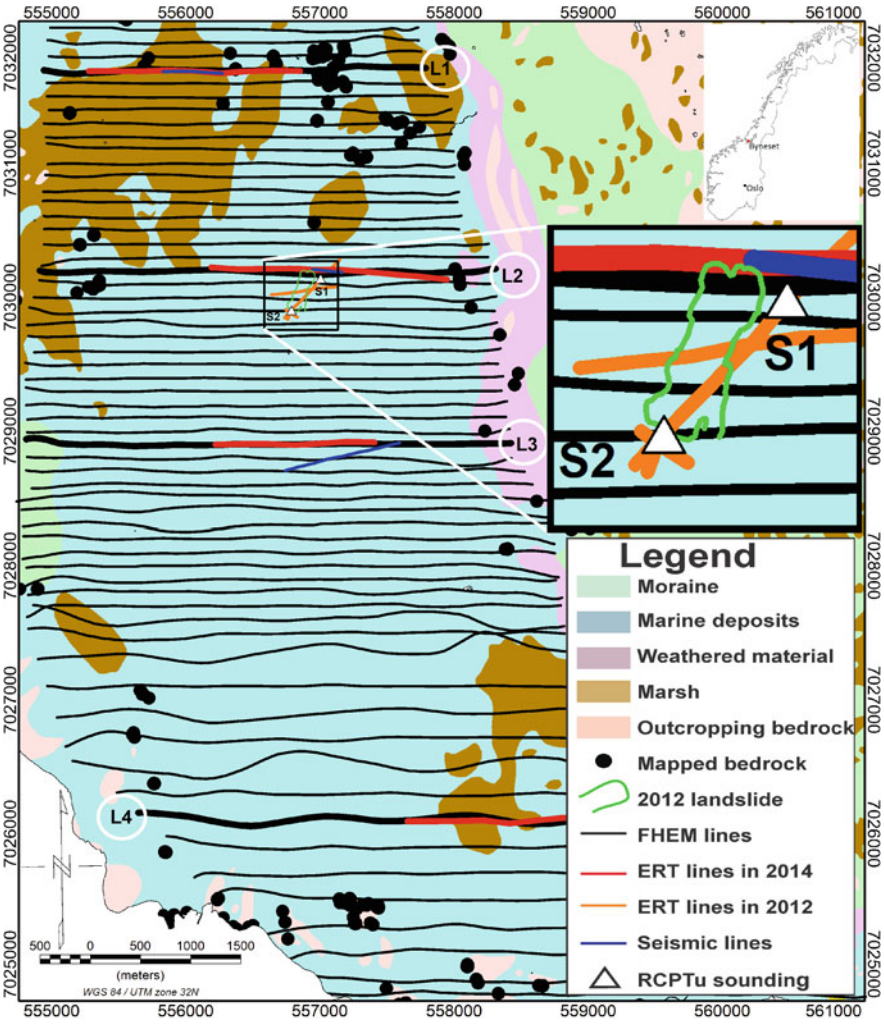

Fig. 42.1 Quaternary geological map of Byneset with locations of geophysical surveys

deglaciation around 10,000 years ago. Due to glacio-isostatic rebound, the sediments are now exposed on land with a ground surface elevation around 160 m a.s.l. (Reite et al. 1999). Central parts of Byneset are dominated by ravines and about one hundred landslide scars (Solberg et al. 2016). Old seabed is also preserved in some parts. The bedrock in the area is dominated by chlorite slate in west and phyllites in the east. The phyllite may contain graphite which is an electronic conductive mineral (Solberg et al. 2015, 2016).

42.3 Geophysical and Geotechnical Surveys

The geophysical and geotechnical surveys performed in the area were FHEM, ERT, resistivity piezocone penetration test unit (RCPTU), refraction seismic, multichannel analysis of surface wave (MASW) and geotechnical soundings including rotary pressure drilling (RPS), total sounding (TS) and soil sample analysis. Large amounts of geotechnical data were collected in Byneset, most of it close to the 2012 landslide scar (Solberg et al. 2015, 2016). As an example, conventional geotechnical soundings e.g. RPS, CPTU and TS performed at S2 indicated presence of quick clay (Fig. 42.1). A good number of core samples were collected for analysis in the laboratory using Swedish fall cone test (NGF 2011). All these samples confirmed quick clay ($s_{ur} < 0.5$) between 5.5 m and 10.5 m depth. The salt content here was ca. 1 g/l down to 10 m depth and increased to about 3.5 g/l below it.

The main purpose of the FHEM survey was to investigate its ability in mapping of clay layers and the subsurface resistivity in a broader area. Some of the FHEM lines were followed by ERT and refraction seismic survey for correlation. FHEM and ground geophysical methods are briefly described in this section. More details, results and interpretation of these and the other methods can be seen in Baranwal et al. (2015) and Solberg et al. (2015, 2016).

42.3.1 Helicopter EM Survey

NGU used a 7.5 m long Hummingbird™ system to collect low altitude (~30–50 m) airborne EM data. Before acquisition, the system was calibrated as described in the system manual (Geotech 1997). After processing and 1D inversion, seawater resistivity from the Trondheimsfjord near the survey area was interpreted correctly to be ca. 0.25 Ωm. FHEM data was collected mostly at 100 m line interval along 60 flight lines shown by black lines in Fig. 42.1. Average ground speed and sensor height were 98 km/h and 59 m, respectively. In-phase and quadrature components of induced secondary magnetic field in part per million (ppm) of transmitted primary field were recorded at 0.1 s interval resulting in ca. 3 m data interval. The data were collected at five different frequencies, three of them in coplanar (34 kHz, 6.6 kHz and 880 Hz) and two of them in co-axial (7 kHz and 980 Hz) setting of transmitter and receiver coils. Details of the instrumentation and processing of FHEM data is discussed in Baranwal et al. (2015). FHEM data was processed using HEM package in Oasis Montaj (Geosoft). Processed FHEM data were inverted using AarhusInv software (Auken and Christiansen 2004; AarhusInv 2015) which can perform laterally constrained inversion (LCI) or spatially constrained inversion (SCI) to give a pseudo-2D or pseudo-3D inversion result, respectively. FHEM data along few single flight lines (e.g. L1 and L2, Fig. 42.1) were inverted using LCI. Later, all the FHEM data were averaged with ten points running average and at 30 m intervals. It was inverted using SCI to give a pseudo-3D resistivity model of the area. Details of the inversion parameters are described in Baranwal et al. (2015).

42.3.2 Ground Geophysical Surveys

RCPTU is a small-scale four electrode sounding technique to perform in-situ electrical resistivity measurements. RCPTU data were collected from the two locations S1 and S2 (Fig. 42.1) and compared with resistivity values from FHEM and ERT surveys. Soil samples were also examined from these two locations to confirm the presence of quick clay in the area.

ERT data was acquired with the Lund system (Dahlin 1993) at 10 m electrode spacing using an ABEM Terrameter LS in multi gradient electrode configuration along parts of four FHEM profile lines (L1-L4 in Fig. 42.1). Six ERT profiles were collected close to the 2012 landslide scar (Solberg et al. 2015, 2016) and some of them are shown in Fig. 42.1. ERT data were inverted using RES2DINV code from Geotomo software (Loke 2010). Standard inversion of L2 norm and V/H filter of 0.5 were used to enhance horizontal structures in the model.

Refraction seismic survey (blue lines in Fig. 42.1) was performed along parts of three of the ERT profiles to estimate the depth to bedrock. The data acquisition was made using a seismic recording system ABEM Terraloc MK6 with 24 channels. Sufficient numbers of shots were made to get refraction from bedrock.

42.4 Interpretation and Results

42.4.1 Geophysical Data

Figures 42.2 and 42.3 present subsurface resistivity models obtained from inversion of ERT and FHEM data along line L1 and L2, respectively. Interpretation along line L3 and L4 are not shown in this paper. Seismic velocity layers interpreted from seismic refraction data are plotted with dashed black lines on the resistivity models. A very shallow upper seismic layer with a velocity of ca. 500 m/s is interpreted as unconsolidated dry layer of clay and partly bog/peat. The middle seismic layer has a velocity of ca. 1500 m/s and corresponds to water-saturated deposits, probably dominated by marine clay. Seismic data cannot differentiate between unleached and leached clay layers. The deepest layer is interpreted as bedrock with seismic velocity of ca. 3200–6500 m/s. The thickness of the seismic layers varies along these two profiles. The depth to bedrock interpreted from seismic refraction data (shown by dashed black lines in Figs. 42.2 and 42.3) is in good agreement with the ERT resistivity models along both lines but not predicted well by FHEM data due to the low depth of investigation (DOI) for FHEM in areas with thick conductive overburden. DOI can be as low as 30 m depending on overburden conductivity and therefore the interpreted resistivity below DOI can be inaccurate.

The results from ERT and FHEM show similar resistivity structures though with slightly different resistivity values. High resistivity areas (ca. 1000 Ωm) at both ends of the ERT and FHEM lines along L1 (Fig. 42.2) corresponds to bedrock exposed

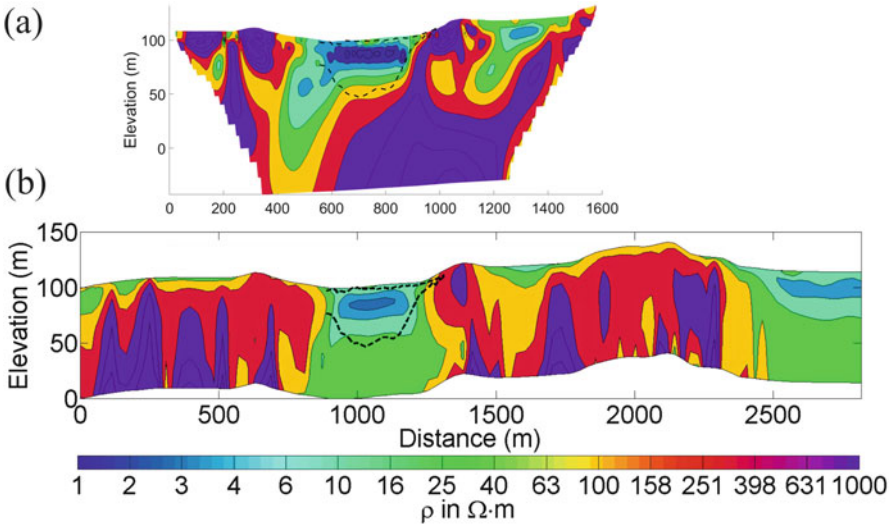

Fig. 42.2 (**a**) Inverted resistivity model from ERT data and (**b**) inverted resistivity model (from LCI) from FHEM data along line L1. (see Fig. 42.1 for location). *Dashed black lines* show seismic velocity boundaries. The figure is slightly modified from Baranwal et al. (2015)

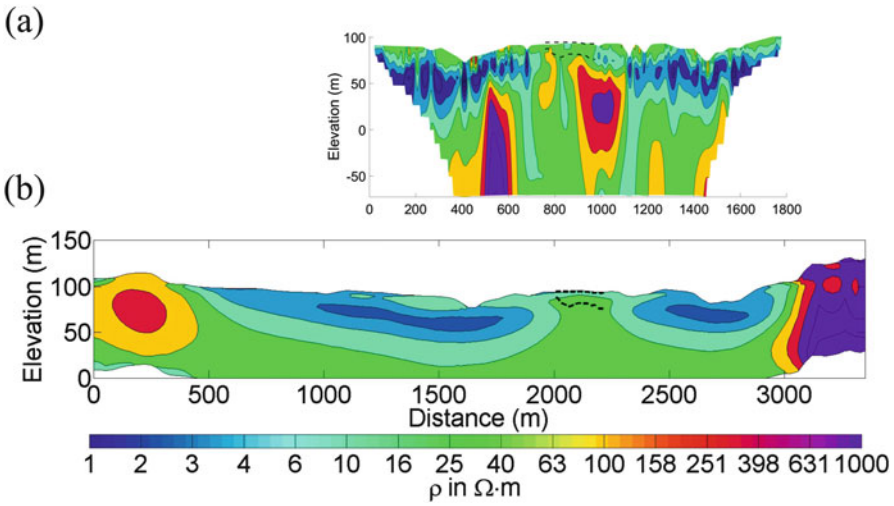

Fig. 42.3 (**a**) Inverted resistivity model from ERT data and (**b**) inverted resistivity model (from LCI) from FHEM data along line L2 (see Fig. 42.1 for location). *Dashed black lines* show seismic velocity boundaries. The figure is slightly modified from Solberg et al. (2016)

at the surface. A 500 m wide and 60 m thick layer along ERT profile L1 (from 500 to 1000 m) with very low resistivity (<10 Ωm) is interpreted as unleached marine clay (Fig. 42.2a). The similar structure is also shown in the FHEM resistivity model (Fig. 42.2b).

The ERT and FHEM resistivity models along line L2 (Fig. 42.3) indicate a 20 m thick leached clay zone with moderate resistivity of ca. 10–50 Ωm (between 800 and 1000 m on ERT profile, Fig. 42.3a). The ERT resistivity model shows a deep high resistivity zone (100–1000 Ωm) in the middle of the profile which matches well with the depth to bedrock interpreted from refraction seismic data. The discontinuity shown at ca. 850 m could be due to the presence of conductive minerals in the bedrock. FHEM data fails to detect the depth to bedrock due to low DOI. Both ERT and FHEM data indicate unleached clay zones (blue coloured from 500 to 2000 m and from 2200 m to 3000 m in Fig. 42.3b and at same location in Fig. 42.3a) below a shallow and inhomogeneous leached clay (green coloured).

FHEM resistivity values obtained from SCI inversion were gridded at 0, 2, 5, 9, 14, 21, 25 and 31 m depth using the inverse distance method in Oasis Montaj (Geosoft). The result, shown as resistivity-depth slices in Fig. 42.4, shows that the area is surrounded by high-resistive structures corresponding to bedrock close to the surface. Outcropping bedrock was observed in the field in the northern part of Byneset as indicated by FHEM data. The central region of the area is conductive due to thick layers of marine deposits. It comprises a thin and moderately resistive (10–100 Ωm) layer at the top interpreted as leached clay or silty sediments with a thick unleached marine clay (<10 Ωm) underneath. In the central part, the layer of unleached marine sediments is thicker.

42.4.2 Comparison of Resistivity from FHEM, ERT and RCPTU

Resistivity values from FHEM, ERT and RCPTU are compared at locations S1 and S2 (Fig. 42.5). FHEM lines were located 25 m and 6 m away from S1 and S2, respectively. FHEM resistivity values were extracted from SCI inversion of FHEM data. ERT resistivity values were extracted at S1 and S2 from ERT lines passing through these locations, as described in Solberg et al. (2016). A good agreement between RCPTU and ERT resistivity values was observed. FHEM resistivity is in good agreement with ERT and RCPTU at S1, and with similar pattern but lower values at S2. The thickness of potential quick clay is overpredicted by ERT and FHEM, as often also done by geotechnical sounding, like RPS and TS (Solberg et al. 2016). The resistivity variation from all three methods at S2 predicts leached clay ca. between 2 and 14 m depth with the resistivity range 10–100 Ωm. However, the sample test result shows a ca. 5 m thick quick-clay layer here. The resistivity value falls below 10 Ωm indicating unleached marine clay below 14 m depth.

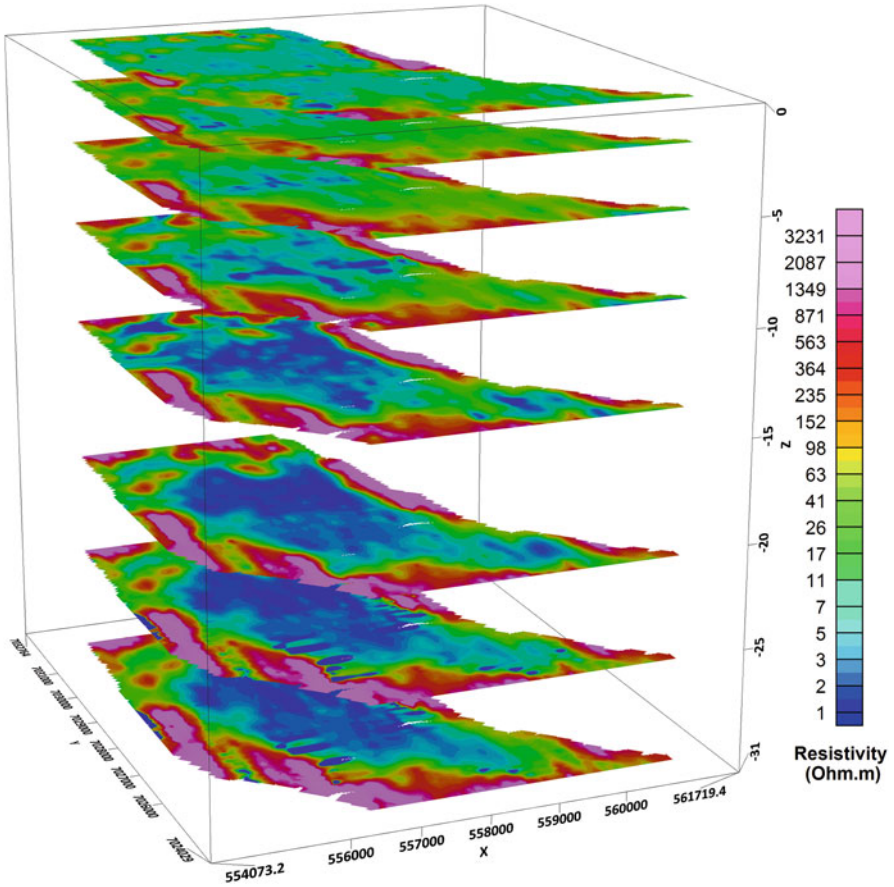

Fig. 42.4 Resistivity-depth slices from 0 to 31 m depth extracted from SCI resistivity models from FHEM data. The figure is slightly modified from Baranwal et al. (2015)

At S1 all three resistivity methods indicates leached clay down to 15 m depth and an ERT resistivity of 8–20 Ωm below this depth, which is close to unleached clay resistivity values (10 Ωm). FHEM show a resistivity variation of 2–50 Ωm at these locations and does not distinguish between leached clay and unleached clay as precisely as by RCPTU and ERT.

42.5 Discussion

Resistivity interpretations are simplified especially in the case of ERT and FHEM when data is interpreted in 2D and 1D. However, the true distribution of resistivity is in 3D. Resistivity profile direction and sampling distance will play an important role in the interpretation and its resolution. There might be sharp changes in resistivity

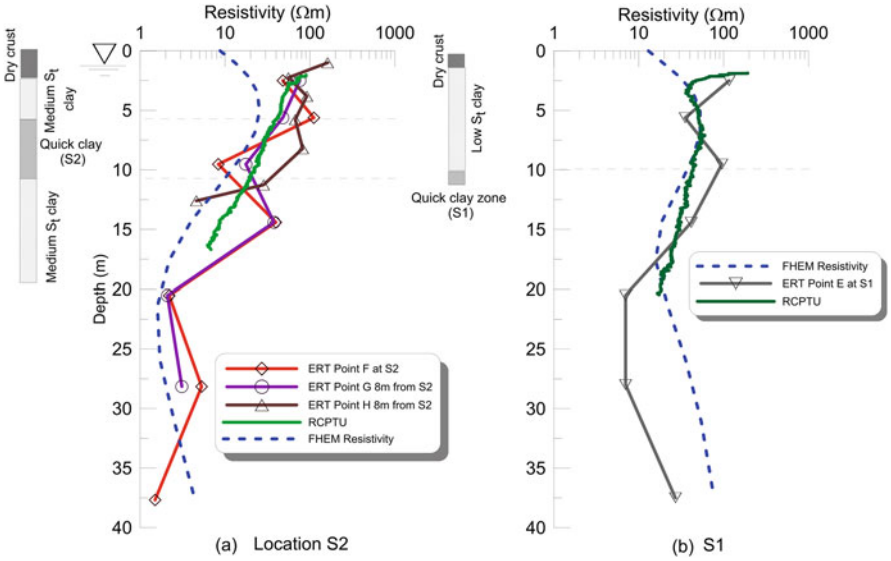

Fig. 42.5 Resistivity values extracted from FHEM and ERT resistivity models close to borehole locations and from RCPTU at borehole (**a**) S2 and (**b**) S1 (see Fig. 42.1 for location). Resistivity values are extracted at points (E-H) from ERT profiles. The figure is slightly modified from Solberg et al. (2016)

values when transiting from bedrock to leached/unleached clay and gradual changes in transiting from leached to unleached clay and vice-versa. There will also be a gradual change in the salt content in the marine clay. The resistivity interpretation is mostly done by smoothly varying resistivity models. Therefore, a sharp boundary between leached and unleached clay in nature should not be expected to be revealed by the resistivity measurements.

Salt content correlates directly with resistivity obtained from RCPTU and ERT (Solberg et al. 2008, 2016). The increase of the resistivity due to leaching makes a strong basis to use resistivity survey methods to differentiate possible quick-clay layers from unleached marine clay. ERT and RCPTU methods could detect unleached and leached zones and FHEM also proved to be a very valuable tool to investigate large areas. Still, these methods normally overpredict the thickness of quick clay, since the quick clay may have been further leached to increase the content of more stabilizing ions from the groundwater. Also, other material like silt or fine-grained till may give resistivity values within the leached clay range (Solberg et al. 2008). Therefore, resistivity methods alone cannot confirm presence of the quick clay.

Resistivity obtained from FHEM, ERT, and RCPTU did not show an exact match but showed a good agreement with each other in spite of the different scale and resolution. RCPTU reveals a very local resistivity within few centimeters, while resolution of ERT and FHEM vary from a meter to tens of meters depending on data collection interval, interpretation technique and sensor height (in case of FHEM) etc.

FHEM cannot reveal accurate resistivity deeper than few tens of meters in areas with conductive overburden due to limitation of depth of investigation (DOI), though it can investigate to hundreds of meters of depth in high-resistive areas. This depth limitation of FHEM interpretation was evident when FHEM results were compared with ERT and refraction seismic results. Seismic refraction interpretation provides more reliable information about depth to bedrock than ERT and FHEM. Some of the disagreement between ERT, FHEM and seismic refraction could be attributed to the presence of conductive minerals in the bedrock (Solberg et al. 2008, 2016). FHEM could clearly differentiate between unleached clay, leached clay and high-resistive bedrock due to detection range of a few Ωm to thousands of Ωm resistivity.

42.6 Conclusion

The study confirms that geophysical techniques are very important tools to investigate areas prone to quick-clay landslides. FHEM could be used as a first-hand reconnaissance survey to get an overview of the area, and later ERT, RCPTU and geotechnical studies can be performed for detailed investigations of clay properties in specific areas of interest. The FHEM data indicated that the central parts of Byneset are relatively conductive comprising a thin and moderately resistive layer of leached clay or silty sediments with thick, unleached marine clay underneath. The area is surrounded by exposed and shallow bedrock with high resistivity.

Geophysical studies cannot replace geotechnical studies for mapping of quick clay. Soil sample analysis is necessary to establish the presence and accurate depth of the proved quick clay. However, the geophysical and geotechnical methods can complement each other very well in the study of a complex geological area investigating different aspects from geological development to material properties. Therefore, a combination of geophysics and geotechnical methods will make investigations more precise and effective.

Acknowledgments The authors wish to express their gratitude to Lena Persson for reviewing the article and giving insightful comments to improve the quality of it.

References

AarhusInv (2015) Manual for inversion program ver. 6.3, HydroGeophysics Group (HGG), University of Aarhus, Denmark, http://www.hgg.geo.au.dk/HGGsoftware/em1dinv/em1dinv_manual.pdf

Auken E, Christiansen AV (2004) Layered and laterally constrained 2D inversion of resistivity data. Geophysics 69:752–761

Baranwal VC, Rønning JS, Dalsegg E, Solberg IL, Tønnesen JF, Rodionov A, Dretvik H (2015) Mapping of marine clay layers using airborne EM and ground geophysical methods at Byneset, Trondheim municipality. NGU Report 2015(006):59

Christensen CW, Pfaffhuber AA, Anschütz H, Smaavik TF (2015) Combining airborne electromagnetic and geotechnical data for automated depth to bedrock tracking. J Appl Geophys 119:178–191

Dahlin T (1993) On the Automation of 2D Resistivity Surveying for Engineering and Environmental Applications. Ph.D. Thesis, Department of Engineering Geology, Lund Institute of Technology, Lund University. ISBN 91-628-1032-4

Geotech (1997) Hummingbird electromagnetic system. User's manual. Geotech Ltd, Canada

Loke MH (2010) Res2DInv ver. 3.59.102. Geoelectrical Imaging 2D and 3D, Instruction Manual. Geotomo Software, www.geoelectrical.com

NGF (Norsk Geoteknisk Forening) (2011) Veilding for symboler og definisjoner i geoteknikk-identifisering og klassifisering av jord- Melding Nr. 2 (in Norwegian)

NVE (Norges vassdrags- og energidirektorat) (2012) Kvikkleireskred ved Esp på Byneset i Trondheim. NVE report 1-2012, preliminary report 2012.01.09 (in Norwegian)

Reite AJ, Sveian H, Erichsen E (1999) Trondheim fra istid til nåtid – landskapshistorie og løsmasser. Geological Survey of Norway (NGU), Gråsteinen 5 (in Norwegian)

Sauvin G, Lecomte I, Bazin S, Hansen L, Vanneste M, L'Heureux JS (2014) On the integrated use of geophysics for quick-clay mapping: The Hvittingfoss case study, Norway. J Appl Geophys 106:1–13

Shan C, Malehmir A, Bastani M, Persson L, Engdahl M (2016) Integration of controlled-source and radio magnetotellurics, electrical resistivity tomography, and reflection seismics to delineate 3D structures of a quick-clays landslide site in southwest of Sweden. Geophysics 81(1):B13–B29

Siemon B, Christiansen AV, Auken E (2009) A review of helicopter-borne electromagnetic methods for groundwater exploration. Near Surf Geophys 7:629–646

Solberg IL, Rønning JS, Dalsegg E, Hansen L, Rokoengen K, Sandven R (2008) Resistivity measurements as a tool for outlining quick clay extents and valley fill stratigraphy: feasability study from Buvika, Central Norway. Can Geotech J 45:210–225

Solberg IL, Baranwal VC, Dalsegg E, Dretvik H, Gasser D, Rønning JS, Tønnesen JF (2015) Geologi på Byneset: en sammenstilling av geologiske, geofysiske og geotekniske data. NGU Report 2015(002):65. (in Norwegian)

Solberg IL, Long M, Baranwal VC, Gylland AS, Rønning JS (2016) Geophysical and geotechnical studies of geology and sediment properties at a quick-clay landslide site at Esp, Trondheim, Norway. Eng Geol 208:214–230

Chapter 43
The Norwegian National Database for Ground Investigations (NADAG): A Tool to Assist in Landslide Hazard Zonation and Other Quick-Clay Related Issues

Inger-Lise Solberg, Bo Nordahl, Louise Hansen, Bjørn Ove Grøtan, and S. Gulbrandsen

Abstract Exploitation of the subsurface is becoming more frequent and the demand for knowledge about ground conditions is increasing. A vast amount of data from ground investigations such as geotechnical drilling, bedrock drilling and ground water wells exists in Norway. However, many of these are not easy to access as they are spread between multiple data owners and users. Following the development of The National Database for Ground investigations (NADAG) during the last years, the registration of geotechnical data has started. With increased accessibility of data, re-use will lead to considerable savings for the society. Importantly, the information will allow for better landslide hazard zonation. In addition, the effectiveness of emergency planning and response will improve with access to relevant, accurate and timely information about the local ground conditions. This may be crucial after landslide events with regard to the assessment of potential landslide expansion and the safe evacuation of people. NADAG aims to collect and make publically available data from ground investigation important for the society. The database contains various amounts of data, depending on availability – ranging from metadata (location, drill type, drill depth, company, date, report no., etc.) to full reports and raw data. NADAG will initially be populated by data from geotechnical investigations. A primary objective for NADAG is to distribute data from all types of ground investigations in Norway and to present the data coverage through a map-enabled web application.

I.-L. Solberg (✉) • B. Nordahl • L. Hansen • B.O. Grøtan • S. Gulbrandsen
Geological Survey of Norway, Trondheim, Norway
e-mail: inger-lise.solberg@ngu.no; bo.nordahl@ngu.no; louise.hansen@ngu.no; bjorn.ove.grotan@ngu.no; snorre.gulbrandsen@ngu.no

V. Thakur et al. (eds.), *Landslides in Sensitive Clays*, Advances in Natural and Technological Hazards Research 46, DOI 10.1007/978-3-319-56487-6_43

43.1 Introduction

In Norway numerous landslides have occurred involving quick clay (e.g. Verdal 1893 (Janbu et al. 1993), Rissa 1978 (Gregersen 1981), Namsos 2009 (Nordal et al. 2009)). Highly sensitive quick clay may develop due to leaching by fresh groundwater altering the chemical composition of the pore water in marine clays (Rosenqvist 1953). An understanding of ground conditions, including the distribution of quick clay, is important for the evaluation of landslide hazards as part of land-use planning, including construction and erosion protection (Fig. 43.1).

Every year large amounts of geotechnical drilling is carried out in order to obtain details about soil properties. Although a significant amount of data exists, these are not easy to access as they are spread between different data owners and users. Within cities, in particular, the exploitation of the subsurface is growing. The need for 3D geological information is increasing, which is important for landslide hazard zonation, and may be crucial for the assessment of safety after landslide events with regard to possible landslide expansion and evacuation of people.

The National Database for Ground investigations (NADAG) has been developed during the last years. NADAG aims to collect and make publically available all data from ground investigations. The fill-in of geotechnical data has started. This makes data access easier and re-use will lead to considerable savings for the society. A cost-benefit analysis has been made for the usefulness of NADAG, which estimates annual savings exceeding NOK 16 mill (about 2 mill Euro) (costs: NOK 2.5 mill per year) (Vennemo et al. 2015). Numerous and expensive investigations may

Fig. 43.1 Construction work in areas of marine clay in Norway is challenging, and requires large amounts of ground investigations. The picture is from building of the new E39 in Børsa, Mid Norway (Photo: NVE 2004)

be necessary to determine ground conditions. Many of these are paid for by the government, and the data should therefore be available for re-use.

The present paper explains how NADAG is highly beneficial for the mapping of quick clay and other sediments, susceptibility and hazard zonation, and emergency management.

43.2 The NADAG Project

The project about the National Database for Ground investigations (NADAG) has been a cooperation between the Geological Survey of Norway (NGU) and three other governmental institutions: the Norwegian Public Roads Administration, the Norwegian Water Resources and Energy Directorate and the Norwegian National Rail Administration. NGU has developed NADAG together with the consulting companies Norkart AS and Trimble. The project began in 2012 (Solberg et al. 2012) and version 2.0 was completed in 2016. Version 1.0 was a proof of technology version and 2.0 is a production version. The development of NADAG is ongoing and will continue.

There are large amounts of data from different types of drilling scattered all over Norway, e.g. bedrock drilling, groundwater wells and energy wells. Geotechnical investigations however, are probably the most common type of drilling, thus it was decided to start to fill NADAG with this data type. The primary objective for NADAG in the future is to store and distribute data from all ground investigations in Norway, and to present the data through a map-enabled web application.

43.3 Structure and Data in NADAG

In Norway standards for geo-referenced information is organised in a system called SOSI. The geotechnical community has made a SOSI standard for geotechnical investigations. This was used to develop the data model for NADAG, and covered a lot of use cases. Figure 43.2 shows the basic structure of the SOSI standard and data model. In a Geotechnical Investigation area (GI) several Geotechnical Boreholes (GB) can be made. Each borehole consists of one or more Geotechnical Borehole Investigations (GBI), e.g. cone penetration test (CPT), total sounding, rotary pressure sounding and sampling.

Some metadata is required for the data that is included in NADAG. This information include location, drilling type, drill depth, company, date and report no. More data is preferable, and if available, NADAG can receive “everything”, from metadata to results and raw data.

Figure 43.3 shows some of the principles for the structure of NADAG. NGU operates the database, and use technology already applied at the survey. The map clients are implemented using a combination of JavaScript (OpenLayers, jQuery

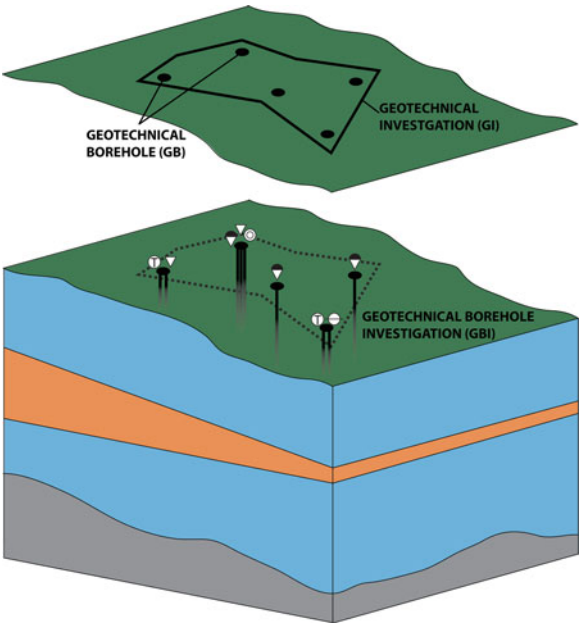

Fig. 43.2 The main structure in the NADAG data model is based on a Norwegian standard for geotechnical investigations. The Geotechnical Investigation (GI) is "the project area", which contains the Geotechnical Boreholes (GB). In each borehole one or more methods may be used, i.e. Geotechnical Borehole Investigations (GBI)

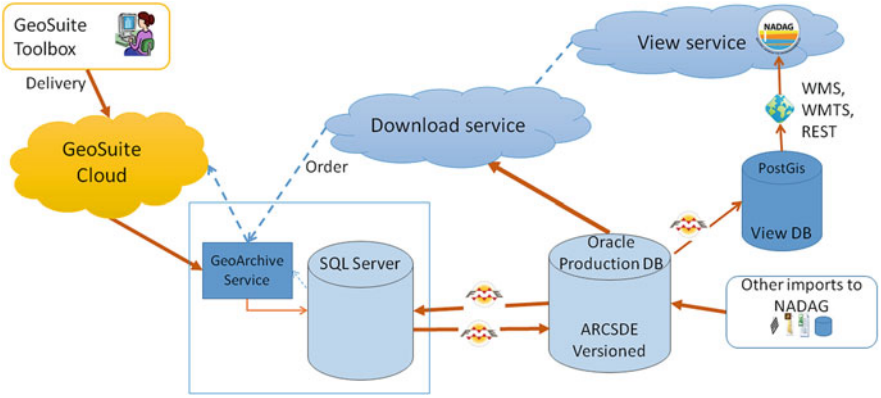

Fig. 43.3 Some of the principles for the structure of NADAG

and other well known frameworks), HTML and PHP. The clients utilize a set of WebServices such as geographical entities – as well as base maps and map data via WMS/WMTS and REST.

Larger geotechnical consultants and some governmental organisations in Norway such as the road authorities, use GeoSuite from Trimble for planning and designing infrastructure. A tool in GeoSuite is developed that will make it easy to deliver all data from a project to NADAG (Fig. 43.3). The road authorities will also use this tool to deliver data from their internal database (GUDB) to NADAG.

The amount of data that is delivered to NADAG is partially dependent on the data owners' individual data management systems. Some data owners only have paper archives of older reports and the digitising of such data will be an expensive and time-consuming process. In that case the first step may be data delivering on the Geotechnical Investigation (GI) level, without details about each drilling (see Fig. 43.2). For newer digital data, it will be easier for data owners to deliver to most or all parts of the database. Therefore, NADAG has the opportunity to receive both old and new data sets. Users of NADAG will be able to download data in different formats, including the GeoSuite format mentioned above.

Another limiting factor for the amount of data that will be imported into NADAG, is the legal rights connected to the use and sharing of the data. In old contracts the data use is often limited to certain projects. However, most consultant companies are willing to publish metadata – as this may also have a beneficial advertising effect for the company. In Norway there is legal requirement for groundwater drill data to be reported to NGU and published, but this is not the case for geotechnical investigations. However, new contract formulations will give the client the opportunity to publish the data. This is an important issue for the governmental institutions.

Figure 43.4 shows an example from the NADAG web application (http://geo.ngu.no/kart/nadag). There are some standard views and it is also possible to choose different layers and backgrounds, or change the order of the layers. The datasets

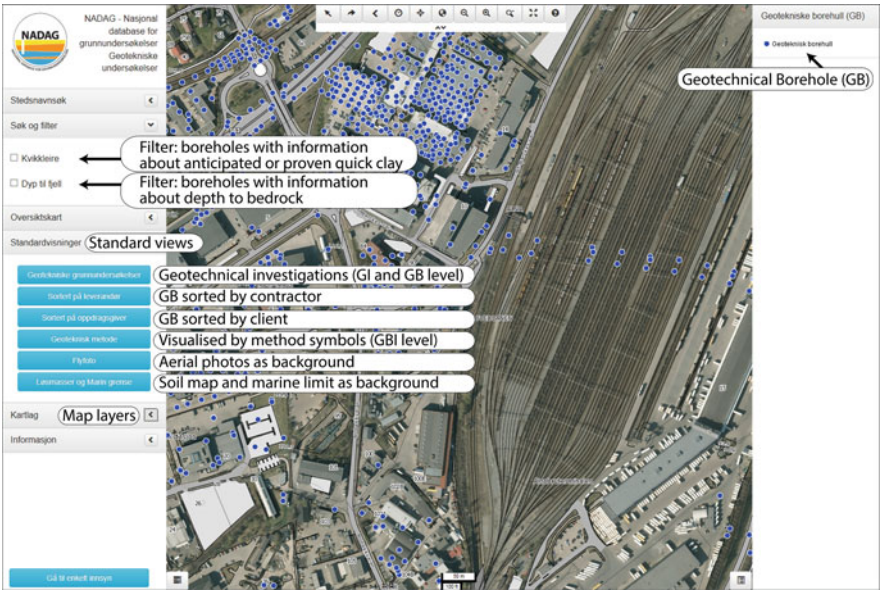

Fig. 43.4 Example of the NADAG web application (http://geo.ngu.no/kart/nadag). The geotechnical boreholes (*black dots*) are shown on aerial photo background. The user can choose between different views and layers

may also be sorted by client or contractor, visualised by method symbols (GBI-level, see Fig. 43.2). There are also two filters: boreholes that have information about anticipated or proven quick clay, and boreholes that have information about depth to bedrock. Information sheets opens in a new tab when clicking a borehole (GB) or an investigation area (GI).

43.4 Use of NADAG Related to Landslide Issues

43.4.1 Quick-Clay Landslide Hazard Zonation

Marine Limit (ML) is the highest sea level after the last ice age and varies throughout Norway. It is as high as 220 m above present sea level in certain areas. Marine sediments and potential quick clay are only found in areas below the ML (Hansen et al. 2014). These areas can be seen as generally susceptible to quick-clay landsliding.

After the Rissa landslide in 1978, a national program was initiated for the mapping of areas where large landslides involving quick clay can potentially occur. The resulting hazard zones have also been risk evaluated (Gregersen 2008). The program is still running.

The landslide hazard mapping is based on Quaternary geological maps (see Hansen et al. 2017), topography, erosion, slope steepness, and geotechnical properties of the soil – among other factors. As geotechnical investigations are expensive, mapping programs often include relatively little sounding and sampling.

When areas are re-evaluated, data from NADAG may be used to aid the investigations from the mapping program. This will potentially change the extent of the zones, classify the zones more accurately and help mapping of new zones. Figure 43.5 shows how quick-clay hazard zones can be displayed together with geotechnical boreholes in NADAG. It is important to notice that quick clay may occur also outside the defined hazard zones. Geotechnical data from NADAG will help to identify smaller areas below ML which potentially can be problematic.

43.4.2 Emergency Preparedness and Management

Landslides in sensitive clays often cause severe damage to infrastructure and threaten human life. Immediately following a quick-clay landslide people are evacuated. The evacuation of people may be inefficient and incorrect, if the ground conditions are poorly identified (Vennemo et al. 2015). The landslide may propagate in an unexpected direction and/or the downstream consequences may be disregarded. Ground investigations are necessary to accurately evaluate the possible extent and direction of landslide expansion. The data can give indications about the

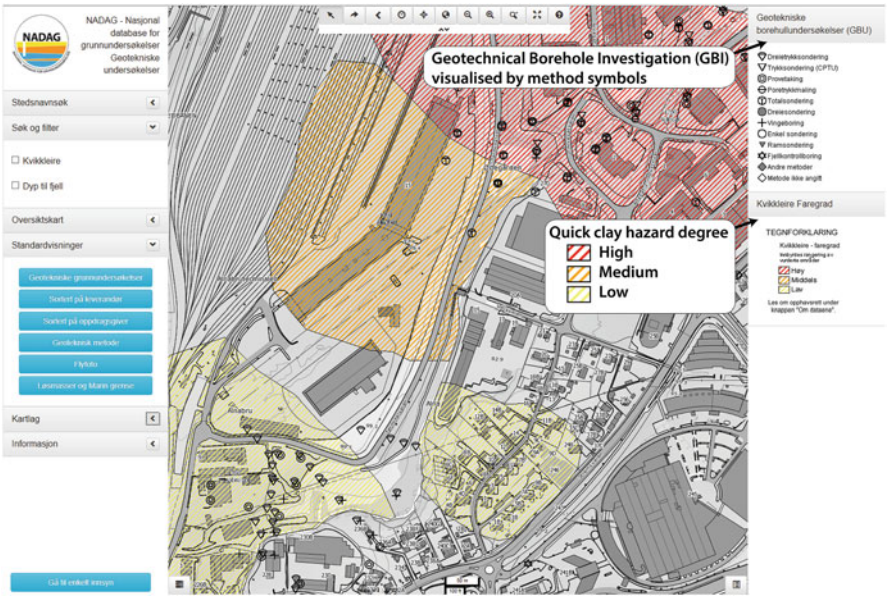

Fig. 43.5 Example from the NADAG web application where geotechnical data is shown (symbolised by method) together with hazard zones for potential quick-clay landsliding. Symbols in the map represent different geotechnical methods. Coloured hachure show hazard zones of different hazard degrees

presence of quick clay or stable materials such as non-quick clay, sand, gravel and bedrock which will act as a barrier to further landslide propagation.

The authorities often use a lot of time to track data from old investigations. In some areas data is very scarce or unavailable and it is necessary to carry out new geotechnical drillings few days after an event. Landslides that hit roads and railways, often lead to closure. Easy access to information about the ground conditions may result in faster management of the situation and reduced closure periods.

Data from earlier investigations in an affected area will therefore be very important. Data in NADAG could allow for a faster overview of the ground conditions and help emergency management.

43.4.3 Safe Construction in Areas with Quick Clay

Construction work in areas of challenging ground conditions requires large amounts of investigations during planning and work. The data are often used for stability calculations and the affected area should have an increased safety factor when the new infrastructure is finished.

Different geotechnical sounding methods provide valuable indications on quick-clay occurrence and sediment stratification. Laboratory testing of core samples gives more detailed information on material properties, like shear strength, and is currently the only method to determine clay sensitivity. However, laboratory tests are more expensive than soundings.

Every year the state, municipalities and private companies use large amounts of money for ground investigations. A few governmental departments and municipalities have their own equipment, but generally the investigations are carried out by geotechnical consultants. The volume of data produced is large; the road authority alone probably has data from over one million geotechnical boreholes throughout the country.

Re-use of data is an essential purpose of NADAG. Easy access to all data from boreholes, or in the least, metadata indicating where more information may be obtained, will lead to major savings for the community. The partners of the NADAG project want to emphasise that data from investigations paid by public funding should be available and free for everyone.

43.5 Concluding Remarks

There are many benefits of a national database for ground investigations, some of which are discussed in this paper. The challenging ground conditions in Norway, with layers of sensitive quick clay within exposed marine deposits, make easy access to information about of geology and soil properties very important for future development and hazard mitigation.

The National Database for Ground investigations (NADAG) aims to collect and make publically available data from ground investigations important for the society. Following the development of NADAG during the last years, the digital registration of geotechnical data has started. NADAG contains various amounts of data, depending on availability – ranging from metadata to full reports and raw data. With increased accessibility of data, re-use will lead to considerable savings for the society. With access to relevant soil property information, mapping of susceptibility, landslide hazard assessment and predictions of landslide propagation below the Marine Limit can be improved. NADAG will also allow authorities to improve emergency evacuation plans and reduce infrastructure closure periods in the event of a landslide.

Acknowledgements Thanks to the Norwegian Public Roads Administration, the Norwegian Water Resources and Energy Directorate, the Norwegian National Rail Administration, The Norwegian Directorate of Public Construction and Property, selected municipalities, Norkart AS, Trimble for the cooperation in the making of NADAG. The authors also wish to express their gratitude to Karin Lundström for reviewing the paper.

References

Gregersen O (1981) The quick clay landslide in Rissa, Norway. NGI Publication 135:1–6

Gregersen O (2008) Program for økt sikkerhet mot leirskred. Metode for kartlegging og klassifisering av faresoner, kvikkleire. NGI report 20001008-2, rev. 3, 2008.10.08

Hansen L, Høgaas F, Sveian H, Olsen L, Rindstad BI (2014) Quaternary geology as a basis for landslide susceptibility assessment in fine-grained, marine deposits, onshore Norway. In: L'Heureux et al (eds) Landslides in sensitive clays – from geosciences to risk management. Advances in natural and technological hazard research 36. Chapter 29, 1st International Workshop on Landslides in Sensitive Clay (IWLSC). Springer, Quebec

Hansen L, Solberg IL, Jarna A, Nordahl B (2017) Developments in mapping and web presentation of fjord-marine deposit distributions for quick-clay related work in Norway. 2nd International Workshop on Landslides in Sensitive Clay (IWLSC), Trondheim, Norway, June 2017

Janbu N, Nestvold JØ, Sveian H (1993) Leirras – årsaksforhold og rasutvikling. In: Walberg, Ø. 1993. Verdalsboka. Ras i Verdal, bind B. Verdal kommune, pp 739–784 (In Norwegian)

Nordal S, Alén C, Emdal A, Jendeby L, Lyche E, Madshus C (2009) Skredet i Kattmarkvegen i Namsos 13. mars 2009. Rapport fra undersøkelsesgruppe satt ned av Samferdselsdepartementet. Institutt for bygg, anlegg og transport, faggruppe for geoteknikk, NTNU (In Norwegian)

Rosenqvist IT (1953) Considerations on the sensitivity of Norwegian clays. Géotechnique 3:195–200

Solberg IL, Ryghaug P, Nordahl B, de Beer H, Hansen L, Høst J (2012) Nasjonal database for grunnundersøkelser (NADAG) – forundersøkelse. NGU report 2012.054 (In Norwegian)

Vennemo H, Magnussen K, Hansen VW, Ibenholt K (2015) Nytte og kostnader av nasjonale databaser: Metodeutvikling og utprøving på nasjonal database for grunnundersøkelser. Vista Analyse Report 2015/03 (In Norwegian)

Chapter 44
Future Strategy for Soil Investigations in Quick Clay Areas

Rolf Sandven, Anders Samstad Gylland, Alberto Montafia, Andreas Aspmo Pfaffhuber, Kristoffer Kåsin, and Mike Long

Abstract The landslides at Rissa in 1978, and more recently at the Skjeggestad bridge in Norway, are devastating reminders of the potential threats related to quick clays. For a geotechnical engineering project it is hence important to determine if there is sensitive clay present and to clarify the extent of the quick clay deposit. Integration of geophysical and geotechnical methods has become more common in ground investigations nowadays, particularly in larger projects. In such integrated measurements, geotechnical engineers and geophysicists can cooperate, and by joint knowledge decide where geotechnical soundings, in situ tests and sampling should be located with optimal cost-efficiency. This paper describes how various investigation methods may be combined to achieve a successful strategy for detecting deposits of quick and sensitive clays. The methods presented herein include conventional soundings, CPTU and field vane test (FVT), supplemented by geophysical methods such as CPTU with resistivity measurements (R-CPTU), Electrical Resistivity Tomography (ERT) and Airborne Electromagnetic Measurements (AEM).

44.1 Introduction

Sensitive clays of Norway, when provoked by manmade or natural causes, have led to several landslide disasters throughout history. These landslides have occurred in highly sensitive clays also known as quick clays, see i.e. L'Heureux (2012).

R. Sandven (deceased) • A.S. Gylland (✉) • A. Montafia
Multiconsult ASA, Trondheim, Norway
e-mail: anders.gylland@multiconsult.no; Alberto.montafia@multiconsult.no

A.A. Pfaffhuber • K. Kåsin
Norwegian Geotechnical Institute (NGI), Oslo, Norway
e-mail: Andreas.a.pfaffhuber@ngi.no; Kristoffer.kaasin@ngi.no

M. Long
School of Civil Engineering, University College Dublin (UCD), Dublin, Ireland
e-mail: Mike.Long@ucd.ie

V. Thakur et al. (eds.), *Landslides in Sensitive Clays*, Advances in Natural and Technological Hazards Research 46, DOI 10.1007/978-3-319-56487-6_44

Indication of quick and sensitive clays is hence an important issue in many projects, since this will change the project assumptions and provide stricter guidelines for the ground investigations. It will also influence geotechnical planning and design, as well as control and documentation routines for the geotechnical work carried out.

The field methods used in Norway today give sufficient indications of brittle materials in many cases. However, sounding profiles obtained by conventional methods may give misleading indications in some situations. This may either be on the conservative side, where results indicate quick clay in the field, but where the laboratory testing show non-sensitive behaviour. More difficult is the opposite, where the sounding profiles show no signs of quick clay, but where such materials are discovered later in the project.

The great efforts undertaken for mapping of quick clay zones have led to an increasing need of quicker and more reliable identification of such materials. Today, there is an increasing tendency of using a combination of geophysical and geotechnical methods in mapping of quick and sensitive clays. In general, one may say that geophysical methods cover large areas in relatively short time, but possibly with poorer resolution and less refinement than most geotechnical tests. Hence, combining geophysical and geotechnical methods may result in a more rational and cost-effective ground investigation, see e.g. Löfroth et al. (2011).

In this paper, quick clay, sensitive clay and brittle materials have been defined according to NGF (2011) and NVE (2014). These definitions are also given in Sandven et al. (2017).

The NIFS project is a joint venture between the Norwegian Water Resources and Energy Directorate (NWRED), The Norwegian Railroad Administration (NNRA) and the Norwegian Public Roads Administration (NPRA). One of the main goals of the project is to coordinate guidelines and develop better tools for geotechnical design in quick clay areas. This paper discusses future strategies for detection of brittle materials from various geotechnical and geophysical field tests. Reference is made to NIFS reports (2015a, b) for detailed results and soil data (http://www.naturfare.no) from the study, summarized by Sandven et al. (2016a, b).

44.2 Toolbox of Geotechnical and Geophysical Methods for Mapping of Quick Clays

The methods applied in mapping of brittle materials must be chosen based on a cost-benefit perspective, the applicability of the methods for the actual ground conditions and the general use of soil data in the project. For use in current practice, it is important to present recommendations based on the experiences and observations made with various detection methods. In particular, this is valid for the resistivity methods R-CPTU, ERT and AEM, where limited experience exists from practical use.

44.2.1 Conventional Geotechnical Soundings

Conventional sounding methods such as rotary pressure and total sounding use, directly or indirectly, the measured total penetration force for indication of brittle materials.

44.2.1.1 Rotary Pressure Sounding (DRT)

Rotary pressure sounding is a method where the drillstring is pushed and rotated into the ground by a drillrig. During penetration, the procedure shall satisfy the following conditions:

- Penetration rate: 3 ± 0.5 m per minute
- Rotation rate: 25 ± 5 rotations per minute

The sounding resistance corresponds to the penetration force required to obtain these normative conditions. Rotary pressure sounding can be used in most types of soils, from clay to gravel.

44.2.1.2 Total Sounding (TOT)

Total sounding is used to determine soil stratification and depth to bedrock or dense strata. The method also enables drilling through larger stones and penetration of the bedrock surface. Total sounding requires a hydraulic drillrig with a percussion hammer and flushing possibilities.

Total sounding combines the sounding principles from rotary pressure sounding and rock control drilling, see Fig. 44.1. In rotary pressure mode, the drill rods are penetrated into the ground with constant penetration and rotation rate. If these methods are not sufficient to advance the drillrods, it is possible to switch to rock control mode with increased rotation, then flushing and hammering.

Detection of brittle materials from rotary pressure and total soundings is mainly based on the slope of the sounding curve, to a lesser degree the magnitude of the recorded penetration force (F_{DT}). In Fig. 44.1, the quick clay layer is typically identified as the section with a vertical, partly negative slope.

44.2.2 Cone Penetration Tests (CPTU)

Cone Penetration Test with pore pressure measurement (CPTU) is performed with an instrumented cylindrical probe that is penetrated into the ground at a constant rate of 20 mm/s. The probe contains electronic transducers for recording of the load against the conical tip, the force against the friction sleeve and the pore pressure

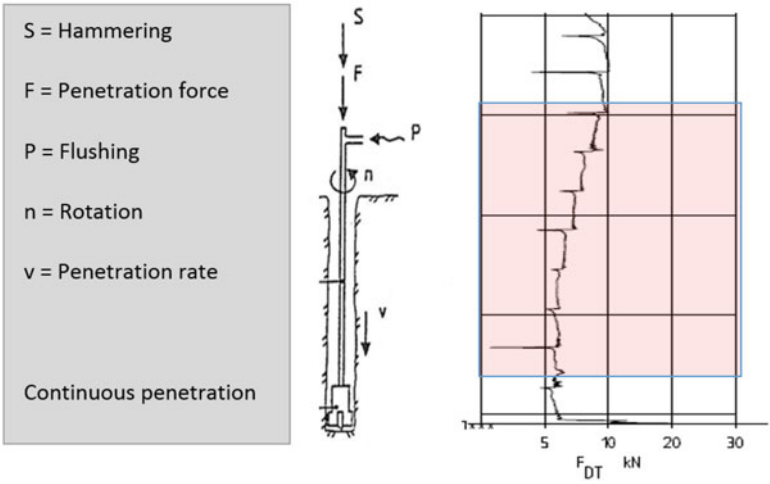

Fig. 44.1 Test principles for total sounding. The *pink-shaded area* is interpreted as potential quick clay

at the location of the porous filter. In addition, the recording of the total penetration force may be used to find the mobilized friction along the drillrods. This information can be used to detect quick and sensitive clay layers.

The presence of quick or sensitive clays from CPTU may be evaluated from the behaviour of cone resistance, sleeve friction and pore-pressure with depth. These, and derived dimensionless parameters, can be used in soil behaviour charts to further indicate soil type (see Sandven et al. 2016b and Gylland et al. 2017).

Despite the obvious potential in these approaches, mixed experiences exist in detection of brittle materials from CPTU (see Sandven et al. 2016b). This is further elaborated in the following sections.

44.2.3 Sleeve Friction f_s

A completely remoulded quick clay has a shear strength $c_{ur} < 0.5$ kPa. Hence, the material is close to being a liquid after full degradation of the soil structure. In CPTU soundings, this should result in very small mobilized sleeve friction, assuming that the clay becomes completely remoulded by the first penetration of the probe. However, analyses of a series of CPTU-profiles show that the sleeve friction can be high even in quick or sensitive clays. This is often the case in silty, lean clays, where the material requires several repeated penetration cycles of the probe before full remoulding is obtained.

44.2.3.1 Pore Pressure Ratio B_q

Due to dilatancy effects, the measured pore pressures behind the cone (u_2) are smaller than the pore pressure in the compression zone beneath the tip (u_1). Due to this influence, the pore pressure ratio B_q is not a unique identification parameter in brittle materials. So, although $B_q \geq 1.0$ is common in quick clays due to the collapsible behaviour at failure, this criterion does not guarantee the presence of quick clay.

44.2.4 Vane Testing

The vane consists of four rectangular plates in cruciform shape which is penetrated into the ground to the desired depth. Then rotation is applied and the torque measured together with rotation. The corresponding maximum torque is recorded and enables determination of the undrained vane strength c_{uv}. The remolded shear strength (c_{rv}), which is valid information for quick clay assessment, is determined after at least 25 full, rapid rotations of the vane.

The vane test is the only in situ test which can be used to determine the remolded shear strength and the sensitivity ($S_t = c_{uv}/c_{rv}$) directly. However, there is not a one-to-one relationship between sensitivity as measured from the vane test and by the falling cone test in the laboratory. The vane appears to measure too high values for the remolded undrained shear strength (Gylland et al. 2016). The torque should therefore preferably be applied and measured down at the vane to avoid friction and deformation in the drillrods.

44.2.5 Resistivity Measurements

The resistivity is a measure of the ability of soils to conduct electric current. The resistivity ρ (Ωm) is defined by the electric field potential E (V/m) over the current density J ((A/m^2)m), and can be computed from the electrical current, a geometry factor and the measured potential. The resistivity gives information about the soil layers, and will in this context give an indication of the salt content in the ground water. The resistivity correlates well with salt content down to concentrations around 1 g/l. For lower salt contents, other influence factors such as clay content and plasticity seem to dominate the measured resistivity (NIFS 2015a).

Resistivity measurements seem to have a great potential for detection and extent of brittle materials (Sandven et al. 2016b). Resistivity profiles give a continuous image of the ground layering, whereas local information from geotechnical borings may be used to support or verify the geophysical interpretation.

Fig. 44.2 CPTU probes and resistivity module for R-CPTU (NIFS 2015a)

So far, the most popular geophysical method for detection of brittle materials has been 2D-resistivity measurements on the surface (Electrical Resistivity Tomography ERT). The resistivity can also be measured locally in a borehole by R-CPTU. Recently, airborne electromagnetic measurements (AEM) have also been introduced for mapping of potential sensitive clays.

44.2.5.1 Downhole Measurements (R-CPTU)

The sounding equipment used for R-CPTU consists of an ordinary CPTU probe and a resistivity module mounted behind the probe, see Fig. 44.2. The module is powered by batteries, and it can read, store and transmit measured data acoustically through the rods, or via an electric cable to a receiver on the surface. The additional time for R-CPTU compared to a conventional CPTU is only a few minutes. Apart from the application of the resistivity module, the sounding procedure is similar to an ordinary CPTU.

Scandinavian manufacturers of R-CPTU equipment have chosen to manufacture their probes with four ring-electrodes (typical range 1–3000 mS/m). The two outer electrodes transmit electric current into the soil, whereas the two inner electrodes measures the difference in potential.

44.2.5.2 Surface Measurements (ERT)

Electrical resistivity tomography (ERT) is a geophysical method that uses DC current for measurement of the resistivity distribution in the ground. The current is applied to the soil volume by using short steel electrodes. These are installed from the surface, penetrating 10–20 cm into the ground. By evaluating the differences in

electric potential, a measurement of the soil resistance is obtained for all electrode locations. With the aid of an inversion algorithm, a 2D or 3D resistivity model of the ground is developed from the results. By comparing the resistivity model with data from geotechnical borings, supported by the geological knowledge of the area, the resistivity can be interpreted in terms of a geological ground model, see Fig. 44.3.

The measurement profiles are organized in one or more straight profiling lines in the terrain. A general estimate of the investigation depth is a reach of about 10–20% of the profile length, depending on the resistivity distribution in the soil. The obtained resolution is dependent on the electrode spacing. It is however possible to measure a profile with several different electrode spacings to obtain a combination of high resolution and sufficient penetration depth. High resolution is particularly important if the aim is to separate the small differences in resistivity between salt and leached clay.

ERT is a robust method that give results of high quality in most cases (see e.g. NIFS 2015a). The measurements are however sensitive to objects in the influenced zone. This may be electrical cables, tubes and other structures influencing the resistivity model. Thus, the use of this method in urban area may be limited.

44.2.5.3 Airborne Measurements (AEM)

AEM (Airborne Electromagnetic Measurements) are used to map the electrical resistivity of the ground in a larger area. Modern systems may have sufficient resolution to be used in hydrological and geotechnical applications. AEM data can be collected both over land and sea areas, and may distinguish between cultivated land, forests and exposed rock. Recent studies show that it is possible to distinguish salt from leached clays with high-resolution measurements, similar to what can be done by R-CPTU and ERT (e.g. Anschütz et al. 2015, Pfaffhuber et al. 2016).

All AEM systems have in common that a magnetic field generated by the primary antenna induces current in the ground, which distributes downward and outwards from the source. The rate of change in the electro-magnetic field these currents produce, is recorded by a secondary coil. The antenna is usually lifted by a helicopter, see Fig. 44.4.

The possible investigation depth may vary from 50 m to about 500 m, depending on the geology and type of soil in the area, the AEM system and the influence of noise from surrounding infrastructure. The vertical resolution may be as good as 3–6 m close to the surface, but gradually gets poorer with depth. Up to 300 km flylines can be gathered daily, which corresponds to an area of about 30 km^2 with line spacing of 100 m. Urban areas cannot be covered by AEM-measurements, since the helicopter or plane is not allowed to fly over human beings with a hanging object.

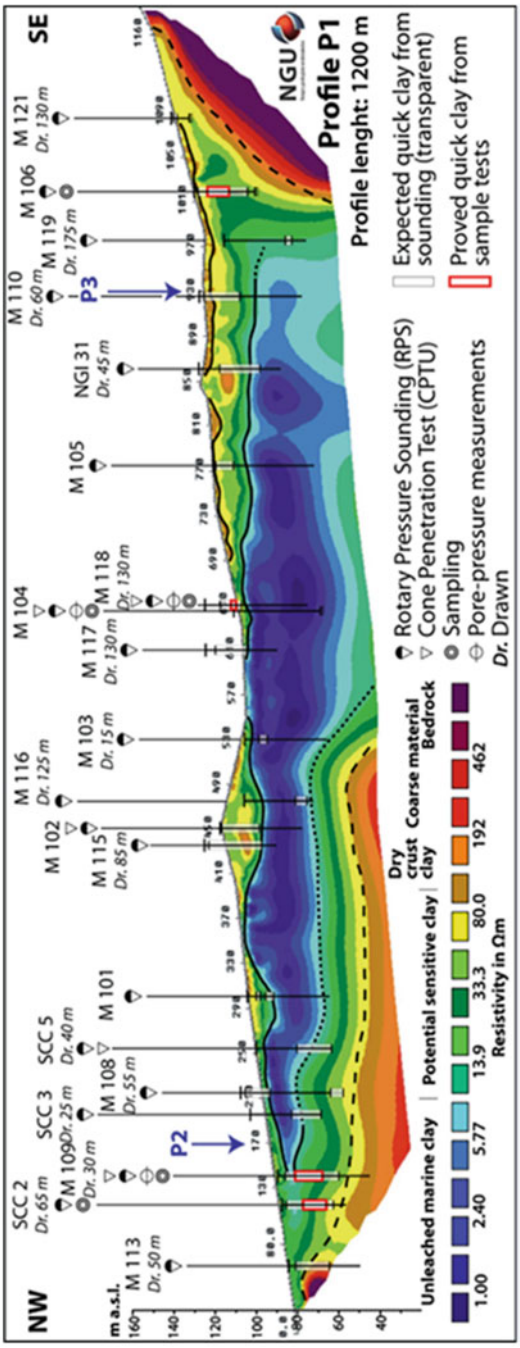

Fig. 44.3 Resistivity profile from ERT measurements (NIFS 2015a)

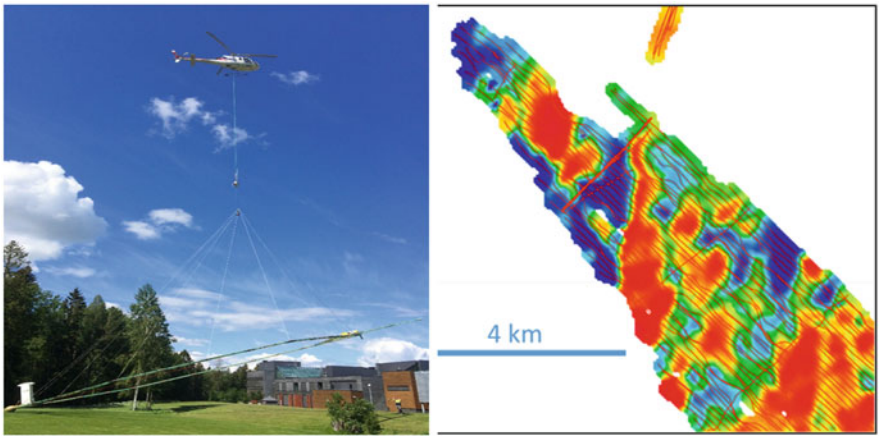

Fig. 44.4 Equipment for and results from AEM measurements (NIFS 2015a)

44.3 Future Strategy for Soil Investigations in Quick Clay Areas

The strategy for mapping of quick clay deposits can be described as a step-by-step procedure. The natural prerequisite is that the zoning plan is beneath the marine limit. If this prerequisite is fulfilled then this strategy is suggested:

44.3.1 Desk Study

A desk study should always be carried out ahead of a geophysical and geotechnical survey. This will help develop an optimal strategy for combination of AEM, ERT and introductory geotechnical borings.

This may include a geotechnical evaluation of the terrain by using existing Quaternary maps. These maps indicate the presence of marine depsoits in the uppermost layers of the soil. An evaluation of the terrain is also mandatory, particularly the presence of slopes or ravines with conditions sufficient to lead to a progressive failures (NIFS 2016).

The geotechnical consultant should collect information about previous soil investigations, particularly providing information about the presence of brittle clay within or adjacent to the area. The available results should be compared to the observations and assumptions made in the map study.

44.3.2 Toolbox for Mapping of Quick Clay Deposits – Choice of Methods

After analysing the existing ground conditions, the geotechnical consultant should evaluate if the distribution of marine clay found in the desk study should be limited or extended, and in which levels beneath the ground surface marine clay could be found. If the information about the quick clay layers is deficient, supplementary investigations have to be carried out.

Conventional sounding methods such as rotary pressure and total sounding, combined with sampling and laboratory testing, will still be important methods for detection of brittle materials. Results should however be checked by other methods.

CPTU, optionally with resistivity measurements (R-CPTU), has great potential for detection of brittle materials through combined recordings of cone resistance, sleeve friction, pore pressure and resistivity. CPTU/R-CPTU are important investigations in strategically important locations, where the results will be used for supplementary classification and determination of soil parameters.

Vane test traditionally gives information about the in situ undrained shear strength (undisturbed and remoulded), and the sensitivity. The determination of the remoulded shear strength may give information about the presence of quick or sensitive clay directly. For reliable measurements of remoulded shear strength it is required that the applied torque is measured down at the vane. This is because systems with torque measurements at the top appears to measure too high values for the remoulded undrained shear strength (Gylland et al. 2016).

Integration of geophysical and geotechnical methods has become more common in ground investigations nowadays, particularly in larger projects. With resistivity measurements, one may cover corridors for road or railway lines in relatively short time and with reasonable accuracy. As an outcome of this, one may detect critical areas with possible quick or sensitive clays, which need further geotechnical investigations by soundings, sampling or in situ tests for verification of the geophysical results. This approach may hence provide more reliable interpretation of the ground conditions.

The continuous results from resistivity measurements can also be used to identify barriers of non-sensitive materials in the ground, for example rock outcrops, massive layers of coarse soil or other continuous layers of non-sensitive material. This information is of crucial importance in stability evaluations, since it enables realistic assessment of potential slide volume and run-out distance for slide debris from a possible quick clay slide.

Acknowledgements The partners in the NIFS project are greatly acknowledged for the financial support and good discussions throughout the study. The board of the Norwegian Geotechnical Society (NGF) are acknowledged for financial support for development of the summary report. The authors want to extend thanks to Rambøll, Multiconsult, NGI, Statens vegvesen (NPRA) and NGU for supplying test data in the study. The authors also wish to express their gratitude to the reviewer Dr. Denis Demers for his valuable comments.

This paper was written by Rolf Sandven before he all too early passed away in October 2016. The authors hope that his legacy and his focus on knowledge and quality in laboratory and field investigations will live on.

References

Anschütz H, Bazin S, Pfaffhuber A (2015) Towards using AEM for sensitive clay mapping – a case study from Norway. 1st European Airborne EM conference. Torino, Italia, Mo AEM 04

Gylland AS, Thakur V, Emdal A (2016) Extended interpretation basis for the vane shear test. In: Proceedings of NGM 2016, May 2016, Reykjavik, Iceland

Gylland AS, Sandven R, Montafia A, Pfaffhuber AA, Kåsin K, Long M (2017) CPTU classification diagrams for identification of sensitive clays. In: Landslides in sensitive clays. Springer, Cham

L'Heureux J-S (2012) A study of the retrogressive behaviour and mobility of Norwegian quick clay landslides. In: Eberhardt E, Froese C, Turner AK, Leroueil S (eds) Landslide and engineered slopes: protecting society through improved understanding. Taylor & Francis Group, London, pp 981–988

Löfroth H, Suer P, Dahlin T, Leroux V, Schälin D (2011) Quick clay mapping by resistivity – surface resistivity, CPTU-R and chemistry to complement other geotechnical sounding and sampling The Swedish Geotechnical Institute GÄU Report 30

NGF (2011) Guideline 2 Symbols and terminology in geotechnics. Rev 2 (In Norwegian)

NIFS (2015a) Detection of brittle materials Summary report with recommendations Final report NIFS Report no 126/2015. http://www.naturfare.no

NIFS (2015b) Detection of quick clay by R-CPTU and electrical field vane tests. Results from field study (in Norwegian). NIFS Report no.101/2015. http://www.naturfare.no

NIFS (2016) Method for evaluation of landslide size and runout NIFS report 14/2016

NVE (2014) Safety against quick clay landslides Guideline 7/2014

Pfaffhuber AA, Bazin S, Kåsin K, Anschütz H, Sandven R, Montafia A, Gylland AS, Long M (2016) In-situ detection of sensitive clays from a geophysical perspective. Proceedings, ICS'5, September 2016, Queensland, Australia

Sandven R, Gylland AS, Montafia A, Kåsin K, Pfaffhuber AA, Long M, Havnen I, Ottesen HB (2016a) In situ detection of sensitive clays – part I: selected test methods. Proceedings of Nordic Geotechnical Meeting 2016, pp 123–132

Sandven R, Gylland AS, Montafia A, Kåsin K, Pfaffhuber AA, Long M, Havnen I, Ottesen HB (2016b) In situ detection of sensitive clays – part II: results. Proceedings of Nordic Geotechnical Meeting 2016, pp 133–142

Sandven R, Kalomoiris K, Furuberg T (2017) Geotechnical evaluation of a quick clay area in Trondheim, Norway. In: Landslides in sensitive clays. Springer, Cham

Part VI
Hazard Assessment and Risk Management

Chapter 45
Reliability of Slopes in Sensitive Clays

Suzanne Lacasse, Zhongqiang Liu, Jihwan Kim, Jung Chan Choi, and Farrokh Nadim

Abstract Risk and probabilistic analyses have now had enough applications that make them effective to use in practice. The approach provides more insight than deterministic analyses alone. They help reduce uncertainty and focus on safety and cost-effectiveness. The paper illustrates the use of reliability methods for the analysis of slopes in sensitive clays with examples of the calculation of probability of failure and run-out for the Finneidfjord and Rissa landslides in Norway. The input, model and results of the probabilistic slope analysis are described, including the uncertainties in the parameters, triggers and calculation model, as well as a brief review of the principles of the reliability approach. Reliability approaches do not remove uncertainty nor do they alleviate the need for judgment. They provide a way to quantify the uncertainties and to handle them consistently. Site investigations, laboratory test programs, limit equilibrium and deformation analyses, instrumentation, monitoring and engineering judgment are necessary inputs to the reliability approach. Landslide events, often unwittingly, are triggered or aggravated by human activity, such as change in topography (e.g. excavation or surcharge) and change in drainage conditions. Climate change can increase the frequency of landslide. The paper proposes that a probabilistic model in an event tree format should be included to ensure that all failure modes and the uncertainties have been covered and that slope failure mitigation measures are quickly available.

45.1 Introduction

Risk is all around us. Landslides, earthquakes, hurricanes. Tornadoes, floods, tsunamis. Dam breach, foundation failures, errors and omissions, climate impact and terrorism. Failures and unexpected events provide us with experience and lessons

S. Lacasse (✉) • Z. Liu • J.C. Choi • F. Nadim
Norwegian Geotechnical Institute (NGI), Oslo, Norway
e-mail: suzanne.lacasse@ngi.no; zhongqiang.liu@ngi.no; jungchan.choi@ngi.no; farrokh.nadim@ngi.no

J. Kim
University of Oslo (UiO), Oslo, Norway

Norwegian Geotechnical Institute (NGI), Oslo, Norway
e-mail: jhkim2@uw.edu

V. Thakur et al. (eds.), *Landslides in Sensitive Clays*, Advances in Natural and Technological Hazards Research 46, DOI 10.1007/978-3-319-56487-6_45

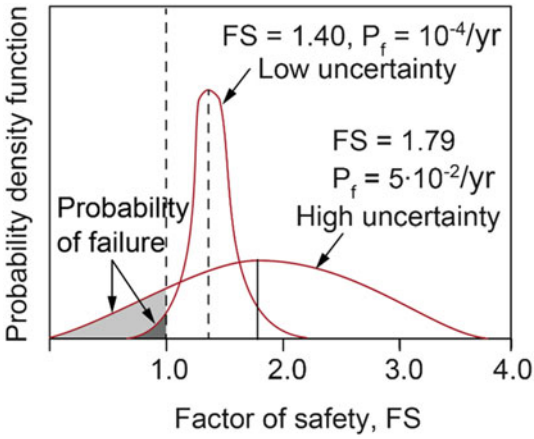

Fig. 45.1 Non-coherence of factor of safety and probability of failure

learned, and prompt the development of new tools and new methods. For example, the 2011 Fukushima-Daiichi incident led nuclear power plants in the USA to design and spend over $4 Billion USD in safety measures and enhancements, according to the Nuclear Energy Institute (ASCE 2016).

Landslides in sensitive materials is a natural hazard that can be triggered by natural causes or by human actions. There are significant uncertainties in the way we calculate factor of safety against failure or the run-out of a landslide. Due to regulation or tradition, the same value of factor of safety is applied to conditions that involve widely varying degrees of uncertainty. That is not logical. The factor of safety against instability is a measure of how far one may be from failure. Factors of safety are applied to compensate for, among others, uncertainties in the calculation. If there were no uncertainties, the factor of safety could be very close to 1.

The implications of Fig. 45.1 are very important. A slope with a central[1] factor of safety of 1.4 may be safer than a slope with a higher factor of safety of 1.8 because uncertainties in an analysis influence differently the probability of failure. Factor of safety alone is therefore not a sufficient measure of the actual safety.

The designer should also be aware that the probability of failure is never equal to zero. In geotechnical evaluations, it is important to not rely on factor of safety alone. Hazard and risk analyses have proven a useful tool to provide an additional assessment and to help making decisions.

Risk and probabilistic analyses have reached a level of maturity that makes them effective to use in practice (Lacasse 2017). The approach provides more insight than deterministic analyses alone. They help reduce uncertainty and focus on safety and cost-effectiveness. Reliability approaches do not remove uncertainty nor do they alleviate the need for judgment. They provide a way to quantify the uncertainties and to handle them consistently. Reliability approaches also provide the basis

[1]Calculated with mean values of all parameters.

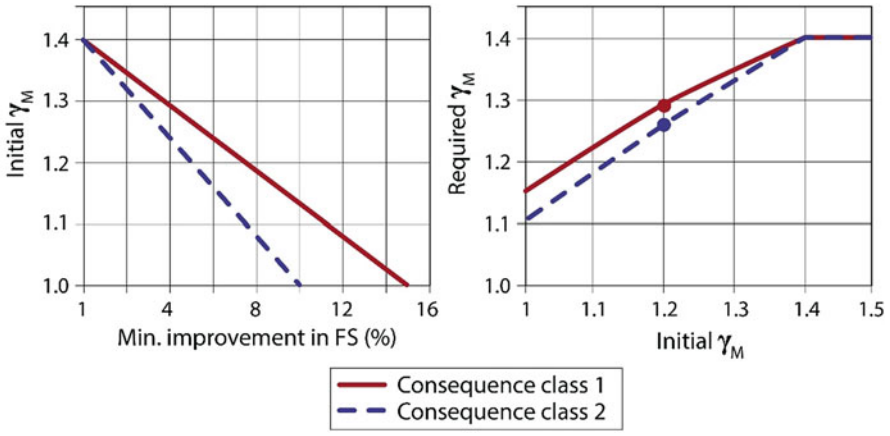

Fig. 45.2 Required improvement of material coefficient for Norwegian clays. Consequence Class 1 is more severe than Consequence Class 2 (After Oset et al. 2014)

for comparing alternatives. Site investigations, laboratory test programs, limit equilibrium and deformation analyses, instrumentation, monitoring and engineering judgment are necessary inputs to the reliability approach (Lacasse 2017).

Oset et al. (2014), at the 1st International Workshop on Landslides in Sensitive Clays (IWSLC) in Québec Canada, presented a regulatory framework for road and railway construction constructed on sensitive clays in Norway. The requirement for the material coefficient γ_M for the overall stability (over an area) of slopes in clays is normally 1.4. For a natural slope with a material coefficient less than 1.4, the regulations require that the material coefficient should be increased, but not necessarily to as much as 1.4. Figure 45.2 provides on the left side the required percentage increase in the material factor and on the right side the actual required material coefficient As an example, for an initial γ_M of 1.2, an improvement from $\gamma_M = 1.2$ to $\gamma_M = 1.29$ is required for Consequence Class 1. Standing slopes with a material factor γ_M of 1.0 require an improvement up to $\gamma_M = 1.15$ for Consequence Class 1.

The reason for allowing a material coefficient less than 1.4 is the fact that the slope is already standing, and is therefore a confirmation that the slope already has a material coefficient of at least 1.0. Any improvement thereof represents a real gain compared to the present situation. This recommendation is a form of Bayesian updating, where a first consideration is updated with additional knowledge.

The paper gives examples of hazard and risk assessment for landslides in sensitive clays. The paper presents three example analyses of Norwegian landslides in sensitive clays: (1) a probabilistic analysis of the sensitive clay landslide at Finneidfjord, (2) a probabilistic run-out modelling of the Finneidfjord landslide and (3) a probabilistic run-out modelling of the Rissa landslide. Basic concepts of risk assessment and management for geotechnical engineering are also briefly mentioned.

Fig. 45.3 Chinese characters to designate risk (After https://vicentesandoval.wordpress.com/2016/02/23/the-origins-of-the-word-risk-etymology)

45.2 Origin of the Word Risk

The origin of the word risk is contested, but the following is believed to be the most commonly accepted (R Skjong 2005, (http://research.dnv.com/skj/Papers/etymology-of-risk.pdf; S.C. Messina 2015), https://www.scmessina.com/2015/02/etymology-of-risk). In Ancient Greek, risk means root, stone or a cut from the firm land. In Latin, the work became "cliff" or "reef". In Ancient Greek, risk was a nautical expression, a metaphor for "difficulty to avoid in the sea" (Homer's Odyssey "Sirens, Scylla, Charybdis and the bulls of Helios"). In the Strait of Messina (Italy), Odysseus tried to save himself from the dangers in the sea by grasping the roots of a wild fig tree. From the sixteenth century on, the term became a technical term for business, with the meaning "to dare, to undertake, enterprise, or hope for economic success". The word for risk in Chinese is constructed from two symbols. "Danger" and "incipient moment, crucial point" (Fig. 45.3), although this has been contested, which is more in line with the modern understanding of risk. Risk assessment is defined by Bernstein (1998) as the "Identification and evaluation of dangers that could prevent us to reach our objectives", which is in line with ISO's (2009) standard definition of risk: "risk is the effect of uncertainties on objectives".

45.3 Probabilistic Stability Analysis of the Finneidfjord Landslide

45.3.1 Description and Triggering of the Landslide

The catastrophic landslide at Finneidfjord in 1996 mobilized 1 million m^3 of sediments and caused four fatalities. Figure 45.4 shows the vicinity of the landslide, with contour lines illustrating the steepness of the embankment down the fjord. Janbu (1996) reconstructed the sliding as a five-stage event on the basis of the available data (Fig. 45.5). Geotechnical investigations before and after the landslide revealed large volumes of quick clay, particularly below the shore and foreshore regions, mobilizing in the later stages of the landslide (Kummeneje 1993, 1996;

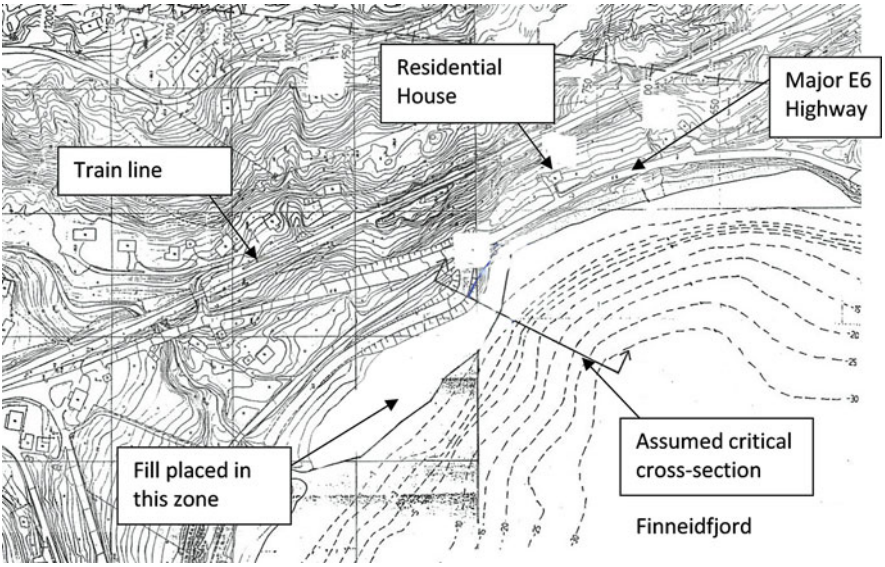

Fig. 45.4 Map of area prior to 1996 Finneidfjord landslide (After Gregersen 1999, 2008)

Janbu 1996; Gregersen 1999). The failed section involved a cap of Holocene silty clay over late glacial clay with the initial detachment within the Holocene succession. The beach was relatively flat before the failure, with the steepest slope about 18° at 5–25 m below sea level. At the shoreline, bedrock was encountered at an elevation of about −15 m. Longva et al. (2003) presented a slightly different interpretation as a three-stage event based on swath bathymetry and seismic data.

Janbu (1996) and Longva et al. (2003) suggested that excess pore pressure triggered the initial landslide. The landslide occurred shortly after about 14 days of heavy rain. Gregersen (1999) documented that, several months before the landslide, the placement of 12–15,000 m^3 of fill, with a total height of 2.5 m, on the foreshore of the Fjord was the triggering mechanism for the landslide. L'Heureux et al. (2012a) and Vanneste et al. (2013) found that a 30-cm weak layer about 3 m below seafloor was sandwiched between clay layers of very low permeability (Fig. 45.6.). This layer is thought to be the initial sliding plane.

45.3.2 Reliability Analysis of Finneidfjord Failure

For the Finneidfjord landslide, the probability of failure was investigated. The level of the fill height, from 0.5 to 2.5 m, was used as governing parameter. The thin weak layer was included in the numerical model used.

The first order second moment (FOSM) approach was used to calculate the probability of failure of the slope. The mean (μ) and variance (σ^2) of the factor of

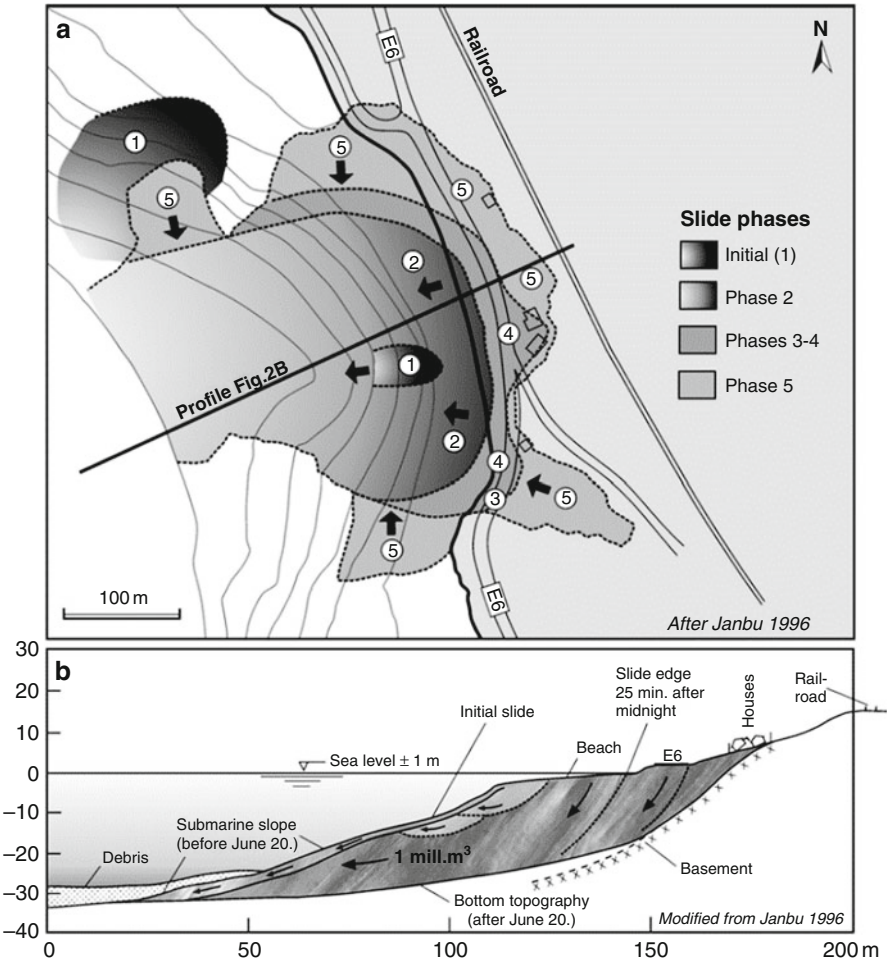

Fig. 45.5 Sliding mechanism interpreted by Janbu (1996) based on 1984 survey: (**a**) Five phases; (**b**) Cross section (Longva et al. 2003)

safety (FS) were calculated with the FOSM procedure described in Ang and Tang (1984). The mean, standard deviation ad coefficient of variation, CoV, defined as the ratio the standard deviation (σ) to the mean, were obtained.

The reliability index β and probability of failure P_f were calculated as:

$$\beta = (\mu_{FS} - 1) / \sigma_{FS} \tag{45.1}$$

$$P_f\,(FS < 1) \approx \Phi\,(-\beta) \tag{45.2}$$

where $\Phi(\cdot)$ is the cumulative standard normal function.

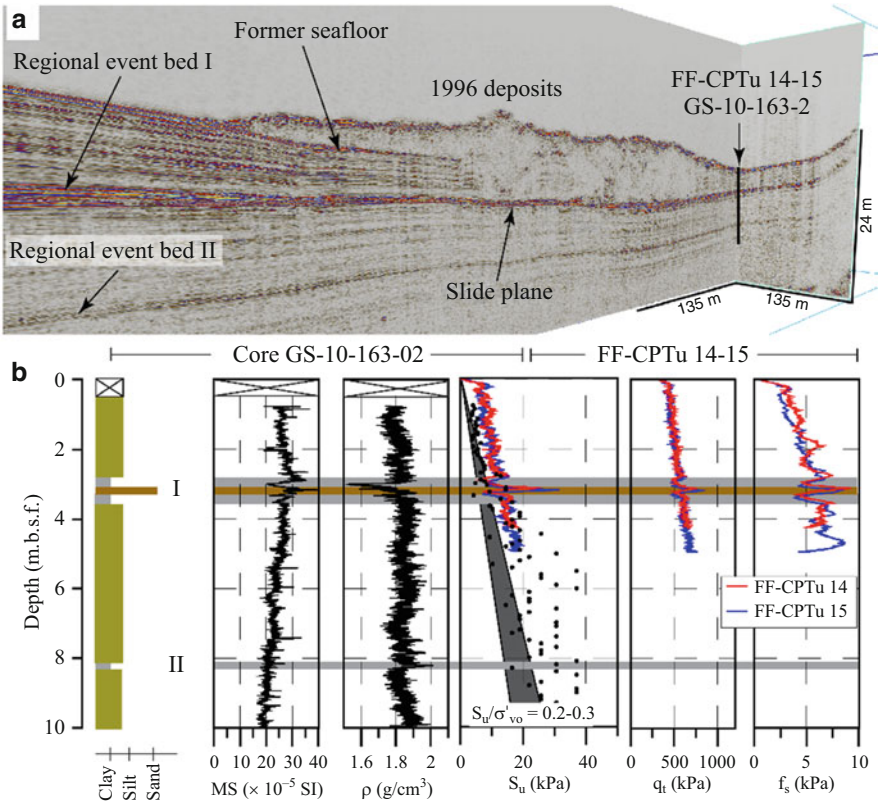

Fig. 45.6 L'Heureux et al. (2012a)'s interpretation: (**a**) Fence diagram of the 1996 landslide deposits from the 3D seismic cube; (**b**) Sedimentological and geotechnical results of core GS-10-163-02 and FF-CPTu-14 and 15. GS-10-163-02 is shifted 0.73 m vertically to match the CPTu data. (*MS* magnetic susceptibility, ρ gamma density, s_u undrained shear strength, q_t total corrected cone resistance, f_s sleeve friction)

45.3.3 Numerical Model and Input Parameters

The material model NGI-ADP (Grimstad et al. 2010) was used in PLAXIS finite element analyses (www.plaxis.nl). The NGI-ADP model is an elasto-plastic model (therefore not accounting for strains-softening) that is able to account the anisotropy of the undrained shear strength. Figure 45.7 shows the finite element model adopted for the analyses. A mesh convergence study was done and showed that the mesh discretisation was sufficiently fine (scales in both directions are in meters).

Table 45.1 summarizes the soil strength profile used in the finite element analyses, including the mean, coefficient of variation and the probability density function. The values were based on the earlier studies of shear strength (Gregersen 1999; Cassidy et al. 2008; L'Heureux et al. 2012a). The anisotropy ratios s_{uDSS}/s_{uC} and s_{uE}/s_{uC} were taken as 0.7 and 0.4 respectively, where s_{uC} stands for the

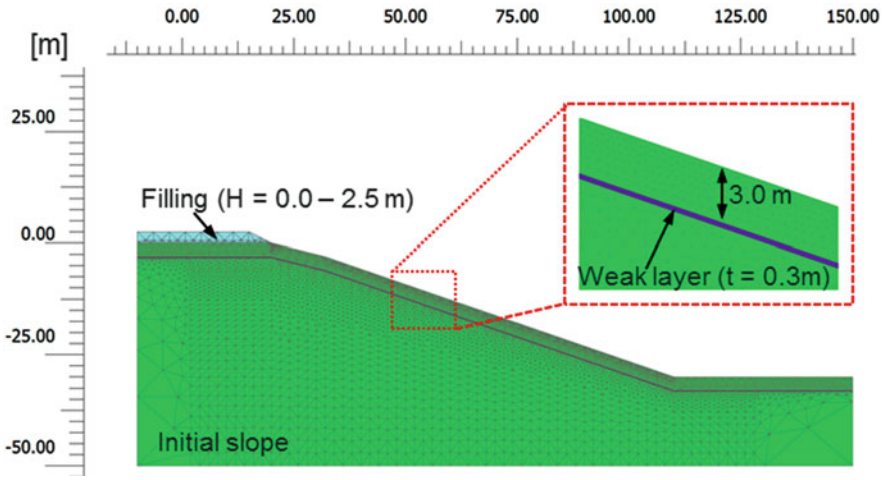

Fig. 45.7 PLAXIS finite element model for the Finneidfjord slope

Table 45.1 Material properties used in assessment of probability of failure of Finneidfjord slope

Parameter	Mean	Distribution	*CoV*
Shear strength in triaxial compression (s_{uC}) and increase in s_u with depth *su_inc*	10 kPa for depths ≤3 m	Lognormal	0.15
	0.33 p'_0 for depths >3 m		
Shear strength weak layer (s_{uC})	8 kPa	Lognormal	0.25
ϕ' of fill material	40°	Lognormal	0.10
Strain-softening correction factor	1.07, range 1.04–1.10	–	–

undrained shear strength in triaxial compression, s_{uDSS} stands for the undrained shear strength in simple shear and s_{uC} stands for the undrained shear strength in triaxial extension.

Results from both laboratory data and cone penetration tests showed that the sensitivity of the 30-cm weaker clay layer is greater than the rest of the clay, with values up to 9 (Vanneste et al. 2013). The uncertainty in s_{uC} was also significantly higher (CoV of 25%, whereas CoV is 15% in the rest of the clay).

As part of the NIFS project (NIFS 2012; Dolva and Petkovic 2017), Fornes and Jostad (2017) proposed to account for the effect of strain-softening in elasto-plastic analyses with a correction factor on the factor of safety, $\gamma_M{}^{softening}$:

$$\gamma_M{}^{\text{softening}} = \gamma_M / F_{\text{softening}} \tag{45.3}$$

where γ_M is the material factor calculated by an elasto-plastic model (as in limit equilibrium analysis) using the peak undrained shear strength, and $F_{softening}$ is the correction required to account for the reduced capacity obtained by a corresponding

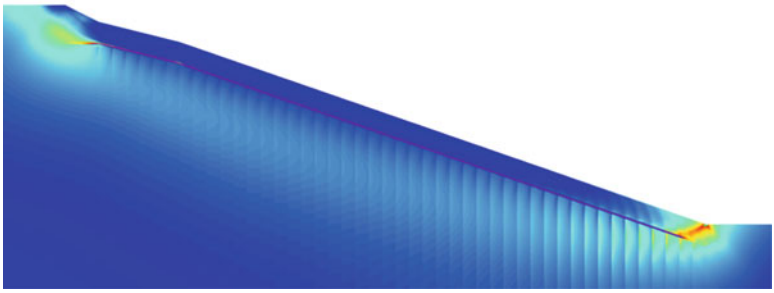

Fig. 45.8 Failure mechanism of the Finneidfjord slope

finite element analyses (FEA) using PLAXIS and the strain-softening material model NGI-ADPSoft that includes the effect of post-peak strain-softening behaviour (Grimstad and Jostad 2010; Jostad and Grimstad 2011).

In the present analyses, the strain-softening correction factor recommended in Fornes and Jostad (2017) and NGI (2014) was used for the clay at Finneidfjord. The factor was introduced as a quotient on the calculated factor of safety to account for the elasto-plastic model used in the PLAXIS analyses. A mean value of 1.07 for the strain-softening correction factor, and a range of 1.04–1.10 was used, and served as model uncertainty.

45.3.4 Results of Probabilistic Analyses of Finneidfjord Slope Failure

An example of the initial failure mechanism is illustrated in Fig. 45.8. The initial failure was located in the thin weak clay layer. The mean factor of safety and nominal probability of failure (at time of failure) for fill heights from 0 to 2.5 m are given in Figs. 45.9 and 45.10. Results from Cassidy et al. (2008) are also plotted. The Cassidy et al. results were obtained with limit equilibrium and the Morgenstern-Price method (Morgenstern and Price 1965).

The factors of safety and the probabilities of failure are comparable to the ones obtained by Cassidy et al. (2008). The reasons for the differences include: the introduction of the strain-softening correction factor and the introduction of the 30-cm weak clay layer and the introduction of a FE model.

The new finite element analyses show that, for the properties and geometry used, the slope was already unstable (FS < 1) before any fill was placed (Fig. 45.9). The values of mean safety factor of 0.99–0.96 are however very close to unity, and, according to the calculation, the addition of 2.5-m of fill reduced the safety factor by only 3%. The difference may be due to the strain-softening correction factor

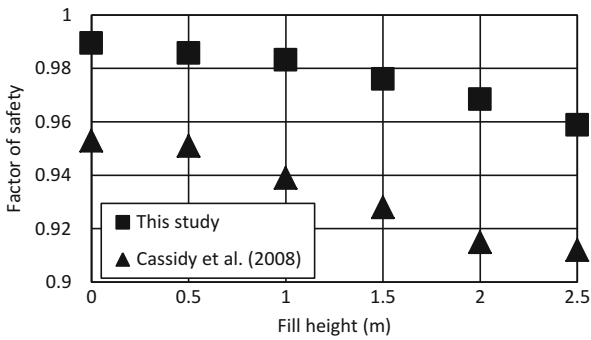

Fig. 45.9 Calculated mean factors of safety of Finneidfjord slope as a function of fill height

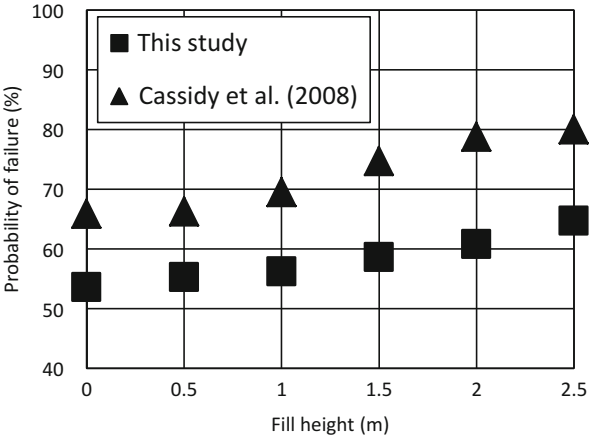

Fig. 45.10 Calculated nominal probability of failure of Finneidfjord slope as a function of fill height

being too high, or to the relatively large uncertainties in the soil parameters within the volume involved in the failure, and a difference between the model and the actual *in situ* behaviour at failure.

The Finneidfjord slope was observed as standing under the condition of "no fill". With the assumption that the addition of the fill was the trigger, this information can be used to further interpret the probability of failure. The probability of slope failure, given an initially stable slope, can be treated as a conditional probability problem, where the probability of the safety factor being less than unity becomes:

$$P\left(FS < 1 \left| FS_{nofill} \geq 1\right.\right) = 1 - \frac{P\left(FS \geq 1\right)}{P\left(FS_{nofill} \geq 1\right)} \tag{45.4}$$

where FS_{nofill} is the factor of safety before the fill is placed and FS is the factor of safety once the fill is placed. The conditional probability calculation are presented in Fig. 45.11. The results show that the probabilities of failure increase from 0 to

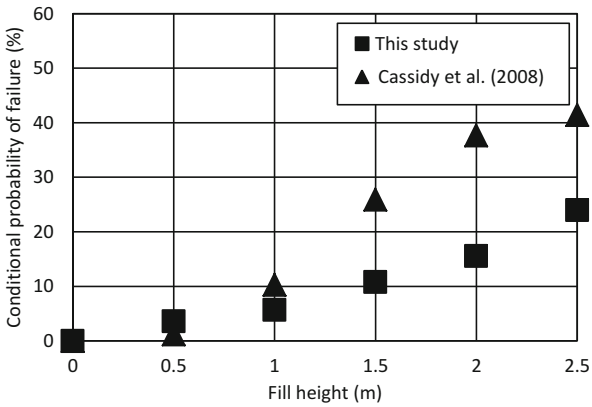

Fig. 45.11 Probability of Finneidfjord slope failure conditioned to the original slope being stable

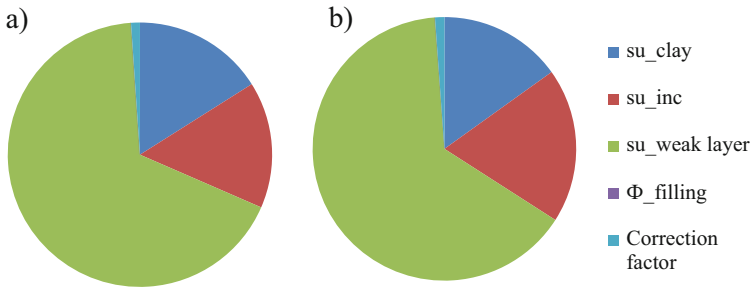

Fig. 45.12 Relative contribution of each random variable to probability of failure of the Finneidfjord slope: (**a**) without fill; (**b**) with 2.5 m fill

24% as the fill height increases from 1 to 2.5 m, which is less than the probabilities of failure obtained in the analyses without consideration of the observed slope condition. The fill height has initially very little effect on the increase in probability of failure but increases significantly as the fill height passes 1.5 m.

Probabilistic analyses provide sensitivity factors for each of the random variables in the analysis. The sensitivity factors quantify the relative contribution of the random variables to the overall uncertainty and the calculated probability of failure. This is the case for the FOSM analyses of the Finneidfjord failure.

The pie-charts in Fig. 45.12 present the sensitivity factors for the analyses of the Finneidfjord slope without fill and with a 2.5-m high fill. In both cases, the undrained shear strength in the weak clay layer at 3 m, *su_weak layer*, is by far the most significant random variable for the calculated probability of failure. A small change in the undrained shear strength, from e.g. 8 kPa to 8.5 to 9 kPa, would probably bring the safety factors in the range from 1.05 to 1.00 for fill heights from 0 to 2.5 m.

45.4 Probabilistic Run-Out of Finneidfjord Landslide

45.4.1 Description of the Finneidfjord Landslide

The first stage of the landslide started 1–9 m below sea level on the steepest part (18°) of the slope, 50–70 m from Highway E6 (Fig. 45.4). Retrogressive sliding was corroborated by eye witnesses seeing waves, bubbles and swirls moving away from the shore for quite a while. As the landslide scar widened to 350 or 450 m, the geometry became that of a "bottleneck" landslide with a gate width of about 150 m (Fig. 45.5). No estimate of the sliding volume of Stage 1 was found in the literature. NGI (2012) documented that the release width was about 400 m and the length roughly 150 m. The stability calculations above showed that the average sliding depth was about 3 m in Stage 1. The total Stage1 volume of 200,000 m^3 was used for the runout simulations. The depletion zone got deeper following retrogression in the later stage, but the analysis was limited to Stage 1.

45.4.2 Numerical Model Used

The numerical model used is an extension of the Bing model (Imran et al. 2001) in Eulerian coordinates with two space dimensions. The Herschel-Bulkley rheology (Imran et al. 2001) was fully implemented to enable the dynamic computation of the depths of the plug and shear layer. The model is described in Annex A. The landslide movement is described with three main parameters: the initial yield stress (peak undrained shear strength), $\tau_{y,0}$, the residual yield stress (remoulded shear strength), $\tau_{y,\infty}$, and the gamma Γ, parameter describing the velocity of the movement. y is the accumulated shear strain at the bottom of the slide.

45.4.3 Input Parameters for Finneidfjord Run-Out Calculations

The landslide movement was controlled mainly by parameters $\tau_{y,0}$, $\tau_{y,\infty}$ and Γ, as well as the initial slide (slab) thickness and the bathymetry. Table 45.2 lists the

Table 45.2 Input parameters for numerical analyses of run-out for the Finneidfjord landslide

Random variable	Mean	Standard deviation	Distribution
Initial yield stress $\tau_{y,0}$ (kPa)	10	1.5	Lognormal
Residual yield stress $\tau_{y,\infty}$ (kPa)	0.1	0.03	Lognormal
Gamma Γ	0.05	0.025	Lognormal

statistics for the three random variables considered in the numerical analyses. The mean and *CoV* of the initial yield stress were taken as 10 kPa and 0.15, respectively, which are identical to the values used for the undrained shear strength in the analyses of the failure. The mean value and CoV of the residual yield stress and parameter Γ were derived based on Natterøy (2011) and NGI (2012). A lognormal distribution was assumed for the three random parameters.

The values of remoulded shear strength from Natterøy (2011) and NGI (2012) were for the quick clay onshore. The analyses herein focused on the mainly underwater initial stage of the landslide. The values used may therefore be on the low side. However, if a larger value of the yield stress is used, no slide gets initiated. Since there was a lack of information on the initial value of the yield stress, the values from the two above references were used.

45.4.4 Results of Run-Out Simulations of the Finneidfjord Landslide

The first stage of the landslide was modelled, and the run-out distance, maximum velocity and deposit height were calculated. A total of 950 Monte Carlo simulations were performed.

Figures 45.13, 45.14. and 45.15. show the histograms of the simulated run-out distance, maximum velocity over the flow domain and average deposit height. The figures give the mean, minimum and maximum values, the standard deviation (SD) and Coefficient of variation (COV) and the number of simulations (*N*). The resulting mean values were 913 m for run-out distance, 8.5 m/s for maximum velocity and 1.0 m average deposit height. Unfortunately, there are no measured data available

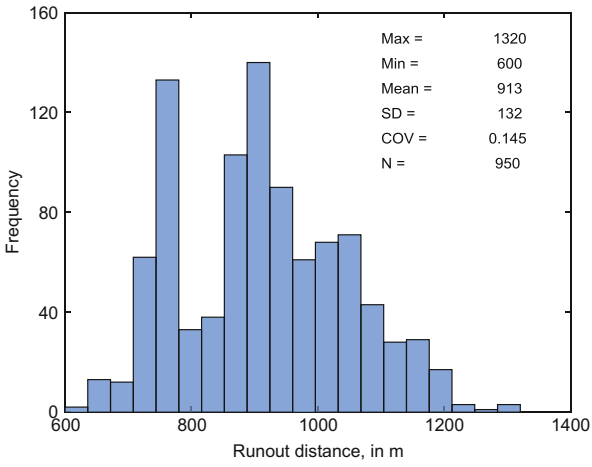

Fig. 45.13 Statistics of runout distance of Finneidfjord landslide from 950 Monte Carlo simulations

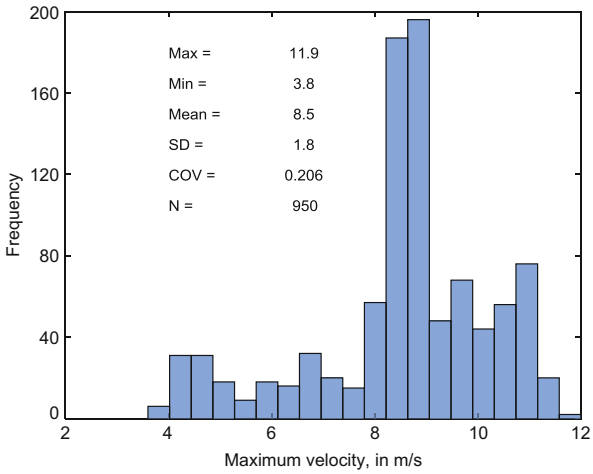

Fig. 45.14 Statistics of maximum velocity of Finneidfjord landslide from 950 Monte Carlo simulations

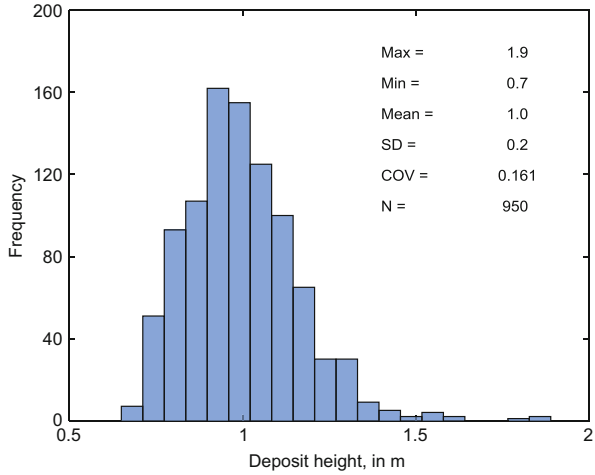

Fig. 45.15 Statistics of deposit height of Finneidfjord landslide from 950 Monte Carlo simulations

for the Finneidfjord landslide. However, no tsunami (or large wave) was observed during the landslide, indicating that velocities and accelerations were moderate. The standard deviations are also shown on the figures.

Figures 45.16, 45.17 and 45.18 suggest that the run-out distance decreases with increasing residual yield stress, maximum velocity decreases with increasing undrained shear strength at failure and with parameter Γ, while deposit height increases slightly with increasing residual yield stress.

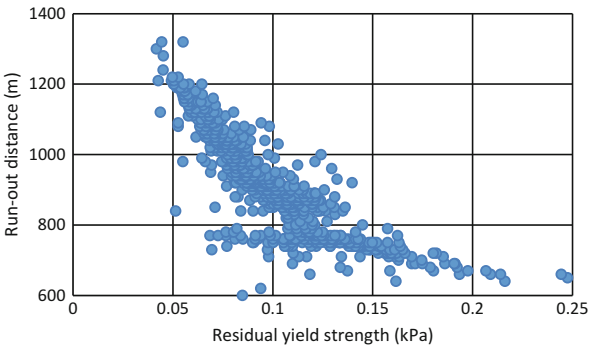

Fig. 45.16 Run-out distance vs residual yield strength for Finneidfjord landslide

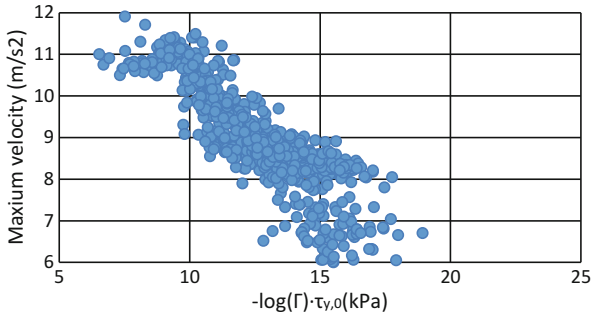

Fig. 45.17 Maximum velocity vs initial yield strength and parameter Γ for Finneidfjord landslide

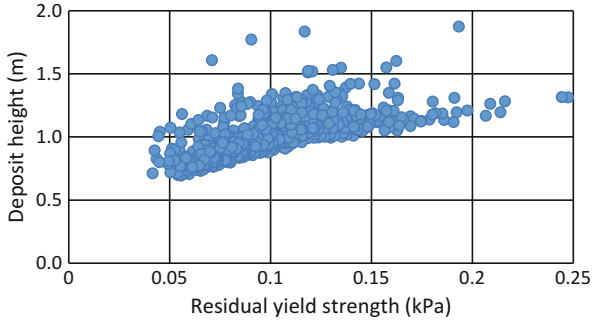

Fig. 45.18 Deposit height vs residual yield strength for Finneidfjord landslide

45.5 Probabilistic Run-Out of Rissa Quick Clay Landside

The 1978 quick clay landslide at Rissa is the largest landslide to have struck Norway during the twentieth century. Seven farms and five single family homes were taken by the landslide or had to be abandoned for safety reasons. Of the 40 people caught in the landslide, one person died.

45.5.1 Description of the Rissa Landslide

A two-stage process of the landslide was described by Gregersen (1981) and was further summarized by L'Heureux et al. (2012b). An initial landslide was triggered by the excavation of clay for the extension of an existing barn and stockpiling the excavated material along the lakeshore. During the initial failure, 70–90 m of the shoreline slid out into the lake, including half of the recently placed earth-fill. The landslide edges were 5–6 m high and extended 15–25 m inland. The landslide developed retrogressively in the southwestern direction over the next 40 min. The sediments completely liquefied during the sliding and the debris literally poured into the lake like streaming water. At this stage, the landslide area took the shape of a long and narrow pit open towards the lake (Fig. 45.19). The length of the sliding area was 450 m, covering an area of 25–30,000 m^2 (at that stage, 6–8% of the final slide area) (Gregersen 1981).

The main landslide started almost immediately after the retrogressive sliding had reached the boundaries of Stage 1 (Fig. 45.19). At this point, large flakes of dry crust (150 × 200 m) started moving towards the lake, not through the existing gate opening, but in the direction of the terrain slope (see flakes A and B, Fig. 45.19). The velocity was initially moderate (flake A), about 10–20 km/h, but increased to 30–40 km/h (flake B). Houses and farms can be seen floating on top of the sliding masses on the videos of the Rissa landslide. A series of smaller and retrogressive slides followed over a short period of time. The sliding process propagated to the mountain side where it stopped. The main sliding stage lasted for approximately 5 min and covered 92–94% of the total landslide area (330,000 m^2). The total volume of mobilized sediment was estimated to be between 5 and 6 × 10^6 m^3.

The observed run-out parameters of the Rissa landslide that will be compared to the results of the simulations were as follows: the run-out distance under Stage 2 was 1150 m from the lakeshore, the maximum velocity over the flow domain was 11 m/s and the average deposit height was 6–8 m.

45.5.2 Input Parameters for Rissa Ruo-Out Calculations Landslide

The run-out analyses were done with the same model as for the Finneidfjord landslide, and with Monte Carlo simulations. The landslide movement was controlled by mainly the combination of the parameters $\tau_{y,0}$, $\tau_{y,\infty}$ and Γ, as well as the initial bathymetric thickness and the bathymetry. Table 45.3 lists the statistics for the three random variables used in the numerical analyses. The initial yield stress (peak undrained shear strength) of the Rissa clay near the sliding surface was varied between 10 and 20 kPa (NGI 2012) and had a CoV of 17%. The residual yield stress was varied over a range typical for quick clays, between 0.1 and 0.5 kPa (with a CoV of also 17%).

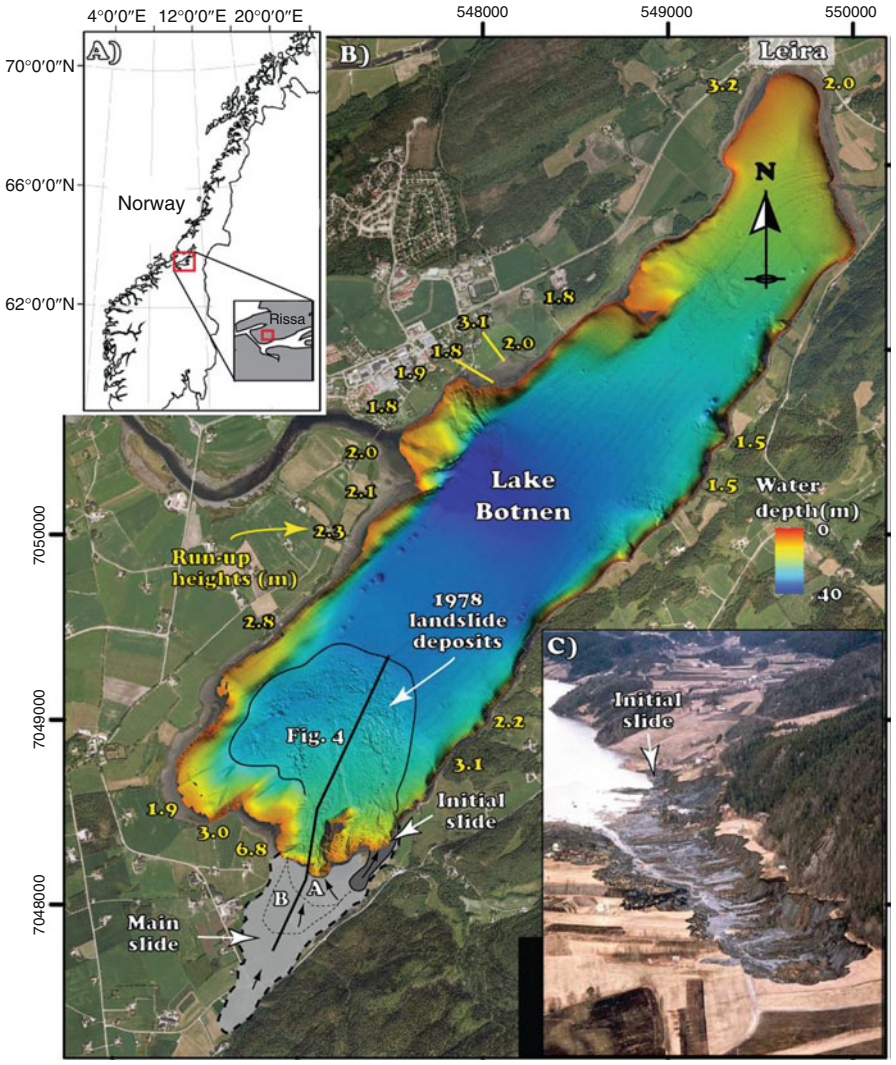

Fig. 45.19 Rissa landslide area: (**a**) Geographic location; (**b**) Map of Lake Botnen with color-coded bathymetry, outline of slide deposits and outline of the areas affected by the initial slide (*dark grey*), the two major flakes A and B and the subsequent retrogressive slide (*light grey*); (**c**) Aerial view of the slide pit (Courtesy Aftenposten. After L'Heureux et al. 2012b)

45.5.3 Results of the Run-Out Simulations of the Rissa Landslide

Stage 2 of the Rissa landslide was simulated, and the run-out distance, maximum velocity and deposit height were calculated with 1000 Monte Carlo simulations.

Table 45.3 Input parameters for numerical analyses

Random variable	Mean	Standard deviation	Distribution
Initial yield stress $\tau_{y,0}$ (kPa)	15	2.5	Lognormal
Residual yield stress $\tau_{y,\infty}$ (kPa)	0.3	0.05	Lognormal
Gamma Γ	0.05	0.025	Lognormal

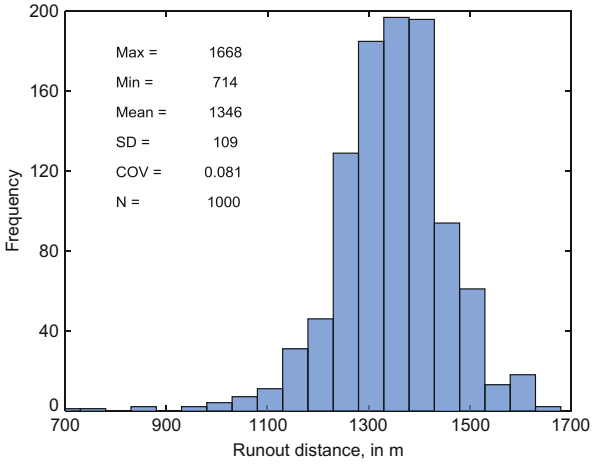

Fig. 45.20 Statistics of run-out distance of Rissa landslide from 1000 Monte Carlo simulations

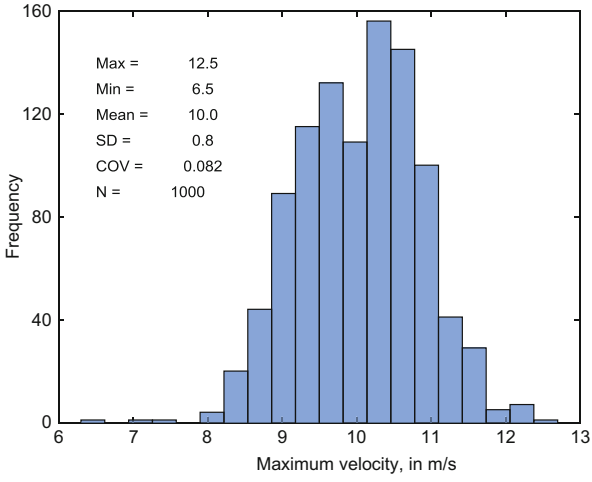

Fig. 45.21 Statistics of maximum velocity of Rissa landslide from 1000 Monte Carlo simulations

Figures 45.20, 45.21 and 45.22 show the histograms of run-out distance from the lakeshore, maximum velocity over the flow domain and average deposit height. The figures give the mean, minimum and maximum values, standard deviation (SD), coefficient of variation (COV) and number of simulations (N). The calculated mean values of run-out distance, maximum velocity and deposit height were 1346 m,

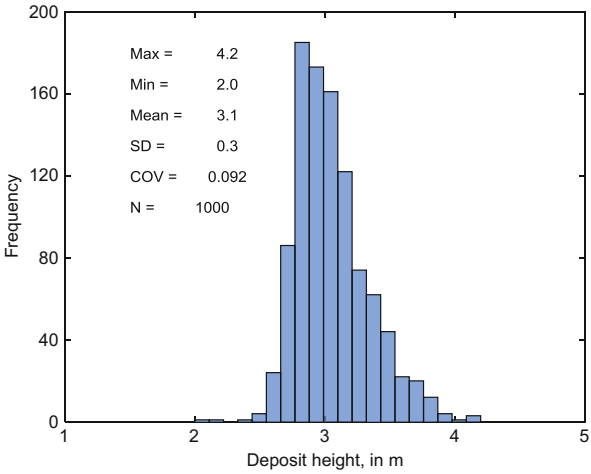

Fig. 45.22 Statistics of deposit height of Rissa landslide from 1000 Monte Carlo simulations

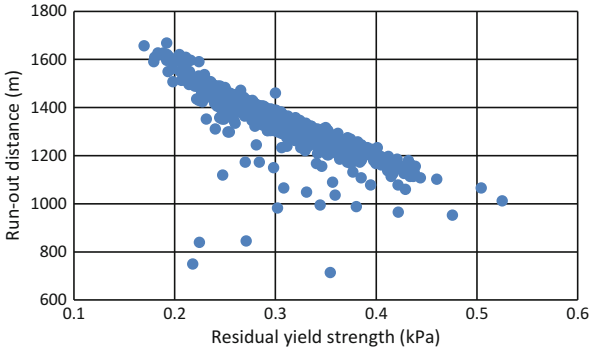

Fig. 45.23 Run-out distance vs residual yield strength for Rissa landslide

10 m/s and 3.1 m, respectively. The mean values[2] are to be compared to the observed run-out distance under Stage 2 (1150 m from the lakeshore, L'Heureux et al. 2012a), maximum velocity over the flow domain (11 m/s) and average deposit height (6–8 m). The mean calculated run-out distance overestimated the observed run-out distance by about one standard deviation. The calculated maximum velocity was close to the observed value and the deposit height was underestimated.

Figures 45.23, 45.24 and 45.25 show that run-out distance decreases with increasing residual yield stress, maximum velocity decreases with increasing initial shear strength and parameter Γ, whereas deposit height increases with increasing residual yield stress.

The visco-plastic model used leads to longer run-out and thinner landslide deposits. There is a reverse correlation between predicted run-out distance and

[2]Since this is a Monte Carlo analysis with limited number of simulations, the most reliable results are the mean ± one standard deviation about the mean.

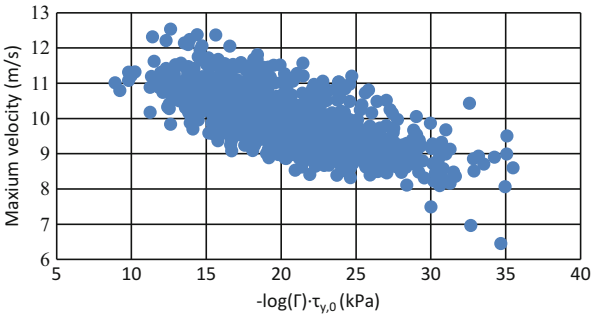

Fig. 45.24 Maximum velocity vs initial yield strength and parameter Γ for Rissa landslide

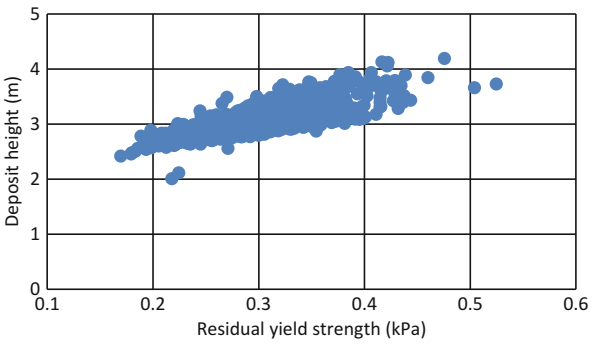

Fig. 45.25 Deposit height vs residual yield strength for Rissa landslide

deposit height (Figs. 45.23. and 45.25), so it is logical that the longer run-out distance resulted in a smaller deposit height. The overestimation of run-out distance comes from the fact that the model assumes that the entire material is quick clay. In reality, there is non-sensitive or less sensitive clay on top of the quick clay. Since the model is depth-averaged, the remoulded yield stress should probably have been selected with a higher value to account for the less sensitive material. This would then give a shorter run-out distance and higher deposit height. New simulations are needed to further document this effect. The results in L'Heureux et al. (2012a) with the Bing model also show a low deposit thickness for the same reason.

45.6 Risk Assessment and Management in Geotechnical Engineering, a Tool for the Future

Risk assessment and risk management have been formalized by ISO (2009) (Fig. 45.26). ISO defines risk as the "effect of uncertainties on the objectives". In engineering practice, one usually defines risk as a product of the hazard by the consequences. Hazard is the temporal probability of occurrence of an event, the consequences are a function of the number of elements at risk, the vulnerability of

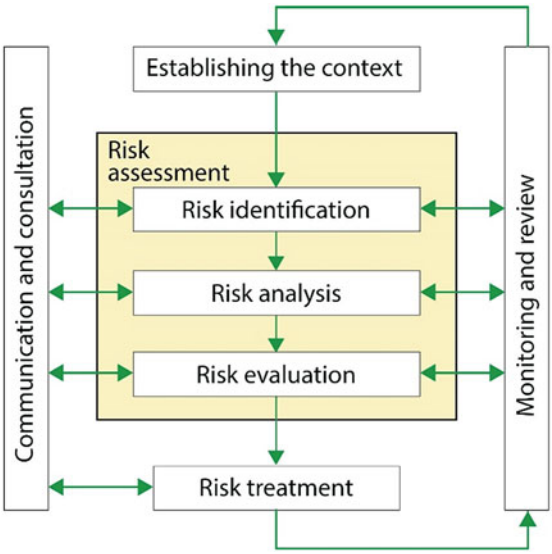

Fig. 45.26 Risk assessment and risk management process (ISO-3100:2009)

elements at risk and the value or utility of the elements at risk. The units of hazard are for example an annual probability or a probability/100 years, vulnerability is a dimensionless parameter usually expressed as a value between 0 (not vulnerable) and 1 (highly vulnerable, e.g. Li et al. 2010) and consequences are expressed as the number of fatalities, monetary values, degree of contamination, or other losses. Risk is then a number of fatalities/year, losses/year or contamination/year.

There are a number of methods available to do the hazard analysis of a slope in sensitive clays, including qualitative risk matrices combining hazard (probability of slope failure) and severity of consequences, for example a 3x3 matrix (Lacasse et al. 2004). Quantitative methods that have been used to study the reliability of slopes include:

- The seven blocks approach called SLOPE (Santamarina et al. 1992)
- The first order second moment approach (Ang and Tang 1984)
- Monte Carlo simulations (Ang and Tang 1984)
- First and second order reliability methods (FORM and SORM) (Nadim and Lacasse 1999)
- The event tree method (Hartford and Baecher 2001; Lacasse et al. 2008)
- The Bayesian network method (Nadim and Liu 2013)

For several of the methods, both the hazard and the consequences can be analyzed. Li et al. (2010) and Corominas et al. (2014) recommended a scenario-based approach to do risk analysis of slopes. Figure 45.27 illustrates the scenario-approach suggested by NGI's EU-project SafeLand project "Living with Landslide Risk in Europe".

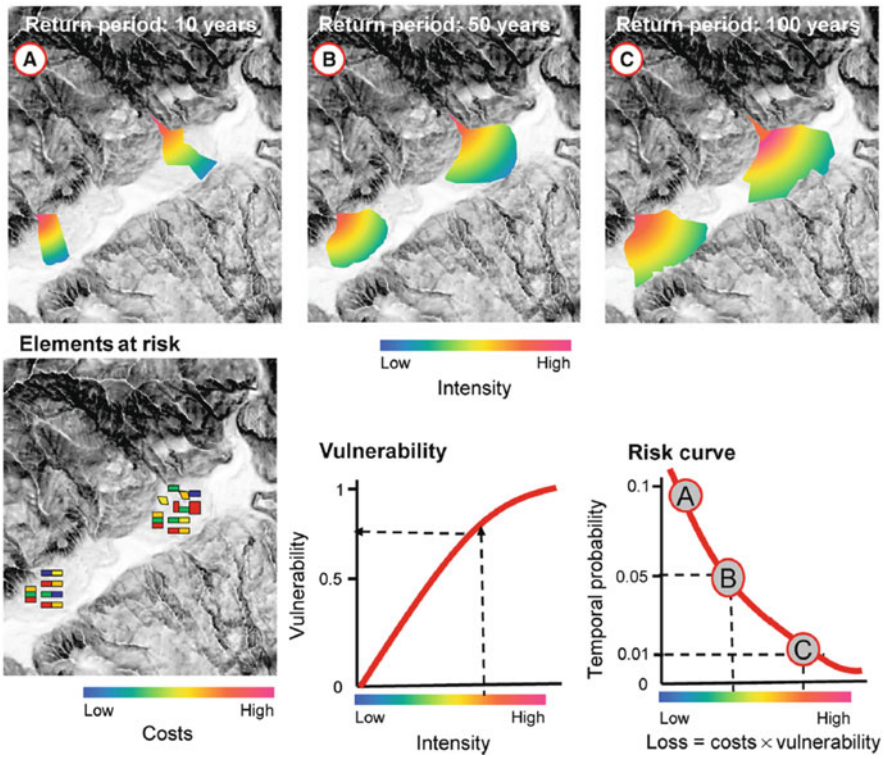

Fig. 45.27 Scenario-based risk assessment in SafeLand project (After Corominas et al. 2014)

45.6.1 Recommendation

Landslides in sensitive clays represent some of the highest risks in Norway (DSB 2014). They occur relatively frequently and the consequences can include loss of life, material losses and environmental damage.

Recently the NIFS project contributed tremendously to advancing the state-of-knowledge in the area of sensitive clays. To ensure that all the uncertainties are taken into account and that all failure modes, whether they are triggered by natural causes or human action, are included in an analysis, it is recommended that a generic probabilistic tool be developed to calculate site-specific annual probability of failure and rank consequences (elements at risk, vulnerability and potential losses).

The generic tool for event tree analysis of slopes in sensitive clays needs to be simple and could be used by practitioners with knowledge of slope stability and sensitive clays. The tool, e.g. an event tree analysis, could be used to study slopes in sensitive clays and for structures or planned earth work in the vicinity of quick clay deposits. Such a tool is both graphical and quantitative, and could easily be implemented in, e.g. EXCEL.

45.6.2 A Tool for the Future

The assessment of hazard and risk is an instrument for the future of our profession. The reliability approach is cross-disciplinary and user-oriented, and it is a communication tool that is common to many fields of expertise. The implementation of the methods allows to prioritise among options and account for different objectives from technology, economy, safety to environment, either separately or jointly. The approach has room to include new moments such as the impact of climate change. Reliability tools are needed because the future is not simply a projection of the present.

In practice, the implementation of reliability concepts and risk analyses allows to make risk-informed, and therefore better, decisions, improve safety and cost-effectiveness, identify potential hazards and aspects could go wrong in a systematic manner, and ultimately seeks to reduce risk and protect people. Those are the requirements for the deliverables in geotechnical engineering.

45.7 Conclusions

The paper gave examples of the application of reliability methods for the evaluation of the probability of failure and run-out of landslides in sensitive clays. In general, the calculated probabilistic values agreed reasonably well with the observed values for the two landslides studied, the Finneidfjord and the Rissa landslides in highly sensitive clays in Norway.

Factor of safety alone is not a sufficient measure of the safety margin because the uncertainties in the analysis influence the probability of failure. In geotechnical evaluations, it is important to not rely on factor of safety alone.

Hazard and risk analyses are useful tools to provide an additional assessment and to help making decisions. The methods applied to geotechnical problems have reached a level of maturity that makes them effective to use in practice. They provide more insight than deterministic analyses alone, and they represent a systematic way to account for all of the uncertainties in an analysis. They are also well suited for comparing alternatives and assisting decision-making.

Responsible future development must include risk assessment and management. Constraints, like difficult mathematics and lack of thrust in probabilistic methods, have now disappeared, with well-tested simple program packages now available. At the same time, the understanding and requests for the quantification of hazard and risk have grown in both the geotechnical profession and the general public.

To further enhance the use of probabilistic and risk methods in slope stability and slope runout in sensitive clays, we need:

- More examples of implementation of probabilistic methods to evaluate hazard and risk, where the results lead to safe and cost-effective solutions.

- Reliability analyses applied to geotechnical problems in university curricula, keeping a balance between theory and practical applications.
- Multi-disciplinary scientific discussion for cross-fertilization of ideas from different areas of risk.
- Publication of databases to improve the statistics of soil parameters, model uncertainties and lessons learned from past landslides.
- Improved communication to enhance the understanding of probabilistic results for the non-specialist.

Ultimately, geotechnical analyses aim at reducing risk and protecting people. Hazard, risk and reliability assessments provide additional insight in geotechnical problems in a systematic manner.

Acknowledgements The authors appreciate the discussions during the preparation of this paper with their NGI colleagues, including Dr. Dieter Issler, Dr. Jean-Sebastien L'Heureux, Dr. Maarten Vanneste and Dr. Kjell Karlsrud, and exchanges with Dr. Vikas Thakur from NTNU.

Annex A: Model Used for Run-Out Analyses

The Herschel-Bulkley rheological model can be described as:

$$\left|\frac{\dot{\gamma}}{\dot{\gamma}_r}\right|^n = \begin{cases} 0, & \text{for } |\tau| \le \tau_y{}' \\ \left(\dfrac{\tau}{\tau_y sgn(\dot{\gamma})} - 1\right), & \text{for } |\tau| > \tau_y \end{cases} \tag{45.A1}$$

Referring to Imran et al. (2001), the set of equations for the plug and shear layers can be derived as,

$$\frac{\partial}{\partial t}\left(h_p + h_s\right) + \nabla \cdot \left(u_p\left(h_p + \alpha_1 h_s\right)\right) = 0 \tag{45.A2}$$

$$\begin{aligned} &\frac{\partial}{\partial t}\left(h_p u_p\right) + \left(\left(h_p u_p \cdot \nabla\right) u_p + u_p\left(\nabla \cdot h_p u_p\right)\right) + g h_p \nabla\left(h + b\right) \\ &\quad + u_p\left(\frac{\partial}{\partial t} h_s + \nabla \cdot \left(\alpha_1 h_s u_p\right)\right) = -\frac{\tau_y sgn\left(u_p\right)}{\rho_d} \end{aligned} \tag{45.A3}$$

$$\begin{aligned} &\alpha_1 \frac{\partial}{\partial t}\left(h_s u_p\right) + \left(\left(h_s \alpha_2 u_p \cdot \nabla\right) u_p + \alpha_2 u_p\left(\nabla \cdot h_s u_p\right)\right) + g h_s \nabla\left(h + b\right) \\ &\quad - u_p\left(\frac{\partial}{\partial t} h_s + \nabla \cdot \left(\alpha_1 h_s u_p\right)\right) = -\frac{\tau_y \beta sgn\left(u_p\right)}{\rho_d}\left|\frac{u_p}{\gamma_r h_s}\right|^n \end{aligned} \tag{45.A4}$$

where h_p and h_s are the height of plug and shear layer, and u_p is the velocity of the plug layer. The height of the entire layer is $h = h_p + h_s$, and α_1, α_2 and β are parameters determined by the exponent n.

Rearranging the model by De Blasio et al. (2005), the model becomes

$$\tau_y(\gamma) = \tau_{y,\infty} + \left(\tau_{y,0} - \tau_{y,\infty}\right) e^{\Gamma\gamma} \tag{45.A5}$$

where $\tau_{y,0}$ and $\tau_{y,\infty}$ are the initial and residual yield stresses and Γ is a parameter describing how fast the movement is. The variable γ is the accumulated shear strain at the bottom given as,

$$\gamma = \int_0^t \left|\frac{\partial u}{\partial z}\right|_{z=0} dt = \frac{n+1}{n} \int \frac{|u_p|}{h_s} dt \tag{45.A6}$$

For numerical implementation, the finite volume method was employed with the total variation diminishing algorithm.

References

Ang AH-S, Tang WH (1984) Probability concepts in engineering planning and design, Volume II-Decision, risk and reliability. Wiley, New York

ASCE (2016) SmartBrief, March 21 2016 e-newsletter

Bernstein PL (1998) Against the Gods: the remarkable story of risk. Wiley, New York, 383 pp

Cassidy MJ, Uzielli M, Lacasse S (2008) Probability risk assessment of landslides: a case study at Finneidfjord. Can Geotech J 45:1250–1267

Corominas J, Van Westen C, Frattini P, Cascini L, Malet JP, Fotopoulou S, Catani F, Van Den Eeckhaut M, Mavrouli O, Agliardi F, Pitilakis K, Winter MG, Pastor M, Ferlisi S, Tofani V, Herva's J, Smith JT (2014) Recommendations for the quantitative analysis of landslide risk. Bull Eng Geol Environ 73:209–263

De Blasio FV, Elverhøi A, Issler D, Harbitz CB, Bryn P, Lien R (2005) On the dynamics of subaqueous clay-rich gravity mass flows—the giant Storegga slide, Norway. *Mar Pet Geol* 22:179–186

Dolva BK, Petkovic G (2017) Natural hazards in changing climate. Second International Workshop on landslides in sensitive clays. In: Thakur V, L'Heureux J-S, Locat A (eds) Landslides in sensitive clays. From research to implementation, Advances on natural and technological hazards research. Springer, Dordrecht, pp 539–547

DSB (2014) National risk analysis – disasters that may affect Norwegian society. 220 pp

Fornes P, Jostad HP (2017) Correction factors for undrained LE analyses of sensitive clays. International Workshop on landslides in sensitive clays. In: Thakur V, L'Heureux J-S, Locat A (eds) Landslides in sensitive clays. From research to implementation. Springer, Dordrecht, pp 225–235

Gregersen O (1981) The quick clay landslide in Rissa, Norway, vol 135. NGI Publications, Oslo, pp 1–6

Gregersen O (1999) Kvikkleireskredet I Finneidfjord 20 juni 1996. NGI report 980005–1. NGI, Oslo, Norway (in Norwegian)

Grimstad G, Jostad HP (2010) Undrained capacity analyses of sensitive clays using the non-local strain approach. 9th HSTAM Intern. Congress on Mechanics Vardoulakis mini-symposium. Limassol, Cyprus

Grimstad G, Andresen L, Jostad HP (2010) NGI ADP: anisotropic shear strength model for clay. Int J Numer Anal Methods Geomech 36(4):483–497

Hartford DND, Baecher GB (2001) Risk and uncertainty in dam safety. Thomas Telfrod Ltd, London, 391 pp

Imran J, Harff P, Parker G (2001) A numerical model of submarine de-bris flow with graphical user interface. Comput Geosci 274:717–729

ISO 31000 (2009) Risk management – principles and guidelines. International Organization for Standardization, Geneva. 24 pp

Janbu N (1996) Raset i Finneidfjord – 20. Juni 1996. Unpublished expert's report prepared for the County Sheriff of Nordland, Norway. Report no. 1, rev. 1 (in Norwegian)

Jostad HP, Grimstad G (2011) Comparison of distribution functions for the non-local strain approach. In: Proceedings of 2nd International Symposium on Computational Geomechanics, Cavtat-Dubrovnik, Croatia

Kummeneje (1993) Grunnundersøkelser Geotekniske vurderinger. Siv. ing. Ottar Kummeneje No. 8994, Rapport nr.1 (in Norwegian)

Kummeneje (1996) Geoteknisk vurdering av: Områder nord og øst for rasgrop-Boliger ved Varpen. Siv.ing.Ottar Kummeneje No. 11445, Rapport nr.3 (in Norwegian).

L'Heureux JS, Eilertsen RS, Glimstad S, Issler D, Solberg IL, Harbitz CB (2012a) The 1978 quick clay landslide at Rissa, mid-Norway: subaqueous morphology and tsunami simulations. In: Yamada Y et al (eds) *Sub-marine mass movements and their consequences*, Advances in natural and technological hazards research 31. Springer, Cham, pp 507–516

L'Heureux JS, Longva O, Steiner A, Hansen L, Vardy ME, Vanneste M, Haflidason H, Brendryen J, Kvalstad TJ, Forsberg CF, Chand S, Kopf A (2012b) Identification of weak layers and their role for the stability of slopes at Finneidfjord, Northern Norway. In: Yamada Y et al (eds) *Submarine mass movements and their consequences*, *Advances in natural and technological hazards research 31*. Springer, pp 321–330

Lacasse S (2017) 55th Rankine Lecture. Hazard, Risk and reliability in geotechnical practice. Paper submitted to *Geotechnique*

Lacasse S, Nadim F, Høeg K, Gregersen O (2004) Risk assessment in geotechnical engineering: the importance of engineering judgment. In: The Skempton conference, proceedings. Thomas Telford, London, UK. vol 2, pp 856–867

Lacasse S, Eidsvig U, Nadim F, Høeg K, Blikra LH (2008) Event TREE ANALYSIS OF Aaknes rock slide hazard. 4th Canadian conference on geohazards, Québec, Canada, pp 551–557

Li Z, Nadim F, Huang H, Uzielli M, Lacasse S (2010) Quantitative vulnerability estimation for scenario-based landslide hazards. Landslides 7:125–134

Longva O, Janbu N, Blikra LH, Bøe R (2003) The 1996 Finneidfjord slide: seafloor failure and slide dynamics. In: Locat J, Mienert J (eds) Submarine mass movements and their consequences. Kluwer Academic, Dordrecht, pp 531–538

Morgenstern NR, Price VE (1965) The analysis of the stability of general slip surface. Geotechnique 15:79–93

Nadim F, Lacasse S (1999) Probabilistic Slope Stability Evaluation. In: Proceedings of geotechnical risk management, Hong Kong Institution of Engineers, Hong Kong, pp 177–186

Nadim F, Liu Z (2013) Quantitative risk assessment for earthquake-triggered landslides using Bayesian network. In: Proceedings of 18th International conference on Soil mechanics and geotechnical engineering, Paris, September 2–6 2013

Natterøy A (2011) Skredkatalog om kvikkleire. Presentasjon av det førebels resultatet i katalogen og utgreiing om typiske kjennetegn ved kvikkleireskred. Project thesis, Institutt for geologi og bergteknikk, Norwegian University of Technology and Science (NTNU), Trondheim, Norway (in Norwegian)

NGI (2012) Back-analyses of run-out for Norwegian quick-clay landslides. NGI report 20120753–01-R, dated 30 November 2012.

NGI (2014) Naturfareprosjekt: Delprosjekt 6. Kvikkleire NGIs anbefaling for krav til effekt av sprøbruddoppførsel NIFS rapport 88/2014, NGI Report 2014 007501R 19 November 2014 (in Norwegian)

NIFS: Natural Hazards – Infrastructure for flood and slides (2012) Programplan 2012–2015 for etatsprogrammet, ISSN: 1501–2832 (in Norwegian)

Oset F, Thakur V, Dolva BK, Aunaas K, Sæter MB, Robsrud A, Viklund M, Nyheim T, Lyche E, Jensen OA (2014) Chapter 37: Regulatory framework for road and railway construction on the sensitive clays of Norway. 1st IWSLC, Québec. In: L'Heureux JS et al (eds) Landslides in sensitive clays: from geosciences to risk management, Advances in natural and technological hazards research 36. Springer, Dordrecht, pp 343–352. doi:10.1007/978-94-007-7079-9_27

Santamarina JC, Altschaefel AG, Chameau JL (1992) Reliability of slopes: incorporating qualitative information. Transp Res Record Issue 1343:5

Vanneste M, Longva O, L'Heureux JS, Steiner A, Vardy ME, Morgan E, Forsberg CF, Kvalstad TJ, Strout JM, Brendryen J, Haflidason H, Lecomte I, Steiner A, Kopf A, Mörz T, Kreiter S (2013) Finneidfjord, a field laboratory for integrated submarine slope stability assessments and characterization of landslide-prone sediments: a review. OTC offshore technology conference, OTC Paper P-686-OTC

Chapter 46
Natural Hazards in a Changing Climate in Norway

Bjorn Kristoffer Dolva and Gordana Petkovic

Abstract In several countries, including Norway, critical transport infrastructure is exposed to natural hazards such as floods, avalanches and landslides. Recent experiences show that these natural hazards have become more frequent primarily due to extreme weather events. These natural hazards have constitute a major threat to human life, surrounding manmade facilities and infrastructure and in Norway. Therefore, decision-making and design processes related to road and railroad construction in Norway rely heavily on an accurate assessment of these natural hazards. From 1900 to date, more than 1100 people have died in Norway due to natural hazards. About 115,000 people live in areas prone to flooding and landslides. According to the statistics, the accumulated cost of damage inflicted in the period 1980–2000 is around 1 billion Euros, and for the periode 2011–2014 the cost of the damage increased by approximately 750 million Euros.

This paper presents some results from the NIFS research program to develop robust approaches to mitigate landslides and minimise the consequences on infrastructure such as roads, railways, housing etc. We present some aspects of real time warning of avalanches, landslides and flooding, application of technology for hazard mapping and early warning, the development of new national databases, and the national strategy for management of natural hazards. It is our belief that some of these technologies and methods adopted for the flood, landslide, and avalanche hazard management are equally applicable for the preparedness and the early warning systems required for landslides in sensitive clays.

46.1 Introduction

The effects of natural hazards on roads have always been a field of work for NPRA, due to ground conditions and topography. An increasing importance of ensuring accessibility and safety, together with the change towards a wetter and uncertain climate, impose higher demands to determine the connection between natural

B.K. Dolva (✉) • G. Petkovic
Norwegian Public Roads Administration (NPRA), Oslo, Norway
e-mail: Bjorn-Kristoffer.Dolva@vegvesen.no; gordana.petkovic@vegvesen.no

V. Thakur et al. (eds.), *Landslides in Sensitive Clays*, Advances in Natural and Technological Hazards Research 46, DOI 10.1007/978-3-319-56487-6_46

hazards, climate change and road construction and management. Since 2006 NPRA have worked systematically on assessing the effects of climate change on roads. It became more and more clear how important it is to provide cross disciplinary collaboration. In 2012 NIFS-programme started, a collaboration between transport agencies and hydrology expertise. The paper will describe the basis for climate adaptation work in Norway, the main features and results from NIFS-programme, and how the collaboration is planned to continue.

46.2 Climate in Norway

Norway has a relatively mild climate for its latitude. Climate change is expected to bring more rain in areas that already are rich with precipitation. The report "Climate in Norway 2100" (NCCS 2015) provides a very valuable basis for all adaptation work in Norway. This report gives a thorough overview of the climate in Norway, past, present, observed trends, and finally the results of modelling of climate change towards the end of this century. Projections of development of climate parameters are given for two scenarios, i.e. representative concentration pathways RCP 4.5 and 8.5, together with indications of uncertainty. This is done for each season and climate change region in Norway.

Climate projections from this work are made available through user friendly web portals and other tools that offer meteorological and hydrological information (Fig. 46.1). A Climate Service Centre is established in Norway, providing updated climate information. This is of great value for everybody working with natural hazards.

An average increase in mean temperature of 4,5 °C, and in precipitation of 18% can be expected by the end of this century, with great seasonal and regional variations. The temperature rise is most pronounced in the winter season and in the northern regions. During the first decades of this century, there will be more snow in the mountain areas. The effect of temperature rise will eventually be more dominant and the snow will be replaced by rain, even at high altitudes.

The main challenges will come from more precipitation generally, and especially from more frequent heavy precipitation. There will be a higher risk of floods and erosion. There will also be a higher risk of landslides, some of them occurring at new locations and in changed forms. More slush avalanches, debris flows and mudflows are expected. Areas exposed to stable winter conditions today may experience higher exposure to repeated freezing and thawing.

The ground conditions in Norway comprise soft clay slopes and steep mountains. The country is prone to many types of natural hazards e.g., landslides, debris- and mudflow, rock fall, snow avalanches, flooding, as illustrated in Fig. 46.2.

From 1900 to date, more than 1100 people have died in Norway due to natural hazards. According to White Paper no.15/2012 about 115,000 people live in areas prone to flood and landslide. Natural hazards have resulted in damage worth about 1 Billion US dollars between years 1980 and 2010. In 2011 alone, the cost of damage increased by about 110 million US dollars (NIFS 2016).

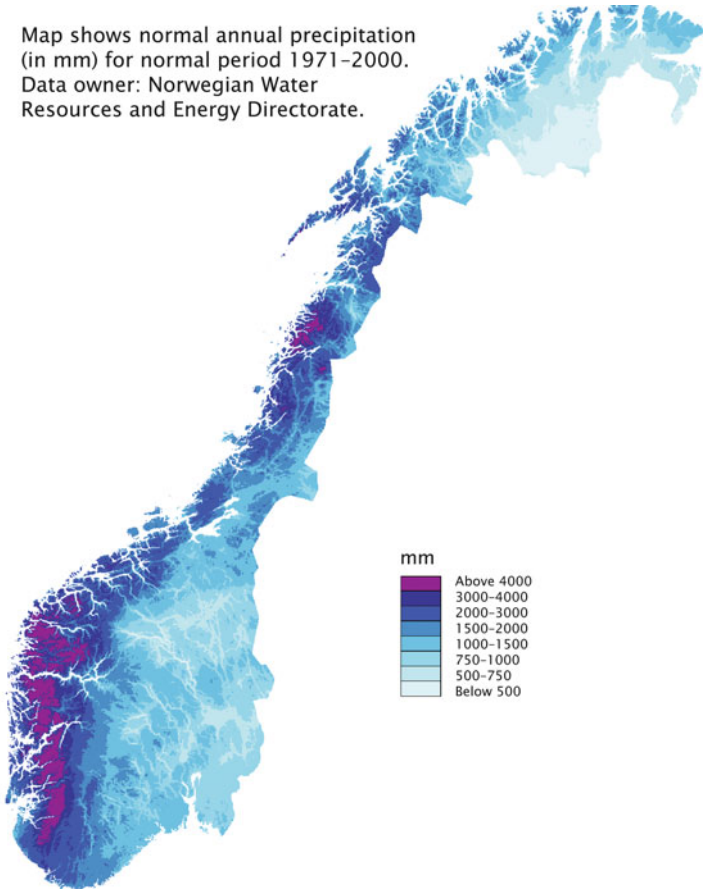

Fig. 46.1 Climate in Norway during 1971–2000

Recent experiences and studies from Norway (e.g. IPCC (2007–2013), Infrarisk (2013); NVE (2010–2011)) suggest there is an increase in the frequency and/or intensity of the Extreme Weather Events (EWEs) such as unusual, severe or unseasonal rainfall, temperature fluctuation and strong wind. In return, the frequencies and the size of debris- and mudflow (DMF) and flooding have increased. Govt. agency report 16 (2011) by Norwegian Water Resources and Energy Directorate (NVE) suggests that there is a significance increase in DMF events in the central and the Northern Norway mainly attributed by the changing climate resulting in EWEs. Moreover, the recent DMFs are occurring at new locations and are larger in size, which demands better preparedness and forecasting strategies for DMF events (see Fig. 46.2b, c). These aspects have been underlined by the White Paper no.15/2012 by the Norwegian parliament titled "How to live with risk of flood and slides". The

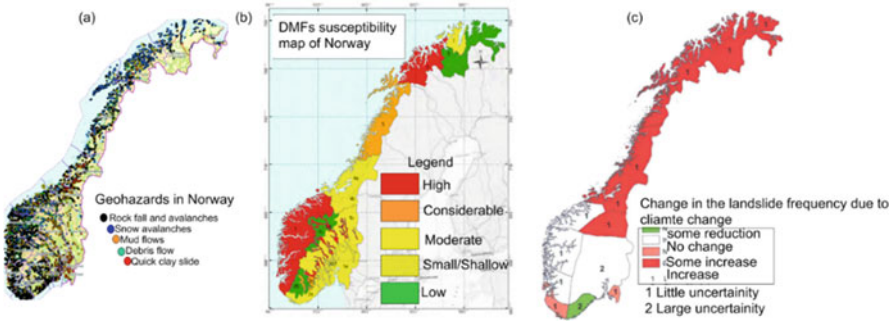

Fig. 46.2 (**a**) Natural hazards challenges in Norway based on www.skrednett.no; (**b**) Debris and mudflows (DMF) susceptibility map of Norway illustrated using a recent study carried out by NIFS (2016); (**c**) Change in landslide frequencies due to climate change triggered EWEs suggested by NVE (2011)

chapter 12.1 and 12.2 of this White paper suggests increasing the research activities related to flood and slides such as DMFs.

46.3 R&D Work for Adaptation to Climate Change and Natural Hazards

The relation between weather, climate and landslide risk and protection methods have been investigated for many years. Since 2006 more systematic work on the effects of climate change of this relation has been studied. The R&D programme "Climate and Transport" had the aim to investigate the impacts climate change could have on the road network in Norway and propose remedial measures. The programme is summarized in a final report (NPRA (2013)). The main outcomes of this programme was a revised edition of NPRA's own manuals of design and practice, proposals of new manuals, a risk management portal, a long list of reports. But most of all – the acknowledgement of interdependencies between transport agencies (roads, railways) and experts on meteorology, hydrology, geology etc. Climate adaptation proved to require inter-disciplinary effort (Fig. 46.3).

46.4 NIFS – Natural Hazards – Infrastructure, Floods and Slides

In 2012, the Norwegian governmental agencies; Norwegian Public Roads Administration (NPRA), Norwegian National Railways Administration (NNRA) and Norwegian Water Resources and Energy Directorate (NVE) initiated a collaborative

Fig. 46.3 Examples of the impact of extreme weather on the Norwegian transportation infrastructure (Source: NNRA and NPRA)

Research Programme named "Natural Hazards – Infrastructure for floods and slides (NIFS)". The program was finalised in 2016. Our final report, NIFS-report nr. 43 (2016), is in Norwegian, but an English translation will be available during 2016 see www.naturfare.no.

46.4.1 Objectives and Scope

The overall objective of the NIFS programme is described in NIFS report no. 57 (2013) as: a safer society with more robust infrastructure, safe buildings, safe transport and good forecasting systems for landslides, avalanches and floods. This was supposed to rely on good and growing partnership platforms, coordinated activities of the agencies and sharing of knowledge. This includes raising awareness of natural hazards, common risk management, adjusting contingency plans for situations that involve unacceptable levels of risk. In addition, coordination and partnership in connection with databases, hazard mapping, forecasting systems and R&D is supposed to ensure efficient use of government funds. The programme took into account current and future climate challenges.

46.4.2 Main Subjects and Results

Both NVE, NPRA and NNRA have key roles in efforts to limit the risk of floods and landslides for buildings and public infrastructure. Many other actors are involved in the work. Understanding of roles, long-term planning and coordination of natural hazard assessments have been a clear objective in NIFS. There is a need for more precise definition of the agencies' roles, at the local and regional level, in construction projects and management of crises and incidents. Good relations between

the agencies, at the local and the regional level, provide a good basis for effective cooperation and interaction, better communication with users and better reputation.

Preliminary work in NIFS revealed the need for a discussion about attitudes concerning the acceptable level of risk, and possibilities for the harmonization risk acceptance criteria. NIFS recommended further coordination of rules and regulation through close contact with the Norwegian Building Authorities (DiBK) on the revision of current technical regulations (TEK 17), which are mostly applicable for buildings.

Mapping of natural hazards and their consequences provides a basis for risk assessment. Cooperation on mapping of flood and landslide risk must be continued. It is important to continue the work on standardization, data coordination, sharing of information from flood and landslide events and ensuring the delivery of ground survey data to a common national database at The Geological Survey of Norway (NGU) and to make them available to the entire society.

Assessment of natural hazards is fundamental to spatial planning and gains importance due to climate change. There is still a need to look into the provisions of the Planning and Building Act (2008) and how the information about natural hazards is communicated and understood. Many of the challenges in spatial planning are related to management of water and impacts of water astray. Handling of natural runoff from the terrain and surface water must be included in all planning phases. Catchment areas should be handled holistically and in cooperation between all involved authorities.

Protection measures for floods and landslides include a wide range of instruments. Closer cooperation regarding protection measures will give more robust infrastructure and less risk of recurrence of damage. The result is fewer delays, better quality of structures and measures, reduced damage risk and improved basis for comprehensive risk and vulnerability analysis. NIFS recommends that the agencies adopt new technology for modelling and further develop and systematize their list of safeguards, with procedures for monitoring and maintenance.

Water astray can cause severe damage and consequences, and yield significant costs. There is a need for comprehensive management of flood and surface water, vs. the whole catchment. Often there are a large number of parties involved and the consequences are often greater for those located “downstream” than where the problem arises. Even small changes in drainage and runoff conditions can cause very serious damage to nearby infrastructure. NIFS program proposes a number of measures to improve future management.

Norway, together with a few other countries such as Sweden and Canada, has a special challenge related to the occurrence of quick clay. Landslides in this type of clay can be triggered by small interventions, and cause large- scale slides even in relatively flat terrain. NIFS has improved methods for mapping of quick clay. This is done by looking at conventional geotechnical probing methods combined with resistivity/electromagnetic measurements and developing these further. NIFS program has worked on coordinating and revising policies and establishing a unified practice for the assessment of stability in quick clay areas. These recommendations should be incorporated into relevant policies, guidelines and regulations.

The climatic and topographical conditions in Norway indicate that 100% protection of infrastructure against floods and landslides is not feasible. Monitoring and forecasting of natural hazards is therefore important to increase predictability and reducing risk. Coordination of the agencies' equipment and services for monitoring the stability has been tested. This has resulted in better utilization of expertise and resources, as well as shorter response time and better quality of services in emergency cases. NIFS has established the basis for a lasting cooperation. Expected future access to radar satellite data, together with other technology, will improve the methods for identification of terrain deformations and for monitoring of infrastructure. NIFS recommends further investments in the use of radar satellite data, through broad cooperation for improved access to data and methodology development.

In case of a natural disaster, it is crucial that society has adequate contingency and is equipped to handle the situation. Effective collaboration between the agencies requires access to adequate information and good communication. NIFS program has prepared a proposal for common term lists and definitions, in order to establish common ground and better understanding. The lists contain terms for avalanche types, preparedness, monitoring and safeguards.

Mutual knowledge concerning contingency plans and organization of emergency is important. NIFS conducted exercises concerning quick clay landslides and rock falls. A manual for field work was published, it covers the most common types of events of floods and landslides in Norway, and includes both small events with limited consequences and major events, involving many agencies or sectors.

Good management of flood and landslide risk requires a high knowledge and competence level. The results from NIFS improve the knowledge base for management of natural hazards and provide directions for further research on selected topics. We have conducted several basic studies within methodology for monitoring and warning, mechanisms within trigging of slides and distribution, quick clay mapping and properties. Further research in these areas is recommended.

46.4.3 Results and Deliverables from NIFS

More than 120 technical reports and over 30 technical papers have been published and are available on the programme's and the agencies' websites. Other dissemination activities consist of presentations on conferences and seminars and outreach activities for recruitment of students. A short film about NIFS and two educational films for secondary schools have also been produced.

The programme has brought increased knowledge and awareness of natural hazards, cause–and-effect relationships, and the need for documentation and verifiability. An example of this is increased avalanche expertise within consulting industry performing avalanche hazard mapping and landslide studies in steep terrain for agencies, municipalities and project owners.

NIFS programme's recommendations for further work, can be summarized in the following main points:

- Collaborative compilation, systematization and storage of data relevant for natural hazard management should be developed further
- Risk and vulnerability analysis should be performed for whole watershed areas. Drainage of roads and flood problems should be taken into all planning phases.
- Unified methodology for assessing social impacts should be further developed.
- Socio-economic analysis should be conducted for natural hazard events with extensive damage.
- Repair and reconstruction after weather related events should contribute to better climate-resilience.
- Further work should be done on harmonization of regulations for stability survey in quick clay areas
- The agencies' contingency plans and preparedness work should be coordinated further.

46.5 Continuing the Collaboration – National Forum for Flood and Landslide Prevention

As stated in the White Paper no. 15/2012 by the Norwegian parliament "How to live with risk of flood and slides", NVE has a coordinating responsibility for establishing a national strategy for the management of natural hazards. This work has to be based on broad cooperation. The collaboration established in NIFS will, therefore, together with new participants, comprise a new forum with the aim of develop and maintain the national strategy. NVE will be responsible for establishing the forum and operating it. The partnership will be based on a project organized approach and involve all relevant national actors.

The strategy will define cooperation areas and identify measures to improve the interaction between agencies. Each participating organisations must contribute within their responsibilities and collaborate on assignments where this is appropriate. Through a national strategy for flood and landslide prevention and associated projects the participants will achieve better common use of resources, better quality of services, greater awareness and understanding across areas of responsibility, and facilitated access to information.

An annual conference/seminar, "National Forum for flood and landslide prevention" will be an important meeting place and venue for exchanging knowledge and experience at national level. In addition, other events will be organised for the local/regional level.

46.6 Closing Remarks

The program's common web site www.naturfare.no will be kept open as the main channel to reach the public. Our results are published in more than 120 different reports and more than 30 scientific articles delivered within the project period. Two Ph.D.-studies are ongoing, and more than 50 M.Sc./B.Sci.-studies have been carried out in collaborating with different NIFS project teams. Our summary report gives our recommendations in a broader context and it will be available in English during 2016.

Acknowledgments The NIFS programme would like to acknowledge the contributions by the Norwegian University of Science and Technology, Norwegian Geotechnical Institute, Multiconsult AS, SINTEF Building and Infrastructure, Norwegian Geological Survey, Rambøll, Snøball, Orbiton. The authors of this paper would like to thank Kari Øvrelid, Eli Katarina Øydvin, Tore Humstad, Steinar Myrabø, Kristian Aunaas and Margareta Viklund for their help and support. Many thanks to our reviewer Ivan Depina.

References

InfraRisk (2013). *Impacts of extreme weather events on infrastructure in Norway (InfraRisk)* – report to NFR-project 200689. Norges Geotekniske Institutt, Oslo

IPCC (2007) Climate change 2007: The physical science basis summary for policymakers, a report of working group I to the fourth assessment report of the Intergovernmental Panel on Climate Change

IPCC (2013) Climate change 2013: The physical science basis. The fifth assessment report of the Intergovernmental Panel on Climate Change, Cambridge University Press

NCCS (2015). Report 2/2015. Climate in Norway 2100. ISSN nr. 2387–3027 (in Norwegian)

NIFS report nr 43 (2016) NIFS – final report. R&D Programme 2012–2015 for the Government Agency Programme. NATURAL HAZARDS – infrastructure for floods and slides (NIFS). ISBN no 978–82–410-1194-8 (in Norwegian)

NIFS report nr 57 (2013) Programme plan 2012–2015 for the Government Agency Programme. NATURAL HAZARDS – infrastructure for floods and slides (NIFS). ISBN no 978–82–410-0931-0

NPRA (2013) Climate and transport 2007–2011. NPRA rapport nr 210. ISSN: 1893–1162

NVE (2011) Plan for landslide hazard mapping – Subreport on soil and debris flows. NVEs Publication nr 16/2011. ISBN no 978–82–410-0757-6. www.nve.no (in Norwegian)

NVE report nr 19 (2010) Strategy for climate adaptation as a basis for further work within the sector. ISBN no 978–82–410-0766-8. www.nve.no (in Norwegian)

The Planning and building Act (2008) https://lovdata.no/dokument/NL/lov/2008-06-27-71

www.naturfare.no

www.vegvesen.no

Chapter 47
Development of a Long Term Monitoring Network of Sensitive Clay Slopes in Québec in the Context of Climate Change

Catherine Cloutier, Pascal Locat, Denis Demers, Alexis Fortin, Jacques Locat, Serge Leroueil, Ariane Locat, Jean-Michel Lemieux, and Chantal Bilodeau

Abstract The Government of Québec recently initiated the deployment of a vast groundwater pressures monitoring network in postglacial marine clays to document their variations in time and improve our understanding of the relationship between failure initiation and climate in clay slopes. This project aims at evaluating the impacts of climate change on clay-slope stability and how it can be integrated in landslide risk management to improve public safety. Hydrogeological data will be acquired at sites located throughout the Québec Province's post-glacial clay deposits to create a public georeferenced index of typical hydrogeological conditions. The project goes beyond the characterization of groundwater pressures and their variations in clay slopes. Indeed, slope deformation will be measured at several sites. Also, two sites in flat terrain will be instrumented in order to evaluate mechanical properties of clay layers in simple 1-D conditions and groundwater recharge. The unsaturated clay crust in slopes susceptible to superficial landslides will be characterized and instrumented. The current lifetime of the monitoring project has been set to a period of 25 years.

C. Cloutier (✉) • J. Locat • J.-M. Lemieux
Département de géologie et de génie géologique, Université Laval, Québec, QC, Canada
e-mail: catherine.cloutier.2@ulaval.ca; jacques.locat@ggl.ulaval.ca

P. Locat • D. Demers • A. Fortin
Ministère des Transports, de la Mobilité durable et de l'Électrification des transports du Québec, Québec, QC, Canada
e-mail: pascal.locat@transports.gouv.qc.ca; denis.demers@mtq.gouv.qc.ca; alexis.fortin@transports.gouv.qc.ca

S. Leroueil • A. Locat
Département de génie civil et de génie des eaux, Université Laval, Québec City, QC, Canada
e-mail: ariane.locat@gci.ulaval.ca

C. Bilodeau
Ministère de la Sécurité publique du Québec, Québec, QC, Canada
e-mail: chantal.bilodeau@msp.gouv.qc.ca

V. Thakur et al. (eds.), *Landslides in Sensitive Clays*, Advances in Natural and Technological Hazards Research 46, DOI 10.1007/978-3-319-56487-6_47

47.1 Introduction

Naturally occurring landslides in sensitive clays are known to result from various causes including erosion (e.g. Lefebvre 1986; Locat et al. 2011), precipitation (e.g. Perret and Bégin 1997) and earthquakes (e.g. Lefebvre et al. 1991; Lamontagne et al. 2007; Locat 2011). For the first two causes, the link with climate can be made quite easily. Firstly, the climate influences the amount of precipitation (snow and water) and other parameters, such as evapotranspiration, which impact groundwater pressures in soil. Secondly, climate and meteorological events control river flow by governing the spring freshet, causing floods and drawdowns, which all influence erosion along river banks (Crozier 2010; Cloutier et al. 2016; Göransson et al. 2016). This concept is well accepted but still little is known about the actual geomechanical response of slopes to short and long term climatic conditions (Terranova 2002; Zêzere et al. 2004; Gauthier and Hutchinson 2012; Segoni et al. 2014; Marefat et al. 2015).

The general stratigraphy of clay deposits in Québec can be simplified to a clay of low permeability lying between more permeable layers consisting of an upper fissured clays or sand and lower till or fluvio-glacial deposits (Lefebvre 1986). Lafleur and Lefebvre (1980) explained how active river erosion deepens valley and influences slope stability by inducing changes to the groundwater regime in such a stratigraphy over hundreds of years. The effect of seasonal and inter-annual groundwater variations on effective stresses have also been studied, but data frequent enough to consider the effect of precipitation are limited. From various studies in clays (Jarrett and Eden 1970; Mitchell and Eden 1972; Berntson and Sällfors 1984; Kenney and Lau 1984; Sällfors and Svensson 1984; Lefebvre 1986; Boyle et al. 2009), we know that rapid variations of pore pressure are taking place in the upper more permeable layer and also, that significant seasonal variation can be observed in the lower permeable layer, but, because of its low permeability, pore pressure in the intact clay cannot follow these rapid variations occurring at its boundaries and the size of the variations decreases with increasing depth. Indeed, time lags are observed in between climatic conditions and the responses of piezometers in clays, which fluctuate with depth and spatial locations. The pore pressure response in clay is a function of its permeability and compressibility. In general, following spring snowmelt, groundwater pressure increases. Precipitation do not necessarily result in significant rises of the groundwater pressure as shown in the study of Boyle et al. (2009), probably due to the impact of vegetation, evapotranspiration and re-wetting of unsaturated soil. Finally, pressure gradient can change through the year (e.g. Berntson and Sällfors 1984).

Dragoni and Sukhija (2008) studied the possible impact of future climate change on water availability and discuss that in areas with increasing groundwater recharge, there will be increased slope instability. However, the ground becomes fully saturated relatively frequently in the environmental context of interest, and thus, ground saturation cannot be the main triggering mechanism for quick clay landslides (Boyle et al. 2009). So, in order to determine if landslide will become

more frequent, the impact of climate change on pore pressure of clays and how they could lead to destabilization must be better understood.

Climate change projections tend towards a general increase in precipitation and in the frequency of extreme precipitation events in Québec (Ouranos 2014), which are known as triggering factors of landslides in clays. However, because climate change also impacts other variables more or less directly, such as evapotranspiration and the timing and magnitude of spring freshet, the impact of climate change on slope stability in post-glacial marine deposits is not straightforward. Key questions arising from mapping landslide susceptibility in this context are (1) how will slopes respond to climate change within the next 50–100 years and (2) how can it be taken into account to reduce landslide hazard. We believe that the first step in answering these questions is to develop a better understanding of the link between the initiation of landslides and the actual climate.

In order to move forward along this goal, the Government of Québec started a vast campaign of instrumentation of post-glacial clay deposits (Fig. 47.1) to characterize groundwater pressures and their variations in time. This project is part of the collaboration between the Ministère de la Sécurité publique du Québec (MSP), the Ministère des Transports, de la Mobilité durable et de l'Électrification des transports du Québec (MTMDET) and Université Laval that aims at contributing to the development of knowledge on slope stability in clay slopes. This collaboration is motivated by the wish to reduce the risk related to landslides in Québec, where 80% of them occur in clays (Fig. 47.1). Indeed, a large part of Québec's population lives on post-glacial marine clay deposits where landslides do occur every year (Demers et al. 2014). Most landslides have low consequences, but some have had high consequences (Potvin et al. 2001; Locat et al. 2014; Transport Québec 2011).

This long term project started in the winter of 2016 by the design of the instrumentation system and the choices of sites with the objective to set up a vast monitoring network. The network installation started in the summer of 2016 and shall continue in the next years. This paper presents the objectives and methodology developed so far to put in place the instrumentation network of groundwater conditions, slope deformations and weather to document climate change impacts on clay slope stability.

47.2 Objectives and Long Term Vision

This project will generate a database of groundwater conditions in post-glacial marine clays now located above sea level in the Province of Québec (Fig. 47.1). The four main objectives are: (1) to increase knowledge on seasonal and long term variations of groundwater pressures in clays, (2) to generate a georeferenced index of typical hydrogeological conditions in clays at different locations in the province to be consulted and used by engineers working with these soils, (3) to study the influence of climate change on slope stability in clays in Québec, and (4) to get a

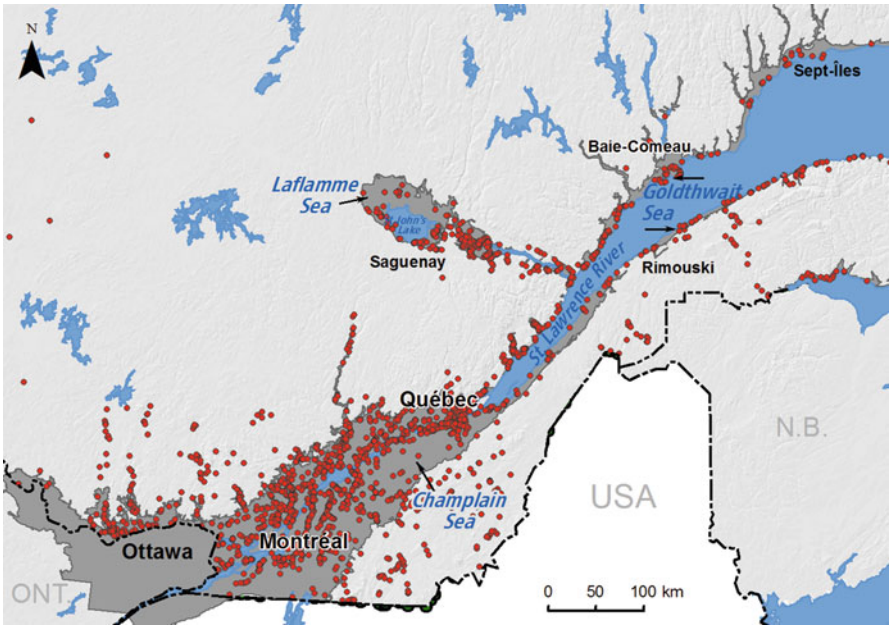

Fig. 47.1 Extent of post-glacial marine deposits (*dark grey zones*) and localization of the known landslides in all types of materials (*red dots*) in the Province of Québec

better understanding of the relationship between variations of groundwater pressures and soil deformations development in clay slopes.

This database should be useful to fill knowledge gaps in the mechanical behaviour of clay slopes. Some potential research themes that should benefit from the database are listed hereunder.

- Characterize mechanical properties, water pressures and deformations in clay soils by instrumenting site in flat ground and in slopes for a 25-year period;
- Improve slope stability analyses in clay slopes;
- Document and study the triggering role of groundwater pressures on deep-seated first-circular failure in clay slopes;
- Evaluate water and weather effects on the triggering of superficial landslides;
- Use climate models to project long term behaviour of clay slopes;
- Define warning criteria for weather and hydrological parameters linked to the landslide triggering;
- Examine the possibility to use real-time monitoring system as a risk management tool.

Keeping in mind theses research themes, five types of sites were conceived to be instrumented. Each type is intended to contribute to some of the listed specific themes, in addition to the four main objectives stated at the beginning of this section.

47.3 Methodology

To reach the scientific objectives, the final geographic distribution of the instrumentation network needs to respect some criteria. Indeed, it should cover the different climatic zones and the different projected climate changes. Moreover, the sites should represent the typical stratigraphy encountered in regions of the Province of Québec; hence, it should represent the various depositional contexts but still within sensitive clay slopes. Lastly, the sites should be placed in various morphologies, such as plains and valleys. The other criteria depend on the types of sites which are characterized by different morphologies and planned instrumentation (Fig. 47.2).

47.3.1 Type 1

Type 1 sites are those that are instrumented either for mapping landslide prone-area or for current slope stability studies carried out by the MTMDET. For mapping purposes, one piezometer nest of three sensors is usually installed at the bottom of valleys; while for stability studies a minimum of two nests of three piezometers are

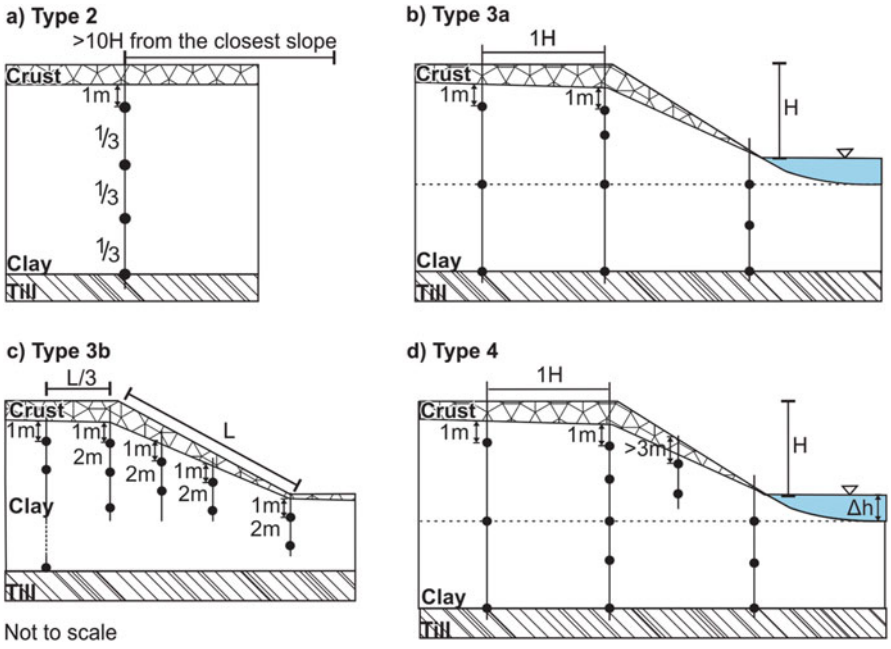

Fig. 47.2 Schematic representation of the 4 site types defined for the project showing the position of the piezometers (*black dots*). The type 1 sites are instrumented by the MTMDET for other purposes and have no typical morphology; this is why they are not drafted on this figure

installed at the top and at the toe of slopes. In both situations, the deepest piezometer often reaches the layer underneath the clay, which can be either till or fluvioglacial deposits. The data are acquired twice a day and saved on a data logger located at the ground surface and manually uploaded on site once a year.

A geotechnical characterization is also conducted, including grainsize distribution, water content, Atterberg limits, oedometer tests, and intact and remoulded undrained shear strength using vane, cone penetrometer test and Swedish fall cone. A digital elevation model (DEM) created from airborne laser scans and time series of aerial orthophotos are available.

Their localisation is chosen independently of the project criteria. Normally, these sites will be instrumented for a period of 3–5 years. However, they can match the criteria of the project, thus, certain type 1 sites could be transformed into types 3a, 3b or 4. Also, because they could offer an interesting spatial dispersion, their acquisition time span could be extended. In May 2016, about fifteen type 1 sites were already instrumented and there should be more in a near future.

47.3.2 Type 2

The instrumentation of the type 2 sites aims at characterizing mechanical properties of clays, hydrological conditions (infiltration, evapotranspiration, freezing depth) and groundwater pressure variations with depth in simple 1-D conditions. The instrumentation will be localized in a post-glacial clay deposit in flat terrain, located away from the closest slope by a distance at least ten times its height, to minimize the horizontal component of groundwater flow. Vegetation cover influence infiltration of water in slope and the vegetation cover will be characterized.

Type 2 sites have the most complex and complete instrumentation system of all five types. They will be located near sites type 3 or 4, as detailed information arising from these sites will help to analyse nearby, less densely instrumented sites.

The geotechnical characterization will include, in addition to what is listed for type 1, hydraulic conductivity, small strain deformation modulus (G_{max}, seismic cone penetrometer) and stratigraphic mapping. The instrumentation will include a minimum of three to four piezometers installed at different depths (Fig. 47.2a), a complete weather station, and sensors to characterize the vadose zone, evaluate water infiltration, and monitor ground temperature.

The acquisition frequency will vary with instruments, but should be around three times per hour for the sensors located in the unsaturated zone and four times per day for the piezometers. This will be adjusted in the final design.

47.3.3 Type 3a

These sites are meant to study groundwater conditions in slopes in sectors prone to deep rotational landslides, hence where recent landslides occurred or where scars were mapped. These sites should be selected with care to cover a range of morphologies, clay properties and regional hydrogeological contexts.

The geotechnical characterization will be similar to the one of type 1, but will include measures of hydraulic conductivity. Moreover, if there is a river, and this should be the case for most sites, its bathymetry should be mapped and water level could be monitored. The groundwater pressures will be monitored by a minimum of three nests of three piezometers (Fig. 47.2b). A weather station should be located nearby; the maximum distance from the site is still under discussion, but should be in the order of 5 km or less.

47.3.4 Type 3b

Sites of type 3b aim at studying superficial (∼3 m thick) landslides in the clay crust. The sites will be clay slopes without active erosion at their toe and where superficial landslides have occurred nearby. Climate change could have a potentially important effect on this type of instability. Indeed, the climate and the weather roles as aggravating and triggering factors of such failure types are well known (Perret and Bégin 1997; Terranova 2002; Crosta and Frattini 2003; Guthrie and Evans 2004).

The geotechnical characterization will be similar to the one of type 3a. In addition, the crust and its fissures should be characterized visually in trenches. The slopes will be monitored by four to five piezometer nests (Fig. 47.2c). The crust should be instrumented to monitor suction and water content. A complete weather station should be located within a close range, defined as less than 1 km.

47.3.5 Type 4

Sites of type 4 (Fig. 47.2d) will have the same geotechnical instrumentation and a similar piezometer installation as type 3a, but slope deformation (surficial displacements and displacement profile with depth) will be measured, potentially with InSAR technology and in-place inclinometers. To increase the chances to measure significant slope deformation, type 4 sites will be located on a riverside which undergoes active erosion and in a sector where recent landslides or past landslides are known. A nearby weather station and monitoring the river water-level are essential.

47.3.6 Piezometers

The network is to be maintained over a long period (25 years), thus, special care must be taken during piezometer installations to maximize the sensors' life span and data accuracy. Vibrating wire piezometers will be used and at least one Casagrande piezometer will be installed per site. Aside from type 1 sites, there should be only one piezometer sensor per borehole in order to limit vertical hydraulic short cuts. The sensor will be installed in a sand lantern with 60 cm-long plug of bentonite cement. The rest of the borehole will be filled with a mix of bentonite and Portland cements adjusted to insure that its permeability will be lower than the one of the soil. A barometer will be installed at sites of types 2 and 3b to correct the groundwater pressure for barometric pressure variations. Elsewhere, these variations will be estimated using data from the nearest weather station.

The piezometers should be installed deeper than frost penetration. For this reasons, the sensors should be at least 1 m below the clay crust (Fig. 47.2).

A hydrogeological model will be created for every site to place the piezometer data in their geotechnical context. This will be part of data validation. This project will generate an important amount of data, so a robust system should be develop to convert, validate and display the measured groundwater pressures.

47.4 Concluding Remarks

The first year of the project (2016) focussed on developing the design of the instrumentation, choosing the sites and starting the installation of piezometers on some sites of types 1 and 3a. Instrumentation of sites of type 2 and 4 were initiated in late 2016 and should be completed through the coming year. The documentation of groundwater pressures and their variations will lead to the creation of an index of hydrogeological conditions in clay deposits in the Province of Québec.

The short and long-term monitoring of clay slopes and the analysis of the data should allow a better evaluation of the occurrence probability of landslides and develop warning criteria adapted for climate change potential impacts.

To conclude, it is this the first time such an extensive monitoring project of sensitive clay slopes of Eastern Canada is being elaborated. The data originating from this monitoring network will benefit different research projects, but first, a little patience is mandatory to obtain data sets long enough to be meaningful.

Acknowledgments The authors would like to thank two reviewers Karin Lundström and Sarah Bouchard and the editor Vikas Takur. The project is financially supported by the Plan d'action des changements climatiques (PACC 15-16) of the Government of Québec.

References

Berntson JA, Sällfors GB (1984) Pore pressure variations in marine clay deposits. In: Proceedings of the IV International symposium on landslides, Toronto 1984, 1, pp 363–365

Boyle S, Karlsrud K, Heydal ØA (2009) Pore-pressure response in a marine clayslope in southeast Norway. Can Geotech J 46:1931–1405

Cloutier C, Locat J, Geertsema M, Jakob M, Schnorbus M (2016) Canadian report on climate change impacts on landslides. In: KKS H, Lacasse S, Picarelli L (eds) Preparedness for climate change impact on slope safety. CRC Press/Balkema, Taylor & Francis Group, Leiden

Crosta GB, Frattini P (2003) Distributed modelling of shallow landslides triggered by intense rainfall. Nat Hazards Earth Syst Sci 3:81–93

Crozier MJ (2010) Deciphering the effect of climate change on landslide activity: a review. Geomorphology 124(3–4):260–267

Demers D, Robitaille D, Locat P, Potvin J (2014) Inventory of large landslides in sensitive clays in the province of Québec, Canada: preliminary analysis. In: L'Heureux J-S (ed) Landslides in sensitive clays: from geosciences to risk management, Advances in natural and technological hazards research 36, pp 77–89

Dragoni W, Sukhija BS (2008) Climate change and groundwater: a short review. Geol Soc Lond, Spec Publ 288:1–12

Gauthier D, Hutchinson DJ (2012) Evaluation of potential meteorological triggers of large landslides in sensitive glaciomarine clay, eastern Canada. Nat Hazards Earth Syst Sci 12(11):3359–3375

Göransson G, Hedfors J, Ndayikengurukiye G, Odén K (2016) Climate change induced river erosion as a trigger for landslide, In: Proceedings of the 17th Nordic geotechnical meeting, Reykjavik, 25–28 May 2016, pp 1193–1192

Guthrie RH, Evans SG (2004) Magnitude and frequency of landslides triggered by a storm event, Loughborougn Inlet, British Colombia. Nat Hazards Earth Syst Sci 4:475–483

Jarrett PM, Eden WJ (1970) Groundwater flow in eastern Ottawa. Can Geotech J 7:326–333

Kenney TC, Lau KC (1984) Temporal changes of groundwater pressure in a natural slope of non-fissured clay. Can Geotech J 20:138–146

Lafleur J, Lefebvre G (1980) Groundwater regime associated with slope stability in Champlain clay deposits. Can Geotech J 17:44–53

Lamontagne M, Demers D, Savopol F (2007) Description et analyse du glissement de terrain meurtrier du 25 octobre 1870 dans le rang des Lahaie, Sainte-Geneviève-de-Batiscan, Québec. Can J Earth Sci 44:947–960

Lefebvre G (1986) Slope instability and valley formation in Canadian soft clay deposits. Can Geotech J 23:261–270

Lefebvre G, Leboeuf D, Hornych P (1991) Slope failures associated with the 1988 Saguenay earthquake, Québec. Canada. Can Geotech J 29:117–130

Locat J (2011) La localisation et la magnitude du séisme du 5 février 1663 (Charlevoix) revues à l'aide des mouvements de terrain. Can Geotech J 48:1266–1286

Locat A, Leroueil S, Bernander S, Demers D, Jostad HP, Ouehb L (2011) Progressive failures in eastern Canadian and Scandinavian sensitive clays. Can Geotech J 48:1696–1712

Locat P, Leroueil S, Locat J, Demers D (2014) Chapter 11: Characterization and post-failure analysis of the 1980 landslide in sensitive clays at Havre-St. Pierre, Québec, Canada. In: L'Heureux J-S et al (eds) Landslides in sensitive clays: from geosciences to risk management, Advances in natural and technological hazards research, 36, pp 133–144

Marefat V, Duhaime F, Chapuis RP (2015) Pore pressure response to barometric pressure change in Champlain clay: prediction of the clay elastic properties. Eng Geol 198:16–29

Mitchell RJ, Eden WJ (1972) Measured movements of clay slopes in the Ottawa area. Can J Earth Sci 9:1001–1013

Ouranos (2014) Vers l'adaptation. Synthèse des connaissances sur les changements climatiques au Québec. Partie 1 : Évolution climatique au Québec. Édition 2014. Montréal, Québec: Ouranos 79 p

Perret D, Bégin C (1997) Inventaire documenté des glissements de terrain associés aux fortes pluies de la mi-juillet 1996, région du Saguenay-Lac Saint-Jean. Institut national de la recherche scientifique (INRS-Géoressources). Report presented to the Bureau de reconstruction et de relance du Saguenay-Lac Saint-Jean

Potvin J, Pellerin F, Demers D, Robitaille D, La Rochelle P, Chagnon J-Y (2001) Revue et investigation supplémentaire du site du glissement de Saint-Jean-Vianney. In: Proceedings of the 54th Canadian geotechnical conference, Calgary 2, pp 792–800

Sällfors GB, Svensson C (1984) Prediction of maximum groundwater pressure. In: Proceedings of the IV International symposium on landslides, Toronto 1984 1:437–440

Segoni S, Battistini A, Rossi G, Rosi A, Lagomarsino D, Catani F, Morretti S, Casagli N (2014) Technical note: an operational landslide early warning system at regional scale based on space-time-variable rainfall thresholds. Nat Hazards Earth Syst Sci 15:853–861

Terranova O (2002) Risk analysis of potentially damaging rainfall events. Instability – planning and management. Thomas Telford, London, pp 389–397

Transports Québec (2011) Rapport MT11–01: Glissement de terrain du 10 mai 2010 à St-Jude, Montérégie. Rapport sur les caractéristiques et les causes. Bibliothèque et Archives Nationales du Québec, Gouvernement du Québec, 101p. ISBN: 978–2–550-63733-2

Zêzere JL, Reais E, Garcia R, Oliveira S, Rodrigues ML, Vieira G, Ferreira AB (2004) Integration of spatial and temporal data for the definition of different landslide hazard scenarios in the area north of Lisbon (Portugal). Nat Hazards Earth Syst Sci 4:133–146

Chapter 48
Practicing Hazard Mitigation Strategies for a Construction on a Sensitive Clay Slope

Samson Abate Degago and Vikas Thakur

Abstract Safety level of sensitive clay slopes can rigorously be established a priori for a given preconstruction state under all foreseeable conditions. However, construction activities may alter the in-situ conditions of the slope and possibly lead to a lower safety level or an increased level of hazard beyond an acceptable level. Therefore, it is crucial to have a thorough follow up during construction activities and implement hazard mitigation measures to ensure or maintain an acceptable safety level. This is illustrated in this paper using a real case involving construction of an infrastructure in highly sensitive clay slope in Rissa, Norway. The work emphasizes that as much as establishing factor of safety or probability of failure is important in design stage, one should also equally focus on trying to reassure the analysis/assessment done in design remains valid during and after construction.

48.1 Introduction

One of the distinct feature of geotechnical engineering is the need to work with uncertainties in analysis and design of geotechnical problems. The uncertainties to be dealt with include uncertainties on soil parameters and loading conditions/resulting stresses. The uncertainties in geotechnical problem can be divided into two, i.e. aleatory (inherent) uncertainty and epistemic uncertainty (reducible) (e.g. Lacasse and Nadim (1996); Phoon and Kulhawy (1999); Nadim (2007)). The current geotechnical practice attempts to address epistemic uncertainties using different ways such as by collecting more ground investigation data of high quality and by making provision for a higher safety margins.

Assessment of slope stability is an important geotechnical problem. In general, stability of natural slopes for a given state can be assessed using either probabilistic

S.A. Degago (✉)
Norwegian Public Roads Administration (NPRA), Trondheim, Norway
e-mail: samson.degago@vegvesen.no

V. Thakur
Department of Civil and Environmental Engineering, Norwegian University of Science and Technology (NTNU), Trondheim, Norway
e-mail: vikas.thakur@ntnu.no

V. Thakur et al. (eds.), *Landslides in Sensitive Clays*, Advances in Natural and Technological Hazards Research 46, DOI 10.1007/978-3-319-56487-6_48

or non-probabilistic methods. Currently there is an increased activity towards introducing probabilistic based reliability approaches to achieve a systematic risk assessment of landslides (e.g. Fell et al. (2005); Lacasse (2015)). The existing practice adopted by the Norwegian transportation agencies, the Norwegian Planning and Building Acts provide design codes and guidelines for assessment of stability of slopes. These design codes require a certain partial factor of safety (FS) which is a function of damage consequence classes should a failure occur and failure mechanisms of soil materials (e.g. see NPRA (2010); Oset et al. (2014)). The required FS vary from 1.4 to 1.6 and are established using best estimate of characteristic values. In this way, an attempt is made to implicitly address epistemic uncertainties controlling slope stability. This implies that, the adopted approach aims to indirectly account for uncertainty and risk within dimensioning principles.

Safety level of natural slopes can rigorously be established a priori for a given preconstruction state and under all foreseeable conditions. Still, construction activities may alter the in-situ conditions of the slope and possibly lead to a lower safety level or an increased level of hazard beyond an acceptable level. Therefore, it is crucial to have a thorough follow up during construction activity and implement hazard mitigation measures whenever necessary to ensure acceptable safety level. Within the framework of landslide risk assessment and management concepts, this article aims to illustrate the significance of qualitative (observation) approach, engineering judgement (experience) and on-site inspection/monitoring for safer execution of a critical infrastructure in sensitive clay slope. The work presents practical implementation of hazard mitigation strategies adopted during a project that involved construction activities on a sensitive clay slope in central part of Norway.

48.2 Brief Project Description

As part of a road construction project, a bridge named *Skaudal Bridge*, is planned to be founded on the sensitive clay deposit located in Rissa municipality, central part of Norway. Skaudal Bridge is 90 m long bridge with three span and four foundation axes where pile groups transfer the load to a bedrock. A longitudinal section of the bridge depicting the slope and the layer of highly sensitive clay is shown in Fig. 48.1. Part of the bridge foundation requires installation of bored steel pipe piles at the top and bottom of the sensitive clay slope. At axis 1, the piles ($2 \times \varnothing 813$ mm) are 23 m long while at axis 2, the piles ($3 \times \varnothing 914$ mm) are 10 m long. An average inclination of the ground slope between axis 1 and 2 is 1:3 towards the river. According to the hazard zonation carried-out by the Norwegian Water Resources and Energy Directorate (NVE) (www.skrednett.no), this area is classified as high hazard level. More on such hazard classification can be referred in Kalsnes et al. (2014).

An extensive geotechnical investigation done for the project (see NPRA 2014) showed that the extent of the sensitive clay is much larger than the one originally mapped by the concerning authority, i.e. NVE. The area is generally characterized

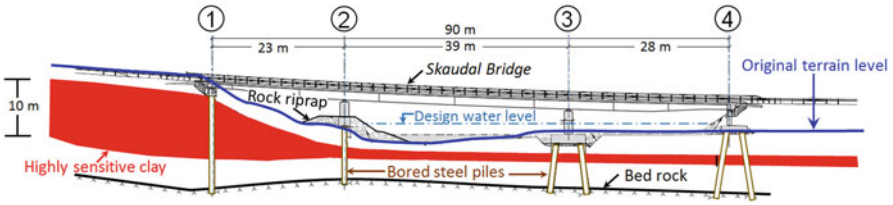

Fig. 48.1 Skaudal Bridge and sketch of extent of the highly sensitive clay layer

Table 48.1 Geostatistical characterization of the highly sensitive clay deposit in the slope

Parameters (symbols)	Unit	Mean	Standard deviation
Unit weight (γ)	kN/m^3	18.9	0.3
Natural water content (w)	%	34.6	2.9
Liquid limit (w_l)	%	30.9	2.5
Plastic limit (w_p)	%	22.9	1.4
Plasticity index (I_P)	%	8.2	2.0
Undrained shear strength (fall cone) (c_u)	kPa	79	18.0
Remolded shear strength (fall cone) (c_{ur})	kPa	0.8	0.4
Friction angle (ϕ)	° (degree)	30.5	0.2
Cohesion (c)	kPa	4.8	0.7
Preconstruction pore pressure ratio (r_u)	–	0.25	0.15

by highly overconsolidated clay with high undrained shear strength at natural state. However, at remolded state the shear strength is seen to be as low as 0.3 kPa. An important feature of this highly sensitive clay layer is that it starts at shallow level, for example, it starts at just 3.5 m depth below the terrain around axis 1 of the bridge. This means that the sensitive clay layer makes part of the slope which is unsupported sideways, Fig. 48.1. The slope is also dominated by under-hydrostatic pore water pressure condition with a ground water table (GWT) that lies at shallow depth, i.e. at the top of the slope the GWT lies at an average depth of 0.7 m from the terrain. Geostatistical data of the highly sensitive clay in the slope are given in Table 48.1. These data were compiled from 23 cylinder samples retrieved from depths between 2 and 15 m in the highly sensitive clay and from 25 pore pressure measurements made between depths 5 m and 20 m. The pore pressure ratio, r_u, is defined as $r_u = \mathrm{u}/(\gamma \mathrm{h})$, where γh is the total overburden pressure at a depth h and u is measured pore water pressure at the same depth h.

48.3 Landslide Hazard Assessment

As a first step in landslide hazard assessment, slope stability analyses are performed to assess local and overall stability condition of the slope. For the critical profile, overall stability analysis yielded minimum FS = 1.34 under preconstruction state

and with measured pore water pressure distribution. This is below the required FS for overall stability, i.e. 1.4. Therefore counter measures, i.e. 1.5 m unloading at the top of the slope and 2 m fill at the toe of the slope, were needed to satisfy the required percentual improvement of the FS as per the NVE (2011) guideline. In addition, landslide hazard is assessed using First-Order Reliability Method (FORM) as implemented in the software Strurel (RCP 2009). In doing so, a limit state function was established for a selected cross-section using Janbu's method (Janbu 1954). This cross-section, with a slope angle of 1:3 and 20 m high, is considered to reflect the overall stability of the slope in this project. The resulting limit state function (f) used for FORM analysis of this cross-section is given in Eq. (48.1) and it is verified using the governing calculation method used for design, i.e. limit equilibrium method based on effective stress analysis. Thus the mean factor of safety (FS_μ) deduced from Eq. 48.1 matches FS results of the slope stability analysis (NPRA 2013).

$$f(\varphi, c, r_u, \gamma, h) = 3.13 \cdot (1 - r_u) \cdot \gamma \cdot h \cdot tan\varphi + 13.3 \cdot c - \gamma \cdot h \tag{48.1}$$

In the FORM analysis, strength and pore water pressure parameters are considered as random variables without correlation among each other and the strength parameters are approximated by lognormal distribution while r_u is modeled by normal distribution. Similar statistical distributions have also been adopted in various literature (e.g. Dai et al. (1993), El-ramly et al. (2005), Nadim (2007)). For simplicity γ and h are modelled as constants. An important part of epistemic uncertainty is referred to as model uncertainty. This is the result of idealization of an actual problem while modeling it numerically. There exist different ways to take into account model uncertainty in a limit state function (e.g. Phoon and Kulhawy (2003), Nadim (2007)). In this study, however, model uncertainty is not considered as the FORM analysis was mainly aimed to assess hazard in relative aspect for various construction stages. In addition, the limit state function, f, in Eq. (48.1) was verified with the governing slope stability method adopted for design.

The relatively large coefficient of variation in r_u indicates that the relative uncertainty in pore pressure is substantial. Furthermore, the value of r_u is expected to be affected by construction activities on the slope. Hence, FORM analysis is made for various selected stages of the slope and the analysis results are presented in Table 48.2. The results are given in terms of probability of failure (P_f), reliability index (β) and factor of safety corresponding to mean values of the input parameters (FS_μ).

For the current study, the relative values of P_f and β are more important than the absolute values as they reflect the relative level of hazard at various construction stages. A scenario where part of the slope experience hydrostatic pore water pressure distribution gave a significant increase in P_f or reduction in β and FS_μ, Table 48.2. This implies that it was crucial to maintain the under-hydrostatic pore water pressure condition during and after construction activity. To control this, it was thus decided to monitor pore water pressure changes in the slope.

Table 48.2 Results of slope stability analyses for various stages of the slope

Stage	r_u (−)		P_f	β	FS_μ	Remark
	Mean	Stdev.				
Preconstruction	0.25	0.15	1/25	1.74	1.34	Based on in-situ data.
Terrain improvement	0.25	0.15	1/33	1.87	1.38	This involves 1.5 m unloading at the top and 2 m filling at the toe of the slope.
During bridge construction	0.43	0.14	1/4	0.73	1.10	Established with an assumption that certain part of the slope experience hydrostatic pore water pressure condition.
Long time after construction	0.25	0.15	1/33	1.87	1.38	Assuming that the pore water pressure comes back to the initial state in the long term.

It has been documented that piling activity can induce disturbances in a sensitive clay slope and trigger large landslide, e.g. Surte landslide in Sweden and others (Bernander (2000), Leroueil (2004)). Should an initial slide occur, the sensitive clay slope in this project has a potential to satisfy the criteria for large landslides (e.g. Tavenas et al. (1983); Trak and Lacasse (1996); Leroueil et al. (1996); Thakur and Degago (2012); Thakur et al. (2014)). It is thus crucial to avoid a possible initial slide that could trigger large landslide. Identifying mechanism that can trigger initial failure is an important aspect of landslide hazard assessment. With this aspect, installation of pile at the top and bottom of the sensitive clay slope are the most critical construction activities. It is also important to avoid erosion at the toe of the slope.

48.4 Framework for the Risk Assessment

Within context of risk management, ISO 31000 defines important steps in risk management process, i.e. risk identification, risk analysis and risk assessment. Elements of these, as related to the project, are briefly mentioned in this section.

Establishing Basis The basis for special attention on this project is the presence of sensitive clay. The extent of the sensitive clay was initially established using maps by NVE; and, this was used in the early planning phase of the project. However, extensive ground investigations revealed that the sensitive clay area was larger than initially indicated by NVE. The updated map, depicting extent of the highly sensitive clay, has formed a basis for subsequent actions and design considerations.

Risk Identification It is worthwhile to mention that the landscape depicts scars of an old landslide indicating that the slope is marginally stable. In addition, the highly sensitive clay layer lies only 3.5 m from the top of the slope implying that it is unsupported sideways and forms part of the slope. In this project, the main hazard

emanates thus from a potential for an initial slide due to the construction activity planned at the critical part of the slope, i.e. pile installations at the crest and toe of the slope. Thus remolding of the highly sensitive clay and pore pressure increase are identified as key aspects of risk sources that can potentially start an initial slide.

Elements at Risk and Consequences Should the construction activity start an initial slide, then this can trigger a much larger landslide. This will primarily endanger the life of the on-site workers (i.e. vulnerability factor is 1.0 when on-site workers are on or near the slope). In addition, a slide can also result in damage of properties, destruction of nearby infrastructure including part of the bridge under construction, loss of agricultural land, flooding in the upstream river and ecological impact. Loss of reputation of the involved companies in the project as well as the resources spent in aftermath of a slide are also considered as part of undesired consequences.

Risk Analysis and Assessment Stability (reliability) analysis has shown that it is important to control pore pressure increase. Thus, the design pore pressure profile was selected to be higher than the characteristics/measured pore pressure distribution to make an allowance for a possible pore water pressure increase due construction activity. Afterwards, the slope is designed such that the local FS is 1.6 and the overall FS is 1.4. In this way, a margin and threshold values are established as an allowance for a possible increase in pore pressure during construction. This approach has also helped to establish values of pore water pressure to stop construction activity and to evacuate on-site workers.

Risk Reduction Measures Aspects of hazard mitigation and risk reduction strategies are presented in the next section.

48.5 Hazard Mitigation and Risk Reduction Strategies

Preparedness and prevention are central part of risk management, as they generally are effective and convenient solutions. The procedures adopted to mitigate hazard and to reduce the associated risk are briefed below.

Communications and Raising Awareness at Different Levels Communication and awareness are key in managing risk. In the early phase of the project, the project leader was made aware of the challenges and complexity of the planned construction activity. This was vital so that sufficient resource, in terms of money and time, are allocated for the geotechnical considerations. It also helped to communicate it further with politicians/decision makers and to manage expectations.

In the initial bridge design, 6 and 4 piles were planned respectively at axis 1 and 2 requiring up to 7 m deep excavation of the highly sensitive clay in the slope. Part of the important communications was thus made with the structural engineers where design modifications had to be made once the extent of the sensitive clay was realized to be wider and lying shallower than expected. As a result, the bridge was re-designed with minimum possible piles in the slope whereby any excavation is avoided at the toe of the slope and an excavation depth is limited to 2.5 m at the

top of the slope (Fig. 48.1). Bored steel pipes with down-the-hole (DTH) drilling method are selected to minimize effect of mass displacement and pore pressure increase.

A series of meetings were held especially with the resident- and assistant resident engineer of the project regarding geotechnical aspects of the project. The aim with these meetings was to define and communicate the key aspect of the project in a clear way and to assign respective roles and responsibilities. This was important since they will be following up and controlling the construction every day. In preparation of the contract document, specific geotechnical requirements were clearly stated so that the contractors consider them in bidding for the project and that the client shall be controlling these activities closely. Before the start of the construction, a meeting was held with all the on-site workers to explain the planned construction sequences and the rationale behind them as well as ways to communicate risks and the related actions. Throughout the project execution, there has been continuous dialog and communications.

Establishing Basis at Early Stage Stability analysis indicated the importance of monitoring pore water pressure conditions so that construction activities do not increase it beyond a level that impairs the stability of the slope. Thus, to establish initial basis, the monitoring started one year before the commencement of the construction to study natural pore pressure variations throughout a year-cycle period. Monitoring was done at six measurement locations containing 22 piezometers at various depths ranging from 5 to 20 m. The data acquisition was made via a remote monitoring service where measurements are registered hourly into a website. The piezometers were kept operative until construction activities were completed.

Decision on the Construction Sequence The construction is planned with a certain sequence with a main objective of maintaining acceptable safety levels at all construction stages. Below is a brief summary of the main construction activities and their sequence as planned during the design phase so that the safety level is not worsened due to construction activity.

1. *Blasting activity*: A blasting activity away from the sensitive clay slope was performed in a controlled way. The aim is that the crushed rocks can then be used for erosion protection and for counter filling at the toe of the sensitive clay slope.
2. *Erosion protection (rock riprap)*: There was an indication of old erosion protection but due to an increased consequence of failure, additional protection was necessary. Approximately 1 m-thick crushed rock riprap was thus designed to be placed on the toe of the slope and along the sensitive clay area adjacent to the river.
3. *Temporary counter filling*: On top of the new erosion protection layer, a 1 m-thick crushed rock layer was designed at the toe of the slope near pile installation points. This was necessary to counterbalance the heavy weight of the drilling machine that weighs 80 ton, i.e. a distributed load of 40 kPa with in an area of 20 m^2.

4. *Unloading at the top of the slope*: After fillings at the toe of the slope, the safety of the slope shall increase to allow construction at the top of the slope. Thus, a 1.5 m-thick terrain unloading at the top of the slope shall be performed. Afterwards, an additional 1 m-thick local excavation around axis 1 shall be performed.
5. *Pile installation at axis 3 and 4*: Axes 3 and 4 of the bridge lies on the flat ground where there is no stability problem (see Fig. 48.1). The piling method shall be evaluated at these locations with respect to induced pore pressure changes, mass displacement and vibrations.
6. *Pile installations at axis 1 and 2*: Based on the experience from axes 3 and 4, the piles shall be installed at axis 1 and 2.
7. *Finalizing the remaining activities:* This includes removing the temporary filling at the toes of the slope, filling back 25 cm-thick fertile soil for crop cultivating at the top of the slope and finalizing construction of the road and the bridge.

On-Site Inspection – Establishing Experience The contractor presented a recently developed down-the-hole (DTH) drilling system. This system is designed to have an enhanced air flushing system such that leakage of compressed air into the surrounding soil body is avoided. The system shall also avoid excess pore pressure development and soil mass displacements. To evaluate the performance of this new method, the client decided to evaluate the drilling system after a well-documented initial experience during installation of piles at axis 3 and 4. During installations in axis 3, vibration measurements were made according to NS 8141–3:2014 guideline. The maximum attained value of 27 mm/s was measured during drilling through the working platform of 1 m-thick crushed rock. This is less than the maximum allowed value of 45 mm/s. However, since vibration can potentially lead to liquefaction of materials, it is rather preferable to minimize it. Hence, the lesson learned from this was to avoid drilling through the working platform (crushed rock) in axes 1 and 2.

Installation of piles at axis 4 was followed up with three piezometrs placed at various locations and depths. Measurements showed that the drilling system did not perform as described and its performance was unacceptable for a sensitive clay slope. A maximum excess pore pressure increase of 107 kPa (from 58 to 165 kPa) was measured at 3.3 m horizontal distance and 6 m depth from the pile center being installed. It was also observed that the compressed air did not always returned inside the casing as desired, i.e. it also leaked via outside of the casing tube and through the adjacent installed piles. Thus, the contractor had to make amendments and validate them with a pile test resembling the condition at axis 1. The pile test was carefully performed with modified procedure while the client followed this up with pore pressure measurements. The measurements were well within acceptable limits and the pile test was deemed successful. The experience established with the pile test was then used to install the piles at axis 1 and 2 (see Degago et al. (2016) for details).

On-Site Inspection – Observational Approach and Judgement It is crucial to do a proper follow up at site, especially for constructions in sensitive clay. As a controlling system, installation of piles at axis 1 and 2 was monitored with five

piezometers installed at various depths and distances from the piles. Initially it was planned to acquire continuous measurement data remotely. However, the system could only make remote measurements at a certain interval, which was deemed too long to use as a basis for early warning or evacuation purpose. Thus, the pore pressure measurement had to be made manually and evaluated during piling. Accordingly, the piling activity was stopped twice due to increase excess pore pressure to threshold values. Piling resumed once the pore pressures were back to their normal values.

Even though a good deal of the homework is done during the desk study a priori, unforeseen changes may still arise during construction. In such cases, it is important to do steps that minimize the probability of failure or reduce actions that may compromise the safety margin. These actions can, at times, be pragmatic solutions that are known to improve stability of a slope. Some examples from this project include: before piling at axis 1, placing of ca. 0.75 m-thick layer of crushed rock to support the slope sideways (between axis 1 and 2); adjusting the 1 m-thick rock working platforms during installation of the two piles at axis 1; removing the platforms right after installations at axis 1 was finished so as to relief the slope for piling at axis 2; protection of the excavations at the top of the slope with geotextile to control water infiltration from rain and melted snows; providing proper drainage around axis 1 to properly drain water from an even bigger slope at the back; controlling temporary fills and excavations; avoiding hammering during piling that may induce vibrations; at points where piles for axis 2 are to be installed, locally excavating and replacing the rock fill layer at the toe of the slope to avoid drilling through it.

48.6 Closing Remarks

Safety level of natural slopes can rigorously be established a priori for a given pre-construction state and under all foreseeable conditions by either probabilistic or non-probabilistic approaches during desk study. Even though probabilistic approaches allow for systematic handling of parameter uncertainty, using a fully probabilistic approach for a stability analysis is a formidable task. The current NPRA guideline is based on non-probabilistic approach where implicit considerations are made to address uncertainty, hazard and risk within dimensioning principles. In this way, an attempt is made to benefit from reliability approaches without performing rigorous probabilistic analyses.

In this work, stability analysis and hazard assessment performed during desk study are briefly presented. These analyses helped to identify major sources of uncertainties that influence stability of the slope with an emphasis on construction scenario that may possibly lead to a lower FS or higher P_f beyond an acceptable level. A certain construction sequence is thus defined with main objective of maintaining an acceptable safety level at all stages. The work advocates that it is crucial to have a thorough follow up during all construction activities and implement

hazard mitigation measures whenever necessary to ensure acceptable safety levels are maintained at all stages of construction. Within the framework of landslide risk assessment and management concepts, this article presents a real case to illustrate the significance of qualitative (observation) approach, sound engineering judgement (experience) and on-site inspection/monitoring for safer execution of a critical infrastructure in sensitive clay slope. The work presents practical implementation of hazard mitigation strategies adopted during a project that involved construction activities on a sensitive clay slope in Rissa municipality, central part of Norway.

Back-analysis of recent slides that have occurred in Norway (e.g. Leistad, Lyngen, E18 Skjeggestad) have generally showed that the slopes were subjected to a condition where *FS* dropped to less than unity (decrease in β or increase in P_f). The authors do not believe that such slides could have been avoided by using either probabilistic or non-probabilistic analyses in design. The occurrences of these slides have more to do with unforeseen events or unplanned activities at the sites than calculation methods. It is important to thus note that *FS* or P_f of a slope are valid only for the given sets of information under all foreseeable conditions. Unplanned activity that were not foreseen during design may alter the in-situ conditions of the slope and result in a different *FS* or P_f. Thus, as much as establishing *FS* or P_f is important in design phase one should also equally focus on trying to reassure the analysis/assessment done during the design phase remains valid during and after construction. This becomes even more crucial for highly sensitive clay slopes.

Acknowledgments Ørjan Edvardsen, Henrik Tømmervik, Steinar Giske, Svein Hove, Per Olav Berg, Frode Oset and several others at Norwegian Public Roads Administration (SVV) are greatly acknowledged for their part in making this project a success. The authors wish to acknowledge Vidar Gjelsvik at Norwegian Geotechnical Institute (NGI) for reviewing this paper.

References

Bernander S (2000) Progressive landslides in long natural slopes. Licentiate thesis: Luleå University of Technology

Dai Y, Fredlund DG, Stolte W (1993) A probabilistic slope stability analysis using deterministic computer software. In: Conference on probabilistic methods in Geotechnical Engineering Canberra, pp 267–274

Degago SA, Giske S, Hove S, Tømmervik S, Edvardsen Ø (2016) Erfaringer med boring av stålrørspeler i kvikkleireskråning. In: 17th Nordic geotechnical meeting, Reykjavik. pp 961–971

EI-Ramly H, Morgenstern NR, Cruden DM (2005) Probabilistic assessment of stability of a cut slope in residual soil. Géotechnique 55(I):77–84

Fell R, Ho KKS, Lacasse S, Leroi E (2005) A framework for landslide risk assessment and management. In: Proceedings of the International conference on landslide risk management, Vancouver, pp 3–25

ISO 31000 (2009) Risk management – principles and guidelines. A standard by International Organization for Standardization (IOC)

Janbu N (1954) Stability analysis of slopes with dimensionless parameters. PhD thesis. Harvard University. Soil Mechanics Series no. 46, 81 p

Kalsnes B, Gjelsvik V, Jostad HP, Lacasse S, Nadim F (2014) Risk assessment for quick clay slides–the Norwegian practice. Adv Nat Technol Hazards Res 36:355–367

Lacasse S (2015) Hazard, risk and reliability in geotechnical practice. In: 55th Rankine Lecture

Lacasse S, Nadim F (1996) Uncertainties in characterising soil properties. Geotechnical special publication No. 58, Proceedings of Uncertainity'96, Shackelford et al., eds., ASCE, pp 49–75

Leroueil, S. (2004) Geotechnics of slopes before failure. Landslides: evaluation and stabilization. In: Proceedings of 9th International symposium on landslides, Rio de Janeiro, vol 1. Side 863–884

Leroueil S, Vaunat J, Picarelli L, Locat J, Faure R, Lee H (1996) A geotechnical characterization of slope movements. In: Proceedings of the 7th International symposium on landslides, Trondheim, pp 53–74

Nadim F (2007) Tools and strategies for dealing with uncertainty in geotechnics. In: Probabilistic methods in geotechnical engineering. Springer, pp 71–96.

NPRA (2010) Guidelines for geotechnical engineering in road constructions – handbook V220. Available at http://www.vegvesen.no/Fag/Publikasjoner/Handboker (in Norwegian)

NPRA (2013) Fv. 715 Keiserås–Olsøy. Geothechnical evaluation report. Norwegian Public Roads Administration (NPRA). Sveis Nr. 2012039995-010 /Ud925Ar10 (in Norwegian)

NPRA (2014) Fv. 715 Keiserås–Olsøy. Geothechnical report for Skaudal Bridge. Norwegian Public Roads Administration (NPRA). Sveis Nr. 2012039995-013 /Ud925Ar13 (in Norwegian)

NS 8141–3:2014 (2014) Norwegian Standard (NS). Vibration and shock guideline. Part 3: Effects of vibration from blasting on triggering landslide in quick clay

NVE (2011) Construction on brittle clays. Guidelines by the Norwegian Water resources and Energy directorate (NVE) (in Norwegian)

Oset F, Thakur V, Dolva BK, Aunaas K, Sæter MB, Robsrud A, Viklund M, Nyheim T, Lyche E, Jensen OA (2014) Regulatory framework for road and railway construction on the sensitive clays of Norway. Adv Natl Technol Hazards Res 36:343–355

Phoon KK, Kulhawy FH (1999) Characterization of geotechnical variability. Can Geotech J 36(4):612–624

Phoon KK, Kulhawy FH (2003) Evaluation of model uncertainties for reliability-based foundation design. In: Proceedings of 9th International conference on applications of statistics and probability in civil engineering, San Francisco, vol 2, pp 1351–135.

RCP (2009) STRUREL – a structural reliability analysis program system. SYSREL users manual. Reliability Consulting Programs (RCP) GmbH, Munich, Germany

Tavenas F, Flon P, Leroueil S, Lebuis, J (1983) Remolding energy and risk of slide retrogression in sensitive clays. In: Proceedings of the symposium slopes on soft clays, Linköping, SGI. pp 423–454

Thakur V, Degago SA (2012) Quickness of sensitive clays. Géotechn Lett 2(3):87–95

Thakur V, Degago SA, Oset F, Aabøe R et al (2014) Characterisation of post-failure movements of landslides in soft sensitive clays. Adv Natl Technol Hazards Res 36:91–103

Trak B, Lacasse S (1996) Soils susceptible to flow slides and associated mechanisms. In: Proceedings of the 7th International symposium on landslides, vol 1, Trondheim, pp 497–506

Chapter 49
Mapping of Landslide Risks in a Changing Climate – Development of Simplified Methodology

Karin Odén, K. Bergdahl, H. Löfroth, G. Göransson, Å. Jönsson, R. Kiilsgaard, and M. Öberg

Abstract The Swedish Geotechnical Institute (SGI) is assigned by the Swedish government to perform risk assessment for landslides in soft soil along priority watercourses as one part of the national climate adaptation funding. From the previously developed landslide risk mapping methodology applied for the Göta River Valley emerged a need for a less extensive methodology that could be implemented at significantly lower cost. Hence, the aim is to develop a sufficiently simplified methodology that could provide a basis for planners in municipalities and county administrative boards in their work with prioritization and preparation of adaptation measures. A criterion was also that such a methodology should ease the interpretation of the landslide risk maps, thereby increasing the societal relevance and usability of the results. The Norsälven River valley was used as a pilot area. The landslide risk analysis along the Norsälven River valley has resulted in a comprehensive overview of the landslide risk in the present and future climate, for built-up as well as undeveloped land and areas with vital infrastructure. The main implications of the climate change for the Norsälven River valley concerns the effect of increased erosion on the slope stability caused by increased water flow. The simplified methodology for landslide risk mapping that has been developed is applicable for landslide risk mapping along other river valleys. However, some modifications will be necessary due to site specific conditions.

49.1 Introduction

The effects of the ongoing climate change will have an impact on the physical environment threatening the safety of buildings and infrastructure. In Sweden, rainfall is expected to increase especially during the winter, while summers may become drier. This will affect groundwater levels and river flows, which can change

K. Odén (✉) • K. Bergdahl • H. Löfroth • G. Göransson • Å. Jönsson • R. Kiilsgaard • M. Öberg
Swedish Geotechnical Institute (SGI), Linköping, Sweden
e-mail: karin.oden@swedgeo.se

V. Thakur et al. (eds.), *Landslides in Sensitive Clays*, Advances in Natural and Technological Hazards Research 46, DOI 10.1007/978-3-319-56487-6_49

the conditions for erosion and landslides. Many communities in Sweden are located along rivers and several areas along these rivers are susceptible to landslides. There is therefore a need for a national mapping along river valleys to identify and prioritize areas in need of action and adaptation.

Between 2009 and 2012 SGI carried out a risk assessment of the Göta River Valley with regard to climate change and with a focus on field investigations, probability and consequences of landslides, assigned by the Swedish government, The Göta River Valley investigation is herein referred to as GÄU. The landslide risk mapping method used in GÄU (SGI 2012) consists of three main parts; (i) assessment of the probability of landslides, (ii) assessment of the consequences of landslides in monetary terms, and (iii) combining probability and consequences into a risk "value". The assessment of the probability of landslides was based on traditional stability analyses and were calculated using a First Order Reliability Method (FORM), where the undrained shear strength, drained shear strength, density as well as the geometry were given uncertainties. And the assumed propagation of a landslide was assessed with respect to the presence of quick clay (Larsson et al. 2008), (Åhnberg et al. 2014). The consequences in GÄU were calculated in monetary values and added up within 100 m squares. The values of the squares were further added up to a likely landslide extent to get a "total" consequence cost at a certain distance from the riverbed.

After completion of the GÄU, SGI subsequently identified and prioritised additional watercourses for landslide risk mapping (Bergdahl et al. 2013). The Norsälven River valley (further referred to by the Swedish name Norsälven) Fig. 49.2, is the first river valley mapping after the GÄU and has served as a pilot study for the development of a less extensive methodology for landslide risk mapping, to a lower cost compared to that of GÄU (Andersson-Sköld et al. 2014), (Löfroth et al. 2012).

The new methodology should result in a general but comprehensive landslide risk mapping that can provide sufficient basis to suggest the need for further analyses within municipalities' and county administrative boards' work with adaptation. The landslide risk mapping contributes to considerable societal benefits by providing basis material to: avoid/mitigate the consequences of landslides; reduce the likelihood of landslides; support the national environmental quality objectives; provide input to planning for adaptation.

In this paper some of the modified parts of the GÄU methodology are described. A detailed description is given in SGI (2015).

49.2 Methodology for Landslide Risk Assessment and Mapping

Landslide risk is here defined as a combination of the probability of a landslide and the consequence of such event. The developed probabilities for landslides and associated consequences are combined in a risk matrix to evaluate the landslide risk level, Fig. 49.1.

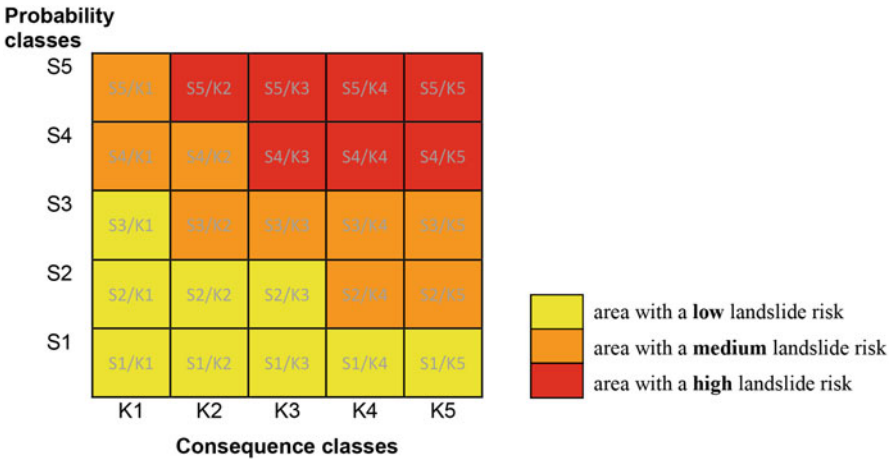

Fig. 49.1 The risk matrix used in Norsälven The risk is classified in three levels; high, medium and low, with corresponding colours, *red*, *orange* and *yellow* in the maps of landslide risk

In this paper, parts of the methodology for landslide risk assessment used in Norsälven is presented, for other parts see Bergdahl et al. (2016) and Göransson et al. (2016). The methodology is based on the extensive GÄU investigation but has been simplified with respect to geotechnical investigations (sparsely distributed investigations in general but detailed in representative areas), prognosis of future river erosion (based on a hydrodynamic model and critical shear stress), assessment of landslide extent (evaluation of historical landslides extent), landslide probability (Point Estimate Method) and consequence analysis (qualitative valuation).

49.2.1 Pilot Study Area

The investigation of Norsälven extends from the Lake Lower Fryken outlet in Kil municipality to Norsälven's estuary in Lake Vänern in the Karlstad municipality, a distance of about 30 km, which is equivalent to 60 km of shoreline, Fig. 49.2. The investigation area has been divided into three sections named South, Middle and North, Fig. 49.2, on the basis of geological conditions as well as for practical reasons, as these sections are divided by two hydropower plants at Frykfors and Edsvalla. The river is slightly meandering and flows in a glacial sediment-filled valley that is characterized by severe gully formation and landslide scars. The sediment consists mainly of fine sediments that in some parts are underlain by coarser glacio-fluvial deposits. Investigation of landslide risks in tributaries or deep valleys that lie within the area of investigation has not been done explicitly, but with assessment based on the results of the calculations along the river.

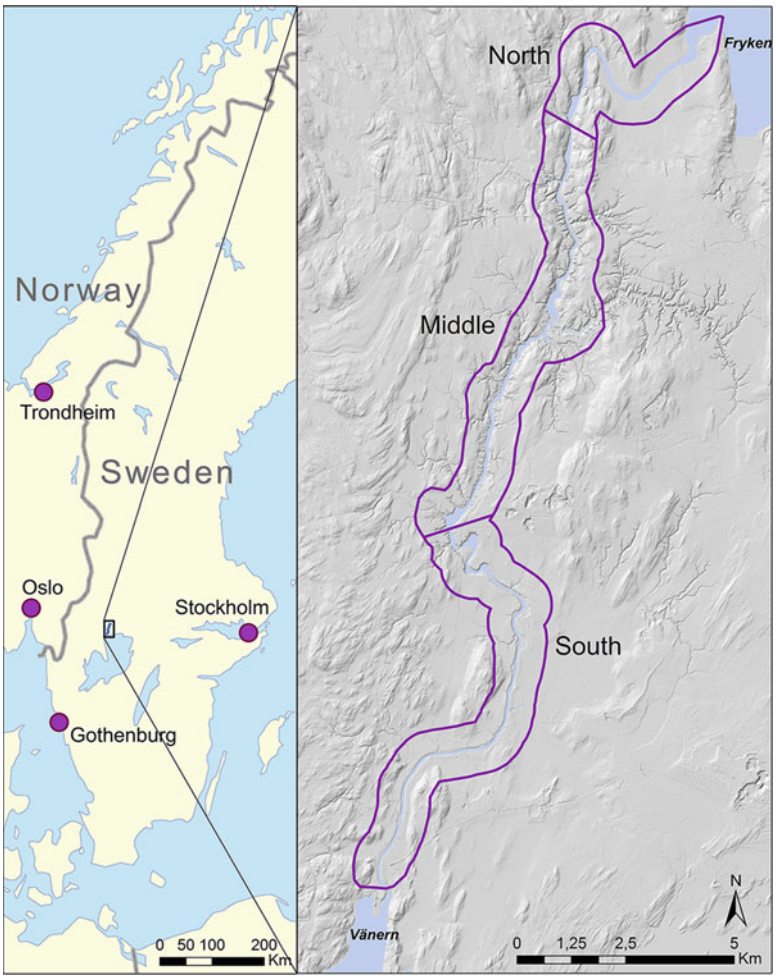

Fig. 49.2 Overview of the investigation area, Norsälven, Sweden (© SGI, Lantmäteriet, Geodatasamverkan)

According to a climate analysis for the county with the most profound increase during the winter months, precipitation will increase by approximately 20% until year 2100. The frequency and intensity of rain burst will increase as well (Persson et al. 2014).

49.2.2 Geotechnical Investigations

Thirty different cross-sections were identified to represent different geological and geometrical conditions along the river. A distance of 1–2 km in between the

investigated sections (compared to 400 m in GÄU) were tried out in order to still get representative geological information, which is quite sparse. Prior to the planning of the field and laboratory work, earlier investigations were gathered and analysed. Based on these results, some areas required supplementary and detailed geotechnical investigations. The methods used in the supplementary investigations were mainly cone penetration tests, CPTu, (including registration of total force for mapping of quick clay (Åhnberg et al. 2014), vane tests, piston sampler and sampling bolt.

49.2.3 River Erosion Due to Climate Change

The magnitude of expected erosion is an important parameter when predicting the stability conditions in a future climate because of its impact on the resisting forces of a slope. A GIS-method for the analysis of bed erosion with respect to the effect of climate change is presented in GÄU. In this study, the method was further developed by combining a bed erosion model with a bank erosion model; one GIS model to compute bed erosion and one spreadsheet model to compute bank and bank toe erosion in some representative geotechnical cross-sections. The method assumes cohesive sediments and formulas for cohesive sediments have been used. The modelling requires, among other things, geological data, bathymetry, sediment properties, hydrodynamic properties, changes in bathymetry with time, data on governing erosive flows, duration of such flows in the future with respect to increased precipitation due to climate change. A concise description of the method is given in Göransson et al. (2016).

49.2.4 Probability Analysis for Slope Stability

The probability of slope failure is based on traditional models for slope stability calculation, incorporating parameter uncertainties determined using experience from similar areas as well as statistics from previous investigations. Both drained and undrained conditions prevail along Norsälven and the Point Estimate Method (PEM) (Sällfors 1990) was chosen to facilitate the calculations for drained conditions. Before the decision, PEM was tested for some of the GÄU analyses to control the suitability and accuracy of the method, which gave results with consistency. Undrained shear strength, drained shear strength as well as the density had been identified having a great impact on stability and were defined with an uncertainty expressed as a mean value and a standard deviation (using a coefficient of variation). The geometry which also has a great impact on stability was not treated as a probabilistic parameter, as the uncertainty of the geometry in each section was regarded as small (the slope geometry determined with great accuracy).

Representative values of the undrained shear strength were based on results from vane shear test and CPT-sounding as well as fall cone tests; direct simple shear tests (DSS) and some triaxial tests. Clearly deviant values were disregarded. The drained shear strength was determined with CPT. Apart from the undrained and drained shear strength as well as the density the rest of the input parameters were seen upon as deterministic.

Firstly, traditional slope stability calculations were made using probable mean values of the parameters to be able to decide if undrained or drained conditions were governing in each analysed section. Thereafter, PEM was used in order to get the mean value, coefficient of variation as well as the relative probability of failure of the safety factor for each section. In this operation, maximum and minimum values of the undrained shear strength, drained shear strength as well as the density are varied in a traditional slope stability program calculating eight different slope stability safety factors per section. In order to assess the change of the probability of failure due to future erosion, similar calculations were performed with conditions applicable to year 2100.

The same classification system as in GÄU for the landslide probability is suggested for Norsälven. The relations between the safety factor, F, and probability of failure, P_f, with respect to the coefficient of variation of the safety factor, V_F, is shown in Fig. 49.3, assuming that lnF is normally distributed. With the results from the analysed representative sections this classification system was then used to assess the probability class along the Norsälven investigation area.

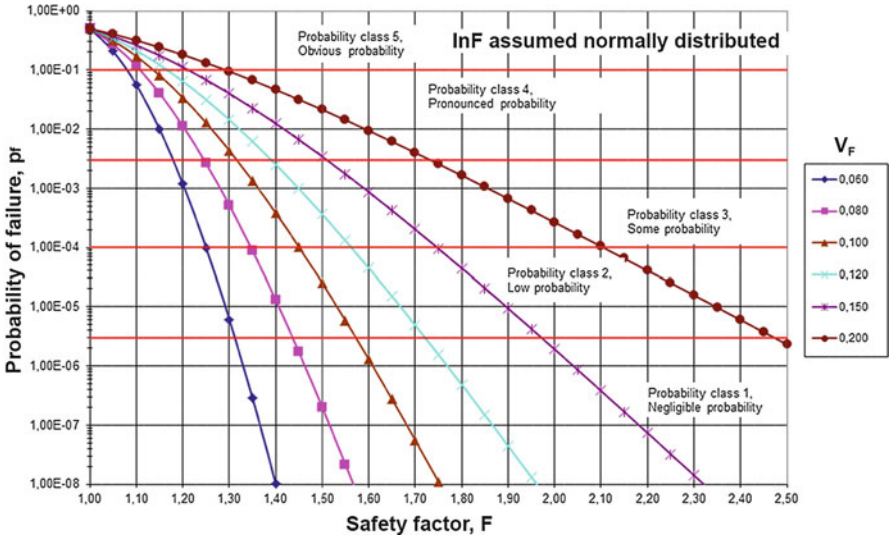

Fig. 49.3 The figure illustrates the relation between the safety factor, F, and probability of failure, P_f, with respect to the coefficient of variation of the safety factor, V_F, from Fig 3.1 in Berggren et al. (2011)

49.2.4.1 Assessment of Landslide Propagation

In order to assess the area for which a particular landslide probability apply, an estimate of landslide retrogression for that area must be considered. A method specially developed for the Göta River valley (Larsson et al. 2008) and modified for GÄU was verified for Norsälven by studying the impact of slope height, type of soil as well as sensitivity (Järvin 2014) and comparing with the extent of older landslides in the region. The extent of landslide retrogression is determined for slopes with an initial slip surface that has a safety factor of 1.3 or lower in an undrained analysis or 1.2 or lower in a combined analysis, if this slip surface includes a soil volume with a sensitivity of 50 or higher (Åhnberg et al. 2014). A modification for Norsälven was made such as the inclination1:15 was used to assess the maximum landslide extent, whereas in GÄU it was assumed that an initial landslide would propagate over the whole area of quick clay for extremely quick clays (St $\geq$ 200), which could result in that it reaches firm ground. The estimation of the landslide extent is thus dependent on the sensitivity of the clay.

49.2.5 Consequences of Landslide

In parallel with the calculation of the probability of landslides, the consequences of landslides along the river have also been assessed. To simplify the analysis in comparison to GÄU, a qualitative valuation of the most important consequences were chosen. The consequences for the buildings and the transport routes in the area (available as GIS-layers) have been valued on the basis of four quality criteria: life, environment, economy and social importance. Landslides in the river valley may affect many people and important social functions. A landslide also means suffering, sorrow or discomfort for many people and thus the overall consequence of a landslide can include various implications for which it is difficult to make a systematic valuation. Possible impact of a changing climate on the consequences has not been assessed since such information is not available.

The consequences have been divided into five consequence classes, K1-K5, see Table 49.1. In the combination of data with various consequences the greatest value within each grid square has determined the consequence class which has been a necessary development of a qualitative method.

49.2.6 Landslide Risk

All parts of the investigation area are assigned a probability class and a consequence class. The combinations of these two classes make pairs of values that describe a risk class. This classification can also be displayed in a matrix to show how various risk classes relate to one another. In order to simplify the risk assessment

Table 49.1 Classification of consequences of landslides

C-class	C-level	Description of consequences
K1	Mild	No persons are injured or killed. No environmentally hazardous activity/enterprises affected and little environmental risk. Small economic losses. Loss of social function with very little social significance. Other/Minor roads (minor road, tractor road, footpath, running tracks, hiking trail, cable car, ferry route)
K2	Large	A few people are injured or killed. No environmentally hazardous activities/enterprises affected and medium environmental risk. Medium-sized economic losses. Loss of social function with low social significance. Public road class III (width < 5 m); Drive/neighborhood road
K3	Very large	Number of wounded or dead persons that corresponds to the number of people in a smaller dwelling with several homes. Environmentally hazardous activities suffer with serious consequences for the environment. Large economic losses. Loss of important social function. Public roads class II (width 5–7 m); Thoroughfare; Road under construction
K4	Extremely large	Number of wounded or dead people that corresponds to the number of people at a larger school, apartment buildings or major railway station. Environmentally hazardous activity involving extremely serious consequences for the environment. Extremely large financial losses. Loss of important social function. Public road separate carriageways; Public road in (width > 7 m)
K5	Catastrophic	Number of wounded or dead people that corresponds to the number of people in an indoor arena (thousands people, high density). Environmentally hazardous activity involving catastrophic consequences for the environment. Catastrophically large economic losses that distinguishes itself from most of the economic losses. Loss of very important social function. All railways; Highways

C Consequence

the risk matrix is divided into three different risk levels: low, medium and high risk level, see Fig. 49.1. The results from the landslide risk analysis represent a general level of probability and consequences, where a qualitative assessment of the consequences has been carried out and, therefore, qualitative evaluation of the landslide risk is given. In Fig. 49.4 an example of a risk map is illustrated. Separate maps are produced in GIS for probability class as well as consequence class to ease the interpretation of the resulting landslide risk maps. The impact of climate change on landslide probability was assessed in the same way as in GÄU, i.e. based on the magnitude in change between landslide probability of today and landslide probability for year 2100 considering expected erosion. Three different categories were used: (a) low sensitivity – climate change generally implicates no change in probability class, (b) moderate sensitivity – climate change causes the probability class to increase by one level in relevant sections along the river, and (c) high sensitivity – climate change causes the probability class to increase by one or two levels in the relevant sections along the river. Note that areas which already have

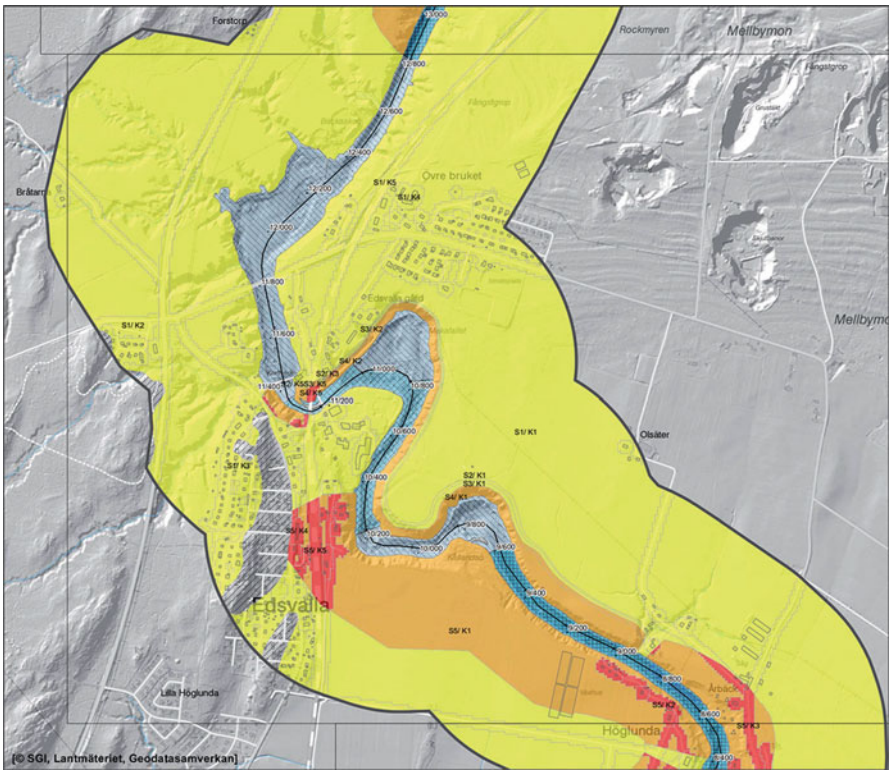

Fig. 49.4 Example of Landslide risk map for part of Norsälven (SGI 2015). *Yellow* indicates a low, *orange* medium and *red* a high landslide risk. The different *blue* colours in the river, indicates different levels of climate impact along the investigation area (© SGI, Lantmäteriet, Geodatasamverkan)

high landslide probability were given high sensitivity since even minor erosion can trigger a landslide. This was not done in the same way in GÄU.

49.3 Conclusions

In comparison with the GÄU the pilot study for Norsälven has resulted in a modified methodology which enables risk analysis at lower cost and yet sufficient accuracy. Although a control of the geometry of the representative cross-sections in comparison to geometry of the areas it represent is crucial as it might have a great impact on the probability of landslides. The used methodology gives a comprehensive overview of the risk of landslides in the present and future climate, for built-up as well as undeveloped land, and areas with vital infrastructure. The methodology is also applicable for other river valleys, although further adjustments

may be needed due to geological and other differences. This will be tested for the next river in line, Säveån in Southwest Sweden, and for the river Ångermanälven representing the Northern parts of Sweden.

Acknowledgement The work has been funded by the governmental climate funding for the Swedish Geotechnical Institute. We would like to express our gratitude to all the employees at the SGI who made this study possible and Ph.D. Marius Tremblay for great revision work.

References

Åhnberg H, Löfroth H, Lundström K (2014) Management of quick clay areas in slope stability investigations – the Göta River valley. In: Landslides in sensitive clays. From geosciences to risk management, Advances in natural and technological hazards research; 36. Springer, Dordrecht, pp 383–394

Andersson-Sköld Y, Falemo S, Tremblay M (2014) Development of methodology for quantitative landslide risk assessment – example Göta river valley. Nat Sci 6(3):130–143

Bergdahl K, Cederbom C, Göransson G (2013) Prioritering av områden för skredriskanalys, Klimatanpassningsanslag 2013, Statens geotekniska institut, SGI, Publikation 6. Linköping, Sweden

Bergdahl K, Odén K, Löfroth H, Göransson G, Jönsson Å, Kiilsgaard R (2016) Landslide risks in a changing climate, Nors River pilot study area. Proceedings of the 17th Nordic geotechnical meeting, Reykjavik 25th–28th May, 2016

Berggren B, Alén C, Bengtsson P-E, Falemo S (2011) Metodbeskrivning sannolikhet för skred: kvantitativ beräkningsmodell. Statens geotekniska institut in Swedish, Göta älvutredningen, GÄU Delrapport 28. Linköping, Sweden

Göransson G, Hedfors J, Ndayikengurukiye G, Odén K (2016) Climate change induced river erosion as trigger for landslide. Proceedings of the 17th Nordic geotechnical meeting, Reykjavik 25th–28th May, 2016

Järvin S (2014) Studie av faktorer som påverkar skredutbredningen vid Norsälven, Värmland, Lunds universitet, Geologiska institutionen, Kandidatarbete nr 392. Lund, Sweden

Larsson R, Bengtsson P-E Edstam T (2008) Vägbyggande med hänsyn till omgivningens stabilitet, Vägverket Region väst, Dnr AL90 B 2007:27435, Statens geotekniska institut, SGI, Slutrapport 08-05-29. Linköping, Sweden

Löfroth H, Lundström K, Schälin D, Åhnberg H, Blied L, Falemo S (2012) Modifiering av metodiker använda inom Göta älvutredningen, Statens geotekniska institut, SGI, Varia 638. Linköping, Sweden

Persson G, Ohlsson A, Eklund D, Sjökvist E, Hallberg K (2014) Klimatanalys – Värmlands Län, Publikationsnummer 2014:2, Länsstyrelsen Värmland, Karlstad, Sweden

Sällfors G (1990) Punktskattningsmetoden, En statistisk metod användbar på geotekniska problem, Chalmers Tekniska Högskola, Geohydrologiska forskningsgruppen, Meddelande nr 89, Göteborg, Sweden

SGI (2012) Skredrisker i Göta älvdalen i ett förändrat klimat, GÄU 2009–2011, Statens geotekniska institut, Linköping, Sweden. Also available in an English version

SGI (2015) Skredrisker i ett förändrat klimat – Norsälven, SGI, Publication 18-1 –4, Statens geotekniska institut, Linköping, Sweden. Also available in an English version

Chapter 50
Quick-Clay Hazard Mapping in Norway

Ingrid Havnen, Hanne Bratlie Ottesen, Ellen D. Haugen, and M. H. Frekhaug

Abstract The Norwegian Water Resources and Energy Directorate (NVE) is responsible for the national quick-clay hazard mapping in Norway, and for the presentation of the quick-clay hazard zones that are identified. The first quick-clay hazard mapping started in the beginning of 1980, in the southeast and middle parts of Norway, initiated by the big quick-clay landslide in Rissa, Norway, in 1978. Today, there are nearly 2000 mapped quick-clay hazard zones in Norway, and the mapping is still ongoing. In the last years (2012–2015), the methods for evaluating quick-clay hazard zones and the presentation of quick-clay areas have been developed through the multi-disciplinary research project Natural Hazards: Infrastructure for Floods and Slides (NIFS), which is a cooperation between the Norwegian National Rail Administration (NNRA), the Norwegian Public Roads Administration (NPRA) and the NVE. New and improved quick-clay hazard maps are one of the positive outcomes of this project. Increased accessibility to geotechnical data is important for the quick-clay mapping, which is improved through the new national database for ground investigations (NADAG). Another outcome of the NIFS project is the quick-clay areas mapped by the NPRA, which are shown together with the quick-clay hazard zones on the NVE website. The NIFS project has also developed new methods for run-out areas and shoreline evaluation, which from now on will be included in the mapping.

I. Havnen (✉)
Norwegian Water Resources and Energy Directorate (NVE), Trondheim, Norway
e-mail: inha@nve.no

H.B. Ottesen • M.H. Frekhaug
Norwegian Public Roads Administration (NPRA), Oslo, Norway
e-mail: hanne.ottesen@vegvesen.no; martine.holm.frekhaug@vegvesen.no

E.D. Haugen
Norwegian Water Resources and Energy Directorate (NVE), Tønsberg, Norway
e-mail: edha@nve.no

V. Thakur et al. (eds.), *Landslides in Sensitive Clays*, Advances in Natural and Technological Hazards Research 46, DOI 10.1007/978-3-319-56487-6_50

50.1 Introduction

Sensitive clays in Norway that have been provoked by manmade or natural causes have led to several landslide disasters throughout history. The most well-known are the landslides in Verdal (1893, 55 million m^3, 116 casualties) (Janbu et al. 1993) and Rissa (1979, 5 million m^3, 1 casualty). These landslides occurred in highly sensitive clays, also known as quick clays, which are defined as clays with remoulded shear strength $\leq$0.5 kPa (NGF 1982). A more conservative definition is sometimes also used: clays with remoulded shear strength $\leq$2.0 kPa and sensitivity $\geq$15, called brittle material (NVE 2014; NIFS 2016d). Quick-clay landslides are characterised by a sudden collapse in the material structure and by a relatively rapid development where the clay becomes liquid and can reach high velocity. To prevent large landslides, mapping of potential areas for quick clay started in the 1980s after the Rissa landslide, and this work is still ongoing.

Landslides can have natural triggering causes, e.g. erosion along rivers or canals, but in some cases, it is difficult to single out an obvious triggering factor. Landslides can also be related to human activity. Some Norwegian governmental agencies, such as the Norwegian Water Resources and Energy Directorate (NVE) and the Norwegian Public Roads Administration (NPRA), present regulatory frameworks for construction in areas with sensitive clay deposits (NVE 2011, 2014; NPRA 2014a, b). The NVE guidelines (NVE 2014) advise on how to assess overall stability in areas with quick and sensitive clays. They focus on site investigations, mapping of quick-clay areas, design procedures and safety precautions for construction works, in addition to design principles for securing natural slopes.

The NVE is responsible for the national quick-clay hazard mapping in Norway, and for the presentation of the resulting hazard and risk zones. This is done by using a risk-based priority approach based on the developed areas that are most exposed to landslides. The national project Natural Hazards: Infrastructure for Floods and Slides (NIFS), which was initiated by the NPRA, the Norwegian National Rail Administration (NNRA) and the NVE (NIFS 2012, 2016a), has led to improved quick-clay maps by compiling data from the NPRA's archive and by developing new mapping methods. The present paper describes the new quick-clay maps, how the new methods for shoreline and run-out areas are being implemented in the national quick-clay mapping, and the current general method for quick-clay mapping in Norway.

50.2 Tools for Quick-Clay Mapping

Today, there are several databases with information about marine clay and quick-clay areas. This includes the NVE website (NVE Atlas and report database), the NPRA reports and ground investigations databases (RapportWeb and GUDB), Geological Survey of Norway (NGU)'s Quaternary geological maps and NADAG (National Database for Ground Investigations).

50.2.1 Quaternary Geological Maps, NGU

Prior to quick-clay hazard zone mapping, sediment mapping has to be carried out. This work is done by the NGU. Marine sediments and marine limit are of particular importance to quick-clay related issues. Data are shown on the NGU website (www.ngu.no). Since quick clay is leached marine clay, it is found below the marine limit. The marine limit is the highest level the sea reached in an area following the Ice Age. Quick clay can also be found underneath other sediment deposits, e.g. sand, gravel or peat. For more information on the marine limit and quaternary geology as a basis for landside susceptibility, see Hansen et al. (2014, 2017) and the NGU website.

50.2.2 NADAG (National Database for Ground Investigations), NGU

For quick-clay mapping, data from previous ground investigations are important for registering new quick-clay zones and for upgrading existing zones. NADAG is a national database that has been developed by the NGU in cooperation with the NIFS project. In time, this database will include data from all the governmental agencies e.g. NPRA, NNRA and NVE. At present, it includes geotechnical data from Statsbygg (the Norwegian government's key advisor in construction and property affairs, building commissioner, property manager and property developer) and from some municipalities. You can find more information about NADAG in Solberg et al. (2017) and on the NGU website (http://www.ngu.no). The NADAG web application: http://geo.ngu.no/kart/nadag.

Due to the quick-clay hazard mapping and the building of physical flood and landslide protection works, the NVE has collected data from ground investigations in a geotechnical report database. The NVE is working on updating and publishing the reports on the NVE website and on transferring the data to NADAG.

The NPRA has registered over 20,000 geotechnical reports in the database "RapportWeb". The reports date from the 1940s and until today. In parallel to RapportWeb, the NPRA has a database for detailed geotechnical data (GUDB). This database includes information about several hundred thousand geotechnical boreholes. The data from RapportWeb and GUDB will be imported into NADAG.

50.3 The National Programme for Quick-Clay Mapping

The first national quick-clay hazard mapping started in the beginning of 1980 in the southeast and middle parts of Norway, initiated by the big quick-clay landslide in Rissa, Norway, in 1978. Since 2000, all of the hazard zones have been classified through the "Programme for increased safety against landslides in clay", which was

developed by the Norwegian Geotechnical Institute (NGI). This employs a method for evaluating hazard, consequence and risk. This method is still in use (NGI 2001; Kalsnes et al. 2014) and the results are shown on the NVE website NVE Atlas.

Today, there are nearly 2000 quick-clay hazard zones in Norway. The focus now is on densely populated areas where quick clay can potentially occur (NVE 2011). GIS analyses facilitate a more detailed selection of which areas to map. The final selection of new areas for mapping is based on the quaternary geological maps from the NGU (areas susceptible to quick-clay landslides), the GIS analysis and some general information on sensitive sediments and relief.

The hazard is an expression of the probability of a landslide, and it is evaluated by the topographical, geotechnical and hydrological conditions and changes due to human activities, climate effects, erosion, etc. The consequence is based on population, settlement, infrastructure, etc. Each of these factors is given a score and is weighted according to its importance in causing a landslide, or according to the consequences a landslide would have, as shown in Table 50.1 for the hazard.

The hazard is divided into 3 classes; "high hazard" (score 26–51), "middle hazard" (score 18–25) and "low hazard" (score 0–17), as shown in Fig. 50.3 (and scores in Table 50.1). As for the hazard, the consequence is also divided into 3 classes: "not severe", "severe" or "highly severe". The risk, which is the product of hazard and consequence, is divided into 5 classes. Tables for the consequence and risk classes are shown in the literature (Kalsnes et al. 2014; NGI 2001).

The national quick-clay mapping is not very detailed, and it focuses on areas that can be exposed to natural large landslides (greater than 1 hectare). It is based on certain terrain criteria:

- Slopes steeper than 1:15
- Terrain height, H > 10 m
- Maximal length of the hazard zone is equivalent to 15 × H from the bottom of the ravine/slope to the back of the zone.

Table 50.1 Evaluation of hazard score

Hazard factor	Weight	Score for hazard			
		3	2	1	0
Earlier landsliding	1	Frequent	Some	Few	None
Height of slope, H (m)	2	>30	20–30	15–20	<15
Overconsolidation ratio (OCR)	2	1.0–1.2	1.2–1.5	1.5–2.0	>2.0
Excess pore pressure (kPa)	3	> + 30	10–30	0–10	Hydrostatic
Under pore pressure (kPa)	−3	> − 50	−(20–50)	−(20–0)	Hydrostatic
Thickness of quick-clay layer	2	>H/2	H/2–H/4	< H/4	Thin layer
Sensitivity, S_t	1	>100	30–100	20–30	< 20
Erosion	3	Active/sliding	Some	Little	None
Landscape worsening	3	Important	Some	Little	None
Landscape improvement	−3	Important	Some	Little	None
Maximum weight score		51	34	17	0

Kalsnes et al. (2014) and NGI (2001)

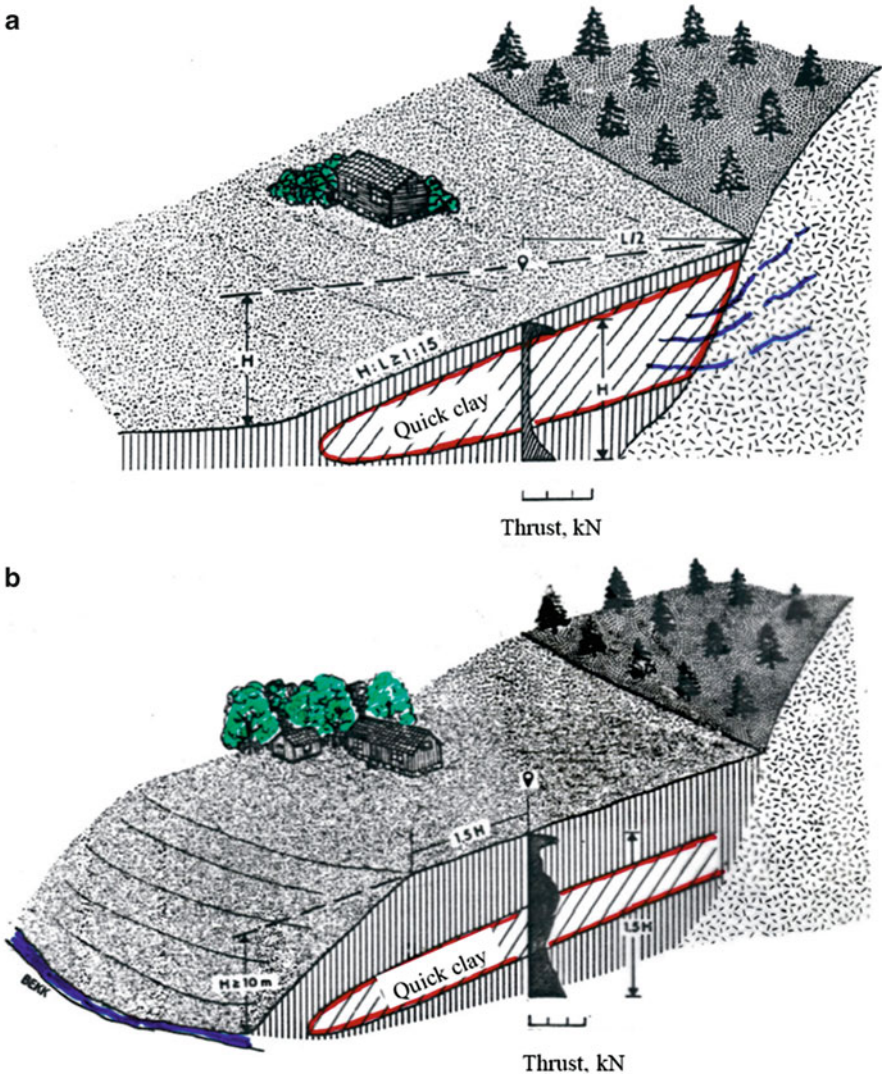

Fig. 50.1 Principles for soundings in quick-clay zones (NGI 2001) (**a**) Perspective in smoothly sloping terrain (**b**) Perspective in ravine terrain

The investigations are conducted based on map studies, field inspections and limited ground investigations, often with only one geotechnical sounding per zone. The sounding interpretation must indicate quick clay at a strategic level. The principles for this are shown in Fig. 50.1 for (a) sloping and (b) ravine terrain, respectively.

With a minimum terrain slope of 1:15 and 10 m terrain height difference, experience shows that most areas with potential for large quick-clay landslides

are covered. Still, obviously, quick-clay landslides can also occur with lower topographic criteria, and a more conservative approach must be used for local mapping and land-use plans, as described in the NVE guidelines (NVE 2014). Therefore, some zones may also be mapped in more detail.

In principle, quick clay may occur in all areas with marine clay, also outside the mapped quick-clay hazard zones. All areas below the marine limit are therefore susceptibility zones for potential landslides in quick clay.

In the last years, as a basis for landslide mitigation in populated areas, priority has been given to investigation and detailed mapping of earlier defined quick-clay hazard zones in the two highest risk classes (4 and 5) and with "high hazard".

Traditionally, the initial mapping approach has been map sheets (as shown in Fig. 50.2). In the last years, the NVE has defined the mapping areas by municipalities.

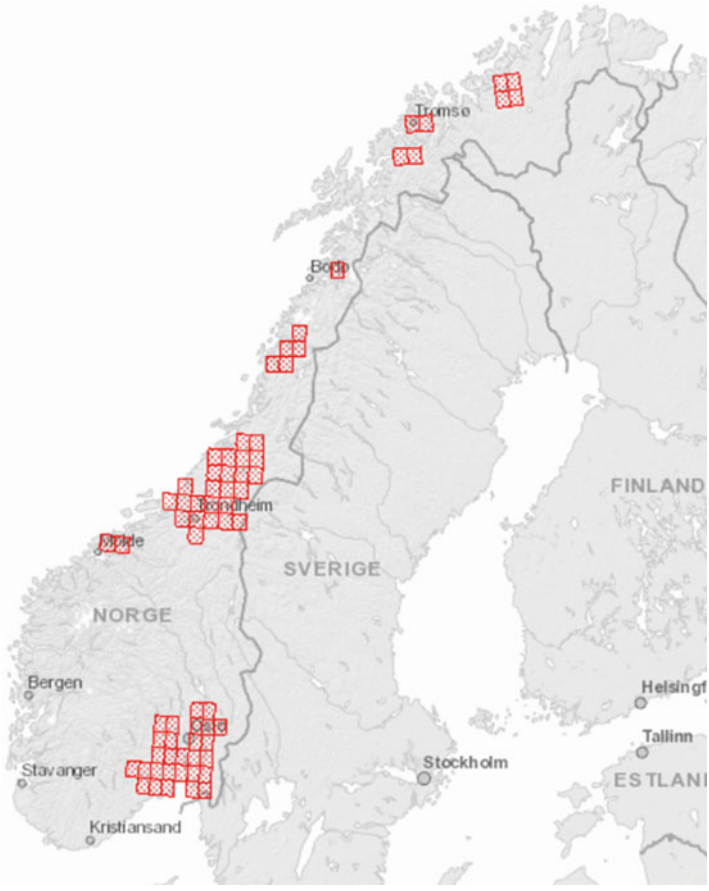

Fig. 50.2 Quick-clay mapping in Norway (NVE Atlas). *Red* areas are mapped

50.4 NVE Quick-Clay Hazard Maps and Cooperation with the NPRA

The quick-clay hazard maps are presented on the NVE website (www.nve.no): "Map services" with "Map catalogue" and "NVE Atlas", as shown in Figs. 50.2 and 50.3. By zooming in on the mapped areas in Fig. 50.2, the NVE quick-clay hazard zones and the NPRA quick-clay areas will be shown, see Fig. 50.3. The NPRA datasets come from the NPRA's report database, "RapportWeb". In the database, it is possible to search for reports related to quick clay. Reports with indicated or proved quick clay are registered. From these, quick-clay areas are drawn (pink shaded areas in Fig. 50.3) on the NVE website. The NPRA has also recorded boreholes with proved quick clay from lab-tested samples, shown as pink dots on the map. Currently, the map is extended with over 1350 quick-clay areas. NOTE that the NPRA quick-clay areas are not quick-clay hazard zones, since they are not classified with hazard, consequence and risk, and the terrain criteria are not considered.

The purpose of showing these datasets together is to improve the quick-clay hazard maps and the system for presenting quick-clay data. The NPRA data are of

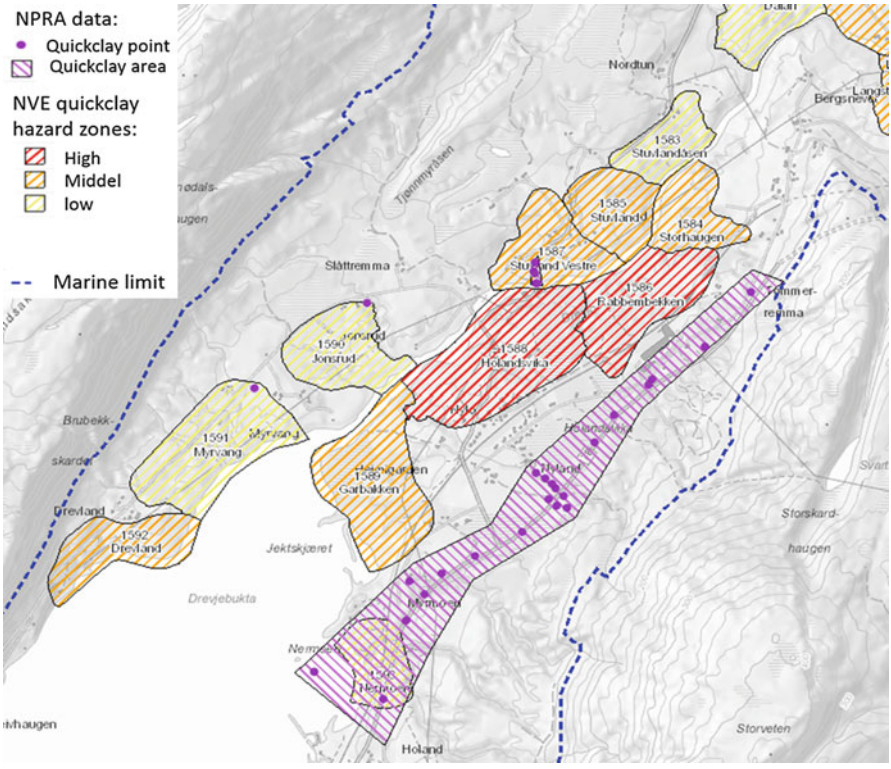

Fig. 50.3 Quick-clay hazard zones and quick-clay areas (NVE Atlas)

great importance in areas where the national quick-clay mapping (done by the NVE) has not been carried out, since the data will indicate hazardous areas. Presenting these data is also important in mapped areas, since areas outside the quick-clay hazard zones also may represent danger, especially in construction situations. In land-use planning, all areas below the marine limit are susceptibility zones for potential landslides in quick clay (NVE 2014). Therefore, by showing all data together, the municipalities get a better tool for land-use planning.

The maps also save time and money when it comes to new mapping and land-use planning, because the NPRA data provide direct information about potential areas for quick-clay hazard zones and will be easily available through the NVE Atlas and NADAG. Fast access to data is also important in emergency preparedness for landslides. With more available data, the quality of the quick-clay hazard zones will improve. The NPRA gives priority to adding to the database in areas where the NVE is planning new mapping.

50.5 New Methods in the National Quick-Clay Mapping

Through the NIFS project, new methods for mapping, which will bring mapping a step further, have been developed. "Tools for quick-clay mapping" provides a better basis for mapping (NIFS 2016c). In addition to basic mapping, new methods have been/are being developed to include the shoreline and to evaluate run-out areas and retrogression distances (NIFS 2014, 2016b). There has also been a project on "Detection of brittle materials", which can be used for better detection of quick clay (NIFS 2016d).

50.5.1 Shoreline Mapping

The principles of shoreline mapping are that both map studies on land and bathymetric data must be included in the evaluation of the hazard zone, see Table 50.1:

- The slope height of the seabed is included. The height is measured between the foot and the top of the most critical slope within the hazard zone.
- Earlier sliding, erosion and human activity (worsening or improving effect) must be evaluated both on land and for the seabed.
- Excess pore pressure can be shown as pockmarks on the seabed, as circular depressions made by water or as gas outflow from the underground.
- The overconsolidation ratio (OCR) tends to be one at the seabed, which gives the highest score.

Including the seabed in the hazard zones is important since Norway has had several landslides along the shore in the last years.

50.5.2 Run-Out Area

Run-out area has not previously been mapped, but this is as important as the quick-clay hazard zones themselves. The extent of damage can be even more catastrophic in the run-out zone, especially if there is a high degree of urbanization and important infrastructure downstream. The landslide debris may dam an area, with large damage and consequences both upstream and downstream as a result. To decide the run-out area, the run-out distance must be considered as a start (Fig. 50.4).

The run-out distance, Lu, depends on the form of the run-out area, what type of landslide that can occur (retrogressive (flow) or rotational/flake) and on how to calculate the retrogression distance. Here, the geometry of the quick-clay pocket and the potential for the remoulded clay to evacuate the landslide scar are considered. The factors are dependent on the amount of ground investigations. For a retrogressive landslide to occur, studies show that more than 40% of the material over the critical slip surface should be quick or sensitive. For a flow slide to occur, the remoulded shear strength should also be less than 1 kPa ($c_{ur} < 1$ kPa) (NIFS 2016b; Thakur et al. 2014). Since the national mapping often has only one geotechnical sounding per quick-clay hazard zone, and often no samples, the run-out distance must be conservative. For these cases, a conservative evaluation of the landslide type and the most conservative retrogression distance must be used. In most cases, this will give a retrogressive slide (flow slide) with at retrogression distance, L, of 15 × H (L/H = 15) from the bottom of the ravine/slope (toe). The run-out distance, Lu, is determined by the terrain type in the run-out area:

Channelized terrain: Lu = 3*L
Open terrain: Lu = 1.5*L
If the landslide type is a rotational/flake, the following run-out distance can be used:
Lu = 0.5*L.

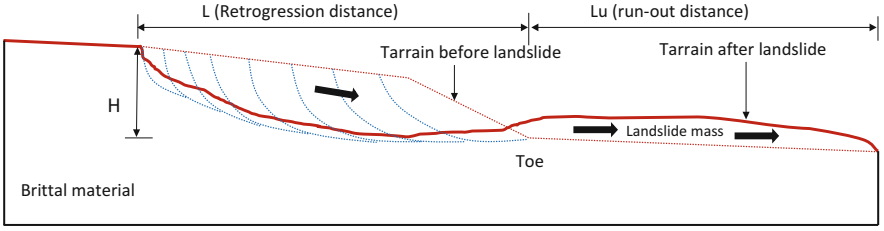

Fig. 50.4 Principles for the evaluation of retrogression and run-out distance of a landslide (NIFS 2016b)

50.6 Conclusions

The national quick-clay hazard mapping has been improved by including evaluations of the shoreline and the run-out areas. The methods are tested in the ongoing mapping. In time, this will provide improved maps for land-use planning, which will result in fewer landslides in the shoreline and better mitigation measures in the run-out areas.

The cooperation with the NRPA, by showing their quick-clay data on the NVE website, has been a success. The quick-clay data, together with data from NADAG, provide more information about areas that are susceptible to quick-clay landslides, as a supplement to the NVE hazard zones. The data are also an important tool for the emergency preparedness system for landslides.

Acknowledgements The cooperative research programme "Natural Hazards: Infrastructure for Floods and Slides (NIFS)" by the NPRA, the NNRA and the NVE is acknowledged for its work. The authors also wish to express their gratitude to the reviewer Inger-Lise Solberg, NGU, for her valuable feedback.

References

Hansen L, Høgaas F, Sveian H, Olsen L, Rindstad BI (2014) Chapter 16: Quaternary geology as a basis for landslide susceptibility assessment in fine-grained, marine deposits, Onshore Norway. In: L'Heureux JS, Locat A, Leroueil S, Demers D, Locat J (eds) Landslides in sensitive clays: from geosciences to risk management, Advances in natural and technological hazards research 36. doi:10.1007/978–94–007-7079-9_13, Springer, Dordrecht

Hansen L, Solberg IL, Jarna A, Nordahl B (2017) Developments in mapping and web presentation of fjord-marine deposit distributions for quick-clay related work in Norway. In: 2nd International Workshop on Landslides in Sensitive Clay (IWLSC), Trondheim, Norway, June 2017

Janbu N, Nestvold J, Røe Ø et al (1993) Leirras – årsaksforhold og rasutvikling. Særtrykk fra Verdalsboka Ras i Verdal, bind B. (Clay slides, causes and development. Offprint from the book "Verdalsboka Ras i Verdal, bind B). ISBN 8–9909500–8-5 (in Norwegian)

Kalsnes B et al (2014) Chapter 16: Risk assessment for quick clay slides – the Norwegian practice. In: L'Heureux JS, Locat A, Leroueil S, Demers D, Locat J (eds) Landslides in sensitive clays: from geosciences to risk management, Advances in natural and technological hazards re-search 36, doi: 10.1007/978–94–007-7079-9_13, Springer, Dordrecht

NGF (Norsk Geoteknisk Forening) (1982) Veiledning for symboler og definisjoner i geoteknikk – presentasjon av geotekniske undersøkelser. Norwegian Geotechnical Society, Oslo. (in Norwegian)

NGI rapport 20001008–2 (2001): Program for økt sikkerhet mot leirskred. Metode for kartlegging og klassifisering av faresoner, kvikkleire, rev 3 2008 (in Norwegian)

NIFS (2012) Programplan 2012–2015 for etatsprogrammet. ISSN: 1501–2832. Available from http://www.naturfare.no (in Norwegian)

NIFS (2014) Skredkartlegging i strandsonen – videreføring Report 27/2014. ISBN: 978–82–410-0974-7. Available from http://www.naturfare.no (in Norwegian)

NIFS (2016a) NIFS – sluttrapport. Report 43/2016. ISSN: 1501–2832. Available from http://www.naturfare.no (in Norwegian)

NIFS (2016b) Metode for vurdering av løsne- og utløpsområder for områdeskred. Report 14/2016. ISSN: 1501–2832. ISBN: 978–82–410-1204-4. Available from http://www.naturfare.no (in Norwegian)

NIFS (2016c) Verktøy for kvikkleirekartlegging. Report 41/2016. ISSN: 1501–2832. Available from http://www.naturfare.no (in Norwegian)

NIFS (2016d) Detection of brittle materials. Summary report with recommendation. Report 27/2016. ISBN: 1501–2832. ISBN: 978–82–410-1218-1. Available from http://www.naturfare.no

NPRA (2014a) Håndbok N200 Vegbygging. Available from http://www.vegvesen.no/Fag/Publikasjoner/Handboker (in Norwegian)

NPRA (2014b) Håndbok V220 Geoteknikk i Vegbygging. Available from http://www.vegvesen.no/Fag/Publikasjoner/Handboker (in Norwegian)

NVE (2011) Plan for skredkarlegging. Report no. 14/2011. ISSN: 1501–0678 (in Norwegian)

NVE (2014) Sikkerhet mot kvikkleireskred. Vurdering av områdestabilitet ved arealplanlegging og utbygging i områder med kvikkleire og andre jordarter med sprøbruddegenskaper. Veileder 7/2014. ISSN: 1501–0678 (in Norwegian)

Solberg IL, Nordahl B, Hansen L, Grøtan BO, Gulbrandsen S (2017) The Norwegian National Database for Ground investigations (NADAG) – a tool to assist in landslide hazard zonation. 2nd International Workshop on Landslides in Sensitive Clay (IWLSC), Trondheim, Norway, June 2017

Thakur V et al (2014) Some discussions related to the post-failure moments for landslides in sensitive clays Geoteknikkdagen 2014 (in Norwegian)

Author Index

V. Thakur et al. (eds.), *Landslides in Sensitive Clays*, Advances in Natural and Technological Hazards Research 46, DOI 10.1007/978-3-319-56487-6

Subject Index

V. Thakur et al. (eds.), *Landslides in Sensitive Clays*, Advances in Natural and Technological Hazards Research 46, DOI 10.1007/978-3-319-56487-6